

MAY 2018

AJNR

VOLUME 39 • PP 797-992

AJNR

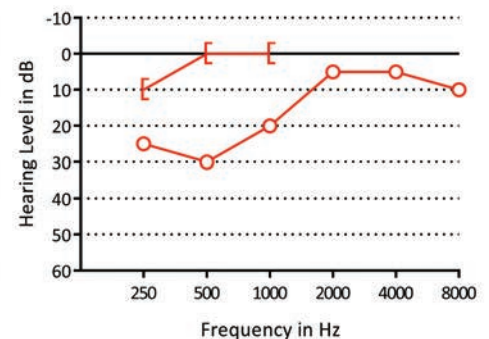
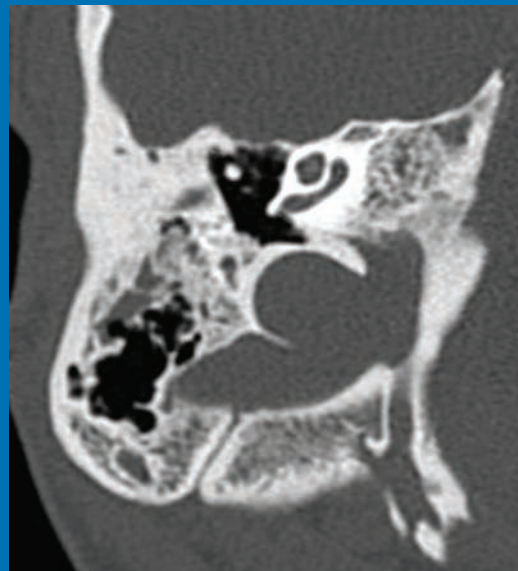
AMERICAN JOURNAL OF NEURORADIOLOGY

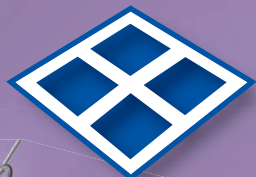
MAY 2018
VOLUME 39
NUMBER 5
WWW.AJNR.ORG

THE JOURNAL OF DIAGNOSTIC AND
INTERVENTIONAL NEURORADIOLOGY

Current status of vertebroplasty and kyphoplasty
Treatment of giant aneurysms with Tubridge flow diverter
Ear malformations in 22q11.2 deletion syndrome

Official Journal ASNR • ASFNR • ASHNR • ASPNR • ASSR





LVIS®

Intraluminal Support Device

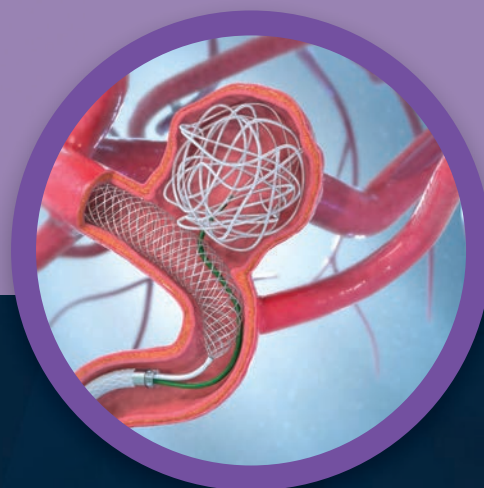
Low-profile Visualized Intرالuminal Support

Stent Deployment. Refined.

Braided Coil Assist Stents with
High Neck Coverage, Excellent Visibility
and Improved Conformability*



Aneurysm
Therapy
Solutions



For more information or a product demonstration,
contact your local MicroVention representative:

**MicroVention Worldwide
Innovation Center**
35 Enterprise

Aliso Viejo, CA 92656 USA

MicroVention UK Limited

MicroVention Europe, S.A.R.L.

MicroVention Deutschland GmbH

microvention.com

PH +1.714.247.8000

PH +44 (0) 191 258 6777

PH +33 (1) 39 21 77 46

PH +49 211 210 798-0

*Humanitarian Device: Authorized by Federal Law for use with bare platinum embolic coils for the treatment of unruptured, wide neck (neck \geq 4 mm or dome to neck ratio < 2), intracranial, saccular aneurysms arising from a parent vessel with a diameter \geq 2.5 mm and \leq 4.5 mm. The effectiveness of this device for this use has not been demonstrated.



Now you have **24 hours** to make a lifetime of difference in stroke patients like Nora



The Trevo Retriever is the only device cleared to **reduce disability in stroke patients up to 24 hours** from time last seen well.

For more information, visit strykerneurovascular.com/trevo24hours

Trevo[®] XP
PROVUE RETRIEVER

Copyright © 2018 Stryker
AP002078 v1.0



Not for sale within the territory of the United States

VISIBLE ADAPTABILITY

DERIVO® Embolisation Device

- Very good visibility
- Excellent navigation and precise positioning
- BlueXide® surface
- Low level artefacts on MRI



www.acandis.com

acandis®
ENGINEERING STROKE SOLUTIONS

A Complete Coil Portfolio

MicroVention's comprehensive portfolio features clinically proven Hydrogel coils, which can be used exclusively or in combination with our trusted Platinum coils to treat a wide range of aneurysms and neurovascular lesions.



Aneurysm
Therapy
Solutions

Breakthrough Hydrogel Technology

- Less Recurrence
- Less Retreatment
- More Progressive Occlusion

Compared to platinum coils with comparable safety¹

REFERENCES:

1. Taschner et al. Second-Generation Hydrogel Coils for the Endovascular Treatment of Intracranial Aneurysm; A Randomized Controlled Trial. 2018;49:00-00. DOI:10.1161/STROKEAHA.117.018707



INDICATIONS FOR USE:

The HydroCoil® Embolic System (HES) and MicroPlex® Coil System (MCS) are intended for the endovascular embolization of intracranial aneurysms and other neurovascular abnormalities such as arteriovenous malformations and arteriovenous fistulae. The HES and MCS are also intended for vascular occlusion of blood vessels within the neurovascular system to permanently obstruct blood flow to an aneurysm or other vascular malformation and for arterial and venous embolizations in the peripheral vasculature.

The device should only be used by physicians who have undergone pre-clinical training in all aspects of HES/MCS procedures as prescribed by MicroVention.



**For more information or a product demonstration,
contact your local MicroVention representative:**



MicroVention Worldwide Innovation Center

35 Enterprise
Aliso Viejo, CA 92656 USA

MicroVention UK Limited

MicroVention Europe, S.A.R.L.

MicroVention Deutschland GmbH

microvention.com

PH +1.714.247.8000

PH +44 (0) 191 258 6777

PH +33 (1) 39 21 77 46

PH +49 211 210 798-0

Balt USA.
The Future of Innovation is Here.

Introducing



Pushing Beyond the Boundaries of
Softness and Speed

Visit balt-usa.com to learn more



Bending expectations of conformability and stability.

Enhanced conformability – The hybrid cell structure is designed to enhance stent opening and conformability in bifurcations and tight curves.

Ease of use – All sizes of the Neuroform Atlas Stent are deliverable through Excelsior® SL-10® and Excelsior XT-17™ Microcatheters.

Higher deployment accuracy – The Neuroform Atlas Stent is designed to have very low foreshortening, which enables very high deployment accuracy.



Neuroform Atlas™ STENT SYSTEM

2017 LUCIEN LEVY BEST RESEARCH ARTICLE AWARD WINNER AND NOMINEES NAMED

This award is named for the late *AJNR* Senior Editor who championed its establishment and recognizes the best original research paper accepted in 2017. The winning paper was published electronically on April 27, 2017 and appeared in the June print issue. It was selected by a vote of the *Journal's* Editor-in-Chief and Senior Editors.



The Editors of *AJNR* are pleased to announce the annual Lucien Levy Best Research Article Award has been presented to

“Synthetic MRI for Clinical Neuroimaging: Results of the Magnetic Resonance Image Compilation (MAGiC) Prospective, Multicenter, Multireader Trial”

by L.N. Tanenbaum, A.J. Tsiouris, A.N. Johnson, T.P. Naidich, M.C. DeLano, E.R. Melhem, P. Quarterman, S.X. Parameswaran, A. Shankaranarayanan, M. Goyen, and A.S. Field

Other nominated papers were:

"Understanding Angiography-Based Aneurysm Flow Fields through Comparison with Computational Fluid Dynamics" by J.R. Cebal, F. Mut, B.J. Chung, L. Spelle, J. Moret, F. van Nijnatten, and D. Ruijters

"Apparent Diffusion Coefficient Histograms of Human Papillomavirus–Positive and Human Papillomavirus–Negative Head and Neck Squamous Cell Carcinoma: Assessment of Tumor Heterogeneity and Comparison with Histopathology" by T. de Perrot, V. Lenoir, M. Domingo Ayllón, N. Dulguerov, M. Pusztaszeri, and M. Becker

"Risk Factor Analysis of Recanalization Timing in Coiled Aneurysms: Early versus Late Recanalization" by J.P. Jeon, Y.D. Cho, D.H. Yoo, J. Moon, J. Lee, W.-S. Cho, H.-S. Kang, J.E. Kim, and M.H. Han

"Prediction of IDH1-Mutation and 1p/19q-Codeletion Status Using Preoperative MR Imaging Phenotypes in Lower Grade Gliomas" by Y.W. Park, K. Han, S.S. Ahn, S. Bae, Y.S. Choi, J.H. Chang, S.H. Kim, S.-G. Kang, and S.-K. Lee

"MR Elastography Analysis of Glioma Stiffness and IDH1-Mutation Status" by K.M. Pepin, K.P. McGee, A. Arani, D.S. Lake, K.J. Glaser, A. Manduca, I.F. Parney, R.L. Ehman, and J. Huston III

"Multiparametric Analysis of Permeability and ADC Histogram Metrics for Classification of Pediatric Brain Tumors by Tumor Grade" by S. Vajapeyam, D. Brown, P.R. Johnston, K.I. Ricci, M.W. Kieran, H.G.W. Lidov, and T.Y. Poussaint

Save the Date!!

The ASNR 57th Annual Meeting & The Foundation of the ASNR Symposium 2019

May 18-23, 2019 • Hynes Convention Center • Boston, Massachusetts



Images provided by Greater Boston Convention & Visitors Bureau



ASNR 57th Annual Meeting

c/o American Society of Neuroradiology

800 Enterprise Drive, Suite 205 | Oak Brook, Illinois 60523-4216

Phone: 630-574-0220 | Fax: 630 574-0661 | meetings@asnir.org

We're Inside Every Great Neuroradiologist!

ASNR MEMBERS RECEIVE

American Journal of Neuroradiology (AJNR)

The leading neuroradiology research journal, published monthly

Neurographics

Bimonthly educational journal with CME for members

ASNR Annual Meeting

Discounts for members on the field's premier conference

eCME

Online collection of lectures and articles with SA-CME and Category 1 credit

Advocacy

Coding/reimbursement, quality standards and practice guidelines; demonstrating neuroradiology's value!

Networking

Access to 5,000 peers

... And More!

Join the leaders in neuroradiology today!

Learn more at www.asnr.org/join

ASNR

American Society of Neuroradiology

800 Enterprise Dr., Suite 205, Oak Brook, IL 60523 • (630)574-0220 • membership@asnr.org • www.asnr.org



52nd Annual Meeting | American Society of

Head & Neck Radiology

**The Westin Savannah Harbor Golf Resort & Spa
Savannah, GA**

September 26 - 30, 2018

Please contact Educational Symposia at 813-806-1000 or ASHNR@edusymp.com or
visit www.ASHNR.org for additional information.

Neuroform Atlas™ Stent System

See package insert for complete indications, contraindications, warnings and instructions for use.

Humanitarian Device. Authorized by Federal law for use with neurovascular embolic coils in patients who are ≥ 18 years of age for the treatment of wide neck, intracranial, saccular aneurysms arising from a parent vessel with a diameter of ≥ 2 mm and ≤ 4.5 mm that are not amenable to treatment with surgical clipping. Wide neck aneurysms are defined as having a neck ≥ 4 mm or a dome-to-neck ratio < 2. The effectiveness of this device for use has not been demonstrated.

INDICATIONS FOR USE

The Neuroform Atlas™ Stent System is indicated for use with neurovascular embolic coils in patients who are ≥ 18 years of age for the treatment of wide neck, intracranial, saccular aneurysms arising from a parent vessel with a diameter of ≥ 2 mm and ≤ 4.5 mm that are not amenable to treatment with surgical clipping. Wide neck aneurysms are defined as having a neck ≥ 4 mm or a dome-to-neck ratio of < 2.

CONTRAINDICATIONS

Patients in whom antiplatelet and/or anticoagulation therapy is contraindicated.

POTENTIAL ADVERSE EVENTS

The potential adverse events listed below, as well as others, may be associated with the use of the Neuroform Atlas™ Stent System with or without the procedure:

Allergic reaction to nitinol metal and medications, Aneurysm perforation or rupture, Coil herniation through stent into parent vessel, Death, Embolus, Headache, Hemorrhage, In-stent stenosis, Infection, Ischemia, Neurological deficit/intracranial sequelae, Pseudoaneurysm, Stent fracture, Stent migration/embolization, Stent misplacement, Stent thrombosis, Stroke, Transient ischemic attack, Vasospasm, Vessel occlusion or closure, Vessel perforation/rupture, Vessel dissection, Vessel trauma or damage, Vessel thrombosis, Vision impairment, and other procedural complications including but not limited to anesthetic and contrast media risks, hypotension, hypertension, access site complications.

WARNINGS

- Contents supplied STERILE using an ethylene oxide (EO) process. Do not use if sterile barrier is damaged. If damage is found, call your Stryker Neurovascular representative.
- For single use only. Do not reuse, reprocess or resterilize. Reuse, reprocessing or resterilization may compromise the structural integrity of the device and/or lead to device failure which, in turn, may result in patient injury, illness or death. Reuse, reprocessing or resterilization may also create a risk of contamination of the device and/or cause patient infection or cross-infection, including, but not limited to, the transmission of infectious disease(s) from one patient to another. Contamination of the device may lead to injury, illness or death of the patient.
- After use, dispose of product and packaging in accordance with hospital, administrative and/or local government policy.
- This device should only be used by physicians who have received appropriate training in interventional neuroradiology or interventional radiology and preclinical training on the use of this device as established by Stryker Neurovascular.
- Select a stent size (length) to maintain a minimum of 4 mm on each side of the aneurysm neck along the parent vessel. An incorrectly sized stent may result in damage to the vessel or stent migration. Therefore, the stent is not designed to treat an aneurysm with a neck greater than 22 mm in length.
- If excessive resistance is encountered during the use of the Neuroform Atlas™ Stent System or any of its components at any time during the procedure, discontinue use of the stent system. Continuing to move the stent system against resistance may result in damage to the vessel or a system component.
- Persons allergic to nickel/titanium (Nitinol) may suffer an allergic response to this stent implant.
- Purge the system carefully to avoid the accidental introduction of air into the stent system.
- Confirm there are no air bubbles trapped anywhere in the stent system.

CAUTIONS / PRECAUTIONS

- Federal Law (USA) restricts this device to sale by or on the order of a physician.
- Use the Neuroform Atlas Stent System prior to the "Use By" date printed on the package
- Carefully inspect the sterile package and Neuroform Atlas Stent System prior to use to verify that neither has been damaged during shipment. Do not use kinked or damaged components; contact your Stryker Neurovascular representative.
- The stent delivery microcatheter and the Neuroform Atlas Stent delivery wire should not be used to recapture the stent.
- Exercise caution when crossing the deployed stent with adjunctive devices.
- After deployment, the stent may foreshorten from up to 8.3%.
- The max OD of the coiling microcatheter should not exceed the max OD of the stent delivery microcatheter.

Copyright © 2017 Stryker

AP001839 v1.0 | Page 2 of 2

Trevo® XP ProVue Retrievers

See package insert for complete indications, complications, warnings and instructions for use.

INDICATIONS FOR USE

- The Trevo Retriever is indicated for use to restore blood flow in the neurovasculature by removing thrombus for the treatment of acute ischemic stroke to reduce disability in patients with a persistent, proximal anterior circulation, large vessel occlusion, and smaller core infarcts who have first received intravenous tissue plasminogen activator (IV t-PA). Endovascular therapy with the device should start within 6 hours of symptom onset.
- The Trevo Retriever is intended to restore blood flow in the neurovasculature by removing thrombus in patients experiencing ischemic stroke within 8 hours of symptom onset. Patients who are ineligible for intravenous tissue plasminogen activator (IV t-PA) or who fail IV t-PA therapy are candidates for treatment.
- The Trevo Retriever is indicated for use to restore blood flow in the neurovasculature by removing thrombus for the treatment of acute ischemic stroke to reduce disability in patients with a persistent, proximal anterior circulation, large vessel occlusion of the internal carotid artery (ICA) or middle cerebral artery (MCA/M1 segments with smaller core infarcts (0-50c for age < 80 years, 0-20c for age ≥ 80 years). Endovascular therapy with the device should start within 6-24 hours of time last seen well in patients who are ineligible for intravenous tissue plasminogen activator (IV t-PA) or who fail IV t-PA therapy.

COMPLICATIONS

Procedures requiring percutaneous catheter introduction should not be attempted by physicians unfamiliar with possible complications which may occur during or after the procedure. Possible complications include, but are not limited to, the following: air embolism; hematoma or hemorrhage at puncture site; infection; distal embolization; pain/headache; vessel spasm, thrombosis, dissection, or perforation; emboli; acute occlusion; ischemia; intracranial hemorrhage; large aneurysm formation; neurological deficits including stroke; and death.

- Standard interventional devices with distal tips > 1.8 F may not be able to pass through the interstices of the stent.
- Safety of the Neuroform Atlas Stent System in patients below the age of 18 has not been established.
- In cases where multiple aneurysms are to be treated, start at the most distal aneurysm first.

MAGNETIC RESONANCE IMAGING (MRI)

Safety Information Magnetic Resonance Conditional

Non-clinical testing and analysis have demonstrated that the Neuroform Atlas Stent is MR Conditional alone, or when overlapped with a second stent, and adjacent to a Stryker Neurovascular coil mass. A patient with the Neuroform Atlas Stent can be safely scanned immediately after placement of this implant, under the following conditions:

- Static magnetic field of 1.5 and 3.0 Tesla
- Maximum spatial gradient field up to 2500 Gauss/cm (25 Tesla/m)
- Maximum MR system reported whole body averaged specific absorption rate of 2 W/kg (Normal Operating Mode) and head averaged specific absorption rate of 3.2 W/kg.

Under the scan conditions defined above, the Neuroform Atlas Stent is expected to produce a maximum temperature rise of 4°C after 15 minutes of continuous scanning. The Neuroform Atlas Stent should not migrate in this MRI environment.

In non-clinical testing, the image artifact caused by the device extends approximately 2 mm from the Neuroform Atlas Stent when imaged with a spin echo pulse sequence and 3 Tesla MRI System. The artifact may obscure the device lumen. It may be necessary to optimize MRI imaging parameters for the presence of this implant.

Excelsior® XT-17™ Microcatheter

See package insert for complete indications, contraindications, warnings and instructions for use.

INTENDED USE / INDICATIONS FOR USE

Stryker Neurovascular's Excelsior XT-17 Microcatheters are intended to assist in the delivery of diagnostic agents, such as contrast media, and therapeutic agents, such as occlusion coils, into the peripheral, coronary and neuro vasculature.

CONTRAINDICATIONS

None known.

POTENTIAL ADVERSE EVENTS

Potential adverse events associated with the use of microcatheters or with the endovascular procedures include, but are not limited to: access site complications, allergic reaction, aneurysm perforation, aneurysm rupture, death, embolism (air, foreign body, plaque, thrombus), hematoma, hemorrhage, infection, ischemia, neurological deficits, pseudoaneurysm, stroke, transient ischemic attack, vasospasm, vessel dissection, vessel occlusion, vessel perforation, vessel rupture, vessel thrombosis

WARNINGS

- The accessories are not intended for use inside the human body.
- Limited testing has been performed with solutions such as contrast media, saline and suspended embolic particles. The use of these microcatheters for delivery of solutions other than the types that have been tested for compatibility is not recommended. Do not use with glue or glue mixtures.
- Carefully inspect all devices prior to use. Verify shape, size and condition are suitable for the specific procedure.
- Exchange microcatheters frequently during lengthy procedures that require extensive guidewire manipulation or multiple guidewire exchanges.
- Never advance or withdraw an intravascular device against resistance until the cause of the resistance is determined by fluoroscopy. Movement of the microcatheter or guidewire against resistance could dislodge a clot, perforate a vessel wall, or damage microcatheter and guidewire. In severe cases, tip separation of the microcatheter or guidewire may occur.
- Contents supplied STERILE using an ethylene oxide (EO) process. Do not use if sterile barrier is damaged. If damage is found, call your Stryker Neurovascular representative.
- For single use only. Do not reuse, reprocess or resterilize. Reuse, reprocessing or resterilization may compromise the structural integrity of the device and/or lead to device failure which, in turn, may result in patient injury, illness or death. Reuse, reprocessing or resterilization may also create a risk of contamination of the device and/or cause patient infection or cross-infection, including, but not limited to, the transmission of infectious disease(s) from one patient to another. Contamination of the device may lead to injury, illness or death of the patient.
- After use, dispose of product and packaging in accordance with hospital, administrative and/or local government policy.
- These devices are intended for use only by physicians trained in performing endovascular procedures.
- Inspect product before use for any bends, kinks or damage. Do not use a microcatheter that has been damaged. Damaged microcatheters may rupture causing vessel trauma or tip detachment during steering maneuvers.
- The shaping mandrel is not intended for use inside the human body.

COMPATIBILITY

3x20mm retrievers are compatible with Trevo® Pro 14 Microcatheters (REF 90231) and Trevo® Pro 18 Microcatheters (REF 90238). 4x20mm retrievers are compatible with Trevo® Pro 18 Microcatheters (REF 90238). 4x30mm retrievers are compatible with Excelsior® XT-27™ Microcatheters (150cm x 6cm straight REF 275081) and Trevo® Pro 18 Microcatheters (REF 90238). 6x25mm Retriever are compatible with Excelsior® XT-27™ Microcatheters (150cm x 6cm straight REF 275081). Recommended minimum vessel ID for all Retriever sizes is 5mm. Compatibility of the Retriever with other microcatheters has not been established. Performance of the Retriever device may be impacted if a different microcatheter is used.

Ballon Guide Catheters (such as Merc® Balloon Guide Catheter and FlowGate® Balloon Guide Catheter) are recommended for use during thrombus removal procedures.

Retrievers are compatible with the Abbott Vascular DOC® Guide Wire Extension (REF 22260).

Retrievers are compatible with Boston Scientific Rotating Hemostatic Valve (REF 421242).

SPECIFIC WARNINGS FOR INDICATION 1

- The safety and effectiveness of the Trevo Retrievers in reducing disability has not been established in patients with large core infarcts (i.e., ASPECTS ≤ 7). There may be increased risks, such as intracerebral hemorrhage, in these patients.
- The safety and effectiveness of the Trevo Retrievers in reducing disability has not been established or evaluated in patients with occlusions in the posterior circulation (e.g., basilar or vertebral arteries) or for more distal occlusions in the anterior circulation.

SPECIFIC WARNINGS FOR INDICATION 2

- To reduce risk of vessel damage, take care to appropriately size Retriever to vessel diameter at intended site of deployment.

SPECIFIC WARNINGS FOR INDICATION 3

- The safety and effectiveness of the Trevo Retrievers in reducing disability has not been established in patients with large core infarcts (i.e., ASPECTS ≤ 7). There may be increased risks, such as intracerebral hemorrhage, in these patients.
- The safety and effectiveness of the Trevo Retrievers in reducing disability has not been established or evaluated in patients with occlusions in the posterior circulation (e.g., basilar or vertebral arteries) or for more distal occlusions in the anterior circulation.
- Users should validate their imaging software analysis techniques to ensure robust and consistent results for assessing core infarct size.

- Discontinue use of microcatheter for infusion if increased resistance is noted. Resistance indicates possible blockage. Remove and replace blocked microcatheter immediately. DO NOT attempt to clear blockage by over-pressure. Doing so may cause the microcatheter to rupture, resulting in vascular damage or patient injury.
- Do not exceed 2,070 kPa (300 psi) infusion pressure. Excessive pressure could dislodge a clot, causing thromboemboli, or could result in a ruptured microcatheter or severed tip, causing vessel injury.

CAUTIONS / PRECAUTIONS

- To reduce the probability of coating damage in tortuous vasculature, use a guide catheter with a minimum internal diameter as specified in Table 1 above, and is recommended for use with Stryker Neurovascular hydrophilically coated microcatheters.
- To control the proper introduction, movement, positioning and removal of the microcatheter within the vascular system, users should employ standard clinical angiographic and fluoroscopic practices and techniques throughout the interventional procedure.
- Exercise care in handling of the microcatheter during a procedure to reduce the possibility of accidental breakage, bending or kinking.
- Use the product prior to the "Use By" date printed on the label.
- Limited testing indicates that Excelsior XT-17 Microcatheter is compatible with Dimethyl Sulfoxide (DMSO). The compatibility of Excelsior XT-17 Microcatheter with individual agents suspended in DMSO has not been established.
- Federal Law (USA) restricts this device to sale by or on the order of a physician.
- Wet dispenser coil or packaging tray and hydrophilically coated outer shaft of microcatheters prior to removal from packaging tray. Once the microcatheter has been wetted, do not allow to dry.
- The packaging mandrel is not intended for reuse. The packaging mandrel is not intended for use inside the human body.
- Check that all fittings are secure so that air is not introduced into guide catheter or microcatheter during continuous flush.
- In order to achieve optimal performance of Stryker Neurovascular Microcatheters and to maintain the lubricity of the Hydrolene® Coating surface, it is critical that a continuous flow of appropriate flush solution be maintained between the Stryker Neurovascular Microcatheter and guide catheter, and the microcatheter and any intraluminal device. In addition, flushing aids in preventing contrast crystal formation and/or clotting on both the intraluminal device and inside the guide catheter and/or the microcatheter lumen.
- Do not position microcatheter closer than 2.54 cm (1 in) from the steam source. Damage to the microcatheter may result.
- Excessive tightening of a hemostatic valve onto the microcatheter shaft may result in damage to the microcatheter. Removing the peel away introducer with a guidewire inserted in the microcatheter lumen might result in damage to the microcatheter shaft.
- To facilitate microcatheter handling, the proximal portion of the microcatheter does not have the hydrophilic surface. Greater resistance may be encountered when this section of the microcatheter is advanced into the RHV.

Excelsior® SL-10® Microcatheter

See package insert for complete indications, contraindications, warnings and instructions for use.

INTENDED USE / INDICATIONS FOR USE

Stryker Neurovascular Excelsior SL-10 Microcatheter is intended to assist in the delivery of diagnostic agents, such as contrast media, and therapeutic agents, such as occlusion coils, into the peripheral, coronary, and neurovasculature.

CONTRAINDICATIONS

None known.

POTENTIAL ADVERSE EVENTS

Potential adverse events associated with the use of microcatheters or with the endovascular procedures include, but are not limited to: access site complications, allergic reaction, aneurysm perforation, aneurysm rupture, death, embolism (air, foreign body, plaque, thrombus), hematoma, hemorrhage, infection, ischemia, neurological deficits, pseudoaneurysm, stroke, transient ischemic attack, vessel dissection, vessel occlusion, vessel perforation, vessel rupture, vessel thrombosis.

WARNINGS

- Contents supplied STERILE using an ethylene oxide (EO) process. Do not use if sterile barrier is damaged. If damage is found, call your Stryker Neurovascular representative.
 - For single patient use only. Do not reuse, reprocess or resterilize. Reuse, reprocessing or resterilization may compromise the structural integrity of the device and/or lead to device failure which, in turn, may result in patient injury, illness or death. Reuse, reprocessing or resterilization may also create a risk of contamination of the device and/or cause patient infection or cross-infection, including, but not limited to, the transmission of infectious disease(s) from one patient to another. Contamination of the device may lead to injury, illness or death of the patient.
 - After use, dispose of product and packaging in accordance with hospital, administrative and/or local government policy.
 - These devices are intended for use only by physicians trained in performing endovascular procedures.
 - Inspect product before use for any bends, kinks or damage. Do not use a microcatheter that has been damaged. Damaged microcatheters may rupture causing vessel trauma or tip detachment during steering maneuvers.
 - The shaping mandrel is not intended for use inside the human body.
- WARNINGS APPLIED TO ALL INDICATIONS**
- Administration of IV t-PA should be within the FDA-approved window (within 3 hours of stroke symptom onset).
 - To reduce risk of vessel damage, adhere to the following recommendations:
 - Do not perform more than six (6) retrieval attempts in same vessel using Retriever devices.
 - Maintain Retriever position in vessel when removing or exchanging Microcatheter.
 - To reduce risk of kinking/fracture, adhere to the following recommendations:
 - Immediately after unsheathing Retriever, position Microcatheter tip marker just proximal to shaped section. Maintain Microcatheter tip marker just proximal to shaped section of Retriever during manipulation and withdrawal.
 - Do not rotate or torque Retriever.
 - Use caution when passing Retriever through stented arteries.
 - The Retriever is a delicate instrument and should be handled carefully. Before use and when possible during procedure, inspect device carefully for damage. Do not use a device that shows signs of damage. Damage may prevent device from functioning and may cause complications.
 - Do not advance or withdraw Retriever against resistance or significant vasospasm. Moving or torquing device against resistance or significant vasospasm may result in damage to vessel or device. Assess cause of resistance using fluoroscopy and if needed resheath the device to withdraw.
 - If Retriever is difficult to withdraw from the vessel, do not torque Retriever. Advance Microcatheter distally, gently pull Retriever back into Microcatheter, and remove Retriever and Microcatheter as a unit. If undue resistance is met when withdrawing the Retriever into the Microcatheter, consider extending the Retriever using the Abbott Vascular DOC guidewire extension (REF 22260) so that the Microcatheter can be exchanged for a larger diameter catheter such as a DAC® Catheter. Gently withdraw the Retriever into the larger diameter catheter.
 - Administer anti-coagulation and anti-platelet medications per standard institutional guidelines.
 - Users should take all necessary precautions to limit X-radiation doses to patients and themselves by using sufficient shielding, reducing fluoroscopy times, and modifying X-ray technical factors where possible.

to injury, illness or death of the patient.

- After use, dispose of product and packaging in accordance with hospital, administrative and/or local government policy.
- **These devices are intended for use only by physicians trained in performing endovascular procedures.**
- Limited testing has been performed with solutions such as contrast media, saline and suspended embolic particles. The use of these catheters for delivery of solutions other than the types that have been tested for compatibility is not recommended. Do not use with glue or glue mixtures.
- The accessories are not intended for use inside the human body.
- Carefully inspect all devices prior to use. Verify shape, size and condition are suitable for the specific procedure.
- Exchange microcatheters frequently during lengthy procedures that require extensive guidewire manipulation or multiple guidewire exchanges.
- Never advance or withdraw an intravascular device against resistance until the cause of the resistance is determined by fluoroscopy. Movement of the microcatheter or guidewire against resistance could dislodge a clot, perforate a vessel wall, or damage microcatheter and guidewire. In severe cases, tip separation of the microcatheter or guidewire may occur.
- Inspect product before use for any bends, kinks or damage. Do not use a microcatheter that has been damaged. Damaged microcatheters may rupture causing vessel trauma or tip detachment during steering maneuvers.
- Shaping mandrel is not intended for use inside the human body.
- Discontinue use of microcatheter for infusion if increased resistance is noted. Resistance indicates possible blockage. Remove and replace blocked microcatheter immediately. DO NOT attempt to clear blockage by over-pressure. Doing so may cause the microcatheter to rupture, resulting in vascular damage or patient injury.
- Do not exceed 2,070 kPa (300 psi) infusion pressure. Excessive pressure could dislodge a clot, causing thromboemboli, or could result in a ruptured microcatheter or severed tip, causing vessel injury.

CAUTIONS / PRECAUTIONS

- Federal Law (USA) restricts this device to sale by or on the order of a physician.
- To facilitate microcatheter handling, the proximal portion of the microcatheter does not have the hydrophilic surface. Greater resistance may be encountered when this section of the microcatheter is advanced into the RHV.
- Exercise care in handling of the microcatheter during a procedure to reduce the possibility of accidental breakage, bending or kinking.
- To reduce the probability of coating damage in tortuous vasculature, use a guide catheter with a minimum internal diameter that is ≥ 1.00 mm (0.038 in) and is recommended for use with Stryker Neurovascular hydrophilically coated microcatheters.
- To control the proper introduction, movement, positioning and removal of the microcatheter within the vascular system, users should employ standard clinical angiographic and fluoroscopic practices and techniques throughout the interventional procedure.
- Flush dispenser coil of hydrophilically coated microcatheters prior to removal from guide cath. Once the microcatheter has been wetted, do not allow to dry. Do not reinsert the microcatheter into dispenser coil.
- Do not position microcatheter closer than 2.54 cm (1 in) from the steam source. Damage to the microcatheter may result.
- Check that all fittings are secure so that air is not introduced into guide catheter or microcatheter during continuous flush.
- In order to achieve optimal performance of Stryker Neurovascular Microcatheters and to maintain the lubricity of the Hydrolene® Coating surface, it is critical that a continuous flow of appropriate flush solution be maintained between the Stryker Neurovascular Microcatheter and guide catheter, and the microcatheter and any intraluminal device. In addition, flushing aids in preventing contrast crystal formation and/or clotting on both the intraluminal device and inside the guide catheter and/or the microcatheter lumen.
- Excessive tightening of a hemostatic valve onto the microcatheter shaft may result in damage to the microcatheter.



Stryker Neurovascular
47900 Bayside Parkway
Fremont, CA 94538

strykerneurovascular.com

Date of Release: NOV/2017

EX_EN_US

PRECAUTIONS

- Prescription only – device restricted to use by or on order of a physician.
- Store in cool, dry, dark place.
- Do not use open or damaged packages.
- Do not use "Use By" date.
- Exposure to temperatures above 54°C (130°F) may damage device and accessories. Do not autoclave.
- Do not expose Retriever to solvents.
- Use Retriever in conjunction with fluoroscopic visualization and proper anti-coagulation agents.
- To prevent thrombus formation and contrast media crystal formation, maintain a constant infusion of appropriate flush solution between guide catheter and Microcatheter and between Microcatheter and Retriever or guidewire.
- Do not attach a torque device to the shaped proximal end of DOC® Compatible Retriever. Damage may occur, preventing ability to attach DOC® Guide Wire Extension.

DOC is a trademark of Abbott Laboratories.



Stryker Neurovascular
47900 Bayside Parkway
Fremont, CA 94538

strykerneurovascular.com

Date of Release: APR/2018

EX_EN_US

Copyright © 2018 Stryker

AP002078 v1.0 | Page 2 of 2

AJNR

AMERICAN JOURNAL OF NEURORADIOLOGY

MAY 2018
VOLUME 39
NUMBER 5
WWW.AJNR.ORG




Publication Preview at www.ajnr.org features articles released in advance of print. Visit www.ajnrblog.org to comment on AJNR content and chat with colleagues and AJNR's News Digest at <http://ajnrdigest.org> to read the stories behind the latest research in neuroimaging.

797 **PERSPECTIVES** *S.M. Schonfeld*

REVIEW ARTICLE

-  798 **Vertebroplasty and Kyphoplasty for Osteoporotic Vertebral Fractures: What Are the Latest Data?** *R.V. Chandra, et al.* **SPINE**

LEVEL 1 EBM EXPEDITED PUBLICATION

-    807 **Parent Artery Reconstruction for Large or Giant Cerebral Aneurysms Using the Tubridge Flow Diverter: A Multicenter, Randomized, Controlled Clinical Trial (PARAT)** *J.-m. Liu, et al.* **INTERVENTIONAL**

GENERAL CONTENTS

-   817 **Localized Marked Elongation of the Distal Internal Carotid Artery with or without PHACE Syndrome: Segmental Dolichoectasia of the Distal Internal Carotid Artery** *Z.Y. Jia, et al.* **ADULT BRAIN**
-   824 **Brain MRI Characteristics of Patients with Anti-N-Methyl-D-Aspartate Receptor Encephalitis and Their Associations with 2-Year Clinical Outcome** *T. Zhang, et al.* **ADULT BRAIN**
-   830 **Fast and Robust Unsupervised Identification of MS Lesion Change Using the Statistical Detection of Changes Algorithm** *T.D. Nguyen, et al.* **ADULT BRAIN**
- 834 **Signal Change of Acute Cortical and Juxtacortical Microinfarction on Follow-Up MRI** *M. Miyata, et al.* **ADULT BRAIN**
-    841 **European Multicenter Study for the Evaluation of a Dual-Layer Flow-Diverting Stent for Treatment of Wide-Neck Intracranial Aneurysms: The European Flow-Redirection Intraluminal Device Study** *M. Killer-Oberpfalzer, et al.* **INTERVENTIONAL**
-  848 **An Update on the Adjunctive Neurovascular Support of Wide-Neck Aneurysm Embolization and Reconstruction Trial: 1-Year Safety and Angiographic Results** *A.M. Spiotta, et al.* **INTERVENTIONAL**
-   852 **Endovascular Treatment of Very Large and Giant Intracranial Aneurysms: Comparison between Reconstructive and Deconstructive Techniques—A Meta-Analysis** *F. Cagnazzo, et al.* **INTERVENTIONAL**

AJNR (Am J Neuroradiol ISSN 0195–6108) is a journal published monthly, owned and published by the American Society of Neuroradiology (ASNR), 800 Enterprise Drive, Suite 205, Oak Brook, IL 60523. Annual dues for the ASNR include \$170.00 for journal subscription. The journal is printed by Cadmus Journal Services, 5457 Twin Knolls Road, Suite 200, Columbia, MD 21045; Periodicals postage paid at Oak Brook, IL and additional mailing offices. Printed in the U.S.A. POSTMASTER: Please send address changes to American Journal of Neuroradiology, P.O. Box 3000, Denville, NJ 07834, U.S.A. Subscription rates: nonmember \$400 (\$470 foreign) print and online, \$320 online only; institutions \$460 (\$530 foreign) print and basic online, \$915 (\$980 foreign) print and extended online, \$380 online only (basic), extended online \$825; single copies are \$35 each (\$40 foreign). Indexed by PubMed/Medline, BIOSIS Previews, Current Contents (Clinical Medicine and Life Sciences), EMBASE, Google Scholar, HighWire Press, Q-Sensei, RefSeek, Science Citation Index, SCI Expanded, and Meta/CZI. Copyright © American Society of Neuroradiology.

	859	The New Low-Profile WEB 17 System for Treatment of Intracranial Aneurysms: First Clinical Experiences <i>S.B.T. van Rooij, et al.</i>	INTERVENTIONAL
	864	Long-Term Outcomes of Patients with Stent Tips Embedded into Internal Carotid Artery Branches during Aneurysm Coiling <i>S.P. Ban, et al.</i>	INTERVENTIONAL
	869	Factors Influencing Confidence in Diagnostic Ratings and Retreatment Recommendations in Coiled Aneurysms <i>M. Ernst, et al.</i>	INTERVENTIONAL
	875	Management of Small Unruptured Intracranial Aneurysms: A Survey of Neuroradiologists <i>A. Malhotra, et al.</i>	INTERVENTIONAL
	881	Diagnosing Early Ischemic Changes with the Latest-Generation Flat Detector CT: A Comparative Study with Multidetector CT <i>I.L. Maier, et al.</i>	INTERVENTIONAL ADULT BRAIN
	887	Endovascular Management of Acute Stroke in the Elderly: A Systematic Review and Meta-Analysis <i>C.A. Hilditch, et al.</i>	INTERVENTIONAL ADULT BRAIN
	892	Accuracy of CT Angiography for Differentiating Pseudo-Occlusion from True Occlusion or High-Grade Stenosis of the Extracranial ICA in Acute Ischemic Stroke: A Retrospective MR CLEAN Substudy <i>M. Kappelhof, et al.</i>	INTERVENTIONAL
	899	Randomized Assessment of the Safety and Efficacy of Intra-Arterial Infusion of Autologous Stem Cells in Subacute Ischemic Stroke <i>V. Bhatia, et al.</i>	INTERVENTIONAL
	905	Under Pressure: Comparison of Aspiration Techniques for Endovascular Mechanical Thrombectomy <i>O. Nikoubashman, et al.</i>	INTERVENTIONAL
	910	Aneurysmal Parent Artery-Specific Inflow Conditions for Complete and Incomplete Circle of Willis Configurations <i>B.M.W. Cornelissen, et al.</i>	INTERVENTIONAL
	916	3D Deep Learning Angiography (3D-DLA) from C-Arm Conebeam CT <i>J.C. Montoya, et al.</i>	INTERVENTIONAL
	923	Evaluation of the Normal Cochlear Second Interscalar Ridge Angle and Depth on 3D T2-Weighted Images: A Tool for the Diagnosis of Scala Communis and Incomplete Partition Type II <i>T.N. Booth, et al.</i>	HEAD & NECK
	928	Anatomic Malformations of the Middle and Inner Ear in 22q11.2 Deletion Syndrome: Case Series and Literature Review <i>E. Verheij, et al.</i>	HEAD & NECK
	935	Brain Diffusion Abnormalities in Children with Tension-Type and Migraine-Type Headaches <i>J.D. Santoro, et al.</i>	PEDIATRICS
	942	Congenital Aqueductal Stenosis: Findings at Fetal MRI That Accurately Predict a Postnatal Diagnosis <i>K.J. Heaphy-Henault, et al.</i>	PEDIATRICS
	949	MRI Characteristics of Primary Tumors and Metastatic Lesions in Molecular Subgroups of Pediatric Medulloblastoma: A Single-Center Study <i>D. Mata-Mbemba, et al.</i>	PEDIATRICS
	956	Cerebellar Growth Impairment Characterizes School-Aged Children Born Preterm without Perinatal Brain Lesions <i>K. Pieterman, et al.</i>	PEDIATRICS
	963	Prenatal Brain MR Imaging: Reference Linear Biometric Centiles between 20 and 24 Gestational Weeks <i>G. Conte, et al.</i>	PEDIATRICS
	968	Differentiating Atypical Hemangiomas and Metastatic Vertebral Lesions: The Role of T1-Weighted Dynamic Contrast-Enhanced MRI <i>K.A. Morales, et al.</i>	SPINE
	974	The Importance of Flexion MRI in Hirayama Disease with Special Reference to Laminodural Space Measurements <i>D.K. Boruah, et al.</i>	SPINE
	981	Percutaneous CT-Guided Biopsies of the Cervical Spine: Technique, Histopathologic and Microbiologic Yield, and Safety at a Single Academic Institution <i>E.L. Wiesner, et al.</i>	SPINE
	986	Transforaminal Lumbar Puncture: An Alternative Technique in Patients with Challenging Access <i>D.R. Nascene, et al.</i>	SPINE
	992	35 YEARS AGO IN AJNR	

ONLINE FEATURES

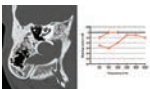
LETTERS

- E54 Pacemakers in MRI for the Neuroradiologist: Revisited** *E. Kanal*
E56 Reply *A.W. Korutz, et al.*
E57 Interaction Should Guide Management Decisions *E. Johansson, et al.*
E58 Reply *A.P. Jadhav, et al.*
E59 Triage in the Angiography Suite for Mechanical Thrombectomy in Acute Ischemic Stroke: Not Such a Good Idea *F. Clarençon, et al.*

BOOK REVIEWS

R.M. Quencer, Section Editor

Please visit www.ajnrblog.org to read and comment on Book Reviews.



Axial CT of right temporal bone (*left*) shows incomplete partition type II of the cochlea. Audiogram (*right*) shows normal hearing.



Indicates Editor's Choices selection



Indicates Fellows' Journal Club selection



Indicates open access to non-subscribers at www.ajnr.org



Indicates article with supplemental on-line table



Indicates article with supplemental on-line photo



Indicates article with supplemental on-line video



Evidence-Based Medicine Level 1



Evidence-Based Medicine Level 2

Official Journal:

American Society of Neuroradiology
American Society of Functional Neuroradiology
American Society of Head and Neck Radiology
American Society of Pediatric Neuroradiology
American Society of Spine Radiology

EDITOR-IN-CHIEF

Jeffrey S. Ross, MD

*Professor of Radiology, Department of Radiology,
Mayo Clinic College of Medicine, Phoenix, AZ*

SENIOR EDITORS

Harry J. Cloft, MD, PhD

*Professor of Radiology and Neurosurgery,
Department of Radiology, Mayo Clinic College of
Medicine, Rochester, MN*

Thierry A.G.M. Huisman, MD

*Professor of Radiology, Pediatrics, Neurology, and
Neurosurgery, Chairman, Department of Imaging
and Imaging Science, Johns Hopkins Bayview,
Director, Pediatric Radiology and Pediatric
Neuroradiology, Johns Hopkins Hospital,
Baltimore, MD*

Yvonne W. Lui, MD

*Associate Professor of Radiology,
Chief of Neuroradiology,
New York University School of Medicine,
New York, NY*

C.D. Phillips, MD, FACR

*Professor of Radiology, Weill Cornell Medical
College, Director of Head and Neck Imaging,
New York-Presbyterian Hospital, New York, NY*

Pamela W. Schaefer, MD

*Clinical Director of MRI and Associate Director of
Neuroradiology, Massachusetts General Hospital,
Boston, Massachusetts, Associate Professor,
Radiology, Harvard Medical School, Cambridge, MA*

Charles M. Strother, MD

*Professor of Radiology, Emeritus, University of
Wisconsin, Madison, WI*

STATISTICAL SENIOR EDITOR

Bryan A. Comstock, MS

*Senior Biostatistician,
Department of Biostatistics,
University of Washington, Seattle, WA*

EDITORIAL BOARD

Ashley H. Aiken, *Atlanta, GA*
Lea M. Alhilali, *Phoenix, AZ*
John D. Barr, *Dallas, TX*
Ari Blitz, *Baltimore, MD*
Barton F. Branstetter IV, *Pittsburgh, PA*
Jonathan L. Brisman, *Lake Success, NY*
Julie Bykowski, *San Diego, CA*
Keith Cauley, *Danville, PA*
Asim F. Choudhri, *Memphis, TN*
Alessandro Cianfoni, *Lugano, Switzerland*
J. Matthew Debnam, *Houston, TX*
Seena Dehkharghani, *New York, NY*
Colin Derdeyn, *Iowa City, IA*
Rahul S. Desikan, *San Francisco, CA*
Yonghong Ding, *Rochester, MN*
Clifford J. Eskey, *Hanover, NH*
Saeed Fakhran, *Phoenix, AZ*
Massimo Filippi, *Milan, Italy*
Allan J. Fox, *Toronto, Ontario, Canada*
Wende N. Gibbs, *Los Angeles, CA*
Christine M. Glastonbury, *San Francisco, CA*
John L. Go, *Los Angeles, CA*
Allison Grayev, *Madison, WI*
Brent Griffith, *Detroit, MI*
Wan-Yuo Guo, *Taipei, Taiwan*
Ajay Gupta, *New York, NY*
Rakesh K. Gupta, *Lucknow, India*
Lotfi Hachein-Bey, *Sacramento, CA*
Christopher P. Hess, *San Francisco, CA*
Andrei Holodny, *New York, NY*
Benjamin Huang, *Chapel Hill, NC*
George J. Hunter, *Boston, MA*
Mahesh V. Jayaraman, *Providence, RI*
Valerie Jewells, *Chapel Hill, NC*
Christof Karmonik, *Houston, TX*
Timothy J. Kaufmann, *Rochester, MN*
Hillary R. Kelly, *Boston, MA*
Toshitomi Kinoshita, *Akita, Japan*
Kenneth F. Layton, *Dallas, TX*
Michael M. Lell, *Nürnberg, Germany*
Michael Lev, *Boston, MA*
Karl-Olof Lovblad, *Geneva, Switzerland*
Franklin A. Marden, *Chicago, IL*
M. Gisele Matheus, *Charleston, SC*
Joseph C. McGowan, *Merion Station, PA*
Stephan Meckel, *Freiburg, Germany*
Christopher J. Moran, *St. Louis, MO*
Takahisa Mori, *Kamakura City, Japan*
Suresh Mukherji, *Ann Arbor, MI*
Amanda Murphy, *Toronto, Ontario, Canada*
Alexander J. Nemeth, *Chicago, IL*
Sasan Partovi, *Cleveland, OH*
Laurent Pierot, *Reims, France*
Jay J. Pillai, *Baltimore, MD*

Whitney B. Pope, *Los Angeles, CA*
M. Judith Donovan Post, *Miami, FL*
Tina Young Poussaint, *Boston, MA*
Joana Ramalho, *Lisbon, Portugal*
Otto Rapalino, *Boston, MA*
Álex Rovira-Cañellas, *Barcelona, Spain*
Paul M. Ruggieri, *Cleveland, OH*
Zoran Rumboldt, *Rovinj-Rovigno, Croatia*
Amit M. Saindane, *Atlanta, GA*
Erin Simon Schwartz, *Philadelphia, PA*
Lubdhra M. Shah, *Salt Lake City, UT*
Aseem Sharma, *St. Louis, MO*
J. Keith Smith, *Chapel Hill, NC*
Maria Vittoria Spampinato, *Charleston, SC*
Gordon K. Sze, *New Haven, CT*
Krishnamoorthy Thamburaj, *Hershey, PA*
Cheng Hong Toh, *Taipei, Taiwan*
Thomas A. Tomsick, *Cincinnati, OH*
Aquila S. Turk, *Charleston, SC*
Willem Jan van Rooij, *Tilburg, Netherlands*
Arastoo Vossough, *Philadelphia, PA*
Elysa Widjaja, *Toronto, Ontario, Canada*
Max Wintermark, *Stanford, CA*
Ronald L. Wolf, *Philadelphia, PA*
Kei Yamada, *Kyoto, Japan*
Carlos Zamora, *Chapel Hill, NC*

EDITORIAL FELLOW

Vahe Zohrabian, *New Haven, CT*

SPECIAL CONSULTANTS TO THE EDITOR

AJNR Blog Editor

Neil Lall, *Denver, CO*

Case of the Month Editor

Nicholas Stence, *Aurora, CO*

Case of the Week Editors

Juan Pablo Cruz, *Santiago, Chile*

Sapna Rawal, *Toronto, Ontario, Canada*

Classic Case Editor

Sandy Cheng-Yu Chen, *Taipei, Taiwan*

Facebook Editor

Peter Yi Shen, *Sacramento, CA*

Health Care and Socioeconomics Editor

Pina C. Sanelli, *New York, NY*

Physics Editor

Greg Zaharchuk, *Stanford, CA*

Podcast Editor

Wende N. Gibbs, *Los Angeles, CA*

Twitter Editor

Jennifer McCarty, *Atlanta, Georgia*

YOUNG PROFESSIONALS ADVISORY COMMITTEE

Asim K. Bag, *Birmingham, AL*
Anna E. Nidecker, *Sacramento, CA*
Peter Yi Shen, *Sacramento, CA*

Founding Editor
Juan M. Taveras

Editors Emeriti
**Mauricio Castillo, Robert I. Grossman,
Michael S. Huckman, Robert M. Quencer**

Managing Editor
Karen Halm

Assistant Managing Editor
Laura Wilhelm

Digital Publications and Social Media Coordinator
Kylie Mason

Executive Director, ASNR
Mary Beth Hepp



Title: Lionesses Sleeping on Rock, Serengeti, Tanzania. We found these lionesses napping in the afternoon heat. It was the only shady place for miles.
Steven M. Schonfeld, MD, FACR, University Radiology Group, PA, East Brunswick, New Jersey

Vertebroplasty and Kyphoplasty for Osteoporotic Vertebral Fractures: What Are the Latest Data?

 R.V. Chandra,  J. Maingard,  H. Asadi,  L.-A. Slater,  T.-L. Mazwi,  S. Marcia,  J. Barr, and  J.A. Hirsch



ABSTRACT

SUMMARY: Osteoporotic vertebral compression fractures frequently result in significant morbidity and health care resource use. For patients with severe and disabling pain, vertebral augmentation (vertebroplasty and kyphoplasty) is often considered. Although vertebroplasty was introduced >30 years ago, there are conflicting opinions regarding the role of these procedures in the treatment of osteoporotic vertebral compression fractures. This review article updates clinicians on the published prospective randomized controlled data, including the most recent positive trials that followed initial negative trials in 2009. Analysis of multiple national claim datasets has also provided further insight into the utility of these procedures. Finally, we considered the recent recommendations of national organizations and medical societies that advise on the use of vertebral augmentation procedures for osteoporotic vertebral compression fractures.

ABBREVIATIONS: NRS = numeric rating scale; PMMA = polymethylmethacrylate; QUALEFFO = Quality of Life Questionnaire of the European Foundation for Osteoporosis; RCT = randomized controlled trial; RDQ = Roland Morris Disability Questionnaire; VAS = Visual Analog Scale; VCF = vertebral compression fracture

Osteoporosis and low bone mass affect >50 million people in the United States: Every other person older than 50 years of age has low bone mass or osteoporosis.¹ The major sources of morbidity and community health care costs from osteoporosis are related to fractures. By 50 years of age, the remaining lifetime fracture risk is 1 in 2 for women and 1 in 5 for men.² By 2025, >3 million osteoporotic fractures and \$25 billion in related health care costs will occur in the United States.³ Of these, vertebral compression fractures (VCFs) will account for one-quarter of osteoporotic fractures.³

Some osteoporotic VCFs result in minimal or mild pain. Symptoms typically subside during 6–8 weeks as healing occurs. For such patients, medical management with analgesics or limiting activities/bed rest, back braces, and physical therapy or a combination of these are the mainstay of treatment. Patients with

more severe pain seek medical attention or require hospitalization. Annually, >60,000 office visits and >70,000 admissions occur from osteoporotic VCFs in the United States.^{4,5} For these patients, medical management often involves bed rest. As few as 2 days of bed rest lead to bone mass loss⁶; by 1 week, the rate of bone loss is 50 times the normal age-related rate.⁷ After 10 days of bed rest, 15% of aerobic capacity and lower extremity strength is lost,⁸ equivalent to 10 years of age-related loss.⁸ Adding narcotic anesthesia and the associated adverse effects of sedation, nausea, and constipation further increases physical deconditioning and fall risk and prolongs recovery. After hospitalization, >50% require ongoing care⁴; chronic pain occurs in 40%.⁹ Thus, while medical management is widely used, there are significant negative effects.

In patients with severe pain, vertebral augmentation (vertebroplasty and/or kyphoplasty) may be considered. In general, patients with severe and disabling back pain with correlating physical examination and advanced imaging findings (MR imaging bone marrow edema or bone-scan/SPECT/CT uptake) are selected for treatment. These minimally invasive procedures involve injection of cement (polymethylmethacrylate [PMMA]) into the VCF. Kyphoplasty involves the additional step of cavity creation; most typically, a balloon tamp is inflated to create a cavity into which PMMA is injected. Both treatments may reduce pain and disability and improve alignment.

Although >3000 articles have been published on vertebral augmentation, there remains debate on whether it is effective. Our aim was to update clinicians with a focused review of published prospective randomized controlled trials (RCTs) of verte-

From the Interventional Neuroradiology Unit (R.V.C., H.A., L.-A.S.), Monash Imaging, Monash Health, Melbourne, Victoria, Australia; Faculty of Medicine, Nursing and Health Sciences (R.V.C., L.-A.S.), Monash University, Melbourne, Victoria, Australia; Interventional Neuroradiology Service (J.M., H.A.), Department of Radiology, Austin Hospital, Melbourne, Victoria, Australia; School of Medicine, Faculty of Health (H.A.), Deakin University, Warrnambool, Victoria, Australia; Neuroendovascular Program (T.-L.M., J.A.H.), Massachusetts General Hospital, Harvard Medical School, Boston, Massachusetts; Department of Radiology (S.M.), SS. Trinità Hospital, Cagliari, Italy; and Interventional Neuroradiology (J.B.), University of Texas Southwestern Medical Center, Dallas, Texas.

Please address correspondence to Ronil V. Chandra, FRANZCR CCINR, Interventional Neuroradiology Unit, Monash Imaging, Monash Health, Monash University, 246 Clayton Rd, Melbourne, Victoria 3168, Australia; e-mail: ronil.chandra@monash.edu

 Indicates open access to non-subscribers at www.ajnr.org

<http://dx.doi.org/10.3174/ajnr.A5458>

broplasty and kyphoplasty for osteoporotic fractures. We considered the inclusion of patients in these trials by fracture age: acute (<6 weeks), subacute (6–12 weeks), and chronic (>12 weeks). We also considered the insights provided by national claims data and recent recommendations of national organizations and medical societies.

Early Observational Data

Successful small European series led to Jensen et al¹⁰ introducing vertebroplasty to the United States in 1993 and their publication in the *American Journal of Neuroradiology* in 1997. Twenty-nine patients with 47 painful osteoporotic VCFs were included. Twenty-six (90%) reported pain relief and improved mobility within 24 hours.¹⁰ Publication of several series followed, which were pooled to more robustly assess clinical outcomes. An analysis of vertebroplasty for osteoporotic VCFs from 1989 to 2004 included 2086 patients.¹¹ Nineteen studies reported pain outcomes; there was significant reduction of pain after vertebroplasty (mean Visual Analog Scale [VAS] score, 8.1–2.6; $P < .001$). Serious complications occurred in <1%. Similar outcomes were described for kyphoplasty; 1710 patients were pooled.¹² There was significant reduction of the VAS score after treatment (weighted mean difference, -5.11 ; 95% CI, -5.72 to -4.49). Alignment was also improved, anterior vertebral height was increased, and kyphosis was reduced.¹²

In 2007, encouraging preliminary data led medical societies to endorse vertebral augmentation as safe and effective for painful osteoporotic VCFs refractory to medical management.¹³ However, there were no RCT data, and there were concerns due to the improvement in back pain for most patients, regression to the mean for patients with severe pain,¹⁴ and the influence of the placebo effect.¹⁵ Further evidence from prospective RCTs was required.

Early RCTs

The Vertebroplasty for Painful Chronic Osteoporotic Vertebral Fractures (VERTOS) trial published in 2007 was the first early prospective RCT of vertebroplasty compared with medical management for osteoporotic VCFs.¹⁶ Inclusion criteria were 50 years of age or older, invalidating pain, subacute and chronic fracture age (6–24 weeks), tenderness on examination, and MR imaging bone marrow edema. Thirty-four patients were enrolled ($n = 18$ in vertebroplasty, $n = 16$ in medical management). At 24 hours, there was significant improvement in the VAS score after vertebroplasty (4.7 versus 7.1; difference, -2.4 ; 95% CI -3.7 to -1.0). At 2 weeks, this was no longer significant. Fourteen (88%) of 16 patients in the medical management arm crossed over to vertebroplasty; no long-term follow-up was possible.

The Fracture Reduction Evaluation (FREE) trial from early 2009 is the only multicenter prospective RCT that compared kyphoplasty with medical management for VCFs.¹⁷ Inclusion criteria were 21 years of age or older, moderate back pain ($\geq 4/10$ on the numeric rating scale [NRS], acute and subacute fracture age [< 3 months]), focal tenderness, and MR imaging bone marrow edema. Three hundred patients were enrolled ($n = 149$ in kyphoplasty, $n = 151$ in medical management). At 1 month, the primary end point was positive: significantly greater improve-

ment in Short-Form-36 physical component summary scores in the kyphoplasty arm (difference, 5.2 points; 95% CI, 2.9–7.4; $P < .001$). These improvements were durable to 6 months. Patients in the kyphoplasty arm gained 60 days without restricted activity and bed rest.

The main limitation of the FREE trial was the lack of blinding, which overestimates treatment benefit due to the placebo response.¹⁸ Moreover, 4 patients had nonosteoporotic fractures. The FREE investigators later reported 2-year outcome data. There was durable reduction in back pain NRS scores but no difference in the Short-Form-36 or Roland Morris Disability Questionnaire (RDQ) scores at 24 months.¹⁹ Anatomic outcomes were durable: The 27% anterior height restoration and 3.3° of kyphosis correction gained was maintained.²⁰

Rousing et al²¹ published a small RCT in mid-2009 designed to compare vertebroplasty with medical management. Inclusion criteria were 65 years of age or older, intractable back pain, and fractures of <8 weeks with plain radiographic confirmation. Forty-nine patients were enrolled ($n = 25$ in vertebroplasty, $n = 24$ in medical management). The primary outcome was the 3-month VAS score. Both groups had similar VAS scores at 3 months ($P = .33$). However, there was a reduction in the VAS within 24 hours (VAS 7.7 versus 2.0, $P < .01$) and shorter hospital stay (7.6 days versus 11.7 days, $P = .01$) after vertebroplasty. Limitations included the small single-center nature and lack of baseline VAS for 27%. A later post hoc analysis favored vertebroplasty at 1 month (VAS 3.5 versus 6.4, $P < .01$).²²

Although the FREE trial provided data to support vertebral augmentation, there remained questions regarding the placebo effect. In August 2009, 2 double-blind multicenter RCTs comparing vertebroplasty with a sham procedure were published in the *New England Journal of Medicine*.^{23,24} The Investigational Vertebroplasty Safety and Efficacy Trial (INVEST) was designed to compare vertebroplasty with a sham procedure for patients with osteoporotic VCFs.²⁴ Inclusion criteria were 50 years of age or older, moderate and severe back pain ($\geq 3/10$ points), and fracture age <1 year confirmed by examination and spine imaging (either plain radiographs or MR imaging). A total of 131 patients were enrolled ($n = 68$ in vertebroplasty, $n = 63$ in sham procedures). In both treatment arms, bupivacaine was injected onto the periosteum. In the sham procedure, vertebroplasty was simulated with verbal cues, manual palpation to simulate needle placement, and simulation of the PMMA smell. Baseline fracture age was 16 weeks and 20 weeks in the vertebroplasty and sham procedure arms, respectively.

The primary end point was back pain NRS and RDQ scores at 1 month. At 1 month, there was no difference in back pain NRS ($P = .19$) or RDQ scores ($P = .49$). There were also no statistically significant differences in secondary outcome measures of pain, disability, and quality of life. Notably, there was a trend toward a higher rate of clinically meaningful improvement in pain (30% reduction) in the vertebroplasty group (64% versus 48%, $P = .06$). By 3 months, 43% of patients crossed over to vertebroplasty; no longer term comparisons were possible.

There were limitations to INVEST: Forty percent of patients had fractures of <3 months, while 36% had fractures of >6 months. Thus, the trial examined acute, subacute, and chronic

VCFs. In addition, because MR imaging edema was not a specific requirement, patients were included after plain radiography. However, there may have been adjacent radiographically occult fractures that could have been identified if MR imaging was performed. In addition, enrollment was slow; 1813 patients were screened, 300 declined, and 131 enrolled during 4 years at 11 centers in the United States, United Kingdom, and Australia. Although these centers were chosen on the basis of established vertebroplasty services, INVEST recruited an average of 3 patients per center per year, and sample size estimates were reduced from 249 to 166. In addition, there was a high proportion of patients with Workers Compensation claims.²⁵

Buchbinder et al²³ published another multicenter double-blind prospective RCT comparing vertebroplasty with a sham procedure. Inclusion criteria were back pain, fracture age <1 year, and MR imaging–confirmed fracture line and/or edema. Seventy-eight patients were enrolled ($n = 38$ vertebroplasties, $n = 40$ sham procedures). In both treatment arms, a 13-ga needle was inserted to the periosteum. In the sham procedure arm, vertebroplasty was simulated with gentle tapping of the needle with the hammer, rotation of the imaging intensifier, and PMMA preparation.²⁶ Baseline fracture age was 9 weeks and 9.5 weeks in the vertebroplasty and sham procedure arms, respectively.

The primary outcome was back pain NRS score at 3 months. At 3 months, there was no difference in NRS scores, with no difference at 1 week, 3 months, or 6 months. Additional secondary outcome measures of pain, disability, and quality of life also did not differ.

There were limitations: Thirty-two percent had fractures of <6 weeks' duration, and one-quarter of patients had fractures between 3 and 12 months (mainly 3–6 months). Thus, acute, subacute, and chronic fractures were included, with limitations similar to those in INVEST. Moreover, a physical examination requirement was not included. From the 468 patients screened, 141 declined and 78 were enrolled during 4 years at 4 Australian centers. Most (68%) were recruited at 1 center; 2 sites enrolled 5 patients. Thus, outcomes may be weighted to this single center. Similar to INVEST, the investigators terminated the trial before reaching the sample size of 82 patients per group for 24-month outcomes; they did achieve their calculated sample size of 24 per group, considered to have 80% power to show a short-term treatment advantage of vertebroplasty.²³

The VERTOS II study followed, another large prospective multicenter RCT designed to compare early vertebroplasty with medical management.²⁷ Inclusion criteria were 50 years of age or older, moderate back pain ($VAS \geq 5$), fracture age (<6 weeks), focal tenderness, and MR imaging bone edema.²⁸ Two hundred two patients were enrolled ($n = 101$ for vertebroplasty, $n = 101$ for medical management). At 1 month, the primary end point was positive: There was a significant improvement in the VAS score in the vertebroplasty arm (VAS , 2.5 versus 4.9; $P < .001$), which was durable at 1 year. Patients achieved pain relief almost 3 months faster and gained 120 pain-free days during a year. There were also improvements for secondary outcomes of the RDQ scores ($P < .001$) and Quality of Life Questionnaire of the European Foundation for Osteoporosis (QUALEFFO) scores ($P < .001$) favoring vertebroplasty.

The main limitation of the VERTOS II trial was the lack of blinding. Further post hoc analysis of the medical cohort revealed that 60% achieved sufficient ($VAS \leq 3$) pain relief by 12 months, with most within 3 months.⁹ There were no predictors to identify the 40% who developed chronic pain. This finding led the investigators to postulate that vertebroplasty may be justified for patients without sufficient pain relief after 3 months of medical management, setting the stage for further trials.

Debate persisted about whether vertebroplasty for recent fractures (≤ 6 weeks) or severe pain (NRS score ≥ 8) provided benefit. Thus, data from INVEST and the trials of Buchbinder et al^{23,26} were pooled. Across these trials, 27% ($n = 57$) had recent-onset (≤ 6 weeks) pain and 47% ($n = 99$) had severe (NRS ≥ 8) pain. There was no difference in pain and disability scores at 1 month.²⁹ Statistical power was increased by pooling the data. However, limitations of the INVEST and Buchbinder trials remained.

In 2011, Farrokhi et al³⁰ published another RCT of vertebroplasty compared with medical management for osteoporotic VCFs. Inclusion criteria were severe pain, fracture age 4 weeks to 1 year, focal tenderness, MR imaging edema or unhealed fracture cleft, and failure of medical management for 4 weeks. Eighty-two patients were enrolled ($n = 40$ in vertebroplasty, $n = 42$ in medical management). There was reduction in the VAS score in the vertebroplasty arm at 1 week (difference, -3.1 ; $P < .001$) and improvement in quality of life measures. All patients in the vertebroplasty arm were ambulatory after 24 hours compared with 2% after medical management. There was a gain in vertebral body height (mean, 8 mm) and reduction of kyphosis (mean, 8°) after vertebroplasty. Blasco et al³¹ followed with their trial of vertebroplasty compared with medical management for osteoporotic VCFs in 2012. Inclusion criteria were moderate pain ($VAS \geq 4$), fracture age <1 year, and MR imaging edema or increased uptake on bone scans. One hundred twenty-five patients were enrolled ($n = 64$ in vertebroplasty, $n = 61$ in medical management). The mean duration of back pain was 4.7 months; 6 (5%) had fractures of <6 weeks. At 2 months, there was greater VAS improvement in the vertebroplasty arm compared with the medical arm ($P = .017$). Rescue anesthesia (intrathecal infusion) was required in 5% of the vertebroplasty arm compared with 25% of the medical arm ($P = .002$). Both groups had similar improvement in VAS and QUALEFFO scores by 12 months. Limitations include the lack of treatment blinding, the 11% crossover rate to vertebroplasty, and the high loss of follow-up rate (24%).

Recent Prospective Randomized Controlled Data

During these early trials, there remained ongoing doubt regarding the influence of the placebo effect. The sham procedure trials were designed to minimize the placebo effect, but patients with acute, subacute, and chronic fractures causing both moderate and severe pain were enrolled. Moreover, there is now increased recognition of placebo, nocebo, and the concept of active control treatments (such as periosteal local anesthetic injection in the early RCTs) that contribute to success or failure of pain relief.³² In addition, clinicians performing vertebral augmentation recognized that older patients with severe pain from recent fracture, particularly those admitted to the hospital, may form a subgroup for which

A comparison of the published prospective multicenter sham procedure RCTs on vertebroplasty for osteoporotic fractures

	Trials of Buchbinder et al ^{23,26}	INVEST ²⁴	VAPOUR ³³
Total enrollment (No.)	78	131	120
Age (yr) inclusion threshold	None	50	60
Mean (SD) age (yr)	76.6 (12.1)	73.8 (9.4)	80.5 (7)
NRS pain score inclusion threshold	None	≥3	≥7
No. (%) with severe pain	38 (49%) NRS ≥8/10	61 (47%) NRS ≥8/10	120 (100%) NRS ≥7/10
Fracture age (wk) threshold	<52	<52	<6
Mean (SD) fracture age (wk)	11.7 (11.1)	22.5 (16.3)	3 (2)
No. (%) fractures <6-weeks	31 (40%)	26 (20%)	120 (100%)
Advanced imaging (MRI or SPECT/CT) required?	Yes	No	Yes
Hospitalized patients	NR	0	57%
Mean (SD) PMMA volume (mL)	2.8 (1.2)	NR	7.5 (2.8)
Primary end point	Mean NRS pain at 3 mo	Mean NRS pain at 1 mo	% NRS pain <4/10 at 2 wk
Primary outcome	No difference	No difference	Vertebroplasty superior

Note:—NR indicates not reported.

vertebroplasty may be of greater benefit. These patients have been included in the recent RCTs.

The Vertebroplasty for Acute Painful Osteoporotic fractures (VAPOUR) trial was designed to compare early vertebroplasty with a sham procedure for patients with severe pain.³³ Inclusion criteria were 60 years of age and older, severe back pain (NRS ≥ 7), fracture age <6 weeks, and MR imaging edema or SPECT/CT uptake within 1 week. One hundred twenty patients were enrolled ($n = 61$ in vertebroplasty, $n = 59$ in sham procedures). The sham procedure was identical to that in INVEST except that a local anesthetic was injected into the subcutaneous tissues, and the PMMA kit did not emit a smell. There was no difference in the baseline pain NRS score; baseline fracture age was also similar (2.8 versus 2.4 weeks).

The primary end point was the proportion of patients whose NRS pain scores were reduced to <4 by 14 days. There was a significant treatment advantage in the vertebroplasty arm (44% versus 21%, $P = .011$) that was durable to 6 months. There were greater reductions in RDQ and QUALEFFO scores favoring vertebroplasty. Notably, 57% of patients were hospital in-patients; the median length of admission was reduced by 5.5 days after vertebroplasty. Anatomic outcomes were also superior: 30% greater vertebral height preservation compared with the sham procedure.

The limitations of VAPOUR include the bias toward a single center, with 85% performed at 1 of 4 recruiting centers.³⁴ Moreover, 8 of 120 patients did not have the 14-day outcome measure due to delirium, being uncontactable, or revoking consent. However, even if these patients (6 in the vertebroplasty arm) were considered treatment failures, the primary outcome remained significant.

VAPOUR had some important differences compared with the earlier sham procedure trials (Table), being the first sham procedure RCT that focused on stringent patient selection. Although all patients had fracture ages of <6 weeks, most (80%) had fractures of <3 weeks. Second, many (57%) were hospitalized and had vertebroplasty <7 days from admission. Third, PMMA volumes (mean, 7.5 mL) were much greater than in the trial of Buchbinder et al.²³ Although this trial had specified that 3–4 mL of PMMA would be injected,²⁶ many patients received less PMMA (mean, 2.8 mL). The INVEST trial investigators did not record PMMA volumes.³⁵ There are conflicting data on whether higher cement

volume or the percentage of vertebral body filled is associated with higher rates of pain relief, with some investigators reporting no association,³⁶ while others reported a positive cement volume–clinical response association.^{37,38} In addition, the sham procedure in VAPOUR involved subcutaneous local anesthetic injection, closer to a true placebo,³² compared with the previous trials that used periosteal local anesthetic, an active control treatment that could relieve secondary facet joint pain.³⁹

Additional small prospective open-label trials were also published in 2016. Yang et al⁴⁰ examined elderly patients with early vertebroplasty. Inclusion criteria were 70 years of age and older and moderate and severe pain (VAS ≥ 5) with MR imaging edema. One hundred thirty-five patients were enrolled ($n = 66$ in vertebroplasty, $n = 69$ in medical management). In the vertebroplasty arm, vertebroplasty was performed at a mean of 8.4 days after symptom onset, with all patients treated <3 weeks from onset. There was significantly greater improvement in the VAS in the vertebroplasty arm from day 1, which was durable to 1 year. There were improvements in the Oswestry Disability Index and QUALEFFO scores. Limitations included the lack of treatment blinding, the 12% crossover rate, and the small single-institution result limiting generalizability. Leali et al⁴¹ examined postmenopausal women with 1 osteoporotic VCF. Inclusion criteria were fracture age <6 weeks and MR imaging edema. Four hundred women were enrolled ($n = 200$ in vertebroplasty, $n = 200$ in medical management). Baseline fracture age and the VAS in each arm were not reported. Although there was improvement in the vertebroplasty arm at 1 day, there was no difference in the VAS and Oswestry Disability Index at ≥6 weeks. Limitations included the significant paucity of data reported and the lack of treatment blinding.

There is also interest in whether chronic unhealed fractures respond to vertebroplasty as examined by Chen et al in 2014.⁴² Inclusion criteria were persistent severe pain for >3 months and MR imaging edema. A total of 96 patients were enrolled ($n = 46$ in vertebroplasty, $n = 50$ on medical management); the mean fracture age was 7 months. From 1 week, there were significantly greater reductions in the VAS score in the vertebroplasty arms that were durable at 1 month, 3 months, 6 months, and 1 year. Similar improvements were evident in RDQ scores. By 1 year, 85% of the patients with vertebroplasty had complete pain relief compared with 35% in the medical arm ($P < .001$). Similar limi-

tations remain: the lack of treatment blinding and the small single-center design.

Upcoming Evidence

Currently, there remain multiple ongoing trials of vertebral augmentation for osteoporotic fractures. The VERTOS investigators initiated VERTOS IV using the same inclusion criteria as VERTOS II but comparing vertebroplasty with a sham procedure. Enrollment commenced in 2011, with the aim of randomizing 180 patients; results have not been published.⁴³ The Vertebroplasty Compared with a Sham-Procedure for Painful Acute Osteoporotic Vertebral Fractures (VOPE) trial is a smaller trial comparing vertebroplasty with periosteal lidocaine injection, which enrolled 52 patients; results have not been published.⁴⁴ VERTOS V will be an important trial for patients with chronic unhealed fractures, comparing vertebroplasty with a sham procedure for patients 50 years of age or older with persistent moderate pain (VAS ≥ 5) from a chronic (≥ 3 months) VCF.⁴⁵

Safety Outcomes

Major symptomatic procedural complications from vertebroplasty are significant hemorrhage or vascular injury, spine infection, symptomatic cement pulmonary emboli, symptomatic hemothorax or pneumothorax, new procedure-related fractures, permanent neurologic deficits occurring within 30 days or requiring an operation, and death.⁴⁶ Across the RCTs reviewed, these major complications occurred in $<1\%$, with no procedural mortality. All procedure-related fractures were managed conservatively.³³ Osteomyelitis occurred in 1 patient who did not receive prophylactic antibiotics,²³ and a symptomatic cement leak occurred in 1 patient, requiring decompressive surgery with neurologic recovery.³⁰ These results have translated to clinical practice: In a large population-based study of elderly patients ($n = 1773$), no spinal cord injury or procedural death occurred.⁴⁷

Cement leakage outside the vertebra is common when assessed with CT (72% in VERTOS II).²⁸ Most occur via the end plates, into the disc or local adjacent veins; symptomatic leakage is very rare. During kyphoplasty, compacted bone at the periphery of the cavity is created by balloon tamp inflation, which allows cement injection at lower pressure and higher viscosity, which reduces the rate of leaks.⁴⁸ Higher rates of leak are likely with cortical disruption or fracture clefts, use of low-viscosity cement, and higher volume injections.⁴⁸

Vertebral augmentation does not increase the baseline risk of new VCFs. Overall, 1 in 5 patients develop a new VCF within 12 months of the initial VCF; the risk is higher in patients with multiple VCFs.⁴⁹ Two meta-analyses of published prospective trials found no difference in subsequent VCF risk between the medical management and vertebroplasty cohorts^{50,51}; baseline low bone mineral density is most consistently associated with increased subsequent VCF risk.⁵²

Medical management for VCFs is not always risk-free: Four patients in 2 trials developed spinal cord compression.^{33,40} Three underwent an operation with neurologic recovery; the other remained paraplegic. These occurrences relate to further VCF height loss. In VAPOUR, in almost 50%, further height loss occurred by 6 months in the sham procedure arm.³³ The rates of

pneumonia and venous thrombosis were not consistently reported but occurred in 12% in 1 trial.⁴⁰ The complications associated with narcotic anesthesia are not reported, but there is growing concern regarding narcotic anesthesia in elderly patients.

Vertebroplasty or Kyphoplasty

Although many RCTs have been published comparing vertebroplasty or kyphoplasty with medical management, there have been few prospective RCTs comparing the safety and efficacy of vertebroplasty with kyphoplasty. The largest RCT was the Kyphoplasty and Vertebroplasty in the Augmentation and Restoration of Vertebral Body Compression Fractures (KAVIAR) trial, which was designed to detect a difference in subsequent radiographic fractures.⁵³ Although this trial was terminated early due to limited enrollment, 361 patients completed 1-month follow-up ($n = 181$ vertebroplasty, 180 kyphoplasty procedures). The mean procedural duration was longer with kyphoplasty, with no difference in clinical outcome or symptomatic complications. Similar results have been reported in 2 smaller prospective RCTs.^{54,55} If clinical outcomes are definitively equivalent, the lower procedural cost of vertebroplasty may be favored over kyphoplasty. However, these trials were underpowered to detect differences in clinical outcomes,⁵⁶ with KAVIAR reaching only 30% of the enrollment target.

More robust data arise from a recent large systematic review and meta-analysis comparing vertebroplasty and kyphoplasty that included 2838 patients (1454 vertebroplasty and 1384 kyphoplasty procedures) across 29 randomized, prospective non-randomized, and retrospective comparative studies.⁵⁷ There were no differences in back pain or disability pain scores at any time point between vertebroplasty and kyphoplasty. There was no difference in the rate of symptomatic cement leakage, but kyphoplasty was associated with a lower rate of overall cement leakage ($P < .01$) and greater kyphosis correction ($P < .01$). Limitations included the heterogeneity of results that probably reflects the largely nonrandomized patient cohort included. Further data are required to determine whether subgroups of patients may benefit from kyphoplasty over vertebroplasty.

Hospital Admission

Most patients admitted with a painful VCF are managed conservatively with significant resource use. In a systematic review that included 622,675 hospitalized patients with VCFs, the median length of admission was 10 days; 1 in 4 patients stayed ≥ 2 weeks.⁵⁸ Hospital mortality ranged from 0.9% to 3.5%; up to 50% were discharged into a care facility.⁵⁸ Moreover, 1 in 5 patients were re-admitted within 30 days.⁵⁹

For hospitalized patients with VCFs, vertebroplasty is associated with a reduced hospital stay and reduced re-admission rates. An analysis of 13,624 hospitalized patients with VCFs from the French Hospital National Database demonstrated that a higher proportion of patients are discharged in 7 days after vertebroplasty compared with medical management (68% versus 47%, $P < .001$).⁶⁰ A large Taiwanese study using National Health Insurance data for 9238 hospitalized patients with VCFs demonstrated a 2-day-earlier discharge and lower 30-day readmission rates after vertebroplasty.⁵⁹

Mortality

Excessive mortality risk after VCF ranges from 2% to 42% for 12 months.⁶¹ In an analysis of the Medicare population in the United States (97,142 patients with VCF, 428,956 controls), the mortality rate for patients with VCF was twice that of matched controls. The 3- and 5-year mortality rates for patients with VCF were 46% and 69%, respectively, compared with 22% and 36% for matched controls.⁶² The cause of this excessive mortality is unknown. However, death may be an avoidable outcome if the etiology and predictive factors are identified. From data from the Swedish National Register of 16,051 hospitalized patients with VCF, 28% of deaths were considered causally related to the VCF.⁶³

Vertebral augmentation also reduces in-hospital and long-term mortality after a VCF compared with medical management. In an analysis of 5766 admissions for non-neoplastic VCFs from the Nationwide Inpatient Sample, kyphoplasty halved the rate of in-hospital mortality (OR 0.52, $P = .003$).⁶⁴ There is a similar effect on long-term mortality. In another analysis of 1,038,956 VCFs from the US Medicare dataset, 75,364 patients treated with vertebroplasty and 141,343 treated with kyphoplasty were identified.⁶⁵ In the subgroup with osteoporotic VCFs who were propensity matched, the mortality risk was significantly higher after medical management compared with both kyphoplasty (adjusted hazard ratio, 1.70; 95% CI, 1.67–1.74) and vertebroplasty (adjusted hazard ratio, 1.32; 95% CI, 1.29–1.35); kyphoplasty had a 17% survival benefit compared with vertebroplasty (adjusted hazard ratio, 0.83; 95% CI, 0.80–0.87).

Similar reductions in mortality after vertebral augmentation have been reported in analyses of German⁶⁶ and Taiwanese health insurance data.⁴⁷ In the Taiwanese dataset that identified 10,785 elderly (older than 70 years) patients hospitalized with a painful VCF, the risk of death was 39% higher in patients receiving medical management (hazard ratio, 1.39; 95% CI, 1.09–1.78; $P = .008$) compared with vertebroplasty. Notably, the risk of respiratory failure was also higher after medical management (hazard ratio, 1.46; 95% CI, 1.04–2.05; $P = .028$), suggesting that pulmonary impairment may play a role in explaining the excess mortality. For patients medically managed who required opiate anesthesia, the risk of death and respiratory failure was double that of patients who underwent vertebroplasty (hazard ratio death, 1.83; 95% CI, 1.28–2.60; $P = .001$; hazard ratio respiratory failure, 2.48; 95% CI, 1.50–4.11; $P < .001$). These increased risks of death and respiratory failure with medical management were observed for up to 12 years of follow-up. The impressive mortality benefit demonstrated in Taiwan could relate to early intervention; 93% received vertebroplasty within 2 weeks of hospital admission.

National Organization and Medical Society Opinions

During the past decade, there has been a clear evolution of the evidence for vertebral augmentation in the treatment of osteoporotic VCFs. At various times, national organizations and medical societies have examined the available evidence and released their recommendations, which have been variable depending on the literature examined and the respective interpretations of the available data.

In Australia, the Medical Services Advisory Committee appraises new medical procedures for public funding by examining

the safety, effectiveness, and cost-effectiveness. After examining the literature between 1987 and 2004, interim public funding was recommended for vertebroplasty in 2005.⁶⁷ A subsequent planned review by the Medical Services Advisory Committee was performed to include literature to August 2010. The INVEST and trials of Buchbinder et al^{23,24} had been published, and public funding for vertebroplasty in Australia was removed in 2011.⁶⁸ In contrast, the National Institute for Health and Care Excellence, which provides evidence-based guidance and advice to the National Health Service in the United Kingdom examined the evidence to November 2011.⁶⁹ In April 2013, the National Institute for Health and Care Excellence recommended vertebroplasty and kyphoplasty as treatment options for patients with severe pain after a recent osteoporotic VCF and concluded that it was reasonable to assume that vertebroplasty and kyphoplasty reduce mortality.⁷⁰

Similarly, medical societies have also varied in their interpretations of the evidence. In 2010, the American Academy of Orthopaedic Surgeons recommended against vertebroplasty, with a limited recommendation for kyphoplasty for symptomatic osteoporotic VCFs after reviewing the literature to December 2009.^{71,72} By comparison, in their 2014 position papers, the American Association of Neurologic Surgeons, Congress of Neurologic Surgeons, American College of Radiology, American Society of Neuroradiology, American Society of Spine Radiology, Canadian Interventional Radiology Association, Society of Neuro-Interventional Surgery, and American Academy of Family Physicians considered vertebral augmentation as a valid treatment option for patients with ongoing pain or disability with medical management.^{73,74} The recent guideline from the Cardiovascular and Interventional Radiologic Society of Europe admits that the evidence for vertebroplasty has been conflicting, but recent data including VAPOUR show a treatment benefit.⁷⁵

CONCLUSIONS

The evidence for vertebroplasty in the treatment of osteoporotic fractures has evolved with time. Early open-label trials were particularly susceptible to bias and the placebo effect, and the early sham procedure trials were designed to minimize the role of the placebo effect. However, these trials included patients with acute, subacute, and chronic fractures with moderate-to-severe pain. Across the years, evidence has shown that patients subject to more rigorous selection—those with severe pain who are treated <6 weeks from fracture onset—are good candidates for vertebroplasty. This has been validated by a recent methodologically rigorous sham procedure RCT. Elderly patients hospitalized for painful VCFs are a subgroup that benefits from vertebroplasty; recent data from national datasets indicate vertebroplasty results in earlier hospital discharge, lower re-admission rates, and reduced mortality.

Disclosures: Hamed Asadi—UNRELATED: Other: participated in the Interventional Neuroradiology meetings sponsored by the industry. Stefano Marcia—UNRELATED: Consultancy: Stryker, Techlamed, Vexim, Spineart. John Barr—UNRELATED: Stock/Stock Options: Medtronic, Stryker, Comments: purchased stock. Joshua A. Hirsch—UNRELATED: Board Membership: Codman Neurovascular, Comments: Data and Safety Monitoring Board; Consultancy: Medtronic, Globus, Comments: These companies make augmentation products.

REFERENCES

- Wright NC, Looker AC, Saag KG, et al. **The recent prevalence of osteoporosis and low bone mass in the United States based on bone mineral density at the femoral neck or lumbar spine.** *J Bone Miner Res* 2014;29:2520–26 CrossRef Medline
- Johnell O, Kanis J. **Epidemiology of osteoporotic fractures.** *Osteoporos Int* 2005;16(suppl 2):S3–7 CrossRef Medline
- Burge R, Dawson-Hughes B, Solomon DH, et al. **Incidence and economic burden of osteoporosis-related fractures in the United States, 2005–2025.** *J Bone Miner Res* 2007;22:465–75 CrossRef Medline
- Gehlbach SH, Burge RT, Puleo E, et al. **Hospital care of osteoporosis-related vertebral fractures.** *Osteoporos Int* 2003;14:53–60 CrossRef Medline
- Ray NF, Chan JK, Thamer M, et al. **Medical expenditures for the treatment of osteoporotic fractures in the United States in 1995: report from the National Osteoporosis Foundation.** *J Bone Miner Res* 1997;12:24–35 Medline
- Baeker N, Tomic A, Mika C, et al. **Bone resorption is induced on the second day of bed rest: results of a controlled crossover trial.** *J Appl Physiol* 2003;95:977–82 CrossRef Medline
- Marie PJ, Kassem M. **Extrinsic mechanisms involved in age-related defective bone formation.** *J Clin Endocrinol Metab* 2011;96:600–09 CrossRef Medline
- Kortebein P, Symons TB, Ferrando A, et al. **Functional impact of 10 days of bed rest in healthy older adults.** *J Gerontol A Biol Sci Med Sci* 2008;63:1076–81 CrossRef Medline
- Venmans A, Klazen CA, Lohle PN, et al. **Natural history of pain in patients with conservatively treated osteoporotic vertebral compression fractures: results from VERTOS II.** *AJNR Am J Neuroradiol* 2012;33:519–21 CrossRef Medline
- Jensen ME, Evans AJ, Mathis JM, et al. **Percutaneous polymethylmethacrylate vertebroplasty in the treatment of osteoporotic vertebral body compression fractures: technical aspects.** *AJNR Am J Neuroradiol* 1997;18:1897–904 Medline
- Hochmuth K, Proschek D, Schwarz W, et al. **Percutaneous vertebroplasty in the therapy of osteoporotic vertebral compression fractures: a critical review.** *Eur Radiol* 2006;16:998–1004 CrossRef Medline
- Bouza C, López T, Magro A, et al. **Efficacy and safety of balloon kyphoplasty in the treatment of vertebral compression fractures: a systematic review.** *Eur Spine J* 2006;15:1050–67 CrossRef Medline
- Jensen ME, McGraw JK, Cardella JF, et al. **Position statement on percutaneous vertebral augmentation: a consensus statement developed by the American Society of Interventional and Therapeutic Neuroradiology, Society of Interventional Radiology, American Association of Neurological Surgeons/Congress of Neurological Surgeons, and American Society of Spine Radiology.** *J Vasc Interv Radiol* 2007;18:325–30 CrossRef Medline
- Whitney CW, Von Korff M. **Regression to the mean in treated versus untreated chronic pain.** *Pain* 1992;50:281–85 CrossRef Medline
- Turner JA, Deyo RA, Loeser JD, et al. **The importance of placebo effects in pain treatment and research.** *JAMA* 1994;271:1609–14 Medline
- Voormolen MH, Mali WP, Lohle PN, et al. **Percutaneous vertebroplasty compared with optimal pain medication treatment: short-term clinical outcome of patients with subacute or chronic painful osteoporotic vertebral compression fractures: the VERTOS study.** *AJNR Am J Neuroradiol* 2007;28:555–60 Medline
- Wardlaw D, Cummings SR, Van Meirhaeghe J, et al. **Efficacy and safety of balloon kyphoplasty compared with non-surgical care for vertebral compression fracture (FREE): a randomised controlled trial.** *Lancet* 2009;373:1016–24 CrossRef Medline
- Schulz KF, Grimes DA. **Blinding in randomised trials: hiding who got what.** *Lancet* 2002;359:696–700 CrossRef Medline
- Boonen S, Van Meirhaeghe J, Bastian L, et al. **Balloon kyphoplasty for the treatment of acute vertebral compression fractures: 2-year results from a randomized trial.** *J Bone Miner Res* 2011;26:1627–37 CrossRef Medline
- Van Meirhaeghe J, Bastian L, Boonen S, et al; FREE investigators. **A randomized trial of balloon kyphoplasty and non-surgical management for treating acute vertebral compression fractures: vertebral body kyphosis correction and surgical parameters.** *Spine (Phila Pa 1976)* 2013;38:971–83 CrossRef Medline
- Rousing R, Andersen MO, Jespersen SM, et al. **Percutaneous vertebroplasty compared to conservative treatment in patients with painful acute or subacute osteoporotic vertebral fractures: three-months follow-up in a clinical randomized study.** *Spine* 2009;34:1349–54 CrossRef Medline
- Rousing R, Hansen KL, Andersen MO, et al. **Twelve-months follow-up in forty-nine patients with acute/semiacute osteoporotic vertebral fractures treated conservatively or with percutaneous vertebroplasty: a clinical randomized study.** *Spine* 2010;35:478–82 CrossRef Medline
- Buchbinder R, Osborne RH, Ebeling PR, et al. **A randomized trial of vertebroplasty for painful osteoporotic vertebral fractures.** *N Engl J Med* 2009;361:557–68 CrossRef Medline
- Kallmes DF, Comstock BA, Heagerty PJ, et al. **A randomized trial of vertebroplasty for osteoporotic spinal fractures.** *N Engl J Med* 2009;361:569–79 CrossRef Medline
- Saxena AP, Hirsch AE, Yoo AJ, et al. **The use of advanced imaging and representation of workers compensation in vertebral augmentation: a single-center comparison with the INVEST trial.** *Pain Physician* 2013;16:E391–96 Medline
- Buchbinder R, Osborne RH, Ebeling PR, et al. **Efficacy and safety of vertebroplasty for treatment of painful osteoporotic vertebral fracture: a randomised controlled trial [ACTRN012605000079640].** *BMC Musculoskelet Disord* 2008;9:156 CrossRef Medline
- Klazen CA, Verhaar HJ, Lampmann LE, et al. **VERTOS II: percutaneous vertebroplasty versus conservative therapy in patients with painful osteoporotic vertebral compression fractures: rationale, objectives and design of a multicenter randomized controlled trial.** *Trials* 2007;8:33 CrossRef Medline
- Klazen CA, Lohle PN, de Vries J, et al. **Vertebroplasty versus conservative treatment in acute osteoporotic vertebral compression fractures (Vertos II): an open-label randomised trial.** *Lancet* 2010;376:1085–92 CrossRef Medline
- Staples MP, Kallmes DF, Comstock BA, et al. **Effectiveness of vertebroplasty using individual patient data from two randomised placebo controlled trials: meta-analysis.** *BMJ* 2011;343:d3952 CrossRef Medline
- Farrokhi MR, Alibai E, Maghami Z. **Randomized controlled trial of percutaneous vertebroplasty versus optimal medical management for the relief of pain and disability in acute osteoporotic vertebral compression fractures.** *J Neurosurg Spine* 2011;14:561–69 CrossRef Medline
- Blasco J, Martinez-Ferrer A, Macho J, et al. **Effect of vertebroplasty on pain relief, quality of life, and the incidence of new vertebral fractures: a 12-month randomized follow-up, controlled trial.** *J Bone Miner Res* 2012;27:1159–66 CrossRef Medline
- Manchikanti L, Giordano J, Fellows B, et al. **Placebo and nocebo in interventional pain management: a friend or a foe—or simply foes?** *Pain Physician* 2011;14:E157–75 Medline
- Clark W, Bird P, Gonski P, et al. **Safety and Efficacy of Vertebroplasty for Acute Painful Osteoporotic Fractures (VAPOUR): a multicentre, randomised, double-blind, placebo-controlled trial.** *Lancet* 2016;388:1408–16 CrossRef Medline
- Hirsch JA, Chandra RV. **Resurrection of evidence for vertebroplasty?** *Lancet* 2016;388:1356–57 CrossRef Medline
- Boszczyk B. **Volume matters: a review of procedural details of two randomised controlled vertebroplasty trials of 2009.** *Eur Spine J* 2010;19:1837–40 CrossRef Medline
- Kaufmann TJ, Trout AT, Kallmes DF. **The effects of cement volume on clinical outcomes of percutaneous vertebroplasty.** *AJNR Am J Neuroradiol* 2006;27:1933–37 Medline

37. Fu Z, Hu X, Wu Y, et al. **Is there a dose-response relationship of cement volume with cement leakage and pain relief after vertebroplasty?** *Dose Response* 2016;14:1559325816682867 CrossRef Medline
38. Nieuwenhuijse MJ, Bollen L, van Erkel AR, et al. **Optimal intravertebral cement volume in percutaneous vertebroplasty for painful osteoporotic vertebral compression fractures.** *Spine* 2012;37:1747–55 CrossRef Medline
39. Wilson DJ, Owen S, Corkill RA. **Facet joint injections as a means of reducing the need for vertebroplasty in insufficiency fractures of the spine.** *Eur Radiol* 2011;21:1772–78 CrossRef Medline
40. Yang EZ, Xu JG, Huang GZ, et al. **Percutaneous vertebroplasty versus conservative treatment in aged patients with acute osteoporotic vertebral compression fractures: a prospective randomized controlled clinical study.** *Spine* 2016;41:653–60 CrossRef Medline
41. Leali PT, Solla F, Maestretti G, et al. **Safety and efficacy of vertebroplasty in the treatment of osteoporotic vertebral compression fractures: a prospective multicenter international randomized controlled study.** *Clin Cases Miner Bone Metab* 2016;13:234–36 CrossRef Medline
42. Chen D, An ZQ, Song S, et al. **Percutaneous vertebroplasty compared with conservative treatment in patients with chronic painful osteoporotic spinal fractures.** *J Clin Neurosci* 2014;21:473–77 CrossRef Medline
43. Firanescu C, Lohle PN, de Vries J, et al; VERTOS IV study group. **A randomised sham controlled trial of vertebroplasty for painful acute osteoporotic vertebral fractures (VERTOS IV).** *Trials* 2011;12:93 CrossRef Medline
44. Hansen E, Simony A, Rousing R, et al. **Vertebroplasty Compared With a Sham-procedure for Painful Acute Osteoporotic Vertebral Fractures (VOPE).** <https://clinicaltrials.gov/ct2/show/NCT01537770>. Accessed July 16, 2017
45. Carli D. **A Trial of Vertebroplasty for Painful Chronic Osteoporotic Vertebral Fractures (VERTOS V).** <https://clinicaltrials.gov/ct2/show/NCT01963039>. Accessed July 16, 2017
46. Baerlocher MO, Saad WE, Dariushnia S, et al; Society of Interventional Radiology Standards of Practice Committee. **Quality improvement guidelines for percutaneous vertebroplasty.** *J Vasc Interv Radiol* 2014;25:165–70 CrossRef Medline
47. Lin JH, Chien LN, Tsai WL, et al. **Early vertebroplasty associated with a lower risk of mortality and respiratory failure in aged patients with painful vertebral compression fractures: a population-based cohort study in Taiwan.** *Spine J* 2017;17:1310–18 CrossRef Medline
48. Zhan Y, Jiang J, Liao H, et al. **Risk factors for cement leakage after vertebroplasty or kyphoplasty: a meta-analysis of published evidence.** *World Neurosurg* 2017;101:633–42 CrossRef Medline
49. Lindsay R, Silverman SL, Cooper C, et al. **Risk of new vertebral fracture in the year following a fracture.** *JAMA* 2001;285:320–23 CrossRef Medline
50. Anderson PA, Froysheter AB, Tontz WL Jr. **Meta-analysis of vertebral augmentation compared to conservative treatment for osteoporotic spinal fractures.** *J Bone Miner Res* 2013;28:372–82 CrossRef Medline
51. Shi MM, Cai XZ, Lin T, et al. **Is there really no benefit of vertebroplasty for osteoporotic vertebral fractures? A meta-analysis.** *Clin Orthop Relat Res* 2012;470:2785–99 CrossRef Medline
52. Cao J, Kong L, Meng F, et al. **Risk factors for new vertebral compression fractures after vertebroplasty: a meta-analysis.** *ANZ J Surg* 2016;86:549–54 CrossRef Medline
53. Dohm M, Black CM, Dacre A, et al; KAVIAR investigators. **A randomized trial comparing balloon kyphoplasty and vertebroplasty for vertebral compression fractures due to osteoporosis.** *AJNR Am J Neuroradiol* 2014;35:2227–36 CrossRef Medline
54. Liu JT, Liao WJ, Tan WC, et al. **Balloon kyphoplasty versus vertebroplasty for treatment of osteoporotic vertebral compression fracture: a prospective, comparative, and randomized clinical study.** *Osteoporosis Int* 2010;21:359–64 CrossRef Medline
55. Evans AJ, Kip KE, Brinjikji W, et al. **Randomized controlled trial of vertebroplasty versus kyphoplasty in the treatment of vertebral compression fractures.** *J Neurointerv Surg* 2016;8:756–63 CrossRef Medline
56. Beall DP. **Response to: Randomized controlled trial of vertebroplasty versus kyphoplasty in the treatment of vertebral compression fractures.** *J Neurointerv Surg* 2016;8:763–64 CrossRef Medline
57. Gu CN, Brinjikji W, Evans AJ, et al. **Outcomes of vertebroplasty compared with kyphoplasty: a systematic review and meta-analysis.** *J Neurointerv Surg* 2016;8:636–42 CrossRef Medline
58. Ong T, Kantachuesiri P, Sahota O, et al. **Characteristics and outcomes of hospitalised patients with vertebral fragility fractures: a systematic review.** *Age and Aging* 2017 May 10. CrossRef
59. Tsai YW, Hsiao FY, Wen YW, et al. **Clinical outcomes of vertebroplasty or kyphoplasty for patients with vertebral compression fractures: a nationwide cohort study.** *J Am Med Dir* 2013;14:41–47 CrossRef Medline
60. Maravic M, Taupin P, Roux C. **Hospital burden of vertebral fractures in France: influence of vertebroplasty.** *Osteoporosis Int* 2013;24:2001–06 CrossRef Medline
61. Sattui SE, Saag KG. **Fracture mortality: associations with epidemiology and osteoporosis treatment.** *Nat Rev Endocrinol* 2014;10:592–602 CrossRef Medline
62. Lau E, Ong K, Kurtz S, et al. **Mortality following the diagnosis of a vertebral compression fracture in the Medicare population.** *J Bone Joint Surg Am* 2008;90:1479–86 CrossRef Medline
63. Kanis JA, Oden A, Johnell O, et al. **Excess mortality after hospitalisation for vertebral fracture.** *Osteoporosis Int* 2004;15:108–12 CrossRef Medline
64. Zampini JM, White AP, McGuire KJ. **Comparison of 5766 vertebral compression fractures treated with or without kyphoplasty.** *Clin Orthop Relat Res* 2010;468:1773–80 CrossRef Medline
65. Edidin AA, Ong KL, Lau E, et al. **Morbidity and mortality after vertebral fractures: comparison of vertebral augmentation and non-operative management in the Medicare population.** *Spine* 2015;40:1228–41 CrossRef Medline
66. Lange A, Kasperk C, Alvares L, et al. **Survival and cost comparison of kyphoplasty and percutaneous vertebroplasty using German claims data.** *Spine* 2014;39:318–26 CrossRef Medline
67. Committee MSA. **Vertebroplasty and kyphoplasty for the treatment of vertebral compression fracture: MSAC reference 27 Assessment report. 2005.** https://www.adelaide.edu.au/ahta/pubs/reportsmonographs/Vertebroplasty_reference_27_assessment_report_final_printready.pdf. Accessed July 16, 2017
68. Doidge J, Merlin T, Liufu Z, et al. **Review of interim funded service: vertebroplasty and new review of kyphoplasty.** MSAC Application 27.1. Canberra, ACT: Commonwealth of Australia; 2011
69. Stevenson M, Gomersall T, Lloyd Jones M, et al. **Percutaneous vertebroplasty and percutaneous balloon kyphoplasty for the treatment of osteoporotic vertebral fractures: a systematic review and cost-effectiveness analysis.** *Health Technol Assess* 2014;18:1–290 CrossRef Medline
70. National Institute for Health and Care Excellence. **NICE technology appraisal guidance TA279. Percutaneous vertebroplasty and percutaneous balloon kyphoplasty for treating osteoporotic vertebral compression fractures.** April 2013. <https://www.nice.org.uk/guidance/ta279>. Accessed July 16, 2017
71. McGuire R. **AAOS Clinical Practice Guideline: the treatment of symptomatic osteoporotic spinal compression fractures.** *J Am Acad Orthop Surg* 2011;19:183–84 CrossRef Medline
72. Esses SI, McGuire R, Jenkins J, et al. **The treatment of symptomatic osteoporotic spinal compression fractures.** *J Am Acad Orthop Surg* 2011;19:176–82 CrossRef Medline
73. Barr JD, Jensen ME, Hirsch JA, et al. **Position statement on percutaneous vertebral augmentation: a consensus statement developed by the Society of Interventional Radiology (SIR), American Association of Neurological Surgeons (AANS) and the Congress of Neurological Surgeons (CNS), American College of**

- Radiology (ACR), American Society of Neuroradiology (ASNR), American Society of Spine Radiology (ASSR), Canadian Interventional Radiology Association (CIRA), and the Society of NeuroInterventional Surgery (SNIS). *J Vasc Interv Radiol* 2014;25:171–81 [CrossRef Medline](#)
74. Chandra RV, Meyers PM, Hirsch JA, et al; Society of NeuroInterventional Surgery. **Vertebral augmentation: report of the Standards and Guidelines Committee of the Society of NeuroInterventional Surgery.** *J Neurointerv Surg* 2014;6:7–15 [CrossRef Medline](#)
75. Tsoumakidou G, Too CW, Koch G, et al. **CIRSE Guidelines on Percutaneous Vertebral Augmentation.** *Cardiovasc Intervent Radiol* 2017;40:331–42 [CrossRef Medline](#)

Parent Artery Reconstruction for Large or Giant Cerebral Aneurysms Using the Tubridge Flow Diverter: A Multicenter, Randomized, Controlled Clinical Trial (PARAT)

J.-m. Liu, Y. Zhou, Y. Li, T. Li, B. Leng, P. Zhang, G. Liang, Q. Huang, P.-f. Yang, H. Shi, J. Zhang, J. Wan, W. He, C. Liang, G. Zhu, Y. Xu, B. Hong, X. Yang, W. Bai, Y. Tian, H. Zhang, Z. Li, Q. Li, R. Zhao, Y. Fang, and K. Zhao, for the PARAT investigators



ABSTRACT

BACKGROUND AND PURPOSE: Although flow diverters have been reported with favorable clinical and angiographic outcomes in various literatures, randomized trials determining their true effectiveness and safety are still in lack. The Parent Artery Reconstruction for Large or Giant Cerebral Aneurysms Using the Tubridge Flow Diverter (PARAT) trial was designed to evaluate the safety and efficacy of the Tubridge flow diverter in the treatment of large or giant aneurysms in comparison with Enterprise stent-assisted coiling.

MATERIALS AND METHODS: This prospective, multicenter, randomized trial was conducted at 12 hospitals throughout China. Enrolled adults with unruptured large/giant intracranial aneurysms were randomly assigned (1:1) to receive either Enterprise stent-assisted coiling or Tubridge flow diverter implantation. The primary end point was complete occlusion at 6-month follow-up, while secondary end points included technical success, mortality, target vessel–related stroke, aneurysm bleeding, in-stent stenosis, parent artery occlusion, and the frequency of all adverse events.

RESULTS: Among 185 enrolled subjects, 41 withdrew before procedure initiation. Overall, 82 subjects underwent Tubridge implantation, and 62 subjects were primarily treated with stent-assisted coiling. The results of 6-month follow-up imaging included complete occlusion rates of 75.34% versus 24.53% for the Tubridge and stent-assisted coiling groups, respectively, with a calculated common odds ratio of 9.4 (95% confidence interval, 4.14–21.38; $P < .001$). There was a higher, nonsignificant frequency of complications for Tubridge subjects. Multivariate analysis showed a decreased stroke rate at the primary investigational site, with a marginal P value ($P = .051$).

CONCLUSIONS: This trial showed an obviously higher rate of large and giant aneurysm obliteration with the Tubridge FD over Enterprise stent-assisted coiling. However, this higher obliteration rate came at the cost of a nonsignificantly higher rate of complications. Investigational site comparisons suggested that a learning curve for flow-diverter implantation should be recognized and factored into trial designs.

ABBREVIATIONS: FD = flow diverter; LTF = lost-to-follow-up; PARAT = Parent Artery Reconstruction for Large or Giant Cerebral Aneurysms Using the Tubridge Flow Diverter; SAC = stent-assisted coiling

Large (10–25 mm) or giant (≥ 25 mm) aneurysms are a very challenging subtype among intracranial aneurysms, with

much higher risks of rupture and poorer outcomes compared with small aneurysms.^{1,2} Despite recent technical advances, the treatment of large or giant aneurysms remains technically disappointing, with high complication and/or recanalization rates.^{3–6}

Received January 16, 2018; accepted after revision February 26.

From the Department of Neurosurgery, (J.-m.L., Y.Z., P.-f.Y., B.H., Y.X., Q.L., R.Z., Y.F., K.Z., Q.H.), Shanghai Changhai Hospital, Shanghai, China; Department of Neurosurgery (Y.L., X.Y.), Tiantan Hospital, Beijing, China; Department of Interventional Radiology (T.L., W.B.), Henan Provincial People's Hospital, Henan Province, China; Department of Neurosurgery (B.L., Y.T.), Huashan Hospital, Shanghai, China; Department of Neurosurgery (P.Z., H.Z.), Xuanwu Hospital, Beijing, China; Department of Neurosurgery (G.L., Z.L.), General Hospital of Shenyang Military, Shenyang Province, China; Department of Neurosurgery (H.S.), First Clinical Hospital affiliated with Harbin Medical University, Heilongjiang Province, China; Department of Neurosurgery (J.Z.), Second Affiliated Hospital of Zhejiang University, Hangzhou Municipality, Zhejiang, China; Department of Neurosurgery (J.W.), Renji Hospital, Shanghai, China; Department of Neurosurgery (W.H.), Second Affiliated Hospital of Guangzhou Medical University, Guangzhou, China; Department of Neurosurgery (C.L.), First Hospital of China Medical University, Shenyang Municipality, Liaoning, China; and Department of Neurosurgery (G.Z.), Southwest Hospital, Chongqing Municipality, China.

Jin-min Liu and Yu Zhou contributed equally to this work.

The PARAT investigators are listed in the On-line Appendix.

The trial was funded by the National Research and Development Project of Key Chronic Diseases (Grant No. 2016YFC1300700), the National Science and Technology Supporting Program (2011BAI08B14), and the project of the Shanghai Science and Technology Commission (11DZ1921603) and was sponsored by unrestricted grants from MicroPort NeuroTech Co, Shanghai, China.

Please address correspondence to Jian-min Liu, Department of Neurosurgery, Changhai Hospital, Second Military Medical University, 168 Changhai Rd, Shanghai 200433, China; e-mail: liujm18@vip.163.com

Indicates open access to non-subscribers at www.ajnr.org

Indicates article with supplemental on-line appendix and tables.

Evidence-Based Medicine Level 1.

<http://dx.doi.org/10.3174/ajnr.A5619>

In recent years, various flow diverter (FD) devices, such as the Pipeline Embolization Device (Covidien, Irvine, California), the Silk flow diverter (Balt Extrusion, Montmorency, France), the Flow-Redirection Endoluminal Device (FRED; MicroVention, Tustin, California), and the Surpass stent (Stryker Neurovascular, Kalamazoo, Michigan), have been increasingly used in >50 countries. These devices were believed to improve long-term effectiveness, due to their capability to alter intrasaccular hemodynamics.⁷ Unfortunately, reported clinical results have varied significantly, with aneurysm occlusion rates and periprocedural complication rates ranging from 49% to 93.4% and 2.8% to 11%, respectively. On the other hand, there is only 1 randomized controlled trial reported until now (Flow Diversion in Intracranial Aneurysm Treatment [FIAT]), which showed very high complication rates and below-expectation effectiveness.⁸ These results confused neurointerventionalists about the true effectiveness and safety of FDs. The recent publication of Raymond et al⁸ echoed these sentiments by suggesting that more randomized trials are needed to determine the role of flow diversion in the management of aneurysms.

In 2012, a lack of prospective data and reports of significant adverse outcomes associated with FD use in treating intracranial aneurysms fueled our interest in leading a multicenter, prospective, randomized, controlled trial (Parent Artery Reconstruction for Large or Giant Cerebral Aneurysms Using the Tubridge Flow Diverter [PARAT]) assessing FD treatment of large and giant intracranial aneurysms. In contrast to the FIAT trial, the PARAT trial focused on unruptured large or giant internal carotid artery or vertebral artery aneurysms, the traditional indication for FD implantation. By comparing it with a well-established treatment, stent-assisted coiling (SAC), we attempted to characterize the safety and effectiveness of the Tubridge FD (MicroPort Neuro-Tech, Shanghai, China) in this specific subset of intracranial aneurysms.

MATERIALS AND METHODS

Study Design and Participants

The PARAT trial used a prospective, multicenter, parallel-group design, with balanced randomization (1:1). The primary trial purpose was to compare outcomes of subjects with unruptured large/giant intracranial aneurysms who were treated with either Enterprise SAC (Codman & Shurtleff, Raynham, Massachusetts) or Tubridge FD implantation. The study was conducted in 12 centers throughout China, each of which was required to have performed >30 stent-assisted coiling procedures per year during the previous 5 years. The PARAT trial protocol was approved by all relevant local ethics boards.⁹ Site investigators generated trial data, with monitoring and data base maintenance completed by a commercial clinical research organization. The corresponding author had full access to all trial data and had final authority for key decisions relevant to this publication.

At each trial center, prospective subjects were screened for trial eligibility, based on having an unruptured ICA or vertebral artery saccular aneurysm (including recanalized aneurysms) measuring ≥ 10 mm in maximum diameter and ≥ 4 mm across the aneurysm neck. Investigators recruited only those who met all inclusion criteria and none with the exclusion criteria. Patients with rup-

tured aneurysms or other intracranial diseases were excluded. Detailed inclusion and exclusion criteria are listed in On-line Table 1. Investigational sites did not record or retain a log of patients who were screened for eligibility. Written informed consent was obtained from each participant before enrollment.

Randomization and Masking

After we obtained each prospective subject's informed consent, treatment allocation was initiated by a researcher contacting a clinical research associate who was independent of the patient-recruitment procedure. Subject randomization was accomplished through an interactive Web response system, which was developed by information technology managers from an independent clinical research organization under the instruction of a clinical trial statistician. The randomization scheme included built-in stratification by the participating center, aneurysm size (≤ 15 mm versus >15 mm), and aneurysm location (anterior circulation versus posterior circulation). The on-line central randomization ensured that the allocation sequence was concealed from investigators who were recruiting patients before the decision to randomize. Treatment groups were balanced using minimization criteria.

Masking of the randomization results to local investigators or trial participants was impossible to achieve. However, members of an independent Core Laboratory and those who followed up with trial subjects via telephone or face-to-face on-site interviews were blinded as to treatment allocation.

Interventions, Treatment, and Evaluation Procedures

For all recruited patients, dual-antiplatelet drugs (300 mg/day of aspirin plus 75 mg/day of clopidogrel) were prescribed for at least 3 days before the pivotal procedure. All FD placement procedures were performed with the patient under general anesthesia and via a transfemoral approach. After sheath placement, heparin (100 u/kg) was administered to maintain an activated clotting time of 250–350 seconds throughout the procedure. Next, a suitable guiding catheter (7F for subjects to be treated with Tubridge and coils) was placed in the distal internal carotid or vertebral artery. Subsequently, treatment group subjects underwent Tubridge FD implantation alone or in combination with bare coils, while control group subjects were treated by Enterprise stent-assisted coiling with bare coils.

The Tubridge Flow Diverter, developed by MicroPort Neuro-Tech, Shanghai, China, is designed to encourage the formation of intra-aneurysmal clot, while concurrently repairing and reconstructing the parent artery. Previously, we have characterized the Tubridge FD and its structural differences from the Pipeline and Silk flow diverters, such as the platinum-iridium material used for the radiopaque microfilaments, more braided microfilaments for the large-sized FD, and a decreased incidence of shortening (Table 1).⁹ Deployment of the Tubridge FD requires a combination “push” and “pull” technique to ensure full opening of the device and to increase the metal coverage across the aneurysm neck, as previously described.⁹

The approach and timing of coil placement and the number of Tubridge devices implanted were left to the discretion of each operator. For control subject aneurysms, Enterprise stents were

Table 1: Structural comparison between different FDs

FD Type	Size	Braided Microfilaments ^a		Radiopaque Microfilaments	Flared End	Metal Coverage	Retrievable
		No.	Material				
Pipeline	3–5.5 mm	48	75% cobalt chromium and 25% platinum	NA	No	30%–35%	Yes ^b
Silk Surpass	2.5–5 mm	48	Nickel-titanium alloy	4 Platinum wires	Yes	35%–55%	Yes
	2.5–5 mm	2.5 mm (36) 3 and 4 mm (60) 5 mm (84)	Cobalt-chromium	12 Platinum wires	No	30%	NA
FRED	2.5–5.5 mm	Inner layer (48) Outer layer (16)	Nickel-titanium alloy	2 Tantalum wires	Yes	NA	Yes
Tubridge	2.5–6.5 mm	<3.5 mm (46)	Nickel-titanium alloy	2 Platinum-iridium wires	Yes	30%–35%	Yes
		≥3.5 mm (62)					

Note:—NA indicates not applicable.

^a Braided microfilaments in this table mean those main wires excluding microfilaments especially for radiopaque usage.

^b Pipeline Flex embolization devices are retrievable.

implanted according to the instructions for use of the product, and all aneurysms were embolized (coiled) to achieve maximum packing density. All subject treatments were well-documented, and details included aneurysm shape and dimensions, width of the aneurysmal neck, diameter of the parent artery, and all relevant treatment outcomes. The postoperative antiplatelet regimen was as follows: <6 weeks: 300 mg of aspirin + 75 mg of clopidogrel; 6 weeks to 3 months: 100 mg of aspirin + 75 mg of clopidogrel; and, ≥3 months: 100 mg of aspirin indefinitely.

Digital copies of angiograms, including 3D rotational angiography as well as working projection images and other anteroposterior/lateral angiographic images, were collected by the clinical research organization—assigned clinical research associate of each site. These were sent to an independent Core Laboratory for analyses by up to 3 experienced neurointerventionalists (“analysts”). On the first pass, 2 analysts separately reviewed each subject’s imaging. If the initial 2 interpretations conflicted, a third analyst provided a tie-breaking assessment. Follow-up angiographic results were classified into 4 categories, according to the immediate degree of embolization: 1) occluded, defined as no contrast filling into the aneurysm sac; 2) improved, defined as decreased contrast filling into the aneurysm sac; 3) stable, defined as unchanged contrast filling into the aneurysm sac; and, 4) recanalized, defined as increased contrast filling into the aneurysm sac. Analysts also documented instances of parent artery occlusion or in-stent stenosis.

At 1, 3, and 6 months postimplantation, experienced site investigators followed up with each subject by telephone or by in-person clinical interviews. To provide some level of objectivity, these interviewers were blinded to the treatment allocation. If any adverse events were identified, investigators documented, in full detail, the following information: symptoms, event duration and severity, possible causes and associations, actions taken, and event resolution/final outcomes. A fully independent Clinical Events Committee evaluated all investigator-documented adverse events and categorized them according to the most likely causal relationship: procedure-related, device-related, disease-related, or unrelated to either disease, device, or procedure.

Study Outcomes

The primary end point was complete aneurysm occlusion at the 6-month follow-up. During reviews of 3D rotational angiography and other angiographic images, members of the Core Laboratory

consistently followed precise analytic criteria for establishing the final effectiveness end point. Only those aneurysms exhibiting no contrast filling in the aneurysm were judged as meeting the complete occlusion designation. End point analysis was expressed as percentage occurrence within the test and control groups.

Secondary end points included the following:

1) Immediate technical success rate, which included successful device delivery, exact stent positioning, and full expansion of the devices.

2) Death or stroke related to target vessel (assessment time points: 30 days, 90 days, and 1 year postoperation). Stroke was defined as sudden symptoms and signs of a focal cerebral function deficit associated with cerebral circulation disorders and including hemorrhagic or ischemic stroke. Hemorrhagic stroke was defined as acute extravasation of blood into the brain parenchyma or subarachnoid space with associated neurologic symptoms, whereas ischemic stroke was defined as rapid onset of a new focal neurologic deficit or rapid worsening of an existing focal neurologic deficit with clinical evidence of infarction not attributable to a nonischemic etiology (not associated with brain infection, trauma, tumor, seizure, severe metabolic disease, or degenerative neurologic disease).

3) Aneurysm bleeding rate (assessment time points: 30 days, 90 days, and 1 year postoperation), including intraoperative rupture and delayed aneurysm rupture confirmed by CT.

4) The rate of in-stent stenosis (assessment time point: 6 months postoperation).

5) The rate of parent artery occlusion (assessment time point: 6 months postoperation).

6) General adverse events (assessment time points: 30 days, 90 days, and 1 year postoperation).

Statistical Analysis

On the basis of an assumption of a 20% lost-to-follow-up (LTF) rate, a 124-subject sample size was planned (62 per group) to obtain a valid result (2-tailed test, significance level of $\alpha = .05$, power of $1 - \beta = 0.80$). However, because postrandomization subject withdrawals were higher than anticipated, the independent Data Monitoring Committee of the trial suggested a larger sample size to reach the required minimum number for each group (62 subjects). Differences between the PARAT trial protocol and a final report were included in the statistical analysis plan.

Data analyses included a modified intention-to-treat approach based on a population of subjects who were recruited and treated (full analysis set). Those who left the trial immediately after randomization and who did not undergo the pivotal procedure were removed from this analysis. Those who completed treatment and the entire follow-up protocol constituted the per-protocol set, while those who were treated and had at least 1 safety evaluation were included in the safety set. To verify intergroup balance, the statisticians compared the baseline characteristics of subjects between the 2 study arms. Proportions were used for categorical variables, and medians with interquartile ranges were used for continuous variables. The categorical variables were compared between study arms using the χ^2 or Fisher exact test. For continuous variables, the t test or Mann-Whitney rank test, as applicable, was used according to the distribution of the data.

Analysis of the primary effectiveness end point involved a comparison of complete occlusion rates at the 6-month follow-up between the treatment and control groups in the full analysis set using the χ^2 method in combination with multivariable logistic regression adjusted for subject age (60 years or younger versus older than 60 years) and aneurysm size (≤ 15 versus > 15 mm). A sensitivity analysis was performed to assess the effect of missing data (ie, those who were partially or wholly LTF after undergoing the pivotal procedure). A per-protocol set analysis was also performed excluding the following: subjects who were enrolled in the trial but who did not undergo the index procedure, those in whom the procedure failed, and those who did not reach the primary end point because they were deemed LTF. Secondary outcomes were compared between groups in the safety set using the χ^2 or Fisher exact test, as applicable. An additional multivariable logistic regression was performed to explore factors potentially affecting subject outcomes.

Statistical analyses were conducted by statisticians at the Institute of Clinical Evaluation, affiliated with Beijing University, and the data were analyzed using Statistical Analysis System software, Version 9.2 (SAS Institute, Cary, North Carolina). All tests were 2-sided, and a P value $< .05$ was considered statistically significant.

An independent Data and Safety Monitoring Committee had unrestricted access to trial data, to allow periodic monitoring of trial progress. This trial was registered on the Chinese Clinical Trial Registry: ChiCTR-TRC-13003127.

RESULTS

Subject Characteristics and Disposition

Between December 18, 2012, and May 9, 2014, one hundred eighty-five subjects were enrolled and randomized. The distribution of subjects among the investigational sites is shown in On-line Table 2. Of considerable surprise and prompting a midstudy revision of enrollment strategy was the high proportion of subjects ($n = 41$) exiting the study after randomization. Details of these LTF subjects are found in the final part of this article in a discussion of trial limitations as well as in the Figure.

Pivotal treatments were initiated in the remaining 144 subjects who formed the full analysis set based on a principle of modified intention-to-treat. Due to a tortuous parent artery or a wide an-

eurysm neck, investigators failed to catheterize the parent artery or deliver devices across the aneurysm neck in 6 instances (3 per trial group). Of 138 treated subjects, 5 died; 1 withdrew after serious procedure-related complications; and 6 were defined as LTF without reason. The remaining 126 subjects were included in the per-protocol analysis. There were no subject crossovers among trial groups. Treatment and follow-up details are shown in On-line Table 3.

A comparison of baseline characteristics between the 2 groups in the full analysis set showed similar distributions except for subject age ($P = .036$, Table 2), which was not considered a prognostic factor for the primary outcome. Because a high proportion of participants quit after randomization, we also compared baseline characteristics between the 41 excluded subjects and the 144 subjects in the full analysis set and determined that the distributions were comparable (On-line Table 4).

Primary Outcome

As shown in Table 3, in the 6-month angiographic follow-up, aneurysms treated with Tubridge FDs were associated with a favorable shift toward a complete occlusion rate. In the per-protocol analysis of 126 cases for the primary effectiveness end point, the complete occlusion rate was 75.34% (55/73) for the Tubridge group and 24.53% (13/53) for the Enterprise control group, with an adjusted common odds ratio of 9.31 (95% confidence interval, 4.00–21.66; $P < .001$). Unadjusted results and sensitivity analyses also showed superior results for the Tubridge group. Table 4 lists 6-month 100% aneurysm occlusion rates in the context of aneurysm location and size.

Secondary Outcomes

Immediate technical success rates did not differ significantly between the 2 trial groups. Three procedures in each group failed due to difficulties in advancing a microcatheter into the distal arteries. The calculated technical success rates were 96.34% (79/82) and 95.16% (59/62) in the Tubridge FD group and Enterprise control group, respectively, with a common odds ratio of 1.34 (95% CI, 0.26–6.87; $P = .726$).

Trial statisticians calculated a trend toward an increased but nonsignificant risk of complications for subjects in the Tubridge group. Hemorrhagic stroke occurred in 7 subjects, including 5/82 (6.1%) in the Tubridge group and 2/62 (3.23%) in the control group. Ischemic stroke, related to target vessels, occurred in 8/82 (9.76%) of the Tubridge group and 6/62 (9.68%) of the control group. These complications resulted in 4 deaths: Three were Tubridge subjects and 1 was an Enterprise-treated subject. In addition, 1 subject in each of the 2 trial groups died during follow-up for reasons unrelated to target vessels. Overall, the rates of death or stroke related to target vessels in 1-year follow up were 14.52% and 17.07% in the control and Tubridge groups, respectively. Statistically, there was no significant difference between the groups ($P = .678$).

The aneurysm bleeding rate was comparable between groups, with 3.66% versus 1.61% for the Tubridge group and Enterprise control group, respectively ($P = .634$). Overall, general adverse events occurred in 46/82 (56.10%) of the Tubridge

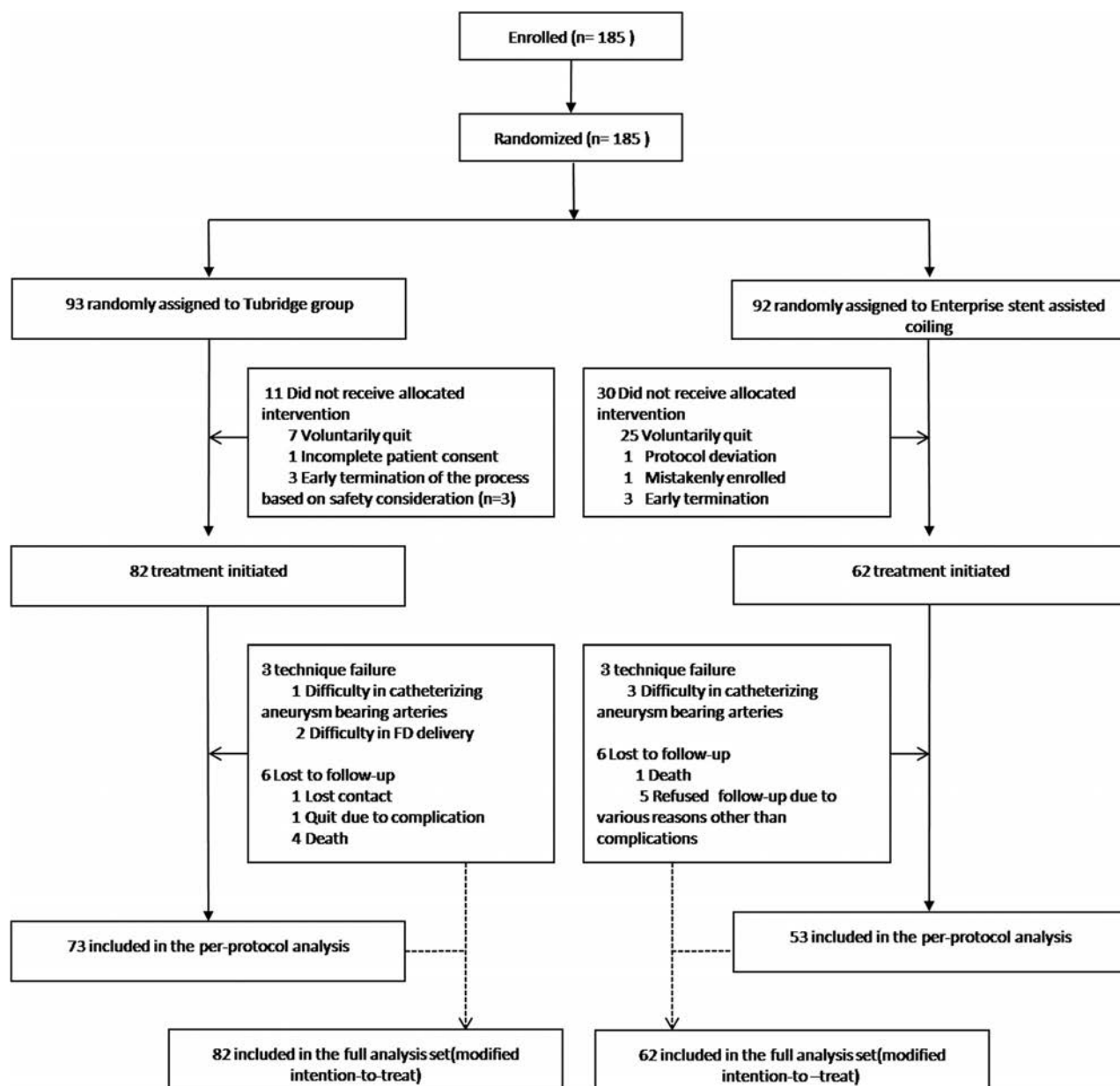


FIGURE. Flow diagram of the PARAT trial.

group and 33/62 (53.23%) of the Enterprise control group; among these, most were symptoms unrelated to the device, index procedure, or aneurysmal disease, such as headache, vomiting, or fever and there was no significant difference between the groups at the 30-day, 90-day, or 1-year follow-up. There was a trend toward a higher rate of in-stent stenosis or parent artery occlusion in the Tubridge group, but the difference was not statistically significant (Table 5).

Additional Complication Details

As shown in On-line Table 5, target vessel-related stroke, both ischemic and hemorrhagic, occurred in 21 subjects. Eight occurred during the procedure; 9, within the first 30 days after the index procedure (procedure-related); and the remaining 4 cases, at 1, 2, 3, and 7 months posttreatment.

Intraoperative bleeding occurred in 3 subjects. One Tubridge

subject had a microwire injury to a distal artery and died, while the other 2 subjects with intraoperative bleeding (1 per group/mRS of 1 at follow-up) recovered well after prompt coil deployment immediately after the onset of rupture. The Clinical Events Committee concluded that these complications, though unrelated to the Tubridge and Enterprise devices per se, were classified as procedure-related complications.

Periprocedural bleeding occurred in 4 cases (3 Tubridge/1 Enterprise). Delayed aneurysm rupture accounted for 2 complications (both large or giant aneurysms treated with FD alone). Of the remaining 2 cases, 1 Enterprise subject presented with cerebral hematoma and 1 Tubridge subject presented with mild subarachnoid hemorrhage in the Sylvian fissure. Both were thought to be unrelated to aneurysm rupture. The patient with a cerebral hematoma died due to prehospital delay, while the other one recovered well.

Overall, there were 14 cases of target vessel-related ischemic

stroke (8 Tubridge/6 Enterprise). Five subjects experienced intraoperative ischemia; another 5, within the first 30 days; and the remaining 4, at 1–7 months posttreatment.

Among those with intraoperative ischemic events, 3 were Tubridge subjects. One had a stroke after anterior choroidal artery occlusion due to coil introduction; another had a frontoparietal acute infarction due to parent artery occlusion caused by intrastent thrombosis; and, the other one was thought to be the result of a thromboembolic event. All of them resulted in contralateral limb weakness, and symptoms resolved in 1 case. In the 2 control subjects, patients had ischemic symptoms after uneventful procedures. Thromboembolic events were considered after further CT and angiographies, and both recovered well after medical therapy.

Among 5 subjects with periprocedural thromboembolic events (2 Tubridge/3 Enterprise), ischemic symptoms were all identified within 1 week after the procedure. Symptoms resulting from these periprocedural ischemia events were characterized as

mild and transient, with all events resolving well after aggressive antiplatelet therapy.

There were no hemorrhagic events after the periprocedural period. However, delayed ischemic stroke occurred in 4, including 3 Tubridge subjects and 1 Enterprise subject. For the 3 Tubridge subjects, 2 strokes were identified with parent artery occlusion after further examination and the patients were treated conservatively; and the other 2 patients (1 per group) had ischemic symptoms 1 and 2 months postprocedure, with patent parent arteries. All these symptoms improved during the follow-up period.

Overall, among all these complications, there were 4 deaths and 2 disabilities identified during the last follow-up. The procedure-related mortality rate was 3.66% (3/82) in the Tubridge group versus 1.61% (1/62) in the Enterprise group, while the procedure-related morbidity rate was 2.4% (2/82) in the Tubridge group versus zero in the control group in 1-year follow-up.

Table 2: Baseline characteristics of the full analysis set^a

Characteristics	Tubridge Group n = 82	Enterprise Group n = 62
Mean age (yr)	52.11 (10.31)	55.66 (9.53)
Sex ratio (male/female)	21:61	13:49
Medical history		
Cerebrovascular stroke	9 (10.98%)	8 (12.90%)
Coronary artery disease	1 (1.22%)	4 (6.45%)
Hypertension	41 (50.0%)	25 (40.32%)
Hypercholesterolemia	4 (4.88%)	3 (4.84%)
Diabetes	5 (6.10%)	2 (3.23%)
Current/previous smoking	12 (14.63%)	7 (11.29%)
Systolic blood pressure (median) (mm Hg)	129.50 (120.0–143.0)	129.50 (120.0–138.0)
Aneurysm location ^b		
Anterior circulation	77 (96.25%)	59 (98.33%)
Posterior circulation	3 (3.75%)	1 (1.67%)
Aneurysm size (median)	18.00 (13.14–26.0)	17.14 (12.44–24.74)
Aneurysm size classification		
Large (10–15 mm)	30 (36.59%)	24 (38.71%)
Very large or giant (>15 mm)	52 (63.41%)	38 (61.29%)

^a Data are No. (%), median (interquartile range), or mean (SD).

^b Of the 6 patients with failed procedures, locations of 2 aneurysms were absent.

Multivariate Analysis

To further explore the factors affecting angiographic outcomes and complication occurrences, trial statisticians performed multivariate analysis, including subject age, aneurysm size, aneurysm location (anterior circulation versus posterior circulation), and treatment technique (FD alone; FD + coils; and Enterprise stent-assisted coiling). The primary investigational site (Shanghai Changhai hospital) showed a decreased stroke rate compared with other trial centers, with a marginal *P* value (OR = 4.81; 95% CI, 0.991–23.335; *P* = .051).

DISCUSSION

Since the introduction of flow diverters to the global neurovascular community,

Table 3: Sensitivity analyses on the composite primary outcome

Factoring in Subjects Who Missed F/U	6-Mo Occlusion Rate		Unadjusted Result			Adjusted Result ^a		
	Tubridge Group	Control Group	OR	95% CI	<i>P</i> Value	OR	95% CI	<i>P</i> Value
Missing F/U excluded (PPS)	55/73, 75.34%	13/53, 24.53%	9.40	4.14–21.38	<.001	9.31	4.00–21.66	<.001
Missing F/U counted as complete occlusion	64/82, 78.05%	22/62, 35.48%	6.47	3.09–13.52	<.001	6.14	2.92–12.91	<.001
Missing F/U counted as not completely occluded	55/82, 67.07%	13/62, 20.97%	7.68	3.57–16.51	<.001	7.34	3.36–16.05	<.001
Missing F/U counted as complete occlusion for control and incomplete occlusion for Tubridge	55/82, 67.07%	22/62, 35.48%	3.70	1.85–7.42	<.001	3.49	1.73–7.03	<.001

Note:—F/U indicates follow-up; PPS, per-protocol set.

^a Adjusted for each subject's age and aneurysm size (≤15 versus >15 mm).

Table 4: Data correlating aneurysm location and size with aneurysm complete occlusion rate

Aneurysm Location	No.	Aneurysm Size (mm)	Proportion of Giant Aneurysms	100% Occlusion Rate at 6-Mo F/U	
				Tubridge	Controls
ICA communicating	19	18.0 ± 7.6 (10.0–33.9)	4/19	76.9%, 10/13	40%, 2/5
ICA ophthalmic	39	15.8 ± 5.6 (10.0–30.0)	4/39	83.3%, 15/18	33.3%, 6/18
ICA paraclinoid or cavernous	73	21.8 ± 7.5 (10.0–45)	25/73	75.7%, 28/37	13.8%, 4/29
ICA petrous	3	21.3 ± 9.3 (15.0–32.0)	1/3	50%, 1/2	0
Vertebral artery	4	14.3 ± 2.2 (12.0–16.3)	0/4	33.3%, 1/3	100%, 1/1

Note:—F/U indicates follow-up.

Table 5: Secondary outcome evaluation

Secondary Outcome	Enterprise n = 62	Tubridge n = 82	Odds Ratio (95% CI)	P Value
Immediate technique success rate	59/62 (95.16%)	79/82 (96.34%)	1.34 (0.26–6.87)	.726
Death or target vessel–related stroke				
30 days	7/62 (11.29%)	11/82 (13.41%)	0.821 (0.299–2.258)	.703
90 days	8/62 (12.90%)	12/82 (14.63%)	0.864 (0.330–2.263)	.766
1 yr	9/62 (14.52%)	14/82 (17.07%)	0.825 (0.332–2.051)	.678
Mortality rate				
30 days	1/62 (1.61%)	3/82 (3.66%)	0.432 (0.044–4.253)	.634
90 days	1/62 (1.61%)	4/82 (4.88%)	0.320 (0.035–2.934)	.391
1 yr ^a	2/62 (3.23%)	4/82 (4.88%)	0.650 (0.115–3.668)	.699
Hemorrhagic stroke related to target vessel				
30 days	2/62 (3.23%)	5/82 (6.1%)	0.531 (0.096–2.738)	.699
90 days	2/62 (3.23%)	5/82 (6.1%)	0.531 (0.096–2.738)	.699
1 yr	2/62 (3.23%)	5/82 (6.1%)	0.531 (0.096–2.738)	.699
Ischemic stroke related to target vessel				
30 days	4/62 (6.54%)	6/82 (7.32%)	0.874 (0.236–3.239)	.874
90 days	5/62 (8.06%)	6/82 (7.32%)	1.111 (0.323–3.822)	.867
1 yr	6/62 (9.68%)	8/82 (9.76%)	0.991 (0.325–3.109)	.987
Aneurysm rupture				
30 days	1/62 (1.61%)	3/82 (3.66%)	0.357 (0.072–1.783)	.634
90 days	1/62 (1.61%)	3/82 (3.66%)	0.357 (0.072–1.783)	.634
1 yr	1/62 (1.61%)	3/82 (3.66%)	0.357 (0.072–1.783)	.634
General adverse events				
30 days	26/62 (41.94%)	42/82 (51.22%)	0.808 (0.293–2.229)	.269
90 days	26/62 (41.94%)	42/82 (51.22%)	0.808 (0.293–2.229)	.269
1 year	33/62 (53.23%)	46/82 (56.10%)	0.938 (0.644–1.365)	.88
Rate of intrastent stenosis	2/53 (3.77%)	4/73 (5.48%)	0.676 (0.119–3.837)	1
Rate of intrastent thrombosis	1/59 (1.69%)	6/79 (7.59%)	0.215 (0.025–1.839)	.273

^a Two subjects died during follow-up for reasons unrelated to the target vessels (1 each in Tubridge and control groups).

many clinical studies were conducted to evaluate the safety and effectiveness of FDs, such as the Pipeline for Uncoilable or Failed Aneurysms (PUFS), Aneurysm Study of Pipeline in an Observational Registry (ASPIRE), and PITA trials.^{8,10–18} Additional effort to evaluate the effectiveness and safety of FDs versus conventional treatments included the Multicenter Randomized Trial on Selective Endovascular Aneurysm Occlusion with Coils versus Parent Vessel Reconstruction using the SILK Flow Diverter (MARCO POLO), FIAT, Flow Diverter Stent for Endovascular Treatment of Unruptured Saccular Wide-necked Intracranial Aneurysms (EVIDENCE), and Complete Occlusion of Coilable Aneurysms (COCOA) trials.^{19–22} However, the number of studies that focused on FD treatment of large or giant intracranial aneurysms is low. The purpose of the PARAT trial was to compare the safety and effectiveness outcomes in the treatment of ICA or vertebral artery large or giant aneurysms with the Tubridge FD (with and without coiling) versus a more conventional approach using Enterprise SAC. The PARAT trial results suggested that in subjects with ICA or vertebral artery large or giant aneurysms, Tubridge FD implantation had a significantly higher 6-month complete occlusion rate compared with conventional stent-assisted coiling. However, there was a trend toward increased risk of stroke with FD implantation.

The treatment of large or giant intracranial aneurysms has evolved significantly during the past few years. Before the emergence of FDs, parent artery occlusion, coiling alone, and stent-assisted coiling were the major treatment modalities for intracranial large or giant aneurysms. According to a meta-analysis by Turfe et al,²³ parent artery occlusion can result in a complete occlusion rate of 93.0% (95% CI, 86.0%–97.0%). However, par-

ent artery occlusion may be a viable treatment option only when there is sufficient compensating blood flow. Even when a balloon occlusion test finding is negative, a 4%–15% complication rate is possible.²³ In addition, there have been concerns about de novo aneurysm occurrence after carotid occlusion.²⁴ In a report by Arambepola et al,²⁵ 4.3% of patients developed de novo aneurysms within a mean of 9 years. Bypass surgery may reduce the incidence of ischemic events, but the procedure may be too complicated, leading to morbidity and mortality rates as high as 7% and 13%, respectively.^{26–28} In this trial, parent artery occlusion was not selected as a feasible control treatment because parent artery sacrifice is considered, throughout most hospitals in China, a last and somewhat futile option for treating intracranial aneurysms. Thus, only those cases posing considerable difficulty or possible failure in parent artery reconstruction would be treated with this method as a salvaging effort. Other than with simple and uncomplicated cases, coiling of large or giant aneurysms without a stent is undertaken far less frequently because of anticipated high recanalization rates.²³

In many prospective multicenter studies, complete occlusion rates at final follow-up varied from 49% to 93.4%, and 6-month complete occlusion rates ranged from 55.7% to 93.3% (On-line Table 6). In the treatment of large or giant aneurysms with FDs, Becske et al¹⁸ reported a complete occlusion rate of 76.4% at 180 days. Chalouhi et al²⁹ reported a complete occlusion rate of 86% at a median angiographic follow-up of 7 months. On the basis of a meta-analysis of 29 studies, including 1451 patients with 1654 aneurysms, Brinjikji et al³⁰ reported that the complete occlusion rate after FD implantation was 74% (95% CI, 63%–83%) for large aneurysms and 76% (95% CI, 53%–90.0%) for giant aneurysms.

Generally, the complete occlusion rate of 75.3% in the Tubridge group at 6 months seems comparable with rates reported in previous publications. The complete occlusion rate of 24.5% for the control group is lower than that reported in previously published articles. In 2 relatively large studies involving large or giant aneurysms, complete occlusion rates of 31% and 41% were reported by Sluzewski et al⁵ and Chalouhi et al,²⁹ respectively. The discrepancies between the latter reports and other published results, as noted above, may be related to variations in patient-selection criteria, study methods, trial design, aneurysm characteristics, and evaluation specifications and procedures. Nevertheless, the effectiveness of Tubridge FD treatment appears to be superior to that of conventional stent-assisted coiling and comparable with reported effectiveness outcomes for other FDs.

Other concerns after FD implantation include technical success rates and overall safety, as well as how FD treatment compares with conventional treatment options. The Enterprise stent is thought to be a safe device for aneurysm treatment, and hemorrhagic complications are assumed to be uncommon.³¹ Although exact causes are not well-understood, delayed aneurysm rupture or intraparenchymal hemorrhage after FD implantation has been recognized.

As shown in On-line Table 6, the hemorrhagic stroke and aneurysm rupture rates were as high as 6.9% and 5.2%, respectively, as reported for multicenter prospective studies. In the International retrospective study of the Pipeline embolization device (IntrePED) study, capturing data from 793 patients among 17 centers, the intraparenchymal hemorrhage rate was 2.4%, while the aneurysm rupture rate was 0.6%.³² In a recent meta-analysis of 3125 treated subjects, the calculated intraparenchymal hemorrhage and aneurysm rupture rates were 2.9% and 1.8%, respectively. These complications are customarily thought to be higher in large or giant aneurysms.³³ Calculated intraparenchymal hemorrhage and aneurysm rupture rates were 5.4% and 7.5%, respectively, in giant aneurysms, and 2.1% and 1.3%, respectively, in small and large aneurysms. The IntrePED study generated similar results, with intraparenchymal hemorrhage and aneurysm rupture rates of 5.8% and 5.8%, respectively, in giant ICA aneurysms; 2.6% and 0.5%, respectively, in large ICA aneurysms; and, 1.9% and 0%, respectively, in small ICA aneurysms. We observed an overall hemorrhagic rate of 6.1% (5/82) in the Tubridge group, of which 2 hemorrhagic occurrences were thought to be the result of procedural injury. Excluding these 2 cases, 2/82 (2.4%) manifested as aneurysm rupture. We did not encounter intraparenchymal hemorrhage, but we observed 1 (1.2%) lateral Sylvian fissure SAH, unrelated to aneurysm rupture. The results of our study are very comparable with those of the above-described studies.

The prospect of ischemic stroke presents additional concerns. A complication rate of 9.68% in the Enterprise control group was consistent with that reported previously by Chalouhi et al,²⁹ as well as our own single-center experience, in the range of 7.58%–11.4%.³⁴ Overall, ischemic rates after FD implantation vary among multiple publications, with a rate of 0%–10.3%. Two recent meta-analyses indicated ischemic rates ranging from 5.5% to 7.5%.^{33,35} However, the occurrence was increased in large or giant aneurysms due to intra-aneurysmal thrombosis or a prolonged procedure time, with a rate ranging from 5.2% to 13.5%.³² Ye et

al³³ indicated an ischemic rate of 9.5% for giant aneurysms. Among Tubridge subjects of the PARAT trial, ischemic complications occurred in 8 (9.76%) subjects. Although the PARAT trial rates are comparable with reported thromboembolic rates in published studies, a 9%–10% incidence of ischemic complications should be anticipated when using FDs for large or giant intracranial aneurysms. In the FIAT study, 12/75 subjects (16.0%; 95% CI, 8.9%–26.7%) treated by flow diversion were dead ($n = 8$) or dependent ($n = 4$) at ≥ 3 months postimplantation.⁸ These results differ from those in our previous experience with FDs. We believe this discrepancy may reflect “real world” early experience with flow diverters for large or giant aneurysms in multiple centers with adjudication by an external imaging Core Laboratory. Similar reports of low procedure-related risks are seen commonly with single-center or retrospective studies, as best exemplified by the recent the Stenting vs. Aggressive Medical Management for Preventing Recurrent Stroke in Intracranial Stenosis (SAMMPRIS) trial.³⁶

To better understand why these complications occurred, we undertook a detailed review of the PARAT trial complications. One possible factor is the role of the learning curve with flow diversion, and physicians’ experience may still play a role in determining the relative safety of FD therapy. The prospect of a learning curve not only encourages a higher skill level in device handling and stent deployment but also leads to more appropriate subject selection. After gaining more experience with a new flow diverter in the treatment of large or giant aneurysms, physicians can avoid many technical failures, make more appropriate FD-size selections, better understand the necessity of appropriate postdeployment balloon dilation to avoid poor apposition or overdistension, and better identify the need for simultaneous coil insertion in the treatment of large or giant aneurysms. As an example, the PARAT trial experienced high rates of parent artery occlusions, and these contributed to 3 ischemic events in the Tubridge FD group. The possibility of malapposition may exist when the devices are underdeployed. In such instances, balloon dilation after initial FD deployment may protect against in-stent thrombosis and parent artery occlusion.

The concept of a PARAT trial learning curve was also supported by our multivariate analysis, which showed significantly lower complication rates in the primary investigational site, where the leading physicians already had gained considerable experience with the Tubridge FD in a previous single-center study. We believe that intensive training of inexperienced physicians on all flow diverters should be advocated before launching a study or introducing use in general neurointerventional practice. We believe that the role that learning curves can play in trials should be increasingly emphasized.

Several recent studies have suggested that antiplatelet regimens may play a role in the occurrence of hemorrhagic or thrombotic complications.^{37,38} In the PARAT trial, investigator management of antiplatelet therapy and subject compliance with prescribed study medications were not investigated.

We have identified some key limitations of the PARAT trial. The most obvious one is the high number of postconsent subject withdrawals ($n = 41$) in both arms, highlighting the delicate balance between physicians and subjects as to what treatment might

be better suited for optimal outcomes in the treatment of highly challenging aneurysms. Seven prospective Tubridge subjects voiced their concerns about the potential adverse effects of flow-diverter use, while 15 subjects did not want to undergo stent-assisted coiling because they feared that the long-term durability was inferior to that anticipated with flow diverters. These subjects preferred to withdraw from the trial and wait to be treated with a commercially available flow diverter. The concept of new or apparently complicated technology can be intimidating for some patients.

Among the remaining subjects who departed from this trial prematurely, 1 dropped out after an incomplete subject consent, 6 had their index procedure terminated early after angiography examination indicated safety concerns, 1 was enrolled mistakenly, 1 violated the trial protocol and did not qualify for the index procedure, and 10 were terminated or withdrew from the trial for unknown reasons. Incomplete trial participation by the above-mentioned subjects led to a need to expand the sample size and prevent unbalanced subject numbers and age. We compared the baseline data of subjects who were LTF with those from the full analysis set and determined that their removal had not affected the overall distribution of characteristics. Moreover, although subject age was not thought to affect outcomes, we used multivariable logistic regression, adjusted for subject age, to eliminate the effect of this imbalance. Second, the results of this study only represent the treatment of a specific subtype of aneurysms and a preliminary application of a novel FD. As discussed above, increasing familiarity with the Tubridge device is expected to lower the rate of clinical complications. Finally, although we included treatment of vertebral artery aneurysms in this trial, only 4 subjects with these aneurysms were enrolled. Thus, generalizations about the use of flow diverters in vertebral arteries should be made with caution. Clearly, additional vertebral artery aneurysm studies are warranted.

CONCLUSIONS

This trial showed that there was a significantly higher obliteration rate of aneurysms treated with the Tubridge FD versus conventional Enterprise SAC treatment in a selected group of patients with large or giant intracranial aneurysms. However, this higher obliteration rate comes at a cost of nonsignificant higher complication rates. For inexperienced operators who are either entering flow-diverter clinical trials or preparing for real-world clinical use, the importance of a learning curve should be emphasized.

ACKNOWLEDGMENTS

We thank Professors Ming-hua Li, Qiu-ping Li, and Liang Shao for their contribution in evaluating the 6-month angiographic results; Professors Yin Jian-hua, Chen Yao, Dong Lin, and Dong-Lei Song for data and safety monitoring; and Professors XiaoYan Yan, Chong Ya Dong, and Yao Chen for their statistical analyses. Professor Jia He gave some guidance when drafting and revising this manuscript. We thank them for their constructive guidance. We are grateful to all principal investigators and delegated physicians who enrolled participants in all participating centers. We also thank the participants and their caretakers and families who consented to participate in the PARAT trial.

REFERENCES

1. International Study of Unruptured Intracranial Aneurysms Investigators. **Unruptured intracranial aneurysm: risk of rupture and risks of surgical intervention.** *N Engl J Med* 1998;339:1725–33 [CrossRef Medline](#)
2. Barrow DL, Alleyne C. **Natural history of giant intracranial aneurysms and indications for intervention.** *Clin Neurosurg* 1995;42: 214–44 [Medline](#)
3. Darsaut TE, Darsaut NM, Chang SD, et al. **Predictors of clinical and angiographic outcome after surgical or endovascular therapy of very large and giant intracranial aneurysms.** *Neurosurgery* 2011;68: 903–15; discussion 915 [CrossRef Medline](#)
4. Gonzalez NR, Duckwiler G, Jahan R, et al. **Challenges in the endovascular treatment of giant intracranial aneurysms.** *Neurosurgery* 2008;62(6 Suppl 3):1324–35 [Medline](#)
5. Sluzewski M, Menovsky T, van Rooij WJ, et al. **Coiling of very large or giant cerebral aneurysms: long-term clinical and serial angiographic results.** *AJNR Am J Neuroradiol* 2003;24:257–62 [Medline](#)
6. Chalouhi N, Tjoumakaris S, Gonzalez LF, et al. **Coiling of large and giant aneurysms: complications and long-term results of 334 cases.** *AJNR Am J Neuroradiol* 2014;35:546–52 [CrossRef Medline](#)
7. Sadasivan C, Cesar L, Seong J, et al. **Treatment of rabbit elastase-induced aneurysm models by flow diverters: development of quantifiable indexes of device performance using digital subtraction angiography.** *IEEE Trans Med Imaging* 2009;28:1117–25 [CrossRef Medline](#)
8. Raymond J, Gentric JC, Darsaut TE, et al. **Flow diversion in the treatment of aneurysms: a randomized care trial and registry.** *J Neurosurg* 2017;127:454–62 [CrossRef Medline](#)
9. Zhou Y, Yang PF, Fang YB, et al. **A novel flow-diverting device (Tubridge) for the treatment of 28 large or giant intracranial aneurysms: a single-center experience.** *AJNR Am J Neuroradiol* 2014;35:2326–33 [CrossRef Medline](#)
10. Kallmes DF, Brinjikji W, Boccardi E, et al. **Aneurysm Study of Pipeline in an Observational Registry (ASPIRe).** *Interv Neurol* 2016;5: 89–99 [CrossRef Medline](#)
11. Becske T, Kallmes DF, Saatci I, et al. **Pipeline for uncoilable or failed aneurysms: results from a multicenter clinical trial.** *Radiology* 2013; 267:858–68 [CrossRef Medline](#)
12. Byrne JV, Beltechi R, Yarnold JA, et al. **Early experience in the treatment of intra-cranial aneurysms by endovascular flow diversion: a multicentre prospective study.** *PLoS One* 2010;5: pii: e12492 [CrossRef Medline](#)
13. Nelson PK, Lylyk P, Szikora I, et al. **The Pipeline embolization device for the intracranial treatment of aneurysms trial.** *AJNR Am J Neuroradiol* 2011;32:34–40 [CrossRef Medline](#)
14. Kan P, Siddiqui AH, Veznedaroglu E, et al. **Early postmarket results after treatment of intracranial aneurysms with the Pipeline embolization device: a U.S. multicenter experience.** *Neurosurgery* 2012;71: 1080–87; discussion 87–88 [CrossRef Medline](#)
15. Wakhloo AK, Lylyk P, de Vries J, et al; Surpass Study Group. **Surpass flow diverter in the treatment of intracranial aneurysms: a prospective multicenter study.** *AJNR Am J Neuroradiol* 2015;36:98–107 [CrossRef Medline](#)
16. Yu SC, Kwok CK, Cheng PW, et al. **Intracranial aneurysms: midterm outcome of Pipeline embolization device—a prospective study in 143 patients with 178 aneurysms.** *Radiology* 2012;265:893–901 [CrossRef Medline](#)
17. Chiu AH, Cheung AK, Wenderoth JD, et al. **Long-term follow-up results following elective treatment of unruptured intracranial aneurysms with the Pipeline embolization device.** *AJNR Am J Neuroradiol* 2015;36:1728–34 [CrossRef Medline](#)
18. Becske T, Potts MB, Shapiro M, et al. **Pipeline for uncoilable or failed aneurysms: 3-year follow-up results.** *J Neurosurg* 2017;127:81–88 [CrossRef Medline](#)
19. ClinicalTrials.gov. Multicenter Randomized Trial on Selective Endovascular Aneurysm Occlusion With Coils Versus Parent Vessel Reconstruction Using the SILK Flow Diverter (MARCO POLO Post-

- Market Clinical Investigation). <https://clinicaltrials.gov/ct2/show/NCT01084681>. Accessed March 17, 2014
20. ClinicalTrials.gov. A Randomized Trial Comparing Flow Diversion and Best-standard Treatment: the FIAT Trial. <https://www.clinicaltrials.gov/ct2/show/NCT01349582>. Accessed January 20, 2016
 21. ClinicalTrials.gov. Multicenter Randomized Study for Medico-economic Evaluation of Embolization With Flow Diverter Stent in the Endovascular Treatment of Unruptured Saccular Wide-necked Intracranial Aneurysms. <https://www.clinicaltrials.gov/ct2/show/NCT01811134>. Accessed January 20, 2016
 22. ClinicalTrials.gov. Complete Occlusion of Coilable Aneurysms. <https://www.clinicaltrials.gov/ct2/show/NCT00777907>. Accessed January 20, 2016
 23. Turfe ZA, Brinjikji W, Murad MH, et al. **Endovascular coiling versus parent artery occlusion for treatment of cavernous carotid aneurysms: a meta-analysis.** *J Neurointerv Surg* 2015;7:250–55 CrossRef Medline
 24. Zhou Y, Yang P, Zhang Y, et al. **Posterior cerebral artery-posterior communicating artery (PCA-PCoA) aneurysms: report of five cases and literature review.** *Neurol India* 2012;60:228–30 CrossRef Medline
 25. Arambepola PK, McEvoy SD, Bulsara KR. **De novo aneurysm formation after carotid artery occlusion for cerebral aneurysms.** *Skull Base* 2010;20:405–08 CrossRef Medline
 26. Jafar JJ, Russell SM, Woo HH. **Treatment of giant intracranial aneurysms with saphenous vein extracranial-to-intracranial bypass grafting: indications, operative technique, and results in 29 patients.** *Neurosurgery* 2002;51:138–44; discussion 44–46 CrossRef Medline
 27. Spetzler RF, Schuster H, Roski RA. **Elective extracranial-intracranial arterial bypass in the treatment of inoperable giant aneurysms of the internal carotid artery.** *J Neurosurg* 1980;53:22–27 CrossRef Medline
 28. Morgan MK, Ferch RD, Little NS, et al. **Bypass to the intracranial internal carotid artery.** *J Clin Neurosci* 2002;9:418–24 CrossRef Medline
 29. Chalouhi N, Tjoumakaris S, Starke RM, et al. **Comparison of flow diversion and coiling in large unruptured intracranial saccular aneurysms.** *Stroke* 2013;44:2150–54 CrossRef Medline
 30. Brinjikji W, Murad MH, Lanzino G, et al. **Endovascular treatment of intracranial aneurysms with flow diverters: a meta-analysis.** *Stroke* 2013;44:442–47 CrossRef Medline
 31. Fargen KM, Hoh BL, Welch BG, et al. **Long-term results of Enterprise stent-assisted coiling of cerebral aneurysms.** *Neurosurgery* 2012;71:239–44; discussion 244 CrossRef Medline
 32. Kallmes DF, Hanel R, Lopes D, et al. **International retrospective study of the Pipeline embolization device: a multicenter aneurysm treatment study.** *AJNR Am J Neuroradiol* 2015;36:108–15 CrossRef Medline
 33. Ye G, Zhang M, Deng L, et al. **Meta-analysis of the efficiency and prognosis of intracranial aneurysm treated with flow diverter devices.** *J Mol Neurosci* 2016;59:158–67 CrossRef Medline
 34. Zhang Y, Zhou Y, Yang P, et al. **Comparison of the flow diverter and stent-assisted coiling in large and giant aneurysms: safety and efficacy based on a propensity score-matched analysis.** *Eur Radiol* 2016; 26:2369–77 CrossRef Medline
 35. Zhou G, Su M, Yin YL, et al. **Complications associated with the use of flow-diverting devices for cerebral aneurysms: a systematic review and meta-analysis.** *Neurosurg Focus* 2017;42:E17 CrossRef Medline
 36. Derdeyn CP, Chimowitz MI, Lynn MJ, et al; Stenting and Aggressive Medical Management for Preventing Recurrent Stroke in Intracranial Stenosis Trial Investigators. **Aggressive medical treatment with or without stenting in high-risk patients with intracranial artery stenosis (SAMMPRIS): the final results of a randomised trial.** *Lancet* 2014;383:333–41 CrossRef Medline
 37. Delgado Almandoz JE, Crandall BM, Scholz JM, et al. **Last-recorded P2Y12 reaction units value is strongly associated with thromboembolic and hemorrhagic complications occurring up to 6 months after treatment in patients with cerebral aneurysms treated with the Pipeline embolization device.** *AJNR Am J Neuroradiol* 2014;35: 128–35 CrossRef Medline
 38. Skukalek SL, Winkler AM, Kang J, et al. **Effect of antiplatelet therapy and platelet function testing on hemorrhagic and thrombotic complications in patients with cerebral aneurysms treated with the Pipeline embolization device: a review and meta-analysis.** *J Neurointerv Surg* 2016;8:58–65 CrossRef Medline
 39. McAuliffe W, Wycoco V, Rice H, et al. **Immediate and midterm results following treatment of unruptured intracranial aneurysms with the pipeline embolization device.** *AJNR Am J Neuroradiol* 2012; 33:164–70 CrossRef Medline

Localized Marked Elongation of the Distal Internal Carotid Artery with or without PHACE Syndrome: Segmental Dolichoectasia of the Distal Internal Carotid Artery

Z.Y. Jia, L.B. Zhao, and D.H. Lee



ABSTRACT

BACKGROUND AND PURPOSE: Segmental intracranial dolichoectasia of the distal ICA is a feature of PHACE syndrome or a sporadic phenomenon. We evaluated the relationship between intracranial dolichoectasia of the distal ICA and PHACE syndrome and illustrated the characteristic radiologic findings of the lesions.

MATERIALS AND METHODS: Intracranial dolichoectasia of the distal ICA was identified in 20 patients at our institution from 2005 to 2016 through a review of diagnostic cerebral angiography results. All radiologic images were reviewed to determine the vascular morphologic dispositions around the distal ICA, including dysplasia, mural calcification, vessel wall enhancement, lumen narrowing, and aneurysm formation. Medical records were reviewed to determine the symptoms of PHACE syndrome. Subsequently, the correlation between radiologic findings and PHACE syndrome was assessed.

RESULTS: In this cohort, which had a strong female predominance (male/female ratio = 2:18), intracranial dolichoectasia had a more ipsilateral vascular morphologic disposition. Mural calcification was detected more frequently in elderly patients, whereas vessel wall enhancement was detected more frequently in younger patients. Follow-up images showed a slow progression of the lesions. However, no significant differences in the vascular morphologic disposition and brain structural changes were observed between patients with ($n = 11$) and without ($n = 9$) PHACE syndrome.

CONCLUSIONS: The striking elongation and tortuosity of the distal ICA generally appeared to be a type of congenital lesion occurring early in embryogenesis as either a sporadic phenomenon or an arterial change associated with PHACE syndrome. Imaging findings revealed various mural abnormalities with a benign clinical course.

ABBREVIATIONS: AChA = anterior choroidal artery; BA = basilar artery; CS = communicating segment; ICDE = intracranial dolichoectasia; PCA = posterior cerebral artery; PcomA = posterior communicating artery; PHACE = posterior fossa malformations, hemangiomas, arterial anomalies, cardiac defects, and eye abnormalities; OA = ophthalmic artery

Marked arterial elongation and tortuosity (intracranial dolichoectasia [ICDE]) have been reported previously as common features of PHACE syndrome^{1–4} or as a sporadic phenomenon.^{5–7} PHACE syndrome refers to conditions associated with posterior fossa malformations, hemangiomas, arterial anomalies, cardiac defects, and eye abnormalities.⁸ ICDE of the intracranial arteries is one of the various features of the arterial cerebrovascular abnormalities.


On cerebrovascular imaging, from time to time, we encounter striking arterial elongations, particularly the distal ICA elongation, regardless of the PHACE syndrome status. This pathologic arterial elongation often co-occurs with marked tortuosity and may even appear as a conglomerated vascular mass to compensate for the limited length of the allocated arterial segment. It is often accompanied by conditions such as multiple stenoses, dilations, or aneurysms and usually features a variable amount of mural calcification.² Angiographically, this vascular morphologic disposition exhibits a more congenital appearance because the unique features cannot be explained by an acquired anatomic alteration. Although these types of arterial changes may present in any arterial segment of the body, we focused on cases of segmental involvement of the distal ICA because in our angiographic experience (limited to the cerebrovascular system), this site is the most frequently affected.

The easily recognizable symptoms and clinical significance of the above-mentioned vascular morphologic disposition completely dif-

Received July 29, 2017; accepted after revision January 1, 2018.

From the Department of Radiology and Research Institute of Radiology (Z.Y.J., L.B.Z., D.H.L.), Asan Medical Center, University of Ulsan College of Medicine, Seoul, Korea; and Department of Radiology (Z.Y.J., L.B.Z.), The First Affiliated Hospital of Nanjing Medical University, Jiangsu Province, China.

Please address correspondence to Deok Hee Lee, MD, PhD, Department of Radiology and Research Institute of Radiology, Asan Medical Center, University of Ulsan College of Medicine, 88, Olympic-ro 43-gil, Songpa-gu, Seoul 138-736, Korea; e-mail: dhlee@amc.seoul.kr

 Indicates article with supplemental on-line table.

<http://dx.doi.org/10.3174/ajnr.A5573>

fer from those of acquired nonsegmental dilative arteriopathy, which is frequently observed in the basilar artery (BA). Accordingly, this study describes angiographic and other imaging characteristics of this peculiar anatomic disposition, particularly in the distal ICA, by reviewing the radiologic findings and medical records of affected patients. We aimed to evaluate the possible associations of the radiologic findings with PHACE syndrome and illustrate the clinical follow-up results of the imaging morphologic abnormalities.

MATERIALS AND METHODS

Definition of ICDE and Segmentation of the ICA

Because pathologic arterial tortuosity cannot be quantified, we subjectively defined segmental ICDE by comparing other arterial segments, particularly those in the same segment on the contralateral side, as unusually marked areas of dolichosis with variable degrees of ectasia on the affected side. Notably, these areas could be easily demarcated from other adjacent segments with normal lengths and tortuosities.

We applied the 7-segment system proposed by Lasjaunias et al⁹ for the ICA to our analysis of the involved segments of the ICA and intracranial arteries. This embryology-based 7-segment system terminates at the origin of the posterior communicating artery (PcomA). Because the system does not name the segment of the adult ICA between the PcomA origin and ICA bifurcation into the MCA and anterior cerebral artery, we designated this specific segment as the “communicating segment” (CS) (Fig 1).

Patient Population and PHACE Syndrome Diagnosis

At our institution (Asan Medical Center), 11,516 patients underwent diagnostic cerebral angiography between January 2005 and December 2016. For our study, we limited the number of candidate cases by applying the search terms “carotid,” “ICA,” “dysplasia,” and “dolichoectasia” and further limited the number to 45 patients by reviewing the angiography reports. Furthermore, all angiographic images of the included cases were reviewed to identify intracranial ICA abnormalities, including marked elongation and tortuosity. Finally, 20 patients were identified.

This retrospective review was approved by our institutional review board, and the requirement for individual patient consent was waived. The included patients’ medical records were reviewed for symptoms and indications of PHACE syndrome and other significant disorders. All data obtained via radiologic imaging modalities (CT, CTA, MR imaging, TOF-MRA, contrast-enhanced MR vessel imaging, and brain perfusion SPECT) were reviewed in our PACS system by 2 radiologists (Z.Y.J. and L.B.Z.). If the individual radiologic analyses differed, the reviewers reached a consensus after discussion with a third reviewer (D.H.L.). Finally, the patients were stratified according to the “Consensus Statement on Diagnostic Criteria for PHACE Syndrome” of 2009 as follows: 1) PHACE syndrome, 2) possible PHACE syndrome, or 3) none.⁸

Image Findings and Statistical Analysis

After recording the laterality and segments of the involved ICA, the morphology of the arterial components around the distal ICA was recorded by reviewing DSA, CTA, and MRA images of the anterior cerebral artery (A1 segment), anterior communicating artery, MCA (M1), anterior choroidal artery (AchoA), PcomA, ophthalmic

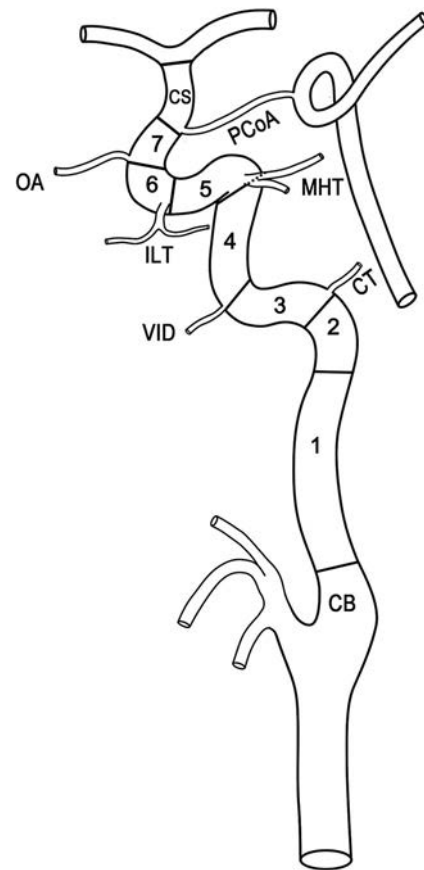


FIG 1. In addition to the 7 segments above, the carotid bulb to the PcomA origin, the segment of the ICA between the PcomA origin and ICA bifurcation before the MCA and anterior cerebral artery, is designated as the CS or distal ICA in adults. ILT indicates inferolateral trunk; MHT, meningohipophyseal trunk; VID, vidian artery; CT, carotico tympanic artery; CB, carotid bulb.

artery (OA), BA, and posterior cerebral artery (PCA) (P1 and P2 segments). The term “dysplasia” encompassed a variety of arterial abnormalities, including looping, coiling, ectasia, dolichoectasia, or simple dolichosis. In addition, the presence of lesions in the contralateral ICA, BA, and/or ipsi- and contralateral vertebral arteries was noted.

DSA, CTA, and MRA were used to analyze vessel stenoses and aneurysms. Stenosis was defined as any narrowing of the vessel lumen compared with the reference vessel as defined in the Warfarin-Aspirin Symptomatic Intracranial Disease trial method.¹⁰ The aneurysm was defined as an eccentric bulging of the vessel wall within the dolichoectatic segment, and the diagnosis was reached with the consensus of 2 doctors (D.H.L. and Z.Y.J.). CT was used to analyze vessel wall calcification. Contrast-enhanced MR imaging of the vessel wall was used to analyze vessel wall characteristics, including enhancement, wall thickening, and luminal narrowing. Brain perfusion SPECT was used to evaluate whether a stenosis or tortuous ICA led to a decrease in brain perfusion.

The patients were divided into 2 groups according to the PHACE syndrome diagnostic criteria: the group positive for PHACE, PHACE (+), and the group negative for PHACE, PHACE (−). The PHACE (+) group included both confirmed and possible cases of PHACE syndrome. The Fisher exact test was used to assess differences between the groups. Descriptive analyses were

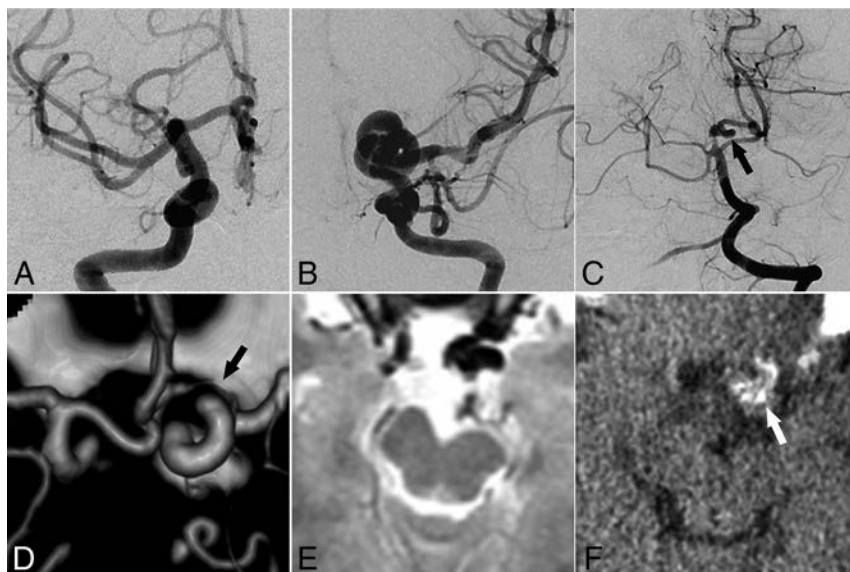


FIG 2. Representative images of ICDE in a patient without PHACE syndrome (patient 6, a 28-year-old woman). A and B, Bilateral ICA angiography shows a tangled arterial mass of the left distal ICA and no observable left A1 segment. C, Left vertebral artery angiography shows a dolichoectasia of the left P1 and P2 segments (arrow). D, CT angiography shows hypoplasia of the left A1 segment (arrow). E, T2-weighted image of the brain shows hypoplasia of the left midbrain. F, CT image of vessel wall calcification in the left distal ICA (arrow).

Table 1: Arterial components and brain structures surrounding the distal ICA on the affected side versus the contralateral side

	Affected Side (n = 20)	Contralateral Side (n = 20)	P Value ^a
A1	Dysplasia = 15 (75.0%)	Dysplasia = 1 (5.0%)	.001
M1	Dysplasia = 2 (10.0%)	Dysplasia = 0 (0.0%)	.487 ^b
OA	Ectopic = 5 (25.0%)	Ectopic = 1 (5.0%)	.219
AchoA	Dysplasia = 5 (25.0%)	Dysplasia = 0 (0.0%)	.047 ^b
PcomA	Dysplasia = 14 (70.0%)	Dysplasia = 3 (15.0%)	.003
BA/PCA	Dysplasia = 14 (70.0%)	Dysplasia = 1 (5.0%)	<.001
Midbrain	Hypoplasia = 9 (45.0%)	Hypoplasia = 0 (0.0%)	.001 ^b

Note:—A1 indicates a segment of the anterior cerebral artery; M1, a segment of the MCA. BA/PCA indicates either BA or PCA, or both.

^a McNemar test.

^b Fisher exact test.

performed to evaluate possible relationships among the following features: age, wall calcification, vessel wall enhancement, stenosis, and aneurysm.

RESULTS

The basic demographic information, presenting symptoms, involved arteries around the distal ICA, acquired changes in affected segments, and PHACE diagnostic statuses of all patients are summarized in the On-line Table. The patients included 18 females and 2 males with a median age of 43.5 years (range, 7–73 years) with varying clinical symptoms that did not appear to be directly related to the arterial abnormality. A systemic review revealed that 3 patients had hypertension, whereas none had systemic vasculitis or autoimmune disease.

All patients had the unique feature, segmental elongation and tortuosity of the distal ICA, resulting in a tangled arterial mass (Fig 2). No differences were observed between the sides of onset (right, 11/20). Two patients presented with bilateral distal ICA dolichoectasia. In these 2 patients, we defined the side with more severe dolichoectasia as the ipsilateral side, while the other side was

the contralateral side. The involved ICA segments ranged from segments 2 to 7, with a mean \pm SD of 3.5 ± 1.6 segments. Fourteen patients had BA ($n = 1$) or ipsilateral PCA ($n = 13$) involvement [BA/PCA (+)]. We observed a significant correlation between ipsilateral A1, PcomA, BA/PCA, and midbrain hypoplasia and segmental ICDE of the distal ICA, unlike the contralateral side (Table 1).

In 9 of the 20 patients, the ipsilateral midbrain was smaller than the contralateral midbrain (Fig 2E). Four and 7 patients were found to have confirmed or possible PHACE syndrome, respectively, when midbrain hypoplasia was excluded as a major or minor criterion for a PHACE syndrome diagnosis (posterior fossa anomaly). The inclusion of this criterion resulted in 4 and 11 patients with confirmed and possible PHACE syndrome, respectively. No significant differences in arterial component dysplasia (including A1, anterior communicating artery, M1, AChoA, PcomA, OA, BA, and PCA) and brain structures were observed between patients positive and negative for PHACE (Table 2).

Calcification was detected in 16 patients with a mean age of 45.9 years; the remaining 4 patients without calcification had a mean age of 17.3 years. Significantly progressive calcification was observed in 1 patient with progressive

arterial stenosis during an interval of 10 years (patient 9; age range, 42–52 years). Stenosis was detected in 11 patients with a mean age of 42.1 years; the 9 patients without stenosis had a mean age of 37.9 years. None of the patients had an ischemic stroke event, and none of the 12 patients who underwent brain perfusion SPECT had hypoperfusion. Aneurysms were detected in 15 patients with a mean age of 38.1 years; the 5 patients without aneurysms had a mean age of 48.8 years.

Ten patients underwent contrast-enhanced high-resolution MR imaging of the vessel wall, which detected enhancement in 6 patients with a mean age of 22.8 ± 13.2 years; the remaining 4 patients had a mean age of 57.0 ± 9.2 years ($P < .001$). One patient (patient 1, Fig 3) exhibited vessel wall enhancement at both 8 and 12 years of age, with no major change in the enhancement pattern. Vessel wall imaging revealed that the stenotic segment exhibited either an eccentric or concentric wall thickening (Fig 4) as well as a potential enhancement of the parent artery and aneurysm neck (Fig 5).

Table 2: Arterial components around the distal ICA on the affected side in patients with and without PHACE syndrome^a

	PHACE (+) (n = 11)	PHACE (-) (n = 9)	P Value ^b
A1	Dysplasia = 8 (72.7%)	Dysplasia = 7 (77.8%)	1.000
M1	Dysplasia = 0 (0.0%)	Dysplasia = 2 (22.2%)	.189
OA	Ectopic = 1 (9.1%)	Ectopic = 4 (44.4%)	.127
AchoA	Dysplasia = 3 (27.3%)	Dysplasia = 2 (22.2%)	1.000
PcomA	Dysplasia = 7 (63.6%)	Dysplasia = 7 (77.8%)	.642
Midbrain	Dysplasia = 5 (45.5%)	Dysplasia = 4 (44.4%)	1.000

^a PHACE includes cases of confirmed and possible PHACE syndrome; a small midbrain was not used as a criterion.

^b Fisher exact test.

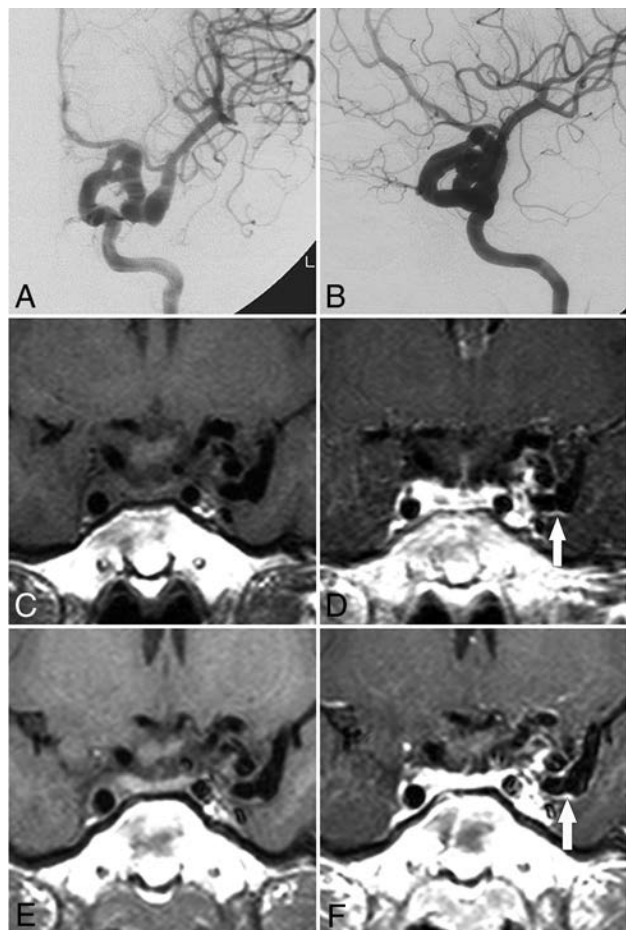


FIG 3. Evolution of vessel wall enhancement with aging in a patient with PHACE syndrome (patient 1, an 8-year-old girl). A and B, Left ICA angiography (anteroposterior and oblique views) reveals tortuosity in the left distal ICA with a small and long A1 segment. C and D, Noncontrast and contrast-enhanced vessel wall imaging at 8 years of age demonstrates vessel wall enhancement and slight vessel wall thickening (arrow in D). E and F, Vessel wall imaging at 12 years of age shows a similar vessel wall enhancement pattern (arrow in F).

DISCUSSION

In our series of patients across a wide range of ages, we observed striking elongation and tortuosity of the distal ICA, regardless of the PHACE diagnostic status. We further observed that compared with the contralateral side, the ipsilateral arterial components and brain structures around the affected distal ICA more frequently showed dysplasia. Furthermore, the affected vessels had various manifestations, including stenosis, aneurysm, calcification, and vessel wall enhancement, and the disease evolved slowly with age according to follow-up radiologic imaging.

Embryologic Pathogenesis of ICDE of the Distal ICA

During the embryologic period of cerebral artery formation, angiogenesis is mainly driven by hypoxia and related growth factors in the target tissue.^{11,12}

We hypothesized that exposure of a specific segment of the intracranial artery to a vasculogenetic trigger resulted in arterial lengthening. According to the ICA developmental anatomy proposed by

Lasjaunias and Santoyo-Vazquez,¹³ the ICA branches into a cranial and caudal rami at stages I and II (3.5–4 weeks); the former gives rise to the anterior cerebral artery and AchoA, whereas the latter gives rise to the PcomA, P1 segment, and upper BA. In this study, dolichoectasia at the anterior (A1 segment, AchoA, and CS segment) and posterior (PcomA, P1 segment, and upper BA) divisions of the ICA suggested that these regions were triggered during embryonic development. We observed no involvement of the superior cerebellar artery in our cases (data not shown); because the superior cerebellar artery existed before ICA branching, the vasculogenetic event may have occurred after the appearance of superior cerebellar artery.¹³ Although the remaining PCA (segments P2–P4) comprises the posterior choroidal branch of the caudal ramus at stage V, the involvement of the P2 segment in several cases suggests that the PCA precursor had also been affected.¹³

PHACE Syndrome

Cerebral arterial anomalies are observed in 91% of patients with PHACE syndrome,¹⁴ and previous studies of PHACE syndrome have reported a presentation of dolichoectasia of the internal carotid arteries similar to that observed in our cases.^{2,4,15,16} Therefore, we searched for common features between our cases and PHACE syndrome cases.

First, we observed a strong female predominance in our patient group in agreement with previous studies of PHACE syndrome (up to 8:1).^{15,17,18} Second, the timing of PHACE syndrome was consistent with our speculated time course. Several studies of PHACE syndrome have reported that the teratogenic influence might occur from gestational weeks 3 to 5.5,^{8,14} concurrent with the regression of the embryonic capillary bed and active stemming of the craniocervical vasculature. Therefore, any influences on these 2 processes may result in a cutaneous hemangioma and trigeminal artery persistence.¹⁹

Third, several vascular anomalies have been reported in both patients with PHACE syndrome and in our patient group. In a previous study, A1 hypoplasia was reported as an intracranial anomaly affecting 8 of 12 patients with PHACE syndrome; this is similar to the findings of our study (15/20).²⁰ ICDE of the ICA was accompanied by dolichoectasia of the posterior circulation in 6 of 7 patients with PHACE syndrome in a previous study.²⁰ An aberrant origin or course of the principal cerebral arteries, a major or minor PHACE syndrome criterion, was observed in 9 of 20 patients (45%; 5 ectopic ophthalmic arteries and 4 other arteries).

Fourth, 4 of the 20 patients in this study met the diagnostic criteria of PHACE syndrome, and an additional 7 patients were classified as possible cases of PHACE syndrome. In addition, some

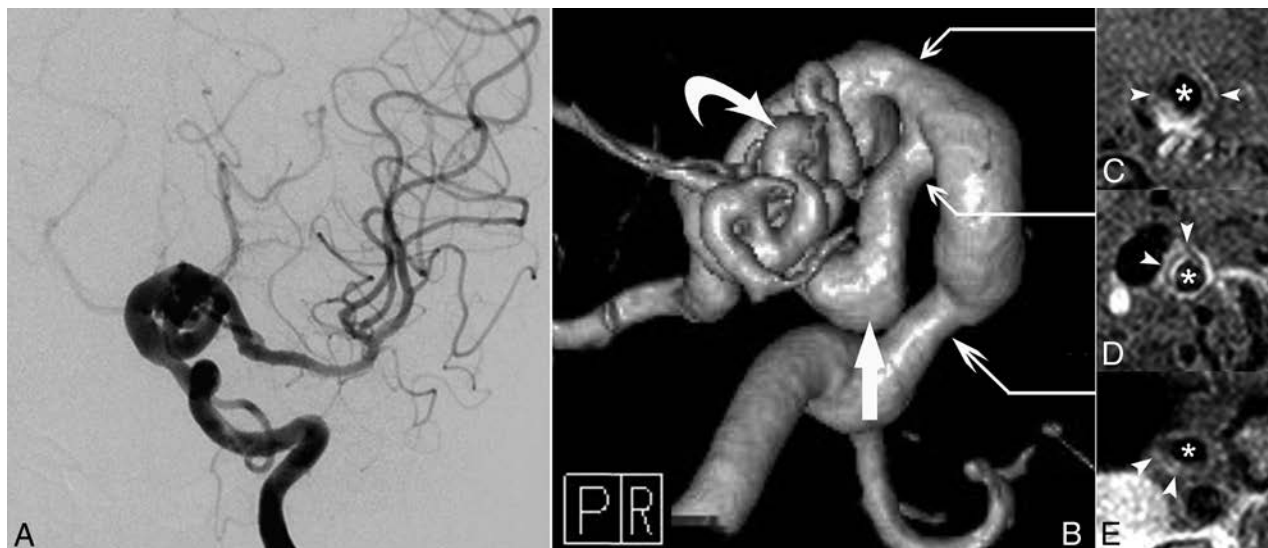


FIG 4. Vessel wall enhancement at the stenotic segment in a patient with possible PHACE syndrome (patient 5, a 23-year-old woman). A and B, Left ICA angiography and TOF-MRA reveal dolichoectasia of the left distal ICA, left PcomA (arrow), and left AchoA (curved arrow). C–E, Section images reveal the vessel wall thickening and enhancing patterns of each corresponding stenotic segment (arrowheads indicate the vessel wall thickening and asterisks indicate vessel lumen; C, sagittal plane; D and E, axial plane). P indicates posterior; R, right.

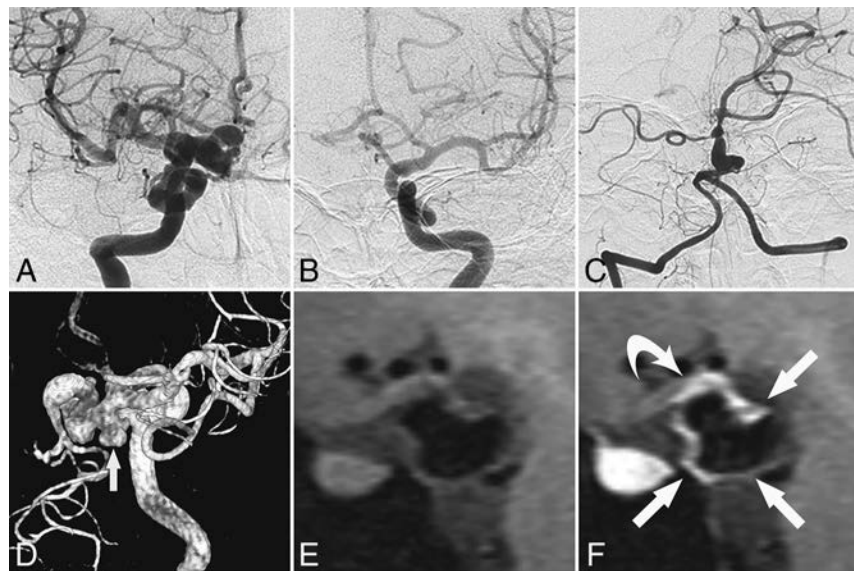


FIG 5. Vessel wall enhancement at the aneurysm wall and the parent artery wall in a patient without PHACE syndrome (patient 11, a 45-year-old woman). A–C, Cerebral angiography shows dolichoectasia in the right distal ICA and basilar artery. D, 3D-DSA shows dolichoectasia in the right distal ICA and right PcomA as well as the formation of multiple aneurysms in the right PcomA (arrow). E and F, Non-contrast-enhanced and contrast-enhanced vessel wall imaging shows enhancement of the aneurysm wall (arrows in F) and the parent artery wall (curved arrow in F).

patients exhibited ipsilateral midbrain hypoplasia. Because a lack of direct contact with the adjacent vessel does not support compression-induced midbrain deformation (Fig 2E), we suspected that dolichoectasia of the arteries feeding the midbrain (BA, P1, or P2) mildly altered the blood supply and caused further hypoplasia. In 1 patient with PHACE (patient 10), hypoplasia of the ipsilateral cerebellum and the ipsilateral midbrain was found to coexist, suggesting that these 2 structural anomalies shared a common origin. Therefore, if a smaller midbrain was defined as a posterior fossa anomaly associated with PHACE syndrome, an additional 4 patients in our study would meet the criteria for possible PHACE syndrome. Such lesions

might broaden the PHACE syndrome phenotype. According to a study by Heyer et al,²⁰ moderate effacement of the right pons (Fig 2C in the article by Heyer et al) and cerebral peduncle along with corresponding vascular anomalies was observed via MR imaging in a patient with PHACE syndrome. However, the author did not propose this finding as an anomaly.²⁰

In our study, we found no significant differences in arterial component dysplasia and brain structures between patients positive and negative for PHACE (Table 2), suggesting that the 2 groups of patients share the same features and pathogenesis. Furthermore, although we did not detect an obvious cutaneous hemangioma in many of our patients, a previous study found that very small cutaneous hemangiomas might be absent or regress spontaneously without prior recognition or reporting.⁴ The above-mentioned aspects raise the intriguing possibility that a marked ICDE of the

ICA might indicate an otherwise-unrecognized partial phenotypic expression of PHACE syndrome. However, the spontaneous regression of cutaneous hemangiomas at an early age may cause the underestimation of the incidence of PHACE syndrome in this group of patients, which further induces underestimation of the relationship between the ICDE and PHACE syndrome.

Acquired Changes in the Involved Arterial Wall

Normally, an abnormal mural angiogenesis likely causes an increase in the luminal caliber because the correct remodeling signals induce apoptosis of the unnecessary vessel wall components.

A lack of remodeling causes centripetal and longitudinal proliferation and luminal reduction; however, this might also cause ectasias, elongated arteries, and aneurysms.¹³ Although many cases involving ICDE of the ICA, with or without PHACE syndrome, have been reported, little is known about the evolution of vessel wall lesions and relevant complications. Results from a follow-up study of vessel lesions may provide valuable prognostic information.

Progressive cerebral arterial stenosis and arterial occlusion and a Moyamoya-like vasculopathy leading to stroke have been described in infants with PHACE syndrome.^{2,20} This progressive cerebral vasculopathy corresponds with the proliferative phase of hemangioma growth, and as a result, the average age of experiencing stroke among patients with PHACE syndrome is 8.8 months.²¹ However, no ischemic stroke events were reported in our present study, even among patients with a Moyamoya-like vasculopathy (patients 4, 8, 12). Notably, we observed vessel wall enhancement more frequently among young patients than older patients, indicating a regression in inflammation with aging. Accordingly, we speculate that most arterial stenoses and occlusions formed within a short time during the prenatal or infant stage. Patients with mild lesions might pass through that period asymptotically, and adult PHACE syndrome diagnoses may be incidental.^{1,22} Due to the long-standing nature of the lesion, there is a good chance of good collateral circulation formation secondary to arterial stenoses, which may present as nonsymptomatic stenooclusive disease.

We further propose that ICDE of the distal ICA, with or without PHACE syndrome, might stabilize after a period of rapid progression. Bracken et al¹⁵ followed up several cases of PHACE in neurodevelopmentally healthy patients for 1–12 years. McLaughlin et al⁵ reported a 24-year-old female patient with a pure arterial malformation involving the distal ICA, PcomA, and PCA that was found on a CT scan obtained to determine the cause of a headache. When this patient was later followed up at 54 years of age, the abnormal vessels had not changed with time on MR images, and no symptoms relevant to the abnormal vessels were reported during the 31-year interval.⁵ Similarly, our review of imaging data collected during a long follow-up demonstrated a slow evolution of vessel wall enhancement (patient 1) and slow progression of both calcification and stenosis (patient 9). The vessel wall enhancement in patient 1 could be explained by the immature nature of the affected vessel wall, which may increase the permeability of the endothelium, with contrast leakage from the lumen into the arterial wall, and may be simultaneously associated with an atherosclerotic-like process in the dysplastic segments.

Treatment and Follow-Up

Many cases of ICDE with tortuous ICAs were identified incidentally, without relevant symptoms^{5,7,15}; in these cases, the lesions appeared stable on follow-up images and the patients did not receive medical treatment. However, several reports and our observations suggested the need for regular imaging follow-up as well as medication in some cases. However, no specific treatment exists for dolichoectasia, and the surgical and medical therapies used to treat this condition have not been systematically evalu-

ated. Although anticoagulation and antiplatelet therapies might help in preventing an ischemic episode, some studies have indicated that aspirin and warfarin or both do not effectively reduce the stroke recurrence rates in patients with dolichoectasia and might increase the risk of hemorrhage in this population.²³ However, we note that these previous data were all with respect to the BAs.

Treatment for PHACE syndrome should address the aforementioned symptoms.² Corticosteroids and interferon have been previously used to treat hemangiomas associated with PHACE syndrome; however, their efficacy in the treatment of acute-phase vessel wall inflammation remains unknown.¹⁶ Occasionally, a pial synangiosis procedure has been suggested for severe stenosis or occlusion of the distal ICA.²⁰

We believe that attention should be paid to several cases in this study. One patient (patient 1) exhibited simultaneous vessel wall enhancement and calcification at 7 years of age, leading to our hypothesis that the affected vessel wall was prone to atherosclerosis formation and secondary calcification. Questions also remain regarding the use of antiatherosclerosis therapies in young patients. Another patient (patient 11, Fig 5) exhibited vessel wall enhancement in an aneurysm and its parent artery, which may be a risk factor for aneurysm rupture; accordingly, a pre-emptive aneurysm embolization was performed.²⁴ In another patient (patient 16), asymptomatic ICDE of the right ICA and hypoplasia of the right A1 segment were detected at 54 years of age, and a blood flow–related aneurysm of the left anterior communicating artery was observed at 69 years of age. This patient was later treated with coiling embolization. Therefore, we suggested a follow-up comprising regular angiography studies (CTA or MRA) to demonstrate overall luminal changes and, if possible, vessel wall imaging to detect inflammation in the lesion.

Limitations

This study had several limitations. First, we found it difficult to objectively define “segmental dolichoectasia.” To overcome this problem, we included only cases with noncontroversial elongation and unusual tortuosity relative to other segments or the contralateral ICA. Accordingly, we might have skipped many mild elongation cases and underestimated the number of relevant cases. Second, the definition of segmental arterial tortuosity is rather subjective. Lasjaunias et al⁹ defined the ICA segments according to embryogenic evolution. In this study, we considered ICDE of the distal ICA to be a congenital disease that may occur segmentally. Although we used this system to describe the observed lesions, we were unable to conclude that the lesions could be attributed to a similar congenital origin. Third, 2 patients in our study had bilateral ICA involvement, which has also been reported in patients with PHACE syndrome. However, a satisfactory interpretation of the bilateral pathogenesis could not be attained.²⁰

CONCLUSIONS

The segmental nature of the striking elongation and tortuosity of the distal ICA suggests a type of congenital lesion representing either a sporadic phenomenon or an arterial change associated with PHACE syndrome. Similar arterial changes were observed in

vascular segments adjacent to the lesions, particularly in the ipsilateral proximal PCA. Imaging findings of affected patients demonstrated various mural abnormalities with a benign clinical course.

REFERENCES

1. Burch EA, Garzon MC, Parikh A, et al. **A 65-year-old woman diagnosed with PHACE syndrome.** *Pediatr Dermatol* 2013;30:e153–56 CrossRef Medline
2. Baccin CE, Krings T, Alvarez H, et al. **A report of two cases with dolichosegmental intracranial arteries as a new feature of PHACES syndrome.** *Childs Nerv Syst* 2007;23:559–67 CrossRef Medline
3. Metry DW, Dowd CF, Barkovich AJ, et al. **The many faces of PHACE syndrome.** *J Pediatr* 2001;139:117–23 CrossRef Medline
4. Rossi A, Bava GL, Biancheri R, et al. **Posterior fossa and arterial abnormalities in patients with facial capillary haemangioma: presumed incomplete phenotypic expression of PHACES syndrome.** *Neuroradiology* 2001;43:934–40 CrossRef Medline
5. McLaughlin N, Raychev R, Duckwiler G, et al. **Pure arterial malformation of the posterior cerebral artery: importance of its recognition.** *J Neurosurg* 2013;119:655–60 CrossRef Medline
6. Yuh SJ, Alkherayf F, Lesiuk H. **Dolichoectasia of the vertebral basilar and internal carotid arteries: a case report and literature review.** *Surg Neurol Int* 2013;4:153 CrossRef Medline
7. Nakahara I, Taki W, Tanaka M, et al. **Dolichoectasia of the middle cerebral artery: case report.** *Neurol Med Chir (Tokyo)* 1995;35:822–24 CrossRef Medline
8. Metry D, Heyer G, Hess C, et al; PHACE Syndrome Research Conference. **Consensus statement on diagnostic criteria for PHACE syndrome.** *Pediatrics* 2009;124:1447–56 CrossRef Medline
9. Lasjaunias PL, Berenstein A, Ter Brugge KG. *Surgical Neuroangiography: Clinical Vascular Anatomy and Variations.* 2nd ed. Vol. 1. Berlin: Springer-Verlag; 2001
10. Samuels OB, Joseph GJ, Lynn MJ, et al. **A standardized method for measuring intracranial arterial stenosis.** *AJNR Am J Neuroradiol* 2000;21:643–46 Medline
11. Menshawi K, Mohr JP, Gutierrez J. **A functional perspective on the embryology and anatomy of the cerebral blood supply.** *J Stroke* 2015;17:144–58 CrossRef Medline
12. Plate KH. **Mechanisms of angiogenesis in the brain.** *J Neuropathol Exp Neurol* 1999;58:313–20 CrossRef Medline
13. Lasjaunias P, Santoyo-Vazquez A. **Segmental agenesis of the internal carotid artery: angiographic aspects with embryological discussion.** *Anat Clin* 1984;6:133–41 CrossRef Medline
14. Haggstrom AN, Garzon MC, Baselga E, et al. **Risk for PHACE syndrome in infants with large facial hemangiomas.** *Pediatrics* 2010;126:e418–26 CrossRef Medline
15. Bracken J, Robinson I, Snow A, et al. **PHACE syndrome: MRI of intracerebral vascular anomalies and clinical findings in a series of 12 patients.** *Pediatr Radiol* 2011;41:1129–38 CrossRef Medline
16. Vermeer S, van Oostrom CG, Boetes C, et al. **A unique case of PHACES syndrome confirming the assumption that PHACES syndrome and the sternal malformation-vascular dysplasia association are part of the same spectrum of malformations.** *Clin Dysmorphol* 2005;14:203–06 CrossRef Medline
17. Metry DW, Haggstrom AN, Drolet BA, et al. **A prospective study of PHACE syndrome in infantile hemangiomas: demographic features, clinical findings, and complications.** *Am J Med Genet A* 2006;140:975–86 Medline
18. Oza VS, Wang E, Berenstein A, et al. **PHACES association: a neuro-radiologic review of 17 patients.** *AJNR Am J Neuroradiol* 2008;29:807–13 CrossRef Medline
19. Pascual-Castroviejo I, Viaño J, Moreno F, et al. **Hemangiomas of the head, neck, and chest with associated vascular and brain anomalies: a complex neurocutaneous syndrome.** *AJNR Am J Neuroradiol* 1996;17:461–71 Medline
20. Heyer GL, Dowling MM, Licht DJ, et al. **The cerebral vasculopathy of PHACES syndrome.** *Stroke* 2008;39:308–16 CrossRef Medline
21. Heyer GL, Millar WS, Ghatan S, et al. **The neurologic aspects of PHACE: case report and review of the literature.** *Pediatr Neurol* 2006;35:419–24 CrossRef Medline
22. Arora SS, Plato BM, Sattenberg RJ, et al. **Adult presentation of PHACES syndrome.** *Interv Neuroradiol* 2011;17:137–46 CrossRef Medline
23. Passero SG, Calchetti B, Bartalini S. **Intracranial bleeding in patients with vertebrobasilar dolichoectasia.** *Stroke* 2005;36:1421–25 CrossRef Medline
24. Edjlali M, Gentric JC, Regent-Rodriguez C, et al. **Does aneurysmal wall enhancement on vessel wall MRI help to distinguish stable from unstable intracranial aneurysms?** *Stroke* 2014;45:3704–06 CrossRef Medline

Brain MRI Characteristics of Patients with Anti-*N*-Methyl-D-Aspartate Receptor Encephalitis and Their Associations with 2-Year Clinical Outcome

T. Zhang, Y. Duan, J. Ye, W. Xu, N. Shu, C. Wang, K. Li, and Y. Liu



ABSTRACT

BACKGROUND AND PURPOSE: Anti-*N*-methyl-D-aspartate receptor encephalitis is an autoimmune-mediated disease without specific brain MRI features. Our aim was to investigate the brain MR imaging characteristics of anti-*N*-methyl-D-aspartate receptor encephalitis and their associations with clinical outcome at a 2-year follow-up.

MATERIALS AND METHODS: We enrolled 53 patients with anti-*N*-methyl-D-aspartate receptor encephalitis and performed 2-year follow-up. Brain MRIs were acquired for all patients at the onset phase. The brain MR imaging manifestations were classified into 4 types: type 1: normal MR imaging findings; type 2: only hippocampal lesions; type 3: lesions not involving the hippocampus; and type 4: lesions in both the hippocampus and other brain areas. The modified Rankin Scale score at 2-year follow-up was assessed, and the association between the mRS and onset brain MR imaging characteristics was evaluated.

RESULTS: Twenty-eight (28/53, 53%) patients had normal MR imaging findings (type 1), and the others (25/53, 47%) had abnormal MRI findings: type 2: 7 patients (13%); type 3: seven patients (13%); and type 4: eleven patients (21%). Normal brain MRI findings were more common in female patients ($P = .02$). Psychiatric and behavioral abnormalities were more common in adults ($P = .015$), and autonomic symptoms ($P = .025$) were more common in pediatric patients. The presence of hippocampal lesions ($P = .008$, OR = 9.584; 95% CI, 1.803–50.931) and relapse ($P = .043$, OR = 0.111; 95% CI, 0.013–0.930) was associated with poor outcome.

CONCLUSIONS: Normal brain MRI findings were observed in half of the patients. Lesions in the hippocampus were the most common MR imaging abnormal finding. The presence of hippocampal lesions is the main MR imaging predictor for poor prognosis in patients with anti-*N*-methyl-D-aspartate receptor encephalitis.

ABBREVIATIONS: anti-NMDA = anti-*N*-methyl-D-aspartate; ICU = intensive care unit; MTA = medial temporal lobe atrophy

Anti-*N*-methyl-D-aspartate (anti-NMDA) receptor encephalitis was first described by Dalmau et al in 2007¹ as a common type of autoimmune-mediated limbic encephalitis that presents

with various clinical symptoms, including behavioral and psychiatric features, memory and cognitive deficits, seizures, central hypoventilation, and movement disorders.^{1–5} The autoantibody of the anti-NMDA receptor can be detected in the CSF and/or the serum of patients and is a specific antibody that correlates with disease severity.² The management of anti-NMDA receptor encephalitis generally includes immunotherapy and tumor detection and removal.⁶ First-line immunotherapy (eg, steroids, plasmapheresis, and intravenous immunoglobulins) and second-line immunotherapy, including cyclophosphamide or rituximab, are treatment choices that depend on the individual patient status.^{4,7}

Received October 26, 2017; accepted after revision January 14, 2018.

From the Departments of Radiology (T.Z., K.L.) and Neurology (J.Y., W.X.), Xuanwu Hospital, Capital Medical University, Beijing, P.R. China; Department of Radiology (Y.D., Y.L.), Beijing Tiantan Hospital, Capital Medical University, Beijing, P.R. China; Tiantan Image Research Center (Y.D., Y.L.), China National Clinical Research Center for Neurological Diseases, Beijing, P.R. China; State Key Laboratory of Cognitive Neuroscience and Learning and International Data Group/McGovern Institute for Brain Research (N.S., C.W.), Beijing Normal University, Beijing, P.R. China; and Beijing Key Lab of MRI and Brain Informatics (K.L.), Beijing, P.R. China.

Tian Zhang and Yunyun Duan contributed equally to this work.

This work was supported by the European Committee for Treatment and Research in Multiple Sclerosis–Magnetic Imaging in Multiple Sclerosis (ECTRIMS-MAGNIMS) Fellowship from ECTRIMS (Y.L.); the National Science Foundation of China (Nos. 81101038, 81401377, 81471221, and 81230028); the National Basic Research Program of China (2013CB966900); the Beijing Natural Science Fund (No. 7133244); the Beijing Nova Programme (xx2013045); the Beijing Municipal Administration of Hospital Clinical Medicine Development of Special Funding Support (code: ZYLX201609); and Key Projects in the National Science and Technology Pillar Program during the Twelfth Five-Year Plan Period (2012BAI10B04).

Please address correspondence to Kuncheng Li, MD, Department of Radiology, Xuanwu Hospital, Capital Medical University, Beijing 100053, China; e-mail: likuncheng@xwh.ccmu.edu.cn; or Yaou Liu, MD, PhD, Department of Radiology, Beijing Tiantan Hospital, Capital Medical University, Beijing, China; Tiantan Image Research Center, China National Clinical Research Center for Neurological Diseases, Beijing, China; e-mail: asiaeurope80@gmail.com

Indicates open access to non-subscribers at www.ajnr.org

<http://dx.doi.org/10.3174/ajnr.A5593>

As reported, normal brain MR imaging results were observed in most patients,⁸ and 33%–55% of patients showed abnormal brain MR imaging results in several previous publications.^{7,9} Brain lesions often occur in the medial temporal lobe, frontal cortex, and parietal cortex, but lesions in the cerebellum, thalamus, basal ganglia, brain stem, and spinal cord have also been occasionally reported.^{1,3,7,10–13} Additionally, pronounced brain atrophy was observed in 2 patients during a 5- to 7-year follow-up.¹⁴ However, dedicated MR imaging research that focuses on lesion characteristics, especially in Chinese anti-NMDA receptor encephalitis, is lacking, and the associations between the MR imaging characteristics and clinical outcomes remain unknown.

In this study, we systematically investigated the MR imaging features, including lesion location, and the visual rating scale of medial temporal lobe atrophy (MTA)^{15,16} of patients with Chinese anti-NMDA receptor encephalitis and correlated the findings with clinical outcomes as measured by the modified Rankin Scale¹⁷ at a 2-year follow-up.

MATERIALS AND METHODS

Standard Protocol Approvals, Registrations, and Patient Consents

The institutional review board of Xuanwu Hospital approved the study, and written informed consent was obtained from each participant before participation.

Subjects

We consecutively enrolled 54 patients in Xuanwu Hospital, Capital Medical University, Beijing, China, from January 2012 to February 2015; one was excluded because of mortality due to cerebrovascular disease. All patients who tested positive for anti-NMDA receptor antibodies were diagnosed with anti-NMDA receptor encephalitis and showed typical clinical presentations, the usual course of symptom development,^{2,4,18,19} as well as CSF and serum that was positive for the associated antibody in tests from 2 independent labs (Tongren Hospital, Capital Medical University, and Peking Union Medical College Hospital in China). Positive antibodies of anti-NMDA receptor in the serum and/or CSF samples were defined according to previously reported criteria,^{2,9,20} including a characteristic pattern of immunostaining of neuropils in the rat brain and specific reactivity with HEK293 cells that express both the NR1 (also named GluN1) and NR2B (also named GluN2B) subunits of the NMDA receptor.

The clinical features were recorded by an experienced neurologist (J.Y., with more than 20 years of experience in neurology). According to the reported manifestations of this disease in previous publications,^{7,9} the symptoms were divided into 4 main groups¹: seizures²; psychiatric and behavioral features³; movement disorders, such as orolingual-facial dyskinesia and uncontrolled motion of the arms and legs⁴; and other symptoms, such as memory deficits, autonomic symptoms (including salivation, urine and/or feces incontinence), central hypoventilation, hemiparesis, and abnormal heart rate. Additionally, the patients were classified into a pediatric group (younger than 18 years of age) or an adult group (18 years of age and older) depending on age.

Brain MR Imaging Acquisition

Brain MRIs were acquired at a mean time interval of 36 ± 15 days (range, 20–90 days) after the presentation onset using a Magnetom Tim Trio or Verio 3T scanner (Siemens, Erlangen, Germany) with an 8-channel phased array head coil in the Department of Radiology, Xuanwu Hospital, Capital Medical University. We obtained the following sequences: axial T2-weighted images (slice = 20, slice thickness = 5.0 mm, TR/TE = 4040/84 ms, flip angle = 160°, FOV = 240 mm), axial T1-weighted images (slice = 20, slice thickness = 5.0 mm, TR/TE = 135/2.55 ms, flip angle = 50°, FOV = 240 mm), coronal T1-weighted images (slice = 20, slice thickness = 5.0 mm, TR/TE = 162/3.09 ms, flip angle = 50°, FOV = 240 mm), and fluid-attenuated inversion recovery images (slice = 20, slice thickness = 5.0 mm, TR/TE = 8500/87 ms, flip angle = 150°, FOV = 230 mm). We defined abnormal brain MR imaging findings as hyperintensity on T2WI and FLAIR and hypointensity on T1WI; we classified abnormalities as hippocampal when hyperintensity or/and volume loss was found in the hippocampus.

Two experienced neuroradiologists (Y.L. and Y.D., both with >10 years of experience) assessed brain MR imaging manifestations, which were categorized into 4 types according to the previous reports⁸ after distinguishing constructed defects—type 1: normal MR imaging findings; type 2: only hippocampal lesions; type 3: lesions not involving the hippocampus; and type 4: lesions in both the hippocampus and other brain areas. Additionally, we measured medial temporal lobe atrophy (Y.L. and Y.D.) by visual assessment on both sides of the brain and used the following 2 categories: normal (MTA = 0–1) and abnormal (MTA \geq 2). After 3 months, all the images were re-evaluated for MTA scores by the 2 raters. The interrater reproducibility was 98% and 96% at the 2 time points of evaluation; the intrarater reproducibility between the 2 raters was 96% and 94%, respectively.

Clinical Outcome Measurement

All 53 patients completed the 2-year follow-up. We used the modified Rankin Scale to define the clinical outcome (good [mRS = 0–1, recovered well] and poor [mRS = 2–5, residual disability])¹⁷ after immunotherapy treatment according to 2 experienced neurologists (J.Y. and W.X., one with more than 20 years of experience and one with 5 years of experience in neurology).

Statistical Analysis

Demographic variables including age (pediatric versus adult), sex, and clinical features were analyzed among the groups using the χ^2 test. The relationship between baseline MR imaging characteristics and 2-year follow-up mRS scores was evaluated using partial correlation, with age, sex, and time interval (interval between the onset of presentation and MR imaging acquisition) as covariates. We assessed factors that may affect the prognosis by univariate and multivariate binary logistic regression (poor outcome defined as mRS = 2–5), using therapy method (surgery and immunotherapy), intensive care unit (ICU) admission, whether there was a relapse, and hippocampal involvement as factors and using age, sex, and time interval (interval between onset of presentation and MR imaging ac-

Table 1: Clinical and MRI features of all 53 patients

	Pediatric (No.)	Adult (No.)	P Value
Sex (female/male)	10:7	18:18	.548
Age (range) (median) (yr)	17 (11–17) (15)	36 (18–60) (32)	–
Symptoms			
Behavioral and psychiatric features	11	33	.015
Seizure	10	26	.329
Autonomic symptoms	3	18	.025
Others	13	29	.732
Normal/abnormal brain MRI findings	9/8	19/17	.991
With/without hippocampal involvement	6/11	12/24	.888
Brain MRI types			
Type 1	9	19	–
Type 2	2	5	–
Type 3	2	5	–
Type 4	4	7	–
With/without tumor	1/16	4/32	.543
Treatment			.088
First-line alone	14	32	–
First-line and second-line	3	1	–
Symptomatic treatment	0	3	–
With/without relapse	5/12	5/31	.178
MTA			
Normal findings (MTA = 0–1)	14	31	.721
One side/both sides (MTA ≥ 2)	3	5	
mRS			
0–1	9	23	.447
≥2	8	13	

quisition) as covariates. Statistical analyses were performed using SPSS 23 (IBM, Armonk, New York). The probability map was calculated with SPM8 (<http://www.fil.ion.ucl.ac.uk/spm/software/spm12>) after drawing the ROI.

RESULTS

Demographic and Clinical Characteristics

In the final analysis, 53 patients with positive antibody titers and definitively diagnosed with anti-NMDA receptor encephalitis were enrolled and completed the 2-year follow-up. For the antibody, the subtype of antibody and how the type of antibody impacts clinical presentation and brain MR imaging warrant exploration in further studies. Twenty-five male patients (age range, 11–47 years; median age, 26.6 years) and 28 female patients (age range, 12–60 years; median age, 26.2 years) were included. Seventeen patients (32%) were pediatric patients, and 36 (68%) were adult patients. Five female patients (9%, 4 adults and 1 child) had an underlying neoplasm, and the tumors were pathologically confirmed as ovarian teratomas.

Within the first month of symptom onset, we categorized the symptoms into 4 main groups, and behavioral and psychiatric features (44/53, 83%) represented the most common symptoms. Seizure was the second most common symptom (36/53, 68%). Movement disorders (37/53), memory deficits (10/53), central hypoventilation (9/53), autonomic symptoms (21/53), and other symptoms (13/53) were also observed. The occurrence of behavioral and psychiatric features and autonomic symptoms were different between the 2 age groups (adult: 33/36, 92%, versus pediatric: 11/17, 65%, $P = .015$; and pediatric: 3/17, 18%, versus adult: 18/36, 50%, $P = .025$, respectively) (Table 1).

In total, 94% of patients (50/53) were treated with immunotherapy (steroids and/or intravenous immunoglobulins or ritux-

imab) and 5 patients underwent tumor removal. Three patients received symptomatic treatment only, such as antiepileptic drugs and antipsychotic drugs. Ten patients (19%) experienced a clinical relapse, which was defined as new-onset or worsening symptoms after 2 months of treatment.⁷ During the 2-year follow-up, 21/53 (40%) patients had residual disability (mRS = 2–5) and 32 (60%) patients recovered well (mRS = 0–1) (Table 1).

Brain MR Imaging Features

Twenty-eight (28/53, 53%) patients with anti-NMDA receptor encephalitis had normal MR imaging (type 1) results at the onset phase, and 25 patients (25/53; 47%) presented with abnormal MR imaging results—type 2: seven patients (7/25, 28%) with lesions in the hippocampus only; type 3: seven patients with lesions in the frontal lobe ($n = 3$); cingulate gyrus and middle cerebellar peduncle ($n = 2$); and corpus callosum, insula, basal ganglia, thalamus, and

brain stem ($n = 1$), without hippocampal lesions; and type 4: 11 patients (11/25, 44%) with lesions in both the hippocampus and other brain areas, including the frontal lobe and temporal lobes ($n = 8$); parietal lobe ($n = 5$); thalamus ($n = 3$); basal ganglia, cingulate gyrus, and brain stem ($n = 2$); and insula, occipital lobe, corpus callosum, and internal capsule ($n = 1$). One patient had only limbic lesions among 18 patients in types 3 and 4. The sample images of the 4 MR imaging types are shown in Fig 1, and the lesion probability map is shown in Fig 2. Normal brain MR imaging results were observed more frequently in female patients (19 of 28, 68%) than in male patients (9 of 25, 36%) ($P = .020$). No difference was observed in brain MR imaging manifestations between age groups (pediatric versus adult groups) ($P = .982$).

Forty-five patients had a normal MTA score (MTA = 0–1) on both sides of the brain, 2 patients showed atrophy (MTA ≥ 2) on both sides, and 6 patients showed atrophy in only 1 side: on the right side in 2 patients (median MTA score = 2) and on the left side in 4 patients (median MTA score = 2).

Association between MR Imaging Characteristics and Clinical Outcome

The patients with hippocampal lesions had higher mRS scores than those without hippocampal lesions after taking age, sex, and time interval as covariates ($P = .032$). Partial correlation analyses showed that the MTA score of the left side was correlated with the mRS score at 2-year follow-up ($r = 0.319$, $P = .020$). In univariate and multivariate logistic regression, both relapse ($P = .040$ versus $P = .043$) and involvement of the hippocampus ($P = .025$ versus $P = .008$) were associated with clinical outcome. Additionally, hippocampal involvement ($P = .008$; OR = 9.584; 95% CI, 1.803–50.931) had a stronger association with clinical outcome than

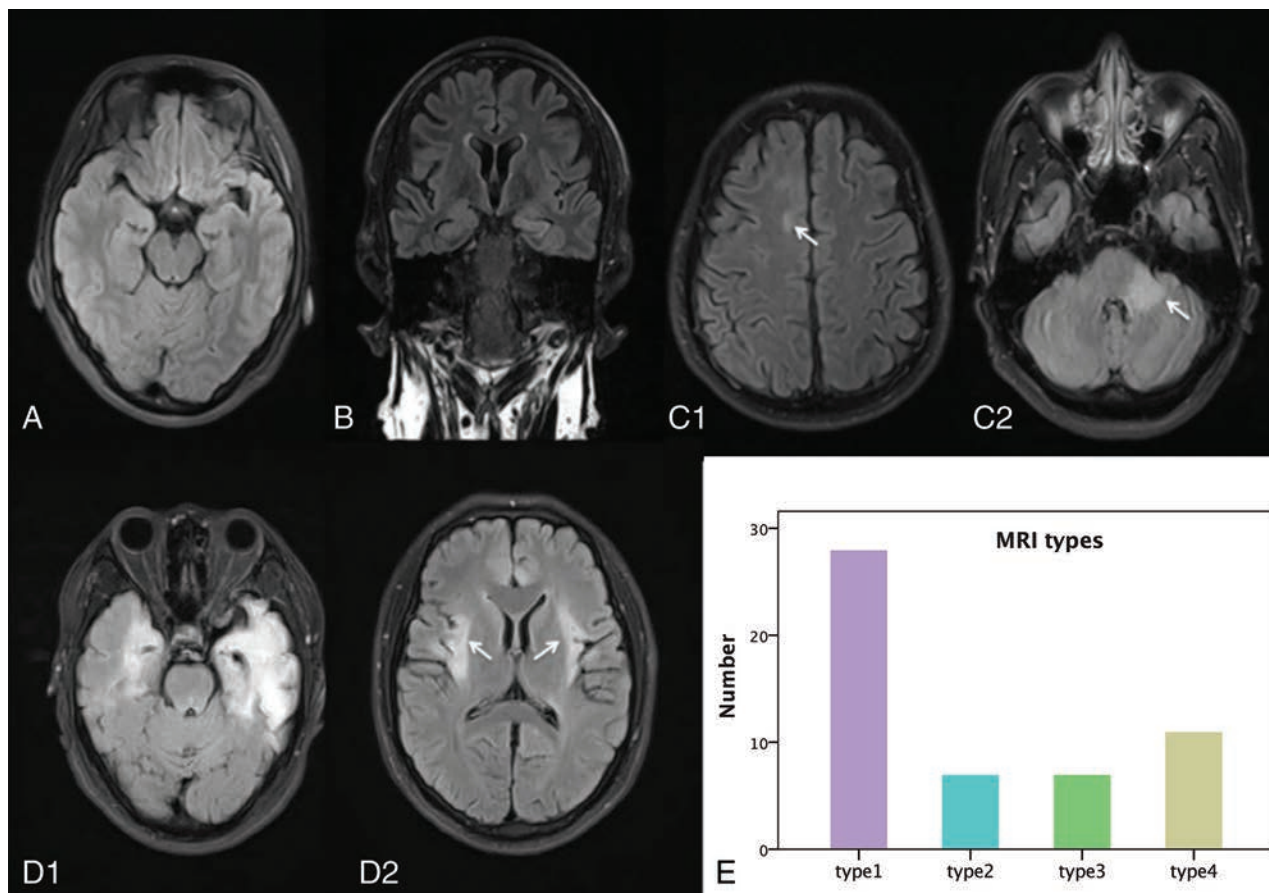


FIG 1. Four types of brain MR imaging appearances in patients with anti-NMDA receptor encephalitis, and the histogram of the 4 types of brain MR imaging appearance. Axial (A, C, and D) and coronal FLAIR images (B) come from 4 patients (C1 and C2 from same patient, D1 and D2 from same patient). A, Type 1, a 23-year-old male patient with anti-NMDA receptor encephalitis, with normal brain MR imaging findings. B, Type 2, a 29-year-old female patient. Lesions are in the left hippocampus with bilateral mild volume loss in the hippocampus. C, Type 3, a 28-year-old male patient. Lesions are in the right frontal lobe (white arrow) and middle cerebellar peduncle (white arrow) and brain stem. D, Type 4, a 25-year-old male patient, with lesions located in the bilateral frontal lobe, temporal lobe, insula (white arrows), hippocampus, and cingulate gyrus, with volume loss in the left hippocampus. E, Histogram of the 4 types of brain MR imaging appearances.

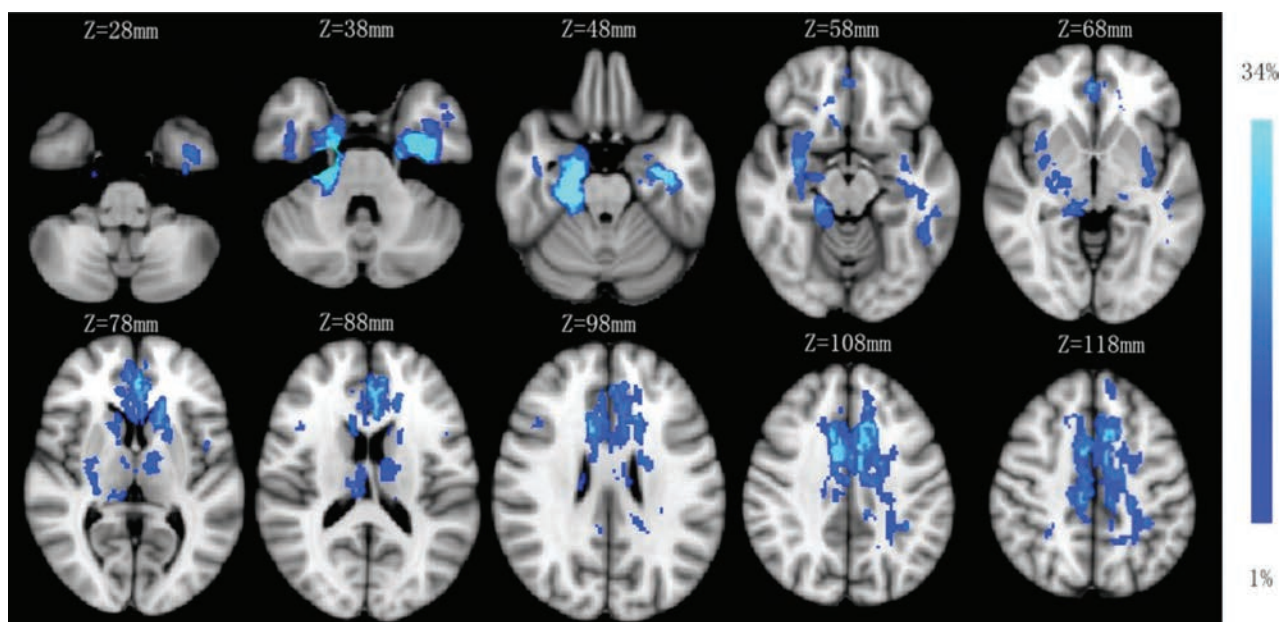


FIG 2. Lesion probability map of brain MR imaging. The mean lesion probability distribution thresholded at 34% is shown in light blue and thresholded at 1% is shown in blue and overlaid on the ICBM152 T1 template in the Montreal Neurological Institute space.

Table 2: Factors associated with poor prognosis (mRS \geq 2)

	P Value	Odds Ratio (95% CI)
Univariate analysis ^a		
Hippocampal involvement	.025	3.929 (1.185–13.021)
Relapse	.040	0.316 (0.060–1.665)
Treatment	.753	1.389 (0.180–10.735)
Admitted to ICU	.352	0.500 (0.116–2.155)
Teratoma	.999	—
Multivariate analysis ^{a,b}		
Hippocampal involvement ^c	.008	9.584 (1.803–50.931)
Relapse	.043	0.111 (0.013–0.930)
Treatment	.753	1.389 (0.180–10.735)
Admitted to ICU	.592	0.636 (0.121–3.334)

^a Using binary logistic regression.

^b Analyzed using the therapy method (operation and immunotherapy), ICU admission, and whether there was relapse and hippocampal involvement as factors and age, sex, and time interval (interval between onset of presentation and MRI acquisition) as covariates.

^c Hippocampal involvement including both types 2 and 4.

relapse ($P = .043$; OR = 0.111; 95% CI, 0.013–0.930). No correlation was observed between clinical outcome and intensive care unit admission, treatment, or teratoma (Table 2).

DISCUSSION

In this study, we demonstrated the MR imaging features of patients with Chinese anti-NMDA receptor encephalitis and their associations with clinical outcomes: 1) We categorized the brain MR imaging of anti-NMDA receptor encephalitis into 4 types and normal brain MR imaging acquisition findings accounted for >50% of cases. Normal brain MR imaging results were observed more frequently in female patients than in male patients. 2) Hippocampal lesions were the most common brain abnormality, and 3) hippocampal lesions and relapse were risk factors that contributed to a poor prognosis.

For demographic and clinical characteristics, the age distribution (range, 11–60 years; mean age, 26.4 years) in our study is similar to that in previous anti-NMDA receptor encephalitis studies,^{7,20,21} but the proportion of male patients is higher (47%) compared with previous studies.^{2,3,7,8} This divergence of sex differences between Chinese and Western patients may be due to racial differences or the relatively small sample size in our study. Therefore, future studies with larger samples are required to compare the demographic features between Chinese and Western patients. The clinical pattern and evolution are similar between adult and pediatric patients.^{22,23} For clinical symptoms, behavioral and psychiatric features were observed in the largest proportion of patients and are the main causes for admission to the hospital. Behavioral and psychiatric features and autonomic symptoms appeared in adults more frequently than in pediatric patients, which is consistent with previous research.³ Clinical relapse appeared in 10 patients (19%), which is similar to the 12%–24% frequency of neurologic relapse observed in previous studies.^{7,8,24}

Normal and abnormal brain MR imaging results were observed in 28 and 25 patients with the anti-NMDA receptor encephalitis, respectively; this finding is consistent with those in previous publications.^{1,2,11} In female patients, normal brain MR imaging findings were encountered more often than male patients, implying the different lesion patterns between sexes. Fur-

ther studies with advanced MR imaging techniques such as diffusion imaging and functional MR imaging should be conducted in the patients with normal routine brain MR imaging findings to reveal the microstructural and functional changes.²⁵ In patients with abnormal brain MR imaging findings, lesions can occur in various locations such as the hippocampus, thalamus, basal ganglia, brain stem, insula, and frontal, temporal, and parietal lobes; and white matter lesions can occur in the corpus callosum, a finding reported by other studies.^{1,3,10–13} In the current study, to simplify the brain MR imaging patterns and characteristics, we classified brain MR imaging appearance into 4 types: type 1 (normal), type 2 (only hippocampal lesion), type 3 (lesions in other brain areas), and type 4 (hippocampal lesion and lesions in other areas). In these 3 abnormal types, type 4 was the most common pattern (21%), implying that lesions in other locations often occur together with hippocampal lesions in patients with anti-NMDA receptor encephalitis.

The hippocampus was the most common lesion site in patients with Chinese anti-NMDA receptor encephalitis, which was observed in approximately one-third of the patients. Previous studies have shown that structural hippocampal damage represented the target change in patients with anti-NMDA receptor encephalitis,^{25,26} which was significantly related to memory deficits and disease severity. Additionally, lesions located in the frontal and temporal lobes were present in approximately 15% of patients (21% and 15%), suggesting that the frontal and temporal lobes were the second most common lesion site after the hippocampus.

Medial temporal lobe atrophy as measured by MTA was observed in 8 patients (15%) on at least 1 side, indicating that structural damage in the hippocampus was relatively common. MTA of the left side was correlated with the mRS; this finding is consistent with that in a previous study showing that left hippocampal volume could predict disease severity.²⁶ The findings suggest MTA as a valuable biomarker for predicting disease severity.

Poor prognosis was correlated with clinical relapse and hippocampal lesions in the present study, and hippocampal involvement had a stronger association with clinical outcome than relapse. Admission to an ICU, the method of treatment, and teratoma had no relationship with the clinical outcome. In several previous studies, some other factors were reported to be associated with clinical outcomes, including lack of a need for admission to an intensive care unit, low severity of the disease within 4 weeks,⁷ and a low titer of serum and CSF NMDA receptor antibodies,^{8,9,27} which were not identified in our study. The discordance between our study and some previous studies was due to the small number of patients, the different definitions of good prognosis,⁷ or the lack of an early mRS assessment.

Limitations

Our study has some limitations. First, the sample size was relatively small, and the significance and reliability of the results need to be improved by enrolling more subjects. Additionally, the data were obtained from a single center. Further studies should focus on multicenter samples to verify the results. Second, brain MR imaging was conducted only at the onset phase, so the MR imaging changes of this disease at different phases or changes with

other auxiliary examinations are not clear. In this study, only routine sequences with slice thicknesses of 5 mm on brain MR imaging were obtained, on which it is difficult to detect small lesions and accurately measure the brain and hippocampal volumes. For MTA score assessment, only 79% of the patients had coronal images. A comprehensive scan and advanced MR imaging techniques with high resolution such as functional MR imaging should be conducted in these patients.²⁸ Third, the assessment of clinical outcome in this study included only mRS scores at the 2-year follow-up. A more systematic assessment²⁹ should be performed in a future study.

CONCLUSIONS

In patients with Chinese anti-NMDA receptor encephalitis, half had normal brain MR imaging findings, and normal brain MRI findings were more common in female patients. Psychiatric and behavioral abnormalities were more common in adults, and autonomic symptoms were more common in pediatric patients. Hippocampal lesions were the most common MR imaging abnormal finding. The presence of hippocampal lesions and relapse were major factors in the prediction of a poor prognosis.

ACKNOWLEDGMENTS

The authors thank Dr Kristofer Wood from Barrow Neurological Institute for language revision and Kun Yang from Xuanwu Hospital, Capital Medical University, for statistics review. The authors also thank the patients in this study and members of Neuroimmunology Team and staff of the Department of Radiology for various kinds of support, especially Drs Jing Huang and Zhuoqing Ren.

REFERENCES

1. Dalmau J, Erdem T, Wu H-y, et al. **Paraneoplastic anti-N-methyl-D-aspartate receptor encephalitis associated with ovarian teratoma.** *Ann Neurol* 2007;61:25–36 CrossRef
2. Dalmau J, Lancaster E, Martinez-Hernandez E, et al. **Clinical experience and laboratory investigations in patients with anti-NMDAR encephalitis.** *Lancet Neurol* 2011;10:63–74 CrossRef Medline
3. Viacoz A, Desestret V, Ducray F, et al. **Clinical specificities of adult male patients with NMDA receptor antibodies encephalitis.** *Neurology* 2014;82:556–63 CrossRef Medline
4. Jones KC, Benseler SM, Moharir M. **Anti-NMDA receptor encephalitis.** *Neuroimaging Clin N Am* 2013;23:309–20 CrossRef Medline
5. Finke C, Kopp UA, Prüss H, et al. **Cognitive deficits following anti-NMDA receptor encephalitis.** *J Neurol Neurosurg Psychiatry* 2012;83:195–98 CrossRef Medline
6. Gultekin SH, Rosenfeld MR, Voltz R, et al. **Paraneoplastic limbic encephalitis: neurological symptoms, immunological findings and tumour association in 50 patients.** *Brain* 2000;123:1481–94 CrossRef Medline
7. Titulaer MJ, McCracken L, Gabilondo I, et al. **Treatment and prognostic factors for long-term outcome in patients with anti-NMDA receptor encephalitis: an observational cohort study.** *Lancet Neurol* 2013;12:157–65 CrossRef Medline
8. Irani SR, Bera K, Waters P, et al. **N-methyl-D-aspartate antibody encephalitis: temporal progression of clinical and paraclinical observations in a predominantly non-paraneoplastic disorder of both sexes.** *Brain* 2010;133:1655–67 CrossRef Medline
9. Dalmau J, Gleichman AJ, Hughes EG, et al. **Anti-NMDA-receptor encephalitis: case series and analysis of the effects of antibodies.** *Lancet Neurol* 2008;7:1091–98 CrossRef Medline

10. Greiner H, Leach JL, Lee KH, et al. **Anti-NMDA receptor encephalitis presenting with imaging findings and clinical features mimicking Rasmussen syndrome.** *Seizure* 2011;20:266–70 CrossRef Medline
11. Günther A, Brodoehl S, Witte OW, et al. **Atypical posthypoxic MRI changes in hypermetabolic regions in anti-NMDA-receptor encephalitis.** *Neurology* 2012;79:720–21 CrossRef Medline
12. Hoffmann LA, Jarius S, Pellkofer HL, et al. **Anti-Ma and anti-Ta associated paraneoplastic neurological syndromes: 22 newly diagnosed patients and review of previous cases.** *J Neurol Neurosurg Psychiatry* 2008;79:767–73 CrossRef
13. Haberlandt E, Bast T, Ebner A, et al. **Limbic encephalitis in children and adolescents.** *Arch Dis Child* 2011;96:186–91 CrossRef Medline
14. Iizuka T, Yoshii S, Kan S, et al. **Reversible brain atrophy in anti-NMDA receptor encephalitis: a long-term observational study.** *J Neurol* 2010;257:1686–91 CrossRef Medline
15. Wahlund LO, Julin P, Johansson SE, et al. **Visual rating and volumetry of the medial temporal lobe on magnetic resonance imaging in dementia: a comparative study.** *J Neurol Neurosurg Psychiatry* 2000;69:630–35 CrossRef Medline
16. Bresciani L, Rossi R, Testa C, et al. **Visual assessment of medial temporal atrophy on MR films in Alzheimer's disease: comparison with volumetry.** *Aging Clin Exp Res* 2005;17:8–13 CrossRef Medline
17. van Swieten JC, Koudstaal PJ, Visser MC, et al. **Interobserver agreement for the assessment of handicap in stroke patients.** *Stroke* 1988;19:604–07 CrossRef Medline
18. Peery HE, Day GS, Dunn S, et al. **Anti-NMDA receptor encephalitis: the disorder, the diagnosis and the immunobiology.** *Autoimmun Rev* 2012;11:863–72 CrossRef Medline
19. Maneta E, Garcia G. **Psychiatric manifestations of anti-NMDA receptor encephalitis: neurobiological underpinnings and differential diagnostic implications.** *Psychosomatics* 2014;55:37–44 CrossRef Medline
20. Sansing LH, Tüzün E, Ko MW, et al. **A patient with encephalitis associated with NMDA receptor antibodies.** *Nat Clin Pract Neurol* 2007;3:291–96 CrossRef Medline
21. Parratt KL, Allan M, Lewis SJ, et al. **Acute psychiatric illness in a young woman: an unusual form of encephalitis.** *Med J Aust* 2009;191:284–86 Medline
22. Florance NR, Davis RL, Lam C, et al. **Anti-N-methyl-D-aspartate receptor (NMDAR) encephalitis in children and adolescents.** *Ann Neurol* 2009;66:11–18 CrossRef Medline
23. Lin JJ, Lin KL, Hsia SH, et al; Children with Encephalitis and/or Encephalopathy Related Status Epilepticus and Epilepsy (CHEESE) Study Group. **Anti-N-methyl-D-aspartate receptor encephalitis in Taiwan: a comparison between children and adults.** *Pediatr Neurol* 2014;50:574–80 CrossRef Medline
24. Gabilondo I, Saiz A, Galán L, et al. **Analysis of relapses in anti-NMDAR encephalitis.** *Neurology* 2011;77:996–99 CrossRef Medline
25. Finke C, Kopp UA, Scheel M, et al. **Functional and structural brain changes in anti-N-methyl-D-aspartate receptor encephalitis.** *Ann Neurol* 2013;74:284–96 CrossRef Medline
26. Finke C, Kopp UA, Pajkert A, et al. **Structural hippocampal damage following anti-N-methyl-D-aspartate receptor encephalitis.** *Biol Psychiatry* 2016;79:727–34 CrossRef Medline
27. Gresa-Arribas N, Titulaer MJ, Torrents A, et al. **Antibody titres at diagnosis and during follow-up of anti-NMDA receptor encephalitis: a retrospective study.** *Lancet Neurol* 2014;13:167–77 CrossRef Medline
28. Baumgartner A, Rauer S, Mader I, et al. **Cerebral FDG-PET and MRI findings in autoimmune limbic encephalitis: correlation with auto-antibody types.** *J Neurol* 2013;260:2744–53 CrossRef Medline
29. Peer M, Prüss H, Ben-Dayán I, et al. **Functional connectivity of large-scale brain networks in patients with anti-NMDA receptor encephalitis: an observational study.** *Lancet Psychiatry* 2017;4:768–74 CrossRef Medline

Fast and Robust Unsupervised Identification of MS Lesion Change Using the Statistical Detection of Changes Algorithm

T.D. Nguyen, S. Zhang, A. Gupta, Y. Zhao, S.A. Gauthier, and Y. Wang



ABSTRACT

SUMMARY: We developed a robust automated algorithm called statistical detection of changes for detecting morphologic changes of multiple sclerosis lesions between 2 T2-weighted FLAIR brain images. Results from 30 patients showed that statistical detection of changes achieved significantly higher sensitivity and specificity (0.964, 95% CI, 0.823–0.994; 0.691, 95% CI, 0.612–0.761) than with the lesion-prediction algorithm (0.614, 95% CI, 0.410–0.784; 0.281, 95% CI, 0.228–0.314), while resulting in a 49% reduction in human review time ($P = .007$).

ABBREVIATIONS: LPA = lesion prediction algorithm; SDC = statistical detection of changes

Patients with multiple sclerosis undergo regular MRIs to monitor disease activity and therapeutic response.¹ Volumetric brain MR imaging protocols with 1-mm³ isotropic resolution have become increasingly common for imaging patients with MS but result in hundreds of images, making detection of new lesions or changes in lesion morphology very time-consuming for radiologists. One approach to overcoming this problem is to extract lesion masks with a lesion-segmentation algorithm²; these masks are subtracted to yield a lesion-change mask. Alternatively, lesion change can be detected on the subtraction of 2 images either by humans³ or with the help of an algorithm relying on the subtraction signal and lesion geometry.⁴ While image subtraction can substantially improve lesion contrast, separating lesion change from background noise requires consideration of the statistical properties of the signal and noise.

Here we propose a rapid and robust algorithm for statistical detection of changes (SDC) in WM lesions. We describe a specific SDC implementation using the Neyman-Pearson detector in sta-

tistics to optimally detect lesion change according to the MR imaging signal-to-noise property.

MATERIALS AND METHODS

SDC Lesion-Detection Algorithm

Given 2 MR images I_1 and I_2 of the same brain acquired at 2 time points, the voxel-subtraction signal $d = I_2 - I_1$ (Fig 1) is assumed to follow a Gaussian distribution $N(\mu, \sigma^2)$ with mean μ and SD σ , in which σ can be estimated from the set of nonlesion WM voxels on the subtraction image. Most of these voxels belong to the intersection of the 2 WM masks obtained by brain segmentation tools (such as FSL; <http://www.fmrib.ox.ac.uk/fsl>) from T1-weighted structural images. These masks typically exclude large lesions that are hypointense on T1WI and therefore consist mainly of nonlesion voxels (On-line Fig 1).

The MR imaging signal-to-noise property can be used to formulate an optimal SDC of lesions as a composite statistical test between 2 hypotheses of the following likelihood functions:

$$H_0 \text{ (voxel is "unchanged")}: p(d | H_0) = N(0, \sigma^2),$$

$$H_1 \text{ (voxel is "changed")}: p(d | H_1) = N(\mu, \sigma^2), \mu \neq 0.$$

In this work, the SDC test statistic was computed over a 3-voxel connected neighborhood based on the currently accepted minimum MS lesion size requirement of 3 mm (3 voxels in 1-mm³ isotropic images)⁶ and on the assumption that the subtraction signals within this small neighborhood are similar. Denoting the subtraction signals at the i -th voxel and its neighbor voxels as d_{i1}, \dots, d_{i3} and assuming $\mu > 0$ (positive change), the test statistic t_i can be computed from the log-likelihood ratio test⁷ and compared with a threshold γ to make a decision:

Received November 21, 2017; accepted after revision January 20, 2018.

From the Department of Radiology (T.D.N., S.Z., A.G., Y.W.), Feil Family Brain and Mind Research Institute (A.G., S.A.G.), and Departments of Healthcare Policy and Research (Y.Z.) and Neurology (S.A.G.), Weill Cornell Medicine, New York, New York.

This work was supported by research grants from the National Institutes of Health (R01 NS090464) and the National MS Society (RG-1602-07671).

Please address correspondence to Thanh D. Nguyen, PhD, 515 East 71st St, Suite S-106, New York, NY 10021, e-mail: tdn2001@med.cornell.edu

Indicates open access to non-subscribers at www.ajnr.org

Indicates article with supplemental on-line photos.

<http://dx.doi.org/10.3174/ajnr.A5594>

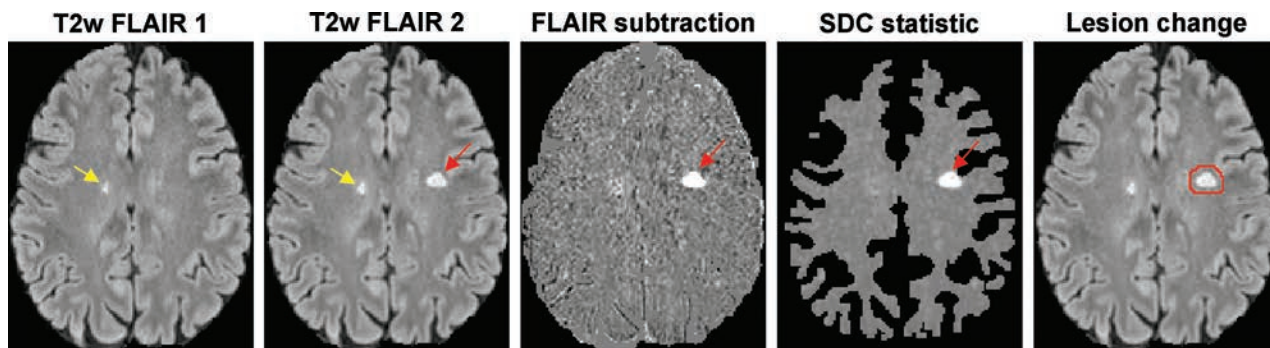


FIG 1. Schematic of the proposed SDC lesion-change detection algorithm on the T2-weighted FLAIR subtraction image. One unchanged lesion (yellow arrow) and 1 new lesion (red arrow) are correctly identified by the SDC. The algorithm automatically generates red ROIs, which encompass the detected areas of change on the second FLAIR image to help the human reader quickly identify lesion changes.

$$1) \quad t_i = \sum_{j=1}^3 d_{ij} \geq \frac{H_1}{H_0} \gamma.$$

Here γ was chosen to control the false-positive rate $P_{FP} = P(t_i > \gamma | H_0)$. According to the Neyman-Pearson lemma, this test provides the best detection power for a given P_{FP} regardless of the unknown mean μ (uniformly most powerful detector).⁷

The test statistic is maximized over all possible neighborhoods surrounding the voxel, to increase the sensitivity of lesion detection:

$$2) \quad t_i = \max(t_{ik}, k \in V_i),$$

where V_i denotes a 3-voxel connected neighborhood system of the i -th voxel (On-line Fig 2). Intuitively, this test statistic encodes in probabilistic terms the expectation that a bright voxel on the subtraction image is more likely to be identified as “changed” if at least 2 of its neighboring voxels also have high signals.

MR Imaging Experiment

This was a retrospective study of 30 patients with MS with 2 consecutive brain MRIs (mean scan interval, 267 ± 104 days; range, 15–410 days) performed on 3T scanners (Magnetom Skyra, VE11A software; Siemens, Erlangen, Germany). The imaging protocol consisted of an MPRAGE T1WI sequence for brain structure (TR/TE/TI = 2300/2.3/900 ms, 1 mm³ isotropic) and a T2WI FLAIR sequence for lesion detection (TR/TE/TI = 7600/446/2450 ms, 1 mm³ isotropic). After skull removal and bias field correction, FLAIR images were coregistered into the half-way space using the FMRIB Linear Image Registration Tool algorithm (FLIRT; <http://www.fmrib.ox.ac.uk/fsl/fslwiki/FLIRT>)⁵ to ensure that the degree of blurring introduced by coregistration was similar between images because this similarity improves subtraction. To account for changes in image contrast or dynamic range (eg, due to different receiver gain settings or slight changes in imaging parameters), we performed image-intensity normalization before subtraction. The robust intensity range (second and 98th percentiles, denoted as m and M , respectively) was computed for each image. The image intensity of the second image I_2 was then scaled linearly to match that of the first image I_1 as follows: $I_{2, \text{scaled}} = \alpha I_2 + \beta$, where $\alpha = (M_1 - m_1) / (M_2 - m_2)$ and $\beta = [(M_1 - \alpha M_2) + (m_1 - \alpha m_2)] / 2$. In addition, brain GM, WM, and CSF masks were obtained from the T1WI using the FMRIB Automated Segmentation Tool (FAST; <https://fsl.fmrib.ox.ac.uk/fsl/fslwiki/>

FAST) algorithm.⁵ The SDC test statistic (Equations 1 and 2) was then computed and thresholded to generate a change mask (Fig 1). The false-positive rate P_{FP} was set to 0.0001, which means that, on average, 50 of approximately 500,000 WM voxels may be incorrectly labeled as “changed.” To reduce the number of false-positives, we imposed additional constraints on lesion size (≥ 3 voxels), location (lesions located within 2 voxels of the CSF border had to be part of a larger lesion that extended outside this border), and intensity on the second FLAIR image (> 2 SDs above the mean normal-appearing WM intensity, ie, WM voxels that do not appear bright on FLAIR were excluded).

For comparison, the lesion prediction algorithm (LPA), part of the Lesion Segmentation Tool toolbox (LST; <http://www.applied-statistics.de/lst.html>),⁸ was used to compute the lesion masks from FLAIR images. This algorithm consists of a binary classifier in the form of a logistic regression model trained on the data of 53 patients with MS.⁸ The lesion masks were then subtracted to obtain the change mask without any human revision. Like the SDC, lesion changes of < 3 voxels were excluded.

Statistical Analysis

A neuroradiologist with 6 years of experience reviewed the 2 FLAIR and the subtraction images with the help of computer-generated color ROIs that encompassed the detected lesion changes (Fig 2). These were labeled as “true-positive” or “false-positive.” The reader also reviewed the images outside these ROIs to count the number of missed (false-negative) and unchanged (true-negative) lesions. Lesion changes detected by the SDC and LPA were presented in randomized order (both by subject and by detection algorithm) to the reader, who was blinded to the algorithm. The image review time was recorded for each subject and algorithm. A 2-tailed paired-sample t test was used to compare the mean review time per subject of SDC and LPA. The sensitivity and specificity of each method were calculated using the generalized estimating equation logistic regression, which accounts for the correlation among the measurements within the same subject.⁹

RESULTS

Figure 2 shows an example of lesion detection, in which the LPA generated more false-positives than the SDC and missed a small

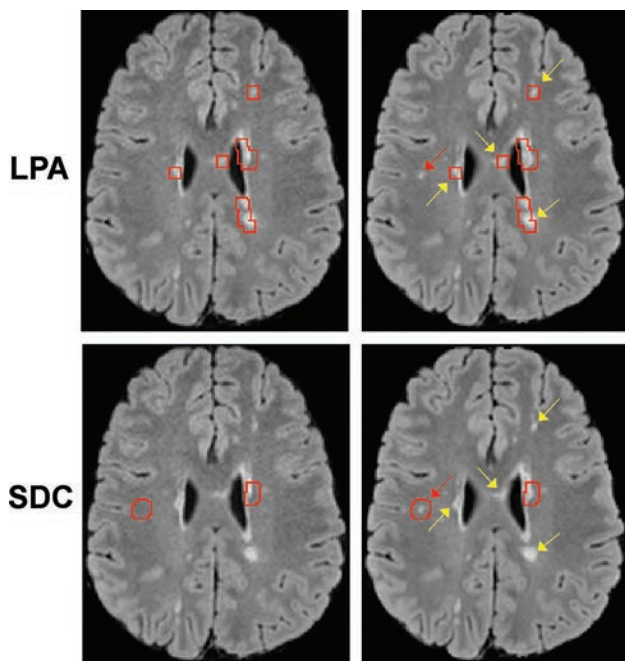


FIG 2. Comparison of lesion changes identified by the LPA and SDC (indicated by the red ROIs generated by the algorithms and superimposed on the T2 source FLAIR images). Each column shows images acquired at a different time points. The LPA identifies more false-positives (yellow arrows) yet misses a new small lesion (red arrow). The SDC correctly classifies positive lesion changes in concordance with the human expert.

new lesion (On-line Fig 3). In 30 subjects, the SDC detected 344 lesion changes, or an average of 11 ± 7 per subject (range, 4–33), while the LPA detected 1506 changes, or an average of 50 ± 38 per subject (range, 5–152). This result led to a 49% reduction in human review time per case (116 ± 44 seconds; range, 50–182 seconds, by SDC versus 229 ± 122 seconds; range, 76–447 seconds, by LPA, $P = .007$). Despite fewer detected changes and decreased review time, the SDC missed only 2 new lesions compared with 34 missed lesions by the LPA. The false-positive rate was 0.241 and 0.735 for SDC and LPA, respectively. With the neuroradiologist's reading used as the reference standard, the SDC achieved both higher sensitivity (0.964; 95% CI, 0.823–0.994 by SDC, versus 0.614; 95% CI, 0.410–0.784 by LPA) and higher specificity (0.691; 95% CI, 0.612–0.761 by SDC, versus 0.281; 95% CI, 0.228–0.314 by LPA). Because the 95% CI for the SDC does not overlap that for the LPA regarding both sensitivity and specificity, we concluded that the difference between the 2 diagnostic methods is statistically significant. The Table summarizes the diagnostic accuracy of each algorithm for lesion-change detection.

DISCUSSION

Our data show that the proposed SDC algorithm based on the optimal Neyman-Pearson detector is a computer-assisted tool that can improve the MS lesion detection rate and decrease image-analysis time, thereby reducing the reader's fatigue. The improved robustness of the SDC can be attributed to its probabilistic approach, which uses the statistical properties of the FLAIR subtraction signal within a connected voxel neighborhood to derive an optimal detection threshold for change detection. Although only

Summary of diagnostic accuracy of the SDC and LPA algorithms for detecting positive lesion change (lesion growth) between 2 FLAIR images with side-by-side image review by a human reader as the reference standard

Predicted Lesion Status	True Lesion Status by a Human Reader	
	Change	No Change
By SDC		
Change	83	261
No change	2	824
By LPA		
Change	52	1454
No change	34	524

positive change (lesion growth) was considered, detecting negative change (lesion shrinkage) can be performed by swapping the order of the FLAIR images. The algorithm was designed to be highly sensitive (0.964 sensitivity) for serving as a screening tool for new lesions while providing a reasonable specificity (only 1 of 3 unchanged lesions was misclassified, compared with 3 of 4 for the LPA). We also considered the longitudinal pipeline implemented in the LST toolbox⁸ and found that it has much lower sensitivity (0.386; 95% CI, 0.269–0.518) though higher specificity (0.994; 95% CI, 0.985–0.999) compared with the LPA mask-subtraction method and therefore is less suited for diagnostic purposes.

This initial feasibility study has several limitations. We have focused on WM lesions to circumvent the limited contrast of cortical or deep GM lesions on FLAIR. Further studies using pulse sequences tailored for GM lesion detection (eg, double inversion recovery at 7T) are warranted to evaluate the SDC for this lesion cohort. Because most subjects (18/30) were imaged at approximately 1-year intervals, it was not possible to assess statistically whether the accuracy of SDC and LPA varies with follow-up intervals. Comparison with other algorithms and further evaluation on the impact of image interpretation in larger patient imaging datasets are also needed, particularly in those with abrupt anatomic changes between scans, which can make image alignment difficult.

CONCLUSIONS

The SDC lesion change detection algorithm has higher sensitivity and specificity than the LPA algorithm.

Disclosures: Thanh D. Nguyen—RELATED: Grant: National Institutes of Health (R01NS090464), National MS Society.* Ajay Gupta—RELATED: Grant: National Institutes of Health (R01NS090464).* Susan A. Gauthier—UNRELATED: Grants/Grants Pending: Mallinckrodt, Genzyme, Novartis.* Yi Wang—RELATED: Grant: National Institutes of Health (R01NS090464), National MS Society. *Money paid to the institution.

REFERENCES

- Wattjes MP, Rovira À, Miller D, et al. Evidence-based guidelines: MAGNIMS consensus guidelines on the use of MRI in multiple sclerosis—establishing disease prognosis and monitoring patients. *Nat Rev Neurol* 2015;11:597–606 CrossRef Medline
- Carass A, Roy S, Jog A, et al. Longitudinal multiple sclerosis lesion segmentation: resource and challenge. *Neuroimage* 2017;148:77–102 CrossRef Medline
- van Heerden J, Rawlinson D, Zhang AM, et al. Improving multiple sclerosis plaque detection using a semiautomated assistive approach. *AJNR Am J Neuroradiol* 2015;36:1465–71 CrossRef Medline
- Battaglini M, Rossi F, Grove RA, et al. Automated identification of

- brain new lesions in multiple sclerosis using subtraction images.** *J Magn Reson Imaging* 2014;39:1543–49 [CrossRef Medline](#)
5. Jenkinson M, Beckmann CF, Behrens TE, et al. **FSL.** *Neuroimage* 2012; 62:782–90 [CrossRef Medline](#)
 6. Filippi M, Rocca MA, Ciccarelli O, et al; MAGNIMS Study Group. **MRI criteria for the diagnosis of multiple sclerosis: MAGNIMS consensus guidelines.** *Lancet Neurol* 2016;15:292–303 [CrossRef Medline](#)
 7. Kay SM. *Fundamentals of Statistical Signal Processing: Detection Theory.* Vol. II. Englewood Cliffs, NJ: Prentice Hall; 1998
 8. Schmidt P. *Bayesian Inference for Structured Additive Regression Models for Large-Scale Problems with Applications to Medical Imaging* [PhD thesis]. Munich: Ludwig-Maximilians-Universität München; 2017
 9. Fleiss JL, Levin B, Paik MC. *Statistical Methods for Rates and Proportions.* Hoboken: Wiley; 2003

Signal Change of Acute Cortical and Juxtacortical Microinfarction on Follow-Up MRI

M. Miyata, S. Kakeda, T. Yoneda, S. Ide, K. Watanabe, J. Moriya, and Y. Korogi

ABSTRACT

BACKGROUND AND PURPOSE: Although the clinical importance of cortical microinfarcts has become well-recognized recently, the evolution of cortical microinfarcts on MR imaging is not fully understood. The aim of this study was to examine the temporal changes in acute cortical microinfarcts using susceptibility-weighted imaging and conventional MR imaging.

MATERIALS AND METHODS: Patients with acute infarcts located in the cortical and/or juxtacortical region measuring ≤ 10 mm in axial diameter based on diffusion-weighted imaging who had a follow-up 3T MR imaging were retrospectively included in the study. All lesions did not show hypointensity on initial T2*WI. For cortical and/or juxtacortical microinfarcts detected on initial DWI, 2 neuroradiologists evaluated the follow-up MR imaging (T2WI, FLAIR, T2*WI, and SWI) and assessed lesion signal intensities and locations (cortical microinfarcts or microinfarcts with juxtacortical white matter involvement).

RESULTS: On initial DWI, 2 radiologists observed 180 cortical and/or juxtacortical microinfarcts in 35 MR imaging examinations in 25 patients; on follow-up, the neuroradiologists identified 29 cortical microinfarcts (16%) on T2WI, 9 (5%) on FLAIR, 4 (2%) on T2*, and 97 (54%) on SWI. All cortical microinfarcts detected with any follow-up MR imaging showed hyperintensity on T2WI/FLAIR and/or hypointensity on T2*WI and SWI.

CONCLUSIONS: SWI revealed conversion (paramagnetic susceptibility changes) of acute cortical microinfarcts, suggesting that a substantial number of cortical microinfarcts may contain hemorrhagic components.

ABBREVIATIONS: AD = Alzheimer disease; CJC = cortical and/or juxtacortical; CMI = cortical microinfarct; GRE = gradient recalled-echo

Accumulating evidence suggests that microinfarcts are a common neuropathologic finding in the aging brain.¹ The prevalence of microinfarcts in patients with probable Alzheimer disease (AD) or vascular dementia is even higher,^{2,3} with a weighted average of 43% in patients with AD.³ Postmortem data from the Adult Changes in Thought (ACT) study, a longitudinal, population-based study of brain aging and dementia, indicated that the most robust pathologic correlate of dementia was an increased number of microinfarcts.⁴ Moreover, Auriel et al⁵ reported that the chance detection of even 1 or 2 lesions using diffusion-weighted imaging suggests an annual incidence of hundreds of new cerebral microinfarcts by a mathematic method for estimating

the total number of microinfarcts based on the presence of incidental DWI lesions. Therefore, microinfarct detection is a vital task in MR imaging. Recently, cortical microinfarcts (CMIs) have generated increased interest.⁶ Kövari et al⁶ assessed the cognitive impact of CMIs, deep white matter and periventricular demyelination, and diffuse and focal gliosis in 43 prospectively evaluated postmortem cases scored as Braak neurofibrillary tangle stage III and found that only CMIs and periventricular demyelination were significantly associated with the Clinical Dementia Rating scale score.⁶

Other previous postmortem studies have also shown an independent relationship between the presence of CMIs and cognitive dysfunction.^{7,8} These findings suggest that CMIs also represent an important mechanistic link between cerebrovascular disease and dementia. Recent studies have shown that it is possible to detect CMIs in vivo using MR imaging. Previous studies have reported that CMIs were detected in 30%–40% of the general older population using 7T MR imaging^{9,10} and in 6% of older individuals with hypertension using high-resolution 3T MR imaging.¹¹ However, these studies have limitations because the authors evaluated

Received October 3, 2017; accepted after revision January 31, 2018.

From the Department of Radiology (M.M., S.K., S.I., K.W., J.M., Y.K.), School of Medicine, University of Occupational and Environmental Health, Kitakyushu, Fukuoka, Japan; and Department of Medical Physics in Advanced Biomedical Sciences (T.Y.), Faculty of Life Sciences, Kumamoto University, Kumamoto, Japan.

Please address correspondence to Shingo Kakeda, MD, PhD, 1-1 Iseigaoka, Yahatanishi-ku, Kitakyushu, Fukuoka, 807-8555, Japan; e-mail: kakeda@med.uoeh-u.ac.jp

<http://dx.doi.org/10.3174/ajnr.A5606>

Table 1: Sequence parameters for DWI, T1WI, T2*WI, FLAIR, and 3D multiecho spoiled GRE sequence^a

	DWI	T2WI	FLAIR	T2*WI	3D Multiecho Spoiled GRE (SWI)
TR (ms)	6000	4000	12,000	800	58.4
Effective TE (ms)	60	85	140	17	No. of TE ^b
Bandwidth (Hz per pixel)	1953	163	98	31	±62.5
Flip angle	90°	90°	90°	30°	15°
Section thickness (mm)	5	5	5	5	2
Matrix size	128 × 192	512 × 512	256 × 224	320 × 192	320 × 416
FOV (mm)	22 × 22	22 × 22	22 × 22	22 × 22	22 × 16.5
Acquisition time (min)	0.5	3.3	3.5	2.5	7
NEX	1	2	1	1	1
Parallel imaging method (reduction factor)	2	2	NA	NA	2

Note:—NA indicates not available.

^a B-values of 0 and 1000 via single-shot multislice spin-echo echo-planar imaging for DWI.

^b Number of echo times, 11; first echo time, 4.5 msec; uniform echo time spacing, 5 msec; repetition time, 58.4 msec.

only chronic lesions in patients with no stroke history or months to years after stroke. Because no firm evidence of the nature of CMIs has been confirmed, particularly during the acute phase, a precise definition or finding of CMIs on MR imaging remains elusive. Furthermore, detection criteria for CMIs on MR imaging are not clearly defined,¹² though accurate diagnosis of CMIs using in vivo MR imaging is desired for appropriate clinical management of patients with dementia.

Many previous MR imaging studies operationally identified CMIs only as cortical hyperintense lesions on T2WI/FLAIR. However, a recent study reported chronic CMIs with hemorrhagic components on histopathologic examination, which were seen as focal accumulations of hemosiderin-containing macrophages accompanied by gliosis and neuronal loss,¹³ suggesting the importance of further evaluating CMIs using MR imaging sequences sensitive to hemorrhagic lesions.

Consequently, we evaluated the imaging evolution of acute CMIs at stroke via MR imaging protocols, including not only T1WI, T2WI, and FLAIR but also T2*WI or susceptibility-weighted imaging.^{14,15} The SWI method, which is more sensitive to magnetic susceptibility, is a useful technique in evaluating patients with cerebrovascular disease.¹⁶ In stroke imaging units, applications of SWI include the detection of hemorrhagic brain lesions. Moreover, even though 7T MR imaging is more sensitive than 3T for CMI detection,⁹ 7T systems are not widely available and can only be used for research. Therefore, the 3T method for the identification of CMIs is preferable for the study of CMIs on a substantially larger scale and in clinical settings, allowing clinically relevant research of CMIs in older individuals and the elucidation of their role in the development of cognitive impairment. In the present study, we identified patients positive for acute CMIs on DWI and evaluated their follow-up MR imaging. The aim of this study was to examine the temporal changes of signal intensities in acute CMIs using SWI and conventional MR imaging.

MATERIALS AND METHODS

Human experiments were performed in accordance with the guidelines provided and approved by the institutional review board of the University of Occupational and Environmental Health School of Medicine (Kitakyushu, Fukuoka, Japan). Our institutional review board approved this retrospective study, which analyzed existing, de-identified patient data and waived informed consent.

In the present analysis, retrospective review of brain MRIs performed between May 2004 and January 2015 was conducted by 2 radiologists (J.M. and M.M., with 15 and 7 years of experience in neuroradiology, respectively), and they selected patients with acute cortical and/or juxtacortical (CJC) microinfarcts. Acute CJC microinfarcts were defined as small hyperintense lesions on DWI measuring ≤10 mm in the axial diameter and restricted to the cortex or juxta cortex, and the lesions did not show hypointensity on initial T2*WI. In previous studies, the appearances of CMIs on T2WI/FLAIR were operationally defined as cortical lesions of <5 mm in greatest dimension.^{3,9,11,17} In general, DWI likely overestimates final infarct size,^{18,19} and an absolute size cutoff of acute CMIs remains controversial. Therefore, in this study, acute CJC microinfarcts were arbitrarily defined as lesions on DWI measuring ≤10 mm in axial diameter. From this cohort, we further selected patients who underwent follow-up brain MR imaging, including the 3D multiecho spoiled gradient recalled-echo (GRE) sequence. At our institution, the 3D multiecho spoiled GRE sequence was introduced in January 2015 as part of the routine brain MR imaging evaluation of vascular disease. Therefore, follow-up MR imaging, including the 3D multiecho spoiled GRE sequence, was not a prespecified study end point, and it was only performed as part of routine patient care if clinically indicated for nonspecific symptoms, worsening existing deficits, or recurrent stroke symptoms. The exclusion criteria were as follows: 1) patients with gross abnormalities, such as infarcts, hemorrhages, or brain tumors; and 2) patients with nondiagnostic imaging.

MR Imaging

All studies were performed on a 3T MR imaging system (Signa Excite 3T; GE Healthcare, Milwaukee, Wisconsin) using a dedicated 8-channel phased array coil (USA Instruments, Aurora, Ohio). All patients underwent 3D multiecho spoiled GRE imaging as well as our standard brain MR imaging protocol, including T1WI, T2WI, FLAIR, T2*WI, and DWI (Table 1). SWI was reconstructed from the 3D multiecho spoiled GRE data. For reconstruction of SWI, a TE of 34.1 ms was chosen from the 11 echoes.

Image Analysis

For CJC microinfarcts detected on initial DWI, 2 neuroradiologists (S.I. and S.K., with 12 and 20 years of neuroradiology experience, respectively) evaluated the follow-up MR imaging findings (T2WI/FLAIR, T2*WI, and SWI) and scored the lesions as

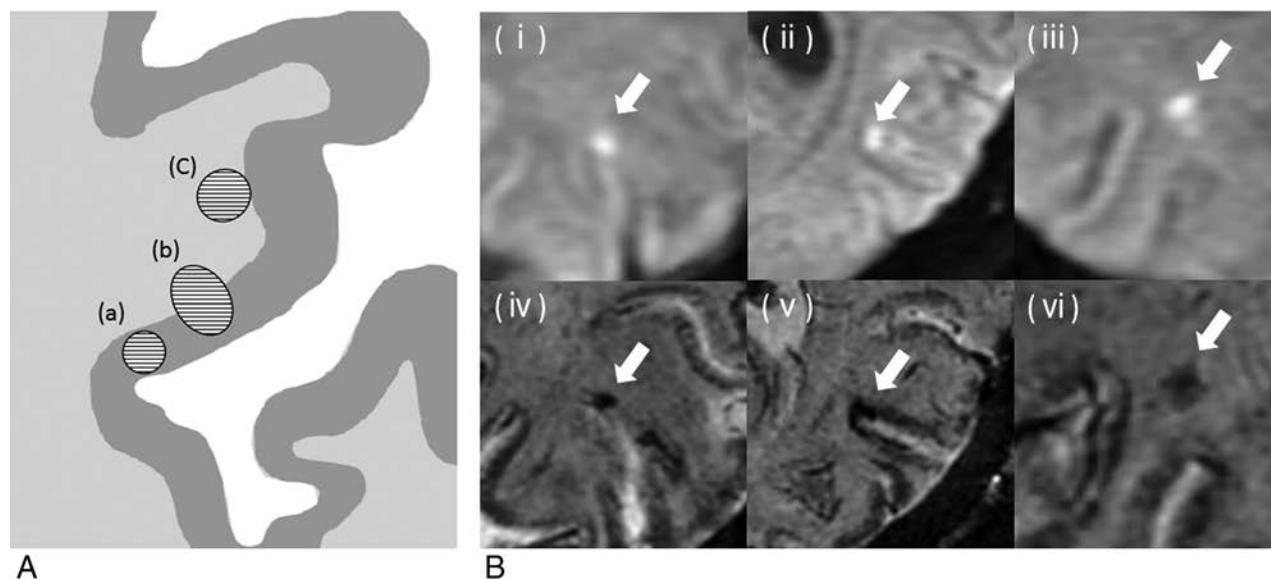


FIG 1. A, Schematic drawing illustrating the classification of lesion location. Involvement of the gray matter alone (a), the GM and juxtacortical white matter (b), and the juxtacortical WM alone (c). B, Reference images for the classification of lesion location. Initial DWIs show acute cortical and juxtacortical microinfarcts (i–iii). Each lesion on follow-up SWI is classified as the involvement of the GM alone (a, iv, arrow), GM and juxtacortical WM (b, v, arrow), or juxtacortical WM alone (c, vi, arrow).

either present or absent. They did not evaluate new lesions on follow-up MR imaging. For the reading session, follow-up MR imaging was always evaluated in conjunction with the initial MR imaging. When the result was scored as present, the neuroradiologists were required to evaluate the signal intensity of the lesions and classify the lesion location into the following 3 patterns: involvement of a) the gray matter alone, b) the GM and juxtacortical WM, or c) the juxtacortical WM alone (Fig 1A).²⁰ We defined the lesions with involvement of the GM [(a) and (b)] as CMIs in this study. Imaging evaluation was performed independently, and final classifications were determined by consensus of the neuroradiologists.

Lesion Detection Rate by the Follow-Up Interval

For SWI, we evaluated the relationship between the lesion detection rate and the follow-up SWI interval. The follow-up SWI interval was defined as the time between initial MR imaging and follow-up SWI. For the follow-up SWI interval, each lesion was classified into group A (<12 months), group B (12–36 months), or group C (>36 months).

Statistical Analysis

The total number of lesions was assessed and expressed as mean \pm SD. The mean number of lesions identified on SWI, T2WI, FLAIR, and T2*WI was expressed as a percentage of the number of lesions identified on DWI at baseline. Lesion-by-lesion analysis compared the number of lesions per category of the lesion location between T2WI and/or FLAIR and SWI. Regarding the follow-up SWI interval, differences between the lesion-detection rate for each group (group A versus B, group B versus C, and group A versus C) were analyzed using the Mann-Whitney *U* test.

Interobserver reliabilities were calculated as weighted κ values. The strength of agreement was considered fair for κ values of 0.21–0.40, moderate for 0.41–0.60, good for 0.61–0.80, and excellent for ≥ 0.80 .

Table 2: Patient characteristics

Characteristic	
Sex (female/male ratio)	8:17
Age on follow-up MRI (range) (yr)	66 (39–86)
MRI examinations (No.) (%) ^a	
1 Time	19 (76)
2 Times	3 (12)
3 Times	2 (8)
4 Times	1 (4)
Follow-up period (range) (mo)	33 \pm 35 (0.5–142)
Symptom on admission (No.) (%)	
None	15 (43)
Pure motor	16 (46)
Hemiplegia	2 (6)
Hemianopsia	2 (6)
Vascular risk factors (No.) (%)	
DM	8 (32)
HL	3 (12)
HT	12 (48)
Smoking	6 (24)

Note:—DM indicates diabetes mellitus; HL, hyperlipidemia; HT, hypertension.

^a Number of initial MRI examination per patients.

RESULTS

The radiologists selected 28 patients with CJC microinfarcts using the initial DWI, 3 of whom were excluded from the study: 1 patient due to major infarction at follow-up MR imaging and 2 patients because of nondiagnostic imaging due to patient motion artifacts at follow-up T2WI and SWI. Thus, 180 CJC microinfarcts on initial DWI were assessed in 25 patients. Each patient had 1 follow-up MR imaging; no patient had multiple follow-up MRIs. The clinical information is summarized in Table 2.

On follow-up of the 180 lesions, the neuroradiologists identified 52 (29%) on T2WI, 39 (22%) on FLAIR, 4 (2%) on T2*WI, and 101 (56%) on SWI (Table 3). The mean number of lesions was significantly larger with SWI than with the other sequences ($P < .05$). The neuroradiologists further identified 29 CMIs on T2WI, 9 on FLAIR, 4 on T2*WI, and 87 on SWI (Fig 2). Over-

Table 3: Follow-up appearances of acute cortical/juxtacortical microinfarcts (n = 180)^a

	CMI ^b	T2WI (n = 52)	FLAIR (n = 39)	T2*WI (n = 4)	SWI (n = 101)
Mean No. of lesions		1.6 ± 2.8	1.2 ± 2.1	0.1 ± 0.4	3.2 ± 4.6 ^c
Lesion locations	(a)	4	3	4	66
	(b)	25	6	0	21
	(c)	23	30	0	14
	(a) + (b)	29	9	4	87

^a Numbers in parentheses are total number of lesions.

^b (a) indicates involvement of the gray matter alone; (b), the GM and juxtacortical white matter; and (c), the juxtacortical WM alone; and (a) + (b) = CMIs.

^c Significantly different from T2WI, FLAIR, and T2*WI ($P < .05$).

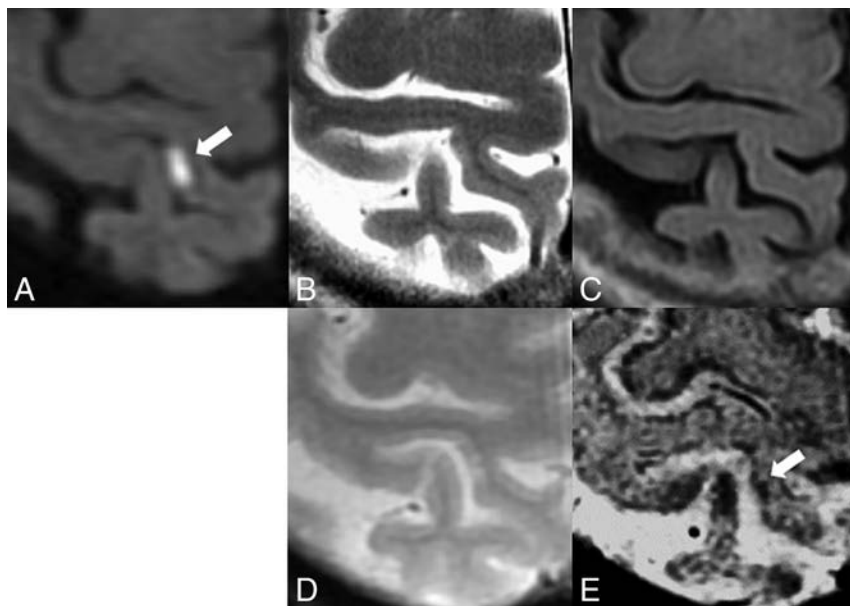


FIG 2. The imaging findings of an 82-year-old woman. The cortical infarct (arrows) shows hyperintensity on the initial DWI (A), hypointensity on the SWI (E), but it is not visible on the follow-up T2WI (B), FLAIR (C), and T2*WI (D).

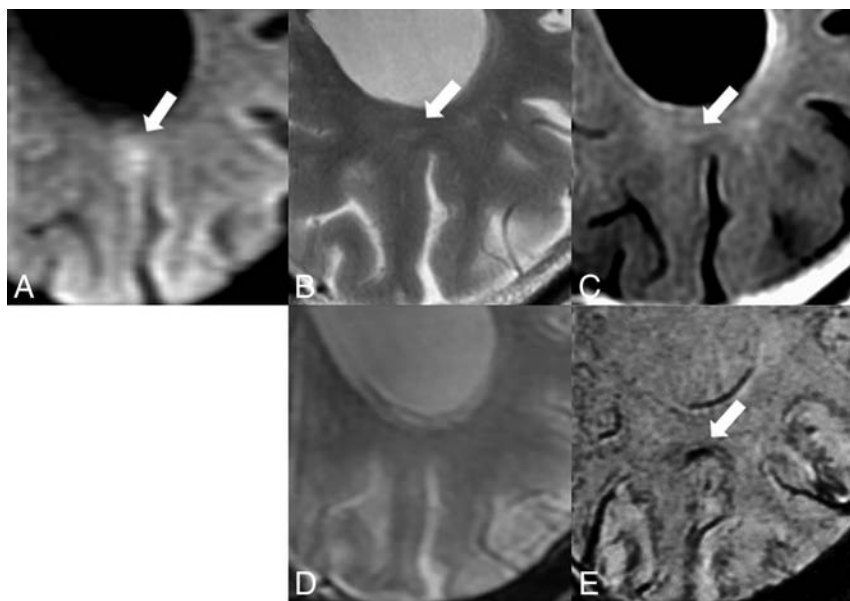


FIG 3. The imaging findings of a 69-year-old man. The acute cortical and juxtacortical microinfarct (arrows) shows hyperintensity on the initial DWI (A). The follow-up T2WI (B) and FLAIR (C) images show juxtacortical white matter hyperintensity (arrows). The hypointensity on SWI (E) was seen only in the gray matter (arrows), but it is not visible on the follow-up T2*WI (D).

all, 23 (44%) lesions on T2WI and 30 (77%) on FLAIR were scored as microinfarcts with sole involvement of the juxtacortical WM (Fig 3).

Lesion-by-lesion analysis (Table 4) demonstrated that of 87 lesions rated as CMIs on SWI, 12 were rated as “juxtacortical WM alone” on T2WI/FLAIR, and 54 lesions were not detected with T2WI/FLAIR. Conversely, 12 of 26 rated as juxtacortical WM alone on T2WI/FLAIR were rated as CMIs on SWI. Moreover, T2WI/FLAIR identified 17 lesions (8 rated as CMIs and 9 as juxtacortical WM alone) that were not seen on SWI.

All of the CMIs detected with any follow-up MR images showed hyperintensity on T2WI/FLAIR and hypointensity on SWI (Fig 3). Regarding the relationship between the lesion-detection rate and the follow-up SWI interval, the lesion-detection rate of group C (>36 months) was significantly lower than those of groups A (<12 months) and B (12–36 months) (36% versus 63% and 69%, respectively, $P < .001$ and $P = .002$) (Table 5). Additionally, there was no significant difference between groups A and B (63% versus 69%, $P = .52$).

The κ value for interobserver variability between the 2 radiologists was 0.736, corresponding to good interobserver agreement.

DISCUSSION

The main strengths of the present study were that we could precisely pinpoint when the CMIs started and follow their evolution with great precision. CMIs are often counted as chronic infarcts in epidemiologic studies.^{3,9,11,17} In previous studies, CMI appearances were defined as small cortical hyperintense lesions on T2WI/FLAIR and hypointense or isointense on T1WI, with a maximum diameter of 5 mm and round or elliptic shape.^{3,9,11,17} To our knowledge, this is the first in vivo study reporting the evolution of DWI positive for acute CMIs on SWI or T2*WI. We found that conversion to cortical hypointensities on follow-up SWI occurred in the DWI positive for acute C/JC microinfarcts.

Regarding the cortical hypointensities on SWI, the main potential explanation is a hemorrhage (hemosiderin de-

Table 4: Results of lesion-by-lesion analysis between the T2WI and/or FLAIR and SWI^a

SWI	T2WI and/or FLAIR		
	Positive		Negative (n = 125)
	(a) + (b) (n = 29)	(c) (n = 26)	
Positive (a) + (b) (n = 87) (c) (n = 14)	21 0	12 5	54 9
Negative (n = 79)	8	9	62

^a Numbers in parentheses are total number of lesions. CMIs: (a) indicates involvement of the gray matter alone; (b), the GM and juxtacortical white matter; (c), the juxtacortical WM alone; and (a) + (b) = CMIs.

Table 5: Relationship between the lesion detection rate and the follow-up interval on SWI

	Follow-Up SWI Interval ^a		
	Group A (0–12 mo)	Group B (12–36 mo)	Group C (36+ mo)
No. of lesions on initial DWI	70	54	56
No. of stroke events on initial DWI	13	9	13
Lesion-detection rate on SWI (No.) (%)	44 (63)	37 (69)	20 (36)

^a The follow-up SWI interval for a lesion was defined as the time between the initial MRI and the follow-up SWI.

position). In a recent extensive review, it was stated that postacute CMIs show as isointense on T2*WI or blood-sensitive scans (eg, gradient-echo or SWI).¹² However, in another study with 7T postmortem MR imaging and histopathology, 12 CMIs could be classified into different types: chronic gliotic CMIs ($n = 5$), chronic gliotic CMIs with cavitation ($n = 3$) or hemorrhagic components ($n = 3$), and acute CMIs ($n = 1$).¹³ Evidence of previous hemorrhage in the form of hemosiderin was present in the chronic gliotic CMIs with hemorrhagic components, but unlike microhemorrhages, the presence of such breakdown products of blood was not the primary feature of the lesions. Moreover, chronic gliotic CMIs with hemorrhagic components appeared hypointense on postmortem T2WI, FLAIR, and T2*WI, supporting our hypothesis, though the differences between pathologic subtypes of cerebral microinfarcts have not yet been linked to specific pathogenic mechanisms.

Another possible explanation may be iron deposition sequestered as ferritin in microglia. Microglia appear to have a high ferritin content,^{21,22} and reactive microglia were strongly stained with antiferritin in formalin-fixed, paraffin-embedded sections.²³ Microglia play an important role in postischemic inflammation.^{15–17} The proliferation of microglia is rapidly induced by cerebral ischemia.^{18,19} Thus, we hypothesized that the signal change of CMI on follow-up SWI may be reflected by ferritin-rich microglial deposition. Moreover, additional factors may lead to an accumulation of other metals within ischemic cells such as copper, zinc, and manganese granules.^{24,25}

Several authors have reported that the paramagnetic susceptibility changes can be more conspicuous on SWI than on T2*WI.^{26,27} In this study, we found conversion to cortical hypointensities on follow-up SWI occurring in 56% (101/180) of the DWIs positive for acute CMIs. Our results suggest that the true burden of CMIs on imaging may thus have been substantially underestimated in previous studies that only counted the cortical

hyperintense lesions on T2WI/FLAIR. On the other hand, we also found CMIs on T2WI/FLAIR that were not visible on SWI, which may correspond to the chronic gliotic CMIs without hemorrhagic components described in the previous histopathologic study.¹³ T2 lengthening caused by gliosis, edema, and cavitation could mask the decrease in T2 from iron-rich macrophages and cause T2WI/FLAIR images to appear hyperintense instead of hypointense.²⁸ Conversely, the paramagnetic field effects of the iron could be enhanced on SWI. Thus, T2WI/FLAIR and SWI provide different information for assessing CMIs; however, this is complementary information. Moreover, our lesion-by-lesion analysis demonstrated that 8 lesions rated as CMIs on SWI were rated as juxtacortical WM alone on T2WI/FLAIR, suggesting that SWI may be more accurate for assessing disease burden, especially GM involvement. In a previous study, phase-weighted MR imaging such as SWI had superior contrast between the GM and the surrounding WM,^{29,30} which may contribute to improved CMI detection. However, CMIs may not be seen on T2WI/FLAIR because they can be obscured from CSF by partial volume effects. Therefore, SWI may provide useful adjunctive information in the evaluation of CMIs.

The follow-up interval for this study was not fixed. The minimum time to follow-up imaging was relatively long (16 days). Therefore, it remains unclear when the signal intensity changes on the phase-weighted images initially appeared. On the other hand, the evaluation of the relationship between the lesion detection rate and the follow-up SWI interval demonstrated that the lesion-detection rate of group C (>36 months) was significantly lower than those of groups A (<12 months) and B (12–36 months). This result may indicate that some lesions on SWI might not persist for >3 years. More recent investigators have identified iron accumulation in multiple sclerosis plaques on Quantitative Susceptibility Mapping and reported that iron accumulation in MS plaques increased rapidly and persisted during its initial few (approximately 4) years and gradually dissipated within 4 years.³¹ Regarding the persistence of the iron accumulation, these results are consistent with our study. Therefore, we should be aware of the possibility of an underlying molecular pathway for brain iron metabolism.

There are some limitations associated with our study. First, in our diagnostic work-up, we selected only patients with microinfarcts due to arterioarterial thromboembolism. Some studies assessed patients with cerebral amyloid angiopathy and found an association with the occurrence of microinfarcts.^{32–34} Others found that CMIs were more common in the watershed areas,^{35,36} suggesting that microinfarcts could be related to intermittent focal ischemic episodes because of marginal brain hypoperfusion. In contrast, microinfarcts were also found in brain regions supplied by large cerebral vessels, and several studies found an association with macroscopic infarcts,^{37–41} implying that some microinfarcts could also have an embolic origin. Therefore, our results might reflect only 1 pathologic aspect of CMIs.

Second, the study was limited by its retrospective nature because it was difficult to identify potential associations among data on neuropsychological examinations and MR imaging findings because clinical findings, such as cognitive function, were uncer-

tain in many cases. Moreover, follow-up MR imaging was performed only as part of routine patient care if clinically indicated for nonspecific symptoms, worsening existing deficits, or recurrent stroke symptoms. Therefore, our results were limited by a lack of follow-up of baseline participants without persisting/new clinical conditions/complaints.

Third, new lesions at follow-up MR imaging were not evaluated because there was no firm evidence of the nature of CMI and no confirmation during the acute phase on initial DWI. Although on initial and follow-up MR imaging, the lesions were compared very carefully, the possibility of including new lesions in the follow-up MR imaging evaluation could not be excluded completely. Finally, the sample size was relatively small; therefore, larger prospective studies with fixed follow-up time points are required.

CONCLUSIONS

We evaluated the evolution of DWI positive for acute CMIs on follow-up MR imaging and found conversion (paramagnetic susceptibility change) to cortical hypointensity on SWI, suggesting that many CMIs may contain hemorrhagic components. Our preliminary results suggest that SWI and T2WI/FLAIR provide complementary information, which may be useful in understanding the pathologic processes underlying CMI subtypes. To confirm this, larger prospective studies with predetermined follow-up intervals are warranted.

REFERENCES

- Vinters HV, Ellis WG, Zarow C, et al. **Neuropathologic substrates of ischemic vascular dementia.** *J Neuropathol Exp Neurol* 2000;59: 931–45 CrossRef Medline
- Smith EE, Schneider JA, Wardlaw JM, et al. **Cerebral microinfarcts: the invisible lesions.** *Lancet Neurol* 2012;11:272–82 CrossRef Medline
- Brundel M, de Bresser J, van Dillen JJ, et al. **Cerebral microinfarcts: a systematic review of neuropathological studies.** *J Cereb Blood Flow Metab* 2012;32:425–36 CrossRef Medline
- Sonnen JA, Larson EB, Crane PK, et al. **Pathological correlates of dementia in a longitudinal, population-based sample of aging.** *Ann Neurol* 2007;62:406–13 CrossRef Medline
- Auriel E, Westover MB, Bisnchi MT, et al. **Estimating total cerebral microinfarct burden from diffusion-weighted imaging.** *Stroke* 2015; 46:2129–35 CrossRef Medline
- Kövari E, Gold G, Herrmann FR, et al. **Cortical microinfarcts and demyelination affect cognition in cases at high risk for dementia.** *Neurology* 2007;68:927–31 CrossRef Medline
- Gold G, Kovari E, Hof PR, et al. **Sorting out the clinical consequences of ischemic lesions in brain aging: a clinicopathological approach.** *J Neurol Sci* 2007;257:17–22 CrossRef Medline
- Kövari E, Gold G, Herrmann FR, et al. **Cortical microinfarcts and demyelination significantly affect cognition in brain aging.** *Stroke* 2004;35:410–14 CrossRef Medline
- van Veluw SJ, Zwanenburg JJ, Engelen-Lee J, et al. **In vivo detection of cerebral cortical microinfarcts with high-resolution 7T MRI.** *J Cereb Blood Flow Metab* 2013;33:322–29 CrossRef Medline
- Brundel M, Reijmer YD, van Veluw SJ, et al; Utrecht Vascular Cognitive Impairment Study Group. **Cerebral microvascular lesions on high-resolution 7-Tesla MRI in patients with type 2 diabetes.** *Diabetes* 2014;63:3523–29 CrossRef Medline
- van Dalen JW, Sciric EE, van Veluw SJ, et al. **Cortical microinfarcts detected in vivo on 3 Tesla MRI clinical and radiological correlates.** *Stroke* 2015;46:255–57 CrossRef Medline
- van Veluw SJ, Shih AY, Smith EE, et al. **Detection, risk factors, and functional consequences of cerebral microinfarcts.** *Lancet Neurol* 2017;16:730–40 CrossRef Medline
- Van Veluw SJ, Zwanenburg JJ, Rozemuller AJ, et al. **The spectrum of MR detectable cortical microinfarcts: a classification study with 7-Tesla postmortem MRI and histopathology.** *J Cereb Blood Flow Metab* 2015;35:676–83 CrossRef Medline
- Haacke EM, Ayaz M, Khan A, et al. **Establishing a baseline phase behavior in magnetic resonance imaging to determine normal vs. abnormal iron content in the brain.** *J Magn Reson Imaging* 2007;26: 256–64 CrossRef Medline
- Haacke EM, Cheng NY, House MJ, et al. **Imaging iron stores in the brain using magnetic resonance imaging.** *Magn Reson Imaging* 2005; 23:1–25 CrossRef Medline
- Huang P, Chen CH, Lin WC, et al. **Clinical applications of susceptibility weighted imaging in patients with major stroke.** *J Neurol* 2012;259:1426–32 CrossRef Medline
- Jouvent E, Poupon C, Gray F, et al. **Intracortical infarcts in small vessel disease: a combined 7-T postmortem MRI and neuropathological case study in cerebral autosomal-dominant arteriopathy with subcortical infarcts and leukoencephalopathy.** *Stroke* 2011;42: e27–30 CrossRef Medline
- Koch S, McClendon MS, Bhatia R. **Imaging evolution of acute lacunar infarction leukoariosis or lacune?** *Neurology* 2011;77:1091–95 CrossRef Medline
- Potter GM, Doubal FN, Jackson CA, et al. **Counting cavitating lacunes underestimates the burden of lacunar infarction.** *Stroke* 2010; 41:267–72 CrossRef Medline
- Kidd D, Barkhof F, McConnell R, et al. **Cortical lesions in multiple sclerosis.** *Brain* 1999;122:17–26 CrossRef Medline
- Connor J, Boeshore K, Benkovic S, et al. **Isoforms of ferritin have a specific cellular distribution in the brain.** *J Neurosci Res* 1994;37: 461–65 CrossRef Medline
- Han J, Day JR, Connor JR, et al. **H and L ferritin subunit mRNA expression differs in brains of control and iron-deficient rats.** *J Nutr* 2002;132:2769–74 CrossRef Medline
- Kaneko Y, Kitamoto T, Tateishi J, et al. **Ferritin immunohistochemistry as a marker for microglia.** *Acta Neuropathol* 1989;79:129–36 CrossRef Medline
- Fujioka M, Taoka T, Matsuo Y, et al. **Novel brain ischemic change on MRI: delayed ischemic hyperintensity on T1-weighted images and selective neuronal death in the caudoputamen of rats after brief focal ischemia.** *Stroke* 1999;30:1043–46 CrossRef Medline
- Siesjö BK. **Pathophysiology and treatment of focal cerebral ischemia, part I: pathophysiology.** *J Neurosurg* 1992;77:169–84 CrossRef Medline
- Tsui YK, Tsai FY, Hasso AN, et al. **Susceptibility-weighted imaging for differential diagnosis of cerebral vascular pathology: a pictorial review.** *J Neurol Sci* 2009;287:7–16 CrossRef Medline
- Haacke EM, DelProposto Z, Chaturvedi S, et al. **Imaging cerebral amyloid angiopathy with susceptibility-weighted imaging.** *AJNR Am J Neuroradiol* 2007;28:316–17 Medline
- Hammond KE, Metcalf M, Carvajal L, et al. **Quantitative in vivo magnetic resonance imaging of multiple sclerosis at 7 Tesla with sensitivity to iron.** *Ann Neurol* 2008;64:707–13 CrossRef Medline
- Futatsuya K, Kakeda S, Yoneda T, et al. **Juxtacortical lesions in multiple sclerosis: assessment of gray matter involvement using phase difference-enhanced imaging (PADRE).** *Magn Reson Med* 2016; 15:349–54 CrossRef Medline
- Kakeda S, Futatsuya K, Ide S, et al. **Improved detection of cortical gray matter involvement in multiple sclerosis with quantitative susceptibility mapping.** *Acad Radiol* 2015;22:1427–32 CrossRef Medline
- Chen W, Gauthier SA, Gupta A, et al. **Quantitative susceptibility mapping of multiple sclerosis lesions at various ages.** *Radiology* 2014;271:183–92 CrossRef Medline
- Olichney JM, Ellis RJ, Katzman R, et al. **Types of cerebrovascular lesions associated with severe cerebral amyloid angiopathy in Alzheimer's disease.** *Ann N Y Acad Sci* 1997;826:493–97 CrossRef Medline
- Soontrornniyomkij V, Lynch MD, Mermash S, et al. **Cerebral microinfarcts associated with severe cerebral β -amyloid angiopathy.** *Brain Pathol* 2010;20:459–67 CrossRef Medline

34. De Reuck J, Deramecourt V, Cordonnier C, et al. **The impact of cerebral amyloid angiopathy on the occurrence of cerebrovascular lesions in demented patients with Alzheimer features: a neuropathological study.** *Eur J Neurol* 2011;18:913–18 [CrossRef Medline](#)
35. Suter OC, Sunthorn T, Kraftsik R, et al. **Cerebral hypoperfusion generates cortical watershed microinfarcts in Alzheimer disease.** *Stroke* 2002;33:1986–92 [CrossRef Medline](#)
36. Strozyk D, Dickson DW, Lipton RB, et al. **Contribution of vascular pathology to the clinical expression of dementia.** *Neurobiol Aging* 2010;31:1710–20 [CrossRef Medline](#)
37. Schneider JA, Arvanitakis Z, Bang W, et al. **Mixed brain pathologies account for most dementia cases in community-dwelling older persons.** *Neurology* 2007;69:2197–204 [CrossRef Medline](#)
38. Schneider JA, Boyle PA, Arvanitakis Z, et al. **Subcortical infarcts, Alzheimer's disease pathology, and memory function in older persons.** *Ann Neurol* 2007;62:59–66 [CrossRef Medline](#)
39. Troncoso JC, Zonderman AB, Resnick SM, et al. **Effect of infarcts on dementia in the Baltimore longitudinal study of aging.** *Ann Neurol* 2008;64:168–76 [CrossRef Medline](#)
40. Longstreth WT Jr, Sonnen JA, Koepsell TD, et al. **Associations between microinfarcts and other macroscopic vascular findings on neuropathologic examination in two databases.** *Alzheimer Dis Assoc Disord* 2009;23:291–94 [CrossRef Medline](#)
41. Arvanitakis Z, Leurgans SE, Barnes LL, et al. **Microinfarct pathology, dementia, and cognitive systems.** *Stroke* 2011;42:722–27 [CrossRef Medline](#)

European Multicenter Study for the Evaluation of a Dual-Layer Flow-Diverting Stent for Treatment of Wide-Neck Intracranial Aneurysms: The European Flow-Redirection Intraluminal Device Study

M. Killer-Oberpfalzer, N. Kocer, C.J. Griessenauer, H. Janssen, T. Engelhorn, M. Holtmannspötter, J.H. Buhk, T. Finkenzeller, G. Fesl, J. Trenkler, W. Reith, A. Berlis, K. Hausegger, M. Augustin, C. Islak, B. Minnich, and M. Möhlenbruch



ABSTRACT

BACKGROUND AND PURPOSE: Endoluminal reconstruction with flow-diverting stents represents a widely accepted technique for the treatment of complex intracranial aneurysms. This European registry study analyzed the initial experience of 15 neurovascular centers with the Flow-Redirection Intraluminal Device (FRED) system.

MATERIALS AND METHODS: Consecutive patients with intracranial aneurysms treated with the FRED between February 2012 and March 2015 were retrospectively reviewed. Complications and adverse events, transient and permanent morbidity, mortality, and occlusion rates were evaluated.

RESULTS: During the defined study period, 579 aneurysms in 531 patients (median age, 54 years; range, 13–86 years) were treated with the FRED. Seven percent of patients were treated in the acute phase (≤ 3 days) of aneurysm rupture. The median aneurysm size was 7.6 mm (range, 1–36.6 mm), and the median neck size 4.5 mm (range, 1–30 mm). Angiographic follow-up of > 3 months was available for 516 (89.1%) aneurysms. There was progressive occlusion witnessed with time, with complete occlusion in 18 (20%) aneurysms followed for up to 90 ± 14 days, 141 (82.5%) for 180 ± 20 days, 116 (91.3%) for 1 year ± 24 days, and 122 (95.3%) aneurysms followed for > 1 year. Transient and permanent morbidity occurred in 3.2% and 0.8% of procedures, respectively. The overall mortality rate was 1.5%.

CONCLUSIONS: This retrospective study in real-world patients demonstrated the safety and efficacy of the FRED for the treatment of intracranial aneurysms. In most cases, treatment with a single FRED resulted in complete angiographic occlusion at 1 year.

ABBREVIATIONS: ASPIRe = Aneurysm Study of Pipeline in an Observational Registry; EuFRED = European Flow-Redirection Intraluminal Device Study; FRED = Flow-Redirection Intraluminal Device; PUFs = Pipeline for Uncoilable or Failed Aneurysms Study

Flow diversion has become a widely accepted treatment option for all kinds of intracranial aneurysms, especially those with a wide neck.¹ High rates of complete aneurysm occlusion have been reported in a number of studies, even for large and giant aneu-

rysms.² Since the inception of the flow-diversion concept, a number of different flow diverters with variations in stent design have been developed and received Conformité Européenne or/and FDA approval. Large multicenter cohort studies using 1 of those flow diverters, the Flow-Redirection Endoluminal Device (FRED; MicroVention, Tustin, California), are currently lacking. The device has a paired, integrated dual-layer self-expanding nitinol braided design with an inner low-porosity stent that acts as the flow diverter and an outer part that serves as a scaffold for the inner stent. This dual-layer design is unique among currently available flow-diverting stents. The Pivotal Study of the FRED Stent System in the Treatment of Intracranial Aneurysms³ is a current trial in the United States with results expected to be pub-

Received October 17, 2017; accepted after revision January 12, 2018.

From the Research Institute of Neurointervention/Department of Neurology (M.K.-O., C.J.G.), Paracelsus Medical University, Salzburg, Austria; Department of Neurology (N.K., C.I.), Cerrahpasa Medical School, Istanbul University, Turkey; Department of Neurosurgery (C.J.G.), Geisinger Health, Danville, Pennsylvania; Institute of Radiology and Neuroradiology (H.J., T.F.), Klinikum Nuernberg Sued, Paracelsus Medical University, Nuernberg, Germany; Department of Neuroradiology (T.E.), University Hospital, Erlangen, Germany; Department of Diagnostic Radiology (M.H.), Rigshospitalet, Copenhagen, Denmark; Department of Neuroradiology (J.H.B.), University Hospital Hamburg, Eppendorf, Germany; Department of Neuroradiology (G.F.), Klinikum Grosshadern, University of Munich, Munich, Germany; Department of Neuroradiology (J.T.), Kepler Universitätsklinikum, Linz, Austria; Klinik für Diagnostische und Interventionelle Neuroradiologie (W.R.), Universitätsklinikum des Saarlandes, Homburg/Saar, Germany; Klinik für Diagnostische Radiologie und Neuroradiologie (A.B.), Klinikum Augsburg, Augsburg, Germany; Department of Diagnostic and Interventional Radiology (K.H.), Klinikum Klagenfurt, Klagenfurt, Austria; Department of Radiology (M.A.), University Hospital, Graz, Austria; Department of Cell Biology and Physiology (B.M.), Universität Salzburg, Salzburg, Austria; and Department of Neuroradiology (M.M.), Universitätsklinikum Heidelberg, Heidelberg, Germany.

M. Killer-Oberpfalzer and N. Kocer contributed equally to this work.

Please address correspondence to Monika Killer-Oberpfalzer, MD, Research Institute of Neurointervention/Department of Neurology, University Hospital Salzburg, Paracelsus Medical University, Salzburg, Austria, Ignaz Harrerstr 79, 5020 Salzburg, Austria; e-mail: m.killer@salk.at

Indicates open access to non-subscribers at www.ajnr.org

Indicates article with supplemental on-line table.

<http://dx.doi.org/10.3174/ajnr.A5592>

lished in 2018. Here, we report the results of the European FRED study (EuFRED), which included 15 European neurovascular centers and evaluated the safety and efficacy of this device in consecutive real-world patients with intracranial aneurysms treated with the FRED.

MATERIALS AND METHODS

Statement of Ethics

Local ethics committees acknowledged this study and the correct use of the patient data. All patients signed consent forms approved by the institutional review boards or the ethics committees.

Study Design

The EuFRED was a retrospective, multicenter postmarket registry of consecutive patients with intracranial aneurysms treated with the FRED between February 2012 and March 2015 at 15 European high-volume neurovascular centers with experienced neurointerventionalists. Centers had to commit to contribute at least 5, preferentially consecutive, cases. The decision to use the FRED was at the discretion of the treating neurointerventionalist to reflect application to real-world patients. Patients were eligible for enrollment in the study under the following conditions: 1) They consented to be treated with the FRED flow-diverting device; 2) they met the requirements for FRED treatment per the instructions for use approved for the country in which the patients were treated; and 3) the center agreed to collect data of all consecutive patients. The principal investigator (M.K.-O.) and a steering committee (C.J.G., B.M.) supervised the study design and operations. This study was not funded by an industrial or governmental source. Some of the patients in the present retrospective dataset were included in previously published single-center case series.⁴⁻⁶

Data Collection

All centers used the same preprinted data-collection sheets, which specified the data to be collected, study end points, and events of interest. An independent study nurse collected all raw data, and an independent statistician performed statistical analysis. Both were not involved in clinical decision-making. The baseline information studied included demographics, medical history, and aneurysm characteristics. The treatment characteristics collected included the number and size of FREDs and parent vessels, concomitant coil embolization, procedure duration, and use of balloon angioplasty. Clinical and imaging follow-up time points were at the discretion of the center. The clinical condition of patients was recorded according to the modified Rankin Scale score. Follow-up intervals were defined as follows: 1) baseline (before interventional treatment), 2) posttreatment (immediately after the procedure), 3) minimum follow-up (90 days), 4) short-term follow-up (90–180 days after the procedure), 5) midterm follow-up (180–365 days after the procedure), and 6) long-term follow-up (>1 year). Vascular imaging was evaluated in the treating center by an independent neuroradiologist who was not involved in the procedure. Digital subtraction angiography or conebeam CT or both with intravenous contrast administration was performed by 1 year. The technique for subsequent neurovas-

cular imaging was at the discretion of the individual center. Aneurysm occlusion grade, in-stent stenosis, and device migration were assessed. Aneurysm occlusion was assessed using a 3-point Raymond-Roy scale and the O'Kelly-Marotta grading scale.⁷ In-stent stenosis was calculated on the basis of the minimal luminal diameter and graded as mild (<50%), moderate (>50 to <75%), or severe (>75%). Device migration was defined as the movement of the device ≥ 5 mm from its originally deployed location.

All complications and adverse events from the time of treatment to last follow-up were registered. The following complications were specifically collected on the data sheets: 1) spontaneous rupture of the FRED-treated aneurysm, 2) spontaneous nonaneurysmal intracranial hemorrhage ipsilateral or contralateral to the treated aneurysm, 3) symptomatic ischemic stroke, 4) stent/parent artery stenosis, 5) stent/parent artery occlusion, 6) permanent cranial neuropathy, and 7) other complications that had to be described. Neurologic symptoms due to a stroke were defined as minor if the symptoms resolved within 1 month and major if the patient experienced a clinical deficit for >1 month. An adverse event was defined as any procedure-related event that resulted in unexpected difficulties without any decline of the patient's baseline neurologic status. Overall morbidity was defined as transient if the clinical sequelae of the complication resolved within 90 days and otherwise as permanent. Mortality was also recorded.

Flow-Redirection Endoluminal Device

The FRED is a flow-diverter stent that was released for clinical use in 2012. It has a paired, integrated dual-layer (stent-within-a-stent) self-expanding nitinol braided design. The inner part of 48 braided nitinol wires determines the working length. It is a low-porosity stent and acts as the active flow-diverting segment at the neck region of the aneurysm, particularly at the inflow zone. The outer part, which determines the total length, is a high-porosity stent with 16 wires, serving as a scaffold for the inner stent. The outer stent is 3 mm longer than the inner flow-diverter mesh at each end so that these proximal and distal parts of the FRED can be used to cover the adjacent perforating arteries or side branches of the parent vessel.

Technique

All elective patients were pretreated with dual-antiplatelet medication or, in acute cases, individually according to the practices of the hospitals. All patients were treated under general anesthesia and followed for 24 hours after the procedure in an intensive care unit. Procedures were performed through a 6F–8F femoral artery access. A guiding-catheter system was placed into the distal cervical segment of the vessel leading to the intracranial vessel targeted for treatment. A standard 0.027-inch ID microcatheter was then manipulated over a 0.014- to 0.018-inch outer diameter microwire into position across the aneurysm neck. When coiling was to be performed in conjunction with FRED treatment, a standard microcatheter was navigated into the aneurysm alongside the 0.027-inch microcatheter within the parent artery in a jailing technique. Once the 0.027-inch microcatheter was positioned distal to the aneurysm, the FRED was loaded via a rotating hemo-

static valve into the hub of the microcatheter and advanced with the delivery wire. The device was then deployed across the targeted landing zone through a process of microcatheter unsheathing and delivery-wire stabilization/advancement. After delivery of approximately two-thirds of the stent length, stent placement was assessed and, if necessary, the stent was resheathed and released again. Once deployed, if coil embolization was to be performed, coils were deployed within the aneurysm through the jailed microcatheter. Following coil embolization, the coiling microcatheter was gently removed from the aneurysm without displacing the construct. Digital subtraction angiography was performed to assess stent placement and the aneurysm occlusion rate immediately after the procedure. Patients continued antiplatelet therapy according to the standard of care in the respective hospital.

Statistical Analysis

All statistical analyses were performed using SigmaPlot 13 (Systat Software, San Jose, California). Data analysis was based on the patient level, except for aneurysm and procedure characteristics, which were based on the number of aneurysms and procedures, respectively. Values are expressed as percentages. Numbers in parentheses are given for better understanding if indicated. Descriptive statistics were used to present the data and summarize the results. Discrete variables are presented using frequency distributions and cross-tabulations. Continuous variables are summarized by presenting the number of observations, median, and range of minimum and maximum values. For correlation of normally distributed variables, the Pearson Product Moment Correlation was used; otherwise, the nonparametric Spearman rank order correlation was used. To indicate the strength and direction of the linear relationship between anterior/posterior circulation aneurysms and transient morbidity, as well as the final occlusion rate, and between aneurysm size and mortality and final occlusion rate, we performed linear regression analysis. For inferential statistics, data were analyzed by either the Student *t* test, Fisher exact test, Mann-Whitney rank sum test, or Kruskal-Wallis 1-way analysis of variance on ranks (if not normally distributed, the Shapiro-Wilk test). For pair-wise multiple comparison procedures, the Dunn method was used. All comparisons of variables were performed at a significance level of .05 or .01 (α) and a power of 0.80 (β).

RESULTS

Baseline Patient and Aneurysm Characteristics

A total of 531 patients with 579 aneurysms were enrolled. The median age was 54 years (range, 13–86 years), and 384 (72.3%) patients were female. In 46.9% of patients, the aneurysm was an incidental finding. Headache was the presenting symptom in 18.4% of patients, and 7% had a cranial nerve palsy. In 10.9%, recanalization of a previously treated aneurysm was the indication for treatment. In 3.8% of patients, a stroke was the reason for diagnosis, while subarachnoid hemorrhage occurred in 12.2%; 7.7% were treated in the acute phase with subarachnoid hemorrhage. Multiple aneurysms were reported in 26.6% of patients (median number of aneurysms per patient, 1; range, 1–5). Not all those aneurysms were treated with the FRED. The median aneu-

Table 1: Baseline characteristics

Characteristics	
No. of aneurysms	579
No. of patients	531
No. of procedures	534
Patient demographics	
Male (No.)	147 (27.7%)
Female (No.)	384 (72.3%)
Age at time of treatment (median) (range) (yr)	54 (13–86)
Presentation of patients (No.)	
Incidental	249 (46.9%)
Headaches	98 (18.4%)
Cranial nerve palsy	37 (7%)
Recanalization of previously treated aneurysm	58 (10.9%)
Subarachnoid hemorrhage	65 (12.2%)
Acute (≤ 3 days)	41 (7.7%)
Stroke	20 (3.8%)
Other	4 (0.8%)
Patients with multiple aneurysms (No.)	141 (26.6%)
Aneurysms per patient (median) (range)	1 (1–5)
Patients with a single aneurysm	390 (73.5%)
Patients with 2 aneurysms	101 (19%)
Patients with 3 aneurysms	30 (5.7%)
Patients with 4 aneurysms	8 (1.5%)
Patients with 5 aneurysms	2 (0.3%)
Pretreatment mRS (per patient) (No.)	
0–2	525 (98.8%)
3–5	6 (1.2%)
Aneurysm characteristics (No.)	
Left	272 (47.0%)
Right	257 (44.4%)
Midline	50 (8.6%)
Anterior circulation (No.)	
Internal carotid artery	
Posterior communicating	50 (8.6%)
Paraophthalmic	270 (46.6%)
Cavernous	45 (7.8%)
Other	67 (11.5%)
Middle cerebral artery	37 (6.4%)
Anterior cerebral artery	16 (2.7%)
Anterior communicating artery	4 (0.9%)
Pericallosal artery	13 (2.2%)
Posterior circulation (No.)	
Basilar artery	36 (6.2%)
Posterior cerebral artery	30 (5.2%)
Superior cerebellar artery	9 (1.6%)
Inferior cerebellar artery	2 (0.3%)
Aneurysm morphology (No.)	
Saccular	
Sidewall	459 (79.2%)
Bifurcation	63 (10.9%)
Fusiform/dissecting/blister	
Fusiform	27 (4.7%)
Dissecting	20 (3.5%)
Blister	10 (1.7%)
Maximal diameter (median) (range) (mm)	7.6 (1–36.6)
Neck diameter (median) (range) (mm)	4.5 (1–30)

rysm size was 7.6 mm (range, 1–36.6 mm). Small (< 10 mm), large (10–20 mm), and giant (> 20 mm) aneurysms were encountered in 76.9%, 17.4%, and 5.7%, respectively. The median aneurysm neck diameter was 4.5 mm (range, 1–30 mm). The median dome-to-neck ratio was 1.4. In 3.8% of aneurysms, partial thrombosis was seen. Aneurysm morphology showed sidewall and bifurcation aneurysms in 79.2% and 10.9%, respectively. In terms of aneurysm location, 86.7% were in the anterior circulation, with most in the internal carotid artery (Table 1).

Table 2: Complications and adverse events per procedure

	Periprocedural (In-Hospital Stay) (No.)	During Follow-Up (after Hospital Discharge) (No.)
Complications		
Spontaneous rupture of the FRED-treated aneurysm	0	2
Spontaneous nonaneurysmal intracranial hemorrhage	3	1
Symptomatic ischemic stroke		
Minor (≤ 1 mo)	8	5
Major (> 1 mo)	2	1
Stent/parent artery stenosis	5	3
Stent/parent artery occlusion	4	8
Permanent cranial neuropathy	0	0
Other complications		
Groin hematoma	1	
Dissection	1	
Aneurysm growth		2
Total	24 (4.5%)	22 (4.1%)
Adverse events		
Detachment in the hub of the microcatheter	2	
Poor opening on deployment	10	
Torquing of stent on deployment	1	
Multiple repositioning	2	
Visible gap between inner and outer stent		1
Fish mouthing of the distal stent end		13
Total	15 (2.8%)	14 (2.6%)
Transient morbidity (≤ 90 days)	10 (1.9%)	7 (1.3%)
Permanent morbidity (> 90 days)	3 (0.6%)	1 (0.2%)
Mortality	4 (0.75%)	4 (0.75%)

Treatment Characteristics

Platelet-function testing was performed in 62.7% of procedures. A combination of aspirin and clopidogrel was the most common dual-antiplatelet regimen (92.1%). The duration of dual-antiplatelet therapy varied among centers from 1 month to 1 year. A total 579 aneurysms in 531 patients were treated in 534 procedures using a median of 1 FRED (range, 1–5). In 515 procedures (96.4%), a single FRED was used. In 5 procedures, the initial stent shortened more than expected and a second stent was placed. In 10 procedures, a second stent was intentionally used because longer stent sizes were not available at the time of the procedure. In 2 procedures, fusiform aneurysms needed 3 and 5 telescoping stents, respectively. Two procedures were for retreatment. Stent deployment was successful on first attempt in 98.3% of single FRED procedures. In 17.6% of aneurysms, concomitant aneurysm coiling was performed. In 15 (2.8%) procedures, balloon angioplasty was performed, 5 of those being intentional in the absence of poor opening. The procedure time was defined from groin puncture to last angiogram and was recorded at a median of 65 minutes (range, 12–536 minutes) (On-line Table).

Adverse Events and Complications

A total of 75 (14%) complications and adverse events were recorded. Of those, 39 (7.3%) adverse events and complications were reported in the periprocedural and 36 (6.7%) in the follow-up period. There were 3 nonaneurysmal intracranial hemorrhages. One major hemorrhage on the ipsilateral side of the treated aneurysm was detected on CT the day of the procedure after sudden neurologic deterioration. Digital subtraction angiography and MR imaging showed stent and parent artery occlusion

and a major infarct with hemorrhagic transformation. This patient died. There were 2 other nonaneurysmal hemorrhages reported from wire perforations during stent delivery, one without neurologic deterioration and one resulting in a slight transient monoparesis of the arm. Eight patients had a minor stroke postoperatively, but symptoms resolved within 1 month. During follow-up, 1 growing aneurysm resulted in a rupture 233 days after the procedure and death of the patient, and another patient died due to unexpected aneurysm rupture 1 week after the confirmation of aneurysm occlusion at 1 month. There were 3 reports of in-stent stenosis (all $< 50\%$) on follow-up. None of the cases of in-stent stenosis were symptomatic and needed treatment. In 12 procedures, complete occlusion of the stent, parent artery, and aneurysm complex was registered periprocedurally and during follow-up. Ten of those were asymptomatic. One patient treated for an internal carotid artery communicating segment aneurysm showed a minor infarct on MR imaging. Only 1 stent occlusion

caused the death of a patient. After routine follow-up at 6 months, a paraophthalmic aneurysm and parent artery showed complete occlusion and the antiplatelet medication was stopped. One month later the patient died from a severe stroke caused by stent occlusion.

Two aneurysms showed enlargement with time. The regrowth of a basilar trunk aneurysm caused brain stem compression. The aneurysm was retreated 2 months later with a Pipeline Embolization Device (Covidien, Irvine, California). The other aneurysm, a fusiform M1 aneurysm treated with 2 telescopic stents, was unchanged in terms of flow and showed slight growth after 9 months. At that time, a decision against retreatment was made and the antiplatelet medication was stopped. There was no change at 1-year follow-up. Clinical outcome at a median follow-up of 6.6 months was favorable. While 515 patients had a good outcome (mRS 0–2), 8 patients had a poor outcome (mRS 3–5) and another 8 patients died (mRS 6). In univariable analysis, posterior circulation location was associated with transient morbidity ($P < .001$), and aneurysms of > 20 mm were associated with mortality ($P = .047$). In multivariable analysis, posterior circulation aneurysm was associated with transient morbidity (OR = 3.661; 95% CI, 1.685–7.953; $P = .001$) (Table 2).

Imaging Outcomes

After a median follow-up time of 6.6 months (range, 0.03–45.6 months), the overall complete occlusion rate was 69.2%. The number of aneurysms followed for > 3 months was 516 (89.1%) aneurysms. There was progressive occlusion witnessed across time, with complete occlusion in 18 (20%) aneurysms followed

for up to 90 ± 14 days, 141 (82.5%) for 180 ± 20 days, 116 (91.3%) for $1 \text{ year} \pm 24$ days, and 122 (95.3%) aneurysms followed for >1 year. The overall aneurysm retreatment rate (using the FRED or alternative techniques and devices) was 1.2%. In univariable analysis, aneurysms of >20 mm were associated with incomplete occlusion using the O'Kelly-Marotta grading scale. No significant predictors of aneurysm occlusion were identified in multivariable analysis.

DISCUSSION

The EuFRED is the largest study to date to evaluate the safety and efficacy of the dual-layer flow-diverting stent, FRED. Fifteen European neurovascular centers contributed 531 patients with 579 aneurysms treated in 534 procedures during 3 years. Any aneurysm deemed suitable for FRED by the treating neurointerventionalist was eligible. The study included a wide variety of aneurysms as encountered in the real-world patient population. Transient and permanent morbidity occurred in 3.2% and 0.8%, respectively, of procedures. The overall mortality rate was 1.5%. Complete occlusion was achieved in 95.3% of aneurysms followed for >1 year.

Aneurysm Characteristics in EuFRED

Flow diversion has clearly revolutionized the endovascular treatment of aneurysms. The 2 main principles on which the concept was founded are diversion of blood flow away from the aneurysm inducing stasis and thrombosis within the aneurysm sac and endothelialization along the stent scaffold and restoration of the integrity of the arterial wall.⁸ These devices have effectively addressed the issue of recanalization and the need for retreatment associated with other endovascular treatment modalities and are continuously gaining popularity among neurointerventionalists.⁹ Whereas treatment of internal carotid artery aneurysms up to the superior hypophyseal segment provided an early experience with flow diverters,¹ use has since expanded to a number of different aneurysm locations. In the EuFRED, 12.2% of aneurysms treated were in the anterior circulation distal to the internal carotid artery, and 13.3%, in the posterior circulation. Thus, more than one-quarter of aneurysms were located outside traditional locations, which mirrors a trend in the literature on flow diversion that advocates its use further distal in the cerebrovascular tree at or beyond the circle of Willis.¹⁰⁻¹² While approximately one-quarter of aneurysms in the EuFRED were large and giant and deemed too difficult to treat using traditional endovascular techniques, the median aneurysm diameter of 7.6 mm is a testament that flow diversion may be suitable for aneurysms traditionally managed with coil embolization with or without assist devices such as stents or balloons.¹³

Along those lines are also the results of a matched analysis comparing flow diversion with coiling of small and uncomplicated aneurysms, demonstrating a potential benefit for the flow diverter even in simple lesions.¹⁴ The 41 (7.7%) aneurysms in the EuFRED treated in acute aneurysmal subarachnoid hemorrhage constitute another important aspect. Nevertheless, the potential risk of rerupture due to a delay in aneurysm occlusion and the need for dual-antiplatelet agents in an acute hemorrhage remain challenges for this indication.¹⁵ There were 63 bifurcation aneurysms treated in 62 patients with a median maximal diameter of 7

mm. Two of those aneurysms were treated in the acute phase of subarachnoid hemorrhage. Likewise, 10 blister aneurysms were treated in the setting of subarachnoid hemorrhage, 8 in the acute phase and 1 each at 1 week and 1 month. In cases of blister aneurysms treated in the acute phase, the patients were loaded with tirofiban and later transitioned to aspirin and clopidogrel.

Aneurysm Occlusion after FRED

The overall rate of complete aneurysm obliteration in EuFRED was 69.2%, with a progressive increase in the proportion of aneurysms occluded with the duration of follow-up. Of aneurysms followed for >1 year, 95.3% were completely occluded. This observation is in line with prior studies that showed progressive aneurysm obliteration after flow diversion. In the Pipeline for Uncoiled or Failed Aneurysms (PUFS) trial, the rate of completely occluded aneurysms at 1 year was 86.8%¹ and climbed to 93.4% at 3 years and 95.2% at 5 years.^{16,17} Aneurysms in PUFS, however, were notably larger at a median aneurysm diameter of 17.5 mm compared with 7.6 mm in the EuFRED. Aneurysms of >20 mm were also associated with a lower rate of occlusion in the EuFRED. The notion that aneurysm size is an important predictor of aneurysm occlusion is also supported by a large multicenter retrospective study of 380 aneurysms treated with Pipeline embolization.¹⁸ In that study, the median aneurysm diameter was 7.7 mm, comparable with that in EuFRED, and the complete occlusion rate in aneurysms followed for at least 1 year was 83.9%. The study also included 13.4% of aneurysms located in the posterior circulation. Both this study and EuFRED found that posterior circulation aneurysms were less likely to occlude compared with their anterior circulation counterparts on univariable analysis. The studies were also comparable regarding the number of flow diverters used. While multiple devices were used in 98.1% of cases in PUFS,¹⁷ most aneurysms in the EuFRED and the aforementioned multicenter study were treated with a single device.

Another study to serve as a reference is the prospective Aneurysm Study of Pipeline in an Observational Registry (ASPIRe).¹⁹ Most aneurysms were also treated with a single device, but aneurysms in ASPIRe were larger than in EuFRED at a median diameter of 12 mm. Complete occlusion rates at 6 months and 1 year were 78.6% and 78.9%, respectively.¹⁷ Similar to EuFRED, size and location criteria followed country-specific instructions for use. ASPIRe also included aneurysms in the posterior circulation.¹⁹ The questions of whether occlusion rates using the FRED are indeed superior to those of other flow diverters such as Pipeline remains unanswered in the absence of a well-designed direct comparison study. Of the bifurcation aneurysms treated in EuFRED, there was progressive occlusion with time that plateaued at 1 year. Complete occlusion was noted in 38.1% at 90 days, 61.5% at 180 days, 88.8% at 1 year, and 85.7% at >1 year from treatment. Of the blister aneurysms, 100% were completely occluded at 3 months.

Adverse Events and Complications with FRED

In EuFRED, transient and permanent morbidity occurred in 3.2% and 0.8% of procedures, respectively, with an overall mortality rate of 1.5%. A pooled analysis of PUFS, ASPIRe, and the International Retrospective Study of the Pipeline Embolization Device,

a retrospective study designed to assess safety-related outcomes, reported major neurologic morbidity from major ipsilateral ischemic stroke and intracranial hemorrhage in 5.7% of patients. The combined major neurologic morbidity and mortality was 7.1%.¹⁷ A meta-analysis including 1654 Pipeline-treated aneurysms and aneurysms treated with the Silk flow diverter (Balt Extrusion, Montmorency, France) reported procedure-related morbidity and mortality rates of 5% and 4%, respectively. Ischemic stroke and perforator infarction rates were significantly higher in the posterior compared with the anterior circulation. Large and giant aneurysms had higher odds of ischemic stroke and subarachnoid hemorrhage.²⁰ Similar relationships were also detected in EuFRED, in which transient morbidity was associated with posterior circulation location and mortality with aneurysms of >20 mm. Of the bifurcation aneurysms treated, 1 patient had a major ipsilateral hemorrhage the day of the procedure. Digital subtraction angiography and MR imaging showed stent and parent artery occlusion resulting in a major infarct with hemorrhagic transformation and death. Except for this patient, all other patients had at least 90 days of follow-up and an mRS score between 0 and 2. Among the patients with blister aneurysms, all had an mRS score between 0 and 1 at last follow-up.

Strengths and Limitations

The main limitation of the present study is selection bias across the different neurovascular centers and individual neurovascular practitioners. No patient- and aneurysm-specific inclusion and exclusion criteria were provided, to mirror the real world. Likewise, periprocedural and follow-up management was at the discretion of the institution, reflected in variations in platelet-function testing, antiplatelet therapy, use of adjunctive coiling, and imaging follow-up schedule. While patients were prospectively enrolled, data collection was retrospective and subject to incomplete datasets. Data collection was performed at the individual institution and not at a central location, a core lab, introducing potential bias. The inclusion of multiple institutions, however, improved the generalizability of the findings. While participating practitioners were encouraged to enroll consecutive cases, it is possible that alternative flow diverters were used occasionally during the study period.

CONCLUSIONS

The EuFRED is the largest study to date assessing the safety and efficacy of the FRED flow-diverting stent. Applied to what may be considered a real-world patient population, FRED performed favorably regarding aneurysm obliteration and complications. Well-designed studies comparing FRED with other flow diverters are required to substantiate those observations.

Disclosures: Monika Killer-Oberpfalzer—UNRELATED: Grant: MicroVention/Terumo, Comments: research grant*; Support for Travel to Meetings for the Study or Other Purposes: MicroVention/Terumo; Travel/Accommodations/Meeting Expenses Unrelated to Activities Listed: MicroVention, Stryker, Medtronic. Naci Kocer—UNRELATED: Consultancy: MicroVention, Medtronic, Comments: consultant and proctorship agreement; Payment for Lectures Including Service on Speakers Bureaus: MicroVention, Comments: lectures on FRED. Hendrik Janssen—UNRELATED: Consultancy: MicroVention/Sequent Medical, Comments: proctor*; Travel/Accommodations/Meeting Expenses Unrelated to Activities Listed: MicroVention, Comments: travel expenses for conferences.* Markus Holtmannspötter—UNRELATED: Consultancy: Medtronic, MicroVention, Sequent Medical, Stryker, Route 92, Comments: consultancy and proctoring agreement; Payment for Lectures Including Service on Speakers

Bureaus: Medtronic, MicroVention, Sequent Medical. Jan-Hendrik Buhk—UNRELATED: Consultancy: Acandis, Codman Neurovascular, Medtronic, MicroVention, Stryker. Johannes Trenkler—UNRELATED: Payment for Lectures Including Service on Speakers Bureaus: MicroVention, Comments: interventional workshops, on-line presentation; Travel/Accommodations/Meeting Expenses Unrelated to Activities Listed: MicroVention, Stryker, Medtronic.* Ansgar Berlis—UNRELATED: Consulting Fee or Honorarium: MicroVention (FRED, Phil, WEB), Comments: proctoring. Markus Möhlenbruch—UNRELATED: Board Membership: Codman Neurovascular; Consultancy: Medtronic*; Grants/Grants Pending: Balt, MicroVention*; Payment for Lectures Including Service on Speakers Bureaus: MicroVention, phenox, Stryker.* *Money paid to the institution.

REFERENCES

1. Becske T, Kallmes DF, Saatci I, et al. Pipeline for uncoilable or failed aneurysms: results from a multicenter clinical trial. *Radiology* 2013; 267:858–68 CrossRef Medline
2. Briganti F, Leone G, Cirillo L, et al. Postprocedural, midterm, and long-term results of cerebral aneurysms treated with flow-diverter devices: 7-year experience at a single center. *Neurosurg Focus* 2017; 42:E3 CrossRef Medline
3. Pivotal Study of the FRED Stent System in the Treatment of Intracranial Aneurysms. ClinicalTrials.gov. <https://www.clinicaltrials.gov/ct2/show/NCT01801007?term=FRED&cond=Aneurysm&rank=1>. Accessed December 18, 2017
4. Luecking H, Engelhorn T, Lang S, et al. FRED flow diverter: a study on safety and efficacy in a consecutive group of 50 patients. *AJNR Am J Neuroradiol* 2017;38:596–602 CrossRef Medline
5. Möhlenbruch MA, Herweh C, Jestaedt L, et al. The FRED flow-diverter stent for intracranial aneurysms: clinical study to assess safety and efficacy. *AJNR Am J Neuroradiol* 2015;36:1155–61 CrossRef Medline
6. Drescher F, Weber W, Berlis A, et al. Treatment of intra- and extracranial aneurysms using the Flow-Redirection Endoluminal Device: multicenter experience and follow-up results. *AJNR Am J Neuroradiol* 2017;38:105–12 CrossRef Medline
7. O'Kelly CJ, Krings T, Fiorella D, et al. A novel grading scale for the angiographic assessment of intracranial aneurysms treated using flow diverting stents. *Interv Neuroradiol* 2010;16:133–37 CrossRef Medline
8. Griessenauer CJ, Gupta R, Shi S, et al. Collar sign in incompletely occluded aneurysms after Pipeline embolization: evaluation with angiography and optical coherence tomography. *AJNR Am J Neuroradiol* 2017;38:323–26 CrossRef Medline
9. Fargen KM, Soriano-Baron HE, Rushing JT, et al. A survey of intracranial aneurysm treatment practices among United States physicians. *J Neurointerv Surg* 2018;10:44–49 CrossRef Medline
10. Dabus G, Grossberg JA, Cawley CM, et al. Treatment of complex anterior cerebral artery aneurysms with Pipeline flow diversion: mid-term results. *J Neurointerv Surg* 2017;9:147–51 CrossRef Medline
11. Bhogal P, Martinez R, Ganslath O, et al. Management of unruptured saccular aneurysms of the M1 segment with flow diversion: a single centre experience. *Clin Neuroradiol* 2016 Dec 11. [Epub ahead of print] CrossRef Medline
12. Lopes DK, Jang DK, Cekirge S, et al. Morbidity and mortality in patients with posterior circulation aneurysms treated with the Pipeline embolization device: a subgroup analysis of the international retrospective study of the Pipeline embolization device. *Neurosurgery* 2017 Sep 18. [Epub ahead of print] CrossRef Medline
13. Brinjikji W, Cloft HJ, Kallmes DF. Difficult aneurysms for endovascular treatment: overwide or undertall? *AJNR Am J Neuroradiol* 2009;30:1513–17 CrossRef Medline
14. Chalouhi N, Daou B, Barros G, et al. Matched comparison of flow diversion and coiling in small, noncomplex intracranial aneurysms. *Neurosurgery* 2017;81:92–97 CrossRef Medline
15. Walcott BP, Koch MJ, Stapleton CJ, et al. Blood flow diversion as a primary treatment method for ruptured brain aneurysms: concerns, controversy, and future directions. *Neurocrit Care* 2017;26: 465–73 CrossRef Medline
16. Becske T, Potts MB, Shapiro M, et al. Pipeline for uncoilable or failed

- aneurysms: 3-year follow-up results. *J Neurosurg* 2017;127:81–88 CrossRef Medline
17. Kallmes DF, Brinjikji W, Cekirge S, et al. **Safety and efficacy of the Pipeline embolization device for treatment of intracranial aneurysms: a pooled analysis of 3 large studies.** *J Neurosurg* 2017;127:775–80 CrossRef Medline
 18. Adeeb N, Moore JM, Wirtz M, et al. **Predictors of incomplete occlusion following Pipeline embolization of intracranial aneurysms: is it less effective in older patients?** *AJNR Am J Neuroradiol* 2017;38:2295–2300 CrossRef Medline
 19. Kallmes DF, Brinjikji W, Boccardi E, et al. **Aneurysm Study of Pipeline in an Observational Registry (ASPIRe).** *Interv Neurol* 2016;5:89–99 CrossRef Medline
 20. Brinjikji W, Murad MH, Lanzino G, et al. **Endovascular treatment of intracranial aneurysms with flow diverters: a meta-analysis.** *Stroke* 2013;44:442–47 CrossRef Medline

An Update on the Adjunctive Neurovascular Support of Wide-Neck Aneurysm Embolization and Reconstruction Trial: 1-Year Safety and Angiographic Results

A.M. Spiotta, M.I. Chaudry, R.D. Turner IV, A.S. Turk, C.P. Derdeyn, J. Mocco, and S. Tateshima



ABSTRACT

BACKGROUND AND PURPOSE: The safety and efficacy of the PulseRider for the treatment of wide-neck, bifurcation aneurysms at the basilar and carotid terminus locations were studied in a prospective trial, the Adjunctive Neurovascular Support of Wide-Neck Aneurysm Embolization and Reconstruction (ANSWER) trial, reporting on initial 6-month angiographic and clinical results. This report provides insight into the longer term durability and safety with 12-month data.

MATERIALS AND METHODS: Aneurysms treated with the PulseRider among enrolled sites were prospectively studied. Updated 12-month data on clinical and imaging end points are included.

RESULTS: Thirty-four patients were enrolled (29 women, 5 men) with a mean age of 60.9 years. The mean aneurysm height ranged from 2.4 to 15.9 mm with a mean neck size of 5.2 mm (range, 2.3–11.6 mm). At 1 year, there were no device migrations or symptomatic in-stent stenoses. Raymond-Roy I occlusion was achieved in 53% of cases at the time of treatment and progressed to 61% and 67% at 6 and 12 months, respectively. Adequate occlusion (Raymond-Roy I/II) progressed from 88% at 6 months to 90% at 12 months. No recanalizations were observed. There was 1 delayed ischemic event. Good outcome (mRS 0–2) was achieved in 90% of patients.

CONCLUSIONS: The updated 1-year results from the ANSWER trial demonstrate aneurysm stability and an acceptable safety profile for aneurysms treated at the basilar apex and carotid terminus. Prospective data from a larger set of aneurysms treated at other locations are required to assess how treatment with PulseRider compares with alternatives for treating wide-neck bifurcation aneurysms.

ABBREVIATION: ANSWER = Adjunctive Neurovascular Support of Wide-Neck Aneurysm Embolization and Reconstruction

The endovascular approach to intracranial aneurysms has been revolutionized with the advent of balloon remodeling and stent-assisted coiling, allowing treatment of geometrically complex aneurysms,^{1–6} but optimization of treatment approaches is still necessary. In particular, wide-neck aneurysms arising at bifurcations still present a challenge with suboptimal rates of adequate occlusion and lower-than-desired safety profiles.⁷ A recently approved device is the PulseRider (Cerenovus, a division of Johnson & Johnson, New Brunswick, New Jersey), de-

signed as an adjunct for the coil embolization of aneurysms arising at bifurcations^{8–12} and to provide an alternative to complex Y-stent reconstruction.^{12–28}

The Adjunctive Neurovascular Support of Wide-Neck Aneurysm Embolization and Reconstruction (ANSWER) trial demonstrated the safety and efficacy²⁹ of the PulseRider at 6 months for the treatment of wide-neck, bifurcation aneurysms arising at the carotid terminus and basilar apex. This report provides an update with 1-year data on clinical and imaging end points.

MATERIALS AND METHODS

Patients were enrolled from 10 US sites, all of which had institutional review board approvals (Medical University of South Carolina; SUNY Buffalo; University of Virginia; Long Beach Memorial Medical Center; University of Kansas Medical Center; Rush University Medical Center; University of Texas Southwestern; Mount Sinai, New York, New York; University of Massachusetts; Baptist Medical Center, Jacksonville, Florida). Aneurysms arising at either the carotid terminus or basilar apex that were relatively wide-neck were considered candi-

Received November 13, 2017; accepted after revision January 10, 2018.

From the Department of Neurosurgery (A.M.S., M.I.C., R.D.T., A.S.T.), Medical University of South Carolina, Charleston, South Carolina; Department of Radiology (C.P.D.), University of Iowa, Iowa City, Iowa; Department of Neurosurgery (J.M.), Mount Sinai Hospital, New York, New York; and Department of Radiology (S.T.), University of California, Los Angeles, Los Angeles, California.

This work was supported by Pulsar Vascular.

Please address correspondence to Alejandro Spiotta, MD, Department of Neurosurgery, Medical University of South Carolina, 96 Jonathan Lucas St, CSB 210, Charleston, SC 29425; e-mail: spiotta@musc.edu

Indicates open access to non-subscribers at www.ajnr.org

<http://dx.doi.org/10.3174/ajnr.A5599>



FIG 1. The PulseRider device is a self-expanding, nitinol implant that is fully retrievable and can be repositioned with radiopaque markers to aid in visibility during deployment and manipulation. The device is available in both Y- and T-configurations, as displayed, and has several different diameters and lengths available. The radiopaque markers are highlighted in red. Photograph provided courtesy of Cerenovus.

dates for inclusion in the trial (clinical trial registration number NCT02312856).

Beyond the primary 6-month FDA end points, extended safety end points for this update included death or stroke in a downstream territory postprocedure at 365 days. Technical success end points included device migration, in-stent stenosis, ability to retain coils within the aneurysm, and rate of aneurysm occlusion using the Raymond-Roy classification. Angiographic evaluation of these technical end points was adjudicated at each time point by a core lab blinded to the site performing the treatment. While all patients underwent angiography at 6 months, imaging follow-up at 1 year included MR angiography ($n = 8$), CT angiography ($n = 1$), and digital subtraction angiography ($n = 21$) (3 lost to follow up). All 12-month imaging was evaluated by a core lab.

PulseRider Device and Coil Embolization Technique

The PulseRider device is a self-expanding, nitinol implant (Fig 1) delivered on a stainless-steel delivery wire within any commercially available 021-diameter microcatheter. The device is fully retrievable and can be repositioned and torqued to fit the relevant anatomy. The device itself has significantly less metal than a conventional stent with most of the surface area coverage focused at the neck of the aneurysm. It has an open leaflet structure, which allows unrestricted microcatheter access to the aneurysm once deployed. The device is available in both T- and Y-configurations, intended to fit the geometry of the daughter vessels arising at the bifurcation. The device is available in different diameters and lengths and is outfitted with 8 radiopaque markers to aid in positioning. It can be positioned with both “wings” within the daughter branches (Fig 2), both within the aneurysm neck itself, or 1 in a daughter branch and 1 in the aneurysm neck. The device is then traversed with the coiling microcatheter for coil embolization.

Details of the procedural technique have been previously reviewed.^{8,9,11}

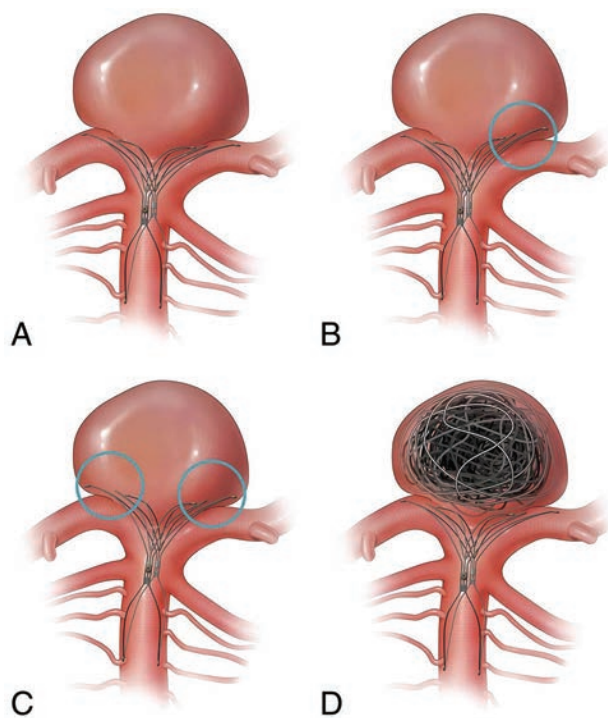


FIG 2. The PulseRider device is versatile and can be positioned with both wings within the daughter branches (A), 1 in a daughter branch and 1 in the aneurysm neck (B), or both within the aneurysm neck itself (C). The device is then traversed with the coiling microcatheter for coil embolization (D). Reprinted from Spiotta AM, Derdeyn CP, Tateshima S, et al. Results of the ANSWER trial using the PulseRider for the treatment of broad-necked, bifurcation aneurysms. *Neurosurgery* 2017;81(1):56–65, by permission of the Congress of Neurological Surgeons.

RESULTS

Patient Demographics and Aneurysm Characteristics

Thirty-four patients were enrolled (29 women and 5 men), with a mean age of 60.9 years (range, 26–86 years). Nine patients had a prior coil embolization procedure to the target aneurysm (8 basilar apex and 1 carotid terminus), and 5 had prior remote subarachnoid hemorrhage.

Aneurysm height ranged from 2.4 to 15.9 mm, and dome size ranged from 2.8 to 16.2 mm. The mean neck size was 5.2 mm (range, 2.3–11.6 mm). Twenty-seven aneurysms were located at the basilar apex and 7 at the carotid terminus. Parent vessel diameter ranged from 2.7 to 3.6 mm (basilar apex) and 2.9 to 4.2 mm (carotid terminus).

Angiographic Outcomes

Of the 34 patients enrolled, 1 patient died of unrelated causes shortly after the 6-month follow-up, and 3 patients were lost to follow-up. Thus, 30 patients in total were imaged at 1 year.

At 1 year, there were no device migrations or vessel stenoses. Raymond-Roy I was achieved in 53% of cases at the time of treatment and progressed to 61% and 67% at 6 and 12 months, respectively. Adequate occlusion (Raymond-Roy I/II) progressed from 88% at 6 months to 90% at 12 months (Table). No recanalizations were observed. No coil herniations or device migrations were observed. At 6 months, there was 1 instance (3.3%) of in-stent stenosis in a daughter vessel, measuring <50%, which was asymp-

Angiographic aneurysm occlusions at treatment (day 0), day 180, and day 365

Raymond-Roy Score	Aneurysm Occlusion (No.) (%)		
	Day 0 (n = 34)	Day 180 ^a (n = 33)	Day 365 ^b (n = 30)
I	18 (53%)	20 (61%)	20 (67%)
II	9 (26%)	9 (27%)	7 (23%)
III	7 (21%)	4 (12%)	3 (10%)
I/II	27 (79%)	29 (88%)	27 (90%)

^a Adequate occlusion was defined as Raymond-Roy I or II occlusion. One subject with a carotid terminus aneurysm had a CTA at 180 days, and occlusion data were not available on the image. The same subject died due to metastatic cancer before the 365-day visit and is not included in the 365-day data.

^b Three subjects were lost to follow-up at the 365-day visit.

tomatic and not flow-limiting. At 1 year, the stenosis had resolved and remained asymptomatic.

Safety End Points

There were no deaths attributed to the device or procedure. There was 1 death involving a patient who was found to have metastatic cancer that was not known before enrollment in the trial, and the death was unrelated to the procedure or the implant. At 12 months, mRS 0–2 was achieved in 90% (27/30) of patients.

One patient (1/30, 3.3%) had a delayed procedure-related ischemic event. Dual-antiplatelet therapy was discontinued after 6 months (per protocol), and at 9 months, the patient reported subjective mild and intermittent visual disturbances. During work-up, a small right thalamic infarct was identified on MR imaging. A thromboembolus from either the coil mass or the limb of the stent positioned in the right posterior cerebral artery was the suspected etiology.

DISCUSSION

The data from the ANSWER trial established the PulseRider as a safe device in the treatment of bifurcation aneurysms.²⁹ This report provides an update on the 12-month results of this trial, previously described at 6 months. Of note, beyond the 6-month follow-up period, the protocol was to discontinue dual-antiplatelet therapy and continue with aspirin, 325 mg daily. Angiographically, there were no device migrations or symptomatic in-stent stenoses identified. The single occurrence of asymptomatic in-stent stenosis of 1 branch vessel was entirely resolved at 1 year. Good outcome (mRS 0–2) was achieved in 90% of patients at a year. There was 1 delayed ischemic complication following discontinuation of dual-antiplatelet therapy.

Aneurysm occlusion rates in patients treated with the PulseRider and evaluated by core lab adjudication were 53% at time of initial treatment and progressed to 67% and 90% for complete and adequate occlusion, respectively. These occlusion rates at 1 year compare favorably with the pooled data from 3 prospective trials using the Woven EndoBridge device (WEB; Sequent Medical, Aliso Viejo, California),³⁰ which demonstrated complete aneurysm occlusion in 52.9%, Raymond-Roy II in 26.1%, and Raymond-Roy III in 20.9%. These angiographic outcomes demonstrate the immediate utility of the PulseRider as an adjunct to coil embolization of these wide-neck aneurysms arising at the basilar apex and carotid terminus, as well as the stability (no recanalizations were observed) and modest degree of flow diversion afforded as reflected in the progressive occlusion at both 6- and 12-month follow-up.

Beyond streamlining the procedure, the results achieved in the ANSWER trial at 12 months compare favorably with the largest, multicenter case series of Y-stent placement ($n = 45$),¹⁵ which reported an 11% intraprocedural complication rate and immediate Raymond-Roy I occlusion rates of 40% that improved to 60% on the latest follow-up imaging, though only 30 of the 45 patients had follow-up imaging available. Among patients in the ANSWER trial, immediate Raymond-Roy I was achieved in 53% of cases at the time of treatment and progressed to 61% and 67% at 6 and 12 months, respectively. However, while the Raymond-Roy I occlusion rates are similar between PulseRider and Y-stent treated cases, Y-stent placement was associated with an 8.9% posttreatment ischemic event rate,¹⁷ compared with 3.3% in this trial.

CONCLUSIONS

The 1-year follow-up data on subjects in the ANSWER trial show that the PulseRider offers a safe and effective adjunctive method of treatment for bifurcation aneurysms of the carotid terminus and basilar apex.

ACKNOWLEDGMENTS

We thank Alyssa Pierce for editorial assistance with manuscript preparation.

Disclosures: Alejandro M. Spiotta—RELATED: Support for Travel to Meetings for the Study or Other Purposes: Pulsar Vascular; UNRELATED: Consultancy: Penumbra, MicroVention, Stryker, Minnetronix, Cerenovus; Stock/Stock Options: Penumbra. M. Imran Chaudry—UNRELATED: Consultancy: Balt, Blockade Medical, EndoStream Medical, Medina, Medtronic, MicroVention, Penumbra, Pulsar Vascular, Synchron, Three Rivers Medical; Stock/Stock Options: Medina, Medtronic, Three Rivers Medical. Raymond D. Turner—RELATED: Grant: Pulsar Vascular; UNRELATED: Consultancy: Codman, Penumbra, MicroVention, Stryker, Medtronic, Q'apel Medical, Rebound Medical, Aquilla S. Turk—UNRELATED: Consultancy: BALT International, Blockade Medical, Cardinal Consulting, Cerebrotech Medical Systems, Codman, Covidien, EndoStream Medical, Lazarus Effect, Medina, MicroVention, Penumbra, Pulsar Vascular, Siemens, The Stroke Project, Three Rivers Medical, Vastrax; Grants/Grants Pending: MicroVention, Penumbra, Stryker, Cerebrotech Medical Systems, Pulsar Vascular, Covidien, Three Rivers Medical, Codman, The Stroke Project; Payment for Lectures Including Service on Speakers Bureaus: MicroVention, Penumbra, Stryker, Pulsar Vascular, Covidien, Three Rivers Medical, Codman, The Stroke Project; Stock/Stock Options: Blockade Medical, Lazarus Effect, Medina, The Stroke Project, Three Rivers Medical, Vastrax; Support for Travel to Meetings for the Study or Other Purposes: MicroVention, Penumbra, Stryker, Pulsar Vascular, Covidien, Three Rivers Medical, Codman, The Stroke Project. Colin P. Derdeyn—UNRELATED: Grant: Washington University, Comments: I directed the core lab for analysis for the ANSWER trial. This lab was supported by Pulsar Vascular.* J. Mocco—UNRELATED: Consultancy: Rebound Medical, EndoStream Medical, Synchron, Cerebrotech Medical Systems; Other: Apama Medical, The Stroke Project, EndoStream Medical, Synchron, Cerebrotech Medical Systems, NeurVana, NeuroTechnology Investors, Comments: investor/ownership. Satoshi Tateshima—UNRELATED: Board Membership: Pulsar Vascular, Comments: Scientific Advisory Board for Pulsar Vascular from 2008 to 2016; Consulting Fee or Honorarium: Pulsar Vascular/Cerenovus; Grant: Cerenovus, Comments: educational grant for neurointervention clinical fellowship; Stock/Stock Options: Pulsar Vascular, Comments: stock option 2008–2016. *Money paid to the institution.

REFERENCES

1. Aletich VA, Debrun GM, Misra M, et al. The remodeling technique of balloon-assisted Guglielmi detachable coil placement in wide-necked aneurysms: experience at the University of Illinois at Chicago. *J Neurosurg* 2000;93:388–96 Medline
2. Lefkowitz MA, Gobin YP, Akiba Y, et al. Balloon-assisted Guglielmi detachable coiling of wide-necked aneurysms, Part II: clinical results. *Neurosurgery* 1999;45:531–37; discussion 537–38 Medline
3. Malek AM, Halbach VV, Phatouros CC, et al. Balloon-assist tech-

- nique for endovascular coil embolization of geometrically difficult intracranial aneurysms. *Neurosurgery* 2000;46:1397–406; discussion 1406–07 Medline
4. Moret J, Cognard C, Weill A, et al. Reconstruction technique in the treatment of wide-neck intracranial aneurysms: long-term angiographic and clinical results—apropos of 56 cases [in French]. *J Neuroradiol* 1997;24:30–44 Medline
 5. Raymond J, Guilbert F, Roy D. Neck-bridge device for endovascular treatment of wide-neck bifurcation aneurysms: initial experience. *Radiology* 2001;221:318–26 Medline
 6. Fiorella D, Albuquerque FC, Han P, et al. Preliminary experience using the Neuroform stent for the treatment of cerebral aneurysms. *Neurosurgery* 2004;54:6–16; discussion 16–17 Medline
 7. Fiorella D, Arthur AS, Chiacchierini R, et al. How safe and effective are existing treatments for wide-necked bifurcation aneurysms? Literature-based objective performance criteria for safety and effectiveness. *J Neurointerv Surg* 2017;9:1197–201 CrossRef Medline
 8. Turk A, Turner RD, Tateshima S, et al. Novel aneurysm neck reconstruction device: initial experience in an experimental preclinical bifurcation aneurysm model. *J Neurointerv Surg* 2013;5:346–50 CrossRef Medline
 9. Spiotta AM, Chaudry MI, Turk AS, et al. Initial experience with the PulseRider for the treatment of bifurcation aneurysms: report of first three cases in the USA. *J Neurointerv Surg* 2016;8:186–89 CrossRef Medline
 10. Gory B, Spiotta AM, Mangiafico S, et al. PulseRider stent-assisted coiling of wide-neck bifurcation aneurysms: periprocedural results in an international series. *AJNR Am J Neuroradiol* 2016;37:130–35 CrossRef Medline
 11. Spiotta AM, Derdeyn CP, Tateshima S, et al. Results of the ANSWER trial using the PulseRider for the treatment of broad-necked, bifurcation aneurysms. *Neurosurgery* 2017;8:56–65 CrossRef Medline
 12. Chow MM, Woo HH, Masaryk TJ, et al. A novel endovascular treatment of a wide-necked basilar apex aneurysm by using a Y-configuration, double-stent technique. *AJNR Am J Neuroradiol* 2004;25:509–12 Medline
 13. Akgul E, Aksungur E, Balli T, et al. Y-stent-assisted coil embolization of wide-neck intracranial aneurysms: a single center experience. *Interv Neuroradiol* 2011;17:36–48 CrossRef Medline
 14. Chalouhi N, Jabbour P, Gonzalez LF, et al. Safety and efficacy of endovascular treatment of basilar tip aneurysms by coiling with and without stent assistance: a review of 235 cases. *Neurosurgery* 2012;71:785–94 CrossRef Medline
 15. Cho YD, Park SW, Lee JY, et al. Nonoverlapping Y-configuration stenting technique with dual closed-cell stents in wide-neck basilar tip aneurysms. *Neurosurgery* 2012;70(2 Suppl Operative):244–49 CrossRef Medline
 16. Darkhabani ZM, Lazzaro MA, Zaidat OO. Pericallosal artery aneurysm treatment using Y-configuration stent-assisted coil embolization: a report of four cases. *J Neurointerv Surg* 2012;4:459–62 CrossRef Medline
 17. Fargen KM, Mocco J, Neal D, et al. A multicenter study of stent-assisted coiling of cerebral aneurysms with a Y configuration. *Neurosurgery* 2013;73:466–72 CrossRef Medline
 18. Martínez-Galdámez M, Saura P, Saura J, et al. Y-stent-assisted coil embolization of anterior circulation aneurysms using two Solitaire AB devices: a single center experience. *Interv Neuroradiol* 2012;18:158–63 CrossRef Medline
 19. Muda AS, Ralib AR, Yaacob Y, et al. Y-stent-assisted coil embolization of wide-necked aneurysms using a new fully retrievable and detachable intracranial stent: report of two cases. *Malays J Med Sci* 2011;18:91–97 Medline
 20. Perez-Arjona E, Fessler RD. Basilar artery to bilateral posterior cerebral artery ‘Y stenting’ for endovascular reconstruction of wide-necked basilar apex aneurysms: report of three cases. *Neurol Res* 2004;26:276–81 CrossRef Medline
 21. Rohde S, Bendszus M, Hartmann M, et al. Treatment of a wide-necked aneurysm of the anterior cerebral artery using two Enterprise stents in “Y”-configuration stenting technique and coil embolization: a technical note. *Neuroradiology* 2010;52:231–35 CrossRef Medline
 22. Sani S, Lopes DK. Treatment of a middle cerebral artery bifurcation aneurysm using a double Neuroform stent “Y” configuration and coil embolization: technical case report. *Neurosurgery* 2005;57(1 Suppl):E209 Medline
 23. Spiotta AM, Gupta R, Fiorella D, et al. Mid-term results of endovascular treatment of wide-necked aneurysms using double stents in Y configuration. *Neurosurgery* 2011;69:421–29 CrossRef Medline
 24. Thorell WE, Chow MM, Woo HH, et al. Y-configured dual intracranial stent-assisted coil embolization for the treatment of wide-necked basilar tip aneurysms. *Neurosurgery* 2005;56:1035–40; discussion 1035–40 Medline
 25. Zhao KJ, Yang PF, Huang QH, et al. Y-configuration stent placement (crossing and kissing) for endovascular treatment of wide-neck cerebral aneurysms located at 4 different bifurcation sites. *AJNR Am J Neuroradiol* 2012;33:1310–16 CrossRef Medline
 26. Cekirge HS, Yavuz K, Geyik S, et al. A novel “Y” stent flow diversion technique for the endovascular treatment of bifurcation aneurysms without endosaccular coiling. *AJNR Am J Neuroradiol* 2011;32:1262–68 CrossRef Medline
 27. Fiorella D, Arthur A, Boulos A, et al. Final results of the US humanitarian device exemption study of the low-profile visualized intraluminal support (LVIS) device. *J Neurointerv Surg* 2016;8:894–97 CrossRef Medline
 28. Hetts SW, Turk A, English JD, et al; Matrix and Platinum Science Trial Investigators. Stent-assisted coiling versus coiling alone in unruptured intracranial aneurysms in the matrix and platinum science trial: safety, efficacy, and mid-term outcomes. *AJNR Am J Neuroradiol* 2014;35:698–705 CrossRef Medline
 29. Spiotta AM, Derdeyn CP, Tateshima S, et al. Results of the ANSWER trial using the PulseRider for the treatment of broad-necked, bifurcation aneurysms. *Neurosurgery* 2017;81:56–65 CrossRef Medline
 30. Pierot L, Moret J, Barreau X, et al. Safety and efficacy of aneurysm treatment with WEB in the cumulative population of three prospective, multicenter series. *J Neurointerv Surg* 2017 Sep 30. [Epub ahead of print] CrossRef Medline

Endovascular Treatment of Very Large and Giant Intracranial Aneurysms: Comparison between Reconstructive and Deconstructive Techniques—A Meta-Analysis

F. Cagnazzo, D. Mantilla, A. Rouchaud, W. Brinjikji, P.-H. Lefevre, C. Dargazanli, G. Gascou, C. Riquelme, P. Perrini, D. di Carlo, A. Bonafe, and V. Costalat



ABSTRACT

BACKGROUND: The safety and efficacy of reconstructive and deconstructive endovascular treatments of very large/giant intracranial aneurysms are not completely clear.

PURPOSE: Our aim was to compare treatment-related outcomes between these 2 techniques.

DATA SOURCES: A systematic search of 3 data bases was performed for studies published from 1990 to 2017.

STUDY SELECTION: We selected series of reconstructive and deconstructive treatments with >10 patients.

DATA ANALYSIS: Random-effects meta-analysis was used to analyze occlusion rates, complications, and neurologic outcomes.

DATA SYNTHESIS: Thirty-nine studies evaluating 894 very large/giant aneurysms were included. Long-term occlusion of unruptured aneurysms was 71% and 93% after reconstructive and deconstructive treatments, respectively ($P = .003$). Among unruptured aneurysms, complications were lower after parent artery occlusion (16% versus 30%, $P = .05$), whereas among ruptured lesions, complications were lower after reconstructive techniques (34% versus 38%). Parent artery occlusion in the posterior circulation had higher complications compared with in the anterior circulation (36% versus 15%, $P = .001$). Overall, coiling yielded lower complication and occlusion rates compared with flow diverters and stent-assisted coiling. Complication rates of flow diversion were lower in the anterior circulation (17% versus 41%, $P < .01$). Among unruptured lesions, early aneurysm rupture (within 30 days) was slightly higher after reconstructive treatment (5% versus 0%, $P = .08$) and after flow diversion alone compared with flow diversion plus coiling (7% versus 0%).

LIMITATIONS: Limitations were selection and publication biases.

CONCLUSIONS: Parent artery occlusion allowed high rates of occlusion with an acceptable rate of complications for unruptured, anterior circulation aneurysms. Coiling should be preferred for posterior circulation and ruptured lesions, whereas flow diversion is relatively safe and effective for unruptured anterior circulation aneurysms.

ABBREVIATIONS: BAC = balloon-assisted coiling; PAO = parent artery occlusion; PRISMA = Preferred Reporting Items for Systematic Reviews and Meta-Analyses; SAC = stent-assisted coiling

Very large (diameter of ≥ 2 cm) and giant (diameter of ≥ 2.5 cm) intracranial aneurysms remain challenging lesions to treat by both surgical and endovascular approaches. Because of

their size, intraluminal thrombosis, neck dimension, and involvement of neural structures, giant aneurysms are often associated with high rates of recurrence and treatment-related morbidity and mortality.^{1,2} Treatment should result in the following³⁻⁵: 1) protection against aneurysm rupture, 2) prevention of thromboembolic complications, 3) improvement of mass effect, and 4) prevention of aneurysm growth. The endovascular strategies can be divided into 2 groups: 1) selective aneurysm treatment with coiling, balloon-assisted coiling (BAC), stent-assisted coiling (SAC), and flow diversion (reconstructive techniques); and 2) parent artery occlusion (PAO) (deconstructive technique). Both techniques have limitations: selective aneurysm embolization is

Received October 13, 2017; accepted after revision January 3, 2018.

From the Neuroradiology Department (F.C., D.M., P.-H.L., C.D., G.G., C.R., A.B., V.C.), University Hospital Gûi de Chauliac, Centre Hospitalier Universitaire de Montpellier, Montpellier, France; Interventional Neuroradiology NEURI Center (A.R.), Hôpital Bichat, Le Kremlin-Bicêtre, France; Department of Neurosurgery (P.P., D.d.C.), University of Pisa, Pisa, Italy; and Department of Radiology (W.B.), Mayo Medical School, Mayo Clinic, Rochester, Minnesota.

Please address correspondence to Federico Cagnazzo, MD, Neuroradiology Department, CHU Gûi de Chauliac, 80 Ave Augustin Fliche, 34000 Montpellier, France; e-mail: f.cagnazzo86@gmail.com



Indicates article with supplemental on-line tables.



Indicates article with supplemental on-line photo.

<http://dx.doi.org/10.3174/ajnr.A5591>

usually associated with high recurrence rates, with important differences in the various available techniques, while, PAO is potentially associated with long-term complications related to vessel sacrifice.^{4,6,7} We performed a meta-analysis of all published series examining endovascular treatments of very large and giant aneurysms with the aim of clarifying the following: 1) occlusion rate, 2) treatment-related complications, and 3) clinical outcome of reconstructive and deconstructive techniques.

MATERIALS AND METHODS

Literature Search

A comprehensive literature search of PubMed, Ovid MEDLINE, and Ovid EMBASE was conducted for studies published from 1990 to September 2017. Guidelines for Preferred Reporting Items for Systematic Reviews and Meta-Analyses (PRISMA)⁸ were followed. The detailed search strategy is reported in On-line Table 1. The inclusion criteria were the following: studies reporting very large (diameter of ≥ 2 cm) and giant (diameter of ≥ 2.5 cm) aneurysms treated endovascularly² (coiling/BAC, SAC, flow diversion, and PAO). Exclusion criteria were the following: 1) studies with <10 patients, 2) review articles, 3) studies published in languages other than English, and 4) treatment with Onyx (Covidien, Irvine, California) or covered stents. In cases of overlapping patient populations, only the series with the largest number of patients or most detailed data were included. Two reviewers independently selected the included studies, and a third author solved discrepancies.

Data Collection

From each study, we extracted the following: 1) treatment-related outcomes, 2) long-term occlusion rates, 3) incidence of early (within 30 days) and late (after 30 days) ruptures after treatment, 4) rate of recurrence, 5) mean and median times between treatment and recurrence, and 6) rate of retreatment. Treatment-related outcomes were dichotomized into 2 groups: reconstructive techniques (coiling/BAC, SAC, flow diversion alone, and flow diversion plus coiling) and deconstructive techniques. In addition, the influence of 4 parameters (age, aneurysm size, location, and shape) on the occlusion and complication rates was analyzed. Finally, good outcome was defined as a modified Rankin Scale score of 0–2 or a Glasgow Outcome Score of 4–5, or it was assumed if the study used terms such as “no morbidity,” “good recovery,” or “no symptoms.”

Outcomes

The primary objectives of this meta-analysis were to compare reconstructive and deconstructive techniques for the following outcomes: 1) aneurysm occlusion rate, 2) treatment-related complications, and 3) clinical outcome. Among the reconstructive group, complications and angiographic outcomes were compared between coiling and flow diversion.

Quality Scoring

The Newcastle-Ottawa Scale⁹ was used to assess the quality of the included studies (On-line Table 2). “High-quality” studies were defined on the basis of the following: 1) the presence of a study and imaging protocol, 2) defined inclusion and exclusion criteria,

3) detailed information about treatment-related outcomes, and 4) adequate length of follow-up. Adequate length of follow-up was considered approximately 12 months because most of the reported outcomes (treatment-related complications and angiographic outcomes) occurred within this time. The quality assessment was performed by 2 authors independently, and a third author solved discrepancies. Studies receiving ≥ 6 stars are considered “high-quality” (score range from 0 to 9).

Statistical Analysis

We estimated, from each cohort, the cumulative prevalence and 95% confidence interval for each outcome. Event rates were pooled across studies with a random-effects meta-analysis. Heterogeneity across studies was evaluated using the I^2 statistic: An I^2 value of $>50\%$ suggests substantial heterogeneity. We also extracted a 2×2 table to calculate P values for the comparisons among the results. Meta-regression was not used in this study. Statistical analysis was performed using OpenMeta[Analyst] (<http://www.cebm.brown.edu/openmeta/>).

RESULTS

Literature Review

Studies included in our meta-analysis are summarized in On-line Table 2. The search flow diagram is shown in the On-line Figure. A total of 39 studies and 894 giant and very large intracranial aneurysms were included in our review. Mean radiologic and clinical follow-ups were 26 months (range, 6–66 months; median, 21 months) and 34 months (range, 6–20 months; median, 28 months).

Quality of Studies

Overall, 20 studies were rated “high quality.” All the high-quality articles reported detailed information about aneurysm occlusion rates, treatment-related complications, factors related to occlusion and complications, and adequate length of follow-up. Three articles were prospective studies, 6 series were obtained from a prospectively maintained data base, and 30 articles were retrospective.

Patient Population and Treatment Characteristics

Detailed information about patient populations is reported in On-line Table 3.

Overall, 75% (95% CI, 72%–78%) and 25% (95% CI, 22%–27%) of aneurysms were treated with reconstructive and deconstructive techniques, respectively. About 70% of unruptured aneurysms were treated with reconstructive techniques. Among these patients, coiling/BAC was performed in 40% of cases; SAC, in about 16% of cases; and flow diversion, in 42% of patients. A deconstructive approach was performed in about 30% of unruptured aneurysms. Ruptured aneurysms were treated with coiling and PAO in 75% and 25% of cases, respectively. No acutely ruptured large and giant aneurysms were treated by flow diversion.

Balloon test occlusion was performed in about 86% of patients before PAO. In about 4% of patients, the occluded vessel was a nondominant vertebral artery and balloon test occlusion was not necessary. In 10% of cases (2 articles), there was not enough information about balloon test occlusion (On-line Table 2). About

Table 1: Angiographic outcomes for unruptured and ruptured very large/giant intracranial aneurysms—comparison between reconstructive and deconstructive treatments

Variables	Unruptured Group (Results of Meta-Analysis)	No. of Articles	P Value	Ruptured Group (Results of Meta-Analysis)	No. of Articles	P Value
Angiographic outcomes						
Long-term aneurysm occlusion (complete/near-complete)	122/175 = 71% (60–81) ($I^2 = 69\%$)	14		23/31 = 72% (57–87) ($I^2 = 0\%$)	5	
Reconstructive						
vs			.003 ^a			.5
Deconstructive	147/158 = 93% (89–98) ($I^2 = 4\%$)	8		13/15 = 80% (60–97) ($I^2 = 42\%$)	4	
Recanalization after reconstructive treatment	45/110 = 40% (13–60) ($I^2 = 95\%$)	9		15/31 = 47% (30–64) ($I^2 = 0\%$)	4	
vs			.001 ^a			.1
Recanalization after deconstructive treatment	3/66 = 5% (1–10) ($I^2 = 0\%$)	6		1/8 = 22% (7–52) ($I^2 = 49\%$)	3	
Time between treatment and recanalization						
Reconstructive			Median, 5 mo; mean, 8.7 mo; IQR, 4–13.5			
vs			vs			
Deconstructive			Median 6 mo; mean 13 mo; IQR, 5–21			
Retreatment after reconstructive treatment	34/105 = 32% (10–55) ($I^2 = 90\%$)	8		14/29 = 48% (30–66) ($I^2 = 0\%$)	3	
vs			.001 ^a			.007 ^a
Retreatment after deconstructive treatment	1/66 = 4% (1–8) ($I^2 = 0\%$)	6		1/8 = 22% (7–52) ($I^2 = 49\%$)	3	
Early aneurysm rupture after reconstructive treatment	8/165 = 5% (1.7–8) ($I^2 = 0\%$)	14		3/37 = 8% (2–22) ($I^2 = 5\%$)	6	
vs			.08			.2
Early aneurysm rupture after deconstructive treatment	0/86	8		0/36	5	
Late aneurysm rupture after reconstructive treatment	3/148 = 3% (0.6–6.2) ($I^2 = 0\%$)	12		0/36	5	
vs			.4			.4
Late aneurysm rupture after deconstructive treatment	0/86	8		0/10	4	

Note:—vs indicates versus; IQR, interquartile range.

^a Significant.

70% of deconstructive treatments in the posterior circulation were performed in the basilar artery/posterior cerebral artery, whereas 30% were performed in the vertebral artery.

Angiographic Outcomes

Unruptured Aneurysms. The rate of long-term complete/near-complete occlusion was 71% (95% CI, 60%–81%) and 93% (95% CI, 89%–98%) after reconstructive and deconstructive treatments, respectively ($P = .003$) (Table 1). The rate of recanalization was higher after reconstructive treatment (40%) compared with the deconstructive technique (5%) ($P = .001$). Similarly, the rate of retreatment was significantly higher among the reconstructive group (32% versus 4%) ($P = .001$). Early and late aneurysm ruptures after reconstructive techniques were 5% and 3%, respectively. No cases of rupture were described after PAO.

Ruptured Aneurysms. There were comparable rates of complete/near-complete occlusion (72% versus 80% after reconstructive and deconstructive treatments, respectively) ($P = .5$). Aneurysm recanalization was 47% after reconstructive and 22% after deconstructive techniques ($P = .1$). There was a significantly higher rate of retreatment after reconstructive compared with deconstructive treatments (48% versus 22%) ($P = .007$). The rate of early aneurysm rupture after coiling was 8%, whereas no cases were described after deconstructive treatment.

Treatment-Related Complications and Clinical Outcomes

Unruptured Aneurysms. Overall, treatment-related complications were 30% (95% CI, 22%–37%) and 16% (95% CI, 7%–

25%) after reconstructive and deconstructive treatments ($P = .05$) (On-line Table 4). Similarly, permanent complications were higher among the reconstructive group (15% versus 8.6%, $P = .01$). Most complications were related to ischemic events (15% and 11% among reconstructive and deconstructive groups, respectively). Worsening of mass effect was comparable between reconstructive and deconstructive treatments (1.7% versus 3.5%). Finally, the rate of hemorrhagic complications was higher after reconstructive techniques (6%) compared with PAO (2%) ($P = .03$). There was no significant difference in mortality rates between the 2 groups (9% versus 6%, $P = .35$).

The rates of good neurologic outcome were 80% and 89% after reconstructive and deconstructive treatments, respectively ($P = .1$). During follow-up, mass effect symptoms were improved in about 48% of patients after reconstructive treatments and in 77% of patients after PAO ($P = .02$).

Ruptured Aneurysms. The overall rates of complications and permanent complications were slightly higher after PAO (38% and 29%) compared with coiling (34% and 20%). The incidence of ischemic events was slightly higher after deconstructive compared with reconstructive treatments (33% versus 18.8%, $P = .3$), as was worsening of mass effect (14% versus 7%, $P = .2$). Hemorrhagic complications were higher after coiling compared with PAO (17% versus 9%, $P = .5$). The rate of good neurologic outcome was close to 60% for both types of treatment. Improvement of compressive symptoms was reported in 24% of reconstructive cases, whereas no data were available among the deconstructive group.

Factors Related to Occlusion and Complication Rates after Treatment

Reconstructive Group. Differences in occlusion rates were not statistically significant in relation to aneurysm size (less or more than 3 cm), anterior-versus-posterior circulation, and saccular-versus-fusiform aneurysms. However, there was a slightly higher incidence of occlusion among younger patients (younger than 60 years) compared with elderly patients (older than 60 years) (82% versus 71%) ($P = .09$, $OR = 1.97$). The incidence of complications was similar among groups of age, aneurysm size, and anterior-versus-posterior circulation. Among saccular aneurysms, the rate of complications was 23% (95% CI, 2%–40%), whereas no data were available for fusiform aneurysms (On-line Table 5).

Deconstructive Group. Complete/near-complete aneurysm obliteration was higher among younger patients (95.9% versus 78%) ($P = .007$, $OR = 2.5$). No differences in occlusion rates were found in relation to aneurysm size, location, and shape. Complication rates were comparable between younger and older patients and aneurysm sizes, whereas posterior circulation aneurysms treated with PAO showed higher rates of complications (36%) compared with anterior circulation aneurysms (15%) ($P = .001$, $OR = 3.6$). Although few studies were available for the analysis, complications were statistically similar between fusiform and saccular aneurysms (On-line Table 5).

Comparison among Coiling/BAC, SAC, and Flow Diversion for the Treatment of Unruptured Aneurysms

Complete/near-complete occlusion was 59% and 73% after coiling/BAC and SAC, respectively ($P = .3$) (On-line Table 6). Flow-diversion treatment resulted in 72% occlusion rates, with comparable rates between treatment with flow diverter alone versus flow diverter with adjunctive coils (75% versus 70%, respectively). The rates of early aneurysm rupture after coiling and SAC were approximately 6% and 9% ($P = .5$), whereas 7% of cases were reported after flow diversion alone, and no cases were described after flow diversion with adjunctive coils. The rate of late aneurysm rupture was 7% after coiling/BAC, whereas there were no cases of late rupture after SAC and flow diversion. The overall rate of treatment-related complications was higher after SAC (39%) compared with coiling/BAC (20%) ($P = .001$). Complications after flow diversion were 29%, and there were no significant differences between flow diversion alone and flow diversion plus coiling (32% versus 26%, $P = .8$). Treatment-related complications among anterior circulation aneurysms were slightly lower compared with posterior circulation aneurysms after coiling/BAC (15% versus 20%, $P = .7$) and SAC (38% versus 43%, $P = .9$), whereas flow diversion was associated with significantly lower rates of complications in the anterior circulation (17% versus 41%, $P = .02$). The most common complications were ischemic events, particularly among the SAC group (32%). Worsening of mass effect was close to 6% after coiling and SAC, whereas it was lower after flow diversion (1.6%). Hemorrhagic complications were between 5% and 10% among the different treatment groups. Overall, the rate of good neurologic outcome was between 60% and 72%.

Study Heterogeneity

High rates of heterogeneity were reported in the following: treatment-related complications, improvement of mass effect among unruptured lesions, rates of occlusion and recanalization among reconstructive treatments of unruptured aneurysms, and factors related to complications and aneurysm occlusion.

DISCUSSION

Our meta-analysis of nearly 900 very large/giant intracranial aneurysms treated endovascularly shows important differences between reconstructive and deconstructive techniques. Overall, among unruptured aneurysms, deconstructive treatments allowed higher rates of occlusion (93% versus 71%) and lower rates of complications (16% versus 30%), compared with reconstructive techniques. However, among posterior circulation aneurysms, treatment-related morbidity was not negligible after PAO (36%). Coil embolization of unruptured lesions was associated with lower rates of complication and aneurysm occlusion (20% and 59%) compared with SAC (39% and 73%) and flow diversion (29% and 72%). Most interesting, flow-diverter stents were significantly safer among anterior circulation aneurysms (17% versus 41% complications), whereas the safety of coiling and SAC was comparable for anterior and posterior circulation lesions. Although ruptured aneurysms were effectively treated with both techniques (70%–80% occlusion), reconstructive treatments were associated with a lower rate of complication and morbidity (34% and 20%) compared with PAO (38% and 29%). Younger patients had higher odds of aneurysm occlusion after reconstructive ($OR = 1.9$) and deconstructive treatments ($OR = 2.5$) compared with older patients. These findings are important, and they provide more information to guide the endovascular treatment/management of these lesions.

Reconstructive Treatments

Although exclusion of aneurysms with preservation of the parent vessel should be the first option, complication rates of reconstructive treatments seem nonnegligible. We found 30% treatment-related complications with 15% morbidity after reconstructive treatments of giant unruptured aneurysms. Most complications were ischemic (15%): They may be related to the complexity of the procedure, longer duration of the treatment, and use of adjunctive devices (SAC, flow diverter and coiling, or multiple flow diverters).^{1,10} Ischemic events were particularly high after SAC (30%), which may be a reflection of a longer procedure time, technical challenges encountered during stent deployment, and the need for dual-antiplatelet therapy. According to our results, in a large series of 512 patients treated with coiling alone and SAC, Yang et al¹¹ showed that larger aneurysm size was a predictor of procedural morbidity after SAC. In our study, the rate of complications after flow-diversion treatment ranged from 25% to 30%, without significant differences between flow diversion alone and flow diversion with adjunctive coils. This finding is in accordance with findings reported in other studies comparing the 2 groups of treatments.¹² Most interesting, flow diversion was safe and effective among anterior circulation lesions, whereas it was associated with a high incidence of complications in the vertebrobasilar region. In the International Retrospective Study of Pipeline Embo-

lization Device (IntrePED), among the subgroup of giant aneurysms, Kallmes et al¹³ reported 40% of complications after Pipeline treatment in the posterior circulation, compared with 23% in the anterior circulation. Among unruptured aneurysms, there was a trend toward higher rates of worsening of mass effect after coiling and SAC (6%) compared with flow diversion (1.6%), whereas the rates were comparable between reconstructive and deconstructive techniques.

Aneurysms presenting with mass effect are usually treated by a surgical approach (and decompression of the mass effect) with evacuation of the aneurysmal sac. However, our meta-analysis showed improvement of mass effect in about 50% and 77% of reconstructive and deconstructive treatments of unruptured aneurysms, respectively. Compressive symptoms in giant aneurysms seem to be a combination between direct compression/deformation of the neural structures and irritation caused by aneurysm sac pulsation. Accordingly, improvement leads independently to aneurysmal shrinkage because of the decreased pulsation, resolution of the perianeurysmal edema, and partial shrinkage.¹⁴ In a series of 19 aneurysms treated with coiling, Hassan and Hamimi¹⁴ reported 63% complete resolution of mass effect and 32% symptom improvement, without strict correlation with aneurysm shrinkage on the MR imaging.

Long-term occlusion of giant aneurysms is notoriously challenging after selective endovascular treatment,^{1,6} and the rates complete/near-complete occlusion are reported to be between 35% and 90%.^{1,3,15-17} Our study, the largest to date, demonstrated roughly 70% complete/near-complete occlusion after reconstructive treatment, with 40% and 32% recanalization and retreatment, respectively. In addition, we found a higher rate of occlusion after flow diversion and SAC (72% and 73%) compared with coiling alone (59%). Although currently it is common practice to perform coil embolization of giant aneurysms in addition to flow diversion, no significant differences in occlusion rates were found between flow diverter alone and flow diverters plus coils. Most interesting, after reconstructive treatments, the occlusion rate seems to be slightly higher among younger patients (80% versus 70%, OR = 1.9) with smaller aneurysms in the anterior circulation. In general, reconstitution of the endothelial lining of the neck with thrombus organization inside the sac is an important factor related to stable aneurysm occlusion. In giant wide-neck aneurysms, insufficient stent wall apposition, low density of coil packing, and coil migration into the thrombotic wall can decrease the neoendothelialization of the neck and the thrombotic process inside the sac.^{1,18,19}

Postprocedural aneurysm rupture is a serious complication, and prior studies demonstrated a higher risk of rupture in giant aneurysms. After reconstructive treatments of unruptured lesions, we found 5% and 3% early and late aneurysm rupture. The incidence of rupture in the first 30 days was slightly higher in the ruptured group (8%, $P = .08$). Most interesting, the rate of rupture was comparable among coiling, SAC, and flow diversion. However, we found 7% early rupture (within 30 days) of aneurysms treated with flow diversion alone, and no cases of rupture in the group of lesions treated with adjunctive coils. These results support the recommendation to treat very large and giant aneurysms with concomitant coiling and flow diverters to prevent de-

layed ruptures. In a recent review of the literature, Rouchaud et al²⁰ reported that 76% of the ruptures after flow diversion occurred in the first month: Giant aneurysms accounted for about 50% of ruptures, and 80% of lesions were not previously coiled.

Overall, the rate of good neurologic outcome was approximately 80% and 60% for unruptured and ruptured treated aneurysms.

Deconstructive Treatments

Among unruptured aneurysms, PAO had lower complications (16%) and morbidity (9%) compared with reconstructive treatments. The most frequent complications were ischemic events (11%), whereas hemorrhagic complications seem to be significantly lower compared with reconstructive treatments (2% versus 6%, $P = .03$). Better results of PAO could be related to a careful patient selection with balloon test occlusion and rigorous postoperative management. In addition, deconstructive treatments allow better results in terms of improvement of mass effect compared with coiling or flow diversion (77% versus 48%, $P = .02$). In a series of 19 patients with giant aneurysms, Clarençon et al⁴ reported an 85% reduction of ocular symptoms, with a complete cure in 75% of cases. However, treatment-related outcomes after PAO in ruptured giant aneurysms were poor, with high rates of complications (38%) and morbidity (29%). The incidence of stroke seems to be high after PAO with SAH (33%). Several factors may explain the high rate of ischemic events in the acute phase: 1) difficulty in testing the hemodynamic tolerance to vessel occlusion, 2) management of the platelet antiaggregation therapy, 3) the hypercoagulability status after SAH, and 4) decreased blood flow compensation after cerebral vasospasm.

Most interesting, posterior circulation giant aneurysms treated with PAO had a remarkable complication rate compared with anterior circulation aneurysms (36% versus 15%, $P = .001$). Lubicz et al²¹ reported 40% early complications and 8% mortality after PAO of 13 giant vertebrobasilar aneurysms. The high morbidity rate can be related to the lower compliance of the posterior cranial fossa to mass effect lesions, high risk of injury to the perforating vessels, and difficulty in assessing the tolerance to occlusion of the vertebrobasilar territory. The size of the posterior communicating arteries represented a good predictor of long-term tolerance to basilar artery occlusion.²² However, giant vertebrobasilar aneurysms are challenging lesions with a poor prognosis after treatment, and survival as low as 20% after a few years if they are left untreated.²²

Overall, long-term occlusion was achieved in about 90% of patients, with low recanalization and retreatment rates among unruptured lesions (5% and 4%, respectively), a low risk of rupture after treatment, and a high rate of good neurologic outcome.

Strength and Limitations

Our study has limitations. There was substantial heterogeneity among the analyzed outcomes ($I^2 > 50\%$). The series are often small, retrospective, and single-institution experiences. Half of the reported studies were of low quality. Details of the antiplatelet therapy were infrequently specified. Finally, the small number of cases in some subgroups may not provide sufficient power to demonstrate a statistically significant difference in the rates of

complications and occlusion among age groups and aneurysm size, location, and shape. However, although retrospective data are low in quality, our meta-analysis is the best available evidence to evaluate reconstructive and deconstructive treatments of very large/giant aneurysms.

CONCLUSIONS

The treatment of very large and giant intracranial aneurysms remains extremely challenging. Sacrifice of the parent artery is a reasonable approach for complex unruptured, anterior circulation aneurysms, allowing high rates of occlusion with an acceptable rate of complications. Among reconstructive techniques, coiling should be preferred for the treatment of posterior circulation aneurysms and for ruptured lesions, whereas flow diversion is relatively safe and effective for unruptured anterior circulation aneurysms.

Disclosures: Federico Cagnazzo—UNRELATED: Employment: University of Florence. Paolo Perrini—UNRELATED: Employment: University of Pisa, Comments: I am an associate professor of neuroradiology. Vincent Costalat—UNRELATED: Grants/ Patents Pending: Medtronic, Stryker*; Payment for Development of Educational Presentations: Medtronic, Stryker, Balt, MicroVent. Alain Bonafe—UNRELATED: Employment: Hôpital Gui de Chauliac service de neuroradiology. Waleed Brinjikji—UNRELATED: Consultancy: Johnson and Johnson, Comments: \$500 consulting fee; Patents (Planned, Pending or Issued): intellectual property in balloon catheter technology; Stock/Stock Options: Superior Medical Editing stock options; Travel/Accommodations/Meeting Expenses Unrelated to Activities Listed: Johnson and Johnson; Other: CEO of Marblehead Medical LLC. Carlos Riquelme—UNRELATED: Employment: Hôpital Gui de Chauliac service de neuroradiology. *Money paid to institution.

REFERENCES

- Adeeb N, Griessenauer CJ, Shallwani H, et al. Pipeline embolization device in treatment of 50 unruptured large and giant aneurysms. *World Neurosurg* 2017;105:232–37 CrossRef Medline
- Gruber A, Killer M, Bavinski G, et al. Clinical and angiographic results of endosaccular coiling treatment of giant and very large intracranial aneurysms: a 7-year, single-center experience. *Neurosurgery* 1999;45:793–803; discussion 803–04 CrossRef Medline
- Gao X, Liang G, Li Z, et al. A single-centre experience and follow-up of patients with endovascular coiling of large and giant intracranial aneurysms with parent artery preservation. *J Clin Neurosci* 2012;19:364–69 CrossRef Medline
- Clarençon F, Bonneville F, Boch AL, et al. Parent artery occlusion is not obsolete in giant aneurysms of the ICA: experience with very-long-term follow-up. *Neuroradiology* 2011;53:973–82 CrossRef Medline
- Jahromi BS, Mocco J, Bang JA, et al. Clinical and angiographic outcome after endovascular management of giant intracranial aneurysms. *Neurosurgery* 2008;63:662–74; discussion 674–75 CrossRef Medline
- Biondi A, Jean B, Vivas E, et al. Giant and large peripheral cerebral aneurysms: etiopathologic considerations, endovascular treatment, and long-term follow-up. *AJNR Am J Neuroradiol* 2006;27:1685–92 Medline
- van Rooij WJ, Sluzewski M. Endovascular treatment of large and giant aneurysms. *AJNR Am J Neuroradiol* 2009;30:12–18 Medline
- Moher D, Liberati A, Tetzlaff J, et al. Preferred reporting items for systematic reviews and meta-analyses: the PRISMA statement. *Int J Surg* 2010;8:336–41 CrossRef Medline
- Wells G SB, O'Connell D. The Newcastle-Ottawa Scale (NOS) for assessing the quality of nonrandomized studies in meta-analyses. Ottawa: Ottawa Hospital Research Institute; 2011 http://www.evidencebasedpublichealth.de/download/Newcastle_Ottawa_Scale_Pope_Bruce.pdf?urlx. Accessed September 5, 2017
- Peschillo S, Caporlingua A, Resta MC, et al. Endovascular treatment of large and giant carotid aneurysms with flow-diverter stents alone or in combination with coils: a multicenter experience and long-term follow-up. *Oper Neurosurg (Hagerstown)* 2017;13:492–502 CrossRef Medline
- Yang H, Liu JX, Zhou ZP, et al. Comparison of the tumor-forming rate between the SCID and NOD/SCID mice used to set up acute myeloid leukemia model [in Chinese]. *Zhongguo Shi Yan Xue Ye Xue Za Zhi* 2015;23:328–34 CrossRef Medline
- Lin N, Brouillard AM, Krishna C, et al. Use of coils in conjunction with the Pipeline embolization device for treatment of intracranial aneurysms. *Neurosurgery* 2015;76:142–49 CrossRef Medline
- Kallmes DF, Hanel R, Lopes D, et al. International retrospective study of the Pipeline embolization device: a multicenter aneurysm treatment study. *AJNR Am J Neuroradiol* 2015;36:108–15 CrossRef Medline
- Hassan T, Hamimi A. Successful endovascular management of brain aneurysms presenting with mass effect and cranial nerve palsy. *Neurosurg Rev* 2013;36:87–97; discussion 97 CrossRef Medline
- Saatci I, Yavuz K, Ozer C, et al. Treatment of intracranial aneurysms using the Pipeline flow-diverter embolization device: a single-center experience with long-term follow-up results. *AJNR Am J Neuroradiol* 2012;33:1436–46 CrossRef Medline
- Strauss I, Maimon S. Silk flow diverter in the treatment of complex intracranial aneurysms: a single-center experience with 60 patients. *Acta Neurochir (Wien)* 2016;158:247–54 CrossRef Medline
- van Oel LI, van Rooij WJ, Sluzewski M, et al. Reconstructive endovascular treatment of fusiform and dissecting basilar trunk aneurysms with flow diverters, stents, and coils. *AJNR Am J Neuroradiol* 2013;34:589–95 CrossRef Medline
- Szikora I, Turányi E, Marosfoi M. Evolution of flow-diverter endovascular treatment and thrombus organization in giant fusiform aneurysms after flow diversion: a histopathologic study. *AJNR Am J Neuroradiol* 2015;36:1716–20 CrossRef Medline
- Rouchaud A, Ramana C, Brinjikji W, et al. Wall apposition is a key factor for aneurysm occlusion after flow diversion: a histologic evaluation in 41 rabbits. *AJNR Am J Neuroradiol* 2016;37:2087–91 CrossRef Medline
- Rouchaud A, Brinjikji W, Lanzino G, et al. Delayed hemorrhagic complications after flow diversion for intracranial aneurysms: a literature overview. *Neuroradiology* 2016;58:171–77 CrossRef Medline
- Lubicz B, Leclerc X, Gauvrit JY, et al. Giant vertebrobasilar aneurysms: endovascular treatment and long-term follow-up. *Neurosurgery* 2004;55:316–23; discussion 323–26 CrossRef Medline
- Sluzewski M, Brilstra EH, van Rooij WJ, et al. Bilateral vertebral artery balloon occlusion for giant vertebrobasilar aneurysms. *Neuroradiology* 2001;43:336–41 CrossRef Medline
- John S, Bain MD, Hussain MS, et al. Long-term effect of flow diversion on large and giant aneurysms: MRI-DSA clinical correlation study. *World Neurosurg* 2016;93:60–66 CrossRef Medline
- Johnson AK, Munich SA, Tan LA, et al. Complication analysis in nitinol stent-assisted embolization of 486 intracranial aneurysms. *J Neurosurg* 2015;123:453–59 CrossRef Medline
- Zhang Z, Lv X, Yang X, et al. Endovascular management of giant aneurysms: an introspection. *Neurol India* 2015;63:184–89 CrossRef Medline
- Labeyrie MA, Lenck S, Bresson D, et al. Parent artery occlusion in large, giant, or fusiform aneurysms of the carotid siphon: clinical and imaging results. *AJNR Am J Neuroradiol* 2015;36:140–45 CrossRef Medline
- Wang B, Gao BL, Xu GP, et al. Endovascular embolization is applicable for large and giant intracranial aneurysms: experience in one center with long-term angiographic follow-up. *Acta Radiol* 2015;56:105–13 CrossRef Medline
- Dumont TM, Levy EI, Siddiqui AH, et al. Endovascular treatment of giant intracranial aneurysms: a work in progress. *World Neurosurg* 2014;81:671–75 CrossRef Medline
- Derrey S, Penchet G, Thines L, et al. French collaborative group

- series on giant intracranial aneurysms: current management. *Neurochirurgie* 2015;61:371–77 [CrossRef Medline](#)
30. Cinar C, Bozkaya H, Oran I. Endovascular treatment of cranial aneurysms with the Pipeline flow-diverting stent: preliminary mid-term results. *Diagn Interv Radiol* 2013;19:154–64 [CrossRef Medline](#)
 31. Yu SC, Kwok CK, Cheng PW, et al. Intracranial aneurysms: midterm outcome of Pipeline embolization device—a prospective study in 143 patients with 178 aneurysms. *Radiology* 2012;265:893–901 [CrossRef Medline](#)
 32. Limaye US, Baheti A, Saraf R, et al. Endovascular management of giant intracranial aneurysms of the posterior circulation. *Neurol India* 2012;60:597–603 [CrossRef Medline](#)
 33. Matouk CC, Kaderali Z, terBrugge KG, et al. Long-term clinical and imaging follow-up of complex intracranial aneurysms treated by endovascular parent vessel occlusion. *AJNR Am J Neuroradiol* 2012;33:1991–97 [CrossRef Medline](#)
 34. Hauck EF, Welch BG, White JA, et al. Stent/coil treatment of very large and giant unruptured ophthalmic and cavernous aneurysms. *Surg Neurol* 2009;71:19–24; discussion 24 [CrossRef Medline](#)
 35. Lv X, Jiang C, Li Y, et al. Treatment of giant intracranial aneurysms. *Interv Neuroradiol* 2009;15:135–44 [CrossRef Medline](#)
 36. Suzuki S, Tateshima S, Jahan R, et al. Endovascular treatment of middle cerebral artery aneurysms with detachable coils: angiographic and clinical outcomes in 115 consecutive patients. *Neurosurgery* 2009;64:876–88; discussion 888–89 [CrossRef Medline](#)
 37. Standhardt H, Boecher-Schwarz H, Gruber A, et al. Endovascular treatment of unruptured intracranial aneurysms with Guglielmi detachable coils: short- and long-term results of a single-centre series. *Stroke* 2008;39:899–904 [CrossRef Medline](#)
 38. Li MH, Li YD, Fang C, et al. Endovascular treatment of giant or very large intracranial aneurysms with different modalities: an analysis of 20 cases. *Neuroradiology* 2007;49:819–28 [CrossRef Medline](#)
 39. Suzuki S, Kurata A, Kan S, et al. Efficacy of endovascular surgery for unruptured internal carotid artery aneurysms presenting with cranial nerve symptoms. *Interv Neuroradiol* 2007;13(Suppl 1):163–69 [CrossRef Medline](#)
 40. Deshaies EM, Adamo MA, Boulous AS. A prospective single-center analysis of the safety and efficacy of the Hydrocoil embolization system for the treatment of intracranial aneurysms. *J Neurosurg* 2007;106:226–33 [CrossRef Medline](#)
 41. Heran NS, Song JK, Kupersmith MJ, et al. Large ophthalmic segment aneurysms with anterior optic pathway compression: assessment of anatomical and visual outcomes after endosaccular coil therapy. *J Neurosurg* 2007;106:968–75 [CrossRef Medline](#)
 42. Cekirge HS, Saatci I, Ozturk MH, et al. Late angiographic and clinical follow-up results of 100 consecutive aneurysms treated with Onyx reconstruction: largest single-center experience. *Neuroradiology* 2006;48:113–26 [CrossRef Medline](#)
 43. Murayama Y, Nien YL, Duckwiler G, et al. Guglielmi detachable coil embolization of cerebral aneurysms: 11 years' experience. *J Neurosurg* 2003;98:959–66 [CrossRef Medline](#)
 44. Sluzewski M, Menovsky T, van Rooij WJ, et al. Coiling of very large or giant cerebral aneurysms: long-term clinical and serial angiographic results. *AJNR Am J Neuroradiol* 2003;24:257–62 [Medline](#)
 45. Ross IB, Weill A, Piotin M, et al. Endovascular treatment of distally located giant aneurysms. *Neurosurgery* 2000;47:1147–52; discussion 1152–53 [CrossRef Medline](#)
 46. Kim SJ, Choi IS. Midterm outcome of partially thrombosed intracranial aneurysms treated with Guglielmi detachable coils. *Interv Neuroradiol* 2000;6:13–25 [CrossRef Medline](#)
 47. Tateshima S, Murayama Y, Gobin YP, et al. Endovascular treatment of basilar tip aneurysms using Guglielmi detachable coils: anatomic and clinical outcomes in 73 patients from a single institution. *Neurosurgery* 2000;47:1332–39; discussion 1339–42 [Medline](#)
 48. Morishima H, Kurata A, Ohmomo T, et al. The efficacy of endovascular surgery for treatment of giant aneurysms with special reference to coil embolization for endosaccular occlusion. *Interv Neuroradiol* 1998;4(Suppl 1):135–43 [CrossRef Medline](#)
 49. Viñuela F, Duckwiler G, Mawad M. Guglielmi detachable coil embolization of acute intracranial aneurysm: perioperative anatomical and clinical outcome in 403 patients. *J Neurosurg* 1997;86:475–82 [CrossRef Medline](#)
 50. Guglielmi G, Viñuela F, Duckwiler G, et al. Endovascular treatment of posterior circulation aneurysms by electrothrombosis using electrically detachable coils. *J Neurosurg* 1992;77:515–24 [CrossRef Medline](#)

The New Low-Profile WEB 17 System for Treatment of Intracranial Aneurysms: First Clinical Experiences

 S.B.T. van Rooij,  J.P. Peluso,  M. Sluzewski,  H.G. Kortman, and  W.J. van Rooij



ABSTRACT

BACKGROUND AND PURPOSE: The Woven EndoBridge (WEB) is an intrasaccular flow diverter intended to treat wide-neck aneurysms. The latest generation WEBs needed a 0.021-inch microcatheter in the small sizes. Recently, a lower profile range of WEBs compliant with a 0.017-inch microcatheter (WEB 17) has been introduced. We present the first clinical results of treatment of both ruptured and unruptured aneurysms with the WEB 17.

MATERIALS AND METHODS: Between December 2016 and September 2017, forty-six aneurysms in 40 patients were treated with the WEB 17. No supporting stents or balloons were used. Twenty-five aneurysms were ruptured (54%). There were 6 men and 34 women (mean age, 62 years; median, 63 years; range, 46–87 years). The mean aneurysm size was 4.9 mm (median, 5 mm; range, 2–7 mm).

RESULTS: There were 2 thromboembolic procedural complications without clinical sequelae and no ruptures. The overall permanent procedural complication rate was 0% (0 of 40; 97.5% CI, 0%–10.4%). Imaging follow-up at 3 months was available in 33 patients with 39 aneurysms (97.5% of 40 eligible aneurysms). In 1 aneurysm, the detached WEB was undersized and the remnant was additionally treated with coils after 1 week. This same aneurysm reopened at 3 months and was again treated with a second WEB. One other aneurysm showed persistent WEB filling at 3 months. Complete occlusion was achieved in 28 of 39 aneurysms (72%), and 9 aneurysms (23%) showed a neck remnant.

CONCLUSIONS: The WEB 17 is safe and effective for both ruptured and unruptured aneurysms. The WEB 17 is a valuable addition to the existing WEB size range, especially for very small aneurysms.

ABBREVIATIONS: WEB = Woven EndoBridge; SL = single layer; SLS = single-layer sphere

Recently, the self-expanding intra-aneurysmal flow disruptor Woven EndoBridge (WEB; Sequent Medical, Aliso Viejo, California) device has been developed primarily for the treatment of wide-neck aneurysms without the need for supporting devices and concomitant dual-antiplatelet therapy.

The first clinical results of the WEB device showed good safety and efficacy profiles. Most of the published series comprised wide-neck, unruptured aneurysms.^{1–14} The first-generation WEBs required 0.027- to 0.033-inch microcatheters for delivery. In 2015, the WEB was redesigned for a 0.021-inch delivery microcatheter (WEB 21) in sizes ranging from 4 to 7 mm.

A new-generation low-profile WEB was introduced in clinical practice in December 2016. This system is compatible with a 0.017-inch microcatheter (WEB 17). Fewer wires were used to construct the device to achieve this lower profile. In benchmark studies, the flow-diverting effect seemed equal to that of the WEB 21 system (MicroVention, Bill Patterson, personal communication, October 27, 2016). The WEB 17 is intended for small aneurysms and comes in sizes of 3–7 mm.

In this study, we present the first clinical results of 46 ruptured and unruptured small aneurysms treated with the new WEB 17 system.

MATERIALS AND METHODS


WEB Device

The WEB device is a self-expanding, oblong or spheric braid of platinum-cored nitinol wires intended to implant inside the aneurysmal sac. The device is electrothermally detachable and is introduced through a microcatheter. In 2010, the device was introduced as the WEB dual-layer, with a second nitinol mesh placed at the bottom inside the primary braid to increase metal

Received December 27, 2017; accepted after revision January 31, 2018.

From the Department of Radiology (S.B.T.v.R.), Noordwest Ziekenhuisgroep, Alkmaar, the Netherlands; and Department of Radiology (J.P.P., M.S., H.G.K., W.J.v.R.), Elisabeth-Tweesteden Ziekenhuis, Tilburg, the Netherlands.

Please address correspondence to S.B.T. van Rooij, MD, Dept of Radiology, Noordwest Ziekenhuisgroep, Wilhelminalaan 12, 1815JD Alkmaar, the Netherlands; e-mail: s.b.t.rooij@gmail.com

 Indicates article with supplemental on-line table.

<http://dx.doi.org/10.3174/ajnr.A5608>

coverage at the neck of the aneurysm. In 2015, the lower profile WEB single-layer (SL) and WEB single-layer sphere (SLS) replaced this high-profile dual-layer version. The WEB-SL has an oblong shape, whereas the SLS version is more spheric. The WEB 21 comes in diameters ranging from 4 (144 wires) to 11 mm (216 wires) in 1-mm increments. The lengths of the SL version range from 3 to 7 mm. The length of the SLS version is 1.6 mm less than its diameter. WEB devices in diameters of 4–7 mm are compatible with a 0.021-inch microcatheter, while the 8- and 9-mm diameter needs a 0.027-inch microcatheter. The largest sizes of 10–11 mm go through a 0.033-inch microcatheter. The VIA microcatheter (Sequent Medical) is available in these different sizes and is specifically designed for the delivery of the WEB device.

Recently, the new low-profile WEB 17 system was introduced. The WEB 17 is especially designed for (very) small aneurysms. This system can be delivered through a 0.017-inch microcatheter. The WEB 17 comes in new smaller sizes starting at 3 mm and more shallow devices of 2-mm height for WEB sizes of 3–5 mm. The WEB 17 has fewer platinum-cored nitinol wires than the WEB 21 (72–108 versus 144) but a similar metal coverage at the neck (57%–59% versus 59%–62%). The WEB 17 SL is available in diameters ranging from 2×3 mm to 7×4 mm, and the WEB 17 SLS, in diameters of 4–7 mm. In the 4- to 7-mm range, there is overlap with the WEB 21 system, both in SL and SLS shapes.

General Indications in This Study

Treatment of patients with both ruptured and unruptured aneurysms is primarily endovascular in our institution. Patients with ruptured aneurysms are treated within 24 hours after admission. Patients with unruptured aneurysms are discussed in a weekly joint meeting with neurologists, neurosurgeons, and neuroradiologists.

The WEB system has been used for endovascular treatment in our institution since early 2015. We started using the WEB for wide-neck bifurcation aneurysms to replace stents, especially in ruptured aneurysms. Encouraging results led us to expand the indication for the WEB to all aneurysms suitable for the device, regardless of location or neck size.¹⁵

With the introduction of the WEB 17, we considered using this WEB in all small aneurysms judged suitable for the device. In general, only shallow aneurysms (height/dome ratio ≤ 0.5) and some aneurysms with vessels coming from the sac were treated otherwise.

WEB 17 Embolization Technique

Embolization was performed on a biplane angiographic system (AlluraClarity; Philips Healthcare, Best, the Netherlands) with the patient under general anesthesia by 3 interventional neuroradiologists with 26, 24, and 12 years of experience (W.J.v.R., M.S., J.P.P.). In unruptured aneurysms, 5000 U of heparin was administered as a bolus at the start of the procedure. In ruptured aneurysms, no anticoagulation was performed except the heparin in the pressure bags used for flushing (1000 U/L).

The required WEB is determined from a 3D angiographic dataset with calibrated distance measurements. Width, height, and

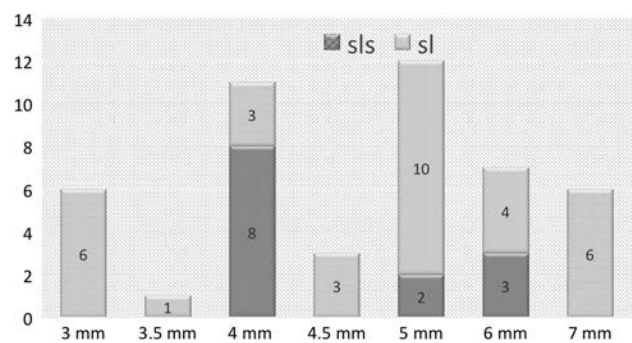


FIG 1. WEB sizes and shapes used in 46 aneurysms treated with WEB 17.

neck size of the aneurysm are measured in 2 orthogonal planes. The WEB is slightly oversized to ensure a stable position inside the aneurysm, and 1 mm was added to the average width of the aneurysm. To correct for increased height caused by horizontal compression, we deducted 1 mm from the average height of the aneurysm (+1/–1 rule).

A VIA 17 microcatheter was placed inside the aneurysmal fundus. The microcatheter could be steam-shaped, depending on vessel geometry. Once it was inside the aneurysm, gentle forward pushing and simultaneous withdrawal of the microcatheter slowly deployed the WEB. After deployment, the position of the WEB device was evaluated with fluoroscopy and an additional angiographic run, sometimes including 3D angiography. When the position of the WEB 17 was considered correct, the device was detached and the catheters were removed.

Data Collection and Angiographic Follow-Up

Patient demographics and treatment and aneurysm characteristics were recorded and retrospectively reviewed. Clinical follow-up was classified with the Modified Rankin Scale at 3-month follow-up. Angiographic follow-up was scheduled at 3 months, and 3T MRA follow-up, at 6 and 12 months according to a previously published protocol.¹⁶ Angiographic results were classified as complete occlusion, neck remnant, or aneurysm remnant.

Categoric variables were expressed as frequencies or percentages with 95% CIs. Quantitative variables were expressed with descriptive statistics.

RESULTS

Patients

Between December 19, 2016, and September 19, 2017, forty patients with 46 aneurysms were treated with the WEB 17 system. Three patients had 2 aneurysms, and 1 patient had 4 aneurysms. Of 46 aneurysms, 25 had ruptured (54%). There were 34 women and 6 men with a mean age of 62 years (median, 63 years; range, 46–87 years). Patient and aneurysm characteristics are shown in the On-line Table.

Aneurysm location was the anterior communicating artery in 17 patients; the middle cerebral artery in 13; the posterior communicating artery in 7; the pericallosal artery in 3; the basilar tip in 3; and the anterior choroidal artery, carotid tip, and superior cerebellar artery each in 1. The mean aneurysm size was 4.9 mm (median, 5 mm; range, 2–7 mm). WEB sizes and shapes used are shown in Fig 1.

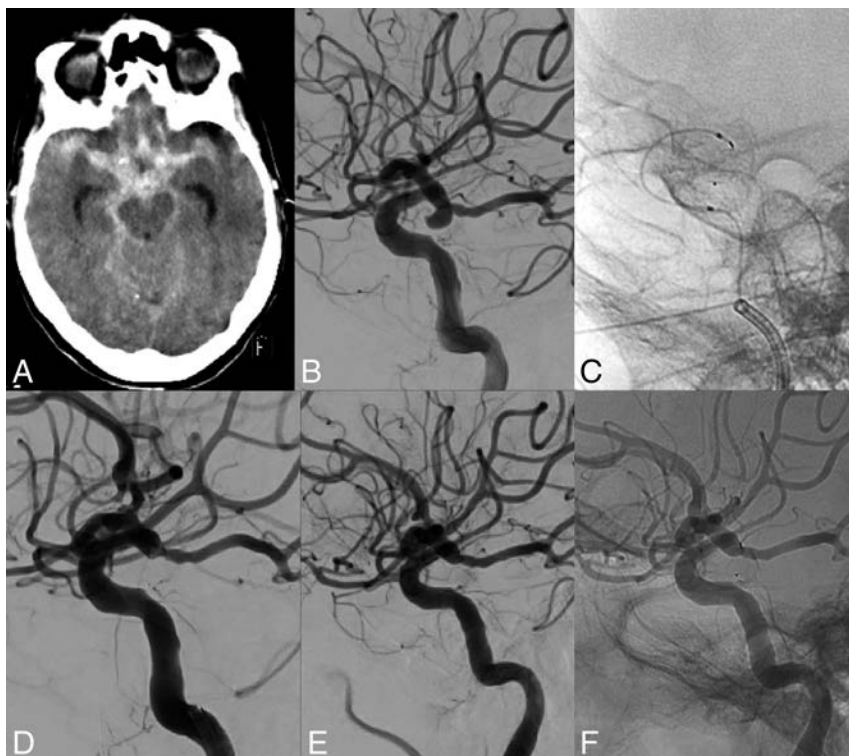


FIG 2. A 71-year-old woman (patient 32) with a ruptured posterior communicating artery aneurysm. A, CT scan shows diffuse subarachnoid blood. B, Lateral right internal carotid angiogram reveals a small posterior communicating artery aneurysm pointing downward. C, VIA 17 in a hairpin configuration after deployment of the WEB 17 SLS 6 mm inside the aneurysm. D, Immediate aneurysm occlusion after WEB 17 placement. E and F, Three-month follow-up angiogram demonstrates persistent complete aneurysm occlusion.

Initial Results and Complications

After WEB placement with sealing of the aneurysm neck, the position of the WEB inside the aneurysm was judged good in 45 of 46 aneurysms without filling of aneurysm remnants. In 1 patient (patient 10), the WEB was undersized, but this was only noticed after detachment. Follow-up angiography after 1 week showed an aneurysm remnant that was then occluded with coils.

There were 2 thromboembolic complications, both in patients with a ruptured anterior communicating artery aneurysm. In a 62-year-old man (patient 25), there was a thromboembolic occlusion of the carotid tip during diagnostic catheterization before WEB placement. This thrombus could be removed with thrombosuction. After the procedure, he had paresis of the left arm that resolved the next day. The other patient was a 54-year-old woman (patient 11) with an ICA dissection during diagnostic angiography followed by thrombotic occlusion of the left A2. During WEB placement, the thrombus migrated distally. After sealing of the aneurysm, she was treated with tirofiban infusion, and she woke up without a deficit.

There were no procedural ruptures. The overall permanent complication rate was 0% (0 of 40; 97.5% CI, 0%–10.4%).

Clinical and Imaging Follow-Up

All 15 patients with 21 unruptured aneurysms treated with WEB 17 remained clinically intact. In 25 patients with a ruptured aneurysm, no early or late rebleeds occurred. Clinical follow-up of these 25 patients was as follows: Six died due to sequelae of SAH (mRS 6), 1 was dependent (mRS 4), 5 had some disability but were independent (mRS 2 and 3), and 13 were independent (mRS 0 and 1).

Six patients died of SAH during hospital admission. Of the 34 surviving patients, 1 refused follow-up angiography. Of the remaining 33 patients, 31 with 37 aneurysms had 3 month-angiographic follow-up. Two patients had MRA follow-up at 3 months. Thus, imaging follow-up at 3 months was available in 33 patients with 39 aneurysms (97.5% of 40 eligible aneurysms).

Two aneurysms (5.1%) were incompletely occluded: Patient 10 had early additional treatment of the WEB 17–treated ruptured aneurysm. At 3-month follow-up, the aneurysm had reopened and was again retreated, now with a WEB 17. One other aneurysm (patient 33) showed persistent WEB filling at 3 months.

Complete occlusion was achieved in 28 of 39 aneurysms (72%), and 9 aneurysms (23%) showed a neck remnant.

Extended MRA follow-up at 6 months was available in 22 aneurysms (Online Table). The occlusion status of those aneurysms was not changed during the time interval.

DISCUSSION

Our preliminary clinical experience with the new low-profile WEB 17 system demonstrates an encouraging safety and efficacy profile. No permanent procedural complications occurred in 40 patients, and no rebleeds occurred in 25 patients with a ruptured aneurysm. Aneurysm occlusion at follow-up was satisfactory with 95% adequate occlusion at 3 months with only 1 aneurysm retreated. Two procedural thromboembolic complications occurred that could be resolved with thrombosuction and tirofiban use and remained without clinical sequelae.

Comparison with other studies is hampered by several factors. The small sample size of this study keeps confidence levels wide. Both ruptured and unruptured aneurysms were included. All aneurysms were small (≤ 7 mm) because the maximum size of the WEB 17 is 7 mm. Because larger aneurysm size is a well-known risk factor for reopening with time, our study only comprising small aneurysms has a bias toward better results at follow-up.

Our first results with the WEB 17 are in line with other studies using previous generations of the WEB or coils to treat intracranial aneurysms.^{1–14} In a meta-analysis by Asnafi et al,⁷ 15 uncontrolled series were included, totaling 565 patients with 588 aneurysms treated with the WEB, of which 127 were ruptured. Initial complete and adequate occlusion rates were 27% and 59%, respectively. Mid-term complete and adequate occlusion rates after a median of 7 months were 39% and 85%, respectively. Perioperative morbidity and mortality rates were 4% and 1%, respectively. Midterm adequate occlusion rates for ruptured aneurysms were 85% compared with 84% for unruptured aneurysms. Both patients with ruptured aneu-

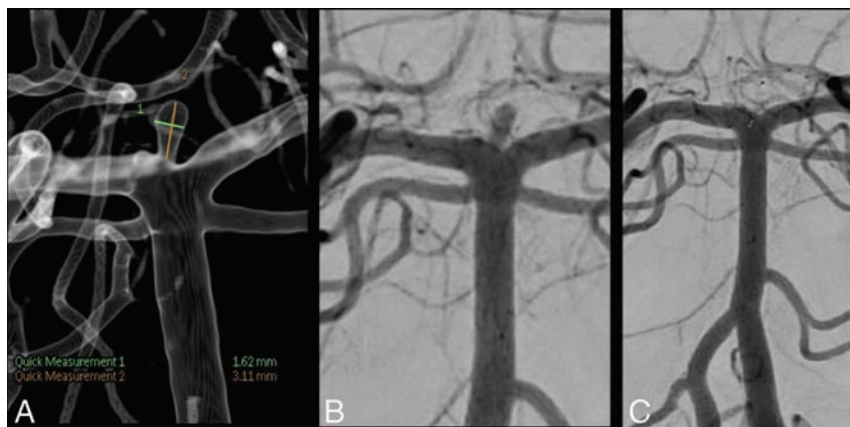


FIG 3. A 62-year-old woman (patient 36) with an unruptured small basilar tip aneurysm. A, Basilar tip aneurysm measuring 1.6×3.1 mm. B, Immediately after placement of WEB 17 (2×3 mm). C, Complete occlusion at 3 months follow-up.

rysms and patients with unruptured aneurysms had perioperative morbidity rates of 2%. Our results of 95% adequate occlusion at 3 months are in the same range as in this meta-analysis, and complication rates were on the same order.

Subjectively, handling of the WEB 17 is smoother than the WEB 21. The WEB 17 is easily introduced through the VIA 17 microcatheter with very low resistance. Unsheathing and deploying the WEB 17 in the aneurysm is smooth, and recapturing is easy with only a little pulling force needed. Because the WEB 17 has fewer and thinner wires than the WEB 21 with weaker memory forces, deployment may sometimes be incomplete, especially when the WEB is angled or rotated. The softer WEB structure makes deformation by pushing or pulling forces easier than with the WEB 21. On the other hand, navigation with the VIA 17 is simpler than with the more rigid VIA 21 microcatheter. The VIA 17 is advantageous in complicated anatomy such as navigating a sharp-angled carotid artery–A1 transition or in situations where a “hairpin” position of the microcatheter is required such as in some posterior communicating artery aneurysms (Fig 2). With very small aneurysms of 2–3 mm, use of the WEB 17 in the smallest sizes is imperative (Fig 3).

There is overlap in WEB 17 and 21 in the 4- to 7-mm sizes. When a WEB in this size range is required to treat the aneurysm, the operator has a choice between the 2 systems. The WEB 21 system is more stable during WEB deployment, and the WEB 21 has better memory forces. Instead, the WEB 17 system can be navigated more easily in complicated anatomy. These considerations may help the operator in the choice between the 2 systems.

Our study confirms the conceptual proof of the WEB 17 system. Despite the construction with fewer platinum-cored nitinol wires, flow disruption proved excellent, with only 1 aneurysm showing persistent WEB filling at follow-up. Adequate aneurysm occlusion was obtained in 95% of aneurysms with imaging follow-up, and no rebleeds occurred in the 25 ruptured aneurysms during clinical follow-up. There were no permanent complications.

Recently, a new intrasaccular flow disruptor has become available in clinical practice (Medina Embolization Device; Medtronic, Minneapolis, Minnesota). This device combines the design of a detachable coil and that of an intrasaccular flow-disruption device. For now, clinical experience is limited, and the first results are encouraging.¹⁷

Our study has several limitations. The limited sample size makes confidence intervals wide and hampers comparison with other studies. Patients were not consecutive but were selected on the basis of the anticipated suitability of the aneurysm for the WEB 17. We, not a core lab, established aneurysm occlusion at follow-up. The follow-up period was limited; this drawback precludes conclusions of effectiveness at mid- and long term. The essential choice of small and very small aneurysms is a bias toward better results at follow-up. Strong points of the study are the complete clinical and almost complete imaging follow-up.

CONCLUSIONS

The new low-profile WEB 17 system is a welcome addition to the existing WEB range. Indications expand to very small aneurysms. The supple VIA 17 microcatheter navigates well in situations with difficult vascular geometry. In the 4- to 7-mm size, there is overlap of the WEB 17 and 21, and the operator may choose between the 2 systems depending on patient-specific factors.

Disclosures: S.B.T. van Rooij—RELATED: Grant: MicroVention, Comments: support of salary and travel expenses directly related to the study.* W.J. van Rooij—RELATED: Consulting Fee or Honorarium: MicroVention; Support for Travel to Meetings for the Study or Other Purposes: MicroVention. *Money paid to the institution.

REFERENCES

1. Armoiry X, Turjman F, Hartmann DJ, et al. **Endovascular treatment of intracranial aneurysms with the WEB device: a systematic review of clinical outcomes.** *AJNR Am J Neuroradiol* 2016;37:868–72 [CrossRef Medline](#)
2. Sivan-Hoffmann R, Gory B, Riva R, et al. **One-year angiographic follow-up after WEB-SL endovascular treatment of wide-neck bifurcation intracranial aneurysms.** *AJNR Am J Neuroradiol* 2015;36:2320–24 [CrossRef Medline](#)
3. Lawson A, Goddard T, Ross S, et al. **Endovascular treatment of cerebral aneurysms using the Woven EndoBridge technique in a single center: preliminary results.** *J Neurosurg* 2017;126:17–28 [CrossRef Medline](#)
4. Lawson A, Molyneux A, Sellar R, et al. **Safety results from the treatment of 109 cerebral aneurysms using the Woven EndoBridge technique: preliminary results in the United Kingdom.** *J Neurosurg* 2018;128:144–53 [CrossRef Medline](#)
5. Gherasim DN, Gory B, Sivan-Hoffmann R, et al. **Endovascular treatment of wide-neck anterior communicating artery aneurysms using WEB-DL and WEB-SL: short-term results in a multicenter study.** *AJNR Am J Neuroradiol* 2015;36:1150–54 [CrossRef Medline](#)
6. Fiorella D, Molyneux A, Coon A, et al; WEB-IT Study Investigators. **Demographic, procedural and 30-day safety results from the WEB Intra-saccular Therapy Study (WEB-IT).** *J Neurointerv Surg* 2017;9:1191–96 [CrossRef Medline](#)
7. Asnafi S, Rouchaud A, Pierot L, et al. **Efficacy and safety of the Woven EndoBridge (WEB) device for the treatment of intracranial aneurysms: a systemic review and meta-analysis.** *AJNR Am J Neuroradiol* 2016;37:2287–92 [CrossRef Medline](#)
8. Pierot L, Moret J, Turjman F, et al. **WEB treatment of intracranial aneurysms: clinical and anatomic results in the French Observatory.** *AJNR Am J Neuroradiol* 2016;37:655–59 [CrossRef Medline](#)

9. Pierot L, Spelle L, Molyneux A, et al. **Clinical and anatomical follow-up in patients with aneurysms treated with the WEB device: 1-year follow-up report in the cumulated population of 2 prospective, multicenter series (WEBCAST and French Observatory).** *Neurosurgery* 2016;78:133–41 [CrossRef Medline](#)
10. Pierot L, Costalat V, Moret J, et al. **Safety and efficacy of aneurysm treatment with WEB: results of the WEBCAST study.** *J Neurosurg* 2016;124:1250–56 [CrossRef Medline](#)
11. Clajus C, Strasilla C, Fiebig T, et al. **Initial and mid-term results from 108 consecutive patients with cerebral aneurysms treated with the WEB device.** *J Neurointerv Surg* 2017;9:411–17 [CrossRef Medline](#)
12. Pierot L, Gubucz I, Buhk JH, et al. **Safety and efficacy of aneurysm treatment with the WEB: results of the WEBCAST 2 study.** *AJNR Am J Neuroradiol* 2017;38:1151–55 [CrossRef Medline](#)
13. Liebig T, Kabbasch C, Strasilla C, et al. **Intrasaccular flow disruption in acutely ruptured aneurysms: a multicenter retrospective review of the use of the WEB.** *AJNR Am J Neuroradiol* 2015;36:1721–27 [CrossRef Medline](#)
14. Popielski J, Berlis A, Weber W, et al. **Two-center experience in the endovascular treatment of ruptured and unruptured aneurysms using the WEB device: a retrospective analysis.** *AJNR Am J Neuroradiol* 2018;39:111–17 [CrossRef Medline](#)
15. van Rooij SB, van Rooij WJ, Peluso JP, et al. **WEB treatment of ruptured intracranial aneurysms: a single-center cohort of 100 aneurysms.** *AJNR Am J Neuroradiol* 2017;38:2282–87 [CrossRef Medline](#)
16. Majoie CB, Sprengers ME, van Rooij WJ, et al. **MR angiography at 3T versus digital subtraction angiography in the follow-up of intracranial aneurysms treated with detachable coils.** *AJNR Am J Neuroradiol* 2005;26:1349–56 [Medline](#)
17. Sourour NA, VandePerre S, Maria FD, et al. **Medina embolization device for the treatment of intracranial aneurysms: safety and angiographic effectiveness at 6 months.** *Neurosurgery* 2018;82:155–62 [CrossRef Medline](#)

Long-Term Outcomes of Patients with Stent Tips Embedded into Internal Carotid Artery Branches during Aneurysm Coiling

 S.P. Ban,  O.-K. Kwon,  S.U. Lee,  J.S. Bang,  C.W. Oh,  H.J. Jeong,  M.J. Cho,  E.-A. Jeong, and  T. Kim



ABSTRACT

BACKGROUND AND PURPOSE: During stent-assisted coiling of ICA aneurysms, stent tips are sometimes unintentionally embedded into ICA branches. Stent tips can be visualized because they have radiopaque markers. Concerns regarding stent tip misplacement include risks of artery perforation and occlusion. The aim of this study was to evaluate the long-term outcomes of ICA branches with embedded stent tips.

MATERIALS AND METHODS: ICA branches with embedded stent tips were identified among 35 patients with unruptured ICA aneurysms treated with stent-assisted coiling between November 2003 and November 2014. Patient clinical and angiographic outcomes associated with the embedded stent tip were analyzed.

RESULTS: Most of the 35 studied aneurysms were paraclinoid ICA aneurysms ($n = 30$). The most commonly involved ICA branch was the posterior communicating artery (26 patients, 74.3%), followed by the anterior choroidal artery (8 patients, 22.9%) and ophthalmic artery (1 patient, 2.9%). During the follow-up period (38.6 ± 17.9 months), no new neurologic deficits developed. Neither hemorrhagic nor thromboembolic events occurred. Angiography was performed during the final follow-up evaluation at a mean of 32.7 ± 18.0 months, and all ICA branches with embedded stent tips showed patent blood flow without severe luminal narrowing.

CONCLUSIONS: In our experience, placement of a stent tip into ICA branches during stent-assisted coiling was not associated with any major adverse events.

ABBREVIATIONS: AChA = anterior choroidal artery; OphA = ophthalmic artery; PcomA = posterior communicating artery; SAC = stent-assisted coiling

Self-expandable stents have provided considerable assistance in increasing the indications for aneurysm coiling. Complex and wide-neck aneurysms, which are considered challenging or impossible to treat with simple coiling, can now be treated.¹

Generally, self-expandable stents for cerebral aneurysm treatment have proximal and distal radiopaque markers to identify the end of the stent. These markers are made from coiled tantalum wire or platinum bands, which are larger than the stent strut itself. The markers are attached to the triangular pointed stent tip wire (strut) part. During stent-assisted coiling (SAC), the stent tip can sometimes be unintentionally em-

bedded into a small arterial branch. We have occasionally encountered this event, particularly during SAC performed for ICA aneurysms, which is well-visualized due to the radiopaque markers. This phenomenon raises concerns regarding the potential risks of arterial perforation due to the sharp end and constant arterial pulsating motion of the stent, as well as the chances of vessel occlusion. Stent tip markers may also disrupt blood flow by themselves or by intimal injury (thrombus formation or intimal hyperplasia), which may then lead to infarction. Despite these concerns, we were unable to find a report regarding the clinical or radiologic outcomes of embedded stent tips within ICA branches. Thus, we reviewed our series of patients who had undergone SAC for unruptured ICA aneurysms and in whom stent tips were embedded within the ICA branch orifice. We analyzed clinical and angiographic data to identify the outcomes of these cases.

MATERIALS AND METHODS


Patients

This study was approved by the institutional review board at our institution. Informed consent from enrolled patients was waived.

Received November 7, 2017; accepted after revision January 3, 2018.

From the Department of Neurosurgery, Seoul National University Bundang Hospital, Seongnam, Gyeonggi-do, Korea.

Please address correspondence to Tackeun Kim, MD, Department of Neurosurgery, Seoul National University Bundang Hospital, 82 Gumi-ro 173 beon-gil, Bundang-gu, Seongnam-si, Gyeonggi-do, 13620, Korea; e-mail: midabo@naver.com

 Indicates article with supplemental on-line table.

<http://dx.doi.org/10.3174/ajnr.A5583>

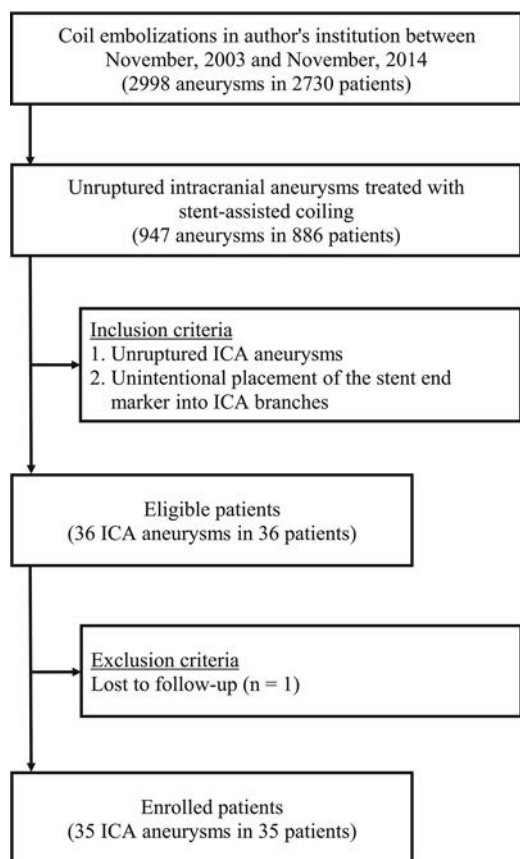


FIG 1. Outline of patient selection.

We retrospectively reviewed patient medical records, including pre- and posttreatment radiologic studies. Our data base contained a series of 2730 patients with 2998 intracranial aneurysms treated with endovascular techniques between November 2003 and November 2014. Among these patients, 886 with 947 unruptured intracranial aneurysms were treated with SAC. In this series, data from 664 patients with 706 ICA aneurysms who were treated with SAC were collected and reviewed. Among these patients, the placement of a stent tip into an ICA branch was identified in 36 aneurysms of 36 patients. In our subsequent analysis, 1 patient who was lost to follow-up was excluded. The patient selection criteria are outlined in Fig 1.

Antiplatelet Therapy Protocol and Endovascular Procedures

Patients with unruptured aneurysms received dual antiplatelet agents (100 mg of aspirin and 75 mg of clopidogrel) for at least 5 days before embolization. One day before coil embolization, P2Y₁₂ reaction units were measured using VerifyNow (Accumetrics, San Diego, California). Patients with clopidogrel resistance (>220 P2Y₁₂ reaction units) received a modified antiplatelet regimen. Details regarding our antiplatelet agent protocol have been previously described.² A 3000-IU bolus dose of intravenous heparin was administered after the placement of the femoral artery sheath, and heparin was later infused at an hourly booster dose of 1000 IU, with monitoring of the activated clotting time. After the procedure, dual antiplatelet treatment continued for 1 year; after

1 year, this therapy was exchanged for daily oral treatment with 100 mg of aspirin for an additional year.

All endovascular procedures were performed with the patient under general anesthesia using an Integris Allura scanner (Philips Healthcare, Best, the Netherlands) before 2014 and an IFNX-8000V scanner (Toshiba, Tokyo, Japan) from 2014. The jailing technique was mainly used for SAC. First, a target aneurysm was selected using a microcatheter (Excelsior SL-10; Stryker Neurovascular, Kalamazoo, Michigan). Then, the parent artery was navigated with another microcatheter (Prowler Select Plus, Codman & Shurtleff, Raynham, Massachusetts; or Neuro Renegade, Stryker Neurovascular) for stent delivery. A stent was deployed into the parent artery across the aneurysm neck. Then, the aneurysm was coiled using platinum detachable coils until complete occlusion was achieved or further coiling was deemed unsafe. Stent type, length, and placement were determined by the neurovascular team and were based on aneurysm location and neck diameter. Among 706 ICA aneurysms treated with SAC, Enterprise stents (Codman & Shurtleff) were most commonly used ($n = 607$, 86.0%), followed by Neuroform stents (Stryker Neurovascular) in 71 cases (10.1%). The other stents used included Low-Profile Visualized Intraluminal Support stents (MicroVention, Tustin, California) in 19 cases (2.7%) and Solitaire AB stents (Covidien, Irvine, California) in 9 cases (1.3%). Of the 35 cases, 32 were treated with a single Enterprise stent and 3 were treated with a single Neuroform stent.

Stent Tips of Enterprise and Neuroform Stents

The Enterprise stent is a laser-cut stent with a closed-cell design. This stent has flared proximal and distal ends, consisting of 4 pointed parts. Each end has 4 radiopaque tantalum coil markers for increased visibility, which flare out for fixation of the stent onto the vascular wall when fully deployed (Fig 2A). Due to the sharp, pointed, flaring parts, these stents can be embedded into the small ICA branches. The radiopaque markers of the tips allow them to be clearly visualized. The diameter of a radiopaque marker was thicker than that of the stent strut. Stent strut width and thickness were approximately 0.0015 inches (0.0381 mm) and 0.0031 inches (0.0787 mm), respectively. The thickness and length of the radiopaque marker were approximately 0.008 inches (0.2032 mm) and 0.043 inches (1.0922 mm), respectively (Fig 2B, -C).

The Neuroform stent is a laser-cut stent with an open-cell or half-open-cell design. This stent has 4 distal and 4 proximal radiopaque platinum markers (Fig 2D). Each open-cell segment may serve as a separate fixing device to enhance the apposition of the stent to the vessel wall like the flared ends of the Enterprise stent. Like the Enterprise stent, the stent tip may be placed and embedded into the branch orifice. Stent strut width and thickness were approximately 0.0027 inches (0.0686 mm). The thickness and length of the radiopaque marker were approximately 0.0116 inches (0.2946 mm) and 0.030 inches (0.762 mm), respectively (Fig 2E, -F).

Evaluation of Clinical and Radiologic Outcomes

The clinical outcomes of all patients were evaluated using the mRS score on admission and at the final outpatient follow-up visit.

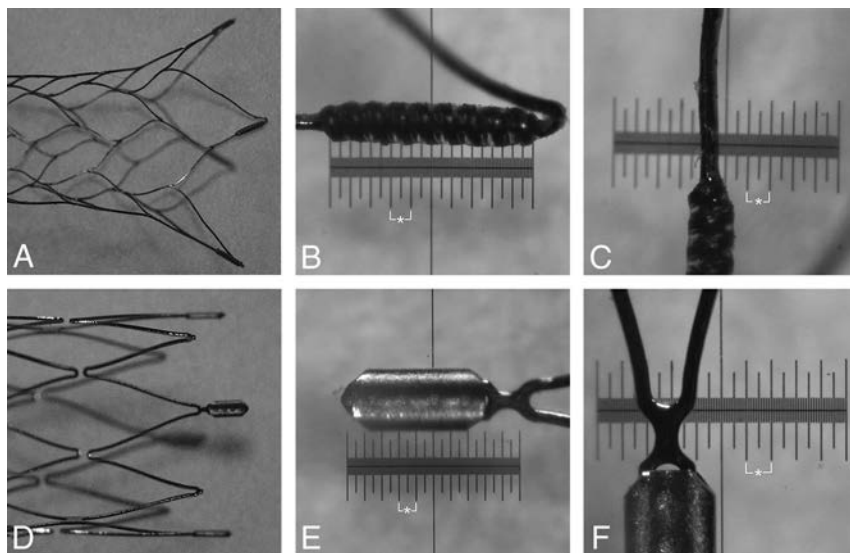


FIG 2. A, Flared ends of the Enterprise stent. B, Length of the flare marker of the Enterprise stent. C, Width of the flare marker and stent strut of the Enterprise stent. D, End of the Neuroform stent. E, Length of the platinum marker of the Neuroform stent. F, Width of the platinum marker and stent strut of the Neuroform stent. Asterisk indicates 0.1 mm.

Newly developed neurologic deficits as well as hemorrhagic and thromboembolic complications during follow-up periods were also reviewed. The placement and embedding of a stent tip with a marker into a branching artery was defined as a stent tip that was placed at the level of branching arteries, with the tip marker clearly visualized within the artery orifice via angiographic views, including rotational angiograms. According to our institutional protocol, patients underwent imaging follow-up at 3, 6, 12, 24, and 36 months with skull plain radiography and at 1, 2, and 3 years with 3D-TOF MRA, including source imaging. Any time a major recanalization was found, DSA was performed. DSA follow-up studies were routinely conducted between 3 and 5 years after coil embolization if no major recanalization of an aneurysm was suspected. In this study, each patient underwent a minimum of 12 months of radiologic follow-up. Vessel patency was documented by follow-up DSA. If follow-up DSA was not performed, vessel patency was confirmed using the follow-up axial MRA source images.

Data Analysis

All statistical analyses were performed using SPSS software (Version 22.0; IBM, Armonk, New York). Continuous variables are presented as mean \pm SD. Binary variables were compared using the Fisher exact test. Statistical significance was set at $P < .05$.

RESULTS

The overview of patients with stent tips embedded into the ICA branches is summarized in the On-line Table. Eight (22.9%) patients were men, and 27 (77.1%) were women. The mean age was 49.3 ± 12.8 years (range, 21–76 years). The cases included 30 (85.7%) paraclinoid ICA aneurysms, 3 (8.6%) ophthalmic artery (OphA) aneurysms, 1 (2.9%) cavernous ICA aneurysm, and 1 (2.9%) posterior communicating artery (PcomA) aneurysm. The most common ICA branching artery with an embedded stent tip

was the PcomA (26 patients, 74.3%). Other involved branching arteries included the anterior choroidal artery (AchoA) in 8 (22.9%) patients and the OphA in 1 (2.9%) patient. The incidence of stent tips embedded within ICA branches was not associated with the type of stent (closed-cell-design stent, 5.3%, versus open-cell-design stent, 4.2%; $P = .424$). Most of these events occurred during deployment of the distal end of the stent at the upward ICA curvature near the ICA branches (32 cases, 91.4%), followed by unintentional stent advancement during microcatheter manipulation (3 cases, 8.6%).

The mean clinical follow-up duration was 38.6 ± 17.9 months (range, 12–91 months). The preoperative mRS score was 0 in 30 (85.7%) patients and 1 in 5 (14.3%) patients. The final follow-up mRS score was 0 in 32 (91.4%) patients and 1 in 3 (8.6%) patients. No

patient experienced mRS score deterioration. No newly developed neurologic deficits were observed. Neither hemorrhagic nor thromboembolic (or ischemic) complications occurred during the follow-up period.

The mean angiographic follow-up duration was 32.7 ± 18.0 months (range, 12–91 months). The mean initial diameter of the ICA branches with embedded stent tips was 1.79 ± 0.69 mm (range, 0.51–2.81 mm). On final follow-up angiography (15 cases were measured by MRA with source imaging and 20 cases were measured by DSA), all ICA branches with an embedded stent tip had persistent blood flow without severe luminal narrowing. In 1 case, the radiopaque stent marker appeared to penetrate the PcomA. In the angiogram, the marker appeared to be located outside the arterial wall. However, no clinical event was observed (case 11).

Illustrative Cases

Case 11. A 64-year-old patient presented with an unruptured left paraclinoid ICA aneurysm (Fig 3A, -B). The aneurysm was treated with coil embolization using a 4.5×20 mm Neuroform stent. Postembolization angiography showed the placement of the stent marker in the PcomA (Fig 3C, -D). Although a radiopaque stent marker appeared to penetrate the PcomA in the 5-year-follow-up angiograms, the PcomA was patent and no hemorrhagic complication occurred (Fig 3E, -F).

Case 13. A 23-year-old patient presented with an unruptured left paraclinoid ICA aneurysm (Fig 4A, -B). The aneurysm was treated with coil embolization using a 4.5×22 mm Enterprise stent. Postembolization angiography showed the placement of the stent marker into the AchoA (Fig 4C, -D). Follow-up angiography at 3 years showed patent blood flow to the AchoA without severe luminal narrowing (Fig 4E, -F).

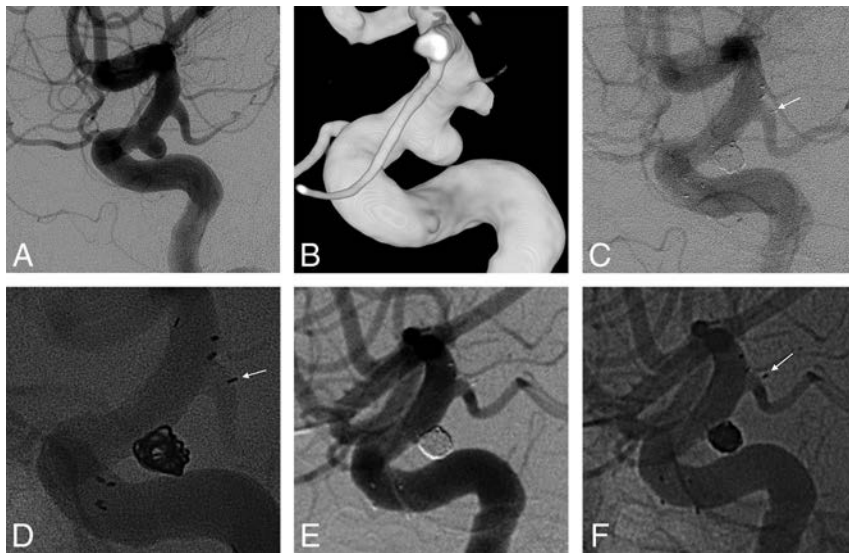


FIG 3. A, An unruptured left paraclinoid ICA aneurysm on pre-embolization DSA. B, 3D image of the aneurysm. C and D, A distal stent marker of the Neuroform stent (arrow) is deployed into the posterior communicating artery, as shown on postembolization angiography. E and F, The blood flow to the PcomA with malposition of the stent marker is patent on 5-year-follow-up cerebral angiography. A radiopaque stent marker appears to penetrate the PcomA (arrow).

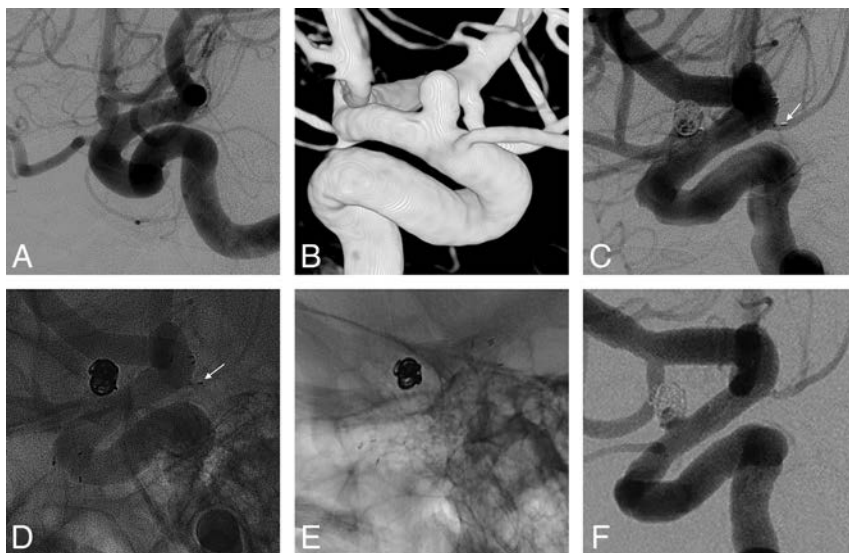


FIG 4. A left paraclinoid ICA aneurysm is shown on pre-embolization DSA (A) and 3D imaging (B). C and D, Postembolization angiography shows the malposition of the Enterprise stent marker in the anterior choroidal artery (arrow). E and F, Follow-up cerebral angiography at 3 years shows persistent blood flow to the AchoA.

DISCUSSION

This study demonstrates that stent tip embedding into the ICA branches during SAC of cerebral aneurysms was not associated with any major adverse events. No arterial rupture or occlusion was observed during at least 1 year (12–91 months) of follow-up.

During SAC of ICA aneurysms, stent tips can be deployed and unintentionally embedded into ICA branching arteries due to their characteristics. In our study, the incidence of this event was 5.1%, and the PcomA was the most commonly involved ICA branch, followed by the AchoA. Although we attempted to deploy stents so as avoid embedding the stent tip into the orifice of these

ICA branches, the distal part of a stent may be deployed flat around the PcomA and AchoA due to the ICA curvature, resulting in stent tips embedding into these ICA branches. In this study, this issue was the most common cause of an embedded stent tip within ICA branches (91.4%). Because the ICA usually starts to curve upward near the PcomA and the diameter of the PcomA is commonly larger than that of the AchoA, it is likely that the stent tips are more easily embedded into the PcomA than into the AchoA.

Regarding the structure of the stents, because a closed-cell-design stent immediately transmits a force from one end to the other end, embedding of a stent tip into ICA branches due to stent advancement during microcatheter manipulation may be more commonly observed in patients receiving a closed-cell-design stent. Concerning this possible mechanism, in this study, all 3 cases (8.6%) in which the distal part of a stent was initially deployed proximally near the PcomA and then advanced and embedded into the PcomA due to microcatheter manipulation were treated with the Enterprise stent (closed-cell design). However, because the most common cause of embedding of a stent tip into ICA branches was the ICA curvature, no association was observed among the types of stents used in this study.

This event raises the following concerns: vessel rupture (perforation) and occlusion. Vessel rupture due to the forceful advancement of stents has been reported. The sharp ends of the stent may contribute to arterial rupture.^{3,4} The lack of this complication in our study suggests that stent ends were inserted into the branching arteries without excessive force. The presence of an

embedded stent tip in small arteries can be a risk factor for further arterial injury with persistent arterial pulsation, at least theoretically. However, this study shows that this risk is not likely in practice.

Vessel occlusion or significant flow disruption may develop through intimal injury by the stent tip in a delayed manner as well as mechanical occlusion by stent tips and large markers themselves during the acute period. Therefore, we can consider several plausible mechanisms of vessel occlusion or flow disruption. A stent covering the small arterial ostium does not usually lead to arterial occlusion.^{5–7} Unlike a simple stent covering the arterial

orifice, embedded stent tips have greater luminal occupancy due to the sharp triangular stent tip labeled with a radiopaque marker. Radiopaque markers at the stent tip have a larger area and volume than the stent. In a coronary artery study of a swine model, 2-fold thicker stents were 49% more thrombogenic and increased flow stagnation and disruption.⁸ Stent markers are 5.3-fold thicker than the stent strut in the Enterprise stent and 4.3-fold thicker than the stent strut in the Neuroform stent. In addition, persistent arterial pulsation with stent tips at the arterial orifice may also lead to further repeat intimal injury and subsequent thrombus formation and neointimal hyperplasia.^{4,9} However, this issue was not detected in our series of patients. The triangular shape of the stent tip may reduce such risks by stopping further advancement of the stent strut into the arterial lumen. The persistent need for blood flow to the ICA branches may also help prevent occlusion or severe stenosis.¹⁰

Furthermore, luminal narrowing by intimal hyperplasia may be spontaneously reversed.¹¹ The proliferated neointima reaches a maximal thickness by 2 months, and this neointimal layer gradually becomes thin, more sclerotic, and less cellular by 8 months. Kim et al⁹ reported that most in-stent stenoses would spontaneously improve to 91% of the initial mean diameter after 24 months. In our series, we did not perform angiographic follow-up until 12 months after SAC. Thus, luminal narrowing before this time was not confirmed. However, neither ischemic symptoms nor infarction developed in our study. One case (case 11) showed a radiopaque stent marker that appeared to be outside the PcomA lumen on 5-year-follow-up angiographic images. It is uncertain whether the stent tip was located outside the artery. However, no clinical symptoms or radiologic findings associated with arterial rupture were observed immediately after coiling, which suggests that the marker was more likely inside the artery and encased by neointimal hyperplasia. Although the mechanism has not yet been clearly determined, this study demonstrates that vessel occlusion by an embedded stent tip into the lumen is not common in practice.

Our study has several limitations including its retrospective nature and small sample size from a single institution. Furthermore, this study showed only the results of placement of stent markers from Enterprise and Neuroform stents, which are only 2 varieties among many expandable stents. In 15 cases, follow-up imaging was performed with TOF-MRA according to our institutional protocol. Although the patency of ICA branches with embedded stent tips was confirmed by MRA images, we did not show the changes in the diameters of ICA branches with embedded stent tips because this would be inaccurate due to the metal artifacts of the embedded stent tip on MRA images. Further research

using computational fluid dynamics is warranted to more completely understand the changes in the diameter of ICA branches with embedded stent tips and the difference in the flow disturbance effect between stent struts and radiopaque markers.

CONCLUSIONS

In our experience, placement of a stent tip into ICA branches during SAC was not associated with any major adverse events. During 12–91 months of follow-up, vessel rupture, significant blood flow reduction, and arterial occlusion were not detected.

REFERENCES

1. Geyik S, Yavus K, Yurttutan N, et al. **Stent-assisted coiling in endovascular treatment of 500 consecutive cerebral aneurysms with long-term follow-up.** *AJNR Am J Neuroradiol* 2013;34:2157–62 [CrossRef Medline](#)
2. Hwang G, Huh W, Lee JS, et al. **Standard vs modified antiplatelet preparation for preventing thromboembolic events in patients with high on-treatment platelet reactivity undergoing coil embolization for an unruptured intracranial aneurysm: a randomized clinical trial.** *JAMA Neurol* 2015;72:764–72 [CrossRef Medline](#)
3. Chalouhi N, Jabbour P, Singhal S, et al. **Stent-assisted coiling of intracranial aneurysms: predictors of complications, recanalization, and outcome in 508 cases.** *Stroke* 2013;44:1348–53 [CrossRef Medline](#)
4. Wang CC, Li W, Feng ZZ, et al. **Preliminary experience with stent-assisted coiling of aneurysms arising from small (<2.5 mm) cerebral vessels using the Low-Profile Visualized Intraluminal Support Device.** *AJNR Am J Neuroradiol* 2017;38:1163–68 [CrossRef Medline](#)
5. D'Urso PI, Lanzino G, Cloft HJ, et al. **Flow diversion for intracranial aneurysms: a review.** *Stroke* 2011;42:2363–68 [CrossRef Medline](#)
6. Masuo O, Terada T, Walker G, et al. **Study of the patency of small arterial branches after stent placement with an experimental in vivo model.** *AJNR Am J Neuroradiol* 2002;23:706–10 [Medline](#)
7. Seong J, Wakhloo AK, Lieber BB. **In vitro evaluation of flow diverters in an elastase-induced saccular aneurysm model in rabbit.** *J Biomech Eng* 2007;129:863–72 [CrossRef Medline](#)
8. Kolandaivelu K, Swaminathan R, Gibson WJ, et al. **Stent thrombogenicity early in high-risk interventional settings is driven by stent design and deployment and protected by polymer-drug coatings.** *Circulation* 2011;123:1400–09 [CrossRef Medline](#)
9. Kim YS, Lee SW, Yeom JA, et al. **Angiographic findings of in-stent intimal hyperplasia after stent-assisted coil embolization: are they permanent findings?** *J Neurosurg* 2016;124:328–33 [CrossRef Medline](#)
10. Iosif C, Berg P, Ponsonnard S, et al. **Role of terminal and anastomotic circulation in the patency of arteries jailed by flow-diverting stents: animal flow model evaluation and preliminary results.** *J Neurosurg* 2016;125:898–908 [CrossRef Medline](#)
11. Schatz RA, Palmaz JC, Tio FO, et al. **Balloon-expandable intracoronary stents in the adult dog.** *Circulation* 1987;76:450–57 [CrossRef Medline](#)

Factors Influencing Confidence in Diagnostic Ratings and Retreatment Recommendations in Coiled Aneurysms

 M. Ernst,  L. Kriston,  M. Groth,  A.M. Frölich,  J. Fiehler, and  J.-H. Buhk



ABSTRACT

BACKGROUND AND PURPOSE: Angiographic occlusion and retreatment of coiled aneurysms are commonly used as surrogate end points in clinical trials. We aimed to evaluate the influence of aneurysm, patient, and rater characteristics on the confidence of visual evaluation of aneurysm coiling and retreatment decisions.

MATERIALS AND METHODS: Twenty-six participants of the Advanced Course in Endovascular Interventional Neuroradiology of the European Society of Neuroradiology were asked to evaluate digital subtraction angiography examinations of patients who had undergone endovascular coiling, by determining the grade of aneurysm occlusion, the change between immediate postprocedural and follow-up angiograms, their level of confidence, the technical difficulty of retreatment, and the best therapeutic approach. The experience, knowledge, and skills of each participant were assessed. The influence of rater and case characteristics on indicated confidence in diagnostic ratings and retreatment recommendations was analyzed.

RESULTS: Interrater reliability was moderate regarding the assessment of aneurysm occlusion grade (intraclass correlation coefficient = 0.581) and substantial regarding change (intraclass correlation coefficient = 0.776). Overall confidence in the diagnostic rating was high (median, “very certain”). Confidence was statistically significantly higher in cases that were generally rated as “worse.” The odds of recommending retreatment were significantly higher in cases that were generally rated with higher mean confidence.

CONCLUSIONS: Although overall confidence in the diagnostic rating was high, our study confirms the suboptimal interrater reliability of visual assessment of aneurysm occlusion as well as retreatment recommendations, rendering both questionable as primary outcome measures. Besides recurrence status, recommendation of retreatment is significantly influenced by patient age, aneurysm neck width, and characteristics of the therapist.

ABBREVIATION: ICC = intraclass correlation coefficient

An important drawback of aneurysm coiling is the possibility of recurrence with a rerupture risk. Previous studies found a low interobserver variability regarding the visual assessment of aneurysm occlusion.^{1,2} In a recent meta-analysis, the interrater reliability of the visual rating of aneurysm occlusion was found to vary significantly as a function of imaging methods, grading scales, occlusion rates, and their interaction.³

Little is known about the confidence of the observers in their ratings, which will probably also influence the retreatment decision in the individual case. However, aneurysm retreatment rate has also been used as a study end point.⁴ Recent studies reported a low interrater reliability of retreatment recommendations in coiled aneurysms^{5,6}; and to this date, there are no guidelines about when and how to retreat a coiled aneurysm. Medical decision-making is a central aspect of neurovascular interventions, and studies analyzing this complex and multifactorial process are limited. A variety of factors such as cognitive biases, personal experiences, prior training, and medicolegal considerations affect decision-making.⁷

We aimed to assess the interrater reliability and the confidence of diagnostic ratings as well as the interrater reliability of retreatment decisions. In a second step, we aimed to evaluate the influence of aneurysm, patient, and rater characteristics on, first, the certainty of visual evaluation of aneurysm coiling and, second, retreatment decisions.

Received November 4, 2017; accepted after revision January 3, 2018.

From the Department of Diagnostic and Interventional Neuroradiology (M.E., M.G., A.M.F., J.F., J.-H.B.), Center for Radiology and Endoscopy, and Department of Medical Psychology (L.K.), University Medical Center Hamburg-Eppendorf, Hamburg, Germany.

Please address correspondence to Marielle Ernst, MD, Department of Diagnostic and Interventional Neuroradiology, University Medical Center Hamburg-Eppendorf, Haus Ost 22 (O22), Martinistr 52, 20246 Hamburg, Germany; e-mail: m.ernst@uke.de

 Indicates article with supplemental on-line appendix and table.

<http://dx.doi.org/10.3174/ajnr.A5581>

MATERIALS AND METHODS

Setting

The study was performed with 26 participants of the Advanced Course in Endovascular Interventional Neuroradiology of the European Society of Neuroradiology, held in Hamburg from January 26 to January 29, 2015, who agreed to participate. The study was approved by the local ethics committee (Ethik-Kommission Ärztekammer Hamburg, WF-030/14), and the requirement for written informed consent was waived. Participants' records and information were anonymized and de-identified before analysis.

Assessment of Experience, Knowledge, and Skills of Participants

Before the course, participants were invited to complete an on-line survey to rate their experience in interventional neuroradiology (On-line Appendix). The on-line survey was a multiple-choice questionnaire with the opportunity to provide commentary for each question. It consisted of 10 questions concerning their qualifications as well as the number of procedures they assisted or performed as a primary operator in aneurysm embolization, mechanical thrombectomy, and endovascular treatment of arteriovenous malformations or dural arteriovenous fistulas. As described in detail elsewhere,⁸ work experience and aneurysm treatment experience were calculated from corresponding items and expressed as standardized scores (*z* scores with a mean of zero and an SD of 1).

To assess knowledge, the participants had to complete an examination consisting of 3 parts at the end of the course. The first part consisted of 20 multiple-choice questions concerning neuroanatomy and neuroembryology, pathophysiology, materials, and techniques as well as studies in interventional neuroradiology. In the second part, participants had to answer 12 questions regarding treatment of a complex incidental aneurysm of the posterior communicating artery region of the internal carotid artery, applying movies derived from live fluoroscopy of the real procedure to simulate a live case scenario. The third part included a semistructured standardized oral examination with questions covering the field of knowledge mentioned above, supplemented by situational perceptivity as well as assessment and management of complications applying standardized case materials. A total knowledge score was calculated from the subdomain scores and expressed as a standardized score.

Practical skills were assessed in aneurysm coiling, thrombectomy, and Woven EndoBridge device (WEB; Sequent Medical, Aliso Viejo, California) treatment as described in detail elsewhere.⁸ For each participant, total skill scores were calculated from these subdomains and expressed as standardized scores.

Cases and Measures

DSAs of patients who had undergone endovascular coiling of either ruptured or unruptured aneurysms at our institution between 2010 and 2015 were evaluated. Only cases with at least 2 comparable angiographic series, one immediately following treatment and another 6 months later, were eligible. Case characteristics are shown in the Figure.

For each case, the angiographic series immediately following

treatment and after 6 months were presented as movies to the participants. Participants were informed about the patient's age and sex as well as whether the aneurysm was ruptured or unruptured and its location, size, and neck width. For each case, the participants answered 6 questions. First, participants were asked to determine the grade of aneurysm occlusion by selecting 1 of 3 options (complete occlusion, neck remnant, residual aneurysm). Second, they were asked to determine the change between the immediate postprocedural angiogram and the follow-up angiogram using a 3-step scale (better, same, worse). Third, they were asked to indicate how confident they were in their diagnostic rating on a 6-step scale (complete guess, very uncertain, somewhat uncertain, somewhat certain, very certain, or completely certain). Then they rated the technical difficulty of retreatment (standard, difficult, unbearable risk) and were asked to recommend the best therapeutic approach for the patient (coiling only, stent-assisted coiling, clipping, other endovascular treatment such as a flow diverter or the WEB device, or no retreatment). Finally, if the presented patient was younger than 50 years of age, the participants were asked to recommend the best therapeutic approach if the patient were 70 years of age; in cases in which the presented patient was older than 50 years of age, they were asked to recommend the best therapeutic approach if the patient were 30 years of age. These cases were treated as "subcases."

Statistical Analyses

For the analysis of confidence ratings, we used a linear mixed model with independent random effects for cases (if applicable, also subcases) and raters. For the analysis of all other outcomes, we used generalized linear mixed models with a binomial (binary outcomes) or multinomial (categorical outcomes) distribution, a logit link, and the random effects described above.

As a measure of interrater reliability, intraclass correlation coefficients (ICCs) were calculated from models with intercept only (baseline model) as the ratio between the variance between cases (if applicable, also subcases) and the total variance.⁹ We determined ICCs for the assessment of aneurysm occlusion grade (complete/neck remnant versus residual aneurysm) and the change between the immediate postprocedure angiogram and the follow-up angiogram (same/better versus worse). We used the following categories for interpreting ICCs: poor to fair (below 0.4), moderate (0.41–0.60), substantial (0.61–0.80), and almost perfect (0.81–1).¹⁰

The influence of various rater characteristics (work experience, aneurysm treatment experience, knowledge, skills), case characteristics (location, bleeding, aneurysm size, aneurysm neck width, patient age), and casewise averaged rating across raters (proportion rating residual grade, proportion rating worsening, proportion rating difficult retreatment, and mean confidence, if applicable) on the indicated confidence in diagnostic rating; any retreatment recommendation; and specific retreatment recommendations was analyzed by adding fixed effects to the baseline model.

Associations with $P < .05$ were considered statistically significant. All analyses were performed with SPSS 21 (IBM, Armonk, New York).

Figure: Case characteristics and retreatment recommendations

Case	Location	Clinic	Size (mm*mm)	Neck width (mm)	Volume (mm ³)	Packing Density	Age	Occlusion (majority) ^a (%)	Change (majority) ^b (%)	Confidence (median) ^c	Retreatment difficulty (median) ^d	Best approach (majority) ^e (%)	
1	Paraophthalmic	asymptomatic	7.8*6.2	6.0	397	12.85	39	3 (64)	3 (92)	5	2	2 (44)	
2	Acom/A2	asymptomatic	11.8*10.2	4.0	422	25.65	31	3 (100)	3 (60)	5	2	2 (52)	
3	Carotid-T	ruptured	12.0*10.0	3.0	544	16.38	35	3 (96)	3 (100)	6	1	1 (52)	
4	A. carotid interna	asymptomatic	8.8*4.6	5.5	188	10.58	41	2 (50)	2 (81)	5	2	5 (42)	
5	A. cerebelli superior	ruptured	4.0*4.5	2.0	38	33.98	38	2 (89)	3 (85)	5	2	5 (58)	
6	Pcom	asymptomatic	8.0*5.0	2.0	167	33.09	32	3 (84)	3 (100)	6	2	5 (77)	
7	Supraophthalmic	ruptured	6.0*5.0	4.3	79	14.20	42	3 (65)	3 (77)	5	2	1 (72)	
8	A. cerebri posterior	asymptomatic	15.2*13.2	4.0	2681	6.97	37	3 (100)	3 (69)	5	2	4 (39)	
9	Basilar tip	ruptured	13.0*12.0	7.0	1062	16.94	30	3 (65)	2 (69)	4	2	5 (46)	
10	A. pericallosa	ruptured	3.0*2.0	1.0	6	80.73	43	3 (53)	2 (65)	5	2	4 (42)	
11	Basilar tip	ruptured	13.0*12.0	7.0	817	19.67	27	3 (96)	3 (100)	6	2	1 (39)	
12	Supraophthalmic	asymptomatic	4.8*4.0	4.1	48	30.88	75	2 (65)	3 (46)	4	2	2 (46)	
13	A. pericallosa	ruptured	5.5*9.0	2.5	141	21.45	31	3 (92)	3 (100)	6	2	4 (50)	
14	Pcom	ruptured	3.0*8.0	2.0	38	24.19	69	3 (81)	3 (96)	6	1.5	1 (77)	
15	Paraophthalmic	ruptured	8.0*4.0	3.0	134	14.33	28	3 (96)	3 (100)	6	2	1 (46)	
16	Pcom	ruptured	10.0*8.0	5.0	268	12.85	68	3 (54)	3 (92)	5	2	4 (58)	
17	Basilar tip	asymptomatic	7.0*5.0	4.0	128	7.84	30	3 (96)	3 (92)	6	1	1 (39)	
18	MCA bifurcation	ruptured	8.2*7.4	3.0	235	14.33	72	3 (100)	3 (96)	6	2	1 (36)	
19	Acom	asymptomatic	4.2*4.3	2.0	42	4.31	71	3 (80)	3 (96)	6	1	1 (60)	
20	Basilar tip	ruptured	5.0*7.0	5.0	98	36.28	29	3 (65)	3 (96)	5	2	1 (64)	
							70					2 (63)	

Note:—Acom indicates anterior communicating artery; Pcom, posterior communicating artery; A., arteria.

^a Rated from complete occlusion, neck remnant, to residual aneurysm.

^b Rated from better, same, to worse.

^c Rated from completely uncertain (1) to completely certain (6).

^d Rated from standard, difficult, to unbearable risk.

^e Rated from coiling only, stent-assisted coiling, clipping, other, or no retreatment.

RESULTS

Participant Characteristics and Experience in Interventional Neuroradiology

All 26 participants answered all questions in the on-line survey, resulting in a response rate of 100%. Twenty participants were younger than 40 years of age (76.9%), and 7 of the 26 participants were women (26.9%). One participant (3.8%) was a neurosurgeon, 1 participant (3.8%) was in his first year of radiology training, 1 (3.8%) was in his fifth year, and 23 participants (88.5%) had completed their radiology residency. Each participant had at least 1 year of experience working in interventional neuroradiology, with 12 (46.2%) reporting at least 4 years. Ten of the 26 participants (38.5%) were certified neuro-radiologists in their country. The high number of certified radiologists is because in most European countries, radiologic certification is a prerequisite for specialization in interventional neuroradiology.

One participant did not attend the final knowledge test. Only 5 participants answered at least 80% of the 20 multiple choice questions correctly (median, 13/65% correct answers). In the second “live case” section of the examination, only 2 participants answered less than 80% of the 12 questions correctly. In the final oral examination, 12 participants answered at least 80% of the 21 questions correctly and 6 participants answered <60%. Median procedural time for coiling of a pos-

terior communicating artery aneurysm was 23 minutes and 29 seconds (14 minutes and 2 seconds to 49 minutes and 53 seconds), and median fluoroscopy time was 13 minutes and 33 seconds (5 minutes and 51 seconds to 31 minutes to 13 seconds). Correct first coil selection was achieved 15 times, and a median of 8 coils was used (minimum 5, maximum 11). In 12 cases, complications occurred.

Interrater Reliability of Occlusion and Change

Interrater reliability was moderate regarding the assessment of aneurysm occlusion grade (ICC = 0.581) and substantial regarding change (ICC = 0.776).

Confidence in Diagnostic Rating

Overall confidence in the diagnostic rating was high (median, “very certain”; mean 5.20). As indicated by substantial variance, some raters were generally more confident in their diagnostic rating regarding the determination of the change between the initial postprocedural angiogram and the follow-up angiogram than others (irrespective of cases). With substantial variance across cases, some cases were rated generally with higher confidence than others (irrespective of raters). As indicated by the poor interrater reliability (ICC = 0.267), each rater reacted individually to each case (On-line Table). Confidence was statistically significantly

Table 1: Results from linear (generalized) mixed modelling investigating the association between case characteristics with confidence in assessment, general retreatment recommendation (any retreatment), and specific retreatment recommendations (coiling, stent and coiling, clipping, other endovascular treatment)

	Confidence ^a β	Any Retreatment ^b Odds Ratio	Coiling Only ^b Odds Ratio	Stent and Coiling ^b Odds Ratio	Clipping ^b Odds Ratio	Other Endovascular Treatment ^b Odds Ratio
Case characteristics						
Location ^c	0.1300	0.6258	0.9887	1.4288	0.0241	0.1635 ⁱ
Bleeding ^d	0.0432	0.7638	0.7022	0.9231	1.7582	0.7084
Aneurysm size (mm)	0.0004	0.9959	1.0006	0.9873 ⁱ	1.0198	1.0072
Aneurysm neck width (mm)	−0.0447	0.9088	0.7354 ⁱ	1.3879 ⁱ	0.4234 ⁱ	0.8492
Patient age ^e	NA	0.2522 ^j	0.3529 ^j	0.2171 ^j	0.1879 ^j	0.2796 ^j
Casewise averaged ratings across raters						
Proportion rating residual grade ^f	0.4683	86.2958 ^j	79.9203 ^j	141.9125 ^j	118.8253	7.3950
Proportion rating worsening ^g	1.1790 ^j	2.2709	1.2754	2.7537	0.2078	8.3006
Proportion rating difficult retreatment ^h	−0.2387	0.4200	0.0282 ⁱ	0.3909	99.9733	1.6362
Mean confidence	NA	2.7197 ^j	2.4697	2.2326	5.1344	0.9219

Note:—NA indicates not analyzed.

^a Rated from completely uncertain (1) to completely certain (6).

^b Binary compared with no treatment; odds ratios of >1 indicate a higher probability of treatment, and odds ratios of <1 indicate a lower probability of treatment with an increase in the predictors.

^c Posterior (1) versus anterior (0).

^d Ruptured (1) versus asymptomatic (0).

^e Elderly, older than 50 years, (1) versus younger, 50 years or younger (0).

^f Proportion of ratings of residual versus complete/neck remnant aneurysm from 0 to 1.

^g Proportion of ratings of worse-versus-the same/better condition from 0 to 1.

^h Proportion of ratings of difficult/unbearably risky versus standard retreatment from 0 to 1.

ⁱ $P < .050$.

^j $P < .00$.

higher in cases that were generally rated as “worse” (versus “same/better”). See Table 1 for detailed results.

Retreatment Recommendation

The distribution and frequencies of retreatment recommendation per case are shown in the Figure. Interrater reliability of the recommendations of any type of retreatment versus no retreatment was substantial (ICC = 0.619). The odds of recommending retreatment were statistically significantly higher in cases that were generally rated as being “residual aneurysm” (versus “complete/neck remnant aneurysm”) and that were generally rated with higher mean confidence. The odds of recommending any retreatment were significantly lower in elderly patients (Table 1).

Interrater reliability was moderate to substantial for coiling (ICC = 0.596), stent and coiling (ICC = 0.561), and clipping (ICC = 0.633), but poor for other endovascular treatments (ICC = 0.342). The odds of recommending coiling were statistically significantly lower in cases that were generally rated as being difficult to retreat and in aneurysms with smaller neck widths. Moreover, a smaller neck width was associated with lower odds of recommending clipping. The recommendation of stent-assisted coiling was more likely in cases with wider necks and less likely in cases with smaller aneurysm size.

Raters with more theoretic knowledge were more likely to recommend coiling only. Raters with more work experience were less likely to recommend clipping (Table 2). For the elderly, all specific retreatment recommendations were less likely than for younger patients.

DISCUSSION

While the overall confidence in their own individual diagnostic rating was high, we found the same low interobserver reliability

regarding the visual assessment of aneurysm as in previous studies.^{1,2} In a recent systematic review and meta-analysis, variability was found to be lower if raters had to comment on change.³ This is in accordance with our findings, because interrater reliability was moderate with regard to the assessment of aneurysm occlusion grade and substantial with regard to change. Moreover, Ernst et al³ found that in studies using DSA, interobserver agreement was significantly better in samples with a higher proportion of completely occluded aneurysms because complete occlusion does not require any further differentiation on the degree of residual flow. Thus, interrater reliability might have been higher in our study if the proportion of completely occluded aneurysms had been higher. Our study also confirms the limited interrater reliability of the recommendation of retreatment of coiled aneurysms in general as well as in the type of retreatment.^{5,6} This finding renders questionable retreatment as a primary outcome measure in studies comparing different types of aneurysm treatment.¹¹ Although the necessity of retreatment is a meaningful outcome parameter for patients, it adds much variability if the recommendation for retreatment varies widely among therapists. The estimation of the need for retreatment is a subjective end point, the basic prerequisite of which is the presence of recanalization as an indicator of higher rupture or rerupture risk. However, the visual assessment of aneurysm occlusion status itself is subjective.

To analyze the underlying reasons behind the wide variation among raters, we evaluated numerous patient and rater variables. Our study shows that the recommendation of retreatment is influenced by not only recurrence status but also case characteristics such as age and neck width as well as rater characteristics such as work experience, theoretic knowledge, and level of confidence in the diagnostic rating.

Table 2: Results from linear (generalized) mixed modelling investigating the association between rater and case characteristics with confidence in assessment, general retreatment recommendation (any retreatment), and specific retreatment recommendations (coiling, stent and coiling, clipping, other endovascular treatment)

	Confidence ^a β	Any Retreatment ^b Odds Ratio	Coiling Only ^b Odds Ratio	Stent and Coiling ^b Odds Ratio	Clipping ^b Odds Ratio	Other Endovascular Treatment ^b Odds Ratio
Rater characteristics						
Work experience ^c	0.0466	0.7280	0.9897	0.8569	0.3882 ^d	0.7475
Aneurysm treatment experience ^c	0.0108	1.0929	1.1190	0.8571	1.2292	1.1915
Knowledge ^c	0.0411	1.4761	1.8102 ^d	1.1198	1.5397	1.3269
Skills ^c	0.0574	0.7945	0.7605	1.0904	0.6667	0.7735

^a Rated from completely uncertain (1) to completely certain (6).

^b Binary compared with no treatment; odds ratios of >1 indicate a higher probability of treatment, and odds ratios of <1 indicate a lower probability of treatment with an increase in the predictors.

^c In SD units.

^d $P < .050$.

As a strength of this study, all angiograms were presented as movies in 2 projections to recreate a more realistic clinical scenario, while previous studies created a case vignette with just 1 single projection per case. Moreover, we focused on coiled aneurysms, while previous studies analyzed a heterogeneous group, including both treated and untreated aneurysms. In contrast to previous studies,⁶ we provided aneurysm-specific information to the raters, including location, size, neck width, and bleeding and found that the recommendation of stent-assisted coiling was more likely in cases with a wider neck and less likely in cases with a smaller aneurysm size. Although in a real-world setting, further factors influence the final retreatment decision such as patient's anxiety and preferences, our experimental setting allowed us to control for these factors and concentrate on the influence of specific rater and aneurysm characteristics.

In contrast to previous studies, we found that rater characteristics have a significant effect on retreatment recommendations.¹² This might be because we involved a larger group of raters and assessed rater characteristics such as knowledge and work experience in more detail compared with previous studies. Thus, we observed that raters with better theoretic knowledge in neurovascular interventions were more likely to recommend coiling and raters with more work experience in endovascular interventions were less likely to recommend clipping.

Similar to previous studies, the recommendation for retreatment was less likely in elderly patients.⁶ The preference of observation in older individuals might be explained by the overall higher treatment risks due to significant comorbidities and shorter life expectancies, though this might not be the appropriate approach in otherwise healthy patients. Clipping was the treatment recommendation of most participants in only 1 case. This might be because most participants were neuroradiologists and recommendations might have been different with more neurosurgical participants. Thus, a recent study found that neurosurgeons were significantly more likely to retreat and recommended different types of treatments compared with neuroradiologists.⁶

Most interesting, cases that were generally rated as being difficult to retreat were not significantly more likely to be recommended for clipping. This finding contradicts the common practice of "negative defensive medicine" (ie, high-risk cases are avoided and sent to other disciplines).¹³ In contrast, the practice of positive defensive medicine might explain the observation that most participants rarely recommended "no retreatment." The

therapist might fear being blamed for undertreatment in case a recurrent aneurysm ruptures. These findings underline the issue of guidelines based on expert opinions, the lowest level of acceptable evidence. Although in the absence of research evidence it might be the only guidance available, it might not be the best.

In recent years, many patients prefer to seek a second opinion on their disease and available treatments by another physician. Second opinion is a common treatment ratification tool that may critically influence diagnosis and treatment. Given the possibility of exchanging and sharing medical images currently, there is no more need for repetitive investigations that would harm the patient. Previous studies have shown that second-opinion interpretations of neuroimaging studies added value by reducing error and optimizing the care of patients.¹⁴ Health care organizations are trying to control costs by urging and even demanding a second opinion before interventions. However, second opinions can provoke unnecessary costs on the medical budget of the community, and dissenting recommendations might confuse and alienate the patient.

In our study, supposing the retreatment recommendation of the majority is the best approach and therefore best for the patient's welfare, the probability of this approach being recommended in a second consultation was only 30%. The probability that the patient gets 2 different treatment recommendations was 61%, and the probability of 3 different treatment recommendations was 23%. Although second opinion as a treatment ratification tool in general might be useful, it appears to be a waste of resources as long as there is no current standard concerning when and how to retreat a coiled aneurysm. Instead, effort should be focused on conducting randomized controlled trials so that clinicians can properly counsel the patients regarding the benefits and relative risks of different management options.

As a recently published objective clinical study end point, aneurysm recurrence volumetry using registered 3D-MRA follow-up datasets was found to be highly sensitive in the detection of aneurysm recurrences and to represent an objective, rater-independent, and highly reliable method and thus a promising approach for future studies.^{15,16}

As a limitation, the number of cases was limited to 20. With 20 cases, the participants voluntarily answered 120 questions. Because concentration diminishes with time and we aimed to guarantee that the participants gave reliable and authentic responses,

we had to limit the number to 20 cases. Future studies with more cases are desirable.

Only 10 of the 26 participants were certified neuroradiologists; therefore, the study does not necessarily represent the interventional neuroradiology community. However, with the detailed assessment of working experience, theoretic knowledge, and practical skills, the group is well-described.

CONCLUSIONS

Although the overall confidence in diagnostic rating was high, our study confirms the suboptimal interrater reliability of visual assessment of aneurysm occlusion as well as retreatment recommendations, rendering both questionable as primary outcome measures. Besides recurrence status, recommendation of retreatment is significantly influenced by patient age, aneurysm neck width, and characteristics of the therapist.

Disclosures: Andreas Frölich—UNRELATED: Consultancy: Philips Healthcare. Jens Fiehler—UNRELATED: Consultancy: Acandis, Boehringer Ingelheim, Cerenovus, Medtronic, MicroVention, Penumbra, Stryker; Grants/Grants Pending: MicroVention, Acandis, Medtronic*; Payment for Lectures Including Service on Speakers Bureaus: Acandis, Boehringer Ingelheim, Cerenovus, Medtronic, MicroVention, Penumbra, Stryker. Jan-Hendrik Buhk—UNRELATED: Consultancy: Acandis, Codman Neuro, Medtronic, MicroVention, Stryker. *Money paid to institution.

REFERENCES

1. Cloft HJ, Kaufmann T, Kallmes DF. **Observer agreement in the assessment of endovascular aneurysm therapy and aneurysm recurrence.** *AJNR Am J Neuroradiol* 2007;28:497–500 [CrossRef Medline](#)
2. Tollard É, Darsaut TE, Bing F, et al. **Outcomes of endovascular treatments of aneurysms: observer variability and implications for interpreting case series and planning randomized trials.** *AJNR Am J Neuroradiol* 2012;33:626–31 [CrossRef Medline](#)
3. Ernst M, Yoo AJ, Kriston L, et al. **Is visual evaluation of aneurysm coiling a reliable study end point? Systematic review and meta-analysis.** *Stroke* 2015;46:1574–81 [CrossRef Medline](#)
4. McDougall CG, Johnston SC, Gholkar A, et al; MAPS Investigators. **Bioactive versus bare platinum coils in the treatment of intracranial aneurysms: the MAPS (Matrix and Platinum Science) trial.** *AJNR Am J Neuroradiol* 2014;35:935–42 [CrossRef Medline](#)
5. Daugherty WP, Rad AE, White JB, et al. **Observer agreement regarding the necessity of retreatment of previously coiled recurrent cerebral aneurysms.** *AJNR Am J Neuroradiol* 2011;32:566–69 [CrossRef Medline](#)
6. McDonald JS, Carter RE, Layton KF, et al. **Interobserver variability in retreatment decisions of recurrent and residual aneurysms.** *AJNR Am J Neuroradiol* 2013;34:1035–39 [CrossRef Medline](#)
7. Bornstein BH, Emler AC. **Rationality in medical decision making: a review of the literature on doctors' decision-making biases.** *J Eval Clin Pract* 2001;7:97–107 [CrossRef Medline](#)
8. Ernst M, Kriston L, Romero JM, et al. **Quantitative evaluation of performance in interventional neuroradiology: an integrated curriculum featuring theoretical and practical challenges.** *PLoS One* 2016;11:e0148694 [CrossRef Medline](#)
9. Shrout PE, Fleiss JL. **Intraclass correlations: uses in assessing rater reliability.** *Psychol Bull* 1979;86:420–28 [CrossRef Medline](#)
10. Landis JR, Koch GG. **The measurement of observer agreement for categorical data.** *Biometrics* 1977;33:159–74 [CrossRef Medline](#)
11. Pierot L, Fiehler J, White P. **Point-TAR: a useful index to follow-up coiled intracranial aneurysms?** *AJNR Am J Neuroradiol* 2015;36:2–4 [CrossRef Medline](#)
12. Darsaut TE, Gentric JC, McDougall CM, et al. **Uncertainty and agreement regarding the role of flow diversion in the management of difficult aneurysms.** *AJNR Am J Neuroradiol* 2015;36:930–36 [CrossRef Medline](#)
13. Studdert DM, Mello MM, Sage WM, et al. **Defensive medicine among high-risk specialist physicians in a volatile malpractice environment.** *JAMA* 2005;293:2609–17 [Medline](#)
14. Hatzoglou V, Omuro AM, Haque S, et al. **Second-opinion interpretations of neuroimaging studies by oncologic neuroradiologists can help reduce errors in cancer care.** *Cancer* 2016;122:2708–14 [CrossRef Medline](#)
15. Ernst M, Buchholz A, Bourcier R, et al. **Voxel based analysis of recurrence dynamics in intracranial aneurysms after coiling.** *J Neurointerv Surg* 2017 Oct 31. [Epub ahead of print] [CrossRef Medline](#)
16. Schönfeldt MH, Schlotfeldt V, Forkert ND, et al. **Aneurysm recurrence volumetry is more sensitive than visual evaluation of aneurysm recurrences.** *Clin Neuroradiol* 2016;26:57–64 [CrossRef Medline](#)

Management of Small Unruptured Intracranial Aneurysms: A Survey of Neuroradiologists

 A. Malhotra,  X. Wu,  B. Geng,  D. Hersey,  D. Gandhi, and  P. Sanelli



ABSTRACT

BACKGROUND AND PURPOSE: The long-term history and management of unruptured intracranial aneurysms is not well understood. Our aim was to determine current practice patterns in the management of unruptured intracranial aneurysms, especially regarding imaging surveillance for conservatively managed aneurysms of this type.

MATERIALS AND METHODS: An on-line survey was designed to examine physician practice and preference regarding the management of small unruptured intracranial aneurysms (≤ 7 mm in diameter). The survey was circulated to members of the American Society of Neuroradiology. Participation was voluntary, and all responses were anonymous.

RESULTS: A total of 227 individual survey responses were obtained and included in the analysis with 54.6% (124/227) from diagnostic neuroradiologists (practicing $>50\%$ neuroradiology) and one-third (29%) from neurointerventional radiologists. One hundred seventy-three of 227 responded that routine, periodic imaging surveillance would be appropriate for conservatively managed unruptured intracranial aneurysms, and 84% of respondents recommended surveillance frequency of at least once a year. Fifty-nine percent favored indefinite, life-long follow-up for small unruptured intracranial aneurysms, and a similar number of respondents favored noncontrast MR angiography for aneurysm follow-up. Significant heterogeneity was found in size measurements used to assess aneurysms and criteria used to define growth on surveillance imaging.

CONCLUSIONS: The natural history of intracranial aneurysms is not well-understood. A large proportion of incidentally detected, unruptured aneurysms are small (< 7 mm). The survey results show significant heterogeneity in practice even among neuroradiologists and underlies the need to standardize imaging practice. Further studies are needed to assess the optimal frequency and duration of surveillance imaging for unruptured intracranial aneurysms. The criteria used to measure aneurysms and define growth on imaging also need to be standardized.

ABBREVIATIONS: AHA = American Heart Association; ASA = American Stroke Association; UIA = unruptured intracranial aneurysm

Unruptured intracranial aneurysms (UIAs) are relatively common in the general population, found in approximately 3.2% of the adult population worldwide.¹ They are being increasingly diagnosed due to more frequent use of less invasive imaging tech-

niques with higher resolution.² The optimal management of UIAs should be decided on the basis of their natural history, which remains poorly understood.³⁻⁵ Observational studies of UIAs suggest that only a fraction of them rupture, though these data have high selection bias, with high-risk aneurysms being treated, resulting in potential underestimation of the rupture rate.^{6,7} Aneurysm size is considered the major risk factor for UIA rupture, with low reported rates of rupture in small (< 7 mm) aneurysms.⁶ A high proportion of unruptured aneurysms are small (< 7 mm in diameter) and incidental.⁸⁻¹⁰ Studies have reported that up to 87.6% of incidental UIAs are tiny, measuring $< 3-4$ mm.⁹ However, small aneurysms are known to rupture, and some recent studies have reported that up to a third of ruptured intracranial aneurysms measure < 5 mm.^{9,11} An increasing number of treating physicians favor preventive treatment of even tiny aneurysms.^{12,13}

The American Heart Association/American Stroke Association

Received September 29, 2017; accepted after revision January 3, 2018.

From the Department of Radiology and Biomedical Imaging (A.M.), Yale School of Medicine, New Haven, Connecticut; Yale School of Medicine (X.W., B.G.), New Haven, Connecticut; Clinical Information Services (D.H.), Cushing/Whitney Medical Library, Yale University, New Haven, Connecticut; Department of Interventional Neuroradiology (D.G.), University of Maryland School of Medicine, Baltimore, Maryland; and Department of Radiology (P.S.), Northwell Health, New York, New York.

Please address correspondence to Ajay Malhotra, MD, MMM, Department of Radiology and Biomedical Imaging, Yale School of Medicine, Box 208042, Tompkins East 2, 333 Cedar St, New Haven, CT 06520-8042; e-mail: ajay.malhotra@yale.edu; @cea_yale



Indicates article with supplemental on-line table.



Indicates article with supplemental on-line photos.

<http://dx.doi.org/10.3174/ajnr.A5631>

tion (AHA/ASA) guidelines for management of patients with UIAs were updated in 2015.⁸ However, these do not specify separate recommendations for small (3–7 mm) and tiny aneurysms (≤ 3 mm), though their natural history, risk of rupture, and success of treatment might be different from aneurysms measuring > 7 mm.^{3,6,14} Patients with no history of SAH with aneurysms of ≤ 7 mm are often followed conservatively with imaging surveillance to assess changes in size and/or morphology, which are known to predict rupture.^{15,16} The AHA/ASA guidelines recommend radiographic follow-up with MRA or CTA at regular intervals. However, the interval and duration of recommended follow-ups are uncertain (Class I; Level of Evidence B).⁸

This lack of clarity in guidelines is reflective of the heterogeneity in the current literature in the preferred imaging technique for surveillance and the best imaging criteria to assess growth.^{3,17} We undertook this survey to assess the practice patterns among diagnostic and interventional neuroradiologists in the surveillance and management of UIAs, particularly small UIAs. To our knowledge, no recent studies have defined current clinical imaging practice to quantify and understand the variability in practice patterns in clinical care.

MATERIALS AND METHODS

A 12-question on-line survey was designed to examine physician practices and preferences regarding the surveillance and management of small UIAs (≤ 7 mm in diameter). The survey was performed using the Qualtrics Survey Software (Qualtrics, Provo, Utah), a Web-based system for surveys. Approval was obtained from the American Society of Neuroradiology to distribute the on-line survey through e-mails to their members soliciting survey completion. A single-click link to the survey was attached. Participation was voluntary, and no compensation was offered to participants. All responses were anonymous. Qualtrics software records the Internet Protocol address, therefore limiting respondents to a single response. The survey was open for 6 weeks. All survey results were summarized and reported by Qualtrics.

All survey results were compiled and graphed using Qualtrics. Using the χ^2 test, we additionally explored the differences in responses between diagnostic neuroradiologists and neurointerventional radiologists/endovascular surgeons in growth measurements, growth definition, and factors that lead to treatment decisions.

RESULTS

A total of 227 individual survey responses were obtained and included in the analysis. The full list of questions and respondent answers is in the On-line Table.

Respondent Characteristics

Most respondents, 54.6% (124/227), were diagnostic neuroradiologists (practicing $> 50\%$ neuroradiology), while 7.5% (17/227) were fellowship-trained diagnostic neuroradiologists practicing $< 50\%$ neuroradiology. Almost one-third (29%) were neurointerventional radiologists (On-line Fig 1). Regarding practice setting, 45% of respondents practiced in academic, tertiary care settings, with 29% in private practice and 20% in hybrid practice settings (combined academic and community setting).

Prevalence of UIAs

Regarding the frequency of small (< 7 mm) aneurysms among all UIAs in clinical practice, the opinion was split in the following manner: Thirty-four percent of respondents thought that small aneurysms constituted 51%–75% of all aneurysms, 26% of respondents favored $> 75\%$ of all UIAs, 20% selected the 26%–50% category, while 19% thought they were $< 25\%$ of all UIAs (On-line Fig 2).

Rupture Rate in Aneurysms (> 1 Option Allowed)

Most respondents (209/227) opined that growing aneurysms are at much higher risk for rupture, irrespective of size. Very few (11/227) responded that the aneurysmal rupture rate is uniform irrespective of size. Forty-four respondents answered that UIAs usually rupture many years (> 10 years) after they form or are discovered. Only 14/227 participants thought that treatment (clipping or coiling) eliminated any chance of subsequent subarachnoid hemorrhage.

Management of Small UIAs (> 1 Option Allowed)

Nearly half the respondents ($n = 101$) commented that small UIAs should be routinely treated with clipping or coiling. One hundred seventy-three of 227 responded that routine, periodic imaging surveillance would be appropriate; 46/227 thought that only high-risk aneurysms needed treatment or imaging follow-up (such as growing aneurysms). A very small minority (2 participants) thought that no imaging follow-up was needed. Forty-seven of 227 responded that the frequency and duration should be similar in ruptured and unruptured aneurysms (Fig 1).

Imaging Surveillance: Frequency of Conservatively Followed Small UIAs

More than half of the respondents (52%) thought that the appropriate imaging surveillance frequency should be every 6 months for the first year, followed by annual imaging thereafter. Thirty-two percent thought annual imaging would be more appropriate. Biannual imaging was favored by 12%, while $< 1\%$ opted for imaging follow-up every 5 years. More aggressive imaging follow-up (every 6 months) was chosen by 3% of the respondents.

Imaging Surveillance: Duration of Conservatively Followed Small UIAs

Most physicians (59%) favored indefinite, life-long follow-up for small UIAs; 8.5% opted for 10-year, 21% opted for 5-year, and 12%, for 2-year follow-up duration for conservatively followed small UIAs (Fig 2).

Imaging Techniques for Conservatively Followed Small UIAs

MR angiography without contrast using a time-of-flight technique was favored by 58%, while contrast MRA was chosen by roughly 10% of respondents. Twenty-one percent chose CT angiography, and 3.2% chose DSA as the technique to follow small UIAs; 8.3% thought that any of these imaging modalities would be equally appropriate for surveillance.

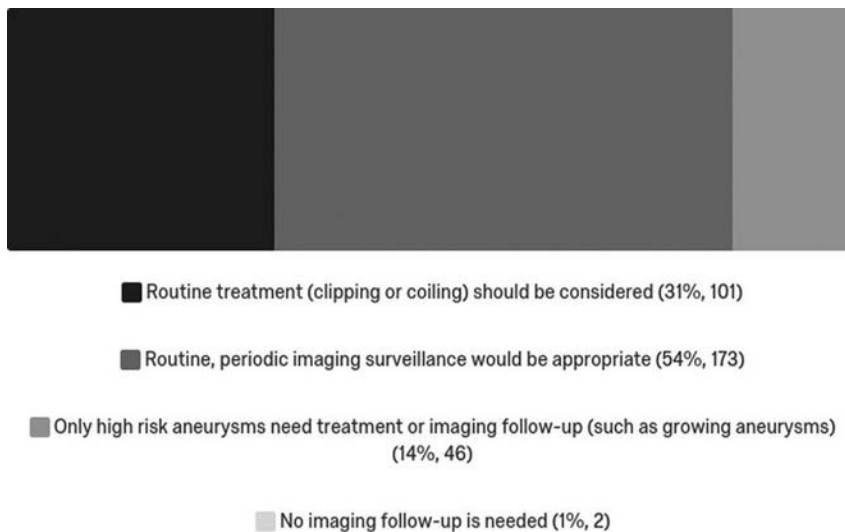


FIG 1. Survey result of management of small UIAs.

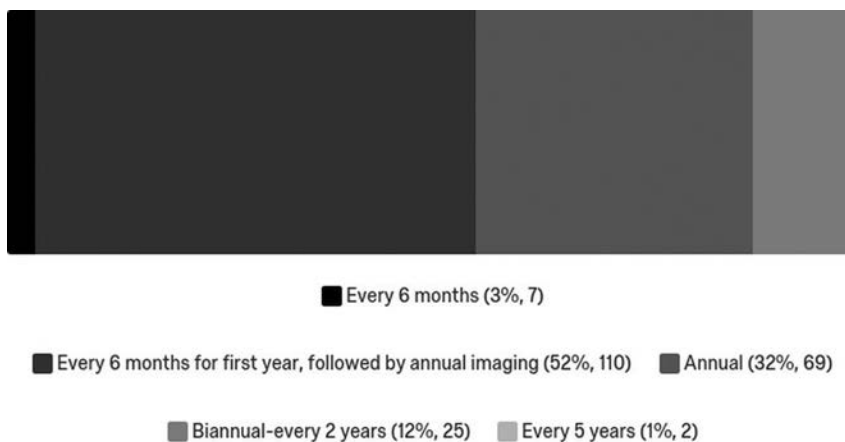


FIG 2. Survey result of imaging follow-up frequency.

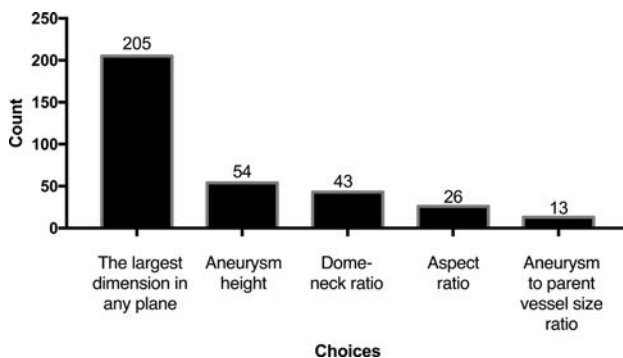


FIG 3. Survey result of measurement of aneurysmal growth.

Preferred Measurement of Aneurysm on Surveillance Imaging (>1 Option Allowed)

The largest dimension in any plane was most frequently used (205/227) followed by aneurysm height (54 participants). Dome-to-neck ratio was chosen by 43, and aspect ratio (aneurysm height divided by aneurysm neck), by 26 respondents. A small minority¹³ reported using size ratio (aneurysm-to-parent vessel size ratio) (Fig 3). There was no significant difference in responses be-

tween diagnostic neuroradiologists and neurointerventional radiologists/endovascular neurosurgeons to any of the choices.

Criteria Used to Define Growth in Small UIAs (>1 Option Allowed)

The most frequently used criterion for growth was growth of >1 mm in at least in 1 direction in 166/227 responses. Forty-three chose growth of the aneurysm of >1.5 times its baseline measurement, while 37 chose an increase of >0.5 mm in 1 dimension. An increase in volume of >5% was used by 18, and 12 chose a change in size to the nearest tenth of a millimeter more than the measurement error per manufacturer's specifications (Fig 4). There was no significant difference in responses between diagnostic neuroradiologists and neurointerventional radiologists/endovascular neurosurgeons.

High-Risk Patients Appropriate for Routine Screening (>1 Option Allowed)

One hundred ninety-five survey participants selected adult polycystic kidney disease, while 169 chose prior history of SAH as an appropriate criterion for screening. Patients with a family member with an unruptured aneurysm was the choice selected by 150, while only 38 thought that patients with ascending aortic aneurysms should be screened for intracranial aneurysms (Fig 5).

Criteria Used to Treat Small UIAs (>1 Option Allowed)

Change in size ($n = 215$), change in morphology ($n = 205$), and complex morphology ($n = 195$) were the criteria most frequently selected for the decision to treat UIAs. Patient preference was chosen by 170, and patient age, by 137 respondents. Smoking history was considered important by 95, and sex, by 32 responding physicians (Fig 6). A statistically significant proportion of neurointerventional radiologists/endovascular neurosurgeons chose age and smoking history compared with diagnostic neuroradiologists.

DISCUSSION

To our knowledge, this survey of practicing neuroradiologists and neurointerventionalists is the first of its kind to assess and quantify practice patterns regarding small unruptured aneurysms. A high degree of respondent variability is evident regarding the perception of prevalence of small UIAs, preferred imaging technique for surveillance, frequency and duration for surveillance, and optimal criteria on imaging to assess aneurysm growth and rupture risk.

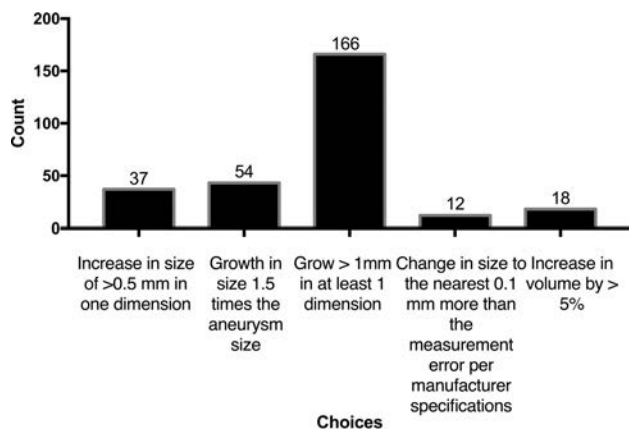


FIG 4. Survey result of the definition of aneurysmal growth.

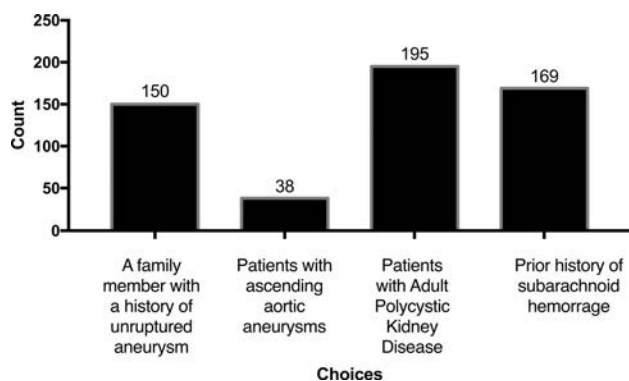


FIG 5. Survey result of the definition of high-risk patients.

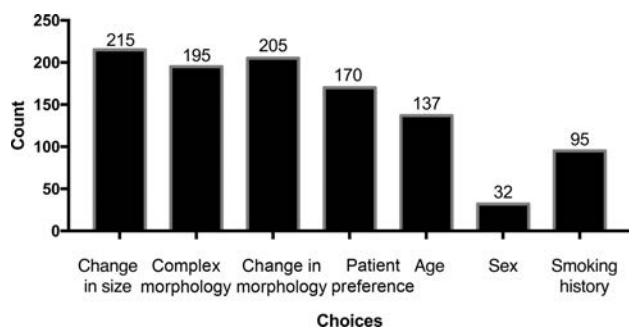


FIG 6. Survey result of factors determining treatment options.

Intracranial aneurysms are acquired lesions, and rupture is the most common etiology of nontraumatic SAH.^{4,18} However, rupture is uncommon and only occurs in 1 of 200–400 patients with a UIA per year.⁵ The natural history of UIAs remains poorly understood, especially for the smaller (3–7 mm) and tiny (≤ 3 mm) aneurysms.¹⁹

A meta-analysis in 2011 including 68 studies reported a prevalence of 3.2% (95% CI, 1.9%–5.2%) in a population without comorbidity and a mean age of 50 years.¹ However, a higher prevalence of up to 7% has been reported in more recent studies using MRA, with a higher prevalence in women and with increasing age.²⁰

Regarding the prevalence of small UIAs, the survey results indicated significant heterogeneity in opinions: Nearly 40% of respondents thought small (<7 mm) aneurysms constituted <50%

of all UIAs. According to a recent review, 93% of UIAs in adults are <10 mm and 66% are <5 mm.¹

Most respondents agreed that size was an important predictor of rupture, and growing aneurysms are at a higher risk for rupture. Size and location of UIAs have been recognized as predictors of rupture in prospective studies of UIAs.^{6,7,21} The International Study of Unruptured Intracranial Aneurysms (ISUIA) reported no ruptures among aneurysms of <7 mm in the anterior circulation in patients with no history of SAH.⁶ However, as with most observational studies on UIAs, the ISUIA has some shortcomings, particularly related to the selection bias resulting from ablation of UIAs thought to be at high risk and conservative treatment of patients thought to be at lower risk of rupture, as well as a poor retention rate of patients used to define the natural history of aneurysms. Only 21% of patients in the observational group were followed up for >4 years. An increased risk of rupture of larger aneurysms, particularly in those measuring >7 mm in diameter, has been reported.^{6,9,21,22}

For assessing growth, 76% (173/227) considered that routine, periodic imaging surveillance would be appropriate for UIAs managed conservatively. Studies have proposed imaging follow-up of all aneurysms (including those of <7 mm) due to up to a 12-fold higher risk of rupture for growing-versus-nongrowing aneurysms.¹⁶ The 2015 AHA guidelines recommend a first follow-up study at 6–12 months after the initial discovery, followed by subsequent yearly or biennial follow-up (Class IIb; Level of Evidence C).⁸ However, the correlation between growth and rupture is relatively poor in small and tiny aneurysms.³ While Villablanca et al¹⁶ reported a good correlation for aneurysms of <7 mm, other studies by Sonobe et al²³ and Bor et al did not.²⁴

Respondents overwhelmingly favored MRA for imaging follow-up of small aneurysms, though 20% preferred CTA. There is considerable variability in the published literature on the optimal imaging technique used to assess growth in UIAs.^{3,17} Although there is literature on the sensitivity and specificity of CTA and MRA for the detection of aneurysms, with DSA considered the criterion standard, there is a paucity of evidence on their accuracy for growth detection. Most studies do not describe interobserver reliability of measurements. Some studies used the average between 2 readers for analysis.²⁵ Other studies reported that the first and last imaging of each patient were assessed for growth in a single session by the same researcher to avoid interobserver and intraobserver reliability.²⁴

For assessing size, the change in the maximum dimension was chosen by 90% (205/227), while 24% (54/227) also chose aneurysm height. Dome-to-neck ratio, aspect ratio, and size ratio were chosen by fewer respondents. A similar degree of heterogeneity was seen in responses to criteria used to assess growth. Most respondents (73%) chose growth of >1 mm in at least 1 direction, but 16% (37/227) chose a 0.5-mm increase as clinically significant. No statistically significant difference was found in responses between diagnostic neuroradiologists and neurointerventional radiologists/endovascular neurosurgeons in size measurements on surveillance imaging and criteria used to define growth.

This variability in the definition of growth was also seen in studies reporting growth in UIAs and becomes even more significant for small UIAs.^{3,17} Very few studies have used different cri-

teria for defining growth in aneurysms of <5 mm compared with larger aneurysms.²⁶ Mehan et al²⁷ selected 2 mm as the criterion for growth in any dimension between CTA examinations because of the high degree of imprecision with smaller measurements.

In addition to size, retrospective studies have identified several morphologic parameters as potential predictors of rupture: aspect ratio (height/neck),²⁸ the bottleneck factor (dome/neck ratio),²⁹ height/width ratio,²⁹ volume-to-ostium area ratio,³⁰ and size ratio.³¹ However, the indices reported were measured after aneurysm rupture, and the results are conflicting.^{32–34} There is substantial variability in the definition and application of aneurysm morphology with multiple criteria, with the Unruptured Cerebral Aneurysm Study criteria reportedly having higher reliability than the ISUIA criteria.³⁵ Alternative aneurysm size definitions have been shown to have significant impact on prediction performance and optimal threshold values.³² In a prospective study, dome-to-neck ratio and multilobar morphology were found to be risk factors for growth in UIAs.²⁴ Aneurysm volume was recently reported to predict future rupture in the only long-term prospective study for UIAs.³⁴

A total of 101/227 (44%) respondents thought that small aneurysms should be routinely treated with coiling or clipping. Roughly 85% thought that surveillance imaging to assess growth should at least be annually. Although only 20% (44/227) of respondents thought that UIAs can rupture ≥ 10 years after they are found, nearly 60% opted for indefinite, life-long imaging surveillance. Only 20% (46/227) responded that only high-risk aneurysms should be treated or have routine imaging surveillance. Age and smoking history were chosen by more neurointerventional radiologists/endovascular neurosurgeons as criteria to treat small aneurysms. These have been shown to be risk factors for growth and rupture of UIAs.⁸

In a 2015 international survey of 203 neurosurgeons, most endorsed treatment of all asymptomatic aneurysms regardless of size.¹² A more recent North American study showed that 11% of treating physicians always or usually recommended treatment of the anterior circulation aneurysms of <5 mm without a family or personal history of SAH.¹³ Another 30% sometimes treated these small aneurysms (40%–60% of the time). A third of the respondents in our survey were practicing neurointerventionalists who treated aneurysms in clinical practice. The utility and cost-effectiveness of routine treatment or close imaging surveillance of all small UIAs are not well-established.³⁶

Surveillance imaging may not detect growth if the intervals are too far apart. Other studies have suggested that aneurysms might bleed shortly after formation, and most aneurysms without early rupture may remain stable for life, thereby questioning the rationale for prophylactic treatment of incidental small UIAs.³⁷ Significant heterogeneity in imaging follow-up protocols has been demonstrated in both untreated and treated aneurysms.^{13,38}

The AHA/ASA guidelines recommend that patients with documented enlargement during follow-up should be offered treatment in the absence of prohibitive comorbidities (Class I; Level of Evidence B). Long-term follow-up imaging may be considered after treatment, given the combined risk of aneurysm recurrence and de novo aneurysm formation (Class IIB; Level of Evidence B). The timing and duration of follow-up is, however, not defined for

treated and untreated aneurysms, and additional investigation has been deemed necessary.⁸

Aneurysm growth is probably an irregular and discontinuous process, with potentially long periods of stability interjected with brief periods of wall instability, permitting growth or aneurysm rupture.^{19,24,39} Some studies have suggested a decreased risk of aneurysm rupture after 5 years. However, in the only long-term study of patients diagnosed with UIAs between 1956 and 1978 and prospectively followed, the median time between diagnosis and a subsequent aneurysm rupture was 10.6 years (range, 1.2–24.4 years), with a median follow-up of 24.4 years.³⁴

The cost-effectiveness of screening for asymptomatic UIAs depends on multiple factors: the likelihood of UIA detection in the study population; the sensitivity and specificity of the imaging technique; the risk of rupture in conservatively followed UIAs; the cost, morbidity, and mortality associated with treatment (such as coiling or clipping); and the risk of subsequent rupture after aneurysm treatment. The AHA/ASA guidelines recommend screening in patients with ≥ 2 family members with intracranial aneurysms or subarachnoid hemorrhage and in patients with a history of autosomal polycystic kidney disease (Class I; Level of Evidence B).⁸

There are several limitations in interpreting the results of this survey. The survey was designed to study general imaging practices and perceptions among specialists in neuroimaging. Each aneurysm has unique characteristics, and each patient needs individual consideration. The survey did not address consideration of specific features such as aneurysm location that may significantly impact treatment decisions. An overrepresentation of neurointerventional radiologists (29%) in the respondents might bias the results toward aggressive, routine treatment of small UIAs. The study was also subject to inherent limitations of survey methodology.

CONCLUSIONS

This survey of practicing neuroradiologists and neurointerventionalists demonstrates significant variability in the perceptions and surveillance practices for small UIAs. This is not surprising given the heterogeneity in the current guidelines and literature coupled with the lack of a clear understanding of the natural history of small UIAs. Better evidence is needed to determine the optimal imaging criteria to assess aneurysm growth and rupture risk. By increasing awareness of the considerable heterogeneity in clinical practice, this study highlights the gap in radiologists' perspectives and the need for standardization of surveillance and treatment practices for patients with UIAs.

REFERENCES

1. Vlak MH, Algra A, Brandenburg R, et al. **Prevalence of unruptured intracranial aneurysms, with emphasis on sex, age, comorbidity, country, and time period: a systematic review and meta-analysis.** *Lancet Neurol* 2011;10:626–36 [CrossRef Medline](#)
2. Qureshi AI, Suri MF, Nasar A, et al. **Trends in hospitalization and mortality for subarachnoid hemorrhage and unruptured aneurysms in the United States.** *Neurosurgery* 2005;57:1–8; discussion 1–8 [Medline](#)
3. Malhotra A, Wu X, Forman HP, et al. **Growth and rupture risk of small unruptured intracranial aneurysms: a systematic review.** *Ann Intern Med* 2017;167:26–33 [CrossRef Medline](#)

4. Steiner T, Juvela S, Unterberg A, et al; European Stroke Organization. **European Stroke Organization guidelines for the management of intracranial aneurysms and subarachnoid haemorrhage.** *Cerebrovasc Dis (Basel, Switzerland)* 2013;35:93–112 CrossRef Medline
5. Go AS, Mozaffarian D, Roger VL, et al; American Heart Association Statistics Committee and Stroke Statistics Subcommittee. **Heart disease and stroke statistics: 2014 update—a report from the American Heart Association.** *Circulation* 2014;129:e28–92 CrossRef Medline
6. Wiebers DO, Whisnant JP, Huston J 3rd, et al; International Study of Unruptured Intracranial Aneurysms Investigators. **Unruptured intracranial aneurysms: natural history, clinical outcome, and risks of surgical and endovascular treatment.** *Lancet* 2003;362:103–10 CrossRef Medline
7. Morita A, Kirino T, Hashi K, et al; UCAS Japan Investigators. **The natural course of unruptured cerebral aneurysms in a Japanese cohort.** *N Engl J Med* 2012;366:2474–82 CrossRef Medline
8. Thompson BG, Brown RD Jr, Amin-Hanjani S, et al; American Heart Association Stroke Council, Council on Cardiovascular and Stroke Nursing, and Council on Epidemiology and Prevention, American Heart Association, American Stroke Association. **Guidelines for the management of patients with unruptured intracranial aneurysms: a guideline for healthcare professionals from the American Heart Association/American Stroke Association.** *Stroke* 2015;46:2368–400 CrossRef Medline
9. Murayama Y, Takao H, Ishibashi T, et al. **Risk analysis of unruptured intracranial aneurysms: prospective 10-year cohort study.** *Stroke* 2016;47:365–71 CrossRef Medline
10. Wardlaw JM, White PM. **The detection and management of unruptured intracranial aneurysms.** *Brain* 2000;123(Pt 2):205–21 CrossRef Medline
11. Wong GK, Teoh J, Chan EK, et al. **Intracranial aneurysm size responsible for spontaneous subarachnoid haemorrhage.** *Br J Neurosurg* 2013;27:34–39 CrossRef Medline
12. Alshafai N, Falenchuk O, Cusimano MD. **Practices and controversies in the management of asymptomatic aneurysms: results of an international survey.** *Br J Neurosurg* 2015;29:758–64 CrossRef Medline
13. Fargen KM, Soriano-Baron HE, Rushing JT, et al. **A survey of intracranial aneurysm treatment practices among United States physicians.** *J Neurointerv Surg* 2018;10:44–49 CrossRef Medline
14. Wermer MJ, van der Schaaf IC, Algra A, et al. **Risk of rupture of unruptured intracranial aneurysms in relation to patient and aneurysm characteristics: an updated meta-analysis.** *Stroke* 2007;38:1404–10 CrossRef Medline
15. Güresir E, Vatter H, Schuss P, et al. **Natural history of small unruptured anterior circulation aneurysms: a prospective cohort study.** *Stroke* 2013;44:3027–31 CrossRef Medline
16. Villablanca JP, Duckwiler GR, Jahan R, et al. **Natural history of asymptomatic unruptured cerebral aneurysms evaluated at CT angiography: growth and rupture incidence and correlation with epidemiologic risk factors.** *Radiology* 2013;269:258–65 CrossRef Medline
17. Backes D, Rinkel GJ, Laban KG, et al. **Patient- and aneurysm-specific risk factors for intracranial aneurysm growth: a systematic review and meta-analysis.** *Stroke* 2016;47:951–57 CrossRef Medline
18. Connolly ES Jr, Rabinstein AA, Carhuapoma JR, et al; American Heart Association Stroke Council, Council on Cardiovascular Radiology and Intervention, Council on Cardiovascular Nursing, Council on Cardiovascular Surgery and Anesthesia, Council on Clinical Cardiology. **Guidelines for the management of aneurysmal subarachnoid hemorrhage: a guideline for healthcare professionals from the American Heart Association/American Stroke Association.** *Stroke* 2012;43:1711–37 CrossRef Medline
19. Chmayssani M, Rebeiz JG, Rebeiz TJ, et al. **Relationship of growth to aneurysm rupture in asymptomatic aneurysms ≤ 7 mm: a systematic analysis of the literature.** *Neurosurgery* 2011;68:1164–71; discussion 1171 CrossRef Medline
20. Li MH, Chen SW, Li YD, et al. **Prevalence of unruptured cerebral aneurysms in Chinese adults aged 35 to 75 years: a cross-sectional study.** *Ann Intern Med* 2013;159:514–21 CrossRef Medline
21. Juvela S, Poussa K, Lehto H, et al. **Natural history of unruptured intracranial aneurysms: a long-term follow-up study.** *Stroke* 2013;44:2414–21 CrossRef Medline
22. Ishibashi T, Murayama Y, Urashima M, et al. **Unruptured intracranial aneurysms: incidence of rupture and risk factors.** *Stroke* 2009;40:313–16 CrossRef Medline
23. Sonobe M, Yamazaki T, Yonekura M, et al. **Small unruptured intracranial aneurysm verification study: SUAVE study, Japan.** *Stroke* 2010;41:1969–77 CrossRef Medline
24. Bor AS, Tiel Groenestege AT, terBrugge KG, et al. **Clinical, radiological, and flow-related risk factors for growth of untreated, unruptured intracranial aneurysms.** *Stroke* 2015;46:42–48 CrossRef Medline
25. Burns JD, Huston J 3rd, Layton KF, et al. **Intracranial aneurysm enlargement on serial magnetic resonance angiography: frequency and risk factors.** *Stroke* 2009;40:406–11 CrossRef Medline
26. Ferns SP, Sprengers ME, van Rooij WJ, et al. **De novo aneurysm formation and growth of untreated aneurysms: a 5-year MRA follow-up in a large cohort of patients with coiled aneurysms and review of the literature.** *Stroke* 2011;42:313–18 CrossRef Medline
27. Mehan WA Jr, Romero JM, Hirsch JA, et al. **Unruptured intracranial aneurysms conservatively followed with serial CT angiography: could morphology and growth predict rupture? J Neurointerv Surg** 2014;6:761–66 CrossRef Medline
28. Nader-Sepahi A, Casimiro M, Sen J, et al. **Is aspect ratio a reliable predictor of intracranial aneurysm rupture?** *Neurosurgery* 2004;54:1343–47; discussion 1347–48 CrossRef Medline
29. Hoh BL, Siström CL, Firment CS, et al. **Bottleneck factor and height-width ratio: association with ruptured aneurysms in patients with multiple cerebral aneurysms.** *Neurosurgery* 2007;61:716–22; discussion 722–23 CrossRef Medline
30. Yasuda R, Strother CM, Taki W, et al. **Aneurysm volume-to-ostium area ratio: a parameter useful for discriminating the rupture status of intracranial aneurysms.** *Neurosurgery* 2011;68:310–17; discussion 317–18 CrossRef Medline
31. Dhar S, Tremmel M, Mocco J, et al. **Morphology parameters for intracranial aneurysm rupture risk assessment.** *Neurosurgery* 2008;63:185–96; discussion 196–97 CrossRef Medline
32. Lauric A, Baharoglu MI, Malek AM. **Ruptured status discrimination performance of aspect ratio, height/width, and bottleneck factor is highly dependent on aneurysm sizing methodology.** *Neurosurgery* 2012;71:38–45 CrossRef Medline
33. Lauric A, Baharoglu MI, Gao BL, et al. **Incremental contribution of size ratio as a discriminant for rupture status in cerebral aneurysms: comparison with size, height, and vessel diameter.** *Neurosurgery* 2012;70:944–51; discussion 951–52 CrossRef Medline
34. Juvela S, Korja M. **Intracranial aneurysm parameters for predicting a future subarachnoid hemorrhage: a long-term follow-up study.** *Neurosurgery* 2017;81:432–40 CrossRef Medline
35. Suh SH, Cloft HJ, Huston J 3rd, et al. **Interobserver variability of aneurysm morphology: discrimination of the daughter sac.** *J Neurointerv Surg* 2016;8:38–41 CrossRef Medline
36. Malhotra A, Wu X, Forman HP, et al. **Management of tiny unruptured intracranial aneurysms: a comparative effectiveness analysis.** *JAMA Neurol* 2018;75:27–34 CrossRef Medline
37. Sato K, Yoshimoto Y. **Risk profile of intracranial aneurysms: rupture rate is not constant after formation.** *Stroke* 2011;42:3376–81 CrossRef Medline
38. Gupta R, Griessenauer CJ, Adeeb N, et al. **Evaluating imaging follow-up strategies and costs of unruptured intracranial aneurysms treated with endovascular techniques: a survey of academic neurovascular centers in the United States.** *World Neurosurg* 2016;94:360–67 CrossRef Medline
39. Koffijberg H, Buskens E, Algra A, et al. **Growth rates of intracranial aneurysms: exploring constancy.** *J Neurosurg* 2008;109:176–85 CrossRef Medline

Diagnosing Early Ischemic Changes with the Latest-Generation Flat Detector CT: A Comparative Study with Multidetector CT

I.L. Maier, J.R. Leyhe, I. Tsogkas, D. Behme, K. Schregel, M. Knauth, M. Schnieder, J. Liman, and M.-N. Psychogios



ABSTRACT

BACKGROUND AND PURPOSE: One-stop management of mechanical thrombectomy–eligible patients with large-vessel occlusion represents an innovative approach in acute stroke treatment. This approach reduces door-to-reperfusion times by omitting multidetector CT, using flat detector CT as pre-mechanical thrombectomy imaging. The purpose of this study was to compare the diagnostic performance of the latest-generation flat detector CT with multidetector CT.

MATERIALS AND METHODS: Prospectively derived data from patients with ischemic stroke with large-vessel occlusion and mechanical thrombectomy were analyzed in this monocentric study. All included patients underwent multidetector CT before referral to our comprehensive stroke center and flat detector CT in the angiography suite before mechanical thrombectomy. Diagnosis of early ischemic signs, quantified by the ASPECTS, was compared between modalities using cross tables, the Pearson correlation, and Bland-Altman plots. The predictive value of multidetector CT– and flat detector CT–derived ASPECTS for functional outcome was investigated using area under the receiver operating characteristic curve analysis.

RESULTS: Of 25 patients, 24 (96%) had flat detector CT with sufficient diagnostic quality. Median multidetector CT and flat detector CT ASPECTSs were 7 (interquartile range, 5.5–9 and 4.25–8, respectively) with a mean period of 143.6 ± 49.5 minutes between both modalities. The overall sensitivity was 85.1% and specificity was 83.1% for flat detector CT ASPECTS compared with multidetector CT ASPECTS as the reference technique. Multidetector CT and flat detector CT ASPECTS were strongly correlated ($r = 0.849$, $P < .001$) and moderately predicted functional outcome (area under the receiver operating characteristic curve, 0.738; $P = .007$ and .715; $P = .069$, respectively).

CONCLUSIONS: Determination of ASPECTS on flat detector CT is feasible, showing no significant difference compared with multidetector CT ASPECTS and a similar predictive value for functional outcome. Our findings support the use of flat detector CT for emergency stroke imaging before mechanical thrombectomy to reduce door-to-groin time.

ABBREVIATIONS: FDCT = flat detector CT; IQR = interquartile range; LVO = large-vessel occlusion; MDCT = multidetector CT; MT = mechanical thrombectomy

In acute major ischemic stroke, the superiority of mechanical thrombectomy (MT) in combination with IV thrombolysis compared with IV thrombolysis alone has been demonstrated in multiple studies.¹ In patients eligible for MT, symptom-to-reperfusion time has been shown to be one of the most impor-

tant determinants for stroke outcome² and influences stroke mortality.³

Thus, the direct transfer of patients with acute cerebral large-vessel occlusions (LVOs) to the angiography suite represents an innovative approach to reduce door-to-reperfusion times and consequently to improve functional outcomes.⁴ A recent retrospective analysis comparing patients with direct referral to the angiography suite for MT and patients with prior admission to the emergency department showed significantly reduced symptom-to-treatment times and demonstrated the feasibility and safety of this approach.⁵ Rather than omitting the emergency department, another approach to direct angiography suite referral is to skip the multidetector CT (MDCT), performing emergency stroke imaging in the angiography suite with flat detector CT (FDCT) and multiphase flat detector CTA followed by MT without delay. This previously reported approach^{6,7} explicitly addresses the delay

Received October 22, 2017; accepted after revision January 24, 2018.

From the Departments of Neurology (I.L.M., M.S., J.L.) and Neuroradiology (J.R.L., I.T., D.B., K.S., M.K., M.-N.P.), University Medical Center Goettingen, Goettingen, Germany.

This study was supported by the Göttinger Kolleg für Translationale Medizini and the Niedersächsische Ministerium für Wissenschaft und Kultur.

Please address correspondence to Marios-Nikos Psychogios, MD, Department of Neuroradiology, University Medicine Goettingen, Robert-Koch-Str 40, 37075 Goettingen, Germany; e-mail: m.psychogios@med.uni-goettingen.de; @MPeyTI

Indicates article with supplemental on-line table.

<http://dx.doi.org/10.3174/ajnr.A5595>

from MDCT imaging to angiography suite referral, which has been identified as a crucial factor concerning in-hospital delays for the treatment of MT-eligible patients.² However, for this approach, not only intracerebral hemorrhage but also ischemic lesions must be reliably diagnosed by FDCT.

An older study comparing MDCT with FDCT after neurointerventional procedures demonstrated the high specificity and sensitivity of FDCT for the detection of intracerebral hemorrhage and hydrocephalus but could not demonstrate diagnostic sufficiency for the diagnosis of ischemic lesions.⁸ Another, more recent study comparing peri-interventional FDCT with postinterventional MDCT after different neurointerventional procedures again showed high sensitivity and specificity for the detection of intracerebral hemorrhage in different locations.⁹ However, this study was limited in the detection of early ischemic changes on FDCT by a long period between modalities (4.3 hours), the use of contrast-/postcontrast agent series, and the use of the ASPECTS as a complete score without the sensitivity/specificity analysis of the predefined brain regions.

The aim of our study was to provide further evidence for the feasibility and reliability of the diagnosis of ischemic changes on FDCT compared with MDCT in patients with acute stroke. Therefore, we compared ASPECTS determined on MDCT and on FDCT performed before MT.

MATERIALS AND METHODS

Ethical Approval

All procedures performed in studies involving human participants were in accordance with the ethical standards of the institutional research committee and with the 1964 Declaration of Helsinki and its later amendments or comparable ethical standards.

Patient Selection

Clinical and neuroradiologic data were analyzed from a prospectively derived, monocentric data base including neuroradiologic and neurologic information of interventional treatment and clinical outcome. Ethics approval was sought from the ethics committee of our tertiary care center, and all patients or next of kin gave informed written consent for the anonymized use of disease-related data on hospitalization.

Patients who presented to a secondary care hospital with acute major ischemic stroke symptoms where they underwent MDCT and CTA were included. After confirmation of LVO, these patients were referred to our tertiary care center for MT. Patients were transferred directly to the angiography suite, where FDCT and MT were performed (“one-stop management” in acute stroke care).⁷ Clinical data including stroke scores (baseline NIHSS score) and baseline/follow-up mRS scores (at discharge or after 90 days) were determined by a certified stroke neurologist. Favorable functional outcome was defined as an mRS ≤ 2 at 90 days or at discharge if the 90-day data were missing.

Data Acquisition

FDCT was performed with a biplane flat detector angiography system (Artis Q; Siemens, Erlangen, Germany) using the following parameters: 20 seconds of rotation, 200° total angle with ap-

proximately 500 projections, 2×2 binning, 109 kV, $1.8 \mu\text{Gy}/\text{frame}$, weighted CT dose index $\sim 60 \text{ mGy}$, effective dose $\sim 2.5 \text{ mSv}$. Initial FDCT projections were then reconstructed on a post-processing workstation (syngo X Workplace; Siemens) with a Hounsfield unit smooth kernel and DynaCT Clear algorithm (Siemens) to images with a 512×512 matrix. MDCT before admission was acquired on Somatom Emotion or Somatom Emotion 16 (Siemens) or Optima CT660 scanner (GE Healthcare, Milwaukee, Wisconsin) using a standard brain scan protocol. Raw FDCT and MDCT data were extracted from the PACS of the department, anonymized, reconstructed parallel to the orbitomeatal plane with a slice thickness of 5 mm and slice distance of 3 mm, and imported for evaluation into the aforementioned postprocessing workstation.

Image Evaluation

All images were analyzed by 2 experienced neuroradiologists (M.-N.P., with >5 years of experience, and K.S., with >3 years of experience) and a trained medical student (J.R.L.). Imaging was qualified using the categories “excellent,” “slightly compromised,” “moderately compromised,” and “severely compromised” (not diagnostic). On all MDCT and FDCT scans with sufficient quality, early ischemic signs were determined using the ASPECTS.¹⁰ The presence of a dense artery sign and intracerebral hemorrhage was noted. FDCT and MDCT images were evaluated with a 4-week break, to limit recall bias.

Statistical Analysis

Statistical analysis was performed using the MedCalc statistical package 16.8 (MedCalc Software, Mariakerke, Belgium). Characteristics of all patients are shown as mean \pm SD if normally distributed and as median with interquartile range (IQR), if not. Sensitivity and specificity were determined using cross tables. ASPECTS ratings on FDCT and MDCT were compared using the Pearson correlation and the Bland-Altman plot. Interrater reliability was determined using the Cohen κ . To assess the predictive value of MDCT and FDCT ASPECTS, we used an area under the receiver operating characteristic curve. Cutoff scores were defined as scores with a maximal Youden index. For all statistical methods, P values $< .05$ were considered significant.

RESULTS

Twenty-five patients with both MDCT and FDCT before MT were identified (Table 1). The mean age was 77.3 ± 10.3 years with a median NIHSS score at admission of 17 points (IQR, 14–19 points). Mean symptom-to-groin time was 249.3 ± 57.1 minutes with a mean period of 143.6 ± 49.5 minutes between MDCT and FDCT. Most patients had an occlusion of either the carotid terminus or the MCA (11 patients [44%] each), and 88% of patients were successfully recanalized. Three (12%) patients were intubated at the time of MT. Median MDCT and FDCT ASPECTSs were 7 (IQR, 5.5–9 and 4.25–8, respectively).

There was no overall difference in the judgment of image quality between MDCT and FDCT (On-line Table). One patient (4.2%) showed extreme motion artifacts, leading to severely compromised FDCT imaging quality on which the ASPECTS could not be determined. FDCT was judged to have slightly compro-

Table 1: Baseline characteristics

Parameter (n = 25)	
Age (mean) (yr)	77.3 ± 10.3
Sex (male) (%)	10 (40)
Occluded vessel	
Proximal ICA (No.) (%)	1 (4)
Carotid terminus (No.) (%)	11 (44)
M1 (No.) (%)	11 (44)
M2 (No.) (%)	2 (8)
IV thrombolysis (No.) (%)	15 (60)
Transfer patients ^a	
Drip and ship (No.) (%)	14 (56)
Ship and drip (No.) (%)	1 (4)
Just ship (No.) (%)	10 (40)
General anesthesia at the time of FDCT (No.) (%)	3 (12)
Arterial hypertension (No.) (%)	19 (76)
Hyperlipoproteinemia (No.) (%)	11 (44)
Diabetes mellitus (No.) (%)	9 (36)
Atrial fibrillation (No.) (%)	8 (32)
Coronary artery disease (No.) (%)	9 (36)
Chronic kidney failure (No.) (%)	7 (28)
NIHSS score on admission (median) (IQR)	17 (14–19)
mRS score on admission (median) (IQR)	5 (4–5)
Successful reperfusion (No.) (%)	22 (88)
Symptom-to-groin time (mean) (min)	249.3 ± 57.1
Symptom-to-reperfusion time (n = 22) (mean) (min)	294.6 ± 66.3
Door-to-groin time (mean) (min)	25.2 ± 8.9
Door-to-reperfusion time (n = 22) (mean) (min)	77.3 ± 30
Symptom-to-MDCT time (mean) (min)	99.4 ± 52.6
Symptom-to-FDCT time (mean) (min)	234.9 ± 55.2
MDCT-to-FDCT time (mean) (min)	143.6 ± 49.5
MDCT ASPECTS (median) (IQR)	7 (5.5–9)
FDCT ASPECTS (median) (IQR)	7 (4.25–8)

^a Drip and ship: transfer patients with IV thrombolysis started in a peripheral stroke center; ship and drip: transfer patients with IV thrombolysis started in our tertiary stroke center; just ship: transfer patients without IV thrombolysis.

mised image quality in 11 (44%) and moderately compromised image quality in 3 (12%) patients. On FDCT, motion artifacts were visible in 15 (60%) patients; streak-artifacts, in 3 (12%) patients; and metal artifacts, in 1 (4%) patient. The remaining 6 (24%) patients had no visible artifacts.

Figures 1 and 2 show MDCT and FDCT examples of 2 representative patients, one with ASPECTS of 9 on MDCT and 8 on FDCT and one with ASPECTS of 0 on MDCT and 2 on FDCT (please refer to the figure legends for further details).

As shown in Fig 3, MDCT and FDCT ASPECTS showed a very strong correlation ($r = 0.849$, $P < .001$). Table 2 gives an overview of all individual ASPECTSs determined on MDCT and FDCT. ASPECTS ratings on FDCT showed a mean difference of 0.8 points (95% CI, 0.28–1.3 points) compared with MDCT ASPECTS on the Bland-Altman plot (Fig 4).

Table 3 depicts the sensitivity and specificity of FDCT ASPECTS compared with MDCT ASPECTS. The overall sensitivity was 85.1% and specificity was 83.2% for FDCT ASPECTS compared with MDCT as the reference method. When we compared the accuracy of FDCT for the determination of early ischemic signs in every single location, sensitivity and specificity were highest for M2, M4, and the caudate nucleus and lowest for M3, the lentiform nucleus, and internal capsule. The diagnostic accuracy of FDCT to detect a dense media sign was lower compared with detection of early ischemic signs (sensitivity = 72.2%, specificity = 66.7%). Interrater agreement for MDCT ASPECTS was

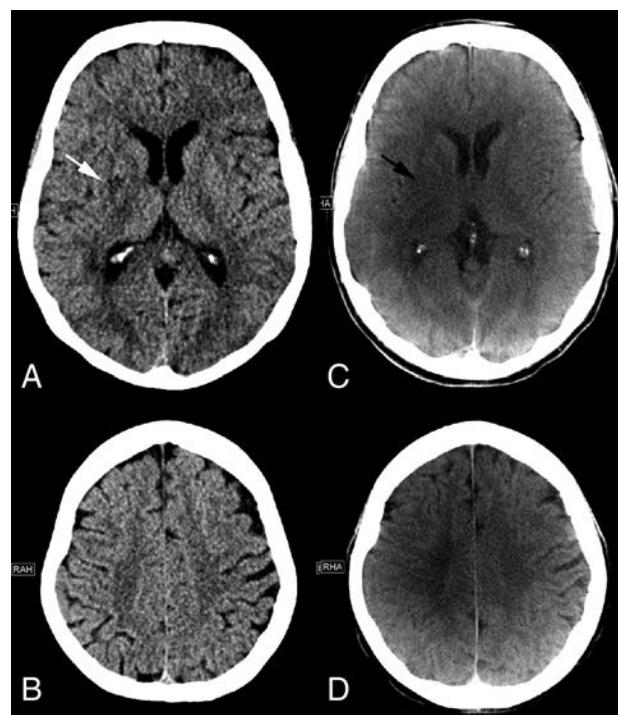


FIG 1. Initial MDCT in the peripheral stroke center shows hypodensity of the right lentiform nucleus (white arrow) and no other early ischemic signs on the ganglionic (A) or supraganglionic (B) level. An ASPECTS of 9 was rated on MDCT images. C, FDCT acquired in our comprehensive stroke center 172 minutes after the initial CT shows hypodensities of the right lentiform nucleus (black arrow) and insula. No early ischemic signs were detected on the supraganglionic level, resulting in an ASPECTS of 8.

excellent between the 2 neuroradiologists ($\kappa = 0.942$, $P < .001$) and between the most experienced neuroradiologist and the trained medical student ($\kappa = 0.843$, $P < .001$). For FDCT ASPECTS, the interrater agreement was also excellent between the 2 neuroradiologists ($\kappa = 0.865$, $P < .001$) and good between the most experienced neuroradiologist and the trained medical student ($\kappa = 0.713$, $P < .001$).

Eight patients (33.3%) had a follow-up mRS of ≤ 2 . Figure 5 shows the receiver operating characteristic curves of both the MDCT and FDCT ASPECTS for the prediction of favorable functional outcome. The predictive value of both MDCT and FDCT ASPECTS was moderate (area under the receiver operating characteristic curve MDCT ASPECTS = 0.738; $P = .007$; FDCT ASPECTS = 0.715; $P = .069$). The comparison of the predictive values of both scores revealed no statistically significant difference ($P = .778$).

DISCUSSION

Innovative approaches to reduce door-to-groin times have been proposed recently for patients with LVO.^{5,6,9,11} These approaches include the direct referral of MT-eligible patients to the angiography suite with a variation of imaging or no imaging proposed by the various authors. We have recently published an innovative one-stop-management protocol, which includes both noncontrast imaging and multiphase CTA (acquired in the angiography suite). Omitting MDCT seems plausible because it has been shown that among 1000 patients with successful MT, for every 15

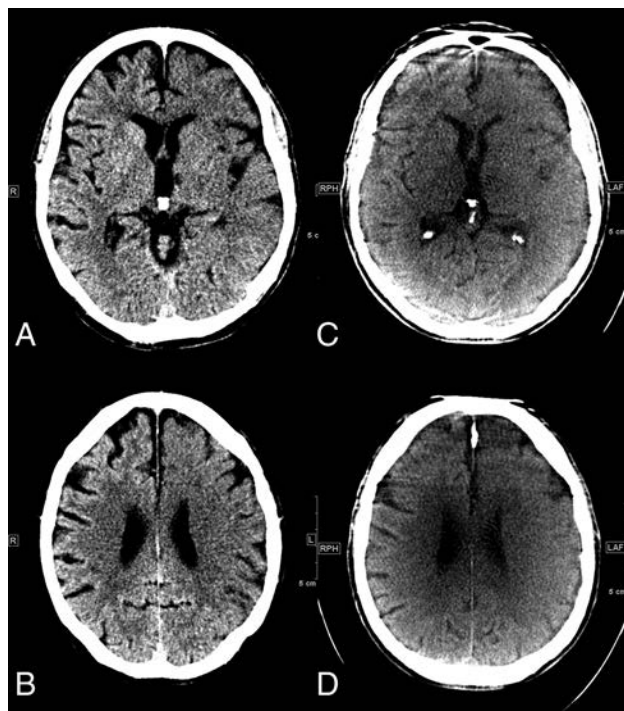


FIG 2. A, Initial MDCT in the peripheral stroke center shows hypodensities of the left striatum, insula, internal capsule, M1, M2, and M3 segments. B, In the supraganglionic levels, we observe early signs in the M4, M5, and M6 segments, resulting in an ASPECTS of 0. C and D, FDCT acquired in our comprehensive stroke center 94 minutes after the initial CT shows early ischemic signs in the left anterior cerebral artery and MCA territories, resulting in an ASPECTS of 2. The M3 and M6 segments are not classified as ischemic on FDCT images.

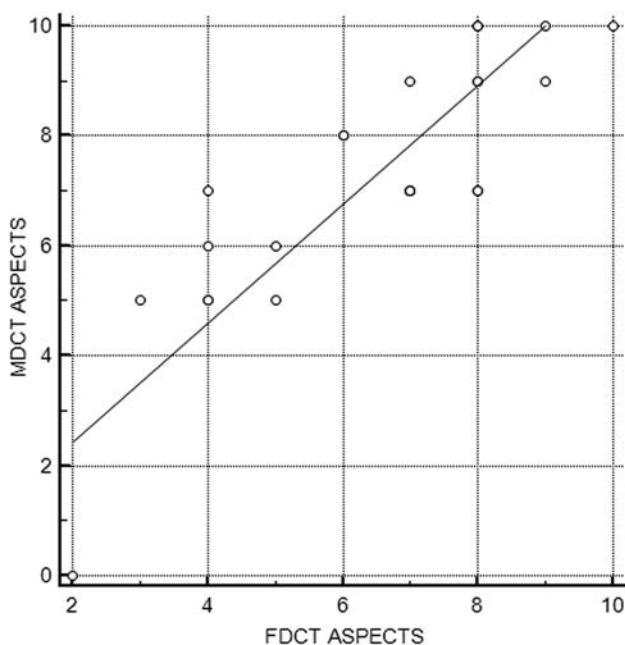


FIG 3. Pearson correlation between MDCT and FDCT ASPECTS.

minutes of faster door-to-reperfusion time, 39 patients would be less disabled at 3-month follow-up, including 25 patients achieving an mRS of 0–2.² In this context, the Highly Effective Reperfusion evaluated in Multiple Endovascular Stroke trials (HERMES) collaborators reported that only 4% of the patients

Table 2: Overview of all individual ASPECTS determined on MDCT and FDCT

Patient No.	ASPECTS	
	MDCT	FDCT
1	10	8
2	9	8
3	7	7
4	10	10
5	10	8
6	7	8
7	7	7
8	8	6
9	9	7
10	5	5
11	3	NA ^a
12	6	5
13	9	8
14	9	9
15	5	4
16	7	4
17	7	7
18	0	2
19	5	3
20	7	7
21	8	6
22	6	4
23	10	9
24	5	4
25	7	8

Note:—NA indicates not applicable.

^a Patient 11 had an FDCT with severely compromised (nondiagnostic) imaging quality.

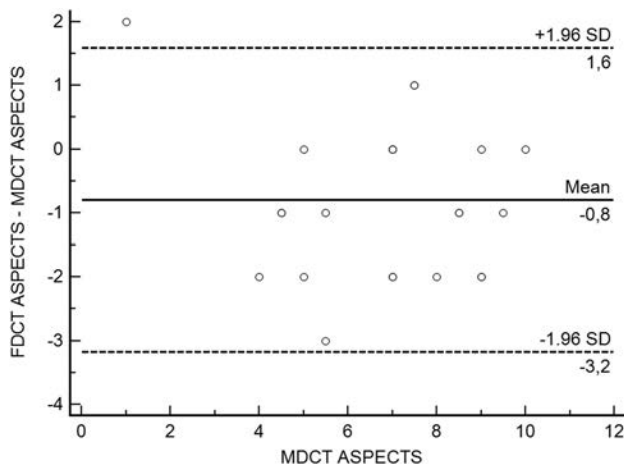


FIG 4. Bland-Altman plot of MDCT and FDCT ASPECTS.

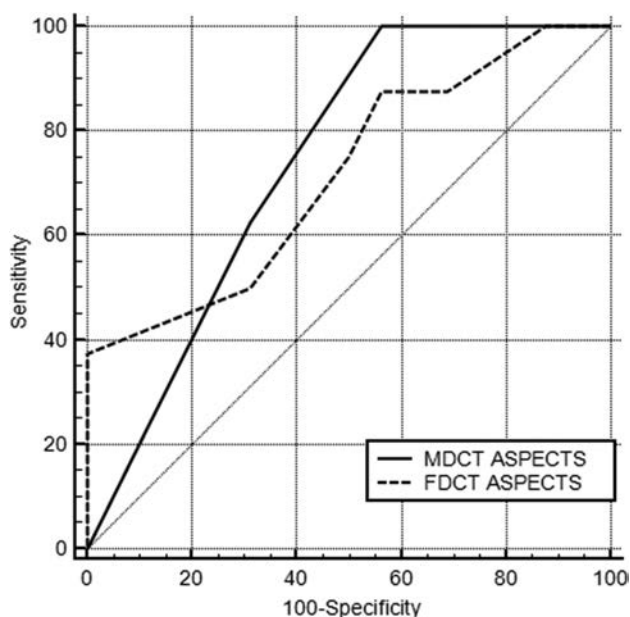
included in the most recent large thrombectomy trials had an MDCT-to-groin puncture time of ≤ 30 minutes, which represents the latest recommendation of the Society of NeuroInterventional Surgery.^{2,12}

However, the approach to perform stroke imaging directly in the angiography suite requires comparable diagnostic accuracy of FDCT and MDCT as the reference method. This includes comparable sensitivity to detect intracerebral hemorrhage, vessel occlusion, and collateral status as well as ischemic changes. For the latter, it can be questioned whether detection of early ischemic signs on initial FDCT is necessary at all because there is evidence that patients with low ASPECTS also benefit from MT.¹³ However, the pre-MT ASPECTS can be very important for the treating

Table 3: Number of patients with early ischemic signs in different regions according to the ASPECTS on MDCT vs FDCT (n = 24)

	ASPECTS				
	Early Ischemic Signs on MDCT	Early Ischemic Signs on FDCT	Early Ischemic Signs on MDCT and FDCT	Sensitivity	Specificity
M1 (No.) (%)	2 (8.3)	3 (12.5)	1 (4.2)	50	90.1
M2 (No.) (%)	2 (8.3)	7 (29.2)	2 (8.3)	100	77.3
M3 (No.) (%)	1 (4.2)	1 (4.2)	0 (0)	0	95.8
C (No.) (%)	14 (58.3)	14 (58.3)	13 (54.2)	92.9	90
L (No.) (%)	15 (62.5)	21 (58.3)	14 (58.3)	93.2	22.2
IC (No.) (%)	3 (12.5)	4 (16.7)	1 (4.2)	33.3	85.7
I (No.) (%)	18 (75)	22 (91.7)	18 (75)	100	33.3
M4 (No.) (%)	5 (20.8)	8 (33.3)	5 (20.8)	100	84.2
M5 (No.) (%)	4 (16.7)	6 (25)	3 (12.5)	75	85
M6 (No.) (%)	3 (12.5)	0 (0)	0 (0)	NA	NA
Overall (No.) (% of 240 locations)	67 (27.9)	86 (35.8)	57 (23.8)	85.1	83.2
Dense media sign (No. positive) (%)	18 (75)	15 (62.5)	13 (54.2)	72.2	66.7

Note:—Anatomic regions according to the Alberta Stroke Program Early CT Score: M1–M6 indicate cortical regions of the medial cerebral artery territory; C, caudate nucleus; L, lentiform nucleus; IC, internal capsule; I, insula; NA, not applicable.

**FIG 5.** Area under the receiver operating curve analysis for the predictive value of MDCT and FDCT ASPECTS for favorable functional outcome (mRS \leq 2).

neurointerventionalist in patients with wake-up strokes or unknown clinical onset as well as in scenarios in which intervention is prolonged and termination of the MT has to be discussed after multiple thrombectomy maneuvers.

There is growing evidence that FDCT can be reliably used to exclude intracerebral hemorrhage^{9,14,15} and that the use of time-resolved flat detector CTA and flat detector CTP is feasible, showing sufficient reliability for decision-making.^{16,17} One of the most recent studies addressing the reliability of FDCT in acute stroke by Eckert et al¹⁵ also reported data on the reliability of detecting ischemic changes on FDCT. This study reported poor sensitivity for FDCT to detect early ischemic signs compared with post-MT MDCT. However, the authors of this study evaluated FDCT images acquired with an older angiography system (Axiom Artis dBA; Siemens) and did not use ASPECTS as a systematic evaluation method to search for early ischemic changes, and only 4 (12.5%) of the 32 patients with ischemic stroke included in this

study had early ischemic changes on the initial MDCT.¹⁵ In contrast, we used a latest-generation angiography suite with 16-bit readout, which allows better contrast resolution compared with the older systems. Additionally, 20 (83.3%) of the 24 patients included in our study had early ischemic signs on initial MDCT (ASPECTS $<$ 10), which renders our cohort more eligible for the comparison of ischemic signs detected on MDCT versus FDCT. Moreover, Eckert et al¹⁵ also included patients with vertebral and basilar artery occlusions, predominantly causing infratentorial ischemia, for which the diagnostic accuracy of FDCT is generally lower compared with the supratentorial region.⁹ In contrast to the study by Eckert et al, our results are in line with findings from a previous study by Leyhe et al,⁹ which showed high sensitivity and specificity for detecting large ischemic changes (ASPECTS \leq 5) on FDCT compared with MDCT.

In our study, FDCT ASPECTS was 0.8 points lower compared with MDCT. This difference could be explained by the delay between both modalities, in which ischemia could have developed in the context of persistent LVO during the transfer from the secondary care hospital to our comprehensive stroke center. This difference is in agreement with findings from a study by Sun et al,¹⁸ which showed an average ASPECTS decline of 1 point if the patient was transferred from another hospital for MT. In the study by Leyhe et al,⁹ a mean ASPECTS difference between peri-interventional FDCT and postinterventional MDCT of 0.5 points was described. The higher difference found in the present study could be explained by ongoing ischemia during the period between MDCT and pre-MT FDCT, while ASPECTS comparison after successful MT (as done by Leyhe et al) is likely to be more stable.⁹

Besides the difference in ASPECTS between both modalities caused by the delay between MDCT and FDCT, increased sensitivity and specificity for FDCT ASPECTS could have been expected with a higher number of patients with general anesthesia during MT. Motion artifacts are a common problem in FDCT imaging because they can affect multiple slices and can occur more often in imaging techniques with prolonged image-acquisition times. Thus, in the latest flat detector systems, image acquisition takes 20 seconds, which increases the risk for motion artifacts.^{9,19} This is a common problem, especially in the acute setting of ischemic stroke, in which patients are often not cooperative due to aphasia or confusion. In our study, most patients underwent

MT without general anesthesia, which explains the high percentage of motion artifacts despite adequate positioning and head fixation, which have been described in detail elsewhere.⁹ These artifacts could also have been the major reason for the lower sensitivity and specificity of FDCT to detect a dense media sign because it is seen in only a small, deep brain region on a few slices. Eckert et al¹⁵ reported a comparable rate of motion artifacts but a significantly lower sensitivity to detect a dense vessel sign (a hyperdense media sign was present in 7 cases, and none were detected on FDCT). These findings underline the diagnostic limitations for the detection of dense media signs and urge combined use with flat detector CTA to reliably diagnose LVO. Additionally, the development of a faster protocol with identical contrast resolution would reduce the presence of motion artifacts.

Our findings must be interpreted considering several limitations of our study. We report retrospective, single-center data, which cannot be applied to other centers using different FDCT systems and imaging-reconstruction methods. In addition, our sample size is small, and ASPECTS raters were not blinded to the ischemic side.

CONCLUSIONS








Our study provides evidence for the feasibility and reliability of ASPECTS determination on FDCT in MT-eligible patients. Given the use of optimized, latest-generation flat detectors and optimal positioning strategies, these findings add to the one-stop approach to acute stroke care, in which emergency stroke imaging is performed in the angiography suite directly before MT, aiming to reduce door-to-groin times.

Disclosures: Ilko L. Maier—RELATED: Niedersächsische Ministerium für Wissenschaft und Kultur. Comments: The first author of this study received a grant from the Göttinger Kolleg für Translationale Medizin, which was supported by the Niedersächsische Ministerium für Wissenschaft und Kultur. Daniel Behme—UNRELATED: Payment for Lectures Including Service on Speakers Bureaus: Penumbra Deutschen Gesellschaft für Neuroradiologie e.V. (DGNR). Acandis DGNR Cologne 2017. Michael Knauth—RELATED: Grant: Siemens. Comments: research cooperation*; Consulting Fee or Honorarium: Siemens. Comments: speakers bureau; Support for Travel to Meetings for the Study or Other Purposes: Siemens. Comments: research cooperation*; UNRELATED: Consultancy: Acandis; Payment for Development of Educational Presentations: Bayer HealthCare. Comments: speakers bureau; Stock/Stock Options: Siemens. Comments: shareholder. Jan Liman—UNRELATED: Payment for Lectures Including Service on Speakers Bureaus: Stryker. Marios-Nikos Psychogios—RELATED: Grant: Siemens*; UNRELATED: Consultancy: Siemens, Stryker, Acandis, Penumbra; Payment for Development of Educational Presentations: pheno. *Money paid to the institution.

REFERENCES

- Goyal M, Menon BK, van Zwam WH, et al; HERMES collaborators. Endovascular thrombectomy after large-vessel ischaemic stroke: a meta-analysis of individual patient data from five randomised trials. *Lancet* 2016;387:1723–31 [CrossRef Medline](#)
- Saver JL, Goyal M, van der Lugt A, et al; HERMES Collaborators. Time to treatment with endovascular thrombectomy and outcomes from ischemic stroke: a meta-analysis. *JAMA* 2016;316:1279–88 [CrossRef Medline](#)
- Rinaldo L, Brinjikji W, McCutcheon BA, et al. Hospital transfer associated with increased mortality after endovascular revascularization for acute ischemic stroke. *J Neurointerv Surg* 2017;9:1166–72 [CrossRef Medline](#)
- Hung SC, Lin CJ, Guo WY, et al. Toward the era of a one-stop imaging service using an angiography suite for neurovascular disorders. *Biomed Res Int* 2013;2013:873614 [CrossRef Medline](#)
- Jadhav AP, Kenmuir CL, Aghaebrahim A, et al. Interfacility transfer directly to the neuroangiography suite in acute ischemic stroke patients undergoing thrombectomy. *Stroke* 2017;48:1884–89 [CrossRef Medline](#)
- Ribo M, Boned S, Rubiera M, et al. Direct transfer to angiosuite to reduce door-to-puncture time in thrombectomy for acute stroke. *J Neurointerv Surg* 2018;10:221–24 [CrossRef Medline](#)
- Psychogios MN, Bähr M, Liman J, et al. One stop management in acute stroke: first mothership patient transported directly to the angiography suite. *Clin Neuroradiol* 2017;27:389–91 [CrossRef Medline](#)
- Psychogios MN, Buhk JH, Schramm P, et al. Feasibility of angiographic CT in peri-interventional diagnostic imaging: a comparative study with multidetector CT. *AJNR Am J Neuroradiol* 2010;31:1226–31 [CrossRef Medline](#)
- Leyhe JR, Tsoqkas I, Hesse AC, et al. Latest generation of flat detector CT as a peri-interventional diagnostic tool: a comparative study with multidetector CT. *J Neurointerv Surg* 2017;9:1253–57 [CrossRef Medline](#)
- Pexman JH, Barber PA, Hill MD, et al. Use of the Alberta Stroke Program Early CT Score (ASPECTS) for assessing CT scans in patients with acute stroke. *AJNR Am J Neuroradiol* 2001;22:1534–42 [Medline](#)
- Psychogios MN, Behme D, Schregel K, et al. One-stop management of acute stroke patients: minimizing door-to-reperfusion times. *Stroke* 2017;48:3152–55 [CrossRef Medline](#)
- McTaggart RA, Ansari SA, Goyal M, et al; Standards and Guidelines Committee of the Society of NeuroInterventional Surgery (SNIS). Initial hospital management of patients with emergent large vessel occlusion (ELVO): report of the standards and guidelines committee of the Society of NeuroInterventional Surgery. *J Neurointerv Surg* 2017;9:316–23 [CrossRef Medline](#)
- Yoo AJ, Berkhemer OA, Franssen PSS, et al; MR CLEAN investigators. Effect of baseline Alberta Stroke Program Early CT Score on safety and efficacy of intra-arterial treatment: a subgroup analysis of a randomised phase 3 trial (MR CLEAN). *Lancet Neurol* 2016;15:685–94 [CrossRef Medline](#)
- Frölich AM, Buhk JH, Fiehler J, et al. Voxel-based sensitivity of flat-panel CT for the detection of intracranial hemorrhage: comparison to multi-detector CT. *PLoS One* 2016;11:e0165794 [CrossRef Medline](#)
- Eckert M, Göllitz P, Lücking H, et al. Optimized flat-detector CT in stroke imaging: ready for first-line use? *Cerebrovasc Dis* 2017;43:9–16 [CrossRef Medline](#)
- Niu K, Yang P, Wu Y, et al. C-arm conebeam CT perfusion imaging in the angiographic suite: a comparison with multidetector CT perfusion imaging. *AJNR Am J Neuroradiol* 2016;37:1303–09 [CrossRef Medline](#)
- Yang P, Niu K, Wu Y, et al. Evaluation of collaterals and clot burden using time-resolved C-arm conebeam CT angiography in the angiography suite: a feasibility study. *AJNR Am J Neuroradiol* 2017;38:747–52 [CrossRef Medline](#)
- Sun CH, Connelly K, Nogueira RG, et al. ASPECTS decay during inter-facility transfer predicts patient outcomes in endovascular reperfusion for ischemic stroke: a unique assessment of dynamic physiologic change over time. *J Neurointerv Surg* 2015;7:22–26 [CrossRef Medline](#)
- Struffert T, Eyupoglu IY, Huttner HB, et al. Clinical evaluation of flat-panel detector compared with multislice computed tomography in 65 patients with acute intracranial hemorrhage: initial results. *Clinical article. J Neurosurg* 2010;113:901–07 [CrossRef Medline](#)

Endovascular Management of Acute Stroke in the Elderly: A Systematic Review and Meta-Analysis

 C.A. Hilditch,  P. Nicholson,  M.H. Murad,  A. Rabinstein,  J. Schaafsma,  A. Pikula,  T. Krings,  V.M. Pereira,  R. Agid, and  W. Brinjikji



ABSTRACT

BACKGROUND: Acute ischemic stroke occurs more frequently, presents with more severe symptoms, and has worse outcomes in elderly patients. The safety and efficacy of endovascular therapy for acute stroke in this age group has not been fully established.

PURPOSE: We present the results of a systematic review and meta-analysis examining clinical, procedural, and radiologic outcomes of endovascular therapy for acute stroke in patients older than 80 years of age.

DATA SOURCES: We searched PubMed, MEDLINE, and EMBASE from 1992 to week 35 of 2017 for studies evaluating endovascular therapy for acute stroke in the elderly.

STUDY SELECTION: Two independent reviewers selected studies and abstracted data. The primary end point was good functional outcome at 3 months defined as modified Rankin Scale score of ≤ 2 .

DATA ANALYSIS: Data were analyzed using random-effects meta-analysis.

DATA SYNTHESIS: Seventeen studies reporting on 860 patients were included. The rate of good functional outcome at 3 months was 27% (95% CI, 21%–32%). Mortality at 3 months was 34% (95% CI, 23%–44%). Successful recanalization was achieved in 78% of patients (95% CI, 72%–85%). Procedure-related complications occurred in 11% (95% CI, 4%–17%). The incidence of intracranial hemorrhage was 24% (95% CI, 15%–32%), and for symptomatic intracranial hemorrhage, it was 8% (95% CI, 5%–10%). The mean time to groin was 251 minutes (95% CI, 224–278 minutes). Procedure time was 99 minutes (95% CI, 67–131 minutes).

LIMITATIONS: I^2 values were above 50% for all outcomes, indicating substantial heterogeneity.

CONCLUSIONS: Good functional recovery in octogenarians treated with endovascular therapy for acute stroke can be achieved in a high proportion of patients despite the higher incidence of comorbidity in this cohort. Outcomes are inferior to those reported for younger patients; however, endovascular therapy can allow at least 1 in 4 patients older than 80 years of age to regain independent function at 3 months. More research is required to improve patient selection in the elderly, but age should not be a discriminator when deciding to offer endovascular therapy for patients with acute stroke.

ABBREVIATION: EVT = endovascular therapy

Due to improvement in health care and better standards of living, the proportion of elderly individuals (older than 80 years of age) is expected to at least double in the United States by

the year 2050, and more than double in the European Union by 2080.^{1,2} With aging of the general population, the burden of cardiovascular and cerebrovascular disease will substantially increase. In fact, prior studies have shown that individuals older than 80 years of age have the highest incidence of acute ischemic stroke.³

Endovascular therapy (EVT) has been proven to improve outcomes in patients with stroke from large-vessel occlusion.⁴ However, 3 of the 6 major trials of EVT for acute stroke excluded older patients.^{5–7} Trials that included octogenarians clearly showed better outcomes among patients treated with EVT in this age sub-

Received November 13, 2017; accepted after revision January 24, 2018.

From the Division of Neuroradiology (C.A.H., P.N., T.K., V.M.P., R.A., W.B.), Joint Division of Medical Imaging, and Division of Neurosurgery (T.K., V.M.P.), Department of Surgery, University Health Network, University of Toronto, Toronto, Ontario, Canada; Evidence-Based Practice Center (M.H.M.) and Department of Neurology (A.R.), Mayo Clinic, Rochester, Minnesota; and Division of Neurology (J.S., A.P.), Toronto Western Hospital, Toronto, Ontario, Canada.

Data could be made available by contacting the corresponding author via e-mail.

Please address correspondence to Christopher Alan Hilditch, MD, Toronto Western Hospital, Department of Neuroradiology, 399 Bathurst St, Toronto, ON M5T 2S8 Canada; e-mail: christopheralan.hilditch@uhn.ca; @hilditchca



Indicates article with supplemental on-line table.

<http://dx.doi.org/10.3174/ajnr.A5598>

group compared with intravenous thrombolysis alone, with odds ratios even more favorable than among younger patients.⁸ Yet, octogenarians were relatively underrepresented even in those trials that did not exclude them, suggesting a possible selection bias (ie, only the octogenarians with greater chances of recovery may have been preferentially enrolled). Meanwhile, there have been several prospective and retrospective observational studies reporting the outcomes of endovascular revascularization in acute stroke in octogenarians. However, many of these studies are limited by small sample sizes or restricted to single centers, thus limiting the generalizability of the results.^{9–24} To better understand the outcomes after EVT in octogenarians, we performed a systematic review and meta-analysis of published observational studies^{9–24} that examined clinical and radiologic outcomes in these patients; we also included data from the Highly Effective Reperfusion evaluated in Multiple Endovascular Stroke trials (HERMES) meta-analysis of randomized controlled trials of EVT in acute stroke.⁸

MATERIALS AND METHODS

Literature Search

A comprehensive literature search of the databases PubMed, Ovid MEDLINE, and Ovid EMBASE was designed and conducted by an experienced librarian with input from the authors. The key words “stroke,” “mechanical thrombectomy,” “elderly,” “octogenarian,” “nonagenarian,” and “outcomes” were used in “AND” and “OR” combinations. The search was limited to articles published from 1992 to week 35 of 2017. All studies reporting outcomes of mechanical thrombectomy in patients older than 80 years of age were included. Inclusion criteria were the following: 1) English language; 2) studies reporting patients with acute stroke treated endovascularly in a patient population 80 years of age or older; and 3) studies reporting at least 3 months of clinical follow-up. Studies including patients treated with older endovascular modalities (ie, Merci retriever [Concentric Medical, Mountain View, California], intra-arterial thrombolysis alone, and so forth) were excluded. Two of the authors selected the included studies (C.A.H., P.N.). Differences were resolved by a senior author with 5 years of experience in meta-analysis (W.B.).

Outcomes and Data Extraction

For each study, we extracted the following baseline information: number of patients, mean or median age, imaging selection criteria, clinical selection criteria, exclusion criteria, mean or median NIHSS score, mean or median ASPECTS, endovascular technique used, type of study (prospective or retrospective), number of patients achieving a good functional outcome (defined as a modified Rankin Scale score of ≤ 2 at 3 months), number of patients in whom successful recanalization was achieved (defined as TICI 3 or 2b), procedure-related complications (eg, vessel perforation and groin complications), number of patients with intracranial hemorrhage and whether this was symptomatic, time from symptom onset to intervention (defined as groin puncture), and procedure time.

The primary end point of this study was good functional outcome at 3 months. Secondary outcomes included the following: mortality at 3 months, rate of successful revascularization, rate of procedure-related complications, rate of intracranial hemorrhage including symptomatic intracranial hemorrhage, time from symptom onset to groin puncture, and procedure time.

METHODOLOGIC QUALITY

We modified the Newcastle-Ottawa Quality Assessment Scale to assess the methodologic quality of the studies included in this meta-analysis. This tool is designed for use in comparative studies; however, because the studies did not include a control group, we assessed study risk of bias based on selected items from the tool, focusing on the following questions: 1) Did the study include all patients or consecutive patients versus a selected sample? 2) Was the study retrospective or prospective? 3) Was clinical follow-up satisfactory, thus allowing ascertainment of all outcomes? 4) Were outcomes clearly reported?

Statistical Analysis

We estimated from each cohort the cumulative incidence (event rate) and 95% confidence interval for each outcome. Confidence intervals were symmetric and 2-sided. Event rates for each intervention were pooled in a meta-analysis using the random-effects model.²⁵ Anticipating heterogeneity between studies, we chose this model a priori because it incorporates within-study variance and between-study variance. Heterogeneity of treatment effect across studies was evaluated using the I^2 statistic, in which $I^2 > 50\%$ suggests substantial heterogeneity.²⁶ A sensitivity analysis was conducted to compare the primary end point (good functional outcome at 90 days) among the included studies, depending on whether they reported an exclusion criterion of a premorbid mRS of ≥ 2 . Statistical analysis was conducted using STATA software, Version 14 (StataCorp, College Station, Texas).

RESULTS

Study Selection and Characteristics

The initial literature search yielded 1072 articles. On review of the abstracts and titles, we excluded 1008 articles. Sixty-four articles were selected for full-text screening. Of these, 24 were excluded (case reports, conference abstracts, review articles, and 1 article written in Russian). In all, 40 potentially relevant articles were identified. Of these, a further 23 were excluded for the following reasons: Some studies did not separate patients by age, the definition of elderly was too young, some studies reported outdated endovascular techniques (primarily those that included patients treated with the first-generation Merci device), and 1 study only provided the mRS score at 30 days rather than at 90 days.

In total, 17 articles including 860 patients aged 80 years or older who underwent EVT for acute stroke were included. In all studies, either a stent retriever alone was used as the primary method of recanalization or a combination of stent retriever plus or minus aspiration. One study included patients who had undergone intra-arterial thrombolysis in addition to stent-retriever and/or aspiration.

Five studies were prospective, and 12 were retrospective. Overall, 3 were considered to have a low risk of bias (using a modified Newcastle-Ottawa Quality Assessment Scale), whereas 14 had limitations. Clinical and imaging inclusion criteria for EVT varied considerably in the studies (On-line Table). Eight of the 17 included studies only performed EVT in patients with acute stroke with a premorbid mRS of ≤ 2 . All except 5 studies clearly defined their inclusion criteria. All included studies reported mRS at 3 months. The smallest study included 16 patients, and the largest study included 111 patients. A summary of included stud-

ies is provided in On-line Table. A flow chart for study selection is provided in Fig 1. The mean/median presentation NIHSS score was 17.8 (available for 16 studies). Seven studies included presentation ASPECTS with their results, the mean of which was 8.5.

Clinical Outcomes

Overall good functional outcome ($mRS \leq 2$) was achieved in 27% of patients (95% CI, 21%–32%). A meta-analysis forest plot for good functional outcome at 3 months is shown in Fig 2. Overall mortality (reported by 14 studies) was 34% (95% CI, 23%–44%). Successful recanalization (reported by 15 studies) was achieved in 78% of patients (95% CI, 72%–85%). Procedure-related complication rates (reported by 4 studies) were 11% (95% CI, 4%–17%). The incidence of intracranial hemorrhage (reported in 10 studies) was 24% (95% CI, 15%–32%), and for symptomatic intracranial hemorrhage (reported by 14 studies), the incidence was 8% (95% CI, 5%–10%). The overall reported mean time to groin (documented in 13 studies) was 251 minutes (95% CI, 224–278 minutes). Procedural time in these elderly patients was 99 minutes

(95% CI, 67–131 minutes). A summary of the results is shown in the Table.

Sensitivity Analysis

Eight of the 17 included studies only performed EVT in patients with a premorbid $mRS \leq 2$. A statistically significantly higher proportion of patients achieved a good functional outcome at 90 days ($mRS \leq 2$) in those studies that only included pre-morbidly independent patients compared with those studies that did not have this prerequisite ($P = .007$). The mean rate of good functional outcome at 90 days in the studies with this inclusion criterion was 31.7% (95% CI, 18.4%–41.1%) compared with 20.4% (95% CI, 16.1%–24.7%) in those studies that did not use this criterion.

Heterogeneity

Heterogeneity of treatment effect across studies was evaluated using the I^2 statistic, in which $I^2 > 50\%$ suggests substantial heterogeneity.²⁶ Substantial heterogeneity was noted for all outcomes. The calculated heterogeneity of treatment effect for good neurologic outcome at 3 months was $I^2 = 70\%$.

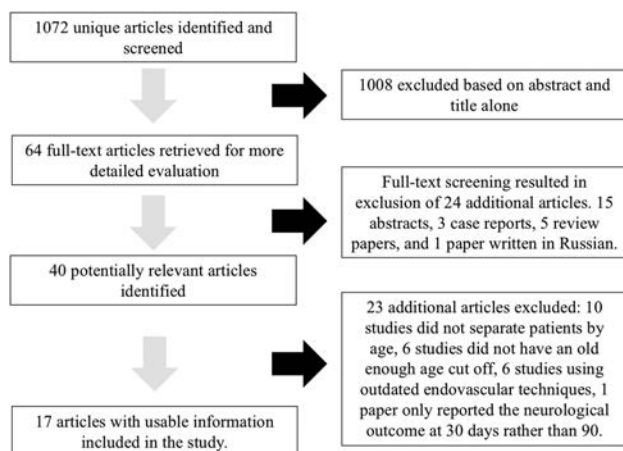


FIG 1. Flow chart for study selection for studies included.

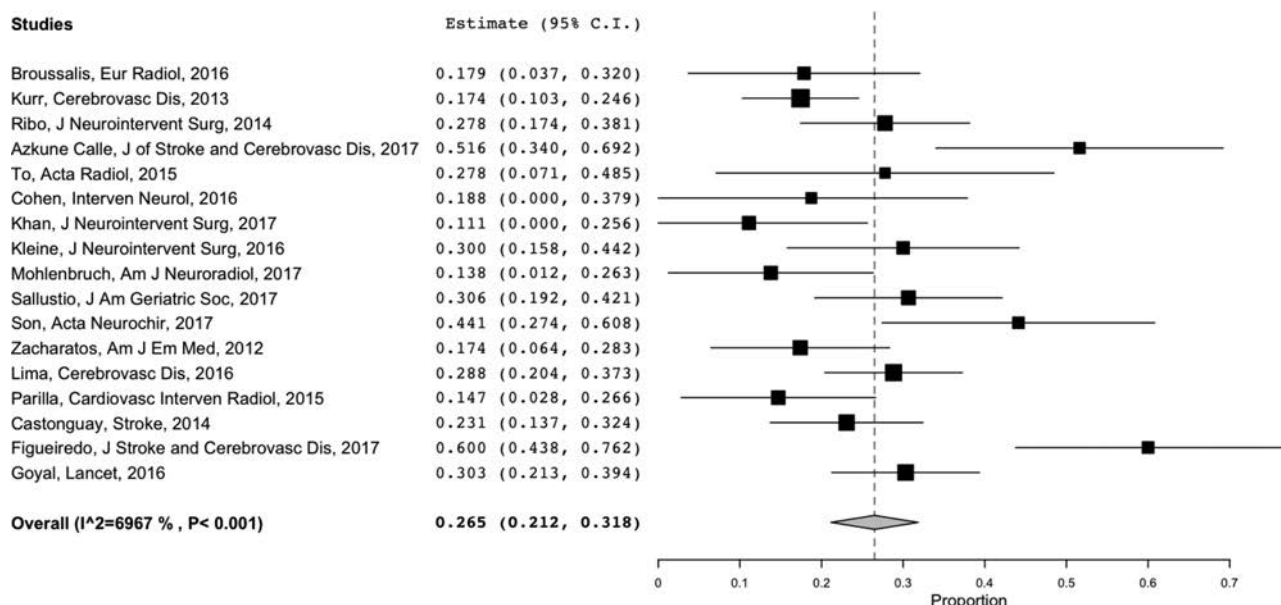


FIG 2. Meta-analysis forest plot for good functional outcomes at 3 months.

DISCUSSION

This systematic review and meta-analysis of 16 observational studies^{9–24} and data from the HERMES study,⁸ including 860 patients 80 years of age or older who underwent mechanical thrombectomy for acute ischemic stroke, has demonstrated a number of compelling findings. First more than one-quarter (27%) of patients achieved good functional outcome (functionally independent) at 90 days, while one-third (34%) of patients died. Excellent rates of TICI 2b/3 recanalization were achieved, close to 80%. Symptomatic intracranial hemorrhage rates were 8%, and procedural complication rates were approximately 11%. These findings suggest that mechanical thrombectomy provides substantial benefit to a sizeable proportion of octogenarians, despite the associated comorbidities in this cohort of patients. More

Summary of clinical outcomes

Outcome		Heterogeneity (I ²)
Good functional outcome at 3 mo	27% (95% CI, 21%–32%)	70%
Mortality within 3 mo	34% (95% CI, 23%–44%)	91%
Successful revascularization	78% (95% CI, 72%–85%)	83%
Procedure-related complication	11% (95% CI, 4%–17%)	56%
Any ICH	24% (95% CI, 15%–32%)	83%
Symptomatic ICH	8% (95% CI, 5%–10%)	61%
Time to groin (min)	251 (95% CI, 224–278)	88%
Procedure time (min)	99 (95% CI, 67–131)	98%

Note:—ICH indicates intracranial hemorrhage.

work is, however, still needed to further improve stroke outcomes in this patient population. These findings are particularly important, given that this demographic group will likely represent a growing proportion of mechanical thrombectomy candidates as the life expectancy of the general population continues to increase.

Ischemic stroke has increasing incidence with age and tends to present with more severe symptoms and has worse outcomes in the elderly compared with younger patients. Thus, it is of interest to determine the safety and efficacy of EVT in this older age group. The randomized trials that have established the remarkable effectiveness of EVT for patients with stroke with large-vessel occlusions do not conclusively answer the question of the value of EVT for octogenarians in daily practice. Exclusion of patients older than 80 years in some trials^{5–7} and the relatively low number of these patients compared with other age groups in those trials that did not consider age among the inclusion criteria^{27–29} are limiting factors that must be taken into consideration when interpreting the data from these randomized controlled studies.

The HERMES meta-analysis⁸ of 5 randomized controlled trials of EVT ($n = 1287$ including 634 assigned to mechanical thrombectomy; mean age, 68 years) reported good functional outcomes in 46% of patients and a mortality rate of 15%. However, among patients 80 years of age and older in the EVT arms, the rates were 29.8% for good 90-day functional outcome and 28% for mortality. These results are comparable with those that we obtained through our meta-analysis of observational studies (which also included data for octogenarians from the HERMES meta-analysis). Our meta-analysis did demonstrate a higher rate of symptomatic intracranial hemorrhage than the randomized trials (8% compared with 2%–5% across all age groups in the trials^{8,30}) as well as high rates of procedure-related complications (11%).

Meta-analysis of trial data clearly demonstrated that octogenarians treated with EVT had markedly better chances of achieving a good functional outcome compared with patients not treated with EVT⁸ (common odds ratio = 3.68; 95% CI, 1.95–6.92), in great part because of the poor outcomes observed in the latter group. Thus, EVT should be offered to patients aged 80 years and older. The challenge remains how to identify those older patients who will not benefit from recanalization to avoid futile and potentially harmful interventions. Eight of the 17 studies, including the HERMES data, included only octogenarians who were premorbidly functionally independent ($mRS \leq 2$). The mean rate of good functional outcome

($mRS < 2$) at 90 days was higher in studies that included only premorbidly independent patients compared with those that did not (20% compared with 32%). This finding highlights the need for careful patient selection for EVT in older patients. An inclusion criterion of only treating patients with a premorbid mRS of ≤ 2 may still exclude a large proportion of patients with stroke (of any age) who could benefit from EVT.

An mRS of 3 may convey a good quality of life in a patient older than 80 years of age, and the potential “shift effect” of EVT toward a lower mRS may still be regarded as a very favorable outcome.

Limitations

While data in this meta-analysis were derived from a strictly defined patient population with at least 3 months of follow-up, our study has limitations. In our assessment of study risk of bias, most of the studies had a medium risk of bias. Publication bias is also possible because centers with better results in treating older patients with stroke may have been more prone to report their results (however, if present, this bias would overestimate the chances of recovery after EVT). I^2 values were $>50\%$ for all outcomes, indicating substantial heterogeneity. Marked variability in patient imaging and clinical inclusion and exclusion criteria across studies may have contributed to this heterogeneity. The 2 studies that reported the worst outcomes included only patients older than 90 years. If these studies were excluded from the meta-analysis, the overall proportion of patients with good neurologic outcome would have slightly increased to 28%. Few studies provided detailed and quantifiable descriptions of the premorbid condition of the patients they treated (On-line Table). Overall, the quality of evidence (confidence in estimates) is low because of imprecision, heterogeneity, and methodologic limitations of the included studies.^{31,32} Due to lack of availability of data from the individual studies, it was not possible to stratify outcomes on the basis of stroke onset-to-recanalization time, concomitant use of thrombolytic therapy, type of anesthesia used, or patient collateral or perfusion mismatch status. It was not possible to perform an mRS shift analysis from the data collected from the included studies, and this issue may have underestimated the benefit of EVT for acute stroke in elderly patients.

CONCLUSIONS

A large proportion of patients 80 years of age or older with severe stroke from large-vessel occlusion can benefit from EVT, and good recanalization rates can be achieved. Our findings suggest that age should not be a discriminator of whether EVT should be attempted in acute stroke. The outcomes in older patients are, however, poorer than in younger patients. When one counsels patients and families, they should be informed that recovery of independent function can be expected in approximately 1 in 4 cases. Further research is necessary to refine selection criteria for EVT in this age group.

REFERENCES

- United States Census Bureau. 2014 National Population Projections Tables. <https://www.census.gov/data/tables/2014/demo/popproj/2014-summary-tables.html>. Accessed August 29, 2017
- Eurostat. Statistics Explained. People in the EU—population projections. http://ec.europa.eu/eurostat/statistics-explained/index.php/People_in_the_EU_-_population_projections#Europop2013_.E2.80.94_population_projections. June 2015. Accessed August 29, 2017
- Writing Group Members, Mozaffarian D, Benjamin E, Go A, et al; American Heart Association Statistics Committee; Stroke Statistics Subcommittee. **Heart Disease and Stroke Statistics: 2015 Update—a report from the American Heart Association.** *Circulation* 2016;133:e38–360 CrossRef Medline
- Saver JL, Goyal M, van der Lugt A, et al; HERMES Collaborators. **Time to treatment with endovascular thrombectomy and outcomes from ischemic stroke: a meta-analysis.** *JAMA* 2016;316:1279–88 CrossRef Medline
- Jovin TG, Chamorro A, Cobo E, et al; REVASCAT Trial Investigators. **Thrombectomy within 8 hours after symptom onset in ischemic stroke.** *N Engl J Med* 2015;372:2296–306 CrossRef Medline
- Saver JL, Goyal M, Bonafe A, et al; SWIFT PRIME Investigators. **Stent-retriever thrombectomy after intravenous t-PA vs. t-PA alone in stroke.** *N Engl J Med* 2015;372:2285–95 CrossRef Medline
- Bracard S, Ducrocq X, Mas JL, et al; THRACE investigators. **Mechanical thrombectomy after intravenous alteplase versus alteplase alone after stroke (THRACE): a randomised controlled trial.** *Lancet Neurol* 2016;15:1138–47 CrossRef Medline
- Goyal M, Menon BK, van Zwam WH, et al; HERMES collaborators. **Endovascular thrombectomy after large-vessel ischaemic stroke: a meta-analysis of individual patient data from five randomised trials.** *Lancet* 2016;387:1723–31 CrossRef Medline
- Broussalis E, Weymayr F, Hitzl W, et al. **Endovascular mechanical recanalization of acute ischaemic stroke in octogenarians.** *Eur Radiol* 2016;26:1742–50 CrossRef Medline
- Kurre W, Aguilar-Pérez M, Niehaus L, et al. **Predictors of outcome after mechanical thrombectomy for anterior circulation large vessel occlusion in patients aged ≥ 80 years.** *Cerebrovasc Dis* 2013;36:430–36 CrossRef Medline
- Ribo M, Flores A, Mansilla E, et al. **Age-adjusted infarct volume threshold for good outcome after endovascular treatment.** *J Neurointerv Surg* 2014;6:418–22 CrossRef Medline
- Azkune Calle I, Bocos Portillo J, Anton-Ladislao A, et al. **Clinical outcome of mechanical thrombectomy for stroke in the elderly.** *J Stroke Cerebrovasc Dis* 2017;26:582–88 CrossRef Medline
- To CY, Rajamand S, Mehra R, et al. **Outcome of mechanical thrombectomy in the very elderly for the treatment of acute ischemic stroke: the real world experience.** *Acta Radiol Open* 2015;4:2058460115599423 CrossRef Medline
- Cohen JE, Gomori JM, Leker RR. **Stent retriever-based thrombectomy in octogenarians.** *Interv Neurol* 2016;5:111–17 CrossRef Medline
- Khan MA, Baird GL, Miller D, et al. **Endovascular treatment of acute ischemic stroke in nonagenarians compared with younger patients in a multicenter cohort.** *J Neurointerv Surg* 2016;9:727–31 CrossRef Medline
- Kleine JF, Boeckh-Behrens T, Prothmann S, et al. **Discrepancy between early neurological course and mid-term outcome in older stroke patients after mechanical thrombectomy.** *J Neurointerv Surg* 2016;8:671–76 CrossRef Medline
- Möhlenbruch M, Pfaff J, Schönenberger S, et al. **Endovascular stroke treatment of nonagenarians.** *AJNR Am J Neuroradiol* 2017;38:299–303 CrossRef Medline
- Sallustio F, Koch G, Motta C, et al. **Efficacy and safety of mechanical thrombectomy in older adults with acute ischemic stroke.** *J Am Geriatr Soc* 2017;65:1816–20 CrossRef Medline
- Son S, Kang DH, Hwang YH, et al. **Efficacy, safety, and clinical outcome of modern mechanical thrombectomy in elderly patients with acute ischemic stroke.** *Acta Neurochir (Wien)* 2017 Jul 2. [Epub ahead of print] CrossRef Medline
- Zacharatos H, Hassan AE, Vazquez G, et al. **Comparison of acute nonthrombolytic and thrombolytic treatments in ischemic stroke patients 80 years or older.** *Am J Emerg Med* 2012;30:158–64 CrossRef Medline
- Lima A, Haussen DC, Rebello LC, et al. **Endovascular therapy for large vessel stroke in the elderly: hope in the new stroke era.** *Cerebrovasc Dis* 2016;42:421–27 CrossRef Medline
- Castonguay A, Zaidat O, Novakovic R, et al. **Influence of age on clinical and revascularization outcomes in the North American Solitaire Stent-Retriever Acute Stroke Registry.** *Stroke* 2014;45:3631–36 CrossRef Medline
- Parrilla G, Carreón E, Zamarro J, et al. **Recanalization and mortality rates of thrombectomy with stent-retrievers in octogenarian patients with acute ischemic stroke.** *Cardiovasc Intervent Radiol* 2015;38:288–94 CrossRef Medline
- Figueiredo S, Carvalho A, Rodrigues M, et al. **Endovascular stroke treatment of patients over 80 years old: cumulative evidence from the “real world.”** *J Stroke Cerebrovasc Dis* 2017;26:2949–53 CrossRef Medline
- DerSimonian R, Laird N. **Meta-analysis in clinical trials.** *Control Clin Trials* 1986;7:177–88 CrossRef Medline
- Higgins JP, Thompson SG, Deeks JJ, et al. **Measuring inconsistency in meta-analyses.** *BMJ* 2003;327:557–60 CrossRef Medline
- Campbell BCV, Mitchell PJ, Kleinig TJ, et al; EXTEND-IA Investigators. **Endovascular therapy for ischemic stroke with perfusion-imaging selection.** *N Engl J Med* 2015;372:1009–18 CrossRef Medline
- Goyal M, Demchuk AM, Menon BK, et al; ESCAPE Trial Investigators. **Randomized assessment of rapid endovascular treatment of ischemic stroke.** *N Engl J Med* 2015;372:1019–30 CrossRef Medline
- Berkhemer OA, Fransen PS, Beumer D, et al. **A randomized trial of intraarterial treatment for acute ischemic stroke.** *N Engl J Med* 2015;372:11–20 CrossRef Medline
- Campbell B, Hill M, Rubiera M, et al. **Safety and efficacy of Solitaire stent thrombectomy: individual patient data meta-analysis of randomized trials.** *Stroke* 2016;47:798–806 CrossRef Medline
- Guyatt GH, Oxman AD, Kunz R, et al. **GRADE guidelines, 6: rating the quality of evidence—imprecision.** *J Clin Epidemiol* 2011;64:1283–93 CrossRef Medline
- Balshem H, Helfand M, Schünemann HJ, et al. **GRADE guidelines, 3: rating the quality of evidence.** *J Clin Epidemiol* 2011;64:401–06 CrossRef Medline

Accuracy of CT Angiography for Differentiating Pseudo-Occlusion from True Occlusion or High-Grade Stenosis of the Extracranial ICA in Acute Ischemic Stroke: A Retrospective MR CLEAN Substudy

M. Kappelhof, H.A. Marquering, O.A. Berkhemer, J. Borst, A. van der Lugt, W.H. van Zwam, J.A. Vos, G. Lycklama à Nijeholt, C.B.L.M. Majoie, and B.J. Emmer, on behalf of the MR CLEAN Investigators



ABSTRACT

BACKGROUND AND PURPOSE: The absence of opacification on CTA in the extracranial ICA in acute ischemic stroke may be caused by atherosclerotic occlusion, dissection, or pseudo-occlusion. The latter is explained by sluggish or stagnant flow in a patent artery caused by a distal intracranial occlusion. This study aimed to explore the accuracy of CTA for differentiating pseudo-occlusion from true occlusion of the extracranial ICA.

MATERIALS AND METHODS: All patients from the Multicenter Randomized Clinical Trial of Endovascular Treatment for Acute Ischemic Stroke in the Netherlands (MR CLEAN) with an apparent ICA occlusion on CTA and available DSA images were included. Two independent observers classified CTA images as atherosclerotic cause (occlusion/high-grade stenosis), dissection, or suspected pseudo-occlusion. Pseudo-occlusion was suspected if CTA showed a gradual contrast decline located above the level of the carotid bulb, especially in the presence of an occluded intracranial ICA bifurcation (T-occlusion). DSA images, classified into the same 3 categories, were used as the criterion standard.

RESULTS: In 108 of 476 patients (23%), CTA showed an apparent extracranial carotid occlusion. DSA was available in 46 of these, showing an atherosclerotic cause in 13 (28%), dissection in 16 (35%), and pseudo-occlusion in 17 (37%). The sensitivity for detecting pseudo-occlusion on CTA was 82% (95% CI, 57–96) for both observers; specificity was 76% (95% CI, 56–90) and 86% (95% CI, 68–96) for observers 1 and 2, respectively. The κ value for interobserver agreement was .77, indicating substantial agreement. T-occlusions were more frequent in pseudo- than true occlusions (82% versus 21%, $P < .001$).

CONCLUSIONS: On CTA, extracranial ICA pseudo-occlusions can be differentiated from true carotid occlusions.

ABBREVIATIONS: EVT = endovascular treatment; MR CLEAN = Multicenter Randomized Clinical Trial of Endovascular Treatment for Acute Ischemic Stroke in the Netherlands; T-occlusion = occluded intracranial ICA bifurcation

Endovascular treatment (EVT) has been proved safe and effective in acute ischemic stroke caused by proximal intracranial occlusion if initiated within 6 hours of symptom onset.¹ The duration and success of EVT are influenced by the ease of access to the intracranial vasculature. In approximately 25% of middle ce-

rebral artery strokes, concomitant intracranial artery and ipsilateral extracranial ICA occlusion occurs, known as tandem occlusion.² A recent study that included patients with tandem occlusions reported a median procedure time of 88 minutes³ versus 30 and 43 minutes in 2 randomized trials that excluded patients with tandem occlusions.^{4,5}

However, not all tandem occlusions identified on CTA represent true occlusions of the extracranial ICA. True occlusion of the extracranial ICA is caused by atherosclerosis or dissection of the vessel wall. So-called pseudo-occlusions mimic occlusion on CTA in the acute phase of ischemic stroke, while the artery is patent on DSA during EVT.⁶ The underlying mechanism of pseudo-occlusion of the extracranial ICA is sluggish or absent contrast flow caused by a distal occlusion of the intracranial vasculature. In these cases, CTA acquisition “outruns” the arrival of contrast material.⁶ Contrast flow can also be impeded by an extracranial ICA stenosis located proximal to the level of apparent occlusion.^{7,8}

The term “pseudo-occlusion” has also been used for chronic high-grade stenosis of the ICA with minimal distal flow.^{9,10} This

Received September 5, 2017; accepted after revision January 15, 2018.

From the Departments of Radiology (M.K., H.A.M., O.A.B., J.B., C.B.L.M.M., B.J.E.) and Biomedical Engineering and Physics (H.A.M.), Academic Medical Center, Amsterdam, the Netherlands; Departments of Radiology (A.v.d.L.) and Neurology (O.A.B.), Erasmus Medical Center, Rotterdam, the Netherlands; Department of Radiology (O.A.B., W.H.v.Z.), Maastricht University Medical Center, Maastricht, the Netherlands; Department of Radiology (J.A.V.), St. Antonius Hospital, Nieuwegein, the Netherlands; and Department of Radiology (G.L.à.N.), Haaglanden Medical Centre, The Hague, the Netherlands.

Paper previously presented at: European Stroke Organization Conference, May 10–12, 2016; Barcelona, Spain.

Please address correspondence to Bart J. Emmer, MD, PhD, Academic Medical Center, Department of Radiology, GI-240, Meibergdreef 9, 1105 AZ Amsterdam, the Netherlands; e-mail: b.j.emmer@amc.uva.nl

Indicates article with supplemental on-line table.

<http://dx.doi.org/10.3174/ajnr.A5601>

phenomenon is markedly different from pseudo-occlusion as an artifact of single-phase CTA, in which there is, in fact, no practically relevant carotid obstruction at all.⁶ To our knowledge, 6 previous studies have described a total of 48 patients with pseudo-occlusions of the extracranial ICA in acute ischemic stroke. They reported that pseudo-occlusion occurs in 6%–15% of patients with acute ischemic stroke.^{6,11–15} It was stated that pseudo-occlusion cannot be discriminated from true occlusion on CTA.¹³ However, certain imaging characteristics may suggest pseudo-occlusion on CTA, such as an ipsilateral occluded intracranial ICA bifurcation (carotid T-occlusion) and good contrast filling of the carotid bulb followed by a gradual contrast decay in the ICA.

In the clinical setting, discrimination of pseudo-occlusion from true occlusion would improve estimation of the procedure time and intervention success by the operator. In case patients arrive late in their treatment window, time to overcome an extracranial ICA occlusion during treatment could be deemed too long for EVT to be beneficial to the patient. This could cause patients with unrecognized pseudo-occlusion on CTA to miss out on endovascular treatment that would have benefited them. Furthermore, better pseudo-occlusion recognition would enable more adequate planning and use of EVT materials such as guiding sheaths, percutaneous transluminal angioplasty balloons, and distal access catheters.

The aim of this retrospective study was to determine whether ICA pseudo-occlusion could be differentiated from atherosclerotic occlusion and dissection on CTA in the Multicenter Randomized Clinical Trial of Endovascular Treatment for Acute Ischemic Stroke in the Netherlands (MR CLEAN) dataset.

MATERIALS AND METHODS

This study was a blinded retrospective analysis of the data from the randomized controlled MR CLEAN trial. MR CLEAN included 500 patients with acute ischemic stroke caused by occlusion of an intracranial artery of the anterior circulation, with an NIHSS deficit of ≥ 2 points, from 16 centers in the Netherlands.^{1,16} After arterial occlusion was demonstrated on vessel imaging, patients were randomized for usual care only or usual care with the addition of EVT. Treatment was initiated within ≤ 6 hours from symptom onset. All imaging data were collected as part of MR CLEAN before the start of the current study.

CTA Analysis

Three raters (O.A.B., J.B., M.K.) assessed all baseline CTA scans for the presence of apparent ipsilateral occlusion of the extracranial ICA, without knowledge of angiographic findings. Images were reviewed in the axial, coronal, and sagittal planes. Only CTA images were assessed; noncontrast CT was not evaluated in this study. Minimum requirements for CTA scans in MR CLEAN were a slice thickness of ≤ 5 mm, the presence of contrast in the intracranial vasculature, and depiction of at least the carotid bulb up to the circle of Willis. Median slice thickness was 0.9 mm (range, 0.5–2.0 mm), median scanner kiloelectron volt was 120 (range, 80–120), and the median number of scanner detector rows was 128 (range, 52–320). The total amount of injected contrast varied from 50 to 100 mL (median, 70 mL) with a median injection speed of 5.0 mL/s (range, 3.5–6.0 mL/s). Detailed CTA

scan protocols per participating center can be found in the Online Table. “Apparent occlusion” was defined as the absence of contrast enhancement in the extracranial ICA ipsilateral to the intracranial occlusion.

Two experienced interventional and diagnostic neuroradiologists (B.J.E., G.L.à.N.), who were also blinded to the angiographic findings, separately reviewed scans with apparent occlusions. They categorized all cases into 1 of 3 underlying causes: atherosclerotic occlusion, dissection, or suspected pseudo-occlusion.

Atherosclerotic Occlusion. If an apparent occlusion was located at the level of the carotid bulb, was sharply demarcated, and/or showed a clear presence of calcifications or plaque, this apparent occlusion was considered as most likely caused by atherosclerosis and classified as such.¹⁷

Dissection. If an apparent ICA occlusion was located above the level of the carotid bulb, without plaque or calcifications at the carotid bulb, and the occlusion was sharply demarcated on CTA, the occlusion was classified as most likely caused by a dissection. Furthermore, young patient age and widening of the ICA under the skull base could suggest the presence of a dissection.

Suspected Pseudo-Occlusion. Pseudo-occlusion was suspected if CTA showed a gradual contrast decay in the ICA above the level of the carotid bulb, in the absence of plaque or calcifications around the carotid bulb, and in the presence of a carotid-T or large M1-occlusion.

Carotid T-Occlusion. T-occlusion presence was determined to compare the prevalence in pseudo- versus true occlusion cases. If a carotid top or terminus was not filled with contrast on CTA, it was classified as a carotid T-occlusion. All cases with apparent extracranial ICA occlusion on CTA and available DSA imaging were reviewed.

DSA Analysis

DSA images of cases with apparent occlusion on CTA were collected. To prevent recall bias, we gave the DSA images new patient identification numbers and rated them 6 months later than the CTAs. One rater (B.J.E.) reviewed all DSA images, checking for atherosclerotic occlusion or dissection. Contrast was injected in the common carotid artery and directly into the ICA in all cases. Dissection was confirmed in case of an irregular vessel wall (at the beginning of the procedure, before vasospasm could have arisen) with a tapering aspect of contrast leading up to an occlusion above the level of the carotid bulb that could not be passed with the guidewire or catheter. Atherosclerotic occlusion was confirmed in case of an abrupt, blunt contrast cutoff at the level of (or slightly above) the carotid bulb, with evidence of circumferential vessel wall involvement that could not be passed easily with a guidewire or catheter. If, despite an apparent occlusion on CTA, DSA showed only high-grade (90%–99%) atherosclerotic stenosis, the underlying reason for the apparent occlusion was deemed an atherosclerotic cause because the practical implications of atherosclerotic high-grade stenosis for EVT are similar to those of atherosclerotic occlusion. If DSA showed no occlusion, a low-grade stenosis, or an apparent occlusion that could be passed unhin-

dered with a guidewire or catheter, the apparent ICA occlusion on CTA was deemed a pseudo-occlusion.

Statistical Analysis

SPSS, Version 24 (IBM, Armonk, New York) and R, Version 3.2 (<http://www.r-project.org>) were used for the statistical analysis. Sensitivity, specificity, and positive and negative predictive values were calculated for detection of pseudo-occlusions, atherosclerotic occlusions, and dissections on CTA. DSA images were used as the criterion standard. Ninety-five percent confidence intervals were calculated using the Clopper-Pearson method for sensitivity and specificity and the asymptotic/adjusted logit intervals for predictive values. Interobserver variability of CTA-based pseudo-occlusion recognition was tested with the κ statistic and the Krippendorff α , to control for the factor of random agreement. The Fisher exact test was used to calculate the statistical significance of the difference in T-occlusion rates in subgroups with and without pseudo-occlusions.

RESULTS

Patients

Figure 1 depicts patient inclusion. CTA images were available for 476 patients. The intervention arm of MR CLEAN com-

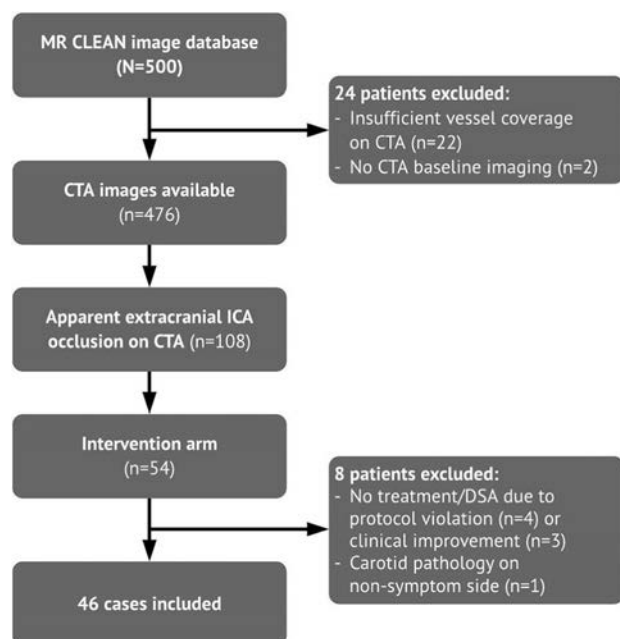


FIG 1. Patient-selection flow chart. *n* indicates number of cases.

prised 233 patients, of whom 216 had DSA images available for analysis.¹ Apparent extracranial ICA occlusion on CTA, regardless of the cause, was found in 108 patients. Forty-six of them had DSA images available and thus were included in the current study.

CTA Analysis

Pseudo-occlusion was identified in 14/17 (82%) cases by both observers (Table 1). For observer 1, the sensitivity and specificity of CTA for identifying pseudo-occlusion were 82% (95% CI, 57%–96%) and 76% (95% CI, 56%–90%). For observer 2, these numbers were 82% (95% CI, 57%–96%) and 86% (95% CI, 68%–96%), respectively (Table 2). The κ value for interobserver agreement on pseudo-occlusions was .77 (95% CI, 0.56–0.97). The Krippendorff α for interobserver agreement on pseudo-occlusions, atherosclerotic occlusions, and dissections was .77 (95% CI, .61–.90).

Dissection and pseudo-occlusion were most frequently not distinguished correctly from each other on CTA. For observers 1 and 2, respectively, 29% (6/21) and 22% (4/18) of suspected pseudo-occlusions turned out to be dissections. Conversely, 23% (3/13) and 20% (3/15) of CTA-diagnosed dissections turned out to be pseudo-occlusions (Table 1). Atherosclerotic pathologies were well-recognized, with a sensitivity of 92% (95% CI, 64%–100%) and 100% (95% CI, 75%–100%) for observers 1 and 2, respectively (Table 2).

Figure 2 shows examples of cases with matching classification of atherosclerotic occlusion, dissection, and pseudo-occlusion, respectively, on CTA and DSA. Figure 3 depicts examples of the most common misinterpretations: cases in which CTA suggested pseudo-occlusion, whereas DSA showed dissection, or CTA suggested dissection, whereas DSA showed pseudo-occlusion. An apparent occlusion located above the level of the carotid bulb, in the absence of extensive amounts of calcifications or plaque, is present in both dissections and pseudo-occlusions, making distinction of the diagnoses more difficult. However, dissections often show a less gradual decline of contrast in the ICA, more tapering of the vessel, and sometimes widening of the ICA contour under the skull base. Furthermore, the presence of carotid T-occlusion may contribute to identification of the right diagnosis.

T-Occlusions

T-occlusions were present in 14 of 17 (82%) pseudo-occlusions versus 2 of 13 (15%) atherosclerotic cases and 4 of 16 (25%) dis-

Table 1: Outcome of diagnoses on CTA for observers 1 and 2 versus final diagnosis on DSA

CTA	DSA (No.)				Total No.
	Atherosclerotic Cause		Pseudo-Occlusion	Dissection	
Occlusion					
Observer 1					
Atherosclerotic occlusion	10	2	0	0	12
Pseudo-occlusion	0	1	14	6	21
Dissection	0	0	3	10	13
Total		13	17	16	46
Observer 2					
Atherosclerotic occlusion	10	3	0	0	13
Pseudo-occlusion	0	0	14	4	18
Dissection	0	0	3	12	15
Total		13	17	16	46

sections ($P < .001$). Of all carotid T-occlusions, 70% (14/20) showed concomitant pseudo-occlusion.

T-occlusions were correctly recognized on CTA in all cases except 1. In that case, CTA showed a floating thrombus in the carotid siphon, which had possibly embolized into the carotid-T by the time DSA images were acquired. Two pseudo-occlusion cases did not show a carotid T-occlusion on DSA. In one, carotid T-occlusion was seen on CTA, and DSA showed an M1 occlusion.

The other case showed M1 and A1 occlusion on CTA, and M2 occlusion on DSA. Migration of the thrombus, possibly under the influence of IV tPA, could explain these cases.

DSA Analysis

The prevalence of pseudo-occlusions in all patients in MR CLEAN with DSA imaging available was 8% (17 of 216 patients). Of 46 included cases with apparent occlusion on CTA, DSA

showed atherosclerotic occlusion or high-grade stenosis in 13 cases (28%, of which 3 [7% in total] were high-grade stenoses) and dissection in 16 (35%). In 17 patients, no carotid occlusion or high-grade stenosis was found; therefore, 37% of apparent extracranial ICA occlusions on CTA were pseudo-occlusions (Table 1). These cases usually showed delayed or absent contrast filling of the vessel distal to the carotid bulb with an indistinct or oscillating contrast border on DSA.

Table 2: Diagnostic accuracy measures for pseudo-occlusion recognition on CTA compared with DSA for observers 1 and 2

	Pseudo-Occlusion	Atherosclerotic Cause	Dissection
Observer 1			
Sensitivity (95% CI)	82 (57–96)	92 (64–100)	63 (35–85)
Specificity (95% CI)	76 (56–90)	100 (89–100)	90 (73–98)
PPV	67 (50–80)	100 (76–100)	77 (52–92)
NPV	88 (72–95)	97 (83–100)	82 (70–90)
Observer 2			
Sensitivity (95% CI)	82 (57–96)	100 (75–100)	75 (47–93)
Specificity (95% CI)	86 (68–96)	100 (89–100)	90 (73–98)
PPV	78 (58–90)	100 (77–100)	80 (57–92)
NPV	89 (75–95)	100 (90–100)	87 (74–94)

Note:—PPV indicates positive predictive value; NPV, negative predictive value.



FIG 2. Examples of carotid pathologies on CTA (upper row) and corresponding DSA (lower row). *A*, Atherosclerotic occlusion of the right ICA in a 79-year-old man. CTA shows extensive calcifications in the carotid bulb with a sharp contrast cutoff at the level of the bifurcation. *B*, DSA of the patient in *A* shows a sharp delineation of contrast at the level of the carotid bulb, and “shouldering,” a convex aspect of the contrast cutoff proximal to the occlusion. *C*, Dissection of the left ICA in a 44-year-old man. CTA shows a sharp, diagonal contrast cutoff above the level of the carotid bifurcation. *D*, DSA of the patient in *C* shows a gradual decline in vessel diameter also known as “tapering,” with a sharp contrast cutoff and irregular vessel wall. It was possible to pass the apparent occlusion with a guidewire, but not with a catheter. *E*, Pseudo-occlusion of the left ICA in a 51-year-old woman. CTA shows a gradual contrast decrease in the left ICA above the level of the carotid bulb (arrowhead) compared with a normal contrast density on the contralateral side, and an ipsilateral carotid T-occlusion. *F*, DSA of the patient in *E* shows a blurred contrast delineation above the level of the carotid bulb. A back-and-forth moving, “oscillating,” contrast border was seen. The apparent occlusion could easily be passed with a guidewire or catheter.

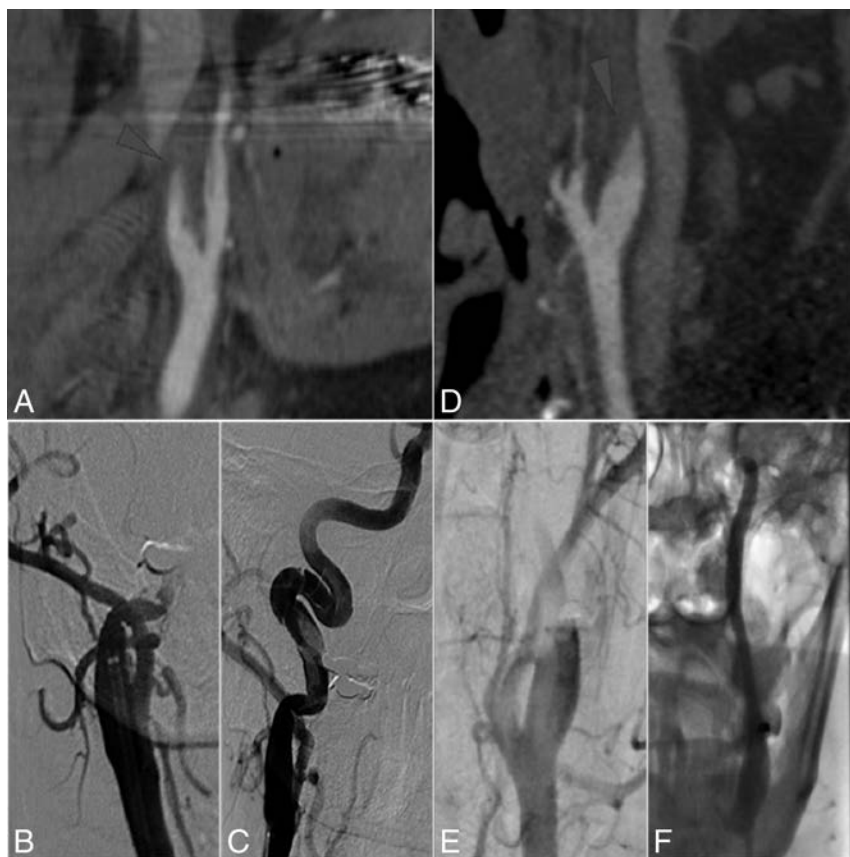


FIG 3. Examples of suspected dissection or pseudo-occlusion on CTA with a noncorresponding cause of apparent occlusion found on DSA. *A*, Dissection of the right ICA in a 65-year-old woman. CTA shows a blurred contrast cutoff above the level of the carotid bulb, suggesting pseudo-occlusion, without T-occlusion present. *B*, DSA of the patient in *A* shows major vessel wall irregularities and the impossibility of passing the occlusion with a catheter (*C*), indicating the presence of a dissection rather than pseudo-occlusion. *D*, Pseudo-occlusion of the left ICA in a 63-year-old man. CTA shows a sharp, diagonal contrast cutoff above the level of the carotid bifurcation, suggesting dissection, with T-occlusion present. *E*, DSA of patient in *D* shows a blurred contrast cutoff slowly moving upward and finally a patent ICA with intracranial carotid T-occlusion present (*F*), indicating pseudo-occlusion.

DISCUSSION

The main finding of this study is that on CTA made in preparation for EVT, extracranial ICA pseudo-occlusion can be well-differentiated from atherosclerotic occlusion and reasonably well from carotid dissection. Additionally, in about one-third of patients with an apparent extracranial internal carotid occlusion on CTA in acute ischemic stroke, the artery is, in fact, patent on DSA during EVT. Finally, the prevalence of a carotid T-occlusion in patients with carotid pseudo-occlusion was high.

To our knowledge, there are no reports on the diagnostic accuracy of CTA on the etiology of apparent tandem lesions in acute stroke with proximal large-vessel occlusions. Previous research^{6,11-13} reported the prevalence of pseudo-occlusions to be 6%–14%. However, these studies included cases in which high-grade extracranial ICA stenosis impeded contrast flow, and they considered them pseudo-occlusions as well.^{6,11-13} Furthermore, previous studies found a high prevalence of carotid T-occlusions in pseudo-occlusion cases.¹¹⁻¹³

We have introduced a CTA-based diagnostic approach that could differentiate pseudo-occlusion from true occlusion or high-grade atherosclerotic stenosis with high sensitivity and specificity. Imaging

characteristics suggestive of pseudo-occlusions were the presence of a carotid T-occlusion and a gradual contrast decline located above the level of the carotid bulb in the absence of atherosclerotic plaque or calcifications. The prevalence of pseudo-occlusions in MR CLEAN was in line with the findings in the studies above. Likewise, in our study, in most pseudo-occlusions, a carotid T-occlusion was present. In a minority of our patients, DSA showed high-grade atherosclerotic stenosis proximal to a gradual contrast decay in the ICA, similar to cases described before.^{6,11,12} However, because high-grade atherosclerotic stenoses usually require a similar approach to atherosclerotic occlusions during EVT, in acute ischemic stroke, one could argue that these cases should be classified as atherosclerotic occlusions.

Several limitations to this study should be noted. First, we have no data on occlusion patterns and characteristics of patients who were not randomized. A selection bias might have occurred because local investigators might have opted not to include patients with extracranial ICA occlusions. Although this might have influenced the prevalence of apparent tandem occlusions in the study sample, it would not have affected the reported sensitivity and specificity measures. Besides, compared with other randomized controlled trials on EVT,^{4,5,18,19} the number of patients with tandem occlusions included in MR CLEAN is relatively high.

Second, the initial selection of apparent ICA occlusions from the dataset was made by 3 researchers who were, though experienced, not certified radiologists. Carotid occlusions might have been missed. However, again this approach would not have affected the sensitivity and specificity numbers because apparent occlusion causes were determined by experienced interventional neuroradiologists.

Finally, this study showed the distinction between carotid dissections and pseudo-occlusions to be the most difficult to make. Both showed a contrast decline above the level of the carotid bifurcation in the absence of carotid plaque or calcifications. A possible discriminating characteristic is a sharp contrast cutoff in dissections versus a gradual contrast decline in pseudo-occlusions. This gradual contrast decline was previously described as the “midcervical flame-shaped extracranial ICA sign.”¹⁴ However, contrast border appearance can be affected by bolus timing, scan acquisition, and low-grade proximal ICA stenosis. These factors may have influenced observers’ decisions on apparent occlusion classification and thereby sensitivity and specificity measures.

CTA scan timing may influence the occurrence and recognition of carotid pseudo-occlusion. Late-phase CTA scans may show a patent ICA by allowing slow contrast flow in the ICA to reach the actual intracranial occlusion. Determining optimal scanning conditions for pseudo-occlusion differentiation on single-phase CTA would require further research. Acquiring a second, late-phase scan after the initial CTA may be of additional value.

Other imaging modalities used in the acute setting of stroke may improve recognition of pseudo-occlusions. For example, 4D-CTA was recently shown to successfully identify slow flow causing pseudo-occlusions.^{13,20,21}

CONCLUSIONS

Extracranial ICA pseudo-occlusion can be well-differentiated from atherosclerotic occlusion and reasonably well from carotid dissection on CTA. The prevalence of pseudo-occlusion in the MR CLEAN trial was high. Several occlusion characteristics can raise suspicion for pseudo-occlusion on CTA, most importantly concomitant carotid T-occlusion.

ACKNOWLEDGMENTS

MR CLEAN trial investigators (all from the Netherlands unless stated otherwise): Peter J. Koudstaal, MD, PhD, and Diederik W.J. Dippel, MD, PhD, Department of Neurology, Erasmus MC University Medical Center, Rotterdam; Yvo B.W.E.M. Roos, MD, PhD, Lucie A. van den Berg, MD, and Paul J. Nederkoorn, MD, PhD, Department of Neurology, Academic Medical Center, Amsterdam; Robert J. van Oostenbrugge, MD, PhD, Debbie Beumer, MD, and Julie Staals, MD, PhD, Department of Neurology, Maastricht University Medical Center, Cardiovascular Research Institute Maastricht; Jelis Boiten, MD, PhD, Department of Neurology, Medisch Centrum Haaglanden, The Hague; Marieke J.H. Wermer, MD, PhD, Department of Neurology, Leiden University Medical Center; L. Jaap Kappelle, MD, PhD, Department of Neurology, University Medical Center Utrecht; Ewoud J. van Dijk, MD, PhD, Department of Neurology, Radboud University Medical Center, Nijmegen; Wouter J. Schonewille, MD, PhD, Department of Neurology, St. Antonius Hospital, Nieuwegein; Willem Jan van Rooij, MD, PhD, Department of Radiology, St. Elisabeth Hospital, Tilburg; Jeannette Hofmeijer, MD, PhD, and Jacques A. van Oostayen, MD, PhD, Department of Radiology, Rijnstate Hospital, Arnhem; Patrick C. Vroomen, MD, PhD, Department of Neurology, University Medical Center Groningen; Paul L.M. de Kort, MD, PhD, Department of Neurology, St. Elisabeth Hospital, Tilburg; Koos Keizer, MD, PhD, Department of Neurology, Catharina Hospital, Eindhoven; Sebastiaan F. de Bruijn, MD, PhD, Department of Neurology, Haga Hospital, The Hague; J.S. Peter van den Berg, MD, PhD, Department of Neurology, Isala Klinieken, Zwolle; Tobien H.C.M.L. Schreuder, MD, Department of Neurology, Atrium Medical Center, Heerlen; Leo A.M. Aerden, MD, PhD, and H. Zwenneke Flach, MD, Department of Neurology, Reinier de Graaf Gasthuis, Delft; Marieke C. Visser, MD, PhD, Department of Neurology, VU Medical Center, Amsterdam; Heleen M. den Hertog, MD, PhD, Department of Neurology, Medical Spectrum Twente, Enschede; Jan S.P. van den Berg, MD, PhD, Department of Neurology, Isala Klinieken, Zwolle;

Patrick A. Brouwer, MD, Department of Radiology, Leiden University Medical Center; Aad van der Lugt, MD, PhD, Department of Radiology, Erasmus MC University Medical Center, Rotterdam; Bart J. Emmer, MD, PhD, Charles B.L.M. Majoie, MD, PhD, Ludo F.M. Beenen, MD, Marieke E.S. Sprengers, MD, PhD, René van den Berg, MD, PhD, and Olvert A. Berkhemer, MD, Department of Radiology, Academic Medical Center, Amsterdam; Wim H. van Zwam, MD, PhD, Department of Radiology, Maastricht University Medical Center; Geert J. Lycklama à Nijeholt, MD, PhD, Department of Radiology, Medisch Centrum Haaglanden, The Hague; Marianne A.A. van Walderveen, MD, PhD, Department of Radiology, Leiden University Medical Center; Rob H. Lo, MD, Department of Radiology, University Medical Center Utrecht; Joost de Vries, MD, PhD, Department of Neurosurgery, Radboud University Medical Center, Nijmegen; Jan Albert Vos, MD, PhD, Department of Radiology, St. Antonius Hospital, Nieuwegein; Omid Eshghi, MD, Department of Radiology, University Medical Center, Groningen; Alexander V. Tielbeek, MD, PhD, Department of Radiology, Catharina Hospital, Eindhoven; Lukas C. van Dijk, MD, Department of Radiology, Haga Hospital, The Hague; Boudewijn A.A.M. van Hasselt, MD, Department of Radiology, Isala Klinieken, Zwolle; Roel J.J. Heijboer, MD, Department of Radiology, Atrium Medical Center, Heerlen; René J. Dallinga, MD, Department of Radiology, Reinier de Graaf Gasthuis, Delft; Joseph C.J. Bot, MD, PhD, Department of Radiology, VU Medical Center, Amsterdam; Dick G. Gerrits, MD, Department of Radiology, Medical Spectrum Twente, Enschede; Puck S.S. Fransen, MD, Departments of Neurology and Radiology, Erasmus MC University Medical Center, Rotterdam; Henk A. Marquering, PhD, Departments of Radiology and Biomedical Engineering and Physics, Academic Medical Center, Amsterdam; Hester F. Lingsma, PhD, and Ewout W. Steyerberg, PhD, Department of Public Health, Erasmus MC University Medical Center, Rotterdam; Albert J. Yoo, MD, Texas Stroke Institute, Plano, Texas; Sjoerd F.M. Jenniskens, MD, PhD, Department of Radiology, Radboud University Medical Center, Nijmegen; Renske M. van den Berg-Vos, MD, PhD, Department of Neurology, St. Lucas Andreas Hospital, Amsterdam; and Giorgos B. Karas, MD, PhD, MBA, Department of Radiology, St. Lucas Andreas Hospital, Amsterdam. The data monitoring and safety board included Martin M. Brown, MD (chair), National Hospital for Neurology and Neurosurgery, London, United Kingdom; Thomas Liebig, MD, Medizinische Fakultät, Universität zu Köln, Germany; and Theo Stijnen, PhD, Leiden University Medical Center (independent statistician). The advisory board included Tommy Andersson, MD (neurointerventionist), Karolinska University Hospital, Stockholm, Sweden; Heinrich Mattle, MD (neurologist), University Hospital, Bern, Switzerland; and Nils Wahlgren, MD (neurologist), Karolinska University Hospital, Stockholm, Sweden. Research nurses and local trial coordinators included Esther van der Heijden and Naziha Ghannouti, Erasmus MC University Medical Center, Rotterdam; Nadine Fleitour and Imke Hooijenga, Academic Medical Center, Amsterdam; Corina Puppels and Wilma Pelliikan, St. Antonius Hospital, Nieuwegein; Annet Geerling, Radboud University Medical Center, Nijmegen; Annemieke Lindl-Velema, Maastricht University Medical Center; Gina van Vemde and Isala Klinieken, Zwolle; Ans de Ridder and Paut

Greebe, University Medical Center, Utrecht; José de Bont-Stikkelbroeck, St Elisabeth Hospital, Tilburg; Joke de Meris, Medisch Centrum Haaglanden, The Hague; Kirsten Janssen, Leiden University Medical Center; Willy Struijk, Haga Hospital, The Hague; and Silvan Licher, Nikki Boodt, Adriaan Ros, Esmee Venema, Ilse Slokkers, Raymie-Jayne Ganpat, Maxim Mulder, Nawid Saiedie, Alis Heshmatollah, Stefanie Schipperen, Stefan Vinken, Tiemen van Boxtel, and Jeroen Koets, Erasmus MC University Medical Center, Rotterdam.

Disclosures: Henk A. Marquering—UNRELATED: Stock/Stock Options; Nico.lab, Comments: founder and shareholder. Olvert A. Berkhemer—UNRELATED: Consultancy: Stryker.* Aad van der Lugt—UNRELATED: Consultancy: Stryker.* Wim H. van Zwam—UNRELATED: Consulting Fee or Honorarium: Stryker, Codman Neuro.* Charles B.L.M. Majoie—UNRELATED: Consultancy: Stryker*; Grants/Grants Pending: TWIN Foundation, CVON/Dutch Heart Foundation.* Bart J. Emmer—UNRELATED: Consultancy: Stryker*; Expert Testimony: DEKRA Certification B.V., Comments: CE Mark review fees; Payment for Lectures Including Service on Speakers Bureaus: Novartis. *Money paid to the institution.

REFERENCES

- Berkhemer OA, Fransen PS, Beumer D, et al. **A randomized trial of intraarterial treatment for acute ischemic stroke.** *N Engl J Med* 2015; 372:11–20 CrossRef Medline
- Dababneh H, Bashir A, Hussain M, et al. **Endovascular treatment of tandem internal carotid and middle cerebral artery occlusions.** *J Vasc Interv Neurol* 2014;14:25–30 Medline
- Behme D, Mpotsaris A, Zeyen P, et al. **Emergency stenting of the extracranial internal carotid artery in combination with anterior circulation thrombectomy in acute ischemic stroke: a retrospective multicenter study.** *AJNR Am J Neuroradiol* 2015;36:2340–45 CrossRef Medline
- Campbell BC, Mitchell PJ, Kleinig TJ, et al; EXTEND-IA Investigators. **Endovascular therapy for ischemic stroke with perfusion-imaging selection.** *N Engl J Med* 2015;372:1009–18 CrossRef Medline
- Saver JL, Goyal M, Bonafe A, et al; SWIFT PRIME Investigators. **Stent-retriever thrombectomy after intravenous t-PA vs. t-PA alone in stroke.** *N Engl J Med* 2015;372:2285–95 CrossRef Medline
- Kim JJ, Dillon WP, Glastonbury CM, et al. **Sixty-four-section multi-detector CT angiography of carotid arteries: a systematic analysis of image quality and artifacts.** *AJNR Am J Neuroradiol* 2010;31:91–99 CrossRef Medline
- Korn A, Bender B, Brodoefel H, et al. **Grading of carotid artery stenosis in the presence of extensive calcifications: dual-energy CT angiography in comparison with contrast-enhanced MR angiography.** *Clin Neuroradiol* 2015;25:33–40 CrossRef Medline
- Fujimoto S, Toyoda K, Kishikawa K, et al. **Accuracy of conventional plus transoral carotid ultrasonography in distinguishing pseudo-occlusion from total occlusion of the internal carotid artery.** *Cerebrovasc Dis* 2006;22:170–76 CrossRef Medline
- Fürst G, Saleh A, Wenserski F, et al. **Reliability and validity of non-invasive imaging of internal carotid artery pseudo-occlusion.** *Stroke* 1999;30:1444–49 CrossRef Medline
- Desole A, Campanile F, Tosato F, et al. **Surgical treatment for pseudo-occlusion of the internal carotid artery.** *Interact Cardiovasc Thorac Surg* 2015;20:636–40 CrossRef Medline
- Marquering HA, Nederkoorn PJ, Beenen LF, et al. **Carotid pseudo-occlusion on CTA in patients with acute ischemic stroke: a concerning observation.** *Clin Neurol Neurosurg* 2013;115:1591–94 CrossRef Medline
- Duijsens HM, Spaander F, van Dijk LC, et al. **Endovascular treatment in patients with acute ischemic stroke and apparent occlusion of the extracranial internal carotid artery on CTA.** *J Neurointerv Surg* 2015;7:709–14 CrossRef Medline
- Ng FC, Choi PM, Datta M, et al. **Perfusion-derived dynamic 4D CT angiography identifies carotid pseudo-occlusion in hyperacute stroke.** *J Neuroimaging* 2016;26:588–91 CrossRef Medline
- Prakkamakul S, Pitakvej N, Dumrongpisutikul N, et al. **Mid-cervical flame-shaped pseudo-occlusion: diagnostic performance of mid-cervical flame-shaped extracranial internal carotid artery sign on computed tomographic angiography in hyperacute ischemic stroke.** *Neuroradiology* 2017;59:989–96 CrossRef Medline
- Akpınar S, Gelener P, Yilmaz G. **Aetiologies of internal carotid artery pseudo-occlusions in acute stroke patients: what neurointerventionalists can expect.** *Br J Radiol* 2017;90:20160352 CrossRef Medline
- Fransen PS, Beumer D, Berkhemer OA, et al; MR CLEAN Investigators. **MR CLEAN, a multicenter randomized clinical trial of endovascular treatment for acute ischemic stroke in the Netherlands: study protocol for a randomized controlled trial.** *Trials* 2014;15:343 CrossRef Medline
- Park ST, Kim JK, Yoon KH, et al. **Atherosclerotic carotid stenoses of apical versus body lesions in high-risk carotid stenting patients.** *AJNR Am J Neuroradiol* 2010;31:1106–12 CrossRef Medline
- Goyal M, Demchuk AM, Menon BK, et al; ESCAPE Trial Investigators. **Randomized assessment of rapid endovascular treatment of ischemic stroke.** *N Engl J Med* 2015;372:1019–30 CrossRef Medline
- Jovin TG, Chamorro A, Cobo E, et al; REVASCAT Trial Investigators. **Thrombectomy within 8 hours after symptom onset in ischemic stroke.** *N Engl J Med* 2015;372:1–11 CrossRef Medline
- Miyazaki Y, Mori T, Tajiri H, et al. **Comparison of four-dimensional CT angiography (4D-CTA) with MRA in acute ischemic stroke patients with probable internal carotid artery occlusion.** *Stroke* 2012;43:A2859
- Zhang S, Chen W, Tang H, et al. **The prognostic value of a four-dimensional CT angiography-based collateral grading scale for reperfusion therapy in acute ischemic stroke patients.** *PLoS One* 2016;11:1–12 CrossRef Medline

Randomized Assessment of the Safety and Efficacy of Intra-Arterial Infusion of Autologous Stem Cells in Subacute Ischemic Stroke

 V. Bhatia,  V. Gupta,  D. Khurana,  R.R. Sharma, and  N. Khandelwal



ABSTRACT

BACKGROUND AND PURPOSE: Stroke is a debilitating illness for which treatment window is limited. Most patients present to the healthcare facility beyond that window. Autologous stem cells have shown some promise for this group of patients. This study was performed to evaluate the safety and the efficacy of intra-arterial infusion of bone marrow–derived mononuclear cells in patients with middle cerebral artery ischemic stroke.

MATERIALS AND METHODS: A prospective, randomized, open-label, blinded–end point study was performed from July 2015 to June 2016. Of 229 patients with acute stroke who presented to the hospital during this period, 20 patients who satisfied the inclusion/exclusion criteria were included and randomized into the control and intervention groups. Intra-arterial stem cell infusion into the ipsilateral MCA was performed in the patients in the intervention group at 8–15 days post-stroke ictus. Final analysis at 6 months was performed for primary (safety) and secondary outcomes (efficacy).

RESULTS: When we compared the primary end point of the study, no procedure-related mortality, complication, new infarct, or symptomatic intracranial hemorrhage was seen in the intervention group. When we compared the secondary end point of good clinical outcome, 8 (80%) patients in the intervention group showed good clinical outcome (modified Rankin Scale score < 2) with 4 (40%) patients in the control group achieving this (95% confidence interval for good outcome in patients with stem cell infusion, 49.03–94.3, and without stem cell infusion, 16.82–68.73; $P = .068$).

CONCLUSIONS: Intra-arterial infusion of stem cells can be carried out safely in the subacute stage of ischemic stroke. Improved clinical outcomes were observed with intra-arterial stem cell therapy; however, studies with larger cohorts are needed to validate the results.

ABBREVIATIONS: BI = Barthel index; BMMNC = bone marrow–derived mononuclear cells

Stroke is a leading cause of mortality and morbidity and is estimated to cause >5 million deaths per year throughout the world. Despite the recent advancement in therapeutic and rehabilitative strategies, stroke remains a major cause of financial burden on the health resources worldwide. Until recently, intravenous tissue plasminogen activator was the only approved therapy for acute stroke with a narrow window of 4.5 hours, and its current reach is to only up to 5% of the population.^{1,2}

Recently, on the basis of multiple randomized trials, the Amer-

ican Heart Association and American Stroke Association have modified stroke treatment guidelines and criteria to include endovascular therapy with stent retrievers in acute stroke in a selected group of patients.² However, only a limited number of patients with stroke reach the hospital in time for stroke revascularization therapies. Even in the dedicated stroke centers and institutions with aggressively organized stroke programs, only about 10% of patients with stroke can receive immediate treatment.³ Thus, most of these patients are eligible for only supportive treatment and rehabilitation. There are no definite pharmacologic or biologic interventions that can reverse impairment in these patients.⁴ Further research is required for treatment dedicated to reducing tissue-injury propagation and hastening clinical and functional recovery in these patients.

Stem cell infusion is a promising novel therapy for acute/subacute ischemic stroke. A few previous studies have examined the effect of bone marrow–derived mononuclear cells (BMMNC) in stroke using different routes of delivery. These studies have shown

Received August 9, 2017; accepted after revision January 5, 2018.

From the Departments of Radiodiagnosis (V.B., V.G., N.K.), Neurology (D.K.), and Transfusion Medicine (R.R.S.), Postgraduate Institute of Medical Education and Research, Chandigarh, India.

Please address correspondence to Vivek Gupta, MD, Department of Radiodiagnosis, PGIMER, Sector-12, Chandigarh, India; e-mail: drvivekgupta.pgi@gmail.com



Indicates article with supplemental on-line tables.



Indicates article with supplemental on-line photo.

<http://dx.doi.org/10.3174/ajnr.A5586>

the safety and feasibility of stem cells in their respective patient cohorts, with good outcomes; but none were randomized.^{5–9} The aim of this research was to analyze in a randomized manner the safety and outcome of autologous BMMNC delivered directly into the ipsilateral middle cerebral artery in patients with ischemic MCA stroke of 8–15 days' duration.

MATERIALS AND METHODS

This prospective, randomized, open-label, blinded–end point study was carried out from July 2015 to June 2016 in a large tertiary care center in India. The study included patients presenting with acute MCA territory stroke. A total of 229 patients with acute stroke were admitted during this period. The initial management for acute stroke was performed in the patients who presented in and out of the therapeutic window according to the institutional protocol. Of these patients, 20 consecutive patients who fulfilled the inclusion and exclusion criteria were randomized into 2 groups (control and intervention groups) in accordance with the study protocol. Inclusion criteria were the following: age range of 20–80 years, symptoms and signs of clinically definite MCA stroke (0–14 days postictus), National Institutes of Health Stroke Scale score of >7 , stroke clinically and on imaging conforming to the MCA territory, recanalization/patency of the involved M1 segment of the MCA on imaging, and patency of the carotid arteries for intra-arterial access of cerebral circulation. Exclusion criteria were the following: cerebral hemorrhage on CT/MR imaging, imaging evidence of M1 MCA segment complete occlusion, hemodynamic instability, known defect of clotting or platelet function, severe comorbidity precluding intra-arterial intervention, hepatic dysfunction, renal dysfunction, pregnancy, patients likely to be unavailable for follow-up, patients with evidence of chronic illness or advanced cancer, patients already dependent in activities of daily living before the present acute stroke (ie, prestroke mRS of >3), and refusal to give informed consent. The major reasons for exclusion included hemorrhagic stroke, scores outside the NIHSS criteria, occluded ipsilateral ICA or M1 MCA, and refusal to give consent.

The approvals were obtained from the ethics and stem cell ethics committees of the institution. A data safety-monitoring board was constituted, comprising 3 members, to report any adverse effects during the study. The data safety-monitoring board evaluated the occurrence of any adverse events, serious adverse events, and treatment-emergent adverse events during a meeting scheduled every 3 months.

Clinical and Imaging Evaluation

The patients were admitted and clinically evaluated by an experienced neurologist. History, detailed clinical examination, and clinical scoring based on the modified Rankin Scale scoring, National Institutes of Health Stroke Scale, and Barthel index (BI) were performed. Blood samples were sent for the following values: complete blood counts, blood urea, creatinine, lipid profile, blood sugar, and the serum electrolytes.

Written informed consent was obtained from the patient or their legal representative for the study. The same clinical and laboratory evaluations were also performed at day 1 postprocedure and at 1, 3, and 6 months in both groups. All patients who were

included underwent a noncontrast head CT and brain MR imaging with an MR angiogram of the brain and neck. Patients were evaluated for infarct location, infarct volume, angiographic findings, the presence of any hemorrhage or new infarct, and the appearance of new lesions or any other findings. The MR imaging follow-up with similar imaging protocol, sequences, and parameters was performed in all patients at 1, 3, and 6 months. An experienced neurologist and a neuroradiologist did the clinical evaluations and the interpretation of the images, respectively. Both were blinded to the initial clinical presentation and the nature of intervention.

Bone Marrow Aspiration, Cell Separation, and Stem Cell Preparation

The bone marrow aspiration was performed from the posterior superior iliac spine under aseptic conditions with the patient under local anesthesia. Each aspiration was transferred into a 350-mL collection bag containing citrate phosphate dextrose adenine, which was transferred to a bone marrow–processing laboratory for the further processing. The BMMNC were separated using a ficoll density gradient centrifugation procedure. Quality control of the final cell product was performed to determine the total number of cells, total BMMNC, total CD34+ cells, CD34+ cell percentage, sterility, and viability. Total nucleated cells and the mononuclear cells were counted using an automated hematology analyzer. CD34 cell enumeration was performed with an anti-CD34 antibody using the International Society of Hematology and Graft Engineering guidelines. Viability was assessed using 0.4% Trypan Blue dye. The criterion set for the BMMNC dosage was a maximum of 5×10^8 cells to be infused.

Intra-Arterial Stem Cell Infusion

The right femoral artery access was through a 6F arterial sheath. With a 5F diagnostic catheter, ipsilateral internal carotid artery angiography was performed to ensure patency of the ICA and M1 segment of the middle cerebral artery to its bifurcation. Then, a 6F Neuron guide catheter (Penumbra, Alameda, California) was placed in the ipsilateral ICA, and an Echelon 10 microcatheter (Covidien, Irvine, California) was navigated in the MCA and placed in the proximal segment (M1) of the MCA. Through the microcatheter, stem cell infusate was slowly injected in the MCA for 10 minutes. After the infusion, a check diagnostic run was performed to ensure patency of all the vessels and rule out any thromboembolic complication. Pre- and postprocedure heart rate, systolic and diastolic blood pressures, respiratory rate, and the presence of rash, urticaria, chills, and rigors or any other complication were noted.

Evaluation of Results

The data were evaluated for the primary and secondary outcomes according to the predetermined criteria. The primary end point (evaluation of safety) was clinically severe procedural complications (increase in the NIHSS score of ≥ 4 points), symptomatic intracerebral hemorrhage, new ischemic lesions on imaging in the intervened territory, or death. The secondary end point (good clinical outcome) was defined as an mRS score of 0–1 in patients

Table 1: Demographics and baseline clinical features of the cohort

	Control Group (No.) (%)	Intervention Group (No.) (%)	P Value
Age (mean) (yr)	66 ± 7.3	57 ± 12.2	.075
Sex ratio (M/F)	6:4	8:2	.329
Hemiparesis (L/R)	5:5	6:4	.653
Thrombolysis	0	1 (10)	.305
Hypertension	5 (50)	5 (50)	1
Diabetes mellitus	6 (60)	7 (70)	.63
Dyslipidemia	9 (90)	8 (80)	.53
Smoking	1 (10)	5 (50)	.051
Atrial fibrillation	0	2 (20)	.13
Coronary artery disease	1 (10)	2 (20)	.53
Mean baseline NIHSS score	10.5	10.6	.94

Note:—L indicates left; R, right.

with an NIHSS score of 8–14 at admission and an mRS score of 0–2 in patients with an NIHSS score of >14 at admission.

Statistical Analysis

The Kolmogorov-Smirnov test was used for normality of distribution of the data. Continuous data were analyzed by a paired *t* test, and discrete data, with χ^2 tests. A value of *P* < .05 was significant.

RESULTS

Baseline Demographic, Laboratory, and Stroke Indices

There was no statistically significant difference between the 2 groups (intervention versus control) regarding the baseline demographic and clinical parameters (Table 1). Also, no statistically significant difference was seen between the 2 groups in relation to baseline stroke severity as assessed by the NIHSS (*P* = .94) and the baseline clinical assessment with the modified Rankin Scale score (*P* = .60) and the Barthel index (*P* = .49). There was a trend toward higher baseline infarct size in the control group, but it was not statistically significant (*P* = .065). On imaging, no statistically significant difference was seen in relation to infarct location, angiography findings, or the presence of hemorrhage or any other imaging findings at baseline and at 6 months.

Stem Cell Infusate Parameters and Comparison with Outcome. The mean poststroke day of intervention was day 10, the mean stem cell harvest volume was 118 mL, the mean infusate volume was 5 mL, and the mean total nucleated cells were 9.3×10^8 . Mean mononuclear cells were 6.1×10^8 , mean CD34 cells were 1.02×10^7 , mean CD34 cell percentage was 1%, and mean viability was 95% (On-line Table 1). There was no statistically significant difference between good outcome and poor outcome in relation to these parameters in the intervention group. There was no significant change in pre- and postprocedural heart rate, respiration rate, blood pressure, and temperature parameters in the intervention group. None of the patients had any allergic reaction such as urticaria, rash, chill, or rigor.

Primary and Secondary Outcome Analysis

Primary End Point Evaluation. No procedure-related complication was seen in any patient. No evidence of any immediate postprocedural or delayed complications related to the procedure or

Table 2: Comparison of primary and secondary outcomes between the 2 groups

Parameter	Control Group (n = 10)	Intervention Group (n = 10)	P Value
Mortality	2	1	.53
Complications	0	0	
New infarct	0	1	.305
SICH	0	0	
Good outcome	4	8	.068

Note:—SICH indicates symptomatic intracerebral hemorrhage.

the infused stem cells was seen. None of the patients in either group had episodes of symptomatic intracerebral hemorrhage immediately after the procedure or at follow-up. No fresh infarct in the involved hemisphere was seen on the follow-up imaging. One patient in the intervention group had an episode of infarction on the contralateral side 2.5 months after the procedure due to a cardioembolic phenomenon (Table 2).

None of the patients in either group had any neoplasms. Two of the patients in the control group died within 1 month of stroke. These patients had initial NIHSS scores of 15 and 18, respectively. Both patients had high initial stroke severity, and the probable cause of death was cardiac arrest. One patient in the intervention group (mentioned above) who had a contralateral stroke at 2.5 months died a month later. This patient had an initial baseline NIHSS score of 11, which had improved to 4 at discharge and up to 1 at the 1-month follow-up. Stroke in the contralateral MCA territory resulted in an NIHSS score of 22 at 3 months, which ultimately led to his death.

Secondary End Point Evaluation. Secondary end point evaluation for clinical improvement was based on the initial NIHSS score and the mRS score at 6 months. There were 8 (80%) patients in the intervention group and 4 (40%) in the control group who achieved good outcome (*P* = .068; odds ratio = 6; 95% CI odds ratio, 0.81–44.31). Seventeen patients had a baseline NIHSS score of 8–14. Of these, 12 patients, including 8 intervention cases and 4 controls, were regarded as having achieved a good clinical outcome (mRS of 0–1) at 6 months (Figs 1 and 2). Three patients in the control group had an NIHSS score of >14. All of them had poor outcome at 6-month follow-up because an mRS score of <2 could not be achieved. Both groups showed improvement in the mRS during a 6-month follow-up; however, intragroup analysis revealed that this improvement was statistically significant only in the intervention group (*P* = .009). There was a significant difference seen in the BI in the intervention group at 6-month follow-up compared with baseline (*P* = .004). No statistically significant differences were seen in the control group (On-line Figure).

DISCUSSION

Ischemic stroke is one of the leading causes of morbidity and mortality worldwide because it leads to irreversible damage to the neuroglial tissue, resulting in functional deficits and chronic sequelae. The only therapy that is FDA-approved for acute stroke is intravenous tPA, which has the limitations of a narrow window (up to 4.5 hours for anterior circulation) and potential hemorrhagic complications. Therefore, it is currently benefiting a limited number of patients with stroke.¹⁰ Recently, the American Heart Association and the American Stroke Association have

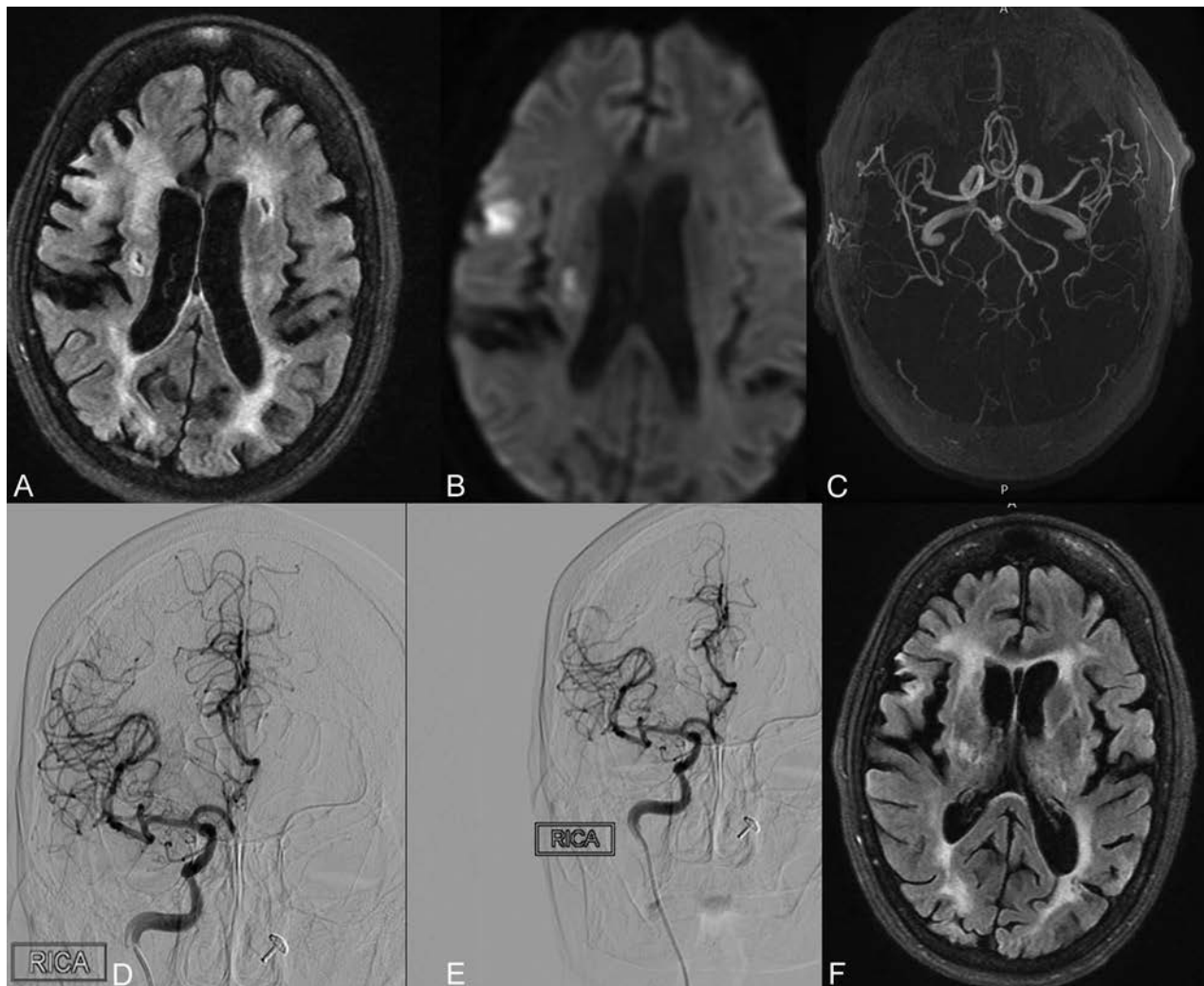


FIG 1. A 70-year-old man with left hemiparesis and a baseline NIHSS score of 10 (intervention group). Axial FLAIR image (A) shows an infarct in the right periventricular and posterior limb of the internal capsule, showing diffusion restriction on diffusion-weighted image (B). MR angiogram shows no evidence of any major branch occlusion (C). Preprocedural right ICA diagnostic run (D) shows normal opacification of the MCA branches. Post-stem cell infusion right ICA run (E) shows similar findings, with normal opacification of all the branches. Axial FLAIR MR imaging at 6-month follow-up shows a reduction in infarct size. This patient had an mRS score of 1 at 6-month follow-up, and his outcome was considered good.

modified their acute stroke treatment guidelines to include mechanical thrombectomy as a first-line treatment for selected patients with large and proximal artery occlusions.² However, a large subset of patients with stroke are either not able to meet these criteria or, due to time or cost constraints, are not able to take advantage of this form of treatment. Therefore, a large number of patients with acute stroke will either not receive any definitive treatment or, even after the treatment, may be left with residual neurologic deficits.

Stem cell therapy is a relatively novel approach in the treatment of patients with stroke, with the fundamental hypothesis coming from the observation that certain brain areas such as the dentate nucleus of the hippocampus and the subventricular zone are capable of regeneration and neurogenesis.¹¹ Patients for stem cell therapy can be selected on the basis of the neuroprotective outcome for acute stroke or neuroreparative outcome for damaged brain tissue to promote neural tissue endogenous repair. Various mechanisms, which potentially produce benefits in pa-

tients with stroke, include reduced apoptosis and inflammation, promotion of angiogenesis and neurogenesis, promotion of neural plasticity, and formation of neural circuitry.^{11,12}

The different methods for transplantation of stem cells in patients with stroke include direct intracranial, arterial, and venous routes.¹³ Intra-arterial transplantation in the affected territory is an invasive approach, but it can directly implant these cells in the affected territory with less risk than direct stereotactic implantation and has the advantage of more dose deployed compared with the intravenous route.^{13,14}

In our study, we obtained autologous BMMNC from the patients with stroke on the day of transplantation, which were then transplanted through an intra-arterial route directly into the ipsilateral MCA. We compared our results with age- and sex-matched controls.

Our study was a prospective, randomized, open-label, blinded-end point study involving 20 patients with acute ischemic stroke, 10 of whom received intra-arterial stem cells (intervention group)

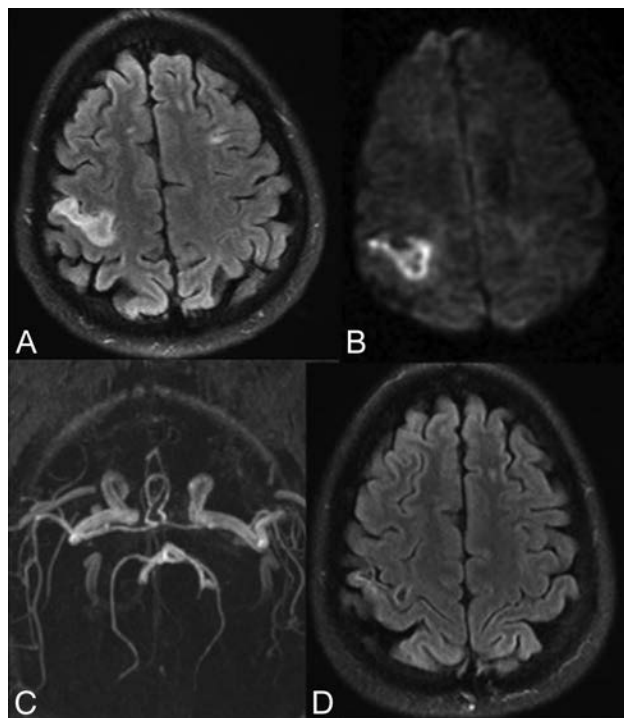


FIG 2. A 50-year-old man with right hemiparesis and an NIHSS score of 7 (intervention group). Axial FLAIR image (A) shows an infarct in the right cortical subcortical location showing diffusion restriction on DWI (B). MR angiogram shows no evidence of any major branch occlusion. Axial FLAIR MR imaging at 6-month follow-up shows a reduction in infarct size. This patient had an mRS score of zero at 6-month follow-up, and his outcome was considered good.

with the rest acting as controls. Previous studies evaluating intra-arterial stem cell therapy in acute stroke either did not have controls or lacked randomization. Also, the results were not evaluated in a blinded fashion.^{5-9,14} The present study has tried to remove the inherent bias by using the prospective, randomized, open-label, blinded-end point study design.

The mean age in our study population was 61.7 years, with a majority of male patients ($n = 14$, 70%). Eleven (55%) patients had left-sided MCA infarct. There was no statistically significant difference between the 2 groups in relation to the age and laboratory values such as hemoglobin, total leukocyte count, platelets, international normalized ratio, urea, creatinine, blood sugar, electrolytes, total cholesterol, and so forth. Both groups received similar stroke care, including pharmacotherapeutics, physiotherapy, and rehabilitation.

Stem cell numbers and viability parameters in our study group were comparable with those in previous studies.^{5,9,14}

We performed the stem cell implantation between 8 and 15 days after stroke. The mean poststroke day of intervention was 10 days in the present study. Previous studies using the intra-arterial route have demonstrated the safety of the procedure from 3 to 9 days.^{5,9,14} Increasing the time for stem cell implantation beyond 1 week of acute stroke as in the present study enables more patients with stroke to be included for the therapeutic benefit of stem cell infusion if proved. The comparison of parameters between the current study and the previous studies is given in On-line Table 2.

The primary end point of the study was the evaluation of the safety of the procedure, which was assessed by reviewing the mor-

tality, symptomatic intracranial hemorrhage, presence of new infarcts/lesions, or any other complications. No intracranial hemorrhage was found in either group on follow-up. These data are consistent with previous studies that have reported the safety of transplanted stem cells in patients with stroke.^{5-9,14} During the course of the study, 1 patient in the stem cell group died at 3.5 months follow-up due to the occurrence of a contralateral MCA infarct. This patient was treated for right-sided MCA infarct with intra-arterial stem cells. At 1-month follow-up, this patient had shown improvement with an mRS score of 2 (the NIHSS score at admission was 13, and at discharge, it was 4). This patient had undergone an operation for atrial septal defect 20 years earlier, and the cause of stroke was probably cardioembolic due to persistent atrial fibrillation. The cause of the new stroke at 2.5 months in this case was again probably cardioembolic, resulting in an occluded left MCA. He was managed at this time with intra-arterial thrombectomy; however, the MCA could not be recanalized and the patient developed infarct and deteriorated. At 3-month follow-up, this patient had an mRS score 5. As in our study, Savitz et al⁸ also found 1 mortality due to pulmonary embolism at 40 days in their study population of 10 patients. The authors concluded that this mortality was not procedural-related because the patient was at high risk of developing deep venous thrombosis due to prolonged limb immobilization and this was the likely source of pulmonary embolism. They reasoned that previous studies have reported that the injected mononuclear cells die within a week of administration and therefore cannot account for the reported episode of pulmonary embolism approximately 1 month after the procedure in their study.¹⁵ Likewise, our patient also had a stroke after 2 and a half months, likely due to atrial fibrillation and not related to the intervention.

There were 2 mortalities in the control group within 1 month of stroke onset. Both had initial high stroke severity with NIHSS scores of 15 and 18, respectively. A previous study with a control population did not find any mortality in the control group.⁵ This difference is likely because of the higher NIHSS scores of these patients at presentation and subsequent deterioration. No other patient developed any other infarct in the intervened side or neoplastic lesion on follow-up, consistent with previous studies.^{5-9,14} We also found no significant changes in the preprocedural and postprocedural parameters such as heart rate, blood pressure, respiratory rate, presence of rash, fever, urticaria, or chills after infusion of BMMNC. No other complication was seen in our study patients, which is consistent with previous similar studies.^{5-9,14}

The secondary end point in the present study was to evaluate clinical improvement based on the improvement in the modified Rankin Scale. Patients with a baseline NIHSS score of 8–14 ($n = 17$) did better than those with a baseline NIHSS score of >14 ($n = 3$). In the former group, 12 patients achieved good clinical outcome (8 in the intervention group and 4 in the control group; $P = .068$). In the latter group, all 3 patients did not achieve the defined good clinical outcome of mRS < 2 .

Friedrich et al⁹ also used similar criteria for good clinical outcome; however, their defined follow-up was 90 days, and there was no control group or randomization. They found good clinical outcome in 8 (40%) of their patients as opposed to 80% in the

present study. Moniche et al⁵ used controls as in our study and found that 20% of the patients who received therapy achieved an mRS of 2 at 6 months versus none in the control group; however, the number of patients showing improvement in mRS did not reach statistically significant levels ($P < .47$).

We also found improving trends in the NIHSS, mRS, and BI in both our stem cell and control groups, which was statistically significant in the intervention group when comparing baseline to 6-month follow-up. Similar trends were also observed in the other studies.^{5-9,14}

There were several limitations of our study. The sample size in our study was small, thus limiting the power of this study to confidently claim clinical benefits in patients who received stem cells compared with controls. Patients with extremes of stroke severity as per the NIHSS were not equally represented due to small sample size; thus, definite conclusions about which patients will benefit the most cannot be made. Although all measures were taken to ensure blinding of the evaluating observers at 6 months, the lack of any sham procedure in the control group might have interfered with the efficacy of blinding.

CONCLUSIONS

The present study demonstrates the safety of intra-arterial BMMNC in patients with acute stroke, with a trend toward improved clinical outcome compared with control patients. Stem cells offer a promising novel therapy in these patients, with reduction in morbidity and improved functional outcome. Further randomized studies with a large patient cohort are needed to validate our findings.

REFERENCES

1. Intercollegiate Stroke Working Party. National Sentinel Stroke Clinical Audit 2010: Public Report for England, Wales and Northern Ireland. London: Royal College of Physicians; 2011. <https://www.rcplondon.ac.uk/projects/outputs/national-sentinel-stroke-audit-2010>. Accessed on March 20, 2017
2. Powers WJ, Derdeyn CP, Biller J, et al; American Heart Association Stroke Council. **2015 Heart Association/American Stroke Association Focused Update of the 2013 Guidelines for the early management of patients with acute ischemic stroke regarding endovascular treatment: a guideline for healthcare professionals from the American Heart Association/American Stroke Association.** *Stroke* 2015; 46:3024–35 CrossRef Medline
3. Morgenstern LB, Staub L, Chan W, et al. **Improving delivery of acute stroke therapy: the TLL Temple Foundation Stroke Project.** *Stroke* 2002;33:160–66 CrossRef Medline
4. Stroemer P, Patel S, Hope A, et al. **The neural stem cell line CTX0E03 promotes behavioral recovery and endogenous neurogenesis after experimental stroke in a dose-dependent fashion.** *Neurorehabil Neural Repair* 2009;23:895–909 CrossRef Medline
5. Moniche F, Gonzalez A, Gonzalez-Marcos JR, et al. **Intra-arterial bone marrow mononuclear cells in ischemic stroke: a pilot clinical trial.** *Stroke* 2012;43:2242–44 CrossRef Medline
6. Battistella V, de Freitas GR, da Fonseca LM, et al. **Safety of autologous bone marrow mononuclear cell transplantation in patients with nonacute ischemic stroke.** *Regen Med* 2011;6:45–52 CrossRef Medline
7. Suárez-Monteagudo C, Hernández-Ramírez P, Alvarez-González L, et al. **Autologous bone marrow stem cell neurotransplantation in stroke patients: an open study.** *Restor Neurol Neurosci* 2009;27: 151–61 Medline
8. Savitz SI, Misra V, Kasam M, et al. **Intravenous autologous bone marrow mononuclear cells for ischemic stroke.** *Ann Neurol* 2011;70: 59–69 CrossRef Medline
9. Friedrich MA, Martins MP, Araujo MD, et al. **Intra-arterial infusion of autologous bone marrow mononuclear cells in patients with moderate to severe middle cerebral artery acute ischemic stroke.** *Cell Transplant* 2012;21(suppl 1):S13–21 CrossRef Medline
10. National Institute of Neurological Disorders and Stroke rt-PA Stroke Study Group. **Tissue plasminogen activator for acute ischemic stroke.** *N Engl J Med* 1995;333:1581–87 CrossRef Medline
11. Jin K, Wang X, Xie L, et al. **Evidence for stroke-induced neurogenesis in the human brain.** *Proc Natl Acad Sci U S A* 2006;103:13198–202 CrossRef Medline
12. Thomson JA, Itskovitz-Eldor J, Shapiro SS, et al. **Embryonic stem cell lines derived from human blastocysts.** *Science* 1998;282:1145–47 CrossRef Medline
13. Banerjee S, Williamson DA, Habib N, et al. **The potential benefit of stem cell therapy after stroke: an update.** *Vasc Health Risk Manag* 2012;8:569–80 CrossRef Medline
14. Banerjee S, Bentley P, Hamady M, et al. **Intra-arterial immunoselected CD34+ stem cells for acute ischemic stroke.** *Stem Cells Transl Med* 2014;3:1322–30 CrossRef Medline
15. Brenneman M, Sharma S, Harting M, et al. **Autologous bone marrow mononuclear cells enhance recovery after acute ischemic stroke in young and middle-aged rats.** *J Cereb Blood Flow Metab* 2010;30: 140–49 CrossRef Medline

Under Pressure: Comparison of Aspiration Techniques for Endovascular Mechanical Thrombectomy

 O. Nikoubashman,  D. Wischer,  H.M. Hennemann,  M. Büsen,  C. Brockmann, and  M. Wiesmann



ABSTRACT

BACKGROUND AND PURPOSE: Blood flow should be interrupted during mechanical thrombectomy to prevent embolization of clot fragments. The purpose of our study was to provide a handy overview of the most common aspiration devices and to quantify their flow characteristics.

MATERIALS AND METHODS: We assessed volumetric flow rates generated by a 60-mL VacLok vacuum pressure syringe, a Pump MAX aspiration pump, and a Dominant Flex suction pump connected to the following: 1) an 8F long sheath, 2) an 8F balloon-guide catheter, 3) an ACE 64 distal aspiration catheter, and 4) an AXS Catalyst 6 Distal Access Catheter. We used a water/glycerol solution, which was kept at a constant temperature of 20°C (viscosity, 3.7 mPa · s).

RESULTS: Aspiration with the syringe and the Dominant Flex suction pump achieved the highest flows, whereas aspiration with the Pump MAX was significantly lower ($P < .001$). Resistors in the aspiration system (tubing, connectors, and so forth) restricted flows, especially when the resistance of the catheter was small (due to its large diameter) and the connected resistors became the predominant resistance ($P < .001$). The syringe achieved an average vacuum pressure of -90 kPa, and the resulting flow was constant during almost the entire procedure of filling the syringe.

CONCLUSIONS: Sixty-milliliter VacLok vacuum pressure syringes and the Dominant Flex suction pump achieved high and constant flows likely sufficient to reverse blood flow during thrombectomy with an 8F sheath or balloon-guide catheter in the ICA and modern distal aspiration catheters in the MCA. The Pump MAX aspiration pump is dedicated for use with distal aspiration catheters and is unlikely to reverse blood flow in the ICA and MCA without balloon protection.

Endovascular mechanical thrombectomy is the most effective treatment option for acute ischemic stroke caused by large-vessel occlusion.¹ In past years, the focus of neurointerventional stroke research has shifted from establishing the method to finding the optimal treatment technique.^{2–6} Effective blood flow management during the procedure is key to safety and effectiveness.⁷ Chueh et al² have shown that there are thousands of small clot fragments during thrombectomy that may occlude small arterioles and capillaries. Even though small infarctions may not be

visible on MR imaging, they can have an important clinical impact.^{8,9} Hence, antegrade blood flow should be interrupted during mechanical thrombectomy to prevent embolization of clot fragments.⁷ For this goal, blood is usually aspirated with syringes or a dedicated aspiration pump proximally through the access catheter and/or distally through an intermediate catheter.

Techniques for flow reversal differ considerably, ranging from pump aspiration through small (5F) guide catheters in the internal carotid artery to syringe aspiration through balloon-guide catheters. Syringes have the advantage of cost-effectiveness and, according to some interventionalists, of subjective feedback of aspiration force when they draw the syringe. However, the actual vacuum pressure is not indicated, and comparably small volumes (usually ≤ 60 mL) restrict aspiration duration and may necessitate the use of multiple syringes, which can be impractical during an acute stroke intervention. Aspiration pumps on the other hand allow pressure-controlled and comparably comfortable aspiration. However, their comparably high cost restricts their availability in many hospitals. The choice between a syringe and aspiration

Received September 20, 2017; accepted after revision January 31, 2018.

From the Department of Diagnostic and Interventional Neuroradiology (O.N., D.W., H.M.H., M.W.), RWTH Aachen University Hospital, Aachen, Germany; Institute of Applied Medical Engineering (M.B.), RWTH Aachen University, Aachen, Germany; and Department of Neuroradiology (C.B.), University Medical Centre, Johannes Gutenberg University, Mainz, Germany.

Please address correspondence to Omid Nikoubashman, MD, Klinik für Neuroradiologie, Universitätsklinikum Aachen, Pauwelsstr 30, 52074 Aachen, Germany, e-mail: onikoubashman@ukaachen.de



Indicates article with supplemental on-line table.

<http://dx.doi.org/10.3174/ajnr.A5605>

pump is usually up to the interventionalist's discretion. However, there is not only no consensus about which method is best but also only a little knowledge about the specific characteristics of each method. For instance, the applied vacuum pressure of aspiration pumps is indicated, but the vacuum pressure of a syringe is not. Furthermore, although the flow through a bare catheter can be calculated using the Hagen-Poiseuille equation, in practice, it is considerably more challenging to determine the effective flow after accounting for resistors such as additional valves and connecting tubes between catheters and pumps. This issue is especially problematic because pump distributors do not indicate the resistance of their tubing.

Because mechanical thrombectomy is about to become more common, many interventionalists are going to deal with the conundrum of which technique to choose. Therefore, the purpose of our study was to provide a handy overview of the most common aspiration devices and to quantify flow characteristics and aspiration volumes through proximal and distal access catheters with a syringe and the 2 aspiration pumps that are currently available on the market (Pump MAX aspiration pump; Penumbra, Alameda, California; and Dominant Flex suction pump; Medela, Baar, Switzerland).

MATERIALS AND METHODS

Experiment

We assessed the volumetric flow rate (simply referred to as "flow" in the article) generated by a 60-mL VacLok vacuum pressure syringe (Merit Medical Systems, South Jordan, Utah), a Penumbra Pump MAX aspiration pump, and a Medela Dominant Flex suction pump, connected to the following: 1) an 8F long sheath (Shuttle Select; Cook, Bloomington, Illinois), 2) an 8F balloon-guide catheter (FlowGate²; Stryker Neurovascular, Kalamazoo, Michigan), 3) an 0.064-inch ACE 64 distal aspiration catheter (Penumbra), and 4) a 0.06-inch AXS Catalyst 6 Distal Access Catheter (Stryker Neurovascular). We connected catheters and aspiration devices with a 3-way valve (Discofix; Braun, Melsungen, Germany) and a hemostatic Y-adapter (Gateway Plus; Boston Scientific, Fremont, California) using the tubing of the manufacturer. Syringes were connected directly to the 3-way valve. No additional resistors (tubing, air filters, and so forth) were added to achieve the highest possible flow.

To simulate the rheologic properties of blood at body temperature, we aspirated a solution of glycerol and water, which was kept at a constant temperature of 20°C to ensure a viscosity of 3.7 mPa · s and a density of 1.11 g/mL.¹⁰ We measured aspiration flow with pumps as reported previously: We aspirated the solution, which was kept in a reservoir, and assessed the weight of the aspirated fluid in grams. The results of 7 measurements were averaged and converted to a volumetric dimension (milliliters). The aspiration flow (milliliters/second) was obtained by dividing the collected volume by the aspiration time.⁵ Aspiration with a syringe was assessed as aspirated volume with time. For measurements through the sheath and balloon catheter, we used an ultrasonic flow meter (HT110 Bypass Flowmeter & Tubing Sensor; Transonic, Ithaca, New York), due to the high flow through these catheters. The Penumbra pump was set on the recommended vacuum pressure of −25.5 inches Hg (\approx −86.4 kPa). The Medela

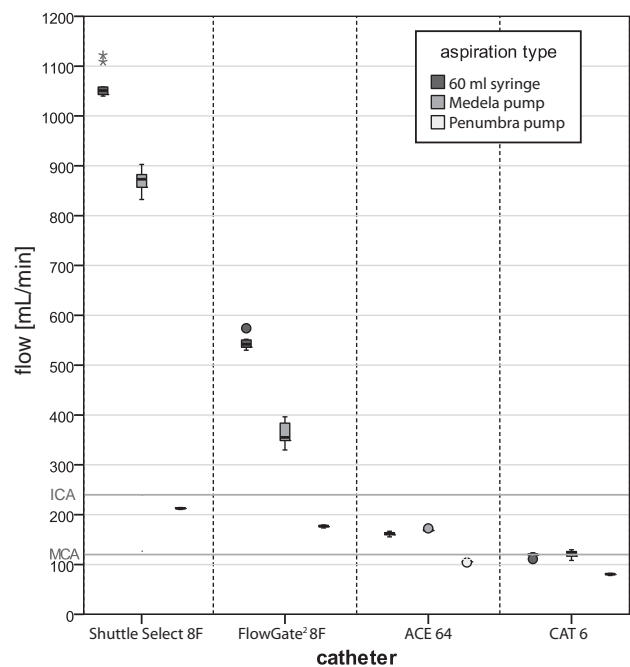


FIG 1. Flow through an 8F long sheath (Shuttle Select), an 8F balloon-catheter (FlowGate² Balloon Guide Catheter), an ACE 64 distal aspiration catheter, and an AXS Catalyst 6 Distal Access Catheter. Left, Syringe; middle, Medela pump; right, Penumbra pump. Dark gray horizontal lines mark the blood flow in the internal carotid artery and the middle cerebral artery in an average patient.

pump was set on a comparable pressure of −86.0 kPa. Measurements were repeated 7 times. The pressure generated with the syringe and the pressure loss from maximal pressure with time was recorded in 20 measurements using an analog manometer (class 1.6; Riegler Customer Solutions, Bad Urach, Germany).

Statistical Analysis

We compared experimental results with each other using the ANOVA test, and we compared experimental results with ideal values using a Student *t* test. *P* values of an α level $\leq .05$ were defined as significant. All statistical analyses were performed with SPSS 23 software (IBM, Armonk, New York).

RESULTS

The results of our flow measurements are summarized in the Online Table and Fig 1. Aspiration with the syringe and the Medela pump achieved the highest flows, whereas aspiration flow with the Penumbra pump was significantly lower. Subtotal vacuum and, first and foremost, the resistors in the aspiration system (tubing, connectors, and so forth) restricted flows, in particular when the resistance of the catheter was small (due to its large diameter) and the connected resistors became the predominant resistance (Online Table and Fig 1). The experimentally determined resistance of the Y-adapter and 3-way valve was approximately 212×10^6 Pa · s/m³ and 1406×10^6 Pa · s/m³, respectively.

Syringe

A fully drawn 60-mL syringe achieved a relatively high maximum average vacuum pressure of −90 kPa. Drawing approximately 7 and 20 mL achieved approximately −50 kPa and −75 kPa, respectively. Flow was constant during almost the entire procedure

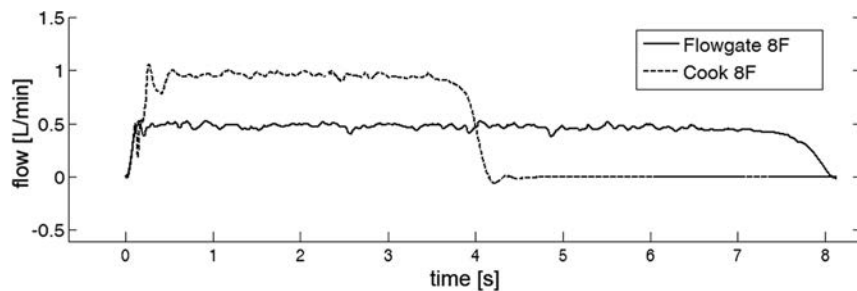


FIG 2. Exemplary flow measurements through an 8F long Shuttle Select sheath and an 8F FlowGate² balloon catheter with a syringe. Note that the flow is comparably constant and the flow decrease occurs within approximately half a second before the syringe has completely filled. Syringes achieve a comparably constant flow despite the unavoidable pressure loss during filling because it is not the pressure loss that predominantly restricts flow but the resistors (syringe tip, 3-way valve, and hemostatic valve).

of filling the syringe (Fig 2). Consequently, the syringe achieved comparably high flows. As anticipated, aspiration duration was limited due to high flow on the one hand and restricted syringe volume on the other. The resistance of the narrow tip of the syringe, as well as the connected Y-adapter and 3-way valve, reduced flows significantly ($P < .001$). When the syringe was drawn but no aspiration was performed, the pressure decreased (from -90 kPa to -60 kPa) by 10 kPa every 91 seconds or 6.6 kPa per minute on average, due to air leakage through the valves and connections.

Aspiration Pumps

The Medela pump achieved high flow, mostly due to the low resistance of the connecting tubing ($3251 \times 10^6 \text{ Pa} \cdot \text{s/m}^3$). Despite a similarly high vacuum pressure, the Penumbra pump achieved significantly lower flow in all experiments ($P < .001$), mostly due to the high resistance of the connecting tubing, which was $18,776 \times 10^6 \text{ Pa} \cdot \text{s/m}^3$ and thus almost 6 times higher than the resistance of the Medela tubing. Notably, the resistance of the old model of the Penumbra tubing ($23,756 \times 10^6 \text{ Pa} \cdot \text{s/m}^3$), which was distributed until 2016, was approximately 20% higher compared with the new tubing and resulted in significantly lower flows ($P < .001$).

DISCUSSION

Syringes and pumps have been established as basic tools used during mechanical thrombectomy. Aspiration with syringes or pumps can be used to generate a pressure gradient that results in a force at the catheter tip, thereby establishing contact between the catheter and the clot (direct aspiration first-pass technique [ADAPT], Stent-retriever Associated Vacuum-locked Extraction [SAVE], and Aspiration-Retriever Technique for Stroke [ARTS] technique, and so forth) and generating backward flow to prevent clot embolization.^{3,6,11} The force at the catheter tip depends on only the catheter diameter and the applied pressure and is therefore not altered by resistors.¹² The flow, however, is highly influenced by additional resistors; thus, any additional tubing and valves should be avoided whenever a backward flow is desired. Minimizing the resistance in the aspiration system is crucial because the necessary flow rate of aspirated blood is rather high: When the aim is to reverse blood flow, antegrade flow in the respective artery should be surpassed. In an average patient and

without a balloon-guide catheter that restricts antegrade flow, aspirated blood flow must surpass 240 mL/min in the ICA and 120 mL in the middle cerebral artery.^{13,14} Given that the flow through a 6F catheter even under ideal conditions (perfect vacuum, no external resistors, no stent retriever in its lumen) barely reaches 240 mL/min , we discourage using small guiding catheters for flow control in the ICA.⁵

In summary, the ideal aspiration system generates a high and constant pressure gradient and has minimal resistance. The latter is particularly important because our results show that pumps

achieve similar pressure gradients but significantly differing effective flows because of their differing tubing systems. The resistance is not an inherent constant, but a coefficient that depends on variables such as flow speed and flow direction as well as fluid density and viscosity. However, because pump distributors do not provide any information about their tubing system, it is impossible for clinicians to estimate effective aspiration flow. We have quantified flow characteristics of various means of flow control and found significant differences among the methods.

Sixty-Milliliter VacLok Vacuum Pressure Syringe

The 60-mL syringe achieved high flows that surpassed blood flow in the ICA with an 8F sheath and an 8F balloon-guide catheter. With the newest generation of distal access catheters (ACE 64), aspiration flow was high enough to surpass blood flow in the MCA. This would even be the case with a stent retriever in the catheter, which reduces flow by approximately 15% .⁵ Syringes provide constant and high flow during an acceptable time (Fig 2), a finding that we did not expect because filling the syringe results in a loss of the pressure gradient. The nonlinear pressure loss, the resistors (syringe tip, 3-way valve, and hemostatic valve), and the inertia of the aspirated blood may be the main reasons for syringes achieving a comparably constant flow despite the unavoidable pressure loss during filling. Whether a syringe should be drawn gradually during the thrombectomy maneuver or drawn and locked before the maneuver has been a subject of discussion. Interventionalists, who draw syringes gradually during the thrombectomy maneuver, report that a tremble during manual aspiration (probably due to the Bernoulli effect) precedes collapse of the vessel and therefore helps anticipate it. However, insufficient flow remains an issue. In our experience, the average interventionalist easily generates approximately 50 kPa (56%) of the maximal 90 kPa vacuum pressure by drawing the first 7 mL of a 60-mL syringe. However, drawing a further 13 mL to achieve 75 kPa and drawing the whole 60-mL syringe for a maximal vacuum pressure of 90 kPa are disproportionately more difficult. Hence, manual feedback when drawing the syringe may give a disproportionate impression of effective flow. Also, maintaining a specific pressure gradient without a pressure gauge is challenging. Furthermore, switching from one syringe to another results in a temporary flow arrest during mechanical thrombectomy.

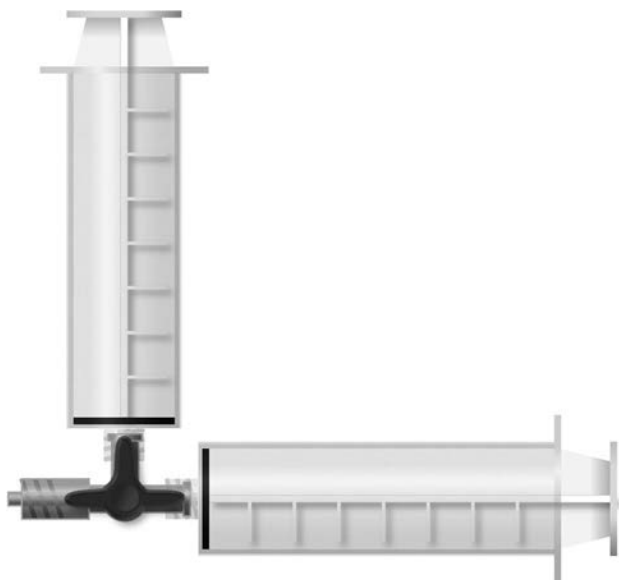


FIG 3. Syringe setup. To avoid flow arrest when switching from one syringe to another, one should connect 2 syringes in parallel to double aspiration volume and thus aspiration time. The 3-way valve, which is in a locked position, is then connected to the hemostatic Y-adapter of the respective aspiration catheter. Before the thrombectomy maneuver starts, the syringes are fully drawn and locked to generate vacuum pressure, while the 3-way valve is still in a locked position. When the thrombectomy maneuver starts, the 3-way valve is set to be open for both syringes at the same time, thereby doubling aspiration volume and thus aspiration time.

Thus, for the sake of simplicity and safety of flow control, we advocate drawing and locking the syringes for aspiration. To avoid flow arrest when switching from one syringe to another, 2 syringes should be connected in parallel and drawn and locked before the thrombectomy maneuver to comfortably double aspiration volume and thus aspiration time (Fig 3). Attention should be paid to drawing the syringes immediately before the thrombectomy maneuver because we found, for our setup, a pressure loss of approximately 10 kPa every 91 seconds or 6.6 kPa per minute on average because the syringes and the valves are not perfectly sealed.

Penumbra Pump

To our surprise, the Penumbra pump achieved a rather low flow through an 8F long sheath or an 8F balloon-guide catheter and is therefore very unlikely to reverse blood flow in the ICA (On-line Table and Fig 1). This low flow is due to the high resistance of the tubing, which has a narrowing at the connection site and at the on/off switch, which are considerably smaller than the diameter of an 8F catheter. The pump is dedicated for use with distal aspiration catheters; nonetheless, many interventionalists use it for aspiration in the ICA, a practice that is not only discouraged by the manufacturer but is also futile according to our experiments. Also, even with the newest generation of distal aspiration catheters (ACE 64), the Penumbra pump barely achieves flow that can reverse blood flow in the MCA. Thus, the pump with its current tubing should not be used for flow control but rather for techniques in which the force at the catheter tip, not the flow, is essential (for example, ADAPT).¹²

Medela Pump

The Medela pump achieved high flow that surpassed blood flow in the ICA with an 8F sheath and an 8F balloon-guide catheter. With the newest generation of distal access catheters (ACE 64), aspiration flow was high enough to surpass blood flow in the MCA, even with a stent retriever in the catheter, which reduces flow by approximately 15%.⁵ Because high flow may cause vessel collapse, attention should be paid during aspiration.

Limitations

The major limitation of our study is the lack of experiments with blood and the limited number of investigated catheters. However, we deliberately chose to conduct a concise study, which captures the essential issues while keeping our results as simple and valid as possible, especially because data in the literature suggest that the viscosity of blood is altered contingently by the necessary anticoagulants.¹⁰ We did not aspirate the water-glycerol solution in a model with tubes that match the diameters of the actual target vessels. Because the vessel diameter has an impact on possible flow volume, we chose to conduct our experiments with a reservoir to reduce the number of possible confounding factors. Hence, our results represent flow rates under ideal conditions; actual flow rates, in particular flow rates in small vessels such the M1 segment of the MCA of a patient, are likely to be even smaller.

CONCLUSIONS

Aspiration with syringes or pumps can be used to generate a pressure gradient with the following results: 1) a force at the catheter tip, thereby establishing contact between the catheter and the clot (ADAPT, SAVE, and ARTS technique, and so forth), or 2) backward flow to prevent clot embolization. The force at the catheter tip depends only on the catheter diameter and the applied pressure and is therefore not altered by resistors. The flow, however, is highly influenced by additional resistors. The ideal aspiration system generates a high and constant pressure gradient and has minimal resistance. The 60-mL VacLok vacuum pressure syringe and the Medela pump achieved constant and high flows that are likely to be sufficient to reverse blood flow during thrombectomy with an 8F sheath or balloon-guide catheter in the ICA and modern distal aspiration catheters in the MCA. The Penumbra pump is dedicated for use with distal aspiration catheters and should not be used with its current tubing for flow control in the ICA and MCA without proximal balloon protection.

ACKNOWLEDGMENTS






The authors thank Arash Nikoubashman for revising the manuscript.

Disclosures: Carolin Brockmann—UNRELATED: Employment: University Hospital Mainz, Germany. Martin Wiesmann—UNRELATED: Consultancy: Stryker; Payment for Lectures Including Service on Speakers Bureaus: Bracco, Medtronic, Siemens, Stryker; Payment for Development of Educational Presentations: Abbott, ab medica, Acandis, Bayer, Bracco, Braun, Codman, Medtronic, Dahlhausen, MicroVention, Penumbra, phenox, Philips Healthcare, Siemens, Silk Road, St. Jude, Stryker*; Support for Travel to Meetings for the Study or Other Purposes: Stryker, Comment: The study was funded by internal funds and we did not receive any support by Stryker. *Money paid to the institution.

REFERENCES

1. Goyal M, Menon BK, van Zwam WH, et al; HERMES collaborators. **Endovascular thrombectomy after large-vessel ischaemic stroke: a meta-analysis of individual patient data from five randomised trials.** *Lancet* 2016;387:1723–31 [CrossRef Medline](#)
2. Chueh JY, Puri AS, Wakhloo AK, et al. **Risk of distal embolization with stent retriever thrombectomy and ADAPT.** *J Neurointerv Surg* 2016;8:197–202 [CrossRef Medline](#)
3. Maus V, Behme D, Kabbasch C, et al. **Maximizing first-pass complete reperfusion with SAVE.** *Clin Neuroradiol* 2017 Feb 13. [Epub ahead of print] [CrossRef Medline](#)
4. Wiesmann M, Brockmann MA, Heringer S, et al. **Active push deployment technique improves stent/vessel-wall interaction in endovascular treatment of acute stroke with stent retrievers.** *J Neurointerv Surg* 2017;9:253–56 [CrossRef Medline](#)
5. Nikoubashman O, Alt JP, Nikoubashman A, et al. **Optimizing endovascular stroke treatment: removing the microcatheter before clot retrieval with stent-retrievers increases aspiration flow.** *J Neurointerv Surg* 2017;9:459–62 [CrossRef Medline](#)
6. Massari F, Henninger N, Lozano JD, et al. **ARTS (Aspiration-Retriever Technique for Stroke): initial clinical experience.** *Interv Neuroradiol* 2016;22:325–32 [CrossRef Medline](#)
7. Chueh JY, Kuhn AL, Puri AS, et al. **Reduction in distal emboli with proximal flow control during mechanical thrombectomy: a quantitative in vitro study.** *Stroke* 2013;44:1396–401 [CrossRef Medline](#)
8. Jouvent E, Poupon C, Gray F, et al. **Intracortical infarcts in small vessel disease: a combined 7-T postmortem MRI and neuropathological case study in cerebral autosomal-dominant arteriopathy with subcortical infarcts and leukoencephalopathy.** *Stroke* 2011;42:e27–30 [CrossRef Medline](#)
9. Shih AY, Blinder P, Tsai PS, et al. **The smallest stroke: occlusion of one penetrating vessel leads to infarction and a cognitive deficit.** *Nat Neurosci* 2013;16:55–63 [CrossRef Medline](#)
10. Mayer GA, Kiss O. **Blood viscosity and in vitro anticoagulants.** *Am J Physiol* 1965;208:795–97 [Medline](#)
11. Hu YC, Stiefel MF. **Force and aspiration analysis of the ADAPT technique in acute ischemic stroke treatment.** *J Neurointerv Surg* 2016;8:244–46 [CrossRef Medline](#)
12. Nikoubashman O, Nikoubashman A, Büsen M, et al. **Necessary catheter diameters for mechanical thrombectomy with ADAPT.** *AJNR Am J Neuroradiol* 2017;38:2277–81 [CrossRef Medline](#)
13. Stock KW, Wetzel SG, Lyrer PA, et al. **Quantification of blood flow in the middle cerebral artery with phase-contrast MR imaging.** *Eur Radiol* 2000;10:1795–800 [CrossRef Medline](#)
14. Schöning M, Walter J, Scheel P. **Estimation of cerebral blood flow through color duplex sonography of the carotid and vertebral arteries in healthy adults.** *Stroke* 1994;25:17–22 [CrossRef Medline](#)

Aneurysmal Parent Artery–Specific Inflow Conditions for Complete and Incomplete Circle of Willis Configurations

 B.M.W. Cornelissen,  J.J. Schneiders,  M.E. Sprengers,  R. van den Berg,  P. van Ooij,  A.J. Nederveen,  E. van Bavel,  W.P. Vandertop,  C.H. Slump,  H.A. Marquering, and  C.B.L.M. Majoie



ABSTRACT

BACKGROUND AND PURPOSE: Hemodynamics are thought to play a role in intracranial aneurysm growth and rupture. Computational fluid dynamics is frequently performed to assess intra-aneurysmal hemodynamics, using generalized flow waveforms of healthy volunteers as inflow boundary conditions. The purpose of this study was to assess differences in inflow conditions for different aneurysmal parent artery locations and variations of circle of Willis configurations.

MATERIALS AND METHODS: In a series of 96 patients with 103 aneurysms, velocity measurements were acquired using 2D phase-contrast MR imaging perpendicular to the aneurysmal parent arteries in the circle of Willis. Circle of Willis configurations were inspected for variations using multiple overlapping thin-slab-acquisition MRAs. Flow rates, velocity magnitudes, and pulsatility indices were calculated for each parent artery location in subgroups of complete and incomplete circle of Willis configurations.

RESULTS: Flow rates, velocity magnitudes, and pulsatility indices were significantly different among aneurysmal parent arteries. Incomplete circle of Willis configurations were observed in 24% of the cases. Significantly lower basilar artery flow rates were observed in configurations with hypoplastic PI segments. Significantly higher A1 flow rates were observed in configurations with a hypoplastic contralateral A1 segment.

CONCLUSIONS: Inflow conditions vary substantially between aneurysmal parent arteries and circle of Willis configurations. We have created a collection of parent artery–specific inflow conditions tailored to the patient-specific circle of Willis configuration that can be used in future computational fluid dynamics studies analyzing intra-aneurysmal hemodynamics.

ABBREVIATIONS: ACA = anterior cerebral artery; AcomA = anterior communicating artery; BA = basilar artery; CoW = circle of Willis; PC-MR = phase-contrast MR imaging; PcomA = posterior communicating artery; PI = pulsatility index; VA = vertebral artery

The incidence of an unruptured intracranial aneurysm in the general population is approximately 3%.¹ Most of these aneurysms are asymptomatic, and 50%–80% of all aneurysms do not rupture during the individual's lifetime.² However, rupture results in subarachnoid hemorrhage, a devastating occurrence associated with high morbidity and fatality rates.² In clinical prac-

tice, large size (≥ 7 mm) and high-risk location (posterior circulation and communicating arteries) are most frequently used to identify aneurysms with a high risk of rupture.³ However, most aneurysms are < 7 mm, and a proportion of these small aneurysms rupture, nevertheless.⁴ Therefore, many studies have been performed to identify additional risk factors for rupture to improve the management of unruptured intracranial aneurysms.

Besides morphologic parameters, intra-aneurysmal hemodynamics are thought to play a role in aneurysm formation, growth, and rupture. Therefore, hemodynamics are frequently assessed to search for differences between ruptured and unruptured aneurysms.^{5,6} To analyze hemodynamic properties, computational fluid dynamics are commonly used to simulate the blood flow in patient-specific aneurysm models. Computational fluid dynamics depend highly on boundary conditions such as geometry and inflow waveforms.^{7–9} Therefore, high-resolution 3D angiographic imaging and


Received October 23, 2017; accepted after revision January 31, 2018.

From the Departments of Radiology and Nuclear Medicine (B.M.W.C., J.J.S., M.E.S., R.v.d.B., P.v.O., A.J.N., H.A.M., C.B.L.M.M.), Biomedical Engineering and Physics (B.M.W.C., E.v.B., H.A.M.), and Neurosurgery (W.P.V.), Academic Medical Center, Amsterdam, the Netherlands; MIRA Institute for Biomedical Technology and Technical Medicine (B.M.W.C., C.H.S.), University of Twente, Enschede, the Netherlands; and Department of Radiology (J.J.S.), Erasmus MC University Medical Center, Rotterdam, the Netherlands.

Henk A. Maquering and Charles B.L.M. Majoie contributed equally to this work.

This work was supported by a grant from the Stichting Toegepast Wetenschappelijk Instituut voor Neuromodulatie (TWIN), the Netherlands. The HEROICA study was supported by a grant from the Nuts-OHRA Foundation, the Netherlands.

Please address correspondence to Bart Cornelissen, Meibergdreef 9, 1105 AZ, Department of Biomedical Engineering and Physics, Academic Medical Center, Amsterdam, the Netherlands; e-mail: b.m.cornelissen@amc.nl

 Indicates article with supplemental on-line table.

<http://dx.doi.org/10.3174/ajnr.A5602>

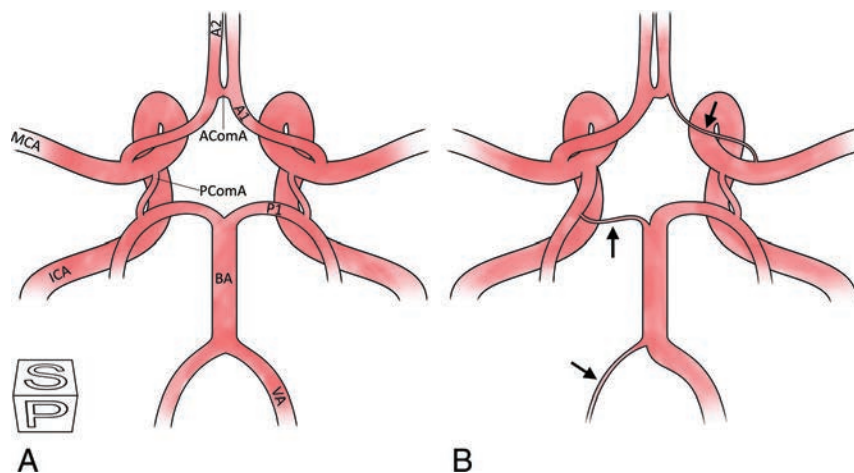


FIG 1. Schematic overview of 2 different CoW configurations. A, Textbook-type. B, Variant-type with hypoplastic VA, P1, and A1 segments, see arrows. VA and A1 segments with diameters $\leq 50\%$ compared with the contralateral side and P1 segments $< \text{PcomA}$ were defined as hypoplastic.

patient-specific data of inflow velocities are needed. Because patient-specific velocity waveforms are rarely available, generalized velocity waveforms of healthy subjects are frequently used.^{10,11} However, intracranial flow velocities vary widely among subjects.^{12,13} A previous study showed that generalized waveforms result in different hemodynamic characteristics, compared with patient-specific velocity waveforms.¹⁴ A similar heterogeneity in flow patterns is expected among variations in location and configuration of the circle of Willis (CoW).¹⁵ This variety of aneurysmal inflow conditions in different aneurysmal parent arteries, considering anatomic variations in the CoW, is insufficiently studied. In this study, we present location-specific aneurysmal inflow waveforms for arteries in the CoW and determine the influence of CoW variations on local flow conditions.

MATERIALS AND METHODS

Patient Selection

All patients treated in the Academic Medical Center Amsterdam for a ruptured or unruptured aneurysm from January 2009 to October 2011 were invited to participate in the Hemodynamics for Rupture Risk Assessment of Intracranial Aneurysms (HEROICA) study.¹⁶ The HEROICA study assessed the additional value of hemodynamics in discriminating ruptured and unruptured aneurysms and was approved by the institutional review board. Written informed consent was obtained from all patients. To assess the variation of inflow in these aneurysms, we included all patients with sufficient quality phase-contrast MR imaging (PC-MR) in the HEROICA dataset.

MR Imaging

MR imaging was performed at 3T (Intera; Philips Healthcare, Best, the Netherlands). 2D PC-MR imaging was performed for velocity measurements perpendicular to the aneurysmal parent arteries. These included the basilar artery (BA), vertebral artery (VA), internal carotid artery, middle cerebral artery, and the A1 and A2 segments of the anterior cerebral artery (ACA). Heart rate monitoring was performed by electrocardiography or by a peripheral pulse unit and was used for cardiac triggering and heart rate calculations. PC-MR imaging resolution was $0.63 \times 0.63 \times 3$ mm. Velocity-encoding was 70–100 cm/s. Velocity measurements were acquired in 23–36 uniformly

spaced cardiac phases. PC-MR imaging was performed before treatment for patients with unruptured aneurysms or at 6-month follow-up after endovascular treatment for cases with acutely ruptured aneurysms. A routine multiple overlapping thin-slab-acquisition MRA sequence with a scan resolution of $0.4 \times 0.4 \times 0.5$ mm was performed to visualize the aneurysm and was used to assess CoW configurations.

Assessment of CoW Configurations

Absence or hypoplasia of arterial components in the CoW was assessed by an experienced neuroradiologist (M.E.S.), using axial reconstructions and volume-renderings of the multiple overlapping thin-slab-acquisition MRA data. A1 and

VA hypoplasia were defined as diameters of $\leq 50\%$ compared with the contralateral side.^{17,18} Hypoplasia of the P1 segment of the posterior cerebral artery was defined as a diameter smaller than that of the feeding posterior communicating artery (PcomA).^{19,20} Hypoplasia of the PcomA and anterior communicating artery (AcomA) was defined as diameters of ≤ 0.8 mm.²¹ A textbook-type CoW configuration and a variant-type CoW configuration with anatomic variations of the VA, P1, and A1 are schematically presented in Fig 1.

CoW configurations were dichotomized into perianeurysmal complete and incomplete groups. Configurations were considered incomplete in case the vascular morphology near the aneurysm presented anatomic variants that were expected to alter local flow rates. For ICA and MCA parent artery locations, configurations with hypoplastic ipsilateral P1 and/or contralateral A1 segments were considered incomplete. For A1 measurement cases, configurations with hypoplastic ipsi- or contralateral A1 segments were considered incomplete. For A2 parent artery locations, azygos ACA or ACA trifurcation configurations were considered incomplete. For the VA, configurations with hypoplastic ipsi- or contralateral VA segments were considered incomplete. For BA cases, 1- or 2-sided hypoplastic P1 segments were considered incomplete configurations.

Flow Parameters

To define the inflow region of the parent artery, we extracted a contour for each cardiac phase using a level-set evolution algorithm²² in the PC-MR magnitude images. Due to arterial pulsatility, the inflow region could have varied between cardiac phases. Spatial-averaged velocity waveforms were calculated for every patient by dividing the sum of the velocity magnitudes in each cardiac phase by the time-averaged inflow area. Flow waveforms were calculated by multiplying the sum of through-slice velocity components by the area of the inflow region for each cardiac phase. High-frequency components in the flow and velocity waveforms were considered noise and therefore suppressed using an eighth-order low-pass Butterworth filter²³ with a half-power frequency of 0.32 Hz. Using the flow- and velocity-waveforms, we

calculated temporally averaged flow rates and mean velocity magnitudes. In addition, the pulsatility index (PI) was calculated to quantify the pulsatile character of the flow waveforms. The PI was defined as the ratio of flow variation to the average flow during a cardiac cycle (Fig 2).²⁴ Parent artery-specific flow parameters were calculated for subgroups with perianeurysmal complete and incomplete CoW configurations.

Location-Representative Waveforms

Eleven features were automatically extracted for each waveform (Fig 2). The waveform was characterized by the diastolic minimum (M) and peak systole (P).²⁵ Additional systolic features were extracted for 25%, 50%, and 75% of the amplitude (S_1 , S_2 , S_3). Diastolic features were extracted for 75% of the amplitude after systole (D_1), half-maximum after systole (H), and 4 uniformly in time-spaced features between H and the end of the cardiac cycle

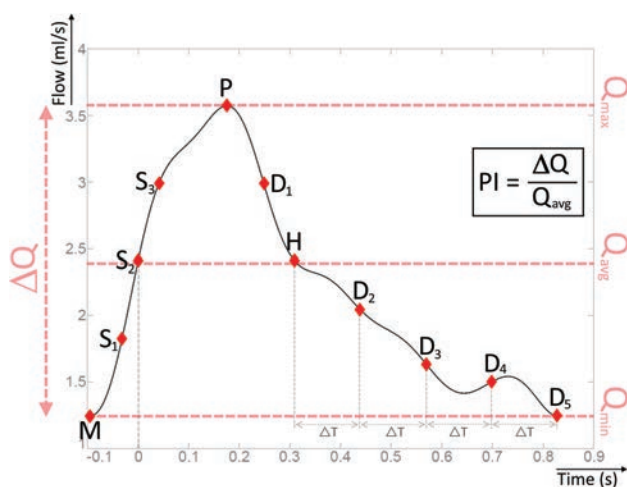


FIG 2. Automatic extraction of 11 waveform features and the PI. M: diastolic minimum. S_1 – S_3 : 25, 50, and 75% of the amplitude before peak systole. P: peak systole. D_1 : 75% of the amplitude after peak systole. H: half-maximum after systole. D_2 – D_5 : late diastolic features, equally spaced in time (ΔT). Feature S_2 was set to time = 0s.

Table 1: Prevalence of anatomic variants in the CoW

CoW Configuration (n = 96)	Absent/Hypoplastic Vascular Components	%
Textbook type	None	10
Variant anatomy	PcomA	73
	AcomA	25
	P1	24
	VA	21
	A1	16
	P1, VA, and/or A1 combined	46

Table 2: Prevalence of perianeurysmal incomplete CoW configurations for each aneurysmal parent artery location

PC-MR Measurement Location (Aneurysm Location)	Incomplete Configuration	No.
ICA (ICA/PcomA)	Hypoplastic ipsilateral P1 and/or contralateral A1	7/30 (23%)
MCA	Hypoplastic ipsilateral P1 and/or contralateral A1	6/30 (20%)
A1 (AcomA)	Hypoplastic contralateral A1	7/28 (25%)
A2 (pericallosal artery)	Azygos ACA	1/4 (25%)
VA	Hypoplastic ipsilateral VA	1/2 (50%)
BA	Hypoplastic P1 (1- or 2-sided)	3/9 (33%)
Total		25/103 (24%)

(D_2 – D_5). Feature S_2 was set to time = 0 seconds. Median feature points were calculated by taking the median flow amplitude at the median time point in the cardiac cycle. Similarly, the interquartile range (IQR) was calculated for each feature point. Location-representative waveforms were generated by cubic spline interpolation of the median feature points for aneurysmal parent arteries in complete and incomplete configurations. The slopes of the first and last feature points were set to zero.

Statistical Analysis

The Kruskal-Wallis test was performed to determine whether flow parameters were different between aneurysmal parent arteries. Subsequently, the Tukey honestly significant difference was performed to analyze differences between combinations of groups. Mann-Whitney U tests were used to assess whether parent artery-specific flow parameters were different between complete and incomplete CoW configurations. In addition, mean velocity magnitudes and PIs were compared between anterior and posterior parent arteries. P values < .05 indicated statistically significant differences.

RESULTS

A total of 96 patients (62 women) with 103 aneurysms (61 ruptured) were included in this study. The median patient age was 53 years (range, 27–76 years). Heart rates ranged between 51 and 109 beats per minute, with a mean of 69 ± 10 beats per minute. The prevalence of anatomic variants in the CoW is shown in Table 1. Only 10% of the patients had a textbook-type CoW configuration, and almost half of the CoW configurations presented with hypoplastic VA, A1, and/or P1 segments.

Table 2 shows the prevalence of perianeurysmal incomplete CoW configurations for each aneurysmal parent artery location. Configurations were incomplete in 24% of the cases. Figure 3 presents boxplots for aneurysmal parent artery-specific flow rates in complete and incomplete CoW configurations. Table 3 shows flow and velocity measures for aneurysmal parent arteries in complete and incomplete configurations. The Location-representative flow and velocity waveforms are shown in Figs 4 and 5, respectively, for aneurysmal parent arteries in perianeurysmal complete and incomplete CoW configurations. Group median (IQR) feature points are shown in the On-line Table.

Flow rates, velocity magnitudes, and PIs were significantly different among parent artery locations: $P < .001$, $P = .008$, and $P = .041$, respectively. VA flow rates were significantly lower compared with ICA flow rates. Furthermore, significantly lower mean velocity magnitudes were observed for the VA arteries

compared with the MCA arteries. No statistically significant differences in PIs were found in pair-wise comparisons among parent artery locations.

BA flow rates were significantly lower for subgroups with 1 or 2 hypoplastic P1 segments. Significantly higher A1 flow rates were observed in configurations with a hypoplastic contralateral A1 segment.

Cases of aneurysmal parent arteries in the posterior circulation showed sig-

nificantly higher PIs ($P = .017$) and lower mean velocity magnitudes ($P = .034$) compared with parent arteries in the anterior circulation.

DISCUSSION

Our study presents location-specific flow rates and velocity magnitudes and shows significant differences among aneurysmal parent artery locations in the CoW. Hypoplastic VA, A1, or P1 segments were observed in almost half of our population. Higher flow rates were observed in A1 segments with an absent or hypoplastic contralateral A1, and lower flow rates for BAs with hypoplastic P1 segments.

Intracranial flow rates have been assessed in several previous PC-MR studies^{26,27} with relatively small study populations of

healthy subjects. In these studies, flow rates were comparable with our findings; however, no information regarding anatomic variations in the CoW configurations was provided in these studies. Other studies investigated relationships between anatomic variations in the CoW and neurovascular diseases; however, no relations with aneurysmal inflow were assessed. The prevalence of VA, A1, and P1 hypoplasia in our study was similar to that reported previously.^{18,19,28} The cerebral blood flow distribution in different configurations of the CoW was assessed previously.²⁹ In this study, decreased BA flow rates were observed in fetal-type posterior cerebral artery configurations, and increased ICA flow rates, in the ipsilateral fetal-type posterior cerebral artery and missing contralateral A1 configurations. Our study also showed significantly lower BA flow rates in hypoplastic P1 configurations, and a trend toward

higher ICA flow rates in ipsilateral hypoplastic P1s and hypoplastic contralateral A1 configurations was seen. The relation between the CoW configuration and flow rates of the ICA and BA has also been studied in healthy volunteers; this study showed similar findings.¹⁵ However, A1 and P1 hypoplasia was only observed in 5% of the study population.

It has been shown that inflow variations of <25% have little effect on flow characteristics in computational fluid dynamics simulations.³⁰ Our study presents larger velocity and flow variations among parent artery locations and CoW configurations. Furthermore, in accordance with previously reported data,³¹ the interpatient variability of peak systolic flow measures was >25%. This finding suggests that those parameters should be taken into account in computational fluid dynamics calculations.³²

Our study has several limitations. The limited imaging resolution of the PC-MR image resulted in partial volume artifacts, which might have led to inaccurate delineations of inflow regions, resulting in inaccurate velocity magnitude calculations.

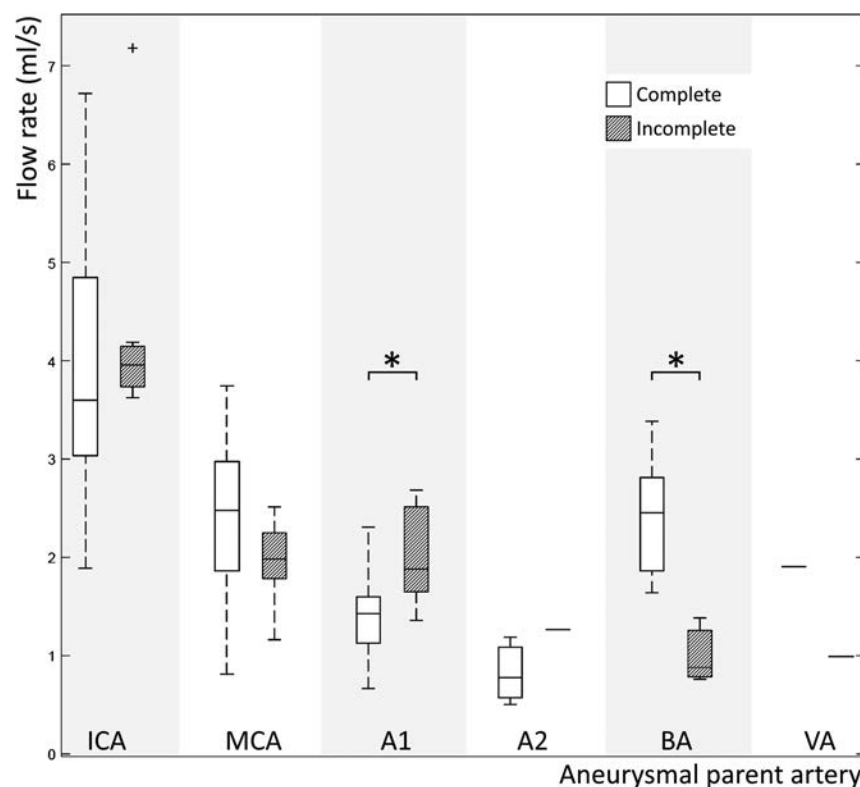


FIG 3. Boxplots for aneurysmal parent artery-specific flow rates in complete (left) and incomplete (right) CoW configurations. The asterisk indicates a statistically significant difference ($P < .05$).

Table 3: Mean velocity magnitudes, flow rates, and PIs for aneurysmal parent arteries in complete and incomplete CoW configurations

Aneurysmal Parent Artery	Perianeurysmal CoW Configuration	Flow Rate (mL/s) (Median) (IQR)	P Value	Mean Velocity Magnitude (cm/s) (Median) (IQR)	P Value	PI (Median) (IQR)	P Value
ICA	Complete	3.60 (3.03–4.84)	.16	36.3 (29.8–46.2)	1.00	0.91 (0.75–1.12)	.49
	Incomplete	3.96 (3.74–4.15)		36.4 (32.7–39.1)		0.98 (0.87–1.18)	
MCA	Complete	2.48 (1.86–2.97)	.15	44.6 (35.4–49.5)	.19	0.80 (0.66–0.94)	.42
	Incomplete	1.98 (1.78–2.25)		38.7 (34.2–42.2)		0.95 (0.74–0.97)	
A1	Complete	1.42 (1.12–1.60)	.01 ^a	34.2 (29.5–38.7)	.52	0.78 (0.69–1.06)	.49
	Incomplete	1.88 (1.65–2.51)		37.9 (29.5–45.3)		0.75 (0.63–0.83)	
A2	Complete	0.78 (0.57–1.08)	.50	21.4 (19.1–33.5)	1.00	0.63 (0.52–0.99)	.50
	Incomplete	1.26		35.2		1.13	
VA	Complete	1.90	1.00	19.1	1.00	1.11	1.00
	Incomplete	0.99		16.5		1.20	
BA	Complete	2.45 (1.87–2.81)	.02 ^a	36.0 (31.3–42.8)	.17	1.00 (0.86–1.06)	.71
	Incomplete	0.88 (0.78–1.26)		25.9 (21.6–30.5)		1.05 (0.98–1.19)	

^a Indicates a statistically significant difference ($P < .05$).

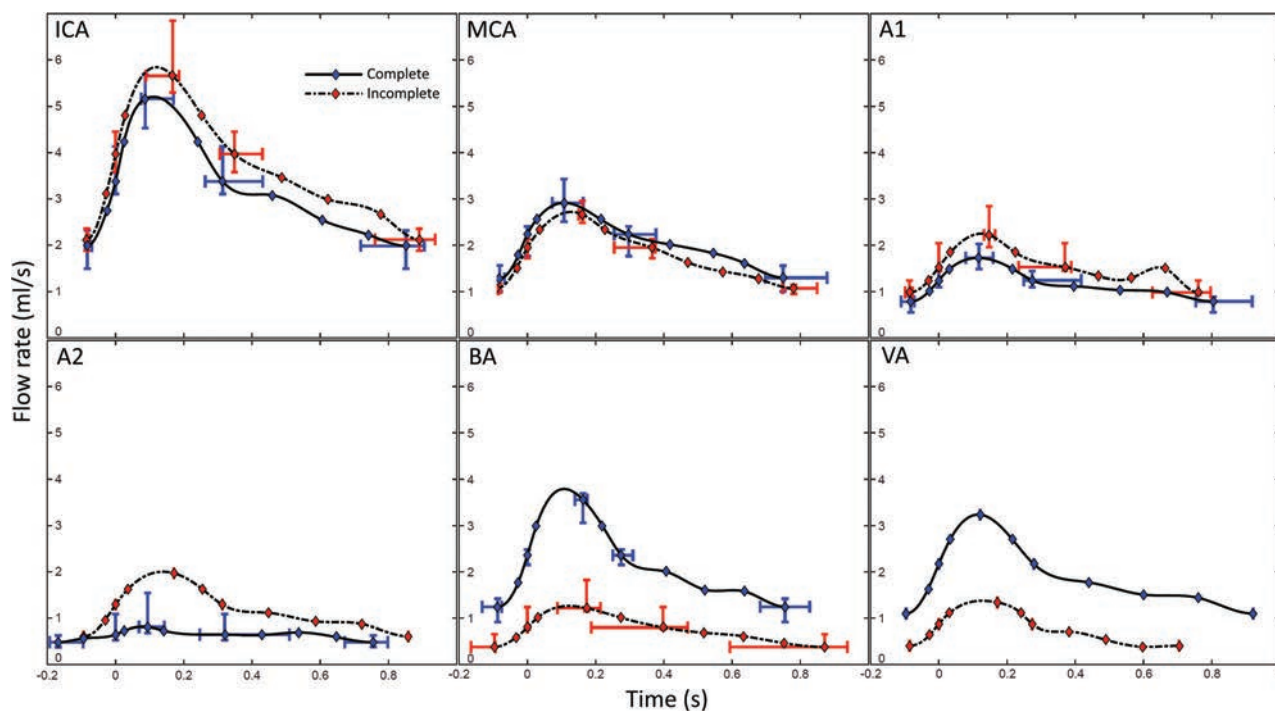


FIG 4. Location-representative flow waveforms for aneurysmal parent arteries in perianeurysmal complete (blue) and incomplete (red, *dashed*) CoW configurations. Interquartile ranges are presented for feature points M, S_2 , P, H, and D_6 .

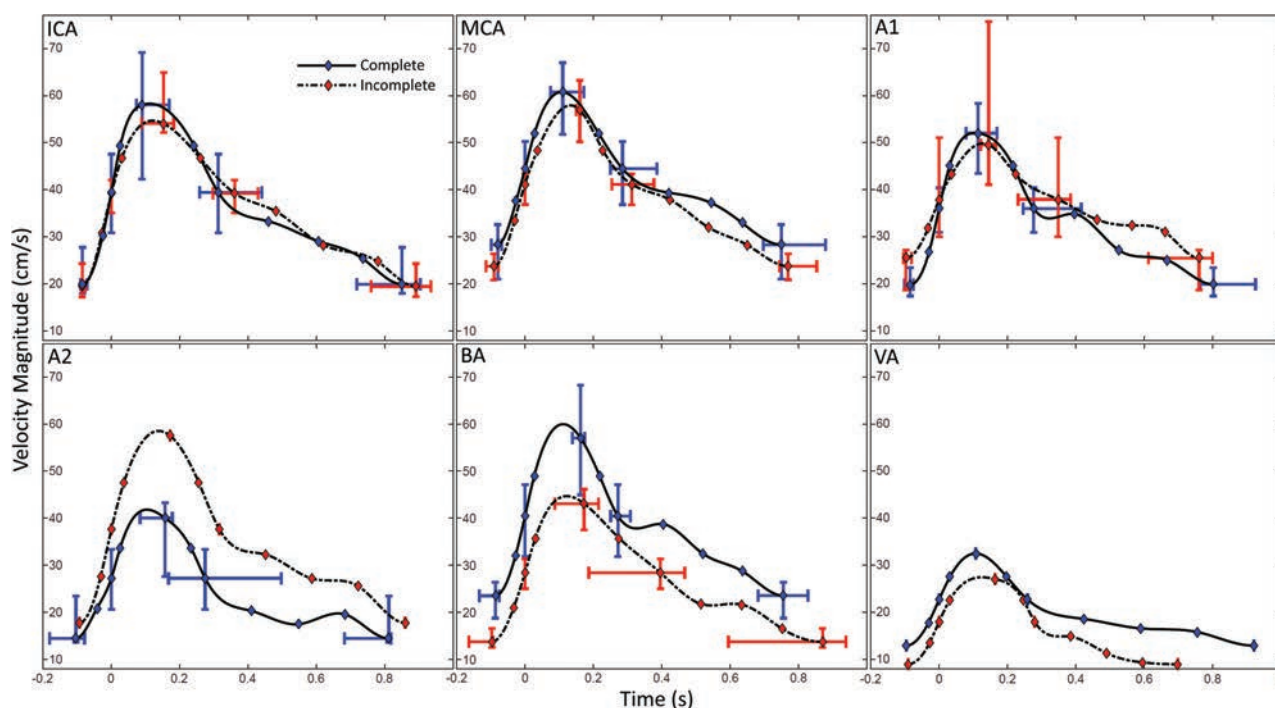


FIG 5. Location-representative velocity waveforms for aneurysmal parent arteries in perianeurysmal complete (blue) and incomplete (red, *dashed*) CoW configurations. Interquartile ranges are presented for feature points M, S_2 , P, H, and D_6 .

We used time-averaged cross-sectional areas of the PC-MRA imaging to calculate temporal velocity profiles, which might not agree with the areas of the 3D rotational angiography-derived vascular models used for computational fluid dynamics because of differences in imaging and segmentation methods. Furthermore, differences in velocity-encoding might have influenced the results, and the quality requirements for the PC-MR imaging might have resulted in a selec-

tion bias. Another limitation of our study was the relatively small sample size. For VA and A2 cases, large differences in flow rates were observed between complete and incomplete configurations, but due to the small sample size, we could not determine whether this was a systematic deviation. Furthermore, low TOF intensities hindered the assessment of hypoplastic segments in some cases due to slow flow or coil artifacts. In addition, CoW assessment was performed by 1 ob-

server only, and comparison with previous results from the literature was hampered by the use of different definitions for hypoplasia of vascular segments.

CONCLUSIONS

There is variation in aneurysmal inflow conditions among parent arteries and CoW configurations. When patient-specific inflow waveforms are not available, we recommend using parent artery-specific flow waveforms, tailored to the patient-specific CoW configuration to improve the accuracy of intra-aneurysmal hemodynamic simulations. We have made a collection available of flow and velocity waveforms that can be used in future computational fluid dynamics studies.

Disclosures: René van den Berg—UNRELATED: Consultancy: Codman Depuy Neurovascular, Comments: coil development,* Henk A. Marquering—OTHER RELATIONSHIPS: cofounder and shareholder of Nico-lab. Charles B.L.M. Majoie—RELATED: Grant: TWIN Foundation*; UNRELATED: Grants/Grants Pending: Dutch Heart Foundation, Stryker.* *Money paid to the institution.

REFERENCES

1. Vlak MH, Algra A, Brandenburg R, et al. **Prevalence of unruptured intracranial aneurysms, with emphasis on sex, age, comorbidity, country, and time period: a systematic review and meta-analysis.** *Lancet Neurol* 2011;10:626–36 [CrossRef Medline](#)
2. Brisman JL, Song JK, Newell DW. **Cerebral aneurysms.** *N Engl J Med* 2006;355:928–39 [CrossRef Medline](#)
3. Wiebers DO, Whisnant JP, Huston J 3rd, et al; International Study of Unruptured Intracranial Aneurysms Investigators. **Unruptured intracranial aneurysms: natural history, clinical outcome, and risks of surgical and endovascular treatment.** *Lancet* 2003;362:103–10 [CrossRef Medline](#)
4. Morita A, Kirino T, Hashi K, et al; UCAS Japan Investigators. **The natural course of unruptured cerebral aneurysms in a Japanese cohort.** *N Engl J Med* 2012;366:2474–82 [CrossRef Medline](#)
5. Xiang J, Natarajan SK, Tremmel M, et al. **Hemodynamic-morphologic discriminants for intracranial aneurysm rupture.** *Stroke* 2011;42:144–52 [CrossRef Medline](#)
6. Chien A, Sayre J. **Morphologic and hemodynamic risk factors in ruptured aneurysms imaged before and after rupture.** *AJNR Am J Neuroradiol* 2014;35:2130–35 [CrossRef Medline](#)
7. Valen-Sendstad K, Steinman DA. **Mind the gap: impact of computational fluid dynamics solution strategy on prediction of intracranial aneurysm hemodynamics and rupture status indicators.** *AJNR Am J Neuroradiol* 2014;35:536–43 [CrossRef Medline](#)
8. Castro MA, Putman CM, Cebal JR. **Computational fluid dynamics modeling of intracranial aneurysms: effects of parent artery segmentation on intra-aneurysmal hemodynamics.** *AJNR Am J Neuroradiol* 2006;27:1703–09 [Medline](#)
9. Venugopal P, Valentino D, Schmitt H, et al. **Sensitivity of patient-specific numerical simulation of cerebral aneurysm hemodynamics to inflow boundary conditions.** *J Neurosurg* 2007;106:1051–60 [CrossRef Medline](#)
10. Cebal JR, Castro MA, Soto O, et al. **Blood-flow models of the circle of Willis from magnetic resonance data.** *J Eng Math* 2003;47:369–86 [CrossRef](#)
11. Steinman DA, Milner JS, Norley CJ, et al. **Image-based computational simulation of flow dynamics in a giant intracranial aneurysm.** *AJNR Am J Neuroradiol* 2003;24:559–66 [Medline](#)
12. Stock KW, Wetzel SG, Lyrer PA, et al. **Quantification of blood flow in the middle cerebral artery with phase-contrast MR imaging.** *Eur Radiol* 2000;10:1795–800 [CrossRef Medline](#)
13. Oktar SO, Yücel C, Karaosmanoglu D, et al. **Blood-flow volume quantification in internal carotid and vertebral arteries: comparison of 3 different ultrasound techniques with phase-contrast MR imaging.** *AJNR Am J Neuroradiol* 2006;27:363–69 [Medline](#)
14. Jansen IG, Schneiders JJ, Potters WV, et al. **Generalized versus patient-specific inflow boundary conditions in computational fluid dynamics simulations of cerebral aneurysmal hemodynamics.** *AJNR Am J Neuroradiol* 2014;35:1543–48 [CrossRef Medline](#)
15. Tanaka H, Fujita N, Enoki T, et al. **Relationship between variations in the circle of Willis and flow rates in internal carotid and basilar arteries determined by means of magnetic resonance imaging with semiautomated lumen segmentation: reference data from 125 healthy volunteers.** *AJNR Am J Neuroradiol* 2006;27:1770–75 [Medline](#)
16. Schneiders JJ, Marquering HA, van Ooij P, et al. **Additional value of intra-aneurysmal hemodynamics in discriminating ruptured versus unruptured intracranial aneurysms.** *AJNR Am J Neuroradiol* 2015;36:1920–26 [CrossRef Medline](#)
17. Kwak R, Niizuma H, Suzuki J. **Hemodynamics in the anterior part of the circle of Willis in patients with intracranial aneurysms: a study by cerebral angiography.** *Tohoku J Exp Med* 1980;69–73 [Medline](#)
18. Rinaldo L, McCutcheon BA, Murphy ME, et al. **Relationship of A1 segment hypoplasia to anterior communicating artery aneurysm morphology and risk factors for aneurysm formation.** *J Neurosurg* 2017;127:89–95 [CrossRef Medline](#)
19. van Raamt AF, Mali WP, van Laar PJ, et al. **The fetal variant of the circle of Willis and its influence on the cerebral collateral circulation.** *Cerebrovasc Dis* 2006;22:217–24 [CrossRef Medline](#)
20. De Monyé C, Dippel DW, Siepmann TA, et al. **Is a fetal origin of the posterior cerebral artery a risk factor for TIA or ischemic stroke? A study with 16-multidetector-row CT angiography.** *J Neurol* 2008;255:239–45 [CrossRef Medline](#)
21. Krabbe-Hartkamp MJ, van der Grond J, de Leeuw FE, et al. **Circle of Willis: morphologic variation on three-dimensional time-of-flight MR angiograms.** *Radiology* 1998;207:103–11 [CrossRef Medline](#)
22. Chunming L, Chenyang X, Changfeng G, et al. **Level set evolution without re-initialization: a new variational formulation.** *Proceedings of the 2005 Institute of Electrical and Electronics Engineers Computer Society Conference on Computer Vision and Pattern Recognition*, San Diego, California. June 20–26, 2005;1:430–36
23. Lieber BB, Stancampiano AP, Wakhloo AK. **Alteration of hemodynamics in aneurysm models by stenting: influence of stent porosity.** *Ann Biomed Eng* 1997;25:460–69 [CrossRef Medline](#)
24. Patti J, Viñuela F, Chien A. **Distinct trends of pulsatility found at the necks of ruptured and unruptured aneurysms.** *J Neurointerv Surg* 2014;6:103–07 [CrossRef Medline](#)
25. Ford MD, Alperin N, Lee SH, et al. **Characterization of volumetric flow rate waveforms in the normal internal carotid and vertebral arteries.** *Physiol Meas* 2005;26:477–88 [CrossRef Medline](#)
26. Cebal JR, Castro MA, Putman CM, et al. **Flow-area relationship in internal carotid and vertebral arteries.** *Physiol Meas* 2008;29:585–94 [CrossRef Medline](#)
27. Wählin A, Ambarki K, Birgander R, et al. **Measuring pulsatile flow in cerebral arteries using 4D phase-contrast MR imaging.** *AJNR Am J Neuroradiol* 2013;34:1740–45 [CrossRef Medline](#)
28. Thierfelder KM, Baumann AB, Sommer WH, et al. **Vertebral artery hypoplasia: frequency and effect on cerebellar blood flow characteristics.** *Stroke* 2014;45:1363–68 [CrossRef Medline](#)
29. Hendrikse J, van Raamt AF, van der Graaf Y, et al. **Distribution of cerebral blood flow in the circle of Willis.** *Radiology* 2005;235:184–89 [CrossRef Medline](#)
30. Cebal JR, Hernandez M, Frangi A, et al. **Subject-specific modeling of intracranial aneurysms.** In: *Proceedings of the Annual Meeting of the International Society for Optics and Photonics Symposium on Electronic Imaging*, San Diego, California. February 14–19, 2004;5369:319–27 [CrossRef](#)
31. Schneiders JJ, Ferns SP, van Ooij P, et al. **Comparison of phase-contrast MR imaging and endovascular sonography for intracranial blood flow velocity measurements.** *AJNR Am J Neuroradiol* 2012;33:1786–90 [CrossRef Medline](#)
32. Xiang J, Siddiqui AH, Meng H. **The effect of inlet waveforms on computational hemodynamics of patient-specific intracranial aneurysms.** *J Biomech* 2014;47:3882–90 [CrossRef Medline](#)

3D Deep Learning Angiography (3D-DLA) from C-arm Conebeam CT

J.C. Montoya, Y. Li, C. Strother, and G.-H. Chen



ABSTRACT

BACKGROUND AND PURPOSE: Deep learning is a branch of artificial intelligence that has demonstrated unprecedented performance in many medical imaging applications. Our purpose was to develop a deep learning angiography method to generate 3D cerebral angiograms from a single contrast-enhanced C-arm conebeam CT acquisition in order to reduce image artifacts and radiation dose.

MATERIALS AND METHODS: A set of 105 3D rotational angiography examinations were randomly selected from an internal data base. All were acquired using a clinical system in conjunction with a standard injection protocol. More than 150 million labeled voxels from 35 subjects were used for training. A deep convolutional neural network was trained to classify each image voxel into 3 tissue types (vasculature, bone, and soft tissue). The trained deep learning angiography model was then applied for tissue classification into a validation cohort of 8 subjects and a final testing cohort of the remaining 62 subjects. The final vasculature tissue class was used to generate the 3D deep learning angiography images. To quantify the generalization error of the trained model, we calculated the accuracy, sensitivity, precision, and Dice similarity coefficients for vasculature classification in relevant anatomy. The 3D deep learning angiography and clinical 3D rotational angiography images were subjected to a qualitative assessment for the presence of intersweep motion artifacts.

RESULTS: Vasculature classification accuracy and 95% CI in the testing dataset were 98.7% (98.3%–99.1%). No residual signal from osseous structures was observed for any 3D deep learning angiography testing cases except for small regions in the otic capsule and nasal cavity compared with 37% (23/62) of the 3D rotational angiographies.

CONCLUSIONS: Deep learning angiography accurately recreated the vascular anatomy of the 3D rotational angiography reconstructions without a mask. Deep learning angiography reduced misregistration artifacts induced by intersweep motion, and it reduced radiation exposure required to obtain clinically useful 3D rotational angiography.

ABBREVIATIONS: CNN = convolutional neural network; 3DRA = 3D rotational angiography; DLA = deep learning angiography; GPU = graphics processing unit

Cerebrovascular diseases are common causes of morbidity and mortality in the adult population worldwide.^{1–3} Most cerebrovascular diseases are found during routine brain imaging with CT or MR imaging; however, 2D-DSA remains the criterion standard for their accurate angiographic evaluation and characterization, in particular for arteriovenous malformations,⁴ cerebral aneurysms,^{5,6} and dural arteriovenous fistulas.⁷ Additional 3D

rotational angiography (3DRA) is used to improve the visualization and spatial understanding of vascular structures during the diagnostic work-up of these conditions. Currently, with many angiographic systems, obtaining a 3DRA still requires 2 rotational acquisitions, one without injection of contrast (mask run) and one during injection of contrast (fill run). These 2 datasets are used to compute log-subtracted projections, which are then used to reconstruct a subtracted 3DRA volume.^{8,9}

Machine learning is a discipline within computer science, closely related to statistics and mathematic optimization, that aims to learn patterns directly from a large set of examples that demonstrate a desired outcome or behavior without the need of explicit instructions.¹⁰ In the context of medical imaging, machine learning methods have been investigated since the early 1990s, initially for computer-aided detection and diagnosis in mammography and pulmonary embolism^{11–14}; however, recent advances in deep learning¹⁵ (ie, a specific machine-learning tech-

Received September 1, 2017; accepted after revision January 26, 2018.

From the Departments of Medical Physics (J.C.M., Y.L., G.-H.C.) and Radiology (C.S., G.-H.C.), University of Wisconsin School of Medicine and Public Health, Madison, Wisconsin.

The work was partially supported by a National Institutes of Health grant U01EB021183.

Please address correspondence to Guang-Hong Chen, PhD, L1167, WIMR, 1111 Highland Ave, Madison, WI 53705; e-mail: gchen7@wisc.edu

Indicates open access to non-subscribers at www.ajnr.org

<http://dx.doi.org/10.3174/ajnr.A5597>

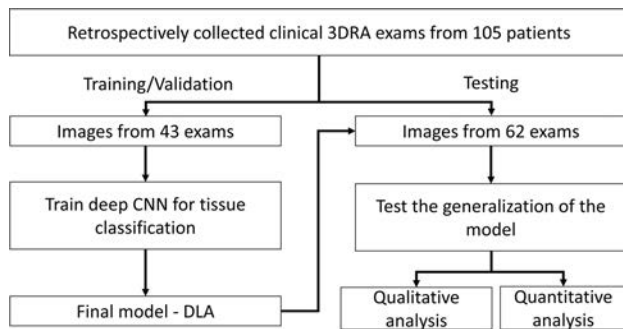


FIG 1. Overall study schema.

nique) have demonstrated unprecedented performance in many applications, including detection of diabetic retinopathy¹⁶ and breast cancer,^{17,18} quantitative analysis of brain tumors in MR imaging,^{19,20} computer-aided detection of cerebral aneurysms in MR angiography,²¹ and computer-aided detection and classification of thoracic diseases.^{22,23}

With recent advances in deep learning and the universal approximation properties of feedforward neural networks,^{24,25} it is hypothesized that a deep neural network is capable of computing cerebral angiograms with only the vascular information contained in the fill scan of a 3DRA examination acquired with a C-arm conebeam CT system. Potential benefits of eliminating the mask scan include the following: 1) reduction of intersweep patient motion artifacts caused by the misregistration of the mask and fill scans, and 2) radiation dose reduction by at least a factor of 2.

The purpose of this work was to develop and test the capability of a deep learning angiography (DLA) method based on convolutional neural networks (CNNs) to generate subtracted 3D cerebral angiograms from a single contrast-enhanced examination without the need for a mask acquisition.

MATERIALS AND METHODS

In the following sections, the patient inclusion criteria and image-acquisition protocols are first presented, followed by a description of the datasets and methods used to train the DLA model. Finally, the image analysis and statistical analysis are described. The overall study schema is shown in Fig 1.

Patient Cohort

All studies were Health Insurance Portability and Accountability Act-compliant and performed under an institutional review board-approved protocol. Clinically indicated rotational angiography examinations for the assessment of cerebrovascular abnormalities of 105 patients, scanned from August 2014 through April 2016, were retrospectively collected. Cases were selected in a random fashion to reduce the potential bias in patient selection. It was thought that the randomized selection during this period would result in a dataset that was representative of the varieties of conditions that are referred for angiographic studies.

Imaging Acquisition and Reconstruction

All subjects were imaged with a standard 3DRA data acquisition protocol using a C-arm conebeam CT system (Axiom Artis zee; Siemens, Erlangen, Germany). The protocol consists of 2

conebeam CT acquisitions (ie, mask and fill acquisitions) with 172 or 304 projection images for a 6- or 13-second rotation time, respectively. Angular coverage for all data acquisitions was 260°, with a tube potential of 70 kVp, detector dose per projection image equal to 0.36 μ Gy per frame, and angular increments of 1.52° or 0.85° per frame. Iodinated contrast medium was injected into the proximal internal carotid artery or vertebral artery just after the initiation of the fill acquisition. For each subject, “native fill” and subtracted 3D volumes were reconstructed using the vendor’s proprietary software (InSpace Reconstruction, syngo Workplace; Siemens). All reconstructions were performed using the standard filtered back-projection with edge enhancement, normal image characteristic, full FOV ($238 \times 238 \text{ mm}^2$) with a 512×512 image matrix, and 0.46-mm image thickness/increment for a 0.46-mm isotropic voxel size. The effective dose for the acquisition protocols used in this study was 1.1 mSv for the 6-second rotation acquisition and 1.8 mSv for 13-second rotation acquisition, which is similar to the dose level reported by others.^{26,27}

Training Dataset

A training dataset consisting of 13,790 axial images from 35 patients with >150 million labeled voxels was generated using the information from both the conebeam CT image of the fill scan and the subtracted images from the subtracted conebeam projection data. For each patient in the training dataset, vasculature extraction was performed by a manual thresholding of the subtracted images. The selection of the threshold was based on the subjective assessment of complete vasculature segmentation while excluding image artifacts and background noise, with threshold values typically in the range of 500–700 HU. Large vessels, specifically the internal carotid artery, middle cerebral artery, anterior cerebral artery, distal branches of the middle cerebral artery and anterior cerebral artery, vertebral artery, and posterior cerebral artery were isolated through 3D connected component analysis.²⁸ Small regions not connected to a large vessel were assumed to be image artifacts and were excluded from the final vasculature volume. After the previous steps, in the event of remaining intersweep patient motion and streak artifacts, the vasculature volume was subjected to manual artifact removal.

The extraction of bone tissue was performed by subtracting the vasculature volume from the contrast-enhanced images (ie, fill scan) and performing manual thresholding and connectivity analysis (like that of vasculature extraction) in the resulting images. Only connected regions including the skull and mandible were considered bone. The remaining streaking artifacts and metal implants in the bone volume were manually removed. Finally, the soft-tissue class was extracted by thresholding the fill images with thresholds of -400 to 500 HU and applying a morphologic erosion.

The procedure described above generates approximately 0.28 million, 6 million, and 15 million voxels of vasculature, bone, and soft tissue, respectively, for each patient. To mitigate the class imbalance (ie, different number of labeled voxels per tissue class) and reduce redundant training data by a similarity of adjacent voxels, we included only 4.3 million labeled voxels per patient for training, consisting of all vasculature voxels and an equal number

of randomly extracted bone and soft-tissue voxels (ie, random undersampling).²⁹

Validation and Testing Datasets

A validation dataset and a testing dataset were created using the remaining image volumes from 70 subjects divided into 8 examinations for the validation dataset and 62 examinations for the testing dataset. These datasets were created with the same procedure used to generate the training dataset; however, the tissue labels were constrained to a region only containing the following anatomy: ICA, middle cerebral artery, anterior cerebral artery, distal branches of the middle cerebral artery and anterior cerebral artery, vertebral artery, posterior cerebral artery, the base and anterior aspect of the skull, temporal bone, otic capsule, and surrounding soft tissue as opposed to the entire head in the training dataset. Each examination in the validation and testing dataset had approximately the same number of labeled voxels for each tissue class.

Neural Network Architecture and Implementation

A 30-layer CNN³⁰ with a ResNet architecture,^{31,32} as shown in Fig 2, was used. All convolutional layers except the input layer used 3×3 filters with rectified linear units for activation function. The input of the network was a $41 \times 41 \times 5$ volumetric image patch extracted from the contrast-enhanced image volume; the network output consisted of a 3-way fully connected layer with softmax activation. Training and inference were performed on a voxelwise basis, in which the input volumetric image patch was labeled with the tissue class of its central voxel. The DLA model was implemented using Tensorflow (Google, Mountain View, California). Network parameters were initialized using the variance scaling method³³ and trained from scratch using a synchronous stochastic gradient descent method with a batch size of 512 volumetric image patches using 2 GTX 1080 Ti (NVIDIA, Santa Clara, California) graphics processing units (GPUs) (256 image patches per GPU). The time required to process 1 case in this study varied from 1 to 3 minutes, depending on the size of the image volume.

Each tissue class had equal probability of being included in a single batch (ie, data resampling), to account for class imbalance.²⁹ The learning rate was initially set to 1×10^{-3} with a momentum of 0.9. The learning rate was reduced to 1×10^{-4} and 1×10^{-5} after 1 and 1.5 epochs, respectively. The validation dataset was used only to monitor the convergence and generalization error during model training. Early stopping was used when the validation error reached a plateau at 2×10^5 iterations.

Statistical Analysis

The trained DLA model was applied for the task of tissue classification in the validation and testing cohorts, consisting of image volumes from 8 and 62 subjects, respectively. The final vasculature tissue class was used to generate the 3D-DLA images. To quantify the generalization error of the trained model, we evaluated the vasculature classification for each labeled voxel in the reference standard for the validation and testing datasets. Two-by-two tables were generated for each patient, and accuracy, sen-

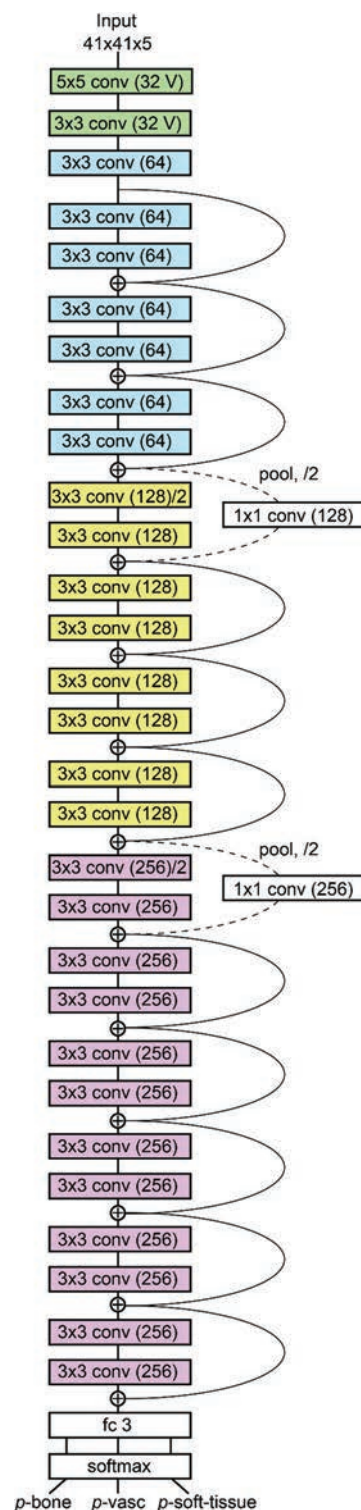


FIG 2. Neural network architecture.

sitivity (also known as recall), positive predictive value (also known as precision), and Dice similarity coefficients were calculated. The 95% CIs for each performance metric were also reported. Finally, the clinical 3DRA and the 3D-DLA images were subjected to a qualitative assessment for the presence of intersweep motion artifacts, and results were expressed as frequencies and percentages.

Summary of performance metrics for vascular classification in the training, validation, and testing datasets

Dataset	Sensitivity (Recall)		PPV (Precision)		DSC (FI Score)		Accuracy	
	TP		TP		2TP		TP + TN	
	TP + FN		TP + FP		2TP + FP + FN		TP + TN + FP + FN	
	Mean	95% CI	Mean	95% CI	Mean	95% CI	Mean	95% CI
Validation ($n = 8$)	97.8%	(96.9%–98.7%)	97.2%	(96.4%–98.1%)	97.5%	(97.0%–98.0%)	98.4%	(98.0%–98.7%)
Testing ($n = 62$)	97.6%	(96.5%–98.6%)	98.5%	(97.6%–99.3%)	98.0%	(97.4%–98.7%)	98.7%	(98.3%–99.1%)

Note:—TP indicates true-positive; FN, false-negative; PPV, positive predictive value; FP, false-positive; TN, true-negative; FI, Dice similarity coefficients.

RESULTS

Contrast-enhanced image volumes from 105 subjects (53.3 ± 13.5 years of age) who underwent clinically indicated rotational angiography examinations for the assessment of cerebrovascular abnormalities were used in the study. Contrast medium was injected via the proximal ICA in 89 patients (85%) and via the vertebral artery in 16 patients (15%). Average and 95% CIs for vasculature classification accuracy, sensitivity, positive predictive value, and Dice similarity coefficient in the testing dataset were 98.7% (95% CI, 98.3%–99.1%), 97.6% (95% CI, 96.5%–98.6%), 98.5% (95% CI, 97.6%–99.3%), and 98.0% (95% CI, 97.4%–98.7%), respectively. The Table summarizes the performance metrics for vascular classification in the training, validation, and testing datasets.

No residual signal from osseous structures was observed for any testing cases generated using 3D-DLA except for small regions in the otic capsule and nasal cavity compared with 37% (23/62) of the 3DRA cases that presented residual bone artifacts. Figure 3 shows a comparison of MIP images derived from 3DRA and the 3D-DLA datasets of a patient evaluated for posterior cerebral circulation. One can see how residual bone artifacts induced by intersweep patient motion are greatly reduced in 3D-DLA, improving the conspicuity of small vessels. Similarly, Fig 4 shows lateral and oblique MIP images derived from 3DRA and the 3D-DLA datasets of a patient evaluated for anterior cerebral circulation. Results show reduced residual bone artifacts for 3D-DLA images, in particular for the anterior aspect of the skull and the temporal bone. Figure 5 shows a comparison of volume-rendering images for both the clinical 3DRA and the 3D-DLA of a patient with a small aneurysm in the anterior communicating artery and a large aneurysm in the middle cerebral artery bifurcation.

DISCUSSION

In this work, a deep CNN was used to learn generic opacified vasculature from contrast-enhanced C-arm conebeam CT datasets to generate a 3D cerebral angiogram, without an explicit definition of cerebrovascular diseases or specific vascular anatomy. The datasets used for model training, validation, and testing were created by applying simple image-processing techniques with minimum manual editing for a total of 82,740 subtracted and contrast-enhanced conebeam CT images from 105 subjects. The proposed DLA method was used to improve image quality by reducing image artifacts caused by misregistration of mask and fill scans in 3DRA, in addition to enabling potential radiation dose reduction.

Many angiographic systems require 2 rotational acquisitions (mask and fill) for reconstruction of a subtracted 3DRA. Others, using vascular segmentation and thresholding algorithms, allow a

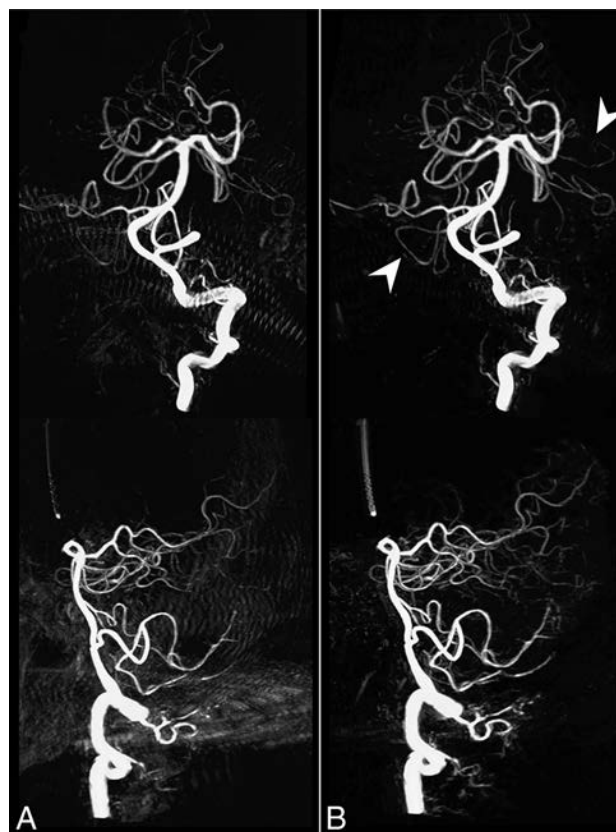


FIG 3. Comparison of anterior and lateral views of MIP images derived from 3DRA (A) and 3D-DLA (B) datasets of a patient evaluated for posterior cerebral circulation. Residual bone artifacts induced by intersweep patient motion are greatly reduced in 3D-DLA, improving the conspicuity of small vessels as indicated by the white arrowheads.

3D vessel reconstruction without the availability of a mask. Those that require 2 rotations are susceptible to artifacts caused by potential misregistrations of the mask and fill projections. Those that require the use of segmentation and thresholding algorithms may be subject to errors related to too little contrast intensity and/or improper segmentation. Together, these techniques remain the standard of care for the diagnosis and treatment planning of cerebrovascular diseases. Misregistration artifacts arise in conventional 3DRA imaging primarily due to the following: 1) small variations in the angular range differences occurring from one rotational acquisition to another, and 2) potential patient motion in both mask and fill runs. The mask-free DLA method, by eliminating the need for one of the rotational acquisitions, in theory, would reduce the chance of motion from both mechanical instability and patient motion and effectively reduce the radiation

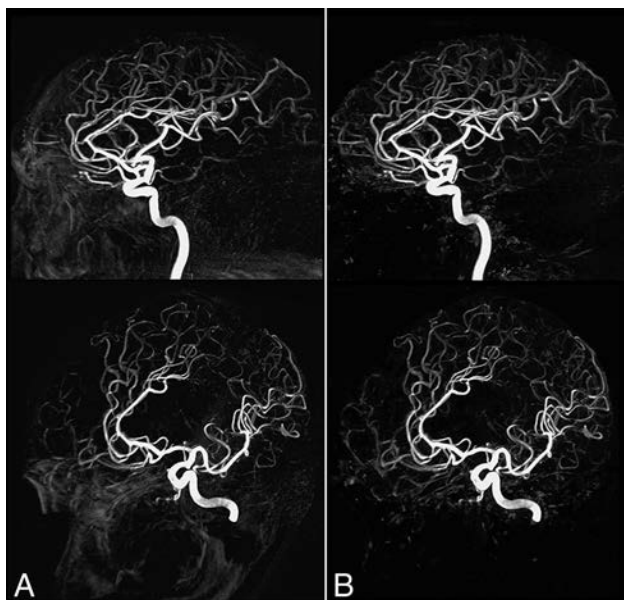


FIG 4. Comparison of lateral and oblique MIP images derived from 3DRA (A) and 3D-DLA (B) datasets of a patient evaluated for anterior cerebral circulation. Results show reduced residual bone artifacts for 3D-DLA images, in particular for the anterior aspect of the skull and the temporal bone.

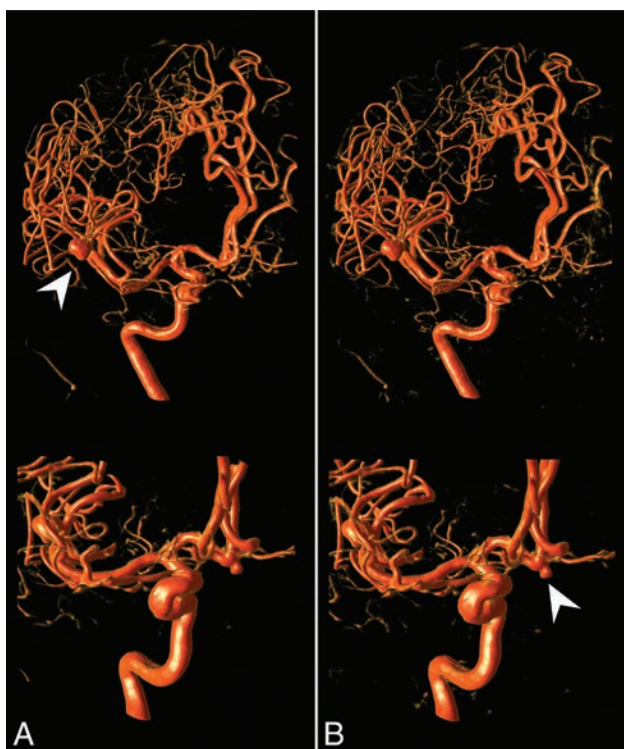


FIG 5. Comparison of volume-rendering images for both the clinical 3DRA (A) and the 3D-DLA (B) of a patient with a small aneurysm in the anterior communicating artery and a large aneurysm in the middle cerebral artery bifurcation as indicated by the *arrowheads*.

dose required to obtain a 3DRA by half in those systems that require 2 rotations.

In the context of medical imaging, machine-learning methods have been investigated since early 1990s^{11–14}; however, the recent unprecedented performance of deep learning has made major

advances in solving very difficult problems in science that were thought to be intractable when approached by other means.^{34,35} In addition to clever mathematical techniques and the availability of large annotated datasets, many authors recognize that the massively parallel computing capabilities of GPUs have played a key role in the success of deep learning applications, providing accelerations of 40× to 250× compared with multicore and single-core CPUs.^{10,15} For example, the training procedure of the network used in this study took approximately 23 hours. This training procedure could have taken 4–5 weeks if only a multicore CPU computation architecture was used, making this application impractical. Fortunately, the training procedure is performed off-line, it only needs to be done once, and GPU computing is already widely available within the medical imaging community or accessible via cloud computing services such as the Google Cloud Platform (<https://cloud.google.com/>) or the Amazon Web Service (<https://aws.amazon.com/>). Also, many standard open-source libraries used for deep learning applications are highly optimized to be used in conjunction with GPUs.

Once the parameters of the model have been learned, the process of analyzing new data that were not used for training the model (ie, inference) can be further optimized for production. The method proposed in this study uses a voxelwise training and inference in which the input of the network is a small image region of $41 \times 41 \times 5$ voxels around the voxel of interest. This approach has multiple benefits: 1) Inference can be parallelized; in other words, the classification of multiple voxels can be performed at the same time. Therefore, the time required to analyze a new case is directly proportional to the number of voxels to be classified (eg, the entire head or a targeted ROI) and the number and generation of available GPUs. The throughput of the particular research implementation of the CNN model used in this study is approximately 2500 voxels/s/GPU. 2) This approach results in a large training dataset consisting of 150 million labeled voxels derived from 13,790 axial images and 35 examinations. In addition to a large training dataset, it is important to have a large testing cohort to assure a good model generalization that better reflects how this technique could be used in practice. Having a large testing cohort also helps to determine whether the training dataset is large enough to achieve a desired level of performance.

Although DLA images were successfully created for all validation and testing cases and were subjected to quantitative and qualitative image analysis, this study still has some limitations: First, the use of a very specific image-acquisition protocol and reconstruction with selective intra-arterial contrast media injection into the proximal internal carotid artery or vertebral artery may limit its clinical application. Fine-tuning of the model and clinical validation with prospective reader studies are required to further generalize these results to the vasculature of other organ systems, to complex or uncommon vascular abnormalities, as well as to angiography studies acquired using different image-acquisition protocols and modalities (eg, injection of IV contrast media, time-resolved 3DRA, multidetector CT, and so forth). This kind of prospective reader study would also overcome the limitation of the current qualitative evaluation in our study by a single reader (C.S.).

Second, in this study, a specific type of deep CNN with 30

layers, implemented with a ResNet^{31,32} architecture, was used to demonstrate the DLA application. The selection of the well-known 30-layer ResNet is only because this architecture won an image contest among computer scientists (ie, ILSVRC 2015 classification task; <http://www.image-net.org/challenges/LSVRC/2015/results>); namely, it outperformed other types of networks such as AlexNet, VGGNet, and GoogLeNet, for the task of natural image classification using the ImageNet (<http://image-net.org/>) dataset. This type of network architecture has also outperformed other types of networks in medical imaging classification tasks with deeper models (ie, increased number of layers) having improved classification accuracy.^{20,22,32,36} However, it remains unknown whether other architectures can be used for DLA and what would be the advantage or disadvantage among all these networks. Furthermore, additional optimization and fine-tuning of the DLA model hyperparameters (eg, number of layers, number of hidden units per layer, learning rate, regularization schemes, and so forth) are required for optimal on-line implementation and compatibility with clinical workflow.

Third, even though metallic objects are automatically subtracted in the 3DRA images that were used to create the training dataset, small movements of metallic implants (eg, an aneurysm clip or a coil mass) that occur during a cardiac cycle are, in the case of subtracted images, usually sufficient to create enough misregistration artifacts to allow detection of an implant presence. This situation, in addition to the high x-ray attenuation and proximity to vasculature of metallic implants, could result in their imitation in the final DLA images. The presence of a high-attenuating object (eg, metal or Onyx [Covidien, Irvine, California]) is also known to be an intrinsic limitation of mask-free angiography (vendors who provide a method to obtain 3DRAs without a mask also offer the ability to perform a mask and fill acquisition in situations in which metal objects are known to be present), and its clinical implications need to be addressed with an expert reader study.

CONCLUSIONS

A DLA method based on CNNs that generates 3D cerebral angiograms from a contrast-enhanced C-arm conebeam CT without mask data acquisition was developed. Results indicate that the proposed method can successfully reduce misregistration artifacts induced by intersweep patient motion and, by eliminating the need for a mask acquisition, can reduce the radiation dose in future clinical 3D angiography.

ACKNOWLEDGMENTS

The authors thank Dr John W. Garrett for technical and editorial assistance.

Disclosures: Guang-Hong Chen—RELATED: Grant: National Institutes of Health*; UNRELATED: Grants/Grants Pending: GE Healthcare, Siemens, Hologic, Comments: Principal Investigator of research contracts for unrelated research topics*; *Money paid to the institution.

REFERENCES

- Go AS, Mozaffarian D, Roger VL, et al; American Heart Association Statistics Committee and Stroke Statistics Subcommittee. **Executive summary: heart disease and stroke statistics—2013 update: a report from the American Heart Association.** *Circulation* 2013;127:143–52 CrossRef Medline
- Wiebers DO. **Unruptured intracranial aneurysms: natural history, clinical outcome, and risks of surgical and endovascular treatment.** *Lancet* 2003;362:103–10 CrossRef Medline
- Mohr JP, Parides MK, Stapf C, et al; international ARUBA investigators. **Medical management with or without interventional therapy for unruptured brain arteriovenous malformations (ARUBA): a multicentre, non-blinded, randomised trial.** *Lancet* 2014;383:614–21 CrossRef Medline
- Ogilvy CS, Stieg PE, Awad I, et al; Special Writing Group of the Stroke Council, American Stroke Association. **AHA scientific statement: recommendations for the management of intracranial arteriovenous malformations: a statement for healthcare professionals from a special writing group of the Stroke Council, American Stroke Association.** *Stroke* 2001;32:1458–71 CrossRef Medline
- Hacein-Bey L, Provenzale JM. **Current imaging assessment and treatment of intracranial aneurysms.** *AJR Am J Roentgenol* 2011;196:32–44 CrossRef Medline
- Anxionnat R, Bracard S, Ducrocq X, et al. **Intracranial aneurysms: clinical value of 3D digital subtraction angiography in the therapeutic decision and endovascular treatment.** *Radiology* 2001;218:799–808 CrossRef Medline
- Gandhi D, Chen J, Pearl M, et al. **Intracranial dural arteriovenous fistulas: classification, imaging findings, and treatment.** *AJNR Am J Neuroradiol* 2012;33:1007–13 CrossRef Medline
- Fahrig R, Fox AJ, Lownie S, et al. **Use of a C-arm system to generate true three-dimensional computed rotational angiograms: preliminary in vitro and in vivo results.** *AJNR Am J Neuroradiol* 1997;18:1507–14 Medline
- Strobel N, Meissner O, Boese J, et al. **3D imaging with flat-detector C-arm systems.** In: Reiser MF, Becker CR, Nikolaou K, et al, eds. *Multislice CT*. Berlin: Springer-Verlag; 2009:33–51
- Erickson BJ, Korfiatis P, Akkus Z, et al. **Machine learning for medical imaging.** *Radiographics* 2017;37:505–15 CrossRef Medline
- Chan HP, Lo SC, Sahiner B, et al. **Computer-aided detection of mammographic microcalcifications: pattern recognition with an artificial neural network.** *Med Phys* 1995;22:1555–67 CrossRef Medline
- Wu Y, Doi K, Giger ML, et al. **Computerized detection of clustered microcalcifications in digital mammograms: applications of artificial neural networks.** *Med Phys* 1992;19:555–60 CrossRef Medline
- Zhang W, Doi K, Giger ML, et al. **Computerized detection of clustered microcalcifications in digital mammograms using a shift-invariant artificial neural network.** *Med Phys* 1994;21:517–24 CrossRef Medline
- Wang S, Summers RM. **Machine learning and radiology.** *Med Image Anal* 2012;16:933–51 CrossRef Medline
- LeCun Y, Bengio Y, Hinton G. **Deep learning.** *Nature* 2015;521:436–44 CrossRef Medline
- Gulshan V, Peng L, Coram M, et al. **Development and validation of a deep learning algorithm for detection of diabetic retinopathy in retinal fundus photographs.** *JAMA* 2016;316:2402–10 CrossRef Medline
- Huynh BQ, Li H, Giger ML. **Digital mammographic tumor classification using transfer learning from deep convolutional neural networks.** *J Med Imaging (Bellingham)* 2016;3:034501 CrossRef Medline
- Antropova N, Huynh BQ, Giger ML. **A deep feature fusion methodology for breast cancer diagnosis demonstrated on three imaging modality datasets.** *Med Phys* 2017;44:5162–71 CrossRef Medline
- Akkus Z, Galimzianova A, Hoogi A, et al. **Deep learning for brain MRI segmentation: state of the art and future directions.** *J Dig Imaging* 2017;30:449–59 CrossRef Medline
- Korfiatis P, Kline TL, Lachance DH, et al. **Residual deep convolutional neural network predicts MGMT methylation status.** *J Dig Imaging* 2017;30:622–28 CrossRef Medline
- Nakao T, Hanaoka S, Nomura Y, et al. **Deep neural network-based computer-assisted detection of cerebral aneurysms in MR angiography.** *J Magn Reson Imaging* 2017 Aug 24. [Epub ahead of print] CrossRef Medline

22. Wang X, Peng Y, Lu L, et al. **ChestX-ray8: hospital-scale chest x-ray database and benchmarks on weakly-supervised classification and localization of common thorax diseases.** In: *Proceedings of the 2017 IEEE Conference on Computer Vision and Pattern Recognition (CVPR)*, Honolulu, Hawaii. July 21–26, 2017
23. Lakhani P, Sundaram B. **Deep learning at chest radiography: automated classification of pulmonary tuberculosis by using convolutional neural networks.** *Radiology* 2017;284:574–82 [CrossRef Medline](#)
24. Cybenko G. **Approximation by superpositions of a sigmoidal function.** *Mathematics of Control, Signals and Systems* 1989;2:303–14 [CrossRef](#)
25. Hornik K. **Approximation capabilities of multilayer feedforward networks.** *Neural Networks* 1991;4:251–57 [CrossRef](#)
26. Struffert T, Hauer M, Banckwitz R, et al. **Effective dose to patient measurements in flat-detector and multislice computed tomography: a comparison of applications in neuroradiology.** *Eur Radiol* 2014;24:1257–65 [CrossRef Medline](#)
27. Lang S, Göllitz P, Struffert T, et al. **4D DSA for dynamic visualization of cerebral vasculature: a single-center experience in 26 cases.** *AJNR Am J Neuroradiol* 2017;38:1169–76 [CrossRef Medline](#)
28. Shapiro LG. **Connected component labeling and adjacency graph construction.** *Machine Intelligence and Pattern Recognition* 1996;19:1–30
29. He H, Garcia EA. **Learning from imbalanced data.** *IEEE Transactions on Knowledge and Data Engineering* 2009;21:1263–84
30. LeCun Y, Boser BE, Denker JS, et al. **Handwritten digit recognition with a back-propagation network.** In: David ST, ed. *Advances in Neural Information Processing Systems* 2. San Francisco: Morgan Kaufmann Publishers;1990:396–404
31. He K, Zhang X, Ren S, et al. **Identity mappings in deep residual networks.** In: Leibe B, Matas J, Sebe N, et al, eds. *Proceedings of Computer Vision—ECCV 2016: 14th European Conference*, Amsterdam, the Netherlands. October 1–14, 2016
32. He K, Zhang X, Ren S, et al. **Deep residual learning for image recognition.** In: *Proceedings of the 2016 IEEE Conference on Computer Vision and Pattern Recognition (CVPR)*, Seattle, Washington. June 27–30, 2016:770–78
33. He K, Zhang X, Ren S, et al. **Delving deep into rectifiers: surpassing human-level performance on ImageNet classification.** In: *Proceedings of the 2015 IEEE International Conference on Computer Vision (ICCV)*, Los Alamitos, California. December 7–13, 2015:1026–34
34. Silver D, Huang A, Maddison CJ, et al. **Mastering the game of Go with deep neural networks and tree search.** *Nature* 2016;529:484–89 [CrossRef Medline](#)
35. Silver D, Schrittwieser J, Simonyan K, et al. **Mastering the game of Go without human knowledge.** *Nature* 2017;550:354–59 [CrossRef Medline](#)
36. Shin HC, Roth HR, Gao M, et al. **Deep convolutional neural networks for computer-aided detection: CNN architectures, dataset characteristics and transfer learning.** *IEEE Trans Med Imaging* 2016;35:1285–98 [CrossRef Medline](#)

Evaluation of the Normal Cochlear Second Interscalar Ridge Angle and Depth on 3D T2-Weighted Images: A Tool for the Diagnosis of Scala Communis and Incomplete Partition Type II

T.N. Booth, C. Wick, R. Clarke, J.W. Kutz, M. Medina, D. Gorsage, Y. Xi, and B. Isaacson



ABSTRACT

BACKGROUND AND PURPOSE: Cochlear malformations may be subtle on imaging studies. The purpose of this study was to evaluate the angle and depth of the lateral second interscalar ridge or notch in ears without sensorineural hearing loss (normal ears) and compare them with ears that have a documented incomplete type II partition malformation.

MATERIALS AND METHODS: The second interscalar ridge notch angle and depth were measured on MR imaging in normal ears by a single experienced neuroradiologist. The images of normal and incomplete partition II malformation ears were then randomly mixed for 2 novice evaluators to measure both the second interscalar ridge notch angle and depth in a blinded manner. For the mixed group, interobserver agreement was calculated, normal and abnormal ear measurements were compared, and receiver operating characteristic curves were generated.

RESULTS: The 94 normal ears had a mean second interscalar ridge angle of $80.86^\circ \pm 11.4^\circ$ and depth of 0.54 ± 0.14 mm with the 98th percentile for an angle of 101° and a depth of 0.3 mm. In the mixed group, agreement between the 2 readers was excellent, with significant differences for angle and depth found between normal and incomplete partition type II ears for angle and depth on average ($P < .001$). Receiver operating characteristic cutoffs for delineating normal from abnormal ears were similar for both readers (depth, 0.31/0.34 mm; angle, $114^\circ/104^\circ$).

CONCLUSIONS: A measured angle of $>114^\circ$ and a depth of the second interscalar ridge notch of ≤ 0.31 mm suggest the diagnosis of incomplete partition type II malformation and scala communis. These measurements can be accurately made by novice readers.

ABBREVIATIONS: IP-II = incomplete partition type II; R2 = second interscalar ridge; SNHL = sensorineural hearing loss

Sensorineural hearing loss (SNHL) can occur due to congenital or acquired conditions. Congenital malformations of the cochlea are generally reported with a descriptive classification using the number of turns and do not specifically include some of the subtler cochlear anomalies. One of the most frequently encountered abnormalities in patients with congenital malformations of the inner ear is enlargement of the endolymphatic duct.^{1,2} Enlargement or increased diameter of the en-

dolymphatic duct is commonly associated the cochlear anomalies with a classic association of incomplete partition type II (IP-II) malformation. This cochlear malformation may be difficult to diagnose, and more objective criteria are needed for accurate assessment.

Anatomically, the continuous osseous spiral lamina separates the cochlea into 2 visible perilymph-containing chambers on MR imaging, the scala tympani and scala vestibuli, with the intervening endolymph-containing scala media not currently demonstrable on imaging. Imaging may demonstrate scalar defects and/or scalar asymmetry with enlargement of the scala vestibuli, which may be seen in association with cochlear malformations. While scala communis can be associated with scalar asymmetry, it is a more extensive malformation that results from a defect of the osseous interscalar septum, which separates the cochlear turns. This is a continuous structure that spans the entire length of the cochlea and results in a continuous ridge along the outer margin, separating it into 3 distinct turns, resulting in 3 distinct indentations or ridges along the

Received September 21, 2017; accepted after revision January 12, 2018.

From the Departments of Radiology (T.N.B., R.C., D.G.) and Otolaryngology (C.W., J.W.K., M.M., B.I.), Children's Medical Center of Dallas, University of Texas Southwestern Medical Center, Dallas, Texas; and Department of Radiology (Y.X.), University of Texas Southwestern Medical Center, Dallas, Texas.

Paper previously presented at: Annual Meeting of the American Society of Neuroradiology and the Foundation of the ASNR Symposium, April 22–27, 2017; Long Beach, California.

Please address correspondence to Timothy N. Booth, MD, Department of Radiology, Children's Medical Center of Dallas, 1935 Medical District Dr, Dallas, TX 75235; e-mail: Tim.booth@childrens.com; @tbooth278

<http://dx.doi.org/10.3174/ajnr.A5585>

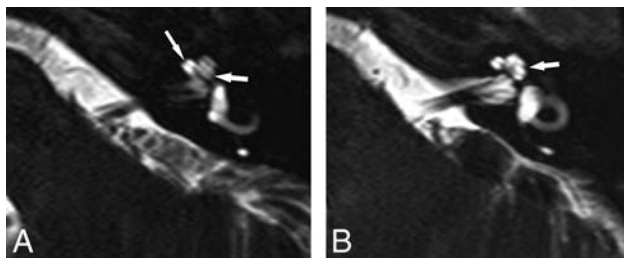


FIG 1. Axial 3D T2-weighted images from inferior to superior showing a normal osseous spiral lamina and interscalar septum. A, A normal osseous spiral lamina separating the scala tympani (posterior) and scala vestibuli (anterior) of the basal (anterior arrow) and middle turns (posterior arrow). B, A normal lateral R2 notch (arrow) associated with the second part of the interscalar septum between the upper basal and upper middle turns of the cochlea.

margins of the cochlea. The second interscalar ridge (R2) or notch, associated with the interscalar septum and located along the lateral margin of the cochlea, is most easily appreciated on imaging (Fig 1).^{3,4}

Scala communis is a common developmental malformation of the cochlea, which manifests as incomplete formation of the distal interscalar septum with resultant incomplete separation of the cochlear turns. This abnormality can be isolated (normal number of cochlear turns) or associated with incomplete partition defects, most commonly type II.^{3,5} The presence of cochlear malformation can result in more intraoperative challenges at the time of and after a cochlear implant operation, with decreased speech perception (outcome) and a risk for a CSF gusher.⁶ A CSF gusher typically occurs secondary to a deficient modiolus and lamina cribrosa, whereas a perilymphatic gusher is usually seen in the presence of an enlarged endolymphatic duct and sac. Appropriate classification of cochlear malformations is important for presurgical planning and in predicting outcomes.⁷ A thorough knowledge of cochlear anatomy and experience in interpreting MR imaging studies is requisite in the diagnosis and classification of inner ear malformations because imaging findings are often subtle.

Using axial 3D T2-weighted MR imaging, one can easily visualize the R2 notch formed by the second portion of the interscalar septum in normal ears; therefore, it is hypothesized that a decrease in depth or increase in the angle of this notch is associated with cochlear scalar malformations. The purpose of this study was to analyze and compare the R2 depth and angle in a group of children with normal hearing (no SNHL) with a subset of patients with ears that have an IP-II malformation. A secondary objective was to determine the feasibility of measuring the R2 angle and depth by comparing the measurements of 2 novice readers.

MATERIALS AND METHODS

This was a retrospective case-control study. The study was approved by the institutional review board and was Health Insurance Portability and Accountability Act-compliant. Axial TSE 3D T2-weighted driven equilibrium MR imaging (TR, 3000 ms; TE, 230 ms; NEX, 1; slice thickness, 1.5 mm at 0.75 mm; matrix, 419 × 364) was performed through the temporal bone as part of a routine cholesteatoma protocol. We retrospectively searched the electronic medical record for this examination code. These patients served as our healthy cohort. Patients were excluded if a 3D

sequence was not present or if the sequence was determined to be of low quality (nonvisualization of the osseous spiral lamina), an audiogram was not available for review, SNHL was present, or the patient was diagnosed with a syndrome known to be associated with SNHL. All audiograms were reviewed by a neurotology fellow (C.W.) for the presence of SNHL defined as a >20-dB mean bone line. Radiology reports and a clinical data base were used to identify patients with an IP-II malformation. The images were reviewed, and the diagnosis was confirmed by an experienced pediatric neuroradiologist and neurotologist (T.N.B., B.I.). If available, genetic results were reviewed for the patients with an IP-II malformation.

In the healthy cohort, the R2 angle and depth measurements were performed using electronic calipers on a PACS station by a pediatric neuroradiologist with 20 years of experience (T.N.B.). The images were magnified 2–3 times to adequately measure the area of interest. A measurement of <0.2 mm was considered zero because electronic calipers would not generate measurement below this value, and the maximum angle was 180°. Additionally, the images from the healthy cohort were evaluated for additional abnormalities of the cochlea, vestibule, and semicircular canals, including visualization of the second portion of the interscalar septum, any partition defects, modiolar deficiency, and scalar asymmetry and/or defects and for the presence or absence of the cochlear nerve. The vestibular labyrinth was evaluated with specific attention to the semicircular canals and the size of the bone island between the vestibule and lateral semicircular canal as well as the size of the endolymphatic duct. An endolymphatic duct midaperture diameter of ≥1 mm was considered abnormal.

A mixed cohort of ears was constructed that included normal ears randomly extracted from the healthy cohort ($n = 23$) and ears with a confirmed IP-II malformation ($n = 17$). The ears were randomly and blindly presented to a pediatric radiology fellow (D.G.) and a third-year otolaryngology resident (M.M.) to measure both the R2 angle and depth. There were a total of 40 ears in the mixed cohort. Three of the IP-II malformation cases were unilateral with normal hearing on the contralateral side. Because readers had limited experience in interpreting MR imaging studies of the temporal bone, they reviewed a reference article³ and completed 5 cases on a normal-hearing ear before measuring the study scans. The blinded readers were told to only evaluate the R2 notch, and cases were presented in 2 sessions with unilateral healthy cases presented to decrease bias.

In the healthy cohort of patients evaluated by the single experienced reader, analysis included determination of the range of measurements of the normal-hearing R2 angle and depth as well as calculating the 98% measurements, upper for angle and lower for depth. Using a mixed cohort of normal-hearing and IP-II malformed ears, we evaluated novice reader agreement by the intraclass correlation coefficient. The average of the 2 readers was used for further analysis. A linear mixed model was used to determine the difference in mean angle and depth between normal and abnormal ears. Interpatient correlation was considered a random effect in the linear model and was subsequently evaluated by the Wald Z-test. A receiver operating characteristic curve was also used to assess the diagnostic performance of angle and depth measurements in detecting abnormalities. The corresponding area under the receiver operating characteristic curve was calculated



FIG 2. Axial 3D T2-weighted image through the cochlea in a normal-hearing ear. A, A normal lateral notch is demonstrated (arrow). B and C, At the same level, angle and depth measurements are demonstrated using electronic calipers (lines). The angle was measured as 84° with a depth of 0.6 mm.

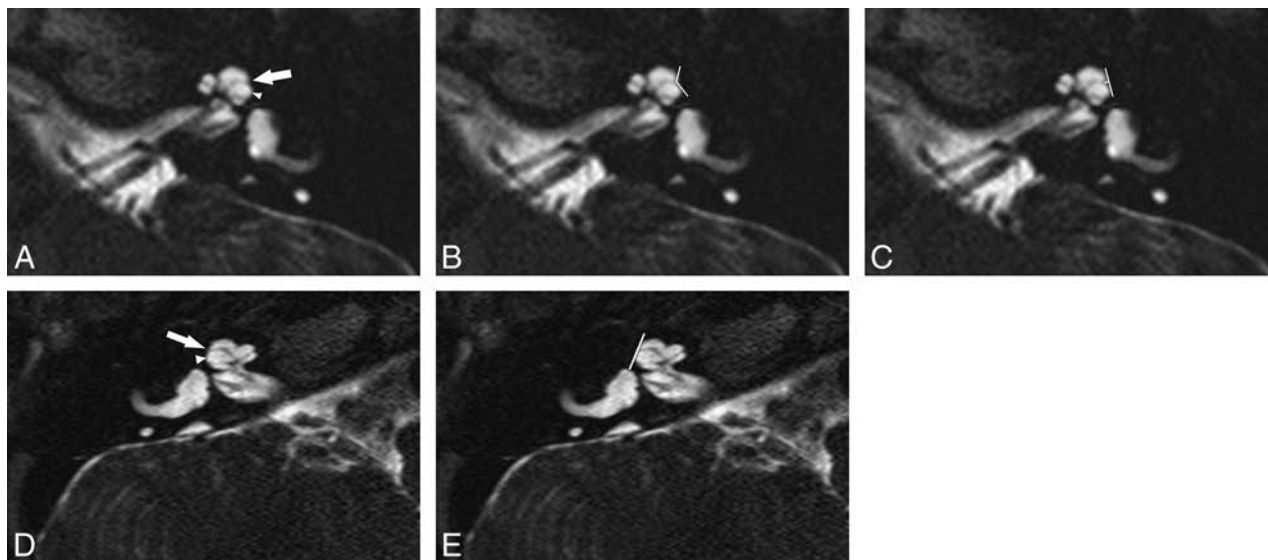


FIG 3. Abnormal R2 notch in 2 different IP-II malformation ears, both with profound SNHL. A–C, A shallow obtuse notch is present (arrow). The scala vestibuli is enlarged (arrowheads) with anterior bowing and high insertion of the second part of the interscalar septum. The measured angle at the same level is 132° (B) with a depth of 0.3 mm (C). D and E, In the other patient, no lateral notch is seen (arrow) and the scala vestibuli is enlarged (arrowhead). At the same level, the angle is 180° and the depth is 0 mm (E).

together with 95% confidence intervals. $P < .05$ was considered statistically significant. The optimal cutoff was determined by the Youden J statistic. The corresponding sensitivity and specificity were also calculated. SAS 9.4 (SAS Institute, Cary, North Carolina) was used for all analyses.

RESULTS

Healthy Cohort

Sixty-nine patients or 138 ears had a 3D T2-weighted MR imaging performed that was considered of good quality. We excluded the following patients: Fourteen patients (28 ears) did not have an audiogram available, and 1 patient (2 ears) had branchio-oto-renal syndrome. After we evaluated the audiogram, 14 ears had SNHL and were excluded, resulting in 94 ears (52 patients) in the healthy cohort. Thirty-four patients were male and 18 were female, with an age at imaging range of 2–17 years (mean, 10.3 years). Most patients were imaged on a 1.5T magnet ($n = 51$).

The 94 normal ears had a mean R2 angle of $80.9^\circ \pm 11.4^\circ$ (range, 57° – 132°) and a depth of 0.54 ± 0.14 mm (range, 0.3–0.9 mm). The 98th percentile angle was 101° with a depth of 0.31 mm (Fig 2). There was no significant difference in any measurement with age ($P = .8$) or sex ($P = .37$). Morphologic analysis of the membranous labyrinth demonstrated a normal cochlea in all nor-

mal ears with normal hearing. The second portion of the interscalar septum was seen in 34 ears (36%). Cochlear nerves were present in all ears. Five ears (5%) showed a diminutive bony island separating the lateral semicircular canal from the vestibule. No patient had a dilated endolymphatic duct.

Mixed Cohort

Seventeen ears with IP-II malformation were confirmed. Seven patients were male, and 3 were female with an age range of 0.8–6 years (mean, 2.9 years) (Fig 3). As per consensus evaluation, a displaced second portion of the interscalar septum was present in 15 ears with associated scalar asymmetry. The second portion of the interscalar septum was not identified in 2 ears. Vestibular abnormalities were present in 8 ears, typically enlargement of the vestibule with diminished size of the bone island in 8 ears and endolymphatic duct enlargement in 12 ears. The bony island was normal and the endolymphatic duct was not enlarged in any of the unilateral IP-II malformation ears ($n = 3$). The cochlear nerve was normal in all ears. Genetic testing was performed in only 2 patients. Connexin was normal in 1 patient, and 1 patient was heterozygous for *SLC26A4* with 2 separate disease-causing mutations.

The mixed group comprising 17 ears with IP-II malformation was combined with 23 ears from the normal-hearing group, in-

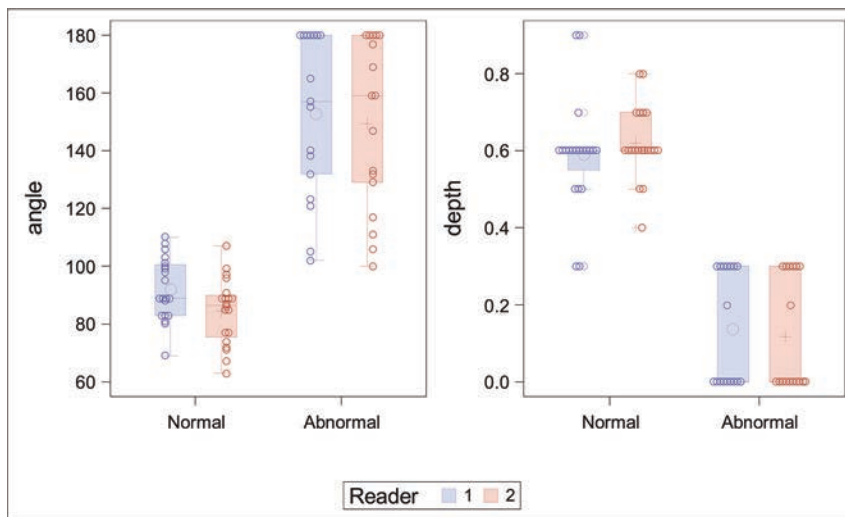


FIG 4. Distribution of measurements of normal and abnormal ears by both novice readers.

ROC analysis for the 2 novice readers

ROC Model	AUC	95% Confidence Interval	Optimal Cutoff	Sensitivity	Specificity
Reader 1					
Angle	0.9676	0.9177–1	114.156	88%	100%
Depth (mm)	0.9588	0.8983–1	0.31294	100%	90%
Reader 2					
Angle	0.9853	0.9593–1	103.874	94%	95%
Depth (mm)	0.9647	0.8953–1	0.33536	100%	95%

Note:—ROC indicates receiver operating characteristic; AUC, area under the curve.

cluding 3 contralateral normal-hearing ears from the patients with unilateral IP-II malformation. The age range was 1–10 years (mean, 5 years), and the sex distribution of 8 males and 5 females of the normal-hearing group was like that in the IP-II group. In this mixed cohort, the agreement between the 2 novice reader measurements was excellent (intraclass correlation coefficient for angle, 0.8; 95% CI, 0.65–0.89; intraclass correlation coefficient for depth, 0.73; 95% CI, 0.54–0.85). Angle was not significantly different either by age ($P = .27$) or sex ($P = .62$). However, younger children had significantly shallower R2 depth ($P = .001$) but not sex ($P = .46$). A significant difference was found between normal-hearing and IP-II malformation ears for angle ($P < .001$) and depth ($P < .001$) (Fig 4). Receiver operating characteristic analysis suggested an excellent area under curve using angle or depth, independent of the observer. Optimal cutoffs for angle and depth were similar between the 2 readers, with high sensitivity and specificity (Table).

DISCUSSION

Inner ear malformations are found in 20% of patients with congenital SNHL.⁸ Cochlear malformations have been subdivided into categories, with cochlear aplasia representing the most severe end of the spectrum and IP-II malformation representing a milder malformation.¹ MR imaging is commonly performed in the evaluation of children with SNHL due to the ability to directly visualize the cochlear nerve.⁹ Appropriate classification of cochlear malformations on MR imaging is clinically important to assess the prognosis for cochlear implantation and for potential complications.⁶

Embryologically, the interscalar septum forms after the formation of the perilymphatic spaces. Membranous bony struts extend toward the modiolus to form the interscalar septum, which separates the turns of the cochlea. The interscalar septum is a continuous structure that can be divided into 3 parts, which form 3 ridges or notches (R1, R2, R3) along the outer margin of the cochlea. The second and third parts of the interscalar septum, which are abnormal in IP-II malformations, form via membranous ossification with the first part of the septum, forming via enchondral ossification.^{4,10} The second part of the interscalar septum divides the upper basal and upper middle turns (lateral), and the third part divides the lower middle from the apical turn (medial). The first part of the interscalar septum divides the lower basal from the lower middle turn (posterior medial). The R2 notch is formed by the associated second part of the interscalar septum and is located along the lateral margin of the cochlea. In our experience, this notch is well-demonstrated on high-resolution MR imaging.

Other cochlear findings such as scalar asymmetry with enlargement of the scala vestibuli, defects in the osseous spiral lamina, and enlargement of the endolymphatic duct are typically seen in IP-II malformation and were commonly present in our IP-II cases. Reported vestibular abnormalities, including decreased size of the lateral semicircular canal bone island with enlargement of the lateral semicircular canal, were found in our affected ears as well.¹¹ The vestibule and semicircular canals were normal in the unilateral cases of IP-II malformation, and dilated endolymphatic ducts were not present. This malformation likely would have been classified as an IP-IIa by one author with associated milder involvement of the cochlea.¹² These ears may benefit even more from a thorough evaluation of the R2 notch because the cochlear abnormality may be subtler and there is a lack of confirmatory vestibular abnormalities.

The second part of the interscalar septum was only visualized in 36% of the normal-hearing ears and appears more difficult to evaluate than the associated notch on MR imaging using our technique. The septum can also be difficult to distinguish from the adjacent osseous spiral lamina in healthy patients, and visualization may be limited due to resolution. Thus, the presence or absence was not evaluated in the mixed-cohort group.

Most interesting, the interscalar septum in IP-II malformations is visualized on histopathology; however, it is often not seen on CT because of a higher insertion point and lack of ossification.^{4,12} Evaluation of the R2 notch on CT would be of value and further research into normal and abnormal values is needed. In IP-II malformation ears, the second portion of the septum bulges anteriorly and is associated with an enlarged scala vestibule, which was commonly found

in our cases (Fig 4).¹³ In a recent study, the second part of the interscalar septum was routinely identified using a higher resolution T2 drive sequence at 3T. The authors proposed evaluating the distance between the osseous spiral lamina of the upper basal turn and the first signal void anteriorly, presumably the second part of the interscalar septum. A cutoff value of ≥ 1.2 mm was found useful for diagnosing the IP-II malformation.¹⁴

The normal R2 notch along the lateral margin of the cochlea was easily appreciated on high-resolution T2-weighted images in the healthy cohort of ears. Identifying abnormalities of the R2 notch may be helpful in the evaluation of children with SNHL, and it has been reported to be abnormal on histologic examination as well as in a few imaging reports.^{3,4} In patients with normal hearing, the notch was measurable in all cochleas, with the 98th percentile for angle and depth being 101° and 0.3 mm, respectively, by an experienced reader.

Using a mixed group of normal ears and ears with an imaging-confirmed diagnosis of IP-II malformation, novice readers had excellent agreement in evaluating the angle and depth of the R2 notch. A significant difference in measurements was found when comparing normal ears with ears with an IP-II malformation, as well as similar cutoffs for angle and depth using receiver operating characteristic analysis (0.31/.34 mm and 114°/104°, respectively). An R2 notch measuring $> 114^\circ$ or ≤ 0.31 mm is suggested as evidence of an IP-II malformation or scala communis. There was a correlation with having a shallower notch with younger age in both groups, maybe due to an imaging-resolution issue or possibly related to postnatal maturation of the interscalar septum. The ability of novice readers to accurately evaluate the R2 notch is important because these examinations can be difficult to interpret and evaluation of the lateral notch is a simple reproducible method to evaluate the integrity of the R2 septum and therefore the presence or absence of scala communis.

Two of the 10 patients with IP-II underwent genetic testing, one of which was for connexin 26 only, which had normal findings, and the remaining patient had a compound heterozygous mutation in the *SLC26A4* gene. The *SLC26A4* gene codes for the protein pendrin, which is a chloride/bicarbonate anion exchanger that serves to increase the pH in the endolymph compartment by secreting bicarbonate.¹⁵ Pendrin protein expression in the endolymphatic sac is critical in the development of the mammalian inner ear as demonstrated in a murine model. The absence or reduction in pendrin expression results in acidification and abnormal expansion of the developing inner ear. Acidification of the developing inner ear results in reduced endolymphatic potassium concentration and subsequent loss of the endocochlear potential. An increase in endolymph calcium also results from acidification and thus results in toxicity to the stria vascularis and the organ of Corti.¹⁵

Potential limitations of the study include bias in the interpretation of the healthy cohort because the experienced reader did have a preconceived theory of the appearance of the normal R2 notch. Also, while the inexperienced readers had minimal prior exposure to interpreting MR imaging of the temporal bone, other findings encountered in IP-II malformation may have been seen and affected their interpretation.

CONCLUSIONS


The R2 notch, formed by the associated second part of the interscalar septum, should be evaluated in all patients being imaged with a diagnosis of SNHL. This notch is easily appreciated with reproducible measurements on high-resolution MR imaging. A R2 angle of $> 114^\circ$ and/or a depth of ≤ 0.31 mm considered abnormal. Measurement of the R2 notch may aid in the evaluation of more subtle IP-II malformations or an isolated scala communis.

Disclosures: Joe W. Kutz—UNRELATED: Consultancy: Medtronic, Purdue Pharma, Achaogen. Brandon Isaacson—UNRELATED: Board Membership: Med-EL, Advanced Bionics, Comments: Advisory Board member; Consultancy: Advanced Bionics, Medtronic, Stryker Corporation, Karl Storz SE & Company KG, Olympus Corporation, Comments: electrode testing, drill testing, and designing an endoscopic ear surgery tool and imaging development.

REFERENCES

1. Sennaroglu L, Saatci I. A new classification for cochleovestibular malformations. *Laryngoscope* 2002;112:2230–41 [CrossRef Medline](#)
2. Adibelli ZH, Isayeva L, Koc AM, et al. The new classification system for inner ear malformations: the INCAV system. *Acta Oto Laryngol* 2017;137:246–52 [CrossRef Medline](#)
3. Makary C, Shin J, Caruso P, et al. A histological study of scala communis with radiological implications. *Audiol Neurotol* 2010;15:383–93 [CrossRef Medline](#)
4. Leung KJ, Quesnel AM, Juliano AF, et al. Correlation of CT, MR, and histopathology in incomplete partition-II cochlear anomaly. *Otol Neurotol* 2016;37:434–37 [CrossRef Medline](#)
5. Merchant SN. Genetically determined and other developmental defects. In: Merchant SN, Nadol JB, eds. *Schuknecht's Pathology of the Ear*. 3rd ed. New York: McGraw-Hill Medical; 2010:545–611
6. Sennaroglu L, Sarac S, Ergin T. Surgical results of cochlear implantation in malformed cochlea. *Otol Neurotol* 2006;27:615–23 [CrossRef Medline](#)
7. Papsin BC. Cochlear implantation in children with anomalous cochleovestibular anatomy. *Laryngoscope* 2005;115(1 Pt 2 Suppl 106):1–26 [Medline](#)
8. Sennaroglu L. Cochlear implantation in inner ear malformation: a review article. *Cochlear Implants Int* 2010;11:4–41 [CrossRef Medline](#)
9. Glastonbury CM, Davidson CH, Harnsberger HR, et al. Imaging findings of cochlear nerve deficiency. *AJNR Am J Neuroradiol* 2002;23:635–43 [Medline](#)
10. Som PM, Curtin HD, Liu K, et al. Current embryology of the temporal bone, part I: the inner ear. *Neurographics* 2016;6:250–65 [CrossRef](#)
11. Davidson CH, Harnsberger HR, Lemmerling MM, et al. MR evaluation of vestibulocochlear anomalies associated with large endolymphatic duct and sac. *AJNR Am J Neuroradiol* 1999;20:1435–41 [Medline](#)
12. Kontorinis G, Goetz F, Giourgas, et al. Radiologic diagnosis of incomplete partition type I versus type II: significance for cochlear implantation. *Eur Radiol* 2012;22:525–32 [CrossRef Medline](#)
13. Sennaroglu L. Histopathology of inner ear malformations: do we have enough evidence to explain pathophysiology? *Cochlear Implants Int* 2016;17:3–20 [CrossRef Medline](#)
14. Reinshagen KL, Curtin HD, Quesnel AM, et al. Measurement for detection of incomplete partition type II anomalies on MR imaging. *AJNR Am J Neuroradiol* 2017;38:2003–07 [CrossRef Medline](#)
15. Wangemann P. Mouse model for pendrin-associated loss of cochlear and vestibular function. *Cell Physiol Biochem* 2013;32(Suppl 1):157–65 [CrossRef Medline](#)

Anatomic Malformations of the Middle and Inner Ear in 22q11.2 Deletion Syndrome: Case Series and Literature Review

 E. Verheij,  L. Elden,  T.B. Crowley,  F.A. Pameijer,  E.H. Zackai,  D.M. McDonald-McGinn, and  H.G.X.M. Thomeer

ABSTRACT

BACKGROUND AND PURPOSE: The 22q11.2 deletion syndrome is characterized by a heterogenic phenotype, including hearing loss. The underlying cause of hearing loss, especially sensorineural hearing loss, is not yet clear. Therefore, our objective was to describe anatomic malformations in the middle and inner ear in patients with 22q11.2 deletion syndrome.

MATERIALS AND METHODS: A retrospective case series was conducted in 2 tertiary referral centers. All patients with 22q11.2 deletion syndrome who had undergone CT or MR imaging of the temporal bones were included. Radiologic images were evaluated on predetermined parameters, including abnormalities of the ossicular chain, cochlea, semicircular canals, and vestibule.

RESULTS: There were 26 patients (52 ears) with a CT or MR imaging scan available. A dense stapes superstructure was found in 18 ears (36%), an incomplete partition type II was suspected in 12 cochleas (23%), the lateral semicircular canal was malformed with a small bony island in 17 ears (33%), and the lateral semicircular canal and vestibule were fused to a single cavity in 15 ears (29%).

CONCLUSIONS: Middle and inner ear abnormalities were frequently encountered in our cohort, including malformations of the lateral semicircular canal.

ABBREVIATIONS: 22q11DS = 22q11.2 deletion syndrome; LSCC = lateral semicircular canal

The 22q11.2 deletion syndrome (22q11DS), also known as velocardiofacial syndrome or DiGeorge syndrome, is caused by a microdeletion on the long arm of chromosome 22 and has a heterogenic phenotype.¹⁻³ Otolaryngologic manifestations are frequently present; the most well-known clinical otolaryngologic features are velopharyngeal insufficiency, cleft palate, recurrent otitis media, and hearing loss. Hearing loss is most commonly the conductive type and might merely be related to recurrent otitis media.⁴⁻⁷ However, sensorineural or mixed hearing loss has also been described.^{4,5,7-11}

The underlying cause of hearing impairment, especially the sensorineural component, is still not understood. There are case

reports describing middle or inner ear malformations on radiologic imaging.¹²⁻¹⁵ Recently, a cohort study was conducted in which CT images of the temporal bones of 11 patients with 22q11DS were analyzed. This study found middle ear malformations as well as cochlear, vestibular, and semicircular canal malformations.¹⁶ The anatomic malformations could be present due to genetic abnormalities leading to an error in the embryologic phase. Mouse studies have identified *Tbx1* as a candidate gene responsible for ear abnormalities in 22q11DS.¹⁶⁻¹⁹ Inactivation of *Tbx1* in the otic vesicle in mice leads to disruption of inner ear development.²⁰

The aim of this study was to describe anatomic malformations of the middle and inner ear in these patients, shown on CT and/or MR imaging.

MATERIALS AND METHODS

We conducted a retrospective study at the University Medical Center Utrecht and Children's Hospital of Philadelphia. All patients diagnosed with 22q11DS, confirmed with a microdeletion, who underwent CT or MR imaging of the temporal bones before May 2017 were included. Radiologic images from Children's Hospital of Philadelphia were de-identified and sent to the University Medical Center Utrecht for analysis. Approval from the institu-

Received August 31, 2017; accepted after revision January 12, 2018.

From the Department of Otorhinolaryngology–Head and Neck Surgery (E.V., H.G.X.M.T.), Brain Center Rudolf Magnus (E.V., H.G.X.M.T.), and Department of Radiology (F.A.P.), University Medical Center Utrecht, Utrecht, the Netherlands; Department of Otorhinolaryngology–Head and Neck Surgery (L.E.), The 22q and You Center (T.B.C., E.H.Z., D.M.M.-M.), and Department of Human Genetics (T.B.C., E.H.Z., D.M.M.-M.), Children's Hospital of Philadelphia, Philadelphia, Pennsylvania; and Department of Pediatrics (E.H.Z., D.M.M.-M.), Perelman School of Medicine at the University of Pennsylvania, Philadelphia, Pennsylvania.

Please address correspondence to E. Verheij, MD, Department of Otorhinolaryngology–Head and Neck Surgery, University Medical Center Utrecht, Heidelberglaan 100, 3584 CX, Utrecht, the Netherlands; e-mail: ent-research@umcutrecht.nl

<http://dx.doi.org/10.3174/ajnr.A5588>

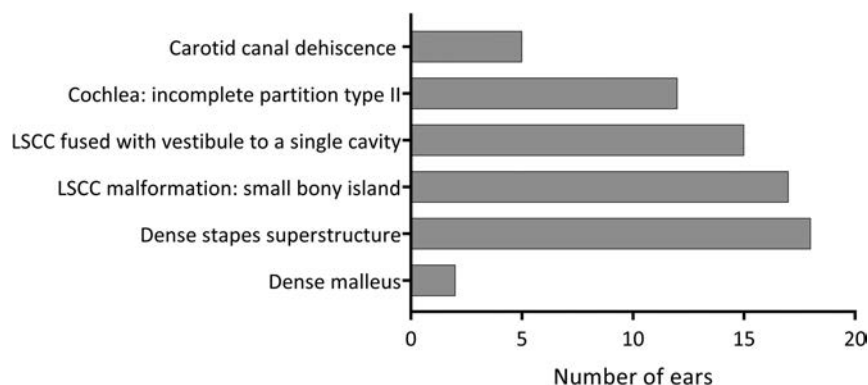


FIG 1. Radiologic malformations of the middle and inner ear encountered in 52 ears.

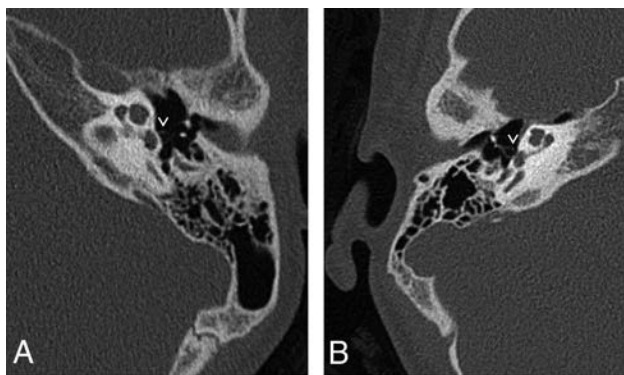


FIG 2. A, Axial CT image of the left mastoid shows a normal stapes superstructure for comparison with B. B, Axial CT image of the right mastoid shows a dense, thick stapes superstructure. The pure tone audiogram of this patient is shown in Fig 5B. The mastoid bones shown in A and B do not belong to the same patient.

tional review board from Children's Hospital of Philadelphia was obtained, and the medical ethics committee of the University Medical Center Utrecht deemed this study exempt from review.

The first author and F.A.P. (head and neck radiologist with >20 years' experience) evaluated the radiologic studies to determine the nature and prevalence of temporal bone abnormalities based on a series of predetermined features. We assessed ossicular chain abnormalities, the course of the facial nerve, malformations of the cochlea, malformations of the semicircular canals, vestibule widening, enlargement of the vestibular aqueduct, and carotid canal dehiscence. We scored features as present, partially present, or absent. We measured the bony island of the lateral semicircular canal (LSCC) and vestibule width to compare with previously defined normal measurements of the bony island of the lateral semicircular canal.²¹ The bony island was considered normal when the axial diameter was between 3.0 and 4.4 mm. For the vestibule width, an axial diameter between 2.8 and 4.0 mm was considered normal. For assessing the density of hearing ossicles, to our knowledge, no normal ranges in densities are described in the literature; therefore, we relied on the expertise of our head and neck radiologist. When one of the hearing ossicles displayed an increased density and/or general thickening on standard windows (especially the stapes superstructure), we recorded this ossicle as "dense."

The medical records were reviewed to determine the primary reason for obtaining CT or MR imaging and to collect data in-

cluding pure tone audiogram information. Furthermore, tympanometry information, history of chronic otitis media, and history of dizziness or balance problems were collected. Hearing loss was defined as a pure tone average (average, 0.5, 1, 2, and 4 kHz) of >20 dB hearing level, in concordance with the American Academy of Otolaryngology–Head and Neck Surgery 1995 guidelines.²² Conductive hearing loss was considered when the average air-conduction threshold was >20 dB, and the air-bone gap was ≥10 dB at ≥1 frequency. Sensorineural hearing loss was

defined as hearing loss with an air-bone gap of <10 dB in all frequencies, and mixed hearing loss, as an average air and bone conduction threshold of >20 dB and an air-bone gap of ≥10 dB at ≥1 frequency. Tympanometry results were classified into type A (representing the normal situation), type B (flat curve, indicating middle ear effusion), type C (negative peak pressure), type As (a small pressure peak, representing a decreased mobility of the ossicular chain), and type Ad (a high pressure peak, indicating an increased mobility of the ossicular chain).

RESULTS

Baseline Characteristics

Of approximately 300 patients followed at the University Medical Center Utrecht and the 1300 patients from Children's Hospital of Philadelphia, 26 patients (52 ears), 14 males and 12 females, underwent radiologic imaging of the temporal bones (11 patients from the University Medical Center Utrecht, 15 patients from Children's Hospital of Philadelphia). The indications for imaging were hearing loss that could not be explained by otoscopic findings ($n = 10$), chronic otitis media ($n = 13$), both unexplained hearing loss and chronic otitis media ($n = 2$), or areal atresia ($n = 1$). MR imaging was performed in 1 patient; all other patients underwent CT of the temporal bones. One patient likely had a second genetic disorder, in addition to a microdeletion on chromosome 22q11.2.

Radiologic Outcomes

Radiologic findings are shown in Fig 1.

Middle Ear

Aural atresia was seen affecting the external auditory canal and middle ear in 1 ear. The middle ear was small and contained 1 rudimentary hearing ossicle. No stapes, stapes footplate, or facial nerve could be identified. This ear belonged to the patient with a possible second genetic disorder. Eighteen ears (36%) (13 patients) were found to have a dense stapes superstructure (Fig 2), and in 2 ears (1 patient), the manubrium of the malleus was dense. No other abnormalities of the malleus or incus were encountered.

Inner Ear

Malformations of the cochlea and vestibular system were seen. As shown in Fig 1, an incomplete partition type II

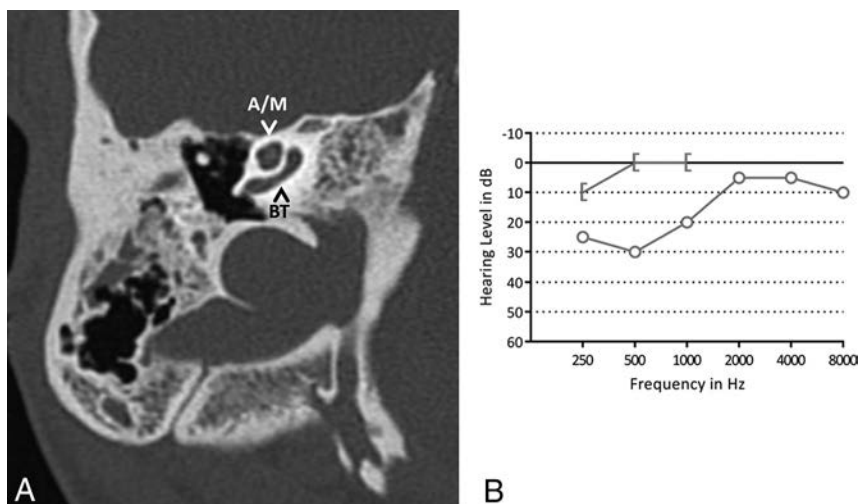


FIG 3. A, Axial CT image of the right mastoid shows an incomplete partition type II of the cochlea. The basal turn (BT) of the cochlea is intact; the apical and middle turn (A/M) seem confluent. B, A pure tone audiogram of the same ear shows normal hearing. The circle indicates an unmasked air-conduction threshold; the bracket, a masked bone-conduction threshold.

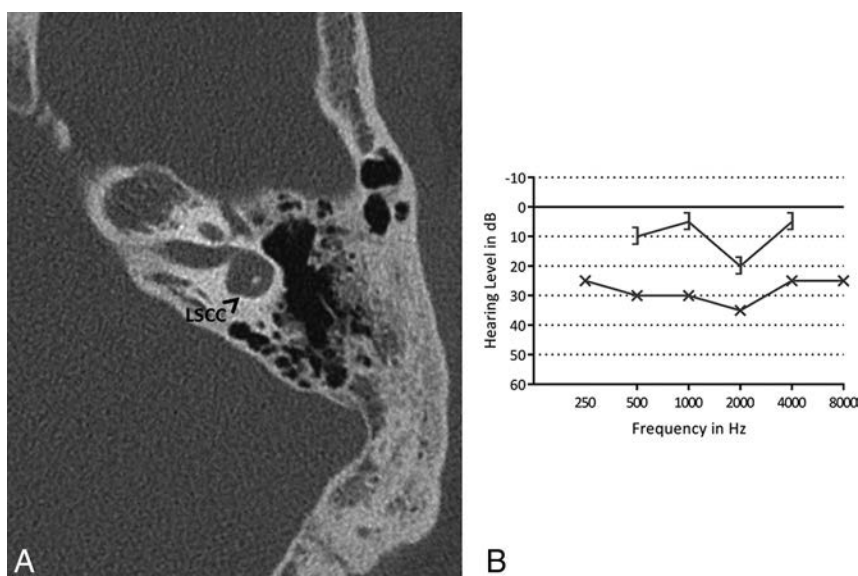


FIG 4. A, Axial CT image of left mastoid bone shows the lateral semicircular canal with a small bony island. B, A pure tone audiogram of the same ear shows a mild conductive hearing loss. The x indicates an unmasked air-conduction threshold; the bracket, a masked bone-conduction threshold.

of the cochlea was suspected in 12 ears (23%) (7 patients). This malformation was frequently subtle and easy to overlook (Fig 3).

In 17 ears (33%) (11 patients), the bony island of the LSCC was small (Fig 4), measuring between 2.6 and 1.1 mm. No evidence of widening of the vestibule was observed, including in the ears with a small bony island (the widest vestibule measured 3.9 mm). In 15 ears (29%) (9 patients), the LSCC and vestibule were fused to a single cavity (Fig 5). Two patients had an LSCC with a small bony island in 1 ear and a single cavity in the contralateral ear. In addition, in 1 ear with a normally formed LSCC, there was a disruption of the posterior semicircular canal, consisting of 2 blind limbs. Superior semicircular canal dehiscence was seen in 1 ear.

Last, in 5 ears (10%) (4 patients), a dehiscence of the carotid canal was present (Fig 6). The vestibular aqueduct and the facial nerve were normal in all cases, except in the ear with an aural atresia, where the facial nerve could not be identified.

Audiologic Findings

Twenty-seven ears belonging to 18 patients showed hearing loss on a pure tone audiogram. Sixteen ears had conductive, 6 ears had sensorineural, and 5 had ears mixed hearing loss. The median pure tone average of the ears with hearing loss was 33.75 dB hearing level (range, 21–100 dB hearing level). In 1 patient, there was no pure tone audiogram available. This patient had undergone a visual reinforcement audiometry and a brain stem evoked response audiometry, which was suspect for a pure sensorineural hearing loss in the right ear and a mixed hearing loss in the left ear. The patient with an aural atresia did not have an audiogram of the atretic ear. The type of hearing loss compared with the encountered anatomic malformations is summarized in Table 1. Tympanometry was performed in 42 ears in 4 ears the test failed, and in the remaining 6 ears, no tympanogram was available in the medical files. A normal tympanogram finding (type A) was present in 18 ears; a type B was present in 5 ears; a type C, in 3 ears; a type As, in 10 ears; a type Ad, in 1 ear; and in 5 ears, a large volume was shown on tympanometry. The tympanometry results from the ears with middle ear abnormalities are shown in Table 1. Of the 12 ears with a dense stapes superstructure and an available tympanogram, 3 ears had a type As tympanogram, indicating decreased mobility of the ossicular chain.

Otologic and Vestibular Findings

Five patients had no history of recurrent otitis media. All other patients ($n = 21$) had either recurrent otitis media with effusion or recurrent acute otitis media or both. All patients with a dense hearing ossicle had a history of recurrent otitis media. One patient was reported to experience occasional dizziness and another patient showed normal compensatory eye movements when tested for the vestibulo-ocular reflex. The patient with occasional dizziness had an LSCC with a small bony island on one side and a single cavity on the other side. In the patient with normal compensatory eye movements, the vestibule and LSCC were bilaterally fused to a single cavity. We presume that no other patient had vestibular symptoms because these symptoms were not mentioned in the medical records.

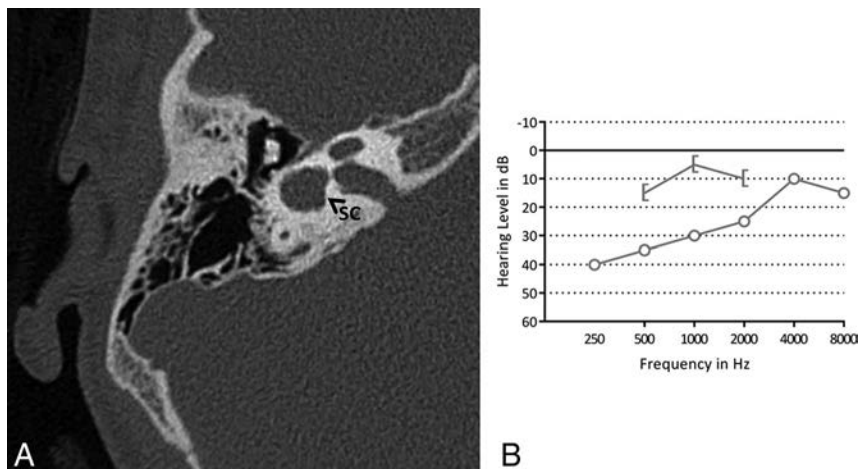


FIG 5. A, Axial CT image of the right mastoid bone. The bony island of the lateral semicircular canal is missing, and the canal and vestibule are composed of a single cavity (SC). B, A pure tone audiogram of the same ear shows conductive hearing loss, more pronounced in the low frequencies. The circle indicates an unmasked air-conduction threshold; the bracket, a masked bone-conduction threshold.

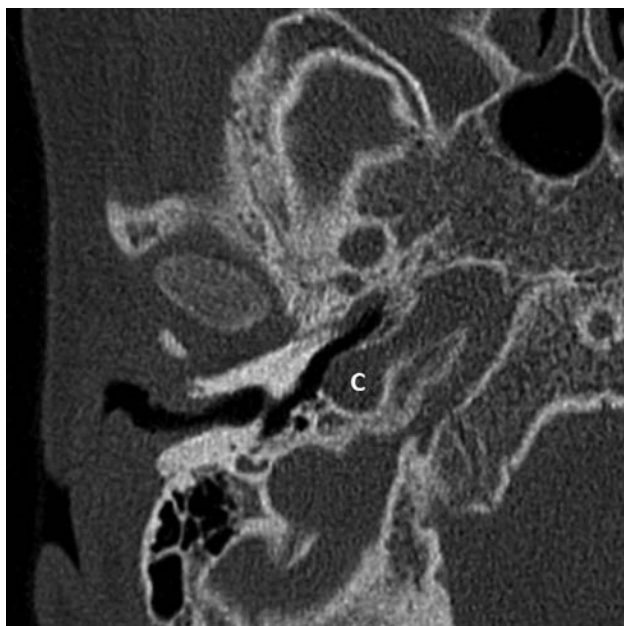


FIG 6. Axial CT image of the right mastoid bone showing a carotid canal dehiscence (C).

DISCUSSION

By pooling data from 2 large centers (University Medical Center Utrecht and Children's Hospital of Philadelphia), we have presented the largest series describing radiographic malformations found in the middle and inner ears of patients with 22q11DS, to our knowledge. In a similar study by Loos et al,¹⁶ CT scans of the temporal bones of 11 patients were analyzed. Table 2 compares the total number of middle and inner ear malformations described in each study. Perhaps the most interesting but incidental finding was when the LSCC and vestibule consisted of a single cavity, as was seen in 29%, and when the LSCC was malformed with a small bony island, present in 33%.

Inner Ear Malformations

Regarding the specific types of vestibular malformations described in the literature, those that resulted in a single cavity have

previously been described in 2 case reports^{13,15} as well as by Loos et al (Table 2).¹⁶ Other vestibular malformations were also reported in the literature. One study retrospectively reviewed brain MR imaging and MRA scans of 24 patients with 22q11DS and found a vestibular dysplasia (the figure in the article showed a single cavity) in 13% of patients. None of these patients had sensorineural hearing loss.²³ This is a lower prevalence than we found. This could be due to the selection of our patients. The indications for radiology in the Bohm et al²³ study were unexplained developmental delay, seizures of unknown etiology, and unilateral weakness, whereas the indications in our population were mainly hearing loss or otitis media. Furthermore, they did not report on a malformed LSCC with a small bony island or an incomplete partition type II of the cochlea.²³ These abnormalities are more subtle and likely more difficult to detect on brain MR imaging compared with an MR imaging of the temporal bones. In addition, 2 case reports described 3 patients who had bilateral poorly formed LSCCs and 1 patient who had bilateral dilation of the vestibule.^{12,24} Loos et al¹⁶ also described 14 ears with a wide vestibule, of which 3 also had a wide LSCC. As described by Casselman et al,²⁵ the vestibule can be considered large when the surface of the bony island of the LSCC is $<6 \text{ mm}^2$. Therefore, we can assume that the malformed LSCC with a small bony island in our series of patients is the same anomaly as a wide vestibule reported by Loos et al, even though the vestibule in our patients, in absolute terms, was not wider than normal considering the measurements described by Purcell et al.²¹

Malformations of the inner ear may result from an error in one of the developmental stages in embryogenesis. A malformed LSCC can occur in combination with normally shaped superior and posterior semicircular canals because the LSCC is developed later compared with the superior and posterior semicircular canals.²⁶ Between 4 and 5 weeks of gestation, the development of the membranous semicircular canals begins. They develop from the dorsal region of the otocyst, which enlarges, and with resorption of the medial walls, a semicircular-shaped duct is formed.²⁷ An error in this resorption will result in a confluent vestibule and canal.²⁸ This was the case in 15 ears in our cohort. In patients with a malformed LSCC with a small bony island, but without a fusion of the canal and vestibule, the development is presumably disrupted at a later stage.^{27,29}

From our chart reviews, clinical findings that may have been directly attributed to inner ear vestibular problems such as vertigo or balance problems were not present in those who had a malformed LSCC on imaging studies. Absent vestibular symptoms in patients without 22q11DS with a malformed LSCC were reported in previous studies.³⁰⁻³² However, more subtle balance problems have frequently been described in the 22q11DS population.³³⁻³⁵ Many of these symptoms can relate to other neuromotor defi-

Table 1: Number of ears with audiometric results per anatomic malformation

Malformation	PTA					Tympanometry ^a					
	No HL (%)	HL				Type					
		C (%)	SN (%)	M (%)	PTA Range in dB	A	B	C	As	Ad	LV
Dense malleus	2 (100)	—	—	—	—	—	—	—	—	—	—
Dense stapes superstructure	7 (39)	6 (33)	1 (6)	4 (22)	21–100	3	3	1	3	—	2
IP type II	5 (42)	3 (25)	1 (8) ^b	3 (25)	38–100	—	—	—	—	—	—
LSCC: small bony island	7 (41)	4 (24)	3 (18) ^b	3 (18) ^b	35–100	—	—	—	—	—	—
LSCC: single cavity	6 (40)	5 (33)	2 (13)	2 (13)	25–96	—	—	—	—	—	—

Note:—HL indicates hearing loss; C, conductive; SN, sensorineural; M, mixed; PTA, pure tone average; A, normal situation; B, flat curve; C, negative peak pressure; As, small pressure peak; Ad, high pressure peak; LV, large volume; IP, incomplete partition.

^a The number of ears does not amount to the total number of ears with a malformation due to missing data.

^b Including 1 ear measured with visual reinforcement audiometry and brain stem evoked response audiometry.

Table 2: Overview of number of ears with middle and/or inner ear abnormalities reported by Loos et al¹⁶ and in the present study

Malformation	Loos et al ¹⁶ ; No. of Ears (%) (Total, 22 Ears)	Present study; No. of Ears (%) (Total, 52 Ears)	Total No. of Ears (%) (Total, 74 Ears)
Malleus, incus, or stapes abnormalities ^a	2 (9)	3 (6) ^b	5 (7) ^c
Dense stapes superstructure	10 (45)	18 (36) ^b	28 (39) ^c
LSCC: single cavity	4 (18)	15 (29)	19 (26)
Wide vestibule/small bony island in LSCC	14 (64)	17 (33)	31 (42)
IP type II	12 (55)	12 (23)	24 (32)
Carotid canal dehiscence	2 (9)	5 (10) ^b	7 (10) ^c

Note:—IP indicates incomplete partition.

^a Other than a dense stapes superstructure.

^b Calculated from a total of 50 ears; bone structures in 2 ears in the present study could not be assessed on MRI.

^c Calculated from a total of 72 ears; bone structures in 2 ears in the present study could not be assessed on MRI.

cits,³³ including motor delay^{36–38} or hypotonia,^{33,38,39} but vestibular problems could also play a role. Prospective research is needed to assess the possible relation among anatomic malformations of the vestibular system, vestibular function, and motor delay in patients with 22q11DS.

A subtle incomplete partition type II was frequently found in our patients. These findings are consistent with those in the study of Loos et al (Table 1).¹⁶ An incomplete partition type II of the cochlea derives from a developmental arrest at the seventh week of gestation. Here the cochlea has 1.5 turns, and there is a defect at the apex of the cochlea between the middle and apical turns. The basal turn and basal part of the modiolus are normally developed.⁴⁰ Other cochlear malformations in 22q11DS have also been previously reported. Loos et al reported on 2 ears with a large basal turn length.¹⁶ One patient described by Devriendt et al¹³ had a malformed cochlea, where the basal turn was broad and the second and apical turns were short.

At a genetic level, both the vestibular and cochlear malformations described in our patients may be associated with *Tbx1*. In patients with 22q11DS, *Tbx1* is hemizygotously deleted. In mutated knockout *Tbx1*^{−/−} mice, the vestibular system and cochlea are absent.^{19,41} Mouse models show an expression of *Tbx1* in the otic vesicle, which forms the membranous inner ear, and in the periotic mesenchyme, which forms the otic capsule and later the bony labyrinth.^{19,41} Studies have indicated that the expression of *Tbx1* in the periotic mesenchyme is necessary for cochlear outgrowth.^{42,43} In addition, *Tbx1* is required for outer and middle ear development.^{20,44}

Hearing impaired as well as normal hearing ears were found to have a dense stapes superstructure, incomplete partition type II of the cochlea, or a malformed LSCC in this study. However, the

relation between hearing loss and abnormalities of the middle or inner ear was not within the scope of this report because selection bias undoubtedly plays a large role. Due to the retrospective design, patients with hearing impairment are more likely to undergo imaging with CT compared with patients with normal hearing. In fact, the indication for the radiologic imaging in 12 patients was unexplained hearing impairment.

We found 5 ears with a dehiscence of the carotid canal. A carotid canal dehiscence is present in approximately 7% of

the general population,^{45,46} in which case our findings suggest a slightly higher prevalence in patients with 22q11DS (10%). In patients with a carotid canal dehiscence, the internal carotid artery is (partly) no longer protected by a bony shield and is exposed in the middle ear. Because patients with 22q11DS often have middle ear infections requiring grommet insertion or even middle ear surgery, otorhinolaryngologists should be aware of the possible presence of a carotid canal dehiscence in patients with 22q11DS.

Middle Ear Abnormalities

We found 1 ear with an aural atresia affecting both the external auditory canal and the middle ear. This patient may have also had a second genetic disorder. Therefore, in this patient, the aural atresia could have been attributed to a disorder other than 22q11DS. Aural atresia has previously been described in 22q11DS by Derbent et al⁴⁷ and Digilio et al.⁴⁸ The patients reported both by Derbent et al and Digilio et al all showed features resembling the oculo-auriculo-vertebral spectrum in addition to 22q11DS.^{47,48} Patients with the oculo-auriculo-vertebral spectrum show defects in organs deriving from the first and second pharyngeal arch. As a result, aural atresia is frequently observed.⁴⁹ Also concluded by Digilio et al,⁴⁸ features resembling the oculo-auriculo-vertebral spectrum could occur in patients with 22q11DS, perhaps more frequently than expected.

In addition, 18 ears with a dense stapes superstructure were encountered. We acknowledge that the diagnosis of a dense stapes superstructure is subjective and these results should be viewed with caution. In the literature, we could not find information on a standardization of the CT density of hearing ossicles. However, when analyzing the CT images of our patients, a dense stapes superstructure was relatively easy to detect by visual analysis. Fur-

thermore, Loos et al¹⁶ found approximately the same number of patients with a dense stapes superstructure (36% versus 45%). This suggests that this finding may be a feature present in patients 22q11DS, though at present, we do not know its clinical significance. We initially assumed that the dense stapes superstructure was a result of chronic otitis media (ie, tympanosclerosis). However, in the study from Loos et al, 1 patient showed this abnormality on day of life 9. This indicated a congenital instead of a postinfectious cause, as stated by the authors.¹⁶ Possibly, the dense stapes superstructures we encountered were also of congenital origin. Moreover, only 3 of the 12 ears with dense stapes superstructures in the present study showed signs of a stiffened ossicular chain on a tympanogram, suggesting a possibly different entity than tympanosclerosis.

Except for a dense manubrium of the malleus and dense stapes, we did not find other abnormalities of hearing ossicles. Many of the affected organs in patients with 22q11DS are derived from the pharyngeal arches.² Although the more caudal arches are more affected in 22q11DS⁵⁰ and hearing ossicles develop from the cranial arches (malleus and incus from the first and stapes from the second pharyngeal arch), we expected to encounter more middle ear malformations. Anomalies of hearing ossicles in 22q11DS are reported in the literature. The first was a patient with conductive hearing loss present since birth, whose imaging revealed “malformation and subluxation of the stapes.”¹⁴ Another report described 2 patients; one patient had a “fusion of the malleus with the incus and a monopodal stapes” shown on CT. CT images of the other patient revealed a “fixation of the malleus at the annulus tympanicus.”¹³ This latter malformation was also encountered by Loos et al¹⁶ in 2 ears where, in addition, the long process of the incus was thin and horizontally oriented. Furthermore, another study described 1 patient with a bilaterally malformed malleus and incus and 1 patient with a unilateral fusion of the malleus with the lateral wall of the middle ear.²⁴

The main limitation of this study is selection bias due to the retrospective design. Only patients with a clinical indication, most likely unexplained hearing loss or chronic or recurrent otitis media, were likely to have undergone radiologic imaging. Therefore, no realistic prevalence should be extracted from this study. The primary purpose of the study was to describe the more common vestibular and cochlear malformations and to consider associations with balance and hearing problems in those who have 22q11DS. Furthermore, some of the encountered abnormalities, especially the incomplete partition type II, are very subtle. Likely, there would be interobserver variability if the same images were also evaluated by a different team.

CONCLUSIONS

Cross-sectional imaging of the temporal bones in a 22q11DS cohort of 26 patients is presented and a review of the literature was performed. A dense stapes superstructure, suspected incomplete partition type II of the cochlea, and LSCC malformations were frequently encountered. Future studies in these patients should preferably include vestibular testing because balance problems are known to contribute to motor development delay in children. Correlation between LSCC malformations and vestibular function would be of interest.

Disclosures: Donna M. McDonald-McGinn—UNRELATED: Grants/Grants Pending: National Institutes of Health, Comments: grants MH087626 and MH087636 for work outside the submitted work*; Payment for Lectures Including Service on Speakers Bureaus: Natera, Comments: lectures on the 22q11.2 deletion syndrome.* *Money paid to the institution.

REFERENCES

1. Kobrynski LJ, Sullivan KE. **Velocardiofacial syndrome, DiGeorge syndrome: the chromosome 22q11.2 deletion syndromes.** *Lancet* 2007;370:1443–52 CrossRef Medline
2. McDonald-McGinn DM, Sullivan KE, Marino B, et al. **22q11.2 deletion syndrome.** *Nat Rev Dis Primers* 2015;1:15071 CrossRef Medline
3. Robin NH, Shprintzen RJ. **Defining the clinical spectrum of deletion 22q11.2.** *J Pediatr* 2005;147:90–96 CrossRef Medline
4. Dyce O, McDonald-McGinn DM, Kirschner RE, et al. **Otolaryngologic manifestations of the 22q11.2 deletion syndrome.** *Arch Otolaryngol Head Neck Surg* 2002;128:1408–12 CrossRef Medline
5. Digilio MC, Pacifico C, Tieri L, et al. **Audiological findings in patients with microdeletion 22q11 (di George/velocardiofacial syndrome).** *Br J Audiol* 1999;33:329–33 CrossRef Medline
6. Ford LC, Sulprizio SL, Rasgon BM. **Otolaryngological manifestations of velocardiofacial syndrome: a retrospective review of 35 patients.** *Laryngoscope* 2000;110:362–67 CrossRef Medline
7. Reyes MR, LeBlanc EM, Bassila MK. **Hearing loss and otitis media in velo-cardio-facial syndrome.** *Int J Pediatr Otorhinolaryngol* 1999;47:227–33 CrossRef Medline
8. Persson C, Friman V, Óskarsdóttir S, et al. **Speech and hearing in adults with 22q11.2 deletion syndrome.** *Am J Med Genet A* 2012;158A:3071–79 CrossRef Medline
9. Van Eynde C, Swillen A, Lambeens E, et al. **Prevalence and nature of hearing loss in 22q11.2 deletion syndrome.** *J Speech Lang Hear Res* 2016;59:583–89 CrossRef Medline
10. Weir FW, Wallace SA, White DR, et al. **Otologic and audiology outcomes in pediatric patients with velo-cardio-facial (22q11 deletion) syndrome.** *Otol Neurotol* 2016;38:73–78 CrossRef Medline
11. Zarchi O, Attias J, Raveh E, et al. **A comparative study of hearing loss in two microdeletion syndromes: velocardiofacial (22q11.2 deletion) and Williams (7q11.23 deletion) syndromes.** *J Pediatr* 2011;158:301–06 CrossRef Medline
12. Junior AT, Haetinger RG, Silva FL, et al. **Middle and inner ear malformations in two cases of velocardiofacial syndrome.** *Intl Arch Otorhinolaryngol* 2009;13:83–86
13. Devriendt K, Swillen A, Schatteman I, et al. **Middle and inner ear malformations in velocardiofacial syndrome.** *Am J Med Genet A* 2004;131:225–26 Medline
14. Cunningham ML, Perry RJ, Eby PR, et al. **Primary pulmonary dysgenesis in velocardiofacial syndrome: a second patient.** *Am J Med Genet A* 2003;121A:177–79 CrossRef Medline
15. Hopsu E, Markkola A, Pitkäranta A. **Labyrinthine malformation in the 22q11.2 deletion syndrome.** *Clin Dysmorphol* 2007;16:67–68 CrossRef Medline
16. Loos E, Verhaert N, Willaert A, et al. **Malformations of the middle and inner ear on CT imaging in 22q11 deletion syndrome.** *Am J Med Genet A* 2016;170:2975–83 CrossRef Medline
17. Fuchs JC, Zinnamon FA, Taylor RR, et al. **Hearing loss in a mouse model of 22q11.2 deletion syndrome.** *PLoS One* 2013;8:e80104 CrossRef Medline
18. Funke B, Epstein JA, Kochilas LK, et al. **Mice overexpressing genes from the 22q11 region deleted in velo-cardio-facial syndrome/DiGeorge syndrome have middle and inner ear defects.** *Hum Mol Genet* 2001;10:2549–56 CrossRef Medline
19. Vitelli F, Viola A, Morishima M, et al. **TBX1 is required for inner ear morphogenesis.** *Hum Mol Genet* 2003;12:2041–48 CrossRef Medline
20. Arnold JS, Braunstein EM, Ohya T, et al. **Tissue-specific roles of Tbx1 in the development of the outer, middle and inner ear, defective in 22q11DS patients.** *Hum Mol Genet* 2006;15:1629–39 CrossRef Medline
21. Purcell D, Johnson J, Fischbein N, et al. **Establishment of normative**

- cochlear and vestibular measurements to aid in the diagnosis of inner ear malformations. *Otolaryngol Head Neck Surg* 2003;128:78–87 CrossRef Medline
22. Monsell EM. **Committee on Hearing and Equilibrium guidelines for the evaluation of results of treatment of conductive hearing loss: American Academy of Otolaryngology-Head and Neck Surgery Foundation, Inc.** *Otolaryngol Head Neck Surg* 1995;113:186–87 CrossRef Medline
23. Bohm LA, Zhou TC, Mingo TJ, et al. **Neuroradiographic findings in 22q11.2 deletion syndrome.** *Am J Med Genet A* 2017;173:2158–65 CrossRef Medline
24. Jiramongkolchai P, Kumar MS, Chinnadurai S, et al. **Prevalence of hearing loss in children with 22q11.2 deletion syndrome.** *Int J Pediatr Otorhinolaryngol* 2016;87:130–33 CrossRef Medline
25. Casselman JW, Delanote J, Kuhweide R, et al. **Congenital malformations of the temporal bone.** In: Lemmerling M, De Foer B, eds. *Temporal Bone Imaging*. Berlin: Springer-Verlag; 2015
26. Rodriguez K, Shah RK, Kenna M. **Anomalies of the middle and inner ear.** *Otolaryngol Clin North Am* 2007;40:81–96, vi CrossRef Medline
27. Lim R, Brichta AM. **Anatomical and physiological development of the human inner ear.** *Hear Res* 2016;338:9–21 CrossRef Medline
28. Jackler R, Luxford W, House W. **Cochlear malformations of the inner ear: a classification based on embryogenesis.** *Laryngoscope* 1987;97:2–14 Medline
29. Jeffery N, Spoor F. **Prenatal growth and development of the modern human labyrinth.** *J Anat* 2004;204:71–92 CrossRef Medline
30. Matsunaga T, Hirota E. **Familial lateral semicircular canal malformation with external and middle ear abnormalities.** *Am J Med Genet A* 2003;116A:360–67 CrossRef Medline
31. Johnson J, Lalwani AK. **Sensorineural and conductive hearing loss associated with lateral semicircular canal malformation.** *Laryngoscope* 2000;110:1673–79 CrossRef Medline
32. Michel G, Espitalier F, Delemazure AS, et al. **Isolated lateral semicircular canal aplasia: functional consequences.** *Eur Ann Otorhinolaryngol Head Neck Dis* 2016;133:199–201 CrossRef Medline
33. Oskarsdóttir S, Belfrage M, Sandstedt E, et al. **Disabilities and cognition in children and adolescents with 22q11 deletion syndrome.** *Dev Med Child Neurol* 2005;47:177–84 CrossRef Medline
34. Roizen NJ, Higgins AM, Antshel KM, et al. **22q11.2 deletion syndrome: are motor deficits more than expected for IQ level?** *J Pediatr* 2010;157:658–61 CrossRef Medline
35. Sobin C, Monk SH, Kiley-Brabeck K, et al. **Neuromotor deficits in children with the 22q11 deletion syndrome.** *Mov Disord* 2006;21:2082–89 CrossRef Medline
36. Van Aken K, De Smedt B, Van Roie A, et al. **Motor development in school-aged children with 22q11 deletion (velocardiofacial/DiGeorge syndrome).** *Dev Med Child Neurol* 2007;49:210–13 CrossRef Medline
37. Roizen NJ, Antshel KM, Fremont W, et al. **22q11.2DS deletion syndrome: developmental milestones in infants and toddlers.** *J Dev Behav Pediatr* 2007;28:119–24 CrossRef Medline
38. Gerdes M, Solot C, Wang PP, et al. **Cognitive and behavior profile of preschool children with chromosome 22q11.2 deletion.** *Am J Med Genet* 1999;85:127–33 Medline
39. Swillen A, Devriendt K, Legius E, et al. **The behavioural phenotype in velo-cardio-facial syndrome (VCFS): from infancy to adolescence.** *Genet Couns* 1999;10:79–88 Medline
40. Sennaroglu L, Saatci I. **A new classification for cochleovestibular malformations.** *Laryngoscope* 2002;112:2230–41 CrossRef Medline
41. Raft S, Nowotschin S, Liao J, et al. **Suppression of neural fate and control of inner ear morphogenesis by Tbx1.** *Development* 2004;131:1801–12 CrossRef Medline
42. Braunstein EM, Monks DC, Aggarwal VS, et al. **Tbx1 and Brn4 regulate retinoic acid metabolic genes during cochlear morphogenesis.** *BMC Dev Biol* 2009;9:31 CrossRef Medline
43. Monks DC, Morrow BE. **Identification of putative retinoic acid target genes downstream of mesenchymal Tbx1 during inner ear development.** *Dev Dyn* 2012;241:563–73 CrossRef Medline
44. Jerome LA, Papaioannou VE. **DiGeorge syndrome phenotype in mice mutant for the T-box gene, Tbx1.** *Nat Genet* 2001;27:286–91 CrossRef Medline
45. Moreano E, Paparella M, Zeltermann D, et al. **Prevalence of carotid canal dehiscence in the human middle ear: a report of 1000 temporal bones.** *Laryngoscope* 1994;104:612–18 CrossRef Medline
46. Wang CH, Shi ZP, Liu DW, et al. **High computed tomographic correlations between carotid canal dehiscence and high jugular bulb in the middle ear.** *Audiol Neurotol* 2011;16:106–12 CrossRef Medline
47. Derbent M, Yilmaz Z, Baltaci V, et al. **Chromosome 22q11.2 deletion and phenotypic features in 30 patients with conotruncal heart defects.** *Am J Med Genet A* 2003;116A:129–35 CrossRef Medline
48. Digilio MC, McDonald-McGinn DM, Heike C, et al. **Three patients with oculo-auriculo-vertebral spectrum and microdeletion 22q11.2.** *Am J Med Genet A* 2009;149A:2860–64 CrossRef Medline
49. Sleifer P, Gorsky Nde S, Goetze TB, et al. **Audiological findings in patients with oculo-auriculo-vertebral spectrum.** *Int Arch Otorhinolaryngol* 2015;19:5–9 CrossRef Medline
50. Baldini A. **Dissecting contiguous gene defects: TBX1.** *Curr Opin Genet Dev* 2005;15:279–84 CrossRef Medline

Brain Diffusion Abnormalities in Children with Tension-Type and Migraine-Type Headaches

J.D. Santoro, N.D. Forkert, Q.-Z. Yang, S. Pavitt, S.J. MacEachern, M.E. Moseley, and K.W. Yeom

ABSTRACT

BACKGROUND AND PURPOSE: Tension-type and migraine-type headaches are the most common chronic paroxysmal disorders of childhood. The goal of this study was to compare regional cerebral volumes and diffusion in tension-type and migraine-type headaches against published controls.

MATERIALS AND METHODS: Patients evaluated for tension-type or migraine-type headache without aura from May 2014 to July 2016 in a single center were retrospectively reviewed. Thirty-two patients with tension-type headache and 23 with migraine-type headache at an average of 4 months after diagnosis were enrolled. All patients underwent DWI at 3T before the start of pharmacotherapy. Using atlas-based DWI analysis, we determined regional volumetric and diffusion properties in the cerebral cortex, thalamus, caudate, putamen, globus pallidus, hippocampus, amygdala, nucleus accumbens, brain stem, and cerebral white matter. Multivariate analysis of covariance was used to test for differences between controls and patients with tension-type and migraine-type headaches.

RESULTS: There were no significant differences in regional brain volumes between the groups. Patients with tension-type and migraine-type headaches showed significantly increased ADC in the hippocampus and brain stem compared with controls. Additionally, only patients with migraine-type headache showed significantly increased ADC in the thalamus and a trend toward increased ADC in the amygdala compared with controls.

CONCLUSIONS: This study identifies early cerebral diffusion changes in patients with tension-type and migraine-type headaches compared with controls. The hypothesized mechanisms of nociception in migraine-type and tension-type headaches may explain the findings as a precursor to structural changes seen in adult patients with chronic headache.

ABBREVIATIONS: ICHD-3 = International Classification of Headache Disorders, Version 3.0; MTH = migraine-type headache; TTH = tension-type headache

Migraine-type headache (MTH) is a common and chronic condition with multifactorial neurovascular etiologies characterized by recurrent paroxysmal attacks of throbbing headache with or without autonomic nervous system dysfunction.¹ Along with tension-type headache (TTH), these are the most common paroxysmal disorders of childhood. Neuroimaging in

these conditions is frequently low yield for clinically relevant findings, with most studies not affecting clinical management.^{2,3}

Neuroimaging in adult patients with MTH with aura has previously demonstrated evidence of subcortical lesions in the deep white matter on DWI.⁴⁻⁷ These studies have been replicated in pediatric populations with similar results and have also identified volumetric white matter changes throughout the brain.⁸ The typical fingerprint of degenerated neuronal tissue is an increase of ADC. However, previous studies investigating diffusion properties in the brain have yielded variable, often transient, findings in adults.^{5,9,10} Given the chronic activation of nociceptive circuits in TTH and MTH and the possible vascular component of MTH, whether these entities are associated with global or regional ADC alterations in the brain tissue is unknown.

In this study, we conducted a retrospective, cross-sectional analysis of changes in the ADC and regional brain volume in various cerebral regions in healthy pediatric controls and in patients with TTH and MTH younger than 18 years of age with prior

Received October 27, 2017; accepted after revision January 1, 2018.

From the Department of Neurology (J.D.S., Q.-Z.Y., S.P.), Division of Child Neurology, and Department of Radiology (M.E.M.), Stanford University School of Medicine, Stanford, California; Departments of Radiology (N.D.F.) and Pediatrics (S.J.M.), Cumming School of Medicine, University of Calgary, Alberta, Canada; and Department of Radiology (K.W.Y.), Lucile Packard Children's Hospital, Stanford University, Stanford, California.

Paper previously presented in part at: Annual Meeting of the Child Neurology Society, October 4–7, 2017; Kansas City, Missouri.

Please address correspondence to Kristen Yeom, MD, Department of Radiology, Lucile Packard Children's Hospital at Stanford, Stanford University School of Medicine, 725 Welch Rd, MC 5654, Palo Alto, CA 94304; e-mail: kyeom@stanford.edu

<http://dx.doi.org/10.3174/ajnr.A5582>

anatomically normal neuroimaging examination findings. We hypothesized that pediatric patients with MTH would differ from healthy controls and patients with TTH in regional ADC properties in limbic and brain stem structures due to the presumed differences in the pathophysiology of TTH and MTH.

MATERIALS AND METHODS

Patient Cohorts

All patients evaluated for TTH or MTH from May 2014 to July 2016 in the pediatric neurology clinics at the Lucile Packard Children's Hospital at Stanford University were retrospectively reviewed after approval by the institutional review board. Because this was a retrospective review, our institutional review board waived the requirement of informed consent. The study cohort was identified using the following inclusion criteria: age 18 years or younger and diagnostic criteria that fit either TTH or MTH as defined by International Classification of Headache Disorders, Version 3.0 (ICHD-3), excluding migraine with brain stem aura, hemiplegic migraine, and retinal migraine (Appendix).¹ Only patients without any prior treatment with prescription medication who underwent diffusion-weighted MR imaging at 3T (as a standard protocol) following initial consultation but before the start of treatment were included. Prior neuroimaging findings must have been read as normal and included no incidental findings or abnormalities (eg, unidentified bright objects, developmental venous anomaly, or Chiari I abnormality). The patients had varying times between diagnosis and neuroimaging. Some patients had multiple neuroimaging examinations, in which case the most recent scan was selected for analysis to ensure consistency. Time to last headache was not collected (not feasible for this retrospective review), but patients' MR imaging intake records were reviewed to exclude patients with active headache or migraine.

Strict exclusion criteria were applied and comprised the following: inadequate data or image-registration quality, any concern for secondary headache, current or prior history of developmental delay, history of medication-overuse headache, underlying cardiac disease, epilepsy, prior or current hemorrhage, vascular lesions (aneurysm, AVM, fistula, or steno-occlusive disease), or prior strokes, given their potential impact on regional diffusion properties in the brain. Additionally, any patient with a previously diagnosed genetic, metabolic, or medical disease was excluded from this study. Patients with any focal neurologic findings, even if incidental, were excluded.

The control group consisted of 100 children with no known neurologic, neurocognitive, developmental, or behavioral deficits who had normal-appearing brains on MR imaging. Control subjects were imaged as a standard of care for evaluation of syncope, nausea, family history of aneurysm or cancers, scalp nevus, isolated facial lesions, orbital strabismus, cholesteatoma of the ear, any neurologic symptoms or deficits, sinus disease or inflammatory nasal obstruction, and familial short stature. This control group study population has been previously described.¹¹

MR Imaging Acquisition

All subjects underwent brain MR imaging at 3T (Discovery 750W; GE Healthcare, Milwaukee, Wisconsin) with an 8-channel head coil on a single MR imaging scanner. Echo-planar whole-brain

DWI was acquired in all cases with TR = 1500 ms, TE = 37 ms, flip angle = 90°, FOV = 24 cm², acceleration factor = 2, in-plane resolution = 0.94 mm², acquisition matrix = 128 × 128 interpolated to a 256 × 256 matrix, 44 sections with 4-mm slice thickness, no skip, 2 diffusion-weightings of $b=0$ s/mm² and $b=1000$ s/mm², with diffusion gradients acquired in 3 directions averaged for the latter. ADC, derived from DWI, has demonstrated high reproducibility and was performed as part of routine institutional neuroimaging.¹²

Image Processing

A custom image-processing pipeline was used in this work to extract quantitative values of regional brain volume and ADC values, previously described in more detail by Forkert et al.¹¹ Briefly described, after motion correction of the DWI dataset acquired with and without diffusion-weighting by rigid registration, the quantitative apparent diffusion coefficient parameter map was calculated using a Stejskal-Tanner equation.¹³ For regional diffusion and volumetric analysis, the Montreal Neurological Institute-152 brain atlas was nonlinearly registered to the DWI dataset and the resulting transformation was used to warp the Harvard-Oxford subcortical atlas brain regions to the subject-specific brain anatomy.¹⁴ Brain regions included in this brain atlas are the cerebral cortex, cerebral white matter, thalamus, caudate, putamen, globus pallidus, amygdala, hippocampus, brain stem, and nucleus accumbens. Two experienced observers checked all registration results to ensure suitable data and registration quality. The aligned brain atlas regions were then used to measure the corresponding regional brain volumes and median ADC values combined for corresponding brain structures in the left and right hemispheres, whereas the lateral ventricles were only used for volumetric assessment.

Statistical Analysis

Multivariate analysis of covariance was used for group comparison of the control group and children with MTH and TTH using the volumetric and median ADC values as dependent variables, age as a covariate, and the class (control/TTH/MTH) as the fixed factor. SPSS (Version 24.0, IBM, Armonk, NY) was used for MANCOVA statistical analyses. A P value < .05 (Bonferroni-corrected) was considered significant.

In addition to the statistical analysis described above, plots with age-related fifth, 10th, 25th, 50th, 75th, 90th, and 95th quantile curves determined using local piecewise regression analysis based on the quantitative analysis of the control cohort were generated individually for each brain structure and parameter along with the corresponding data points extracted from the children with MTH and TTH.¹⁵ The plots were generated using the R statistical software package of The R Foundation of Statistical Computing (Version 3.2.2; www.r-project.org).

RESULTS

Clinical Characteristics

A total of 214 patients with TTH or MTH were reviewed for inclusion in this study. Seventy-four patients (35%) were excluded due to medical comorbidity; 51 (24%), due to secondary or medication overuse-type headache; 25 (12%), due to abnormal neu-

Demographics and diffusion and volumetric analysis by region

	Control (n = 100)	TTH (n = 31)	MTH (n = 23)
Demographics			
Median age (range) (mo)	98 (4–213)	99 (24–209)	83 (12–212)
Sex (M/F)	36:64	13:18	6:17
Family history of any headache (No.) (%)		6 (19%)	10 (43%)
ADC on neuroimaging ([mean $\times 10^{-6}$ mm ² /s], standard error, ^a P value vs control)			
Cerebral cortex	899.05 (3.44)	901.78 (7.04) >.5	907.29 (8.22) >.5
Thalamus	812.48 (3.51)	815.44 (6.26) >.5	833.11 (7.11) .045 ^b
Caudate	815.16 (3.98)	821.42 (7.11) >.5	833.99 (8.64) .149
Putamen	799.94 (3.48)	792.42 (6.21) >.5	800.75 (7.55) >.5
Pallidum	836.62 (4.05)	822.09 (7.22) .24	838.30 (8.78) >.5
Hippocampus	935.52 (4.50)	965.45 (8.03) .013 ^b	970.46 (9.76) .038 ^b
Amygdala	885.83 (3.79)	882.75 (6.78) >.5	904.48 (8.24) .113
Nucleus accumbens	856.83 (4.72)	841.45 (8.43) .34	850.75 (8.43) >.5
Brain stem	806.72 (3.43)	825.01 (6.13) .05 ^b	840.71 (7.45) <.001 ^b
Volume on neuroimaging (mean [in mL], standard error, ^a P value vs control)			
Cerebral cortex	344.33 (4.19)	350.56 (3.92) >.5	362.54 (9.08) .212
Thalamus	6.62 (0.08)	5.54 (0.12) .148	5.71 (0.15) >.5
Caudate	2.68 (0.04)	2.64 (0.06) >.5	2.71 (0.08) >.5
Putamen	4.49 (0.06)	4.46 (0.06) >.5	4.63 (0.12) >.5
Pallidum	1.46 (0.02)	1.42 (0.03) >.5	1.50 (0.04) >.5
Hippocampus	3.10 (0.04)	3.07 (0.07) >.5	3.21 (0.08) >.5
Amygdala	1.53 (0.02)	1.55 (0.04) >.5	1.59 (0.04) >.5
Nucleus accumbens	0.37 (0.01)	0.38 (0.04) >.5	0.039 (0.01) >.5
Brain stem	22.79 (0.30)	22.51 (0.53) .108	22.97 (0.64) >.5

^a Means and standard error were corrected to an age of 97 months in all groups.

^b Significant.

roimaging findings; and 10 (5%), due to developmental delay. Twenty-three patients with MTH (median age, 83 months; ranging from 30 to 212 months), 31 patients with TTH (median age, 99 months; ranging from 32 to 209 months), and 100 controls (median age, 98 months; ranging from 4 to 213 months) were included in this study. Thirteen males and 18 females were in the TTH group, and 6 males and 17 females were in the MTH group (Table). None of the patients had aura-preceding onset of symptoms at the time of diagnosis.

Statistical Analysis

The MANCOVA analysis using the volume and median ADC values as dependent variables, age as a covariate, and the class as a fixed factor revealed a statistically significant difference among patients with MTH, patients with TTH, and healthy controls ($P < .001$). A secondary MANCOVA did not reveal a statistical difference between patients with MTH and patients with TTH, indicating that both headache types are represented by similar imaging findings compared with healthy controls regarding both volume and diffusion metrics.

In pair-wise analysis, no statistically significant differences regarding the volume of the cerebral cortex, cerebral white matter, thalamus, caudate, putamen, globus pallidus, amygdala, hippocampus, brain stem, and nucleus accumbens were found among patients with MTH, those with TTH, and controls ($P > .135$).

Post hoc pair-wise analysis of the median ADC values revealed significant differences in ADC for the hippocampus and brain stem. More precisely, patients with TTH ($P = .013$) and those with MTH ($P = .038$) showed significantly increased ADC values

in the hippocampus compared with healthy controls (age-corrected means: MTH, $962.6 \pm 9.6 \times 10^{-6}$ mm²/s; TTH, $963.2 \pm 8.2 \times 10^{-6}$ mm²/s; controls, $935.8 \pm 4.6 \times 10^{-6}$ mm²/s). Likewise, patients with TTH ($P = .05$) and patients with MTH ($P < .001$) showed significantly increased ADC values in the brain stem compared with healthy controls (age-corrected means: MTH, $838.3 \pm 7.2 \times 10^{-6}$ mm²/s; TTH, $824.2 \pm 6.1 \times 10^{-6}$ mm²/s; controls, $807.2 \pm 3.4 \times 10^{-6}$ mm²/s). Additionally, patients with MTH were noted to have increased ADC in the thalamus compared with controls ($P = .045$; MTH, $833.1 \pm 7.1 \times 10^{-6}$ mm²/s; controls, $812.5 \pm 3.5 \times 10^{-6}$ mm²/s). No other parameter reached a statistically significant difference among groups (Table).

Qualitative Analysis

The results of the statistical evaluation can be also confirmed by visual analysis of the plots generated using local piecewise regression analysis (Figure). Overall, no obvious difference between patients with MTH (red dots) and TTH (blue boxes) is obvious for any parameter analyzed. The plots clearly show the significantly increased ADC values in the hippocampus and brain stem in patients with MTH and TTH compared with healthy controls, while no clear difference is obvious for any other parameter.

DISCUSSION

We hypothesized that patients with MTH may exhibit different diffusion values in the limbic and brain stem circuitry compared with those with TTH and healthy controls, given the underlying differences in pathophysiology of patients with MTH and TTH. Most interesting, this study identified increased diffusion patterns

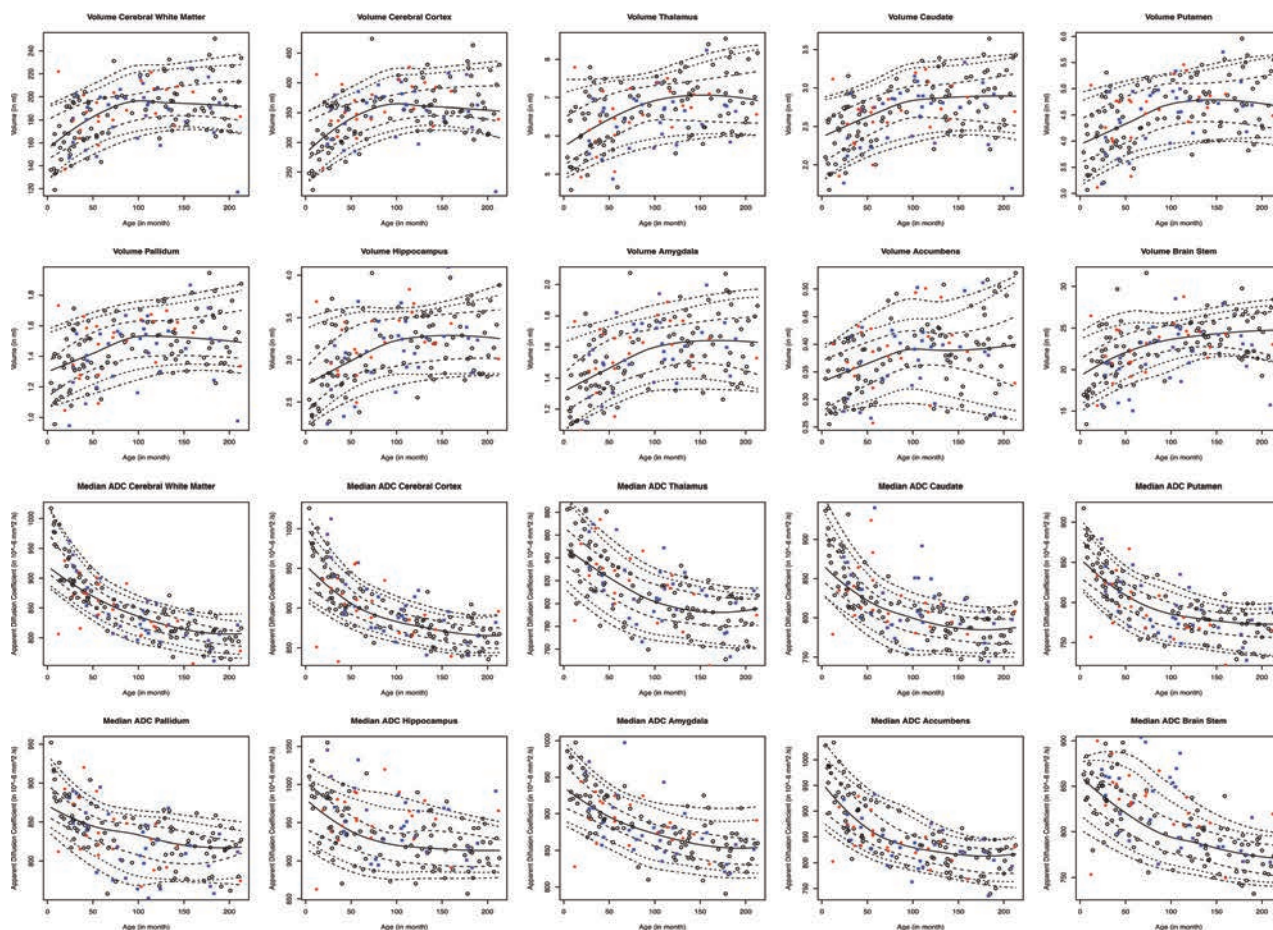


FIGURE. Visual analysis of all plots generated using local piecewise regression analysis for healthy control children (*black circles*) and patients with TTH (*blue boxes*) and MTH (*red dots*).

in those with both TTH and MTH in the hippocampus and brain stem as well as in the thalamus in only those with MTH compared with controls, without any concurrent volume abnormalities. These regions are involved with both pain nociception circuitry and the limbic system, which has been previously implicated in the perception of pain in adult patients with MTH at the functional, mechanistic, and electrophysiologic levels.^{16,17} The involvement of TTH abnormalities, which was unexpected, indicates that diffusion abnormalities in the hippocampus and thalamus may potentially reflect enhanced pain circuitry as opposed to intrinsic pathophysiologic differences between MTH and TTH.

This study is the first to describe early ADC diffusion changes in several areas involved in the limbic circuit in pediatric patients with MTH and TTH. While no volumetric abnormalities were identified, the median age of patients with MTH and TTH was 83 months and 99 months, respectively, which is younger than the median age of 168 months in a prior study.⁸ This finding may explain the lack of volumetric change in our cohort.⁸ Therefore, the difference in age between these 2 study groups may suggest that the early diffusion changes found in this work may become more pronounced with continued headaches and manifest as volumetric abnormalities into adolescence and adulthood.⁵⁻⁸

Of specific interest in our study was the involvement of the brain stem in patients with MTH and TTH. Mechanistically, this

area of the brain has bidirectional connections between the diencephalic structures and the trigeminovascular system, which could either be activated by these areas or be a primary pacer for activation of these structures.¹⁸ Increased flow and activation of the brain stem on PET imaging have been previously observed in adult patients with MTH, indicating another potential component in MTH pain circuitry.¹⁹ Finally, while this area has been identified in previous studies to be functionally activated in acute migraine, long-standing diffusion changes have not been previously identified in pediatric patients.^{19,20}

The hippocampus has been previously noted to exhibit reduced volume in adult patients with high-frequency TTH and MTH.^{21,22} The thalamus seemed to be only significantly altered in patients with MTH in this study, though recently published reports have identified the significance of this brain region as a functional pain-signaling relay.^{23,24} Additionally, the thalamus volume has been found to be altered in patients with medication overuse headache and MTH with and without aura.²³⁻²⁵ The amygdala has also been demonstrated to have volumetric decreases in patients with chronic MTH, demonstrating an inverse relationship to the frequency of migraine.²⁶ These structures are more prominently implicated in the limbic circuitry, which is presumed to be more related to pain perception than pain sensation.^{18,24} Both the hippocampus and amygdala are bidirectionally linked to the brain stem and thalamus; thus, the involvement of

these structures in our study may demonstrate functional preanatomic linkage in migraine physiology. Our findings may indicate a propensity toward volumetric abnormalities in adulthood in patients previously reported with long-standing diffusion abnormalities beginning in childhood, though this propensity requires further investigation. The isolated significance of the thalamus in MTH compared with TTH and controls in our study is consistent with prior studies that have not demonstrated involvement of this region in TTH and may be a more specific factor in migraine, given previously established thalamocortical circuitry in experience processing.^{25,27}

There are several limitations to this study. As a retrospective case-control study, we can only speculate on differences at a single time point. Both the TTH and MTH groups are small, given that this is a single-center study, but the large number of healthy controls allows a unique comparison. Additionally, although validated in pediatric patients, the International Classification of Headache Disorders, Version 3.0 criteria has come under scrutiny for both under- and overdiagnosis of paroxysmal pain disorders in this patient population.²⁸ As a retrospective review, there is the risk of diagnostic inaccuracy, specifically less severe migraine headache diagnosed as tension-type headache. Furthermore, there are no clinical data to correlate the imaging findings with headache severity, because more severe or protracted headaches could potentially demonstrate greater diffusion changes. Furthermore, our inclusion criteria of head imaging before starting treatment might result in a bias toward more severe headache phenotypes. Because previous studies have indicated that diffusion findings may be transient in adults, whether the patient was having a headache at the time of scanning or near the time of scanning may affect the quantitative imaging findings.^{5,9,10} For analysis, we combined data from both the left and right hemispheres to reduce the number of hypotheses tested, which omitted trends in laterality. In addition, we recognize that segmentation of small cerebral structures can be imperfect, but an automated approach (with visual quality control) was used to ensure reproducibility, given that manual segmentation is prone to observer bias. A final limitation of this study is that we did not assess patients with MTH with aura. This assessment was not performed due to the lower prevalence of "pure" MTH with aura and higher rates of mixed-type MTH in pediatric populations.²⁹⁻³¹

CONCLUSIONS

This study identifies early cerebral diffusion changes in patients with TTH and MTH compared with healthy children. The hypothesized underlying pathophysiologic mechanisms of nociception in MTH and TTH may help explain this finding and may be a precursor to the structural changes seen in adult patients with chronic pain syndromes and MTH.

APPENDIX

Criteria for Diagnosis of Tension-Type Headache

1) Infrequent episodic tension-type headache

- a) At least 10 episodes of headache occurring on <1 day per month on average (<12 days per year) and fulfilling criteria b–d
- b) Lasting from 30 minutes to 7 days
- c) At least 2 of the following 4 characteristics:

- i) Bilateral location
 - ii) Pressing or tightening (nonpulsating) quality
 - iii) Mild or moderate intensity
 - iv) Not aggravated by routine physical activity such as walking or climbing stairs
 - d) Both of the following criteria:
 - i) No nausea or vomiting
 - ii) No more than 1 of photophobia or phonophobia
 - e) Not better accounted for by another ICHD-3 diagnosis
- #### 2) Frequent episodic tension-type headache
- a) At least 10 episodes of headache occurring on 1–14 days per month on average for >3 months (>12 and <180 days per year) and fulfilling criteria b–d
 - b) Lasting 30 minutes to 7 days
 - c) At least 2 of the following 4 characteristics:
 - i) Bilateral location
 - ii) Pressing or tightening (nonpulsating) quality
 - iii) Mild or moderate intensity
 - iv) Not aggravated by routine physical activity such as walking or climbing stairs
 - d) Both of the following criteria:
 - i) No nausea or vomiting
 - ii) No more than 1 of photophobia or phonophobia
 - e) Not better accounted for by another ICHD-3 diagnosis
- #### 3) Chronic tension-type headache
- a) Headache occurring on >15 days per month on average for >3 months (>180 days per year) and fulfilling criteria b–d
 - b) Lasting hours to days, or unremitting
 - c) At least 2 of the following 4 characteristics:
 - i) Bilateral location
 - ii) Pressing or tightening (nonpulsating) quality
 - iii) Mild or moderate intensity
 - iv) Not aggravated by routine physical activity such as walking or climbing stairs
 - d) Both of the following criteria:
 - i) No nausea or vomiting
 - ii) No more than 1 of photophobia or phonophobia
 - e) Not better accounted for by another ICHD-3 diagnosis
- #### 4) Probable tension-type headache
- a) Tension-type-like headache missing 1 of the features required to fulfill all criteria for a subtype of tension-type headache coded above, and not fulfilling the criteria for another headache disorder.

Criteria for Diagnosis of Migraine-Type Headache

1) Migraine without aura

- a) At least 5 attacks fulfilling criteria b–d
- b) Headache attacks lasting 4–72 hours (untreated or unsuccessfully treated)
- c) Headache has at least 2 of the following 4 characteristics:
 - i) Unilateral location
 - ii) Pulsating quality
 - iii) Moderate or severe pain intensity
 - iv) Aggravation by or causing avoidance of routine physical activity (eg, walking or climbing stairs)
- d) During headache at least 1 of the following:
 - i) Nausea and/or vomiting

- ii) Photophobia and phonophobia
 - e) Not better accounted for by another ICHD-3 diagnosis
- 2) Migraine with aura
 - a) At least 2 attacks fulfilling criteria b and c
 - b) One or more of the following fully reversible aura symptoms:
 - i) Visual
 - ii) Sensory
 - iii) Speech and/or language
 - iv) Motor
 - v) Brain stem
 - vi) Retinal
 - c) At least 2 of the following 4 characteristics:
 - i) At least 1 aura symptom spreading gradually for >5 minutes and/or ≥ 2 symptoms occurring in succession
 - ii) Each individual aura symptom lasting 5–60 minutes
 - iii) At least 1 unilateral aura symptom
 - iv) The aura accompanied or followed within 60 minutes by headache
 - d) Not better accounted for by another ICHD-3 diagnosis, and transient ischemic attack excluded
- 3) Chronic migraine
 - a) Headache (tension-type-like and/or migraine-like) on >15 days per month for >3 months and fulfilling criteria b and c
 - b) Occurring in a patient who has had at least 5 attacks fulfilling criteria b–d for either migraine without aura and/or criteria b and c for migraine with aura
 - c) On >8 days per month for >3 months, fulfilling any of the following:
 - i) Criteria c and d for migraine without aura
 - ii) Criteria b and c for migraine with aura
 - iii) Believed by the patient to be migraine at onset and relieved by a triptan or ergot derivative
 - d) Not better accounted for by another ICHD-3 diagnosis
- 4) Probable migraine
 - a) Attacks fulfilling all but 1 of the criteria a–d for migraine without aura or all but 1 of the criteria a–c for migraine with aura
 - b) Not fulfilling the ICHD-3 criteria for any other headache disorder
 - c) Not better accounted for by another ICHD-3 diagnosis.

ACKNOWLEDGMENTS

We wish to thank the Division of Child Neurology for their support in the production of this article.

Disclosures: Nils Daniel Forkert—UNRELATED: Grants/Grants Pending: Natural Sciences and Engineering Research Council of Canada; National Institutes of Health, Heart and Stroke Foundation; MS Society.*Money paid to the institution.

REFERENCES

1. Headache Classification Committee of the International Headache Society (IHS). **International Classification of Headache Disorders, 3rd edition (beta version)**. *Cephalalgia* 2013;33:629–808 CrossRef Medline
2. Lewis DW, Dorbad D. **The utility of neuroimaging in the evaluation of children with migraine or chronic daily headache who have normal neurologic examinations**. *Headache* 2000;40:629–32 CrossRef Medline
3. Schwedt TJ, Guo Y, Rothner AD. **“Benign” imaging abnormalities in children and adolescents with headache**. *Headache* 2006;46:387–98 CrossRef Medline
4. Fazekas F, Koch M, Schmidt R, et al. **The prevalence of cerebral damage varies with migraine type: a MRI study**. *Headache* 1992;32:287–91 Medline
5. Jäger HR, Griffin NJ, Goadsby PJ. **Diffusion and perfusion weighted MR imaging in persistent migrainous visual disturbances**. *Cephalalgia* 2005;25:323–32 Medline
6. Oberndorfer S, Wober C, Nasel C, et al. **Familial hemiplegic migraine: follow-up findings of diffusion-weighted magnetic resonance imaging (MRI), perfusion-MRI and [99mTc] HMPAO-SPECT in a patient with prolonged hemiplegic aura**. *Cephalalgia* 2004;24:533–39 Medline
7. Rocca MA, Colombo B, Pratesi A, et al. **A magnetization transfer imaging study of the brain in patients with migraine**. *Neurology* 2000;54:507–09 Medline
8. Messina R, Rocca MA, Colombo B, et al. **White matter microstructure abnormalities in pediatric migraine patients**. *Cephalalgia* 2015;35:1278–86 CrossRef Medline
9. Degirmenci B, Yaman M, Haktanir A, et al. **Cerebral and cerebellar ADC values during a migraine attack**. *Neuroradiology* 2007;49:419–26 CrossRef Medline
10. Belvis R, Ramos R, Villa C, et al. **Brain apparent water diffusion coefficient magnetic resonance imaging during a prolonged visual aura**. *Headache* 2010;50:1045–49 CrossRef Medline
11. Forkert ND, Li MD, Lober RM, et al. **Gray matter growth is accompanied by increasing blood flow and decreasing apparent diffusion coefficient during childhood**. *AJNR Am J Neuroradiol* 2016;37:1738–44 CrossRef Medline
12. Grech-Sollars M, Hales PW, Miyazaki K, et al. **Multi-centre reproducibility of diffusion MRI parameters for clinical sequences in the brain**. *NMR Biomed* 2015;28:468–85 CrossRef Medline
13. Stejskal EO, Tanner JE. **Spin diffusion measurements: spin echoes in the presence of a time-dependent field gradient**. *Journal of Chemical Physics* 1965;42:288–92
14. Mazziotta J, Toga A, Evans A, et al. **A probabilistic atlas and reference system for the human brain: International Consortium for Brain Mapping (ICBM)**. *Philos Trans R Soc Lond B Biol Sci* 2001;356:1293–322 CrossRef Medline
15. Sakov A, Golani I, Lipkind D, et al. **High-throughput data analysis in behavior genetics**. *Ann Appl Stat* 2010;4:743–63 CrossRef
16. Wilcox SL, Veggeberg R, Lemme J, et al. **Increased functional activation of limbic brain regions during negative emotional processing in migraine**. *Front Hum Neurosci* 2016;10:366 CrossRef Medline
17. Demarquay G, Mauguière F. **Central nervous system underpinnings of sensory hypersensitivity in migraine: insights from neuroimaging and electrophysiological studies**. *Headache* 2016;56:1418–38 CrossRef Medline
18. Akerman S, Holland PR, Goadsby PJ. **Diencephalic and brain-stem mechanisms in migraine**. *Nat Rev Neurosci* 2011;12:570–84 CrossRef Medline
19. Cutrer FM, O'Donnell A, Sanchez del Rio M. **Functional neuroimaging: enhanced understanding of migraine pathophysiology**. *Neurology* 2000;55(9 suppl 2):S36–45 Medline
20. Weiller C, May A, Limmroth V, et al. **Brain stem activation in spontaneous human migraine attacks**. *Nat Med* 1995;1:658–60 CrossRef Medline
21. Maleki N, Becerra L, Brawn J, et al. **Common hippocampal structural and functional changes in migraine**. *Brain Struct Funct* 2013;218:903–12 CrossRef Medline
22. Schmidt-Wilcke T, Leinisch E, Straube A, et al. **Gray matter decrease in patients with chronic tension type headache**. *Neurology* 2005;65:1483–86 CrossRef Medline
23. Amin FM, Hougaard A, Magon S, et al. **Altered thalamic connectivity during spontaneous attacks of migraine without aura: a resting state fMRI study**. *Cephalalgia* 2017 Jan 1. [Epub ahead of print] CrossRef Medline
24. Magon S, May A, Stankewitz A, et al. **Morphological abnormalities**

- of thalamic subnuclei in migraine: a multicenter MRI study at 3 Tesla. *J Neurosci* 2015;35:13800–06 [CrossRef Medline](#)
25. Chen Z, Jia Z, Chen X, et al. Volumetric abnormalities of thalamic subnuclei in medication overuse headache. *J Headache Pain* 2017; 18:82 [CrossRef Medline](#)
 26. Schmitz N, Admiraal-Behloul F, Arkink EB, et al. Attack frequency and disease duration as indicators for brain damage in migraine. *Headache* 2008;48:1044–55 [CrossRef Medline](#)
 27. Coppola G, Di Renzo A, Tinelli E, et al. Thalamo-cortical network activity between migraine attacks: insights from MRI-based microstructural and functional resting-state network correlation analysis. *J Headache Pain* 2016;17:100 [CrossRef Medline](#)
 28. Genizi J, Khourieh Matar A, Zelnik N, et al. Frequency of pediatric migraine with aura in a clinic-based sample. *Headache* 2016;56: 113–17 [CrossRef Medline](#)
 29. Split W, Neuman W. Epidemiology of migraine among students from randomly selected secondary schools in Lodz. *Headache* 1999; 39:494–501 [CrossRef Medline](#)
 30. Zwart JA, Dyb G, Holmen TL, et al. The prevalence of migraine and tension-type headaches among adolescents in Norway: the Nord-Trøndelag Health Study (Head-HUNT-Youth), a large population-based epidemiological study. *Cephalalgia* 2004;24:373–79 [CrossRef Medline](#)
 31. Fendrich K, Vennemann M, Pfaffenrath V, et al. Headache prevalence among adolescents: the German DMKG headache study. *Cephalalgia* 2007;27:347–54 [CrossRef Medline](#)

Congenital Aqueductal Stenosis: Findings at Fetal MRI That Accurately Predict a Postnatal Diagnosis

 K.J. Heaphy-Henault,  C.V. Guimaraes,  A.R. Mehollin-Ray,  C.I. Cassady,  W. Zhang,  N.K. Desai, and  M.J. Paldino



ABSTRACT

BACKGROUND AND PURPOSE: Congenital aqueductal stenosis is a common cause of prenatal ventriculomegaly. An accurate diagnosis provides prognostic information and may guide obstetric management. The purpose of this study was to identify specific anatomic findings on prenatal MR imaging that can be used as predictors of congenital aqueductal stenosis.

MATERIALS AND METHODS: Prenatal and postnatal MRIs of fetuses referred to our institution for ventriculomegaly between June 2008 and August 2015 were reviewed. Imaging findings in postnatally confirmed congenital aqueductal stenosis (disease group) were compared with those of ventriculomegaly cases from other causes (control group). Univariate analysis was performed using the Fisher exact test and the Wilcoxon rank test, and multivariate analysis, via the random forest method.

RESULTS: Forty-three cases of ventriculomegaly had a confirmed postnatal diagnosis of congenital aqueductal stenosis. Thirty-two ventriculomegaly cases negative for congenital aqueductal stenosis were included in the control group. Dominant findings associated with an accurate prenatal diagnosis of congenital aqueductal stenosis on multivariate analysis included the following: enlarged inferior third ventricular recesses, enlargement of the lateral ventricles and third ventricle, and an abnormal corpus callosum. Findings that significantly increase the probability of congenital aqueductal stenosis (high positive predictive value) included the following: enlarged third ventricular recesses, aqueduct funneling, hemorrhage in the cerebral aqueduct, ventricular diverticulum, rhombencephalosynapsis, and dystroglycanopathy-related cerebellar dysplasia.

CONCLUSIONS: Our study identified specific characteristics on fetal MR imaging that can be used as predictors of the diagnosis of congenital aqueductal stenosis. Most of these findings are secondary to the obstructive nature of the resulting hydrocephalus. Common associated malformations such as rhombencephalosynapsis and dystroglycanopathies should also increase the suspicion of congenital aqueductal stenosis when present with ventriculomegaly.

ABBREVIATION: CAS = congenital aqueductal stenosis

Ventriculomegaly is the most common CNS abnormality identified by prenatal imaging.^{1,2} Lateral ventricular atria diameter allows classification as mild (10–12 mm), moderate (12–15 mm), or severe (>15 mm).³ Severe ventriculomegaly has been associated with poor neurodevelopmental outcomes, the extent of which is related to the underlying etiology of the ventriculomegaly itself, including obstructive hydrocephalus,


parenchymal disruption, cerebral malformation, and the presence of coexisting anomalies.^{4,5} A study performed by Hannon et al⁴ demonstrated the incidence of severe ventriculomegaly to be 3.6 per 10,000 singleton births. Most cases are accompanied by other anomalies (nonisolated), as Nyberg et al⁶ demonstrated in their study, with 84% of patients having at least 1 major CNS malformation and/or extra-CNS anomaly.

Congenital aqueductal stenosis is a form of noncommunicating hydrocephalus in which a complete or partial obstruction of CSF flow at the aqueduct of Sylvius during fetal life results in dilation of the lateral and third ventricles and increased intracranial pressure. Given the obstructive nature of the hydrocephalus, progressive ventricular enlargement often occurs prenatally and may lead to delivery via cesarean section. This is different from nonobstructive causes of prenatal ventriculomegaly. Therefore, an accurate prenatal diagnosis is desirable because it may affect prognosis and obstetric management.

Received October 6, 2017; accepted after revision January 12, 2018.

From the Department of Radiology (K.J.H.-H.), Hartford Hospital, Hartford, Connecticut; Department of Radiology (C.V.G., A.R.M.-R., C.I.C., N.K.D., M.J.P.) and Outcomes and Impact Service (W.Z.), Texas Children's Hospital, Houston, Texas; and Department of Radiology (C.V.G.), Stanford University School of Medicine, Lucile Packard Children's Hospital, Stanford, California.

Please address correspondence to Carolina V. Guimaraes, MD, Stanford University School of Medicine, Department of Radiology, Lucile Packard Children's Hospital, 300 Pasteur Dr, Stanford, CA 94304; e-mail: cguimaraes@stanford.edu

 Indicates article with supplemental on-line tables.

<http://dx.doi.org/10.3174/ajnr.A5590>

Table 1: Imaging findings associated with AS

Direct Findings	Findings Secondary to Obstructive Hydrocephalus	Findings of Associated Malformations
Aqueduct funneling	Enlarged third ventricular recesses	Abnormal sulcation
Blood in the aqueduct	Enlarged ventricular temporal horns	Brain stem abnormality
Tectal thickening	Perforated septum pellucidum	Cerebellar hypoplasia
	Lateral ventricular diverticulum	Cerebellar dysplasia
	Callosal thinning and/or dysgenesis	Rhombencephalosynapsis
	Macrocephaly	Fourth ventricular dilation
		Vermian hypoplasia

Note:—AS indicates aqueductal stenosis.

Prior studies have cited congenital aqueductal stenosis (CAS) as a diagnosis of exclusion.⁷ However, we propose that there are specific MR imaging findings in the fetal CNS that allow a definitive diagnosis of CAS, both in isolated and nonisolated forms. Our goal was to analyze multiple prenatal MR imaging characteristics in fetuses with CAS and identify specific findings that will increase the prenatal accuracy for this diagnosis.

MATERIALS AND METHODS

Selection Criteria

This retrospective study was approved by the local institutional review board. Patients were identified from a data base of in-utero ventriculomegaly cases referred to our institution between June 2008 and August 2015. Inclusion in the study group was based on the following criteria: 1) prenatal ventriculomegaly, 2) existence of both pre- and postnatal brain MR imaging, and 3) diagnosis of aqueductal stenosis at postnatal imaging.

A control group of patients with ventriculomegaly not due to aqueductal stenosis was selected from the remaining cases on the basis of similar criteria: 1) prenatal ventriculomegaly, 2) existence of both pre- and postnatal brain MR imaging, and 3) postnatal imaging negative for CAS.

Visualization of the cerebral aqueduct on a sagittal high-resolution sequence of postnatal MR imaging was considered the reference standard for the diagnosis of aqueductal stenosis. Cases were considered positive when there was complete loss of aqueductal CSF signal at any level (obstruction) or when subjective stenosis was observed in association with the loss of the normal aqueductal luminal anatomy,^{8,9} such as seen with aqueductal funneling (dilation of the proximal aqueduct with distal narrowing). Cases suspected of CAS on prenatal MR imaging and not confirmed on postnatal imaging were ultimately included in the control group. Cases in which primary CAS could not be differentiated from compression by a large ventricular diverticulum or an enlarged third ventricular suprapineal recess were excluded from further analysis.

MR Imaging

Fetal MR imaging was performed on a 1.5T magnet (Achieva or Ingenia; Philips Healthcare, Best, the Netherlands). Postnatal MRIs were performed on both 1.5T and 3T magnets (Achieva or Ingenia; Philips Healthcare). Representative prenatal imaging protocols were as follows: 3-plane T2-weighted single-shot fast spin-echo, sagittal T2-weighted balanced steady-state free precession, and axial T1-weighted gradient echo, all at 3- to 4-mm slice thickness with no gap. All studies performed after 2010 also had axial DWI and axial EPI for the evaluation of ischemia and blood products, respectively. Postnatal imaging included sagittal T1-weighted, axial and coronal T2-

weighted, axial DWI, and axial gradient echo sequences. The sagittal T1-weighted sequence was performed as either routine resolution (4 mm, 1-mm gap) or high resolution (1-mm, no gap). Additional sagittal 3D high-resolution balanced steady-state free precession imaging (0.3-mm, no gap) was used when initial protocol did not include a high-resolution T1-weighted sequence or aqueduct patency was uncertain on the basis of initial sequences.

Image Review and Analysis

First, a catalog of imaging findings that might be expected to be relevant in aqueductal stenosis was generated on the basis of the literature.^{8,10} These categorical findings fell into 3 main categories: 1) direct findings related to aqueductal stenosis, 2) indirect findings related to obstructive hydrocephalus, and 3) findings related to associated malformations (Table 1).

Second, postnatal imaging in all subjects was reviewed, blinded to the initial interpretation, to assign each patient to either the CAS group or the control group. All imaging examinations were reviewed by 2 pediatric neuroradiologists (C.V.G. and N.K.D.) with dedicated subspecialty expertise in fetal neuroimaging and 9 and 7 years of post-training experience, respectively. Next, the 2 readers reviewed the prenatal MR imaging in all subjects for the presence/absence of each of the categorical findings described in Table 1. Discrepancies were settled by consensus. Enlarged inferior third ventricular recesses, aqueductal funneling, and tectal thickening were primarily evaluated on the sagittal plane. All other imaging findings were reviewed using a combination of all imaging sequences. Findings not adequately evaluated for any reason, including technical limitations (eg, excessive fetal motion or lack of adequate sequence), were tabulated as negative. In addition to the categorical findings, lateral and third ventricular dimensions were measured and recorded. Ventriculomegaly was defined as a width of >10 mm of the lateral ventricular atria at any gestation measured in the axial plane according to standard method.¹¹ Severe ventriculomegaly was defined as an atrial diameter of >15 mm.³ The third ventricle was measured on the coronal plane using the technique described by Garel¹² and Kline-Fath et al.¹³

Statistical Analysis

All statistical analyses were performed with R statistical and computing software, Version 3.0.2 (<http://www.r-project.org/>). First, univariate associations of individual categorical imaging findings with the diagnosis of aqueductal stenosis were assessed across all gestational ages and compared between the second and third trimester using the Fisher Exact test ($\alpha = .05$, corrected for multiple comparisons according to the Bonferroni method).¹⁴ In addition, sensitivity and specificity as well as the positive and negative predictive values of each imaging finding for the diagnosis of aqueductal stenosis were calculated using standard methods. Ventricular measurements in patients with aqueductal stenosis were compared with those of controls using the Wilcoxon rank sum test ($\alpha = .05$, corrected). Classification Tree Analysis¹⁵ was



FIG 1. Sagittal single-shot fast spin-echo sequence of a 32-week fetus demonstrating normal midline anatomy. Note the fully formed corpus callosum (white arrows), normal tectum (black arrow), a patent cerebral aqueduct with normal intraluminal proportions (white arrowhead), and a normal fourth ventricle (asterisk). Note also the normal expected midline morphology of the third ventricle (light gray shaded area) with normal supraoptic and infundibular third ventricular recesses (black arrowheads).

used to assess the optimal thresholds for the diagnosis of aqueductal stenosis based on lateral and third ventricular size. Finally, a multivariate analysis was used to quantify the importance of each prenatal imaging finding to the diagnosis of aqueductal stenosis using a random forest approach. Random forest is a machine-learning algorithm for classification and regression that uses multiple decision trees (decision forest) at training time in a random fashion. This method can estimate the independent contribution of an individual variable while accounting for the contribution of all the other studied variables.¹⁶

RESULTS

Patients

Seventy-five patients with ventriculomegaly met the criteria for inclusion. After blinded review of postnatal imaging, only a single case of suspected CAS prenatally was not confirmed on postnatal MR imaging and therefore was included in the control group. The final study group comprised 43 patients with CAS (gestational age range, 19–36 weeks; median age, 23 weeks), and the final control group comprised 32 cases of ventriculomegaly not related to CAS (gestational age range, 20–38 weeks; median age, 23 weeks). The CAS group included isolated ($n = 15$) and nonisolated ($n = 28$) cases of aqueductal stenosis. A normal sagittal midline view of the fetal brain and representative examples of findings seen in CAS are provided in Figs 1–6. A summary of the associated CNS abnormalities observed in the CAS group and in the ventriculomegaly control group is shown in On-line Table 1.

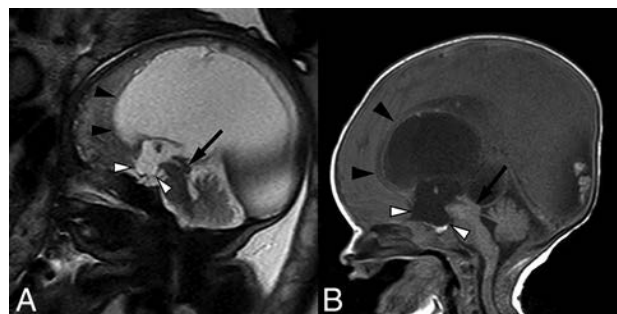


FIG 2. Sagittal balanced steady-state free precession sequence from fetal MR imaging (A) of a 33-week fetus and a postnatal sagittal T1-weighted sequence (B) of the same patient demonstrating stenosis of the inferior cerebral aqueduct with associated aqueductal funneling (arrow). As a result, there is marked enlargement of the lateral and third ventricles with dilation of the inferior third ventricular recesses (white arrowheads) depicted by bowing of the lamina terminalis and inferior third ventricular floor. The corpus callosum is thin and superiorly bowed (black arrowheads). Note also the normal size of the fourth ventricle.

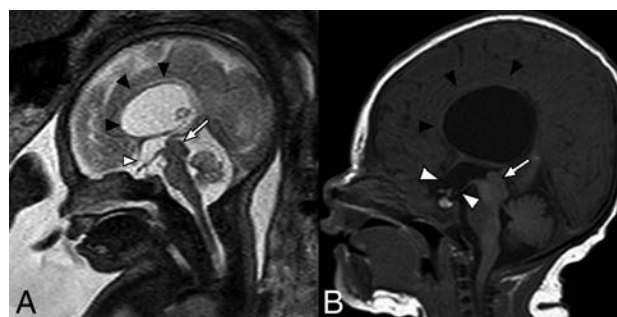


FIG 3. Fetal MR imaging of a 30-week fetus (A) and postnatal MR imaging correlation (B) of prenatally diagnosed aqueductal stenosis with tectal thickening and loss of intercollicular sulcus (arrows). There is subtle early prominence of the supraoptic recess of the third ventricle on fetal MR imaging (white arrowhead), which progressed to more obvious dilation of both supraoptic and infundibular recesses on postnatal imaging (white arrowheads). Note also the presence of a superiorly bowed and thinned corpus callosum (black arrowheads).

Prenatal MR Imaging Findings

The association of categorical prenatal MR imaging findings with CAS is summarized in Table 2. All relevant findings were observed across the range of gestational ages included in this study. Frequencies of each finding did not differ significantly when patients with aqueductal stenosis were imaged in the second trimester versus those imaged in the third trimester. Statistically significant findings associated with aqueductal stenosis at univariate analysis included the following: enlargement of the inferior recesses of the third ventricle ($P < .0023$), an abnormally thinned and/or dysgenetic corpus callosum ($P < .0023$), and the presence of a lateral ventricular diverticulum ($P = .0276$) (Figs 2–4). Along similar lines, enlargement of the third ventricular recesses and the presence of a lateral ventricular diverticulum were both highly specific (97% specificity) for a diagnosis of CAS (Table 2). Direct findings of stenosis of the aqueduct, including a funnel-shaped morphology of the aqueduct (Fig 2) and hemorrhage within the aqueduct (Fig 5), were also highly predictive of the diagnosis but rarely detected (100% positive predictive value; 48%/44% negative predictive value, respectively). Finally, ventriculomegaly in the setting of rhombencephalosynapsis (Fig 4) or dystroglycanopathy

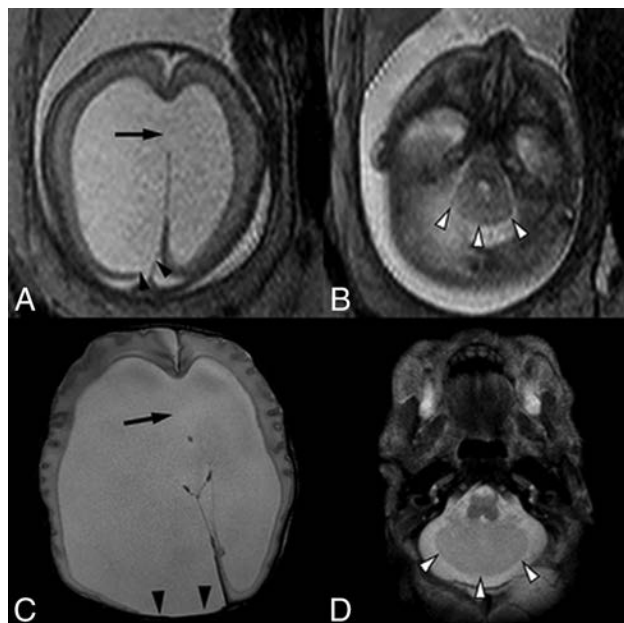


FIG 4. A single-shot fast spin-echo sequence in the axial planes (A and B) through the fetal head in a 23-week fetus and postnatal axial T2-weighted sequence (C and D) demonstrate asymmetric lateral ventriculomegaly with focal parenchymal disruption resulting in a posterior ventricular diverticulum (black arrowheads). Note also performance of the septum pellucidum in A and C (arrow). Within the posterior fossa (B and D), there are a small transverse cerebellar diameter, absence of the cerebellar vermis, midline fusion of cerebellar folia, and a convex posterior cerebellar contour (white arrowheads), compatible with rhombencephalosynapsis.

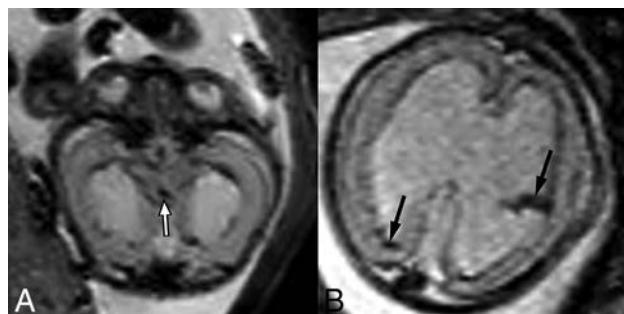


FIG 5. T2-weighted EPI sequences of 2 different fetuses with aqueductal stenosis demonstrating T2-hypointense hemorrhage within the cerebral aqueduct (A) in a 21-week fetus (white arrow) and within the lateral ventricles (B) in a 23-week fetus (black arrows).

(Fig 6) was highly likely to be related to CAS (100% positive predictive value).

On the other hand, the value of callosal abnormalities lies in their high negative predictive value (84%) and low specificity (50%) (Table 2). Most interesting, dilation of the temporal horns of the lateral ventricles, a finding seen with obstructive hydrocephalus, also demonstrated a high negative predictive value (80%) and low specificity (38%) for the diagnosis of CAS.

Third and lateral ventricular sizes were all significantly larger in patients with CAS than in ventriculomegaly controls (On-line Table 2). Classification Tree Analysis identified an optimal threshold of 14 mm for the size of the smaller lateral ventricle, meaning that a measurement of the smaller of the 2 lateral ventricles exceeding 14 mm was very likely to represent aque-

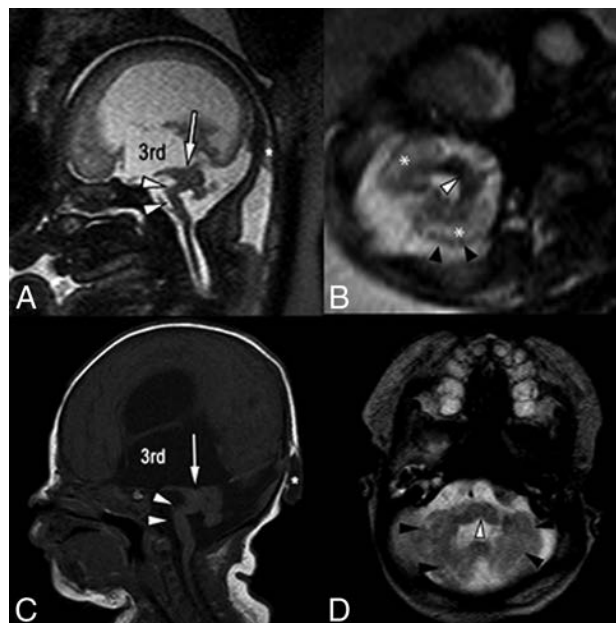


FIG 6. Single-shot fast spin-echo sagittal midline (A) and axial posterior fossa (B) images in a 34-week fetus with multiple findings of dysglycogenopathy suggesting Walker-Warburg syndrome. Postnatal correlation includes a sagittal T1-weighted sequence (C) and an axial T2-weighted sequence (D). Sagittal views of both pre- and postnatal MR imaging demonstrate a hypoplastic kinked brain stem (white arrowheads) and a markedly hypoplastic cerebellar vermis. Note also the dysplastic midbrain with thickening of the tectum causing stenosis of the cerebral aqueduct (arrows). Lateral and third ventricles are markedly enlarged. Incidentally noted was a small occipital cephalocele (asterisk). Axial views show cerebellar dysplasia with irregular cerebellar margins (black arrowheads) and multiple small cerebellar cysts, which account for the increased white matter T2 signal on fetal MR imaging (asterisk). Note also a midline pontine cleft (white arrowheads in B and D), another common finding in Walker-Warburg syndrome.

ductal stenosis in our cohort. No statistically significant size threshold for the larger lateral ventricle or third ventricle could be identified.

Multivariate analysis demonstrated that though several categorical findings did contribute independently, enlargement of the inferior recesses of the third ventricle, size of the lateral and third ventricles (especially enlargement of the smaller lateral ventricle), and an abnormally thin and/or dysgenetic corpus callosum were the dominant imaging findings driving an accurate diagnosis of CAS (Fig 7).

DISCUSSION

Congenital aqueductal stenosis is the most common cause of prenatal obstructive hydrocephalus.¹⁰ Fetal MR imaging has become a major problem-solving tool in the evaluation of ventriculomegaly based on its ability to define the underlying etiology as well as any associated abnormalities.¹⁷

The etiology of CAS is multifactorial, including both genetic and acquired forms.⁷ Acquired causes can be intrinsic (obstruction of the aqueduct lumen) or extrinsic (external compression). Prenatally, acquired causes are most commonly intrinsic, resulting from infection (aqueduct gliosis/web) or intraventricular hemorrhage. Extrinsic causes are less common in the prenatal

Table 2: Univariate analysis of categorical variables on prenatal MRI

Categorical Variable	Control (n = 32)	AS (n = 43)	Adjusted P Value	Sensitivity (95% CI)	Specificity (95% CI)	PPV (95% CI)	NPV (95% CI)
Enlarged inferior 3rd ventricular recesses	1 (3.1%)	31 (72%)	<.0023 ^a	72 (56–85)	97 (84–100)	97 (84–100)	72 (56–85)
Lateral ventricular diverticulum	1 (3.1%)	15 (35%)	.0276 ^a	35 (21–51)	97 (84–100)	94 (70–100)	53 (39–66)
Callosal thinning and/or dysgenesis	16 (50%)	40 (93%)	<.0023 ^a	93 (81–99)	50 (32–68)	71 (58–83)	84 (60–97)
Aqueductal funneling	0 (0%)	9 (21%)	.1909	21 (10–36)	100 (89–100)	100 (60–100)	48 (36–61)
Blood in the aqueduct	0 (0%)	3 (7%)	1	7.0 (1.5–19)	100 (89–100)	100 (29–100)	44 (33–57)
Rhombencephalosynapsis	0 (0%)	4 (9.3%)	1	9.3 (2.6–22.1)	100 (89–100)	100 (40–100)	45 (33–57)
Cerebellar dysplasia	0 (0%)	7 (16%)	.4117	16 (6.8–31)	100 (89–100)	100 (59–100)	47 (35–60)
Tectal plate thickening	2 (6.3%)	12 (28%)	.437	28 (15–44)	94 (79–99)	86 (57–98)	49 (36–62)
Intracranial hemorrhage	2 (6.3%)	15 (35%)	.1035	35 (21–51)	94 (79–99)	88 (64–99)	52 (38–65)
Enlarged ventricular temporal horns	20 (63%)	40 (93%)	.0575	93 (81–99)	38 (21–56)	67 (53–78)	80 (52–96)
Macrocephaly	4 (13%)	17 (40%)	.2484	40 (25–56)	88 (71–96)	81 (58–95)	52 (38–66)
Cerebellar hypoplasia	12 (38%)	5 (12%)	.2714	12 (3.9–25)	63 (44–79)	29 (10–56)	34 (22–48)
Vermian hypoplasia	4 (13%)	9 (21%)	1	21 (10–36)	88 (71–96)	69 (39–91)	45 (32–58)
Brain stem abnormality	4 (13%)	10 (23%)	1	23 (12–39)	88 (71–96)	71 (42–92)	46 (33–59)
Fourth ventricle dilation	3 (9.4%)	4 (9.3%)	1	9.3 (2.6–22)	91 (75–98)	57 (18–90)	43 (31–55)
Abnormal sulcation	8 (25%)	10 (23%)	1	23 (12–39)	75 (57–89)	56 (31–78)	42 (29–56)
Perforated septum pellucidum	14 (44%)	29 (67%)	1	67 (51–81)	56 (38–74)	67 (51–81)	56 (38–74)

Note:—NPV indicates negative predictive value; PPV, positive predictive value; AS, aqueductal stenosis.

^a Significant.

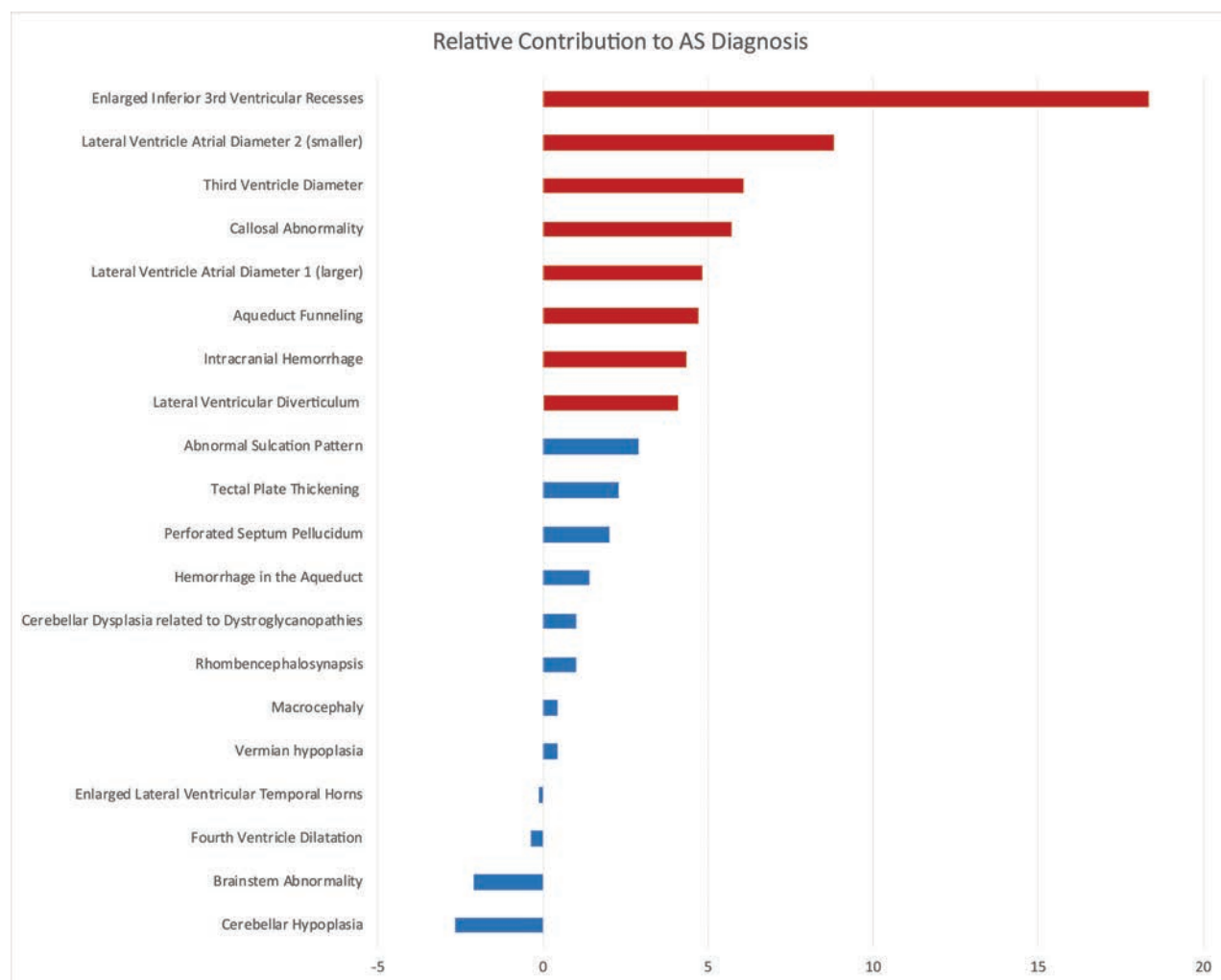


FIG 7. Random forest variable importance plot. This graphic shows the importance (x-axis) of each evaluated prenatal MR imaging finding (y-axis) with respect to the diagnosis of CAS. The independent contribution of each prenatal finding was estimated as the error of CAS classification by the machine-learning algorithm compared with the error that results when that finding is negated. The most important imaging findings associated with an accurate diagnosis of CAS are highlighted in red. Dominant findings include enlargement of the third ventricle inferior recesses, size of the lateral and third ventricles (especially enlargement of the smaller lateral ventricle), and an abnormally thin and/or dysgenetic corpus callosum. AS indicates aqueductal stenosis.

period and include tectal plate mass, periaqueductal vascular malformation, or compression from a ventricular diverticulum.^{8,18}

Of the genetic causes, X-linked and autosomal recessive disorders have been described.¹⁹ X-linked mutation in the gene for the L1 cell adhesion molecule is a known association with CAS as part of what has been described as callosal hypoplasia, retardation, adducted thumbs, spasticity (from absent or hypoplastic corticospinal tracts), and hydrocephalus syndrome.²⁰ Other described malformative and genetic abnormalities associated with CAS include rhombencephalosynapsis, diencephalic-mesencephalic dysplasia, dystroglycanopathy, Chiari II malformation, and Dandy-Walker malformation.^{21,22} We observed a similar spectrum of associated malformations. Furthermore, ventriculomegaly in rhombencephalosynapsis or dystroglycanopathy was highly likely to be caused by aqueductal stenosis (100% specificity and positive predictive value in our cohort). These results are in line with previous reports on CAS, suggesting that approximately 10% of cases have associated rhombencephalosynapsis and most rhombencephalosynapsis cases have CAS, with an incidence reaching near 100% in some series.^{23,24} Dystroglycanopathies can often present with CAS as a result of midbrain-hindbrain dysplasia and tectal plate thickening.²⁵ A dysplastic cerebellum is also a common finding seen in dystroglycanopathies. This feature showed 100% positive predictive value in our cohort, suggesting a strong association between CAS and dystroglycanopathies presenting with prenatal ventriculomegaly. Although we observed cases of Chiari II malformation and diencephalic-mesencephalic dysplasia with midline fusion (diencephalo-mesencephalosynapsis), their association with the diagnosis of CAS was not statistically significant in this cohort.

The spectrum of imaging findings seen in prenatally diagnosed CAS depends on the underlying cause, severity of stenosis, and gestational age. CAS commonly presents with moderate-to-severe ventriculomegaly due to its obstructive nature. Given that patients with severe ventriculomegaly often have poor neurodevelopmental outcomes, it is not surprising that patients with CAS are at an elevated risk for long-term neurologic dysfunction.^{5,26} Neurologic deficits in CAS result in large part, from the effects of CSF obstruction: Reduced or abolished third ventricular outflow leads to an increase in upstream intraventricular pressure; increased pressure results in decreased periventricular cerebral blood flow, regional ischemia, an altered neuronal microenvironment, and, ultimately, axonal shear and gliosis.²⁷

Morphologic abnormalities originate due to similar phenomena. Ventricular enlargement and hypertension tend to stretch and bow the corpus callosum superiorly, often with disruption of normal callosal formation, resulting in varying degrees of thinning and dysgenesis.²⁸ In severe cases, periventricular parenchymal injury based on increased intraventricular pressure can cause focal destruction of the cerebral mantle, leaving only a thin gliotic membrane, allowing the formation of a diverticulum.²⁹

Consistent with this pathogenesis, we observed that the most predictive findings associated with an accurate diagnosis of CAS were related to increased intraventricular pressure resulting from obstructive hydrocephalus. These findings, especially the degree of ventricular enlargement and formation of ventricular diverticula, imply a severe obstructive pathophysiology in CAS compared

with control patients with ventriculomegaly. Prenatally, an enlarged third ventricle in the setting of lateral ventriculomegaly and a normal fourth ventricle have been used as a key finding suggesting stenosis of the cerebral aqueduct. This is particularly important in the early second trimester, when direct visualization of aqueduct patency may fall below the resolution of fetal MR imaging. The normal size for gestational age of the third ventricle has been previously described on both sonography and MR imaging methods.^{12,13,30-32} An MR imaging measurement on the coronal plane of >4 mm is considered enlarged at any gestational age.¹³ In our cohort, the mean lateral third ventricular diameter in CAS cases was 7.37 ± 3.61 mm compared with 3.78 ± 1.89 mm in the control group. Another important aspect in the prenatal evaluation of the third ventricle is the assessment of the third ventricular recesses. Enlargement of the inferior recesses of the third ventricle is a morphologic finding that tends to result in obstructive hydrocephalus and is thought to reflect the absence of brain tissue surrounding these recesses, precluding enlargement on an ex vacuo basis. Although we expected this finding to be seen in both CAS and non-CAS cases with obstructive physiology, recess enlargement was highly specific for CAS in our cohort, which may reflect the tendency for patients with CAS to present with a greater degree of hydrocephalus.

In the postnatal setting, the diagnosis of CAS relies heavily on direct findings related to aqueduct narrowing or obstruction, including a funnel-shaped morphology of the proximal aqueduct reflecting distal obstruction. These findings, although highly predictive on fetal MR imaging when present, were rarely identified on prenatal imaging, which may be due to the small size of these structures relative to the spatial resolution typical of fetal MR imaging.

Although it is not without risk, it has been hypothesized that decompression of the ventricular hypertension with in-utero ventriculoamniotic shunting may normalize cerebral blood flow and ventricular size, thus preventing progressive neurologic injury in cases in which aqueductal stenosis is an isolated finding.²⁶ A study of in-utero intervention for aqueductal stenosis in the 1980s, however, failed to demonstrate value in this approach.²⁹ Many attribute this failure to poor patient selection, in that ventriculomegaly cases caused by CNS malformations other than CAS were not adequately identified and excluded before surgical intervention.^{27,33} Recent studies have demonstrated that CAS can be accurately diagnosed prenatally by sonography.²⁶ Our study further solidifies this diagnostic accuracy using a larger sample size to analyze specific characteristics of CAS found on prenatal MR imaging.

Limitations of this study include those related to the retrospective design and the intrinsic limitations of fetal MR imaging, including low spatial resolution and the effects of fetal motion. In particular, the small size of some of the structures evaluated in this study can present a challenge at fetal imaging. This limitation may explain the relatively poor sensitivity of direct imaging findings for the diagnosis of aqueductal stenosis in our cohort. Last, there was inconsistent postnatal genetic evaluation in our cohort, resulting in an unknown incidence of specific genetic causes of CAS.

CONCLUSIONS

We have presented fetal MR imaging findings that can contribute to a reliable prenatal diagnosis of CAS. Findings related to the severity of obstruction, especially enlargement of the inferior recesses of the third ventricle, the degree of lateral and third ventricular enlargement, and the presence of a lateral ventricular diverticulum, were most predictive for the diagnosis of CAS in our cohort. Direct findings related to stenosis of the aqueduct, such as a funnel-shaped morphology of the aqueduct and hemorrhage within the aqueduct, are highly specific for the diagnosis of CAS but are rarely detected prenatally. Last, identification of certain brain malformations, such as rhombencephalosynapsis and those seen in dystroglycanopathy, should raise suspicion for CAS as the cause of prenatal ventriculomegaly. An accurate diagnosis may provide prognostic information and obstetric guidance and can potentially improve patient selection for any future studies of in-utero intervention for ventriculomegaly.

REFERENCES

1. Beeghly M, Ware J, Soul J, et al. **Neurodevelopmental outcome of fetuses referred for ventriculomegaly.** *Ultrasound Obstet Gynecol* 2010;35:405–16 CrossRef Medline
2. Coakley FV, Glenn OA, Qayyum A, et al. **Fetal MRI: a developing technique for the developing patient.** *AJR Am J Roentgenol* 2004;182:243–52 Medline
3. Chu N, Zhang Y, Yan Y, et al. **Fetal ventriculomegaly: pregnancy outcomes and follow-ups in ten years.** *Biosci Trends* 2016;10:125–32 CrossRef Medline
4. Hannon T, Tennant PW, Rankin J, et al. **Epidemiology, natural history, progression, and postnatal outcome of severe fetal ventriculomegaly.** *Obstet Gynecol* 1953;120:1345 Medline
5. Gaglioni P, Danelon D, Bontempo S, et al. **Fetal cerebral ventriculomegaly: outcome in 176 cases.** *Ultrasound Obstet Gynecol* 2005;25:372–77 CrossRef Medline
6. Nyberg DA, Mack LA, Hirsch J, et al. **Fetal hydrocephalus: sonographic detection and clinical significance of associated anomalies.** *Radiology* 1987;163:187–91 CrossRef Medline
7. Levitsky DB, Mack LA, Nyberg DA, et al. **Fetal aqueductal stenosis diagnosed sonographically: how grave is the prognosis?** *AJR Am J Roentgenol* 1995;164:725–30 Medline
8. Barkovich AJ, Newton TH. **MR of aqueductal stenosis: evidence of a broad spectrum of tectal distortion.** *AJNR Am J Neuroradiol* 1989;10:471–76 Medline
9. Woolam DH, Millen JW. **Anatomical considerations in the pathology of stenosis of the cerebral aqueduct.** *Brain* 1953;76:104–12 CrossRef Medline
10. Cinalli G, Spennato P, Nastro A, et al. **Hydrocephalus in aqueductal stenosis.** *Childs Nerv Syst* 2011;27:1621–42 CrossRef Medline
11. International Society of Ultrasound in Obstetrics and Gynecology Education Committee. **Sonographic examination of the fetal central nervous system: guidelines for performing the 'basic examination' and the 'fetal neurosonogram.'** *Ultrasound Obstet Gynecol* 2007;29:109–16 CrossRef Medline
12. Garel C. *MRI of the Fetal Brain, Normal Development and Cerebral Pathologies.* Berlin: Springer-Verlag; 2004:28, 103
13. Kline-Fath BM, Bulas DI, Bahado-Singh R. *Fundamental and Advanced Fetal Imaging, Ultrasound and MRI.* Philadelphia: Wolters Kluwer; 2015:189, 861
14. Weisstein EW. Bonferroni Correction. *MathWorld*—A Wolfram Web Resource. <http://mathworld.wolfram.com/BonferroniCorrection.html>. Accessed February 28, 2018
15. Breiman L. *Classification and Regression Trees.* Belmont: Wadsworth International Group; 1984:358
16. Breiman L. **Random forests.** *Machine Learning* 2001;45:5–32 CrossRef
17. Sefidbakht S, Dehghani S, Safari M, et al. **Fetal central nervous system anomalies detected by magnetic resonance imaging: a two-year experience.** *Iran J Pediatr* 2016;26:e4589 CrossRef Medline
18. Marcotelles P, Fallet-Bianco C, Oury JF, et al. **Fetal aqueductal glioneuronal hamartoma: a clinicopathological and physiopathological study of three cases.** *Clin Neuropathol* 2005;24:155–62 Medline
19. Zhang J, Williams MA, Rigamonti D. **Genetics of human hydrocephalus.** *J Neurol* 2006;253:1255–66 CrossRef Medline
20. Yamasaki M, Thompson P, Lemmon V. **CRASH syndrome: mutations in LICAM correlate with severity of the disease.** *Neuropediatrics* 1997;28:175–78 CrossRef Medline
21. Weinzierl MR, Coenen VA, Korinth MC, et al. **Endoscopic transtentorial ventriculocystostomy and cystoventriculoperitoneal shunt in a neonate with Dandy-Walker malformation and associated aqueductal obstruction.** *Pediatr Neurosurg* 2005;41:272–77 CrossRef Medline
22. Wong SK, Barkovich AJ, Callen AL, et al. **Supratentorial abnormalities in the Chiari II malformation, III: the interhemispheric cyst.** *J Ultrasound Med* 2009;28:999–1006 CrossRef Medline
23. Ishak GE, Dempsey JC, Shaw DWW, et al. **Rhombencephalosynapsis: a hindbrain malformation associated with incomplete separation of midbrain and forebrain, hydrocephalus and a broad spectrum of severity.** *Brain* 2012;135:1370–86 CrossRef Medline
24. Whitehead MT, Choudhri AF, Grimm J, et al. **Rhombencephalosynapsis as a cause of aqueductal stenosis: an under-recognized association in hydrocephalic children.** *Pediatr Radiol* 2014;44:849–56 CrossRef Medline
25. Jissendi-Tchofo P. **Midbrain-hindbrain involvement in lissencephalies.** *Neurology* 2009;72:410–18 CrossRef Medline
26. Emery SP, Hogge WA, Hill LM. **Accuracy of prenatal diagnosis of isolated aqueductal stenosis.** *Prenat Diagn* 2015;35:319–24 CrossRef Medline
27. Emery SP, Greene S, Hogge WA. **Fetal therapy for isolated aqueductal stenosis.** *Fetal Diagn Ther* 2015;38:81–85 CrossRef Medline
28. Humphreys P. **Focal cerebral mantle disruption in fetal hydrocephalus.** *Pediatr Neurol* 2007;36:236–43 CrossRef Medline
29. Manning FA, Harrison MR, Rodeck C. **Catheter shunts for fetal hydronephrosis and hydrocephalus: report of the International Fetal Surgery Registry.** *N Engl J Med* 1986;315:336–40 CrossRef Medline
30. Hertzberg BS, Kliewer MA, Freed KS, et al. **Third ventricle: size and appearance in normal fetuses through gestation.** *Radiology* 1997;203:641–44 CrossRef Medline
31. Sari A, Ahmetoglu A, Dinc H, et al. **Fetal biometry: size and configuration of the third ventricle.** *Acta Radiol* 2005;46:631–35 CrossRef Medline
32. Andescavage NN, DuPlessis A, McCarter R, et al. **Cerebral fluid and parenchymal brain development and growth in the healthy fetus.** *Dev Neurosci* 2016;38:420–29 CrossRef Medline
33. von Koch CS, Gupta N, Sutton LN, et al. **In utero surgery for hydrocephalus.** *Childs Nerv Syst* 2003;19:574–86 CrossRef Medline

MRI Characteristics of Primary Tumors and Metastatic Lesions in Molecular Subgroups of Pediatric Medulloblastoma: A Single-Center Study

 D. Mata-Mbemba,  M. Zapotocky,  S. Laughlin,  M.D. Taylor,  V. Ramaswamy, and  C. Raybaud



ABSTRACT

BACKGROUND AND PURPOSE: Molecular grouping of medulloblastoma correlates with prognosis and supports the therapeutic strategy. We provide our experience with the imaging features of primary and metastatic disease in relation to the molecular groups.

MATERIALS AND METHODS: One hundred nineteen consecutive patients (mean age, 7.3 ± 3.8 years at diagnosis; male, 79 [66.4%]) with a confirmed diagnosis of medulloblastoma and interpretable pretreatment MRIs were retrieved from our data base from January 2000 to December 2016. Each patient was assigned to *wingless*, *sonic hedgehog*, group 3, or group 4 molecular groups. Then, we determined the imaging features of both primary and metastatic/recurrent disease predictive of molecular groups.

RESULTS: In addition to recently reported predictors based on primary tumor, including cerebellar peripheral location for *sonic hedgehog* (adjusted odds ratio = 9, $P < .0001$), minimal enhancement of primary group 4 tumor (adjusted odds ratio = 5.2, $P < .0001$), and cerebellopontine angle location for *wingless* (adjusted odds ratio = 1.4, $P = .03$), ependymal metastasis with diffusion restriction and minimal postcontrast enhancement (“mismatching pattern”) (adjusted odds ratio = 2.8, $P = .001$) for group 4 and spinal metastasis for group 3 (adjusted odds ratio = 1.9, $P = .01$) also emerged as independent predictors of medulloblastoma molecular groups. Specifically, the presence of a metastasis in the third ventricular infundibular recess showing a mismatching pattern was significantly associated with group 4 ($P = .02$).

CONCLUSIONS: In addition to imaging features of primary tumors, some imaging patterns of metastatic dissemination in medulloblastoma seem characteristic, perhaps even specific to certain groups. This finding could further help in differentiating molecular groups, specifically groups 3 and 4, when the characteristics of the primary tumor overlap.

ABBREVIATIONS: aOR = adjusted odds ratio; CPA = cerebellopontine angle; *SHH* = *sonic hedgehog*; *WNT* = *wingless*

Medulloblastoma is a highly malignant tumor (World Health Organization grade IV) and is also the most common malignant posterior fossa tumor in children. It has a high propensity for leptomeningeal spread. Approximately 20%–

35% of patients present with metastatic disease at diagnosis^{1–3}; and 30%–50%, late during the treatment/surveillance period.⁴ In 1 series of 86 patients with medulloblastoma, 19 (22.1%) patients had metastases at diagnosis and 22 (25.6%) patients had metastases late during the surveillance period.⁵

Recent molecular studies have shown that medulloblastoma is not a single entity but rather a constellation of groups, each with a distinct developmental origin, meaning that each may therefore benefit from subgroup-specific treatments.^{6–8} These groups are *wingless* (*WNT*), *sonic hedgehog* (*SHH*), group 3, and group 4.^{3,7,8} However, high cost and lack of access to this molecular grouping in most centers in the world constitute a main limitation in its routine clinical use to guide treatment. MR imaging of the brain and spine is however routinely performed in all patients with medulloblastoma before treatment to characterize the primary tumor, to aid with surgical neuronavigation, and to assess intracranial and spinal metastases. The presence of the latter worsens the prognosis

Received November 1, 2017; accepted January 2, 2018.


From the Department of Diagnostic Imaging (D.M.-M., S.L., C.R.), Division of Neuro-oncology (M.Z., V.R.), and Department of Neurosurgery (M.D.T.), Hospital for Sick Children, University of Toronto, Toronto, Ontario, Canada.

Daddy Mata-Mbemba and Michal Zapotocky are co-first authors and contributed equally to this work.

Vijay Ramaswamy and Charles Raybaud are co-senior authors and contributed equally to this work.

Previously presented, in part, orally at: Annual Meeting of the American Society of Neuroradiology and the Foundation of the ASNR Symposium, April 33–27, 2017; Long Beach, California.

Please address correspondence to Charles Raybaud, MD, Department of Radiology, Hospital for Sick Children, 555 University Ave, Toronto, ON, M5G 1X8, Canada; e-mail: charles.raybaud@sickkids.ca

 Indicates article with supplemental on-line tables.

<http://dx.doi.org/10.3174/ajnr.A5578>

and would upstage therapeutic strategies from average risk to high risk.⁹

A handful of recent reports based on a smaller number of patients investigated the possibility of using imaging features of the primary tumor on MR imaging as surrogate markers for molecular groups.^{10,11} None of them have evaluated the relationship between imaging features of metastatic disease and molecular grouping.

The aim of this single-institution study was 2-fold: 1) to validate the predictive value of imaging features of primary tumor with respect to their molecular group assignment, and 2) to test the hypothesis that imaging patterns of metastatic disease spread also correlate with the molecular groups.

MATERIALS AND METHODS

Patients

After institutional review board approval and a waiver of consent, 119 consecutive patients (mean age at diagnosis, 7.3 ± 3.8 years; male, 79 [66.4%]) with a confirmed diagnosis of medulloblastoma and interpretable pretreatment MRIs were retrieved from the data base at the Hospital for Sick Children, Toronto, Canada, during a 17-year period (from January 2000 to December 2016). The pathologic diagnosis and the subtypes (large-cell anaplastic, classic, or desmoplastic) of the primary tumor based on hematoxylin-eosin-stained slides of formalin-fixed paraffin-embedded material were also available in our data base for all 119 included patients. Patients referred from outside hospitals without an initial MR imaging study available were excluded.

Molecular Analysis

The 4 molecular groups (*WNT*, *SHH*, group 3, and group 4) of medulloblastoma were determined using NanoString nCounter system (NanoString Technologies, Seattle, Washington), as previously described from both formalin-fixed paraffin-embedded tissue and frozen tissue.^{7,12,13} Molecular grouping data were available for all 119 patients.

MR Imaging

All patients underwent brain and spine MR imaging at either 1.5 or 3T on different magnets and using different protocols during the 17-year period. The MR imaging protocol used presently for brain tumor in our institution includes at least the sequences shown in On-line Tables 1 and 2.

Most patients included in this study underwent DWI, except for 24 (20.2%) patients who were examined before the implementation of DWI in our routine MR imaging protocol.

Imaging Analysis of the Primary Tumor

A neuroradiology fellow and 2 attending neuroradiologists reviewed the MR images. Before starting the review, the 3 readers defined the imaging features to be assessed, including the location and the degree of enhancement of the primary tumor. Ten randomly selected cases were assessed by each reviewer to refine and standardize the definition of these parameters. Afterward, 2 of these readers independently reviewed the MR images blinded to clinical, pathologic, and molecular data. For discordant readings between the 2 first readers, the third reader reviewed the cases and

a consensus was reached among the 3 readers at the end. The initial results of the 2 first readers were used to generate the inter-reader agreement.

The readers evaluated the following MR imaging features: tumor location in relation to the fourth ventricle, tumor size, tumor margin, diffusion restriction, enhancement pattern, cyst/cavitation change, hemorrhage or calcification, the presence of peritumoral vasogenic edema, and the presence of supratentorial hydrocephalus.

The tumor location was categorized as follows: 1) fourth ventricle, which was further divided in 3 groups: fourth ventricle-midline, fourth ventricle with unilateral extension along the lateral recess, and fourth ventricle with bilateral extension along the lateral recesses; 2) cerebellopontine angle (CPA); 3) cerebellar periphery, which was defined as tumor involving the cerebellar cortex; and 4) paraventricular region, which was defined as tumor located close to the fourth ventricle in the deep cerebellar white matter without extending into it. The tumor size was a mean of the 3 orthogonal diameters of the primary tumor. The tumor margin was characterized as ill-defined if >50% of the margin could not be distinguished from the surrounding cerebellar parenchyma on the basis of all imaging sequences.¹¹ The diffusion restriction was characterized by the presence of any low signal area within the tumor on ADC maps, which was determined visually. The degree of diffusion restriction was quantified by ROI-based ADC analysis following the approach of Yeom et al.¹⁴ The degree of tumor enhancement was defined as one of the following: 1) none or minimal (if less than one-third of the mass was enhanced), 2) incomplete (between one-third and two-thirds of the mass was enhanced), and 3) diffuse (if more than two-thirds of the mass was enhanced). Hemorrhage or mineralization was defined as foci of blooming on 2D gradient recalled-echo sequence.

Imaging Analysis of Metastatic Disease

Blinded to molecular and pathologic data, a neuroradiology fellow and another attending neuroradiologist reviewed the imaging features of metastatic disease, which were defined as early (at diagnosis, ie, before the treatment including chemotherapy, radiation, and/or an operation) or late/recurrent (after treatment initiation including chemotherapy, radiation, and/or an operation) metastases, which were further characterized as ependymal or leptomeningeal. Ependymal metastases were searched specifically along the ependyma of the lateral and third ventricles, especially in the third ventricular infundibular recess. The recurrent tumor was searched at the site of primary tumor, including within the fourth ventricle. Leptomeningeal metastases were divided into supratentorial, infratentorial, and spinal. Furthermore, signal patterns of all intracranial metastatic disease were evaluated and characterized as diffusion restricting or not and as postcontrast enhancing or not. Imaging characteristics of metastases were called “mismatching pattern” when the metastatic lesion showed diffusion restriction but no/minimal postcontrast enhancement and “matching pattern” when the lesion showed both diffusion restriction and postcontrast enhancement. Consensus was used to resolve disagreement among the readers.

Table 1: Patient demographics with respect to molecular groups

Parameters	WNT (n = 15) (%)	SHH (n = 26) (%)	Group 3 (n = 29) (%)	Group 4 (n = 49) (%)	Total (n = 119) (%)	P
Sex						.02 ^a
Male	7 (46.7)	13 (50)	20 (69)	39 (80)	79 (66.4)	
Female	8 (53.3)	13 (50)	9 (31)	10 (20)	40 (33.6)	
Age at diagnosis (yr) ^b	8.7 (3.1)	6.2 (4.6)	6.1 (3.8)	8.1 (3.2)	7.3 (3.8)	<.0001 ^a
Histology						.02 ^a
LCA	1 (6.7)	9 (34.6)	13 (44.8)	7 (14.3)	30 (25.2)	
Classic	14 (93.3)	8 (30.8)	15 (51.7)	39 (79.6)	76 (63.9)	
Desmoplastic	0 (0)	9 (34.6)	1 (3.5)	3 (6.1)	13 (10.9)	

Note:—LCA indicates large-cell anaplastic.

^a Statistically significant.

^b Mean with SDs.

Table 2: Locations of primary tumors with respect to molecular groups

Subgroup	Fourth Ventricle					CPA (n = 6) (%)	Paraventricular (n = 12) (%)	Cerebellar Periphery (n = 19) (%)
	No. (n = 119) (%)	Midline-Vermis (n = 40) (%)	4th-uniCPA (n = 25) (%)	4th-biCPA (n = 17) (%)	Subtotal (n = 81) (%)			
WNT	15 (12.6)	5 (12.5)	3 (12)	1 (5.9)	8 (9.9)	3 (50)	3 (25)	0 (0)
SHH	26 (21.8)	3 (7.5)	0 (0)	0 (0)	3 (3.7)	3 (50)	2 (16.7)	18 (94.7)
Group 3	29 (24.4)	11 (27.5)	8 (32)	6 (35.3)	25 (30.9)	0 (0)	4 (33.3)	0 (0)
Group 4	49 (41.2)	21 (52.5)	14 (56)	10 (58.8)	45 (55.5)	0 (0)	3 (25)	1 (5.3)

Note:—4th-uniCPA indicates fourth ventricle with unilateral extension along the lateral recess toward the CPA; 4th-biCPA, fourth ventricle with bilateral extension along bilateral recesses toward the CPAs.

Statistics and Analysis

First, we evaluated the relationship between the molecular groups and MR imaging features of primary or metastatic disease using the Fisher exact test. Afterward, to test the overall performance of MR imaging patterns of metastatic disease spread in predicting the molecular grouping, we conducted a stepwise multivariable multinomial logistic regression in which variables related to the patterns of metastatic disease spread were put in the model along with the previously reported predictors (ie, MR imaging features of primary tumors previously reported as independent predictors of molecular grouping, including CPA location for WNT, minimal enhancement of group 4 tumors, and cerebellar peripheral location for SHH) to determine the overall independent predictors of molecular grouping. All statistical analyses were performed using JMP Pro version 13 software (SAS Institute, Cary, North Carolina), and *P* values <.05 were considered statistically significant.

RESULTS

Patients

The results of our patients, including the distribution of their demographic data and pathologic subcategorization of the primary tumor, are shown in Table 1.

Of the 119 patients, NanoString assay revealed 15 WNT (12.6%), 26 SHH (21.8%), 29 group 3 (24.4%), and 49 group 4 (41.2%) medulloblastoma molecular groups. SHH and group 3 patients were younger (*P* = .02). Male patients were predominant (*P* = .02).

Primary Tumor

There was an almost perfect (reference, 0.81–1.0) agreement among the readers in determining both the location (κ = 86%) and the degree of enhancement (κ = 82%) of the primary tumor.¹⁰

Depending on the group, tumor locations were highly associated with molecular groups. Their distribution is shown in

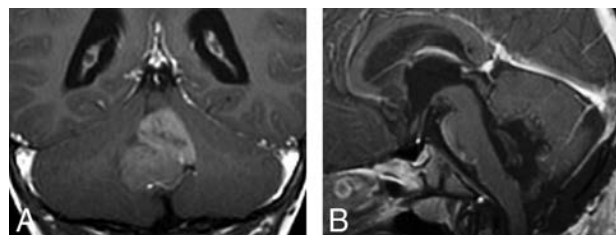


FIG 1. Coronal postcontrast T1WI (A) showing SHH tumor within the fourth ventricle. The postoperative sagittal postcontrast T1 (B) confirmed that the tumor was arising from the flocculonodular lobe.

Table 2. In 20% (3/15), WNT tumors were strictly limited to the CPA, but this was not exclusive to WNT because 3 (11.5%) of 26 SHH tumors were also centered in the CPA. Four of 15 WNT tumors were centered in the fourth ventricle while extending laterally along 1 (in 3 cases) or both (in 1 case) lateral recesses. This location was also observed in groups 3 and 4. The cerebellar periphery (cerebellar cortex) was the primary location of 69% of SHH tumors (*P* < .0001); this corresponds to a positive predictive value of 94.7% (95% CI, 84%–100%) for SHH. Three SHH tumors were located in the fourth ventricular midline (Fig 1), but none them extended from the fourth ventricle into the CPA via the lateral recess (*P* = .0002).

Groups 3 and 4 were primarily located in the fourth ventricle (*P* < .0001) and remained within the midline of the fourth ventricle in 80% of cases (*P* = .02). Of the 12 tumors noted in paraventricular locations, 4 (33.3%) were group 3, but this association was not statistically significant (*P* = .45).

There was a statistically significant difference in the degree of primary tumor enhancement among molecular groups (*P* < .0001)—that is, minimal enhancement was noted in 55.1% of group 4 patients (*P* < .0001), showing a positive predictive value of 75% (95% CI, 60%–89%). Only 4 (13.8%) group 3 patients demonstrated minimal enhancement. On the other hand, 86.3% of SHH tumors demonstrated strong avid enhancement (*P* < .0001).

No significant statistical difference was found among the molecular groups regarding the following tumor characteristics: tumor margin, ADC value, cystic change/necrosis, hemorrhage or calcification, the presence of a peritumoral vasogenic edema, and the presence of supratentorial hydrocephalus ($P > .05$).

Metastatic Disease

Of the 119 patients, 34 patients (28.6%) were diagnosed with metastatic disease, including 25/34 (73.5%) initial and 9/34 (26.5%) later metastases. These metastatic diseases were distributed as follows: 1 of 15 *WNT* (6.7%) (none at diagnosis, 1 late); 2 of 26 *SHH* (7.7%) (2 late), 13 of 29 group 3 (44.8%) (8 at diagnosis, 5 late); 15 of 49 group 4 (30.6%) (14 at diagnosis, 1 late). In 3 cases, multi-

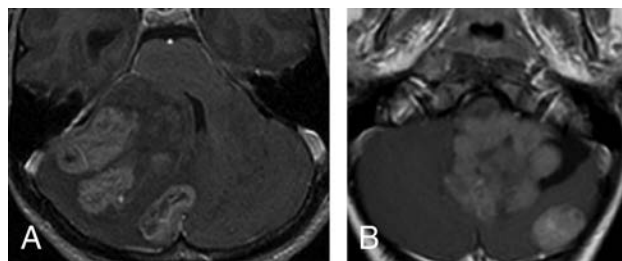


FIG 2. Multifocal (synchronous) *SHH* tumors at diagnosis. The multiple tumors on this axial postcontrast T1 are located in, and presumably originate within, the cerebellar cortex (A). In the second patient (B), there is 1 large fourth ventricular mass with an associated separate cortical mass posteriorly. In this case, the main tumor is lobulated and appears more like a conglomerate of multiple masses.

Table 3: Imaging features of initial metastases with respect to their molecular group assignment^a

MRI Signals	Initial Metastasis (n = 25)				P Value ^b
	<i>WNT</i> (n = 0) (%)	<i>SHH</i> (n = 3) (%)	Group 3 (n = 8) (%)	Group 4 (n = 14) (%)	
Ependymal C−/D+	0 (0)	0 (0)	(0)	6 (42.8)	.01 ^c
3rd V.I.R., C−/D+ ^d	0 (0)	(0)	(0)	4 (28.6)	.02 ^c
Ependymal C+/D+	0 (0)	0 (0)	3 (37.5)	0 (0)	.02 ^c
Leptomeningeal C−/D+	0 (0)	0 (0)	0 (0)	3 (21.4)	.05
Leptomeningeal C+/D+	0 (0)	3 (100)	5 (62.5)	5 (35.7)	.17
Leptomeningeal C+/D−	0 (0)	0 (0)	0 (0)	4 (28.6)	.02 ^c

Note:—C— indicates no contrast enhancing; D+, diffusion-restricting; D−, no diffusion-restricting; C+, contrast enhancing; 3rd V.I.R., third ventricle infundibular recess.

^a The sum of metastases in some locations is higher than the total number of patients in the group because each case could have multiple metastases in >1 compartment.

^b P value determined using the Fisher exact test.

^c Statistically significant.

^d Subgroup of patients with mismatching ependymal metastasis in the third ventricle infundibular recess.



FIG 3. Metastatic group 3 tumor. In the first patient (A and B), the leptomeningeal “sugar coating” metastases demonstrate both diffusion restriction (A) and leptomeningeal enhancement on an axial postcontrast T1 image (B). In the second patient, the primary tumor appears smaller than its leptomeningeal suprasellar, avidly enhancing metastasis (C). An avidly enhancing nodular metastasis involving the cortex in the cerebellum posteriorly is also noted.

nodular *SHH* tumors were initially diagnosed at presentation as metastases; it is now thought that this pattern may rather represent multicentric primary tumors, which were all confined within the cerebellar cortex (Fig 2). This feature distinguished *SHH* from others ($P = .002$), with a positive predictive value of 100%.

Initial Metastasis

Imaging characteristic of initial metastases are shown in Table 3, and the locations of initial metastases are shown in On-line Table 3.

In group 3, metastases demonstrated a matching pattern regardless of their ependymal and leptomeningeal locations and were often massive ($P = .003$), fitting the so-called descriptive “sugar coating” pattern (Fig 3A, -B). In 25% of group 3 patients, the primary tumor was smaller than the largest metastatic tumor ($P = .01$) (Fig 3C). Seven (87.5%) of the 8 group 3 patients showed initial spinal metastases ($P = .02$).

In group 4, of the 14 patients with initial metastasis, 6 (42.9%) showed ependymal metastases with a mismatching pattern (Table 3 and Fig 4A, -B). Four of these 6 patients showed a mismatching metastatic lesion in the ependyma of the third ventricular infundibular recess, a finding that was specific for group 4 ($P = .02$) (Fig 4C), corresponding to a positive predictive value of 100% for group 4. One group 4 patient (7.1%) showed an ependymal metastasis, which did not restrict or enhance.

On the other hand, leptomeningeal metastases were seen in 12 (85.7%) of 14 group 4 patients and demonstrated 3 different imaging patterns: metastases showing a matching pattern in 5 patients, a mismatching pattern in 3 patients, and postcontrast enhancement and no diffusion restriction in 4 patients.

This mixture of patterns of leptomeningeal metastases was significantly associated with group 4 ($P = .0002$) only.

Late Metastases/Recurrence

Of the 9 patients with late metastasis, local tumor recurrence was seen in only 1 group 4 patient, who showed a mass lesion within the surgical bed (Fig 5A, -B). In the 8 remaining patients, recurrent metastatic disease in the posterior fossa presented as multiple scattered lesions.

One patient in the *WNT* group had ependymal metastases that demonstrated diffusion restriction and post-contrast enhancement, with an enhancing leptomeningeal metastasis in the anterior interhemispheric fissure. Of the 2 patients in the *SHH* group, one showed only 1 spinal metastasis, while the other showed multiple supra- and infratentorial leptomeningeal metastases.

Five of the 9 late metastases were from group 3 ($P = .02$). Four (80%) of these 5

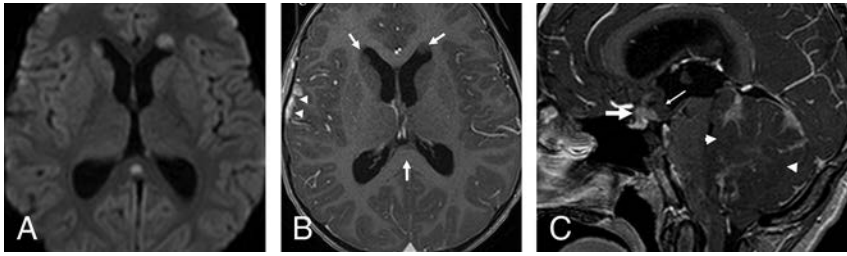


FIG 4. Metastatic group 4 tumors. In the first patient (A and B), the ependymal metastases seen in the anterior horns of the lateral ventricles and in the splenium of corpus callosum demonstrate diffusion restriction (B) without enhancement on contrast-enhanced T1 (arrows, B), while the leptomeningeal metastasis seen along the right temporal lobe demonstrates enhancement without appreciable diffusion restriction (arrowheads, B). In the second patient (C), the primary tumor demonstrates minimal enhancement on the contrast-enhanced T1 (arrowheads). The patient has a metastatic tumor in the suprasellar region with 2 components: One is ependymal in the infundibular recess and shows no enhancement (thin arrow), while the second is leptomeningeal and enhances strongly (thick arrow) like other metastasis in the posterior fossa, or supratentorially.

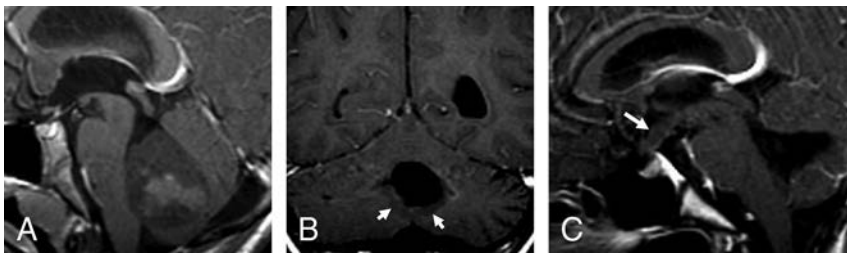


FIG 5. A recurrent group 4 tumor. A, The primary tumor demonstrates minimal postcontrast enhancement. Four years later, a recurrent tumor appeared along the lower margin of the postoperative cavity (arrows, B) as well as a metastasis in the infundibular recess and along the tuber cinereum (arrow, C), both of which are nonenhancing.

patients had spinal metastases ($P = .003$). Of the 5 group 3 patients with late metastases, 4 (80%) showed leptomeningeal and ependymal metastases demonstrating a matching pattern ($P = .003$).

One group 4 patient (the same patient described above who had a local recurrence within the fourth ventricle) showed a late single metastasis in the third ventricular infundibular recess, demonstrating a mismatching pattern (Fig 5C), as well as diffuse spinal intradural extramedullary and intramedullary metastases.

Overall Predictors of Molecular Groups

The stepwise multivariable multinomial logistic regression model revealed that in addition to recently reported predictors based on primary tumor, including cerebellar peripheral location for *SHH* (adjusted odds ratio [aOR] = 9, $P < .0001$), minimal enhancement of primary group 4 tumor (aOR = 5.2, $P < .0001$), and CPA location for *WNT* (aOR = 1.4, $P = .03$), ependymal metastasis with diffusion restriction and minimal postcontrast enhancement (mismatching pattern) (aOR = 2.8, $P = .001$) for group 4 and spinal metastasis for group 3 (aOR = 1.9, $P = .01$) also emerged as independent predictors of medulloblastoma molecular groups. Specifically, the presence of a metastasis in the third ventricular infundibular recess showing mismatching pattern was significantly associated with group 4 ($P = .02$).

DISCUSSION

In this article, we evaluated the relationship between the molecular groups and the imaging features of both primary and metastatic pediatric medulloblastoma tumors and found that some

imaging features of these tumors are reliable in predicting the molecular groups. For the primary tumors, for instance, we validated the previous reports¹¹—that is, *SHH* tumors were mainly located in the cerebellar periphery with strong postcontrast enhancement, and group 4 tumors were located mainly in the fourth ventricles with usually minimal enhancement. However, in our series, only a small proportion (3/15, 20%) of *WNT* tumors were truly located in the CPA; the CPA site was not specific for *WNT* tumors because *SHH* tumors may develop in the same location when they originate from the flocculus (2/26) (Fig 1).

Our findings are concordant with the report by Patay et al,¹⁰ who found that most *WNT* tumors were close to the midline but might lateralize toward the CPA. Gibson et al¹⁵ stated that *WNT* tumors develop in the midline within the fourth ventricle, while on the contrary, Perreault et al¹¹ reported a positive predictive value of 100% for CPA tumors being *WNT*. Indeed, the lateral recess contains the portion of the lower rhombic lip, which has a strong *WNT* expression.¹⁶ The tumor might originate from

there and extend either laterally to the CPA or, more often, develop medially to finally appear centered within the fourth ventricle, while other tumors centered in the fourth ventricle may extend laterally into 1 lateral recess or both.

Most (69.2%) *SHH* tumors were located at the periphery of the cerebellar hemisphere. This result matches the existing literature that states that *SHH* tumors originate from the glutamatergic neuron precursor granule cells of the upper rhombic lip and form the external granular layer, a secondary proliferative zone that persists on the surface of the cerebellum until the second year.¹⁷ *SHH* tumors therefore develop from the cerebellar cortex and are commonly associated with a leptomeningeal desmoplastic reaction. Most develop in the cerebellar convexity of the hemispheres and vermis, but they may also develop from the flocculus, which is located within the CPA, or from the nodulus, which is located within the fourth ventricle.¹⁶ In our patients, 30.8% of *SHH* tumors were located either in the CPA or the lumen of the fourth ventricle. Even in atypical locations, *SHH* tumors may still be distinguished from the other groups because they commonly present with a very strong postcontrast enhancement (seen in 86.3% of *SHH* tumors), which is thought to be due to leptomeningeal desmoplasia, which is associated with this cortical location. Another distinguishing feature of the *SHH* group tumor is the multinodularity and/or synchronous multifocal tumors at presentation. In 3 cases, patients presented with cortical cerebellar masses that were associated with several large cortical nodules scattered in other parts of the cerebellum, initially considered as metastases present at diagnosis. However, these may, in fact, rep-

resent metachronous primary tumors rather than metastatic dissemination. In our data, this feature appears to be specific for the *SHH* group because nothing comparable was observed in the other groups.

In our series, most of the group 3 and 4 medulloblastomas were located in the fourth ventricular midline (89.7%) or, uncommonly, in a paraventricular location (9%). In 25% of the cases, the primary tumor in group 3 was small, possibly smaller than their largest metastasis, and then was unassociated with hydrocephalus. This finding suggests an aggressive malignancy with early metastases in a “young” tumor that did not give the ventricles time to expand. One may speculate that metastatic dissemination in group 3 could be an early clonal event, meaning that the tumor metastasizes earlier during its growth, which is consistent with the very poor prognosis of group 3 patients compared with other groups.^{18,19} Regarding tumors of group 4, they typically show no or only minimal enhancement, as was reported by Perreault et al.¹¹ This contrasts with the usual demonstration in these tumors of prominent intratumoral vessels, consistent with high perfusion; it reflects a preserved blood-tumor barrier, an unexpected finding for a highly malignant embryonal tumor. This minimal or lack of enhancement, though not absolutely specific (found in 18.8% of group 3 tumors as well), is still a good identification mark of group 4 as opposed to other groups.

Regarding metastases, group 3 metastases showed a matching pattern (restricting and enhancing) regardless of their ependymal or leptomeningeal location. This contrasted with most (but not all) ependymal metastases of group 4 tumors, which showed a mismatching pattern (restricting but not enhancing), while most of their leptomeningeal metastases enhanced. The biologic meaning of this finding is not known.

Evaluation of late metastases also demonstrated different features for different molecular groups. Most the late metastatic disease belonged to group 3 and spread away from the primary site into the spinal theca. On the other hand, only 1 of the group 4 patients showed late metastases, including a local recurrence within the surgical site and metastasis in the third ventricular recess. Also, only 1 patient with a *WNT* tumor and 2 with *SHH* tumors showed late metastases; this finding is consistent with the less malignant character of the tumors of these groups compared with group 3.^{18,19}

Third ventricular metastases have been known for a long time to occur in medulloblastoma.²⁰ Most reports are case reports published before the era of molecular grouping, some of which were based on CT images, making it difficult to differentiate leptomeningeal from intraventricular masses.^{21–25} The description of Shelton et al²³ resembles what we noted in at least 1 of our patients (Fig 4C): a suprasellar metastasis with an enhancing leptomeningeal component associated and contrasting with a non-enhancing infundibular ependymal component; molecular grouping was not available then. Recently, Nagashima et al²⁵ reported a case of a large suprasellar metastasis from a non-*SHH*/non-*WNT* type, without further determination of group 3 or 4. In our series, it was clearly significant that all tumors that presented with a metastasis in the anterior third ventricular infundibulum belonged to group 4 tumors. Besides medulloblastoma, suprasellar, third ventricular seeding is known to occur for high-grade gliomas and pineoblastomas. For some authors, the pattern of

“bifocal germinoma” also corresponds to a pattern of metastatic disease spread.²⁶ Therefore, it is not so much the suprasellar/anterior third ventricular location that is surprising in medulloblastoma but that this seemingly occurs in group 4 tumors and not in other groups. Another peculiarity of group 4 metastases is that they enhance in the subarachnoid space but not in the ventricles and that in the ventricles, they may even demonstrate no diffusion restriction. Metastases that do not enhance or show restricted diffusion would be easily missed in the leptomeninges, but not in the ventricles.

This study provides further indications that some of the imaging patterns of primary tumors and metastatic spread in medulloblastoma may be characteristic, though further studies may be needed. This finding is consistent with the idea that medulloblastomas of different groups are biologically different diseases, with different behavior and, possibly, distinct preferences for specific environments. The findings of group-specific patterns of metastatic disease spread complements the already described group-specific radiologic features of the primary tumors.

The main limitation to this study is that it is retrospective; and because it covers a 17-year period, it includes cases with very different MR imaging. Diffusion imaging was not routinely used during the earlier reviewed cases. Similarly, postcontrast FLAIR, which may allow detection of more leptomeningeal metastatic lesions, was not part of the MR imaging protocol during the period covered by this study. In addition, fewer spinal metastases detected in this study may be because we used only contrast-enhanced T1WI. The ongoing development of MR imaging sequences such as spine DWI and steady-state free precession could help in detecting more spinal metastases in the future.

CONCLUSIONS

In addition to imaging features of primary tumors, some of imaging patterns of metastatic dissemination in medulloblastoma seem characteristic, perhaps even specific to certain groups. This finding could further help in differentiating molecular groups, specifically groups 3 and 4, when the characteristics of the primary tumor overlap.

ACKNOWLEDGMENTS

We thank our department of MR imaging Quality Specialist, Mr Manoj Singh, for the technical support in advanced MR imaging and protocols and our department Clinical Research Project Assistant, Ms Olga Carpio Pinto, for her support in editing this article.

REFERENCES

1. Taylor RE, Bailey CC, Robinson KJ, et al. **Outcome for patients with metastatic (M2–3) medulloblastoma treated with SIOP/UKCCSG PNET-3 chemotherapy.** *Eur J Cancer* 2005;41:727–34 [CrossRef](#) [Medline](#)
2. Zeltzer PM, Boyett JM, Finlay JL, et al. **Metastasis stage, adjuvant treatment, and residual tumor are prognostic factors for medulloblastoma in children: conclusions from the Children's Cancer Group 921 randomized phase III study.** *J Clin Oncol* 1999;17:832–45 [CrossRef](#) [Medline](#)
3. Gajjar A, Chintagumpala M, Ashley D, et al. **Risk-adapted craniospinal radiotherapy followed by high-dose chemotherapy and stem-cell rescue in children with newly diagnosed medulloblastoma (St**

- Jude Medulloblastoma-96): long-term results from a prospective, multicentre trial.** *Lancet Oncol* 2006;7:813–20 [CrossRef Medline](#)
4. Bouffet E. **Embryonal tumours of the central nervous system.** *Eur J Cancer* 2002;38:1112–20 [CrossRef Medline](#)
 5. Torres CF, Rebsamen S, Silber JH, et al. **Surveillance scanning of children with medulloblastoma.** *N Engl J Med* 1994;330:892–95 [CrossRef Medline](#)
 6. Cavalli FM, Remke M, Rampasek L, et al. **Intertumoral heterogeneity within medulloblastoma subgroups.** *Cancer Cell* 2017;31:737–54.e6 [CrossRef Medline](#)
 7. Ramaswamy V, Remke M, Adamski J, et al. **Medulloblastoma subgroup-specific outcomes in irradiated children: who are the true high-risk patients?** *Neuro Oncol* 2016;18:291–97 [CrossRef Medline](#)
 8. Thompson EM, Hielscher T, Bouffet E, et al. **Prognostic value of medulloblastoma extent of resection after accounting for molecular subgroup: a retrospective integrated clinical and molecular analysis.** *Lancet Oncol* 2016;17:484–95 [CrossRef Medline](#)
 9. Ramaswamy V, Taylor MD. **Medulloblastoma: from myth to molecular.** *J Clin Oncol* 2017;35:2355–63 [CrossRef Medline](#)
 10. Patay Z, DeSain LA, Hwang SN, et al. **MR imaging characteristics of wingless-type-subgroup pediatric medulloblastoma.** *AJNR Am J Neuroradiol* 2015;36:2386–93. [CrossRef Medline](#)
 11. Perreault S, Ramaswamy V, Achrol AS, et al. **MRI surrogates for molecular subgroups of medulloblastoma.** *AJNR Am J Neuroradiol* 2014;35:1263–69 [CrossRef Medline](#)
 12. Northcott PA, Shih DJ, Remke M, et al. **Rapid, reliable, and reproducible molecular sub-grouping of clinical medulloblastoma samples.** *Acta Neuropathol* 2012;123:615–26 [CrossRef Medline](#)
 13. Northcott PA, Korshunov A, Witt H, et al. **Medulloblastoma comprises four distinct molecular variants.** *J Clin Oncol* 2011;29:1408–14 [CrossRef Medline](#)
 14. Yeom KW, Mobley BC, Lober RM, et al. **Distinctive MRI features of pediatric medulloblastoma subtypes.** *AJR Am J Roentgenol* 2013;200:895–903 [CrossRef Medline](#)
 15. Gibson P, Tong Y, Robinson G, et al. **Subtypes of medulloblastoma have distinct developmental origins.** *Nature* 2010;468:1095–99 [CrossRef Medline](#)
 16. Raybaud C, Ramaswamy V, Taylor MD, et al. **Posterior fossa tumors in children: developmental anatomy and diagnostic imaging.** *Childs Nerv Syst* 2015;31:1661–76 [CrossRef Medline](#)
 17. Ramaswamy V, Remke M, Shih D, et al. **Duration of the pre-diagnostic interval in medulloblastoma is subgroup dependent.** *Pediatr Blood Cancer* 2014;61:1190–94 [CrossRef Medline](#)
 18. Wu X, Northcott PA, Dubuc A, et al. **Clonal selection drives genetic divergence of metastatic medulloblastoma.** *Nature* 2012;482:529–33 [CrossRef Medline](#)
 19. Ramaswamy V, Remke M, Bouffet E, et al. **Risk stratification of childhood medulloblastoma in the molecular era: the current consensus.** *Acta Neuropathol* 2016;131:821–31 [CrossRef Medline](#)
 20. Newton TH, Potts DG. *Radiology of the Skull and Brain. Ventricles and Cisterns.* Vol 4. St. Louis: C.V. Mosby; 1978
 21. Fukusumi A, Maehara F, Hayashi T, et al. **Two cases of cerebellar medulloblastoma associated with seeding in the suprasellar cistern [in Japanese].** *Rinsho Hoshasen* 1985;30:901–04 [Medline](#)
 22. Blaser SI, Harwood-Nash DC. **Neuroradiology of pediatric posterior fossa medulloblastoma.** *J Neurooncol* 1996;29:23–34 [CrossRef Medline](#)
 23. Shelton CH 3rd, Phillips CD, Laws ER, et al. **Third ventricular lesion masquerading as suprasellar disease.** *Surg Neurol* 1999;51:177–80 [CrossRef Medline](#)
 24. Helton KJ, Gajjar A, Hill DA, et al. **Medulloblastoma metastatic to the suprasellar region at diagnosis: a report of six cases with clinicopathologic correlation.** *Pediatr Neurosurg* 2002;37:111–17 [CrossRef Medline](#)
 25. Nagashima H, Nagashima T, Kawamura A, et al. **Medulloblastoma with suprasellar solitary massive metastasis: case report.** *Neurol Neurochir Pol* 2016;50:211–14 [CrossRef Medline](#)
 26. Phi JH, Kim SK, Lee J, et al. **The enigma of bifocal germ cell tumors in the suprasellar and pineal regions: synchronous lesions or metastasis?** *J Neurosurg Pediatr* 2013;11:107–14 [CrossRef Medline](#)

Cerebellar Growth Impairment Characterizes School-Aged Children Born Preterm without Perinatal Brain Lesions

 K. Pieterman,  T.J. White,  G.E. van den Bosch,  W.J. Niessen,  I.K.M. Reiss,  D. Tibboel,  F.E. Hoebeek, and  J. Dudink



ABSTRACT

BACKGROUND AND PURPOSE: Infants born preterm are commonly diagnosed with structural brain lesions known to affect long-term neurodevelopment negatively. Yet, the effects of preterm birth on brain development in the absence of intracranial lesions remain to be studied in detail. In this study, we aim to quantify long term consequences of preterm birth on brain development in this specific group.

MATERIALS AND METHODS: Neonatal cranial sonography and follow-up T1-weighted MR imaging and DTI were performed to evaluate whether the anatomic characteristics of the cerebrum and cerebellum in a cohort of school-aged children (6–12 years of age) were related to gestational age at birth in children free of brain lesions in the perinatal period.

RESULTS: In the cohort consisting of 36 preterm (28–37 weeks' gestational age) and 66 term-born infants, T1-weighted MR imaging and DTI at 6–12 years revealed a reduction of cerebellar white matter volume ($\beta = 0.387, P < .001$), altered fractional anisotropy of cerebellar white matter ($\beta = -0.236, P = .02$), and a reduction of cerebellar gray and white matter surface area ($\beta = 0.337, P < .001$; $\beta = 0.375, P < .001$, respectively) in relation to birth age. Such relations were not observed for the cerebral cortex or white matter volume, surface area, or diffusion quantities.

CONCLUSIONS: The results of our study show that perinatal influences that are not primarily neurologic are still able to disturb long-term neurodevelopment, particularly of the developing cerebellum. Including the cerebellum in future neuroprotective strategies seems therefore essential.

ABBREVIATIONS: FA = fractional anisotropy; MD = mean diffusivity

Preterm birth and related complications are considered major risk factors for long-term functional impairment^{1–3} and have been associated with substantially increased health risks from birth to adulthood.^{4,5} Survival rates following preterm birth have substantially increased due to advances in perinatal care. How-

ever, among survivors, neurocognitive and motor impairments are still frequent,^{6–8} despite a shift from large macroscopic white matter lesions toward subtler punctate lesions and microstructural abnormalities.^{9,10}

Advanced imaging techniques have been widely adopted to study brain development and microstructure following preterm birth, with a predominant focus on studying cerebral structures. A limited number of studies assessing neurodevelopment following preterm birth have incorporated the cerebellum in imaging analysis. More attention toward cerebellar structures seems desirable now that recent evidence shows a potential role of the cerebellum in various nonmotor functions, including attention, cognition, and behavior^{11–14}; disturbances of cerebellar development have been associated with a variety of nonmotor disorders, including autism spectrum disorder,¹⁵ schizophrenia,¹⁶ dyslexia,¹⁷ and attention deficit disorders.¹⁸


Disruptive influences on cerebellar microstructure and structures are likely to occur during perinatal stages, when growth and develop-


Received September 21, 2017; accepted after revision January 12, 2018.

From the Departments of Radiology and Medical Informatics (K.P., W.J.N.), Biomedical Imaging Group Rotterdam; Departments of Child and Adolescent Psychiatry (T.J.W.), Radiology (T.J.W.), Intensive Care and Paediatric Surgery (G.E.v.d.B., D.T.); Division of Neonatology, Department of Pediatrics (I.K.M.R.); and Department of Neuroscience (F.E.H.), Erasmus Medical Centre, Rotterdam, the Netherlands; Department of Imaging Physics (W.J.N.), Faculty of Applied Sciences, Delft University of Technology, Delft, the Netherlands; Quantib BV (W.J.N.), Rotterdam, the Netherlands; and Department of Perinatology (J.D.), Wilhelmina Children's Hospital and Brain Center Rudolf Magnus, University Medical Center Utrecht, Utrecht, the Netherlands.

The research of K.P. was funded by the Royal Dutch Medical Association, *Erasmus Journal of Medicine* grant. T.J.W. and F.E.H. are supported by ZON-MW TOP and Dutch Science Organization-VIDI grants.

Please address correspondence to Freek Hoebeek, MD, Erasmus Medical Center, Department of Neuroscience, Room Eel2-20A, Westzeedijk 353, 3015 AA, Rotterdam, the Netherlands; e-mail: f.hoebeek@erasmusmc.nl; or Jeroen Dudink, MD, Utrecht University Medical Centre, Department of Neonatology; Wilhelmina Children's Hospital, Lundlaan 6, 3584 EA, Utrecht, the Netherlands; e-mail: j.dudink@umcutrecht.nl

 Indicates open access to non-subscribers at www.ajnr.org

 Indicates article with supplemental on-line tables.

<http://dx.doi.org/10.3174/ajnr.A5589>

ment rates are highest and cerebellar microstructure is vulnerable.^{19,20} Imaging studies conducted thus far have suggested that cerebellar lesions within this period disturb cerebellar development and may secondarily impact cerebral development^{21,22}; these findings suggest the existence of trophic interactions between the cerebellum and cerebrum during neurodevelopment and are in line with animal experiments showing the regulatory effects of the cerebellum on the development of supratentorial brain structures.^{23–25} Neonatal events that can disturb this complex interplay between cerebellar and cerebral development may be detrimental and may lead to functional impairment in later life.

To date, few neuroimaging studies have assessed the impact of preterm birth on the cerebellum and were, in great part, conducted during early perinatal stages, following major neurologic perinatal events (eg, hypoxic-ischemic encephalopathy, hemorrhages) and in infants born extremely preterm (<28 weeks of gestation). Studies assessing the long-term impact of birth age on cerebellar structures are sparse, and only a few studies have attempted to quantify the long-term effects of preterm birth on cerebellar anatomy and microstructures. Whether preterm birth in children born after 28 weeks of gestation without brain injury on perinatal imaging influences cerebellar structures long-term remains to be elucidated.

In this study among preterm and term-born infants 6–12 years of age at the time of follow-up, we report neuroimaging data supporting the hypothesis that the cerebellum is particularly sensitive to even subtle perinatal disturbances.

MATERIALS AND METHODS

Subjects

MR imaging scans and neuropsychological assessment scores of 102 children scanned between 6 and 12 years of age were collected and analyzed. The included cohort was scanned as part of a prospective cohort study among children in Rotterdam and consisted of 36 preterm-born infants (28–37 weeks' gestational age) and 66 term-born controls (On-line Table 1).²⁶ Exclusion criteria were the following: macroscopic brain injury seen on sonography during the hospital or neonatal intensive care stay of the infants born preterm (intraventricular hemorrhage, intraparenchymal lesions, stroke) and congenital abnormalities that could affect normal brain development negatively. Perinatal conditions of the infants and eventual adverse events are summarized in On-line Table 2.

All preterm infants had routine sonography assessment in the neonatal intensive care unit, which included scans at days 1, 3, and 7 after birth and once every other week during their neonatal intensive care unit stay. Ultrasounds were performed by expert neonatologists who had at least 2 years of experience with neonatal sonography. For cerebellar evaluation, the mastoid fontanelle was used as the acoustic window. Convex 5–10 MHz and linear 15–18 MHz probes (Esaote Diagnostic Imaging Systems, Genova, Italy) were used to assess the neonatal brain. Research ethics committee approval and written informed consent of parents and children were obtained before MR imaging.

MR Imaging and Data Processing

MR imaging at 6–12 years of age was performed between June 2011 and March 2013, using a 3T MR imaging system and consisted of T1-weighted MR imaging and DWI. T1-weighted imag-

ing was performed using the following settings: TR = 10.3 ms, TE = 4.2 ms, TI = 350 ms, matrix = 256×256 mm, isotropic resolution = $0.9 \times 0.9 \times 0.9$ mm, scan time = 5 minutes 40 seconds. Diffusion-weighted imaging was performed using an echo-planar imaging sequence with the following settings: TR = 11,000 ms, TE = 83 ms, flip angle = 90° , matrix = 128×128 , FOV = 256×256 mm, slice thickness = 2 mm, number of slices = 77, acquisition time = 7 minutes 40 seconds, 35 diffusion-weighted volumes ($b=1000$ s/mm²), 3 volumes without diffusion-weighting ($b=0$ s/mm²), scan time = 7 minutes 40 seconds.²⁷ All scans were obtained without sedation of the patient on a 3T MR imaging system using cushions to minimize head motion.

Preprocessing consisted of visual inspection of raw diffusion-weighted images and T1-weighted MR imaging in 3 orthogonal planes. Motion-corrupted images were excluded before analysis ($n = 2$). T1-weighted images were brain-extracted and registered to the diffusion-weighted images while correcting for EPI-induced deformities using the T1-weighted image as a reference. Diffusion-weighted data were corrected for motion-induced outliers, and tensors were calculated robustly using the REKINDLE (robust extraction of kurtosis indices with linear estimation) approach.^{28–31} Artifacts correction included correction for eddy currents, motion, and EPI-induced distortions. Preprocessing was performed using ExploreDTI, Version 4.8.5 (<http://exploredti.com/>) running in Matlab (R2015; MathWorks, Natick, Massachusetts).²⁹

Following preprocessing, we performed ROI analysis of cerebellar and cerebral regions based on automated white and gray matter segmentations (see On-line Tables 3 and 4 for more information on segmentation procedures and software). For each region, surface area and volume were calculated. Furthermore, probabilistic tractography of the following white matter tracts was performed using FSL (<http://www.fmrib.ox.ac.uk/fsl>) in conjunction with the AutoPtx plugin (<https://fsl.fmrib.ox.ac.uk/fsl/fslwiki/AutoPtx>) for automated probabilistic tractography^{32,33}: cerebellar peduncles (superior, middle, and inferior), thalamic radiation (anterior, superior, and posterior), longitudinal fasciculus (superior and inferior), forceps (major and minor), and corticospinal tract. Fractional anisotropy (FA) and median diffusivity (MD) values were computed for each tract. For more information on toolboxes, ROI placement, and MR imaging atlases that were used, see On-line Tables 3 and 4. Segmentation of the cerebellum was performed using the spatially unbiased infratentorial and cerebellar template segmentation toolbox (SUIT; <http://www.diedrichsenlab.org/imaging/propatlas.htm>). Segmentation results in a representative subject are shown in Fig 1.^{34,35}

Statistical Analysis

Statistical analysis was performed with SPSS Statistics for Windows, Version 22.0 (IBM, Armonk, New York). Linear regression analysis was performed to study the relationship between each structure that was delineated and gestational age, corrected for age at follow-up scanning and sex differences. The standardized regression coefficients and corresponding levels of significance are reported for each structure studied. Statistical results were corrected for multiple testing using a false discovery rate control procedure.³⁶

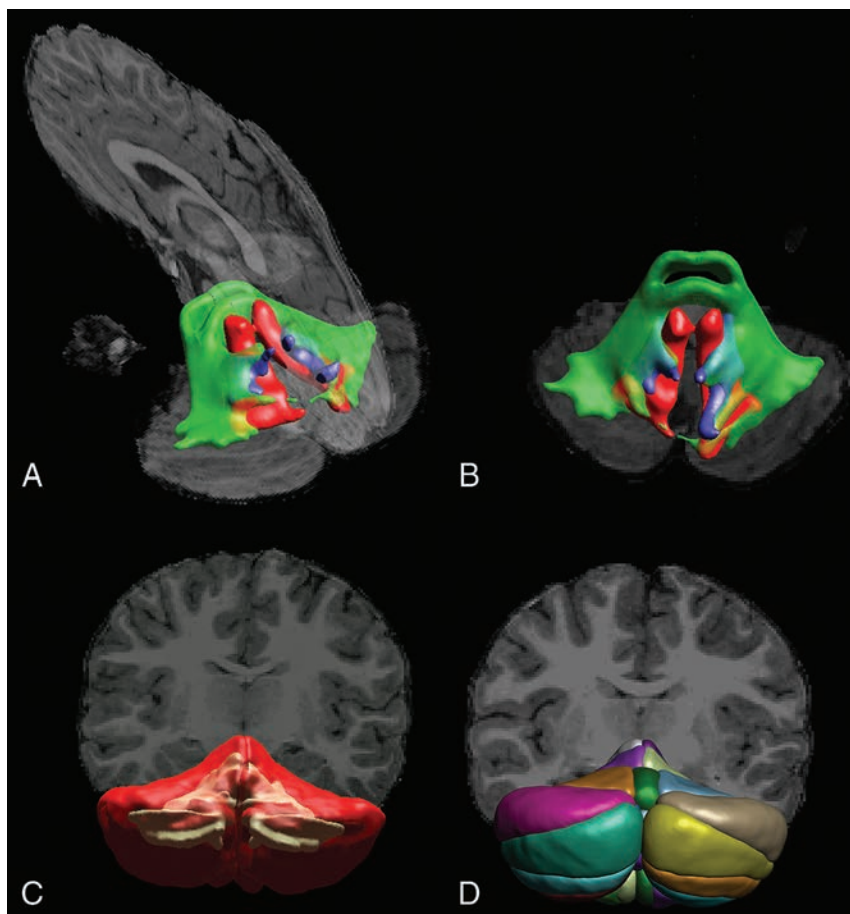


FIG 1. DTI-based tractography of the cerebellar peduncles (A and B) and T1-weighted image segmentation of white and gray matter (C) and cerebellar lobules (D) in a representative subject.

Table 1: Coefficients of the regression model for cerebral volumes and surface areas when accounting for age at scanning and sex differences as covariates

Dependent Variable ^a	Standardized Regression Coefficient (β)	Partial Correlation Coefficient (r)	T Statistics	Significance (2-Tailed)
Total cerebral volume (mm ³)	0.066	0.072	0.712	.48
Cerebral WM volume (mm ³)	0.148	0.130	1.271	.21
Cerebral cortex GM volume (mm ³)	0.058	0.054	0.526	.60
Cerebral WM surface area (mm ²)	0.148	0.130	1.271	.21
Cerebral cortex surface area (mm ²)	0.098	0.089	0.865	.39

^a Predictors in the model that were held constant: age at follow-up MRI (years) and sex (M/F).

Table 2: Coefficients of the regression model for cerebellar volumes and surface areas when accounting for age at scanning and sex differences as covariates

Dependent Variable ^a	Standardized Regression Coefficient (β)	Partial Correlation Coefficient (r)	T Statistics	Significance (2-Tailed)
Total cerebellar volume (mm ³)	0.224	0.195	1.945	.06
Cerebellar WM volume (mm ³)	0.387	0.357	3.703	<.001 ^b
Cerebellar GM volume (mm ³)	0.134	0.118	1.150	.25
Cerebellar WM surface area (mm ²)	0.387	0.357	3.703	<.001 ^b
Cerebellar cortex surface area (mm ²)	0.375	0.350	3.621	<.001 ^b

^a Predictors in the model that were held constant: age at follow-up MRI (years) and sex (M/F).

^b Significant.

RESULTS

Volumetric Analysis

Regression analysis of cerebellar and cerebral structures revealed significant alterations of cerebellar white and gray matter struc-

tures in relation to birth age, but not of analogous cerebral components (Tables 1 and 2). While we corrected for age at MR imaging and sex differences, lower gestational age at birth was associated with lower total cerebellar volume (standardized regression coefficient, $\beta = 0.191$, $P = .04$), whereas this was not found for the cerebral volume ($\beta = 0.057$, $P = .54$). When we evaluated gray and white matter separately, this relation was consistently observed; cerebellar white matter volume ($\beta = 0.336$, $P < .001$) and surface area ($\beta = 0.346$, $P < .001$) were significantly reduced in relation to lower gestational age at birth (Fig 2E, -G), while for cerebral white matter volume ($\beta = 0.098$, $P = .27$) and surface area ($\beta = 0.127$, $P = .17$), no significant relationship was observed (Fig 2A, -C). When comparing cerebellar and cerebral gray matter, we again found a significant negative correlation between the cerebellar gray matter surface area and gestational age at birth ($\beta = 0.337$, $P < .001$) (Fig 2H), while cerebral cortex surface area was not significantly correlated with gestational age at birth ($\beta = 0.073$, $P = .43$) (Fig 2D). Further subdivision of the cerebellar cortex in anatomic lobules according to the Schmahmann et al (1999)³⁷ atlas definitions did not highlight specific parts of the cerebellar cortex as being more predominantly affected in relation to gestational age than others (On-line Table 5).

After false discovery rate correction, which was performed to minimize the risk of false-positive significant findings, the volume and surface areas of cerebellar white matter ($\beta = 0.336$, $P < .001$) as well as cerebellar gray matter surface area ($\beta = 0.337$, $P < .001$) were consistently identified as being significantly associated with gestational age at birth.

DTI Analysis and Tractography

When we looked at diffusion properties of cerebral white matter, cerebral white matter FA and MD were not significantly associated with gestational age ($\beta = -0.016$, $P = .88$ and $\beta = -0.119$, $P = .22$), while for cerebellar white matter, a significant association was observed between cerebellar white matter fractional anisotropy and gestational age at birth ($\beta = -0.266$, $P = .008$). When we looked at gray matter, neither cerebral nor cerebellar FA and MD were

served between cerebellar white matter fractional anisotropy and gestational age at birth ($\beta = -0.266$, $P = .008$). When we looked at gray matter, neither cerebral nor cerebellar FA and MD were

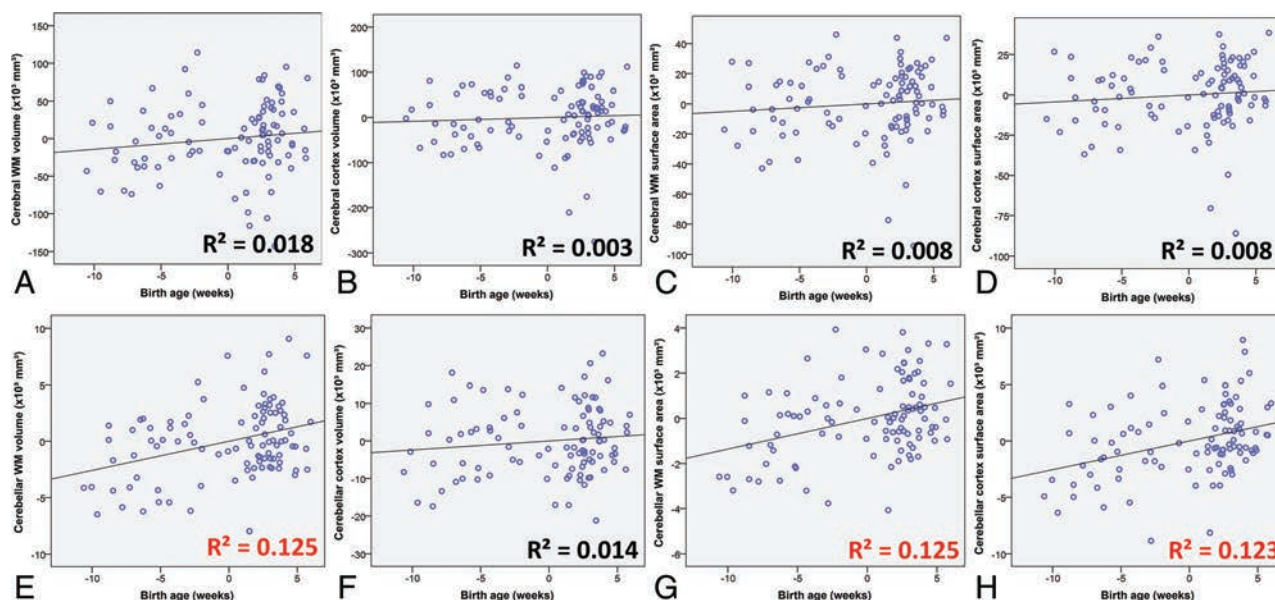


FIG 2. Linear regression analysis plots of cerebral and cerebellar structures in infancy in relation to birth age. Sex and age at follow-up MR imaging were included in the partial regression model as covariates. Significant R^2 correlation coefficients are highlighted in red. The horizontal axis indicates age at birth in weeks relative to term-equivalent age (37 weeks).

Table 3: Coefficient of the regression model for diffusion MRI measurements of the cerebellum and cerebrum corrected for age at scanning and sex differences

Dependent Variable ^a	Standardized Regression Coefficient (β)	Partial Correlation Coefficient (r)	T Statistics	Significance (2-Tailed)
Cerebellar white matter FA	−0.236	−0.238	−2.379	.02 ^b
Cerebellar white matter MD	−0.049	−0.049	−0.476	.64
Cerebellar gray matter FA	−0.104	−0.102	−0.992	.32
Cerebellar gray matter MD	−0.098	−0.095	−0.922	.36
Cerebral white matter FA	0.008	0.008	0.078	.94
Cerebral white matter MD	−0.109	−0.104	−1.014	.31
Cerebral cortex FA	−0.129	−0.123	−1.205	.23
Cerebral cortex MD	−0.059	−0.058	−0.568	.57

^a Predictors in the model that were held constant: age at scanning (years) and sex (M/F).

^b Significant.

significantly associated with gestational age at birth (Table 3). Tractography results of neither cerebellar nor cerebral tracts revealed obvious trends in diffusion characteristics in relation to gestational age at birth (On-line Table 6).

DISCUSSION

In this study, we have performed a structural assessment to evaluate cerebral and cerebellar structures in a cohort of preterm and term-born infants at school age who were free of intracranial lesions in the perinatal period. Our results show profound, long-term trophic effects on cerebellar structures related to birth age in infants free of neurologic complications in the perinatal period. In previous research, perinatal stages were shown to be essential for cerebellar morphogenesis, growth, and development, in that cerebellar aberrations were commonly described in infants with non-cerebellar neurologic pathologies (eg, hemorrhages, stroke) or major perinatal events such as profound hypoxia.^{20,21} Studies evaluating the consequences of prematurity on the cerebellum and cerebrum in the absence of perinatal brain lesions were mostly conducted during the early postnatal stages and were

therefore unable to differentiate between delayed maturation and persistent cerebellar changes.¹

In our cohort, trophic effects related to birth age were most pronounced in cerebellar white matter volume and cerebellar cortex surface area, as well as in cerebellar white matter microstructures as measured by DTI. These results suggest that particularly the cerebellum is sensitive to perinatal disturbances and that even in the absence of neurovascular events, long-term brain development is affected by perinatal circumstances related to prematurity. Possible mechanisms underlying impaired development are suboptimal oxygen levels due to lung immaturity, inflammation due to infections, and impaired regulation of essential nutrients.^{38–42}

The negative impact on cerebellar development that was observed in this study is of particular relevance for child health because disrupted cerebellar development has been associated with a variety of debilitating disorders, including autism spectrum disorder,¹⁵ schizophrenia,¹⁶ dyslexia,¹⁷ and attention deficit disorders.¹⁸ The provided evidence for developmental disturbances of the cerebellum in the absence of neurovascular events demands larger cohort studies with sufficient power to characterize underlying injury mechanisms.

Due to advances in neonatal care, the most commonly seen brain injuries in current clinical practice are shifting from large intracranial lesions toward more subtle disturbances. Therefore, a better understanding of more subtle injury mechanisms would allow further improvement in neonatal care and would help in targeting future neuroprotective strategies toward anatomic regions that are considered most vulnerable. The apparent sensitivity of the cerebellum to perinatal influences that was found in this study is consistent with scientific litera-

ture^{15,19,20,43} and indicates that a dedicated focus on the cerebellum is desirable in future research toward new neuroprotective strategies.

No significant relations were observed between tract profiles of white matter pathways and age at birth in our cohort. A limited number of diffusion-encoding directions in the applied imaging protocol restricted the ability of tracking through crossing-fiber regions in the brain. Future studies using more advanced tractography methods may allow a more detailed characterization of white matter tracts connecting cerebellar hemispheres to contralateral cerebral cortices. In the literature, it has been hypothesized that during the early stages of development, impairment in cerebellar structures might affect cerebral development and vice versa.^{21,43,44} It is therefore possible that alterations in supratentorial brain regions that have been reported in many studies of infants born preterm to some extent relate to impaired cerebellar development and related impaired trophic interactions.^{21,45} Advanced neuroimaging or axonal tracing experiments in human postmortem tissue may provide more insight about cerebello-cerebral connectivity.^{46–48}

For cerebellar white matter, we found a significant increase in white matter FA in infants born earlier, while tractography results of cerebellar tracts were not related to gestational age at birth. The latter finding is remarkable given that our data also showed clear associations between gestational age at birth and cerebellar white matter volume and gray matter surface area. It may be that an increase in FA of total cerebellar white matter in infants born earlier reflects higher fiber coherence and myelination or that the increase in FA results from a decreased complexity of fiber orientations. In the latter case, the extent of fanning and/or crossing fibers is lower in children born earlier, which in turn results in higher FA when using a diffusion tensor model that is inherently unable to adequately represent complex fiber configurations.^{49–51} Future studies using recently developed advanced imaging techniques that can capture more complex fiber orientations are needed to clarify this issue.^{46–48}

Persistent abnormalities in cerebellar volume and surface area that were observed in this study are likely a result of irreversible cellular changes during perinatal stages, when cerebellar proliferation and differentiation rates are highest. In the period between 24 and 40 weeks of gestation, cerebellar volume and surface area increase exponentially due to highly active proliferative zones and rapid migration and differentiation of precursor cells. Preterm birth occurs within this critical timeframe and is likely able to disturb these delicate processes, even in the absence of observable cerebellar lesions. Although infants with intraparenchymal lesions on perinatal sonography were excluded from analysis, we acknowledge that it is unknown whether subtler cerebellar lesions and punctate cerebellar hemorrhages (<4 mm diameter) that are quickly resolved are overlooked in current neuroimaging approaches due to limited spatial resolution of both MR imaging and sonography.^{52–55}

Future studies using more advanced imaging approaches that would allow a more detailed assessment of cerebello-cerebral connectivity and interaction are needed to elucidate whether changes in cerebellar microstructures and structures result in impaired cerebello-cerebral connectivity.

CONCLUSIONS

We have demonstrated the long-term effects of neurologically uncomplicated preterm birth at ≥ 28 weeks' gestational age on cerebellar structures and microstructure. The results of our study suggest a particular vulnerability of the cerebellum to adverse effects of preterm birth, even in the absence of neurologic complications. A special focus on the cerebellum seems therefore essential in fundamental research toward the development of future neuroprotective strategies and predictive models of outcome.

ACKNOWLEDGMENTS

We thank the participants of the study.

Disclosures: Kay Pieterman—RELATED: Grant: Royal Dutch Medical Association, Erasmus Journal of Medicine grant, Comments: research grant of €5000 offered by the university to honors class students.* Tonya J. White—RELATED: Grant: Netherlands Organization for Health Research and Development, Comments: TOP project number 91211021*. Wiro J. Niessen—UNRELATED: Consultancy: Quantib BV, Comments: scientific advisor*; Stock/Stock Options: Quantib BV, Comments: cofounder and stockholder. Freek E. Hoebeek—UNRELATED: Grants/Grants Pending: Dutch Science Organization, Comments: individual fellowship (VIDI-scheme)*. *Money paid to the institution.

REFERENCES

1. de Kieviet JF, Zoetebier L, van Elburg RM, et al. **Brain development of very preterm and very low-birthweight children in childhood and adolescence: a meta-analysis.** *Dev Med Child Neurol* 2012;54:313–23 CrossRef Medline
2. Bos AF, Van Braeckel KN, Hitzert MM, et al. **Development of fine motor skills in preterm infants.** *Dev Med Child Neurol* 2013;55(Suppl 4):1–4 CrossRef Medline
3. Svedenkrans J, Henckel E, Kowalski J, et al. **Long-term impact of preterm birth on exercise capacity in healthy young men: a national population-based cohort study.** *PLoS One* 2013;8:e80869 CrossRef Medline
4. Abitbol CL, Rodriguez MM. **The long-term renal and cardiovascular consequences of prematurity.** *Nat Rev Nephrol* 2012;8:265–74 CrossRef Medline
5. Ali K, Greenough A. **Long-term respiratory outcome of babies born prematurely.** *Thorax* 2012;67:115–20 CrossRef Medline
6. Grisaru-Granovsky S, Reichman B, Lerner-Geva L, et al. **Population-based trends in mortality and neonatal morbidities among singleton, very preterm, very low birth weight infants over 16 years.** *Early Hum Dev* 2014;90:821–27 CrossRef Medline
7. Marlow N, Wolke D, Bracewell MA, et al. **Neurologic and developmental disability at six years of age after extremely preterm birth.** *N Engl J Med* 2005;352:9–19 CrossRef Medline
8. Platt MJ, Cans C, Johnson A, et al. **Trends in cerebral palsy among infants of very low birthweight (<1500 g) or born prematurely (<32 weeks) in 16 European centres: a database study.** *Lancet* 2007;369:43–50 CrossRef Medline
9. Hamrick SE, Miller SP, Leonard C, et al. **Trends in severe brain injury and neurodevelopmental outcome in premature newborn infants: the role of cystic periventricular leukomalacia.** *J Pediatr* 2004;145:593–99 CrossRef Medline
10. Ferriero DM. **Neonatal brain injury.** *N Engl J Med* 2004;351:1985–95 CrossRef Medline
11. Brossard-Racine M, du Plessis AJ, Limperopoulos C. **Developmental cerebellar cognitive affective syndrome in ex-preterm survivors following cerebellar injury.** *Cerebellum* 2015;14:151–64 CrossRef Medline
12. E KH, Chen SH, Ho MH, et al. **A meta-analysis of cerebellar contributions to higher cognition from PET and fMRI studies.** *Hum Brain Mapp* 2014;35:593–615 CrossRef Medline
13. Koziol LF, Budding D, Andreasen N, et al. **Consensus paper: the**

- cerebellum's role in movement and cognition. *Cerebellum* 2014;13:151–77 CrossRef Medline
14. Mazzola V, Vuilleumier P, Latorre V, et al. Effects of emotional contexts on cerebello-thalamo-cortical activity during action observation. *PLoS One* 2013;8:e75912 CrossRef Medline
15. Wang SS, Kloth AD, Badura A. The cerebellum, sensitive periods, and autism. *Neuron* 2014;83:518–32 CrossRef Medline
16. Wagner G, De la Cruz F, Schachtzabel C, et al. Structural and functional dysconnectivity of the fronto-thalamic system in schizophrenia: a DCM-DTI study. *Cortex* 2015;66:35–45 CrossRef Medline
17. Eckert MA, Leonard CM, Richards TL, et al. Anatomical correlates of dyslexia: frontal and cerebellar findings. *Brain* 2003;126:482–94 CrossRef Medline
18. Berquin PC, Giedd JN, Jacobsen LK, et al. Cerebellum in attention-deficit hyperactivity disorder: a morphometric MRI study. *Neurology* 1998;50:1087–93 CrossRef Medline
19. Volpe JJ. Cerebellum of the premature infant: rapidly developing, vulnerable, clinically important. *J Child Neurol* 2009;24:1085–104 CrossRef Medline
20. Limperopoulos C, Soul JS, Gauvreau K, et al. Late gestation cerebellar growth is rapid and impeded by premature birth. *Pediatrics* 2005;115:688–95 CrossRef Medline
21. Limperopoulos C, Soul JS, Haidar H, et al. Impaired trophic interactions between the cerebellum and the cerebrum among preterm infants. *Pediatrics* 2005;116:844–50 CrossRef Medline
22. Limperopoulos C, Chilingaryan G, Sullivan N, et al. Injury to the premature cerebellum: outcome is related to remote cortical development. *Cereb Cortex* 2014;24:728–36 CrossRef Medline
23. Martin GF, Cabana T, Hazlett JC, et al. Development of brainstem and cerebellar projections to the diencephalon with notes on thalamocortical projections: studies in the North American opossum. *J Comp Neurol* 1987;260:186–200 CrossRef Medline
24. Lotto RB, Price DJ. The stimulation of thalamic neurite outgrowth by cortex-derived growth factors in vitro: the influence of cortical age and activity. *Eur J Neurosci* 1995;7:318–28 CrossRef Medline
25. Hisanaga K, Sharp FR. Marked neurotrophic effects of diffusible substances released from non-target cerebellar cells on thalamic neurons in culture. *Brain Res Dev Brain Res* 1990;54:151–60 CrossRef Medline
26. van den Bosch GE, White T, El Marroun H, et al. Prematurity, opioid exposure and neonatal pain: do they affect the developing brain? *Neonatology* 2015;108:8–15 CrossRef Medline
27. White T, El Marroun H, Nijs I, et al. Pediatric population-based neuroimaging and the Generation R Study: the intersection of developmental neuroscience and epidemiology. *Eur J Epidemiol* 2013;28:99–111 CrossRef Medline
28. Irfanoglu MO, Walker L, Sarlls J, et al. Effects of image distortions originating from susceptibility variations and concomitant fields on diffusion MRI tractography results. *Neuroimage* 2012;61:275–88 CrossRef Medline
29. Leemans A, Jeurissen B, Sijbers J, et al. ExploreDTI: a graphical toolbox for processing, analyzing, and visualizing diffusion MR data. In: *Proceedings of the 17th Annual Meeting of International Society for Magnetic Resonance in Medicine*, Honolulu, Hawaii. April 18–24, 2009;209:3537
30. Leemans A, Jones DK. The B-matrix must be rotated when correcting for subject motion in DTI data. *Magn Reson Med* 2009;61:1336–49 CrossRef Medline
31. Tax CM, Otte WM, Viergever MA, et al. REKINDLE: robust extraction of kurtosis indices with linear estimation. *Magn Reson Med* 2015;73:794–808 CrossRef Medline
32. Jenkinson M, Beckmann CF, Behrens TE, et al. FSL. *Neuroimage* 2012;62:782–90 CrossRef Medline
33. de Groot M, Vernooij MW, Klein S, et al. Improving alignment in tract-based spatial statistics: evaluation and optimization of image registration. *Neuroimage* 2013;76:400–11 CrossRef Medline
34. Diedrichsen J, Balsters JH, Flavell J, et al. A probabilistic MR atlas of the human cerebellum. *Neuroimage* 2009;46:39–46 CrossRef Medline
35. Diedrichsen J. A spatially unbiased atlas template of the human cerebellum. *Neuroimage* 2006;33:127–38 CrossRef Medline
36. Benjamini Y, Hochberg Y. Controlling the false discovery rate: a practical and powerful approach to multiple testing. *Journal of the Royal Statistical Society Series B (Methodological)* 1995;57:289–300
37. Schmahmann JD, Doyon J, McDonald D, et al. Three-dimensional MRI atlas of the human cerebellum in proportional stereotaxic space. *Neuroimage* 1999;10:233–60 CrossRef Medline
38. Baraldi E, Filippone M. Chronic lung disease after premature birth. *N Engl J Med* 2007;357:1946–55 CrossRef Medline
39. Keunen K, van Elburg RM, van Bel F, et al. Impact of nutrition on brain development and its neuroprotective implications following preterm birth. *Pediatr Res* 2015;77:148–55 CrossRef Medline
40. Beardsall K, Dunger D. The physiology and clinical management of glucose metabolism in the newborn. *Endocr Dev* 2007;12:124–37 Medline
41. Schmid MB, Hopfner RJ, Lenhof S, et al. Cerebral oxygenation during intermittent hypoxemia and bradycardia in preterm infants. *Neonatology* 2015;107:137–46 CrossRef Medline
42. Rizzo T, Metzger BE, Burns WJ, et al. Correlations between antepartum maternal metabolism and intelligence of offspring. *N Engl J Med* 1991;325:911–16 CrossRef Medline
43. Limperopoulos C, Chilingaryan G, Guizard N, et al. Cerebellar injury in the premature infant is associated with impaired growth of specific cerebral regions. *Pediatr Res* 2010;68:145–50 CrossRef Medline
44. Bolduc ME, Du Plessis AJ, Evans A, et al. Cerebellar malformations alter regional cerebral development. *Dev Med Child Neurol* 2011;53:1128–34 CrossRef Medline
45. Ball G, Boardman JP, Rueckert D, et al. The effect of preterm birth on thalamic and cortical development. *Cereb Cortex* 2012;22:1016–24 CrossRef Medline
46. Pieterman K, Batalle D, Dudink J, et al. Cerebello-cerebral connectivity in the developing brain. *Brain Struct Funct* 2017;222:1625–34 CrossRef Medline
47. Palesi F, Tournier JD, Calamante F, et al. Contralateral cerebello-thalamo-cortical pathways with prominent involvement of associative areas in humans in vivo. *Brain Struct Funct* 2015;220:3369–84 CrossRef Medline
48. Palesi F, Tournier JD, Calamante F, et al. Reconstructing contralateral fiber tracts: methodological aspects of cerebello-thalamocortical pathway reconstruction. *Funct Neurol* 2016;31:229–38 Medline
49. Descoteaux M, Deriche R, Knösche TR, et al. Deterministic and probabilistic tractography based on complex fibre orientation distributions. *IEEE Trans Med Imaging* 2009;28:269–86 CrossRef Medline
50. Kristo G, Leemans A, Raemaekers M, et al. Reliability of two clinically relevant fiber pathways reconstructed with constrained spherical deconvolution. *Magn Reson Med* 2013;70:1544–56 CrossRef Medline
51. Tournier JD, Yeh CH, Calamante F, et al. Resolving crossing fibres using constrained spherical deconvolution: validation using diffusion-weighted imaging phantom data. *Neuroimage* 2008;42:617–25 CrossRef Medline
52. Plaisier A, Raets MM, Ecury-Goossens GM, et al. Serial cranial ultrasonography or early MRI for detecting preterm brain injury? *Arch Dis Child Fetal Neonatal Ed* 2015;100:F293–300 CrossRef Medline
53. Plaisier A, Govaert P, Lequin MH, et al. Optimal timing of cerebral MRI in preterm infants to predict long-term neurodevelopmental outcome: a systematic review. *AJNR Am J Neuroradiol* 2014;35:841–47 CrossRef Medline
54. Heemskerk AM, Leemans A, Plaisier A, et al. Acquisition guidelines and quality assessment tools for analyzing neonatal diffusion tensor MRI data. *AJNR Am J Neuroradiol* 2013;34:1496–505 CrossRef Medline

55. Ecury-Goossen GM, Camfferman FA, Leijser LM, et al. **State of the art cranial ultrasound imaging in neonates.** *J Vis Exp* 2015:e52238 CrossRef Medline
56. Destrieux C, Fischl B, Dale A, et al. **Automatic parcellation of human cortical gyri and sulci using standard anatomical nomenclature.** *Neuroimage* 2010;53:1–15 CrossRef Medline
57. Behrens TE, Woolrich MW, Jenkinson M, et al. **Characterization and propagation of uncertainty in diffusion-weighted MR imaging.** *Magn Reson Med* 2003;50:1077–88 CrossRef Medline
58. Behrens TE, Berg HJ, Jbabdi S, et al. **Probabilistic diffusion tractography with multiple fiber orientations: what can we gain?** *Neuroimage* 2007;34:144–55 CrossRef Medline

Prenatal Brain MR Imaging: Reference Linear Biometric Centiles between 20 and 24 Gestational Weeks

 G. Conte,  S. Milani,  G. Palumbo,  G. Talenti,  S. Boito,  M. Rustico,  F. Triulzi,  A. Righini,  G. Izzo,  C. Doneda,  A. Zolin, and  C. Parazzini



ABSTRACT

BACKGROUND AND PURPOSE: Evaluation of biometry is a fundamental step in prenatal brain MR imaging. While different studies have reported reference centiles for MR imaging biometric data of fetuses in the late second and third trimesters of gestation, no one has reported them in fetuses in the early second trimester. We report centiles of normal MR imaging linear biometric data of a large cohort of fetal brains within 24 weeks of gestation.

MATERIALS AND METHODS: From the data bases of 2 referral centers of fetal medicine, accounting for 3850 examinations, we retrospectively collected 169 prenatal brain MR imaging examinations of singleton pregnancies, between 20 and 24 weeks of gestational age, with normal brain anatomy at MR imaging and normal postnatal neurologic development. To trace the reference centiles, we used the CG-LMS method.

RESULTS: Reference biometric centiles for the developing structures of the cerebrum, cerebellum, brain stem, and theca were obtained. The overall interassessor agreement was adequate for all measurements.

CONCLUSIONS: Reference biometric centiles of the brain structures in fetuses between 20 and 24 weeks of gestational age may be a reliable tool in assessing fetal brain development.

ABBREVIATIONS: BPD = biparietal diameter; LLD = latero-lateral diameter; CSA = clivo-supraoccipital angle; FOD = fronto-occipital diameter; GA = gestational age; LCC = length of the corpus callosum; APD = antero-posterior diameter; CCD = cranio-caudal diameter

Prenatal MR imaging plays an important role in the evaluation of the fetal brain, being usually performed as a second-look investigation when suspected brain abnormalities are detected by prenatal sonography. Prenatal MR imaging has been demonstrated to improve the diagnostic accuracy of brain anomalies, leading to changes in clinical management in many cases.¹ Prenatal MR imaging results may also affect parental counseling. In several countries, imaging is

usually performed in the early second trimester (within 24–25 weeks of gestation) because laws and regulations require crucial decisions to be made within such deadline, and additional MR imaging follow-up is not compatible with time constraints.²


Prenatal brain MR imaging, in addition to morphologic assessment, relies on biometry evaluation. In particular, linear biometry is a fundamental step in clinical routine practice. Biometry is relatively easy to assess as far as reference parameters are established. Thus, normative data of the main fetal brain dimensions are necessary to detect possible disorders in brain development. Different studies have reported normative MR imaging biometric data of fetuses in the late second and third trimesters of gestation.^{3–5} In contrast, few studies have reported them in fetuses in the early second trimester, and these had some methodologic limitations: small number of fetuses^{5–7}; inadequate descriptive analysis based on maximum and minimum values rather than on centiles of each measurement^{5,7}; and volumetric measurements difficult to apply clinically (fetal movements during MR imaging acquisition, time-consuming postprocessing analysis).^{6–12}


The purpose of our study was to report centiles of reference MR imaging linear biometric data of a large cohort of fetal brains within 24 weeks of gestation.

Received October 23, 2017; accepted after revision January 1, 2018.

From the Neuroradiology Unit (G.C., G.P., F.T.) and Division of Prenatal Diagnosis (S.B.), Istituto Di Ricovero e Cura a Carattere Scientifico Fondazione Ca' Granda Ospedale Policlinico, Milan, Italy; Department of Clinical Sciences and Community Health (S.M., A.Z.), Laboratory of Medical Statistics, Biometry and Epidemiology "G.A. Maccacaro," and Department of Pathophysiology and Transplantation (F.T.), Università degli Studi di Milano, Milan, Italy; Neuroradiology Unit (G.T.), Padua University Hospital, Padua, Italy; and Fetal Therapy Unit "Umberto Nicolini" (M.R.), Department of Woman Mother and Neonate, and Department of Paediatric Radiology and Neuroradiology (A.R., G.I., C.D., C.P.), Ospedale dei Bambini "V. Buzzi," Milan, Italy.

Please address correspondence to Giorgio Conte, MD, Fondazione IRCCS Ca' Granda Ospedale Maggiore Policlinico, Neuroradiology Unit, Via Francesco Sforza 35, 20122 Milan, Italy; e-mail: giorgioconte.unimed@gmail.com

 Indicates article with supplemental on-line tables.

 Indicates article with supplemental on-line photos.

<http://dx.doi.org/10.3174/ajnr.A5574>

Table 1: Indications for prenatal MR imaging

Indication for Prenatal MRI	No. of Fetuses (%)
Unclear CNS findings at ultrasound	80 (47)
Extra-CNS disease or malformation	30 (18)
Previous child with a confirmed CNS malformation	59 (35)

MATERIALS AND METHODS

Population

We reviewed the prenatal brain MR imaging data bases of 2 referral centers of fetal medicine, accounting for the examinations performed between 2005 and 2016: three hundred fifty examinations at Istituto Di Ricovero e Cura a Carattere Scientifico Fondazione Ca' Granda Ospedale Maggiore Policlinico (Milan, Italy) and 3500 examinations at Ospedale dei Bambini "Vittore Buzzi" (Milan, Italy). The prenatal MR imaging data bases were approved by the institutional review boards of the 2 hospitals, and all women signed an informed consent for the research use of data.

We collected prenatal brain MR imaging examinations of singleton pregnancies, between 20 and 24 weeks of gestational age (GA), which were performed for the indications reported in Table 1. Exclusion criteria were the following: 1) clear or suspected brain abnormalities at prenatal MR imaging, 2) poor image quality, 3) chromosomal abnormalities, 4) pregnancies complicated by infections, and 5) extra-CNS malformations frequently associated with CNS malformations (eg, cardiac rhabdomyoma). Gestational age was calculated by obstetricians and gynecologists on the basis of the menstrual period and ultrasound criteria and expressed as completed weeks.

Image Acquisition and Analysis

In both hospitals, prenatal MR imaging examinations were performed at 1.5T with the same scanner model (Achieva; Philips Healthcare, Best, the Netherlands) and phased-array abdominal or cardiac coils. Prenatal MR imaging protocols were standard clinical and state-of-the-art, were identical for both hospitals, and included the following: T2-weighted single-shot fast spin-echo multiplanar sections (3- to 4-mm-thick sections; gap = 0.1 mm; TR/TE = 3000/180 ms; in-plane resolution = 1.1-mm²); balanced fast-field echo multiplanar sections (3-mm-thick contiguous sections; TR/TE = 7/3.5 ms; in-plane resolution = 1.5 mm²); T1-weighted fast spin-echo multiplanar sections (5.5-mm-thick sections; TR/TE = 300/14 ms; turbo factor = 3; in-plane resolution = 1.4 mm²); in some cases, T2-weighted 3D fast-field echo sections (1.1-mm-thick sections; TR/TE = 2.5/4.7 ms; in-plane resolution = 1.1 × 1.1 mm²); single-shot fast spin-echo fluid-attenuated inversion recovery sections (4-mm-thick sections; TR/TE = 600/54 ms; in-plane resolution = 1.25 × 3.1 mm²); and diffusion-weighted imaging sections (5.5-mm-thick sections; TR/TE = 1000/90 ms; b factor = 0–600 s/mm²; FOV = 320 × 320 mm, matrix = 128 × 128).

Image analysis was performed on dedicated PACS workstations equipped with professional monitors. All images were independently reviewed for evaluation of biometry with respect to GA by 1 fetal neuroradiologist and 1 resident with >2 years of experience in prenatal MR imaging. In accordance with the method described in previous studies,^{5,13,14} each reader evaluated the following measurements: thecal fronto-occipital diameter (FOD),

thecal biparietal diameter (BPD), length of the corpus callosum (LCC), cerebral FOD, cerebral BPD, width of the atria of the lateral ventricles, mesencephalic antero-posterior diameter (APD), vermian APD, vermian cranio-caudal diameter (CCD), cerebellar latero-lateral diameter (LLD), latero-lateral diameter of the posterior cranial fossa (PCF), pontine APD and pontine CCD, and clivo-supraoccipital angle (CSA). All MR imaging measures were expressed in millimeters, with the only exception being the CSA (degree). The ratio between the LCC and cerebral FOD was also calculated (LCC/cerebral FOD). For details about measurements, see On-line Figs 1A–6B. Each measure was taken twice or thrice on the same or different acquisitions, preferably on balanced fast-field echo images in consideration of their higher spatial resolution (thinner sections) compared with single-shot fast spin-echo T2-weighted images. The average of the measures of each reader was regarded as his best (ie, most reliable) measure. The average of these best measures was used to trace the reference charts.

Statistical Analysis

The lack of precision (random error) of MR imaging assessments was expressed as standard error of measurements (ie, the SD of the measures of the same subject).¹⁵ The difference between the averages of measures made by the 2 assessors (A and B) participating in this study was regarded as an estimate of the difference in their accuracy (systematic error).

The estimates of the size attained at 22 weeks of GA and of the mean weekly increase from 20 to 24 weeks were derived from the following linear model:

$$E(\text{MR trait}) = \mu + \alpha \times s + \beta \times t + \gamma \times s \times t,$$

where $E(\text{MR trait})$ is the expected value of the MR imaging trait, s is 0 for females and 1 for males, $t = \text{GA} - 22$, μ is size attained by females at 22 weeks, α is the "male-versus-female" difference in size attained at 22 weeks, β is mean weekly increase shown by females from 20 to 24 weeks, and γ is the "male-versus-female" difference in an average weekly increase from 20 to 24 weeks.

To trace the reference centiles, we used the CG-LMS method.¹⁶ This expresses the centiles in terms of GA-specific curves called $L(t)$, $M(t)$, and $S(t)$. The $M(t)$ and $S(t)$ curves correspond to the median and coefficient of variation of the MR imaging trait at each age, whereas the $L(t)$ curve allows for the GA-dependent skewness of the distribution of the trait. The value (y) of the MR imaging trait at a given age can be transformed into a SD score (SDS):

$$\text{SDS} = \frac{[y/M(t)]^{L(t)} - 1}{L(t) \times S(t)}.$$

The value $y(p, t)$ of the p th centile at $\text{GA} = t$ is given by $y(p, t) = M(t) \times [1 + z_p \times L(t) \times S(t)]^{1/L(t)}$, where z_p is the standard normal deviate corresponding to probability p .

Centiles were calculated using the software LMS program, Version 1.29 (Medical Research Council, Leicester, UK).

RESULTS

A total of 169 fetuses (23 fetuses of 20 weeks, 73 of 21 weeks, 43 of 22 weeks, 22 of 23 weeks, 8 of 24 weeks) satisfied all the inclusion criteria. One-hundred fifty-nine of 169 fetuses were followed to term and

Table 2: Accuracy and precision of MR imaging measurements

	No. ^a	Mean ^b	B-A ^c	B-A (%) ^d	t Test ^e	P	SEM ^f	CV _{SEM} ^g	r ^h	P
PCF	165	28.61	0.022	0.08	0.17		1.148	4.01	0.059	
Cerebral FOD	168	56.77	-3.258	-5.74	-18.53	<.01	1.611	2.84	0.158	<.05
Cerebral BPD	169	42.12	-1.263	-3.00	-11.68	<.01	0.995	2.36	-0.141	
Vermian APD	167	7.08	0.014	0.20	0.21		0.611	8.64	0.192	<.05
Cerebellar LLD	166	21.81	-1.020	-4.68	-10.41	<.01	0.893	4.09	0.111	
Vermian CCD	168	10.13	-0.934	-9.22	-13.29	<.01	0.644	6.36	-0.004	
CSA	168	72.25	1.020	1.41	1.77		5.278	7.30	0.192	<.05
LCC	152	17.97	0.176	0.98	1.75		0.878	4.89	0.071	
LCC/cerebral FOD (%)	151	31.69	2.252	7.11	11.87	<.01	1.648	5.20	0.238	<.01
Thecal FOD	167	63.47	0.360	0.57	2.97	<.01	1.106	1.74	0.002	
Thecal BPD	169	49.74	0.682	1.37	4.45	<.01	1.410	2.83	0.106	
Mesencephalic APD	118	4.46	0.197	4.41	3.08	<.01	0.490	10.99	0.143	
Pontine APD	159	6.69	-0.074	-1.10	-1.34		0.491	7.34	0.241	<.01
Pontine CCD	158	7.53	-0.384	-5.10	-6.24	<.01	0.547	7.27	0.184	<.05
Lateral ventricles	161	6.76	0.568	8.40	8.15	<.01	0.625	9.25	-0.214	<.01

Note:—SEM indicates standard error of the measurements; APD, antero-posterior diameter; BPD, biparietal diameter; CCD, cranio-caudal diameter; CV, coefficient of variation; CSA, clivus-supraoccipital angle; LCC, length of the corpus callosum; LLD, latero-lateral diameter; FOD, fronto-occipital diameter; PCF, latero-lateral diameter of the posterior cranial fossa.

^a The number of observations.

^b Mean of all measurements.

^c Mean difference between assessor B and assessor A (difference in accuracy of assessors A and B).

^d Percentage interassessor difference [$100 \times (B-A) / \text{mean}$].

^e t test for difference in B-A.

^f Measuring error—that is, the SD of the measures of the same fetus (lack of precision).

^g Measuring error expressed as coefficient of variation (%) of ($100 \times \text{SEM} / \text{mean}$).

^h Correlation coefficient between interassessor B-A difference and the mean of the measurements made on a single fetus.

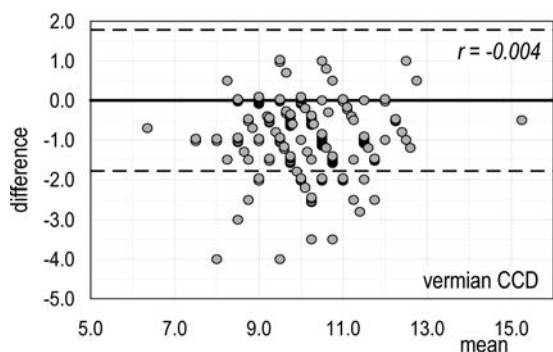


FIG 1. Vermian CCD (the MR imaging trait with the worst percentage disagreement in accuracy between the 2 assessors). Bland-Altman plot of the interassessor B-A difference versus the mean of the measures made on a single fetus. *Dashed lines* are the limits of agreement for the B-A difference: Ninety-five percent of these differences are expected to lie within these limits when the agreement between the 2 assessors is perfect.

determined to be healthy postnatally. Ten of 169 fetuses were missed at postnatal follow-up, and their sex was unknown because their parents did not want to know the sex at the time of the MR imaging and only head-targeted MR imaging was performed.

Reliability

As reported in Table 2, assessor B provided measures slightly higher than assessor A for most MR imaging traits and slightly lower for the cerebrum (cerebral FOD and BPD), vermis (vermian APD and CCD), and pons (pontine APD and CCD). The interassessor disagreement in accuracy ranged from -9.2% (vermian CCD) to +8.4% (width of the atria of the lateral ventricles). The measuring error ranged from 1.7% (thecal FOD) to 11.0% (mesencephalic APD). A weak positive correlation emerged between the interassessor B-A difference and the mean of the measures made on a single fetus for most traits (maximum

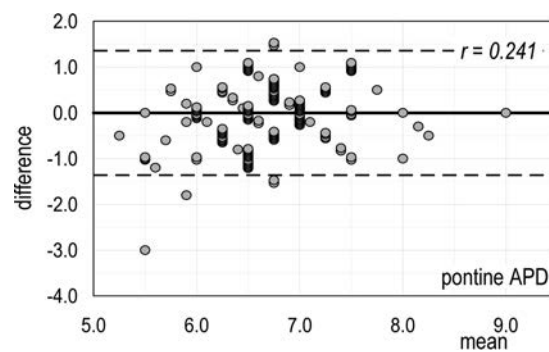


FIG 2. Pontine APD (the MR imaging trait with the highest correlation of disagreement in accuracy between the 2 assessors and size of MR imaging trait). Bland-Altman plot of the interassessor B-A difference versus the mean of the measures made on a single fetus. *Dashed lines* are the limits of agreement for the B-A difference: Ninety-five percent of these differences are expected to lie within these limits when the agreement between the 2 assessors is perfect.

$r = +0.241$, pontine APD). On the contrary, cerebral BPD, vermian CCD, and the width of the atria of the lateral ventricles showed a weak negative correlation (maximum $r = -0.214$).

The Bland-Altman plot for vermian CCD (Fig 1) (ie, the MR imaging trait with the worst percentage disagreement in accuracy between the 2 assessors) shows that 16.1% (27/168) of differences are below the lower agreement limit instead of the expected 2.5%. The Bland-Altman plot for pontine APD (Fig 2) (ie, the MR imaging trait with the highest correlation of disagreement in accuracy between the 2 assessors and size of MR trait) shows that the number of differences within the agreement limits (153/159) is close to the expected one (151/159). Thus, we can conclude that for all the MR imaging traits here considered, both systematic and random errors of measurements can be regarded as negligible. Bland-Altman diagrams for all MR imaging traits are reported in On-line Figs 7).

Table 3: Median and reference limits (5th and 95th centiles) for MR imaging traits between 20 and 24 completed weeks of gestation

	20 Weeks			21 Weeks			22 Weeks			23 Weeks			24 Weeks		
	5th	50th	95th	5th	50th	95th	5th	50th	95th	5th	50th	95th	5th	50th	95th
PCF	23.3	26.3	29.3	24.6	27.8	31.1	25.9	29.3	32.9	27.2	30.8	34.7	28.5	32.4	36.5
Cerebral FOD	46.7	51.2	56.4	50.1	54.8	60.2	53.4	58.4	64.1	56.8	62.0	67.9	60.2	65.5	71.7
Cerebral BPD	36.2	38.7	41.6	37.8	40.9	44.5	39.4	43.0	47.4	40.9	45.2	50.5	42.4	47.3	53.6
Vermian APD	5.5	6.3	7.2	6.0	6.8	7.8	6.4	7.3	8.4	6.8	7.8	9.0	7.2	8.3	9.6
Cerebellar LLD	18.2	19.9	21.8	19.1	21.1	23.4	20.1	22.4	25.0	21.0	23.6	26.6	21.9	24.9	28.3
Vermian CCD	7.7	9.0	10.0	8.3	9.8	10.9	8.9	10.6	11.9	9.5	11.4	12.8	10.1	12.1	13.8
CSA	63.7	71.0	79.9	63.6	71.6	81.5	63.4	72.1	83.2	63.2	72.7	85.0	63.1	73.2	86.8
LCC	13.3	15.3	17.1	14.7	17.1	19.2	16.0	18.9	21.4	17.3	20.7	23.6	18.6	22.5	25.8
LCC/cerebral FOD (%)	27.3	29.9	32.5	27.8	31.1	34.3	28.3	32.3	36.1	28.7	33.5	38.0	29.1	34.7	39.9
Thecal FOD	53.4	57.5	62.1	56.7	61.3	66.6	60.0	65.2	71.2	63.2	69.0	75.7	66.4	72.8	80.4
Thecal BPD	42.1	45.7	49.9	44.4	48.3	52.9	46.7	50.9	56.0	49.0	53.6	59.1	51.3	56.2	62.1
Mesencephalic APD	3.6	4.4	5.2	3.7	4.5	5.2	3.8	4.5	5.3	3.8	4.6	5.3	3.9	4.6	5.3
Pontine APD	5.5	6.2	6.9	5.7	6.5	7.3	6.0	6.8	7.7	6.3	7.1	8.0	6.5	7.4	8.4
Pontine CCD	6.3	7.1	7.9	6.5	7.4	8.3	6.7	7.7	8.7	6.8	8.0	9.0	7.0	8.2	9.4
Lateral ventricles	5.7	7.0	8.4	5.3	6.8	8.4	5.0	6.6	8.4	4.7	6.4	8.5	4.5	6.3	8.5

Note:—APD indicates antero-posterior diameter; BPD, biparietal diameter; CCD, cranio-caudal diameter; CSA, clivus-supraoccipital angle; LCC, length of the corpus callosum; LLD, latero-lateral diameter; FOD, fronto-occipital diameter; PCF, latero-lateral diameter of the posterior cranial fossa.

Encephalic Growth

At 22 weeks of gestation, the MR imaging traits under study attained a size ranging from 4.5 mm (mesencephalic APD) to 65.2 mm (thecal FOD). The CSA was 72.5°, and the LCC/cerebral FOD ratio was 31.7%. The average weekly increase from 20 to 24 weeks was highly significant for all traits except for CSA and mesencephalic APD and ranged from 0.31 mm/week (pontine APD and CCD) to 3.81 mm/week (thecal FOD). The growth rate (ie, weekly increase/size at 22 weeks) ranged from 0.69% (CSA) to 9.22% (LCC). The only MR imaging trait that was found to decrease with increasing GA was the width of the atria of the lateral ventricles (-0.20 mm/week, -3.0%). Details are reported in On-line Table 1.

Difference between Sexes in Encephalic Growth

At 22 weeks of gestation, male fetuses are already larger for all MR imaging traits, with only the exception of the vermian APD and LCC/cerebral FOD ratio. The maximum difference was observed in the PCF, where males are larger than females by 5.2%. As for the weekly increase of MR imaging traits, males appeared to grow faster than females from 20 to 24 weeks of GA for 9 of the 15 MR imaging traits under study, with a maximum of 17.9% for PCF (On-line Table 3). Possibly because of the shortness of the GA interval considered, none of the differences between the sexes in growth velocity were significant. Details are given in On-line Tables 2 and 3.

Reference Centiles

The sex differences reported above, though extremely interesting from an ontogenetic point of view, were not large enough to suggest the need for different reference charts for females and males. Thus, MR imaging traits were fitted with a CG-LMS model independent of sex. In the short GA interval under study, $M(t)$ and $S(t)$ were assumed to change linearly with GA, whereas $L(t)$ was assumed to be constant. The use of more flexible CG-LMS models did not improve the goodness of fitting. All the diameters of the cerebrum, cerebellum, and theca were found to have a positively skewed distribution, as well as the CSA. The remaining MR imaging traits were negatively skewed. The coefficient of variation appeared to increase slightly with increasing GA in all MR imaging traits, with the only exception being the cerebral FOD and mesencephalic APD. De-

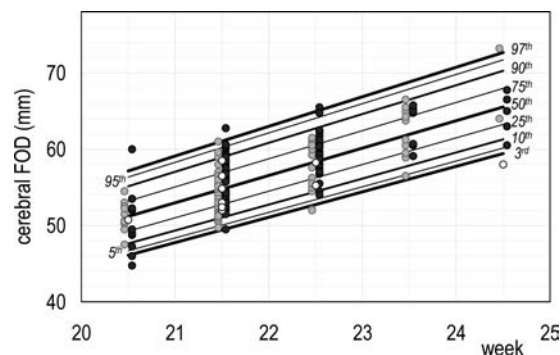


FIG 3. Reference chart for cerebral FOD growth: a whole set of computed centiles (3rd, 5th, 10th, 25th, 50th, 75th, 90th, 95th, 97th) with observed values. Females are denoted by light gray dots, males by dark gray dots, and fetuses of sex unknown by white dots.

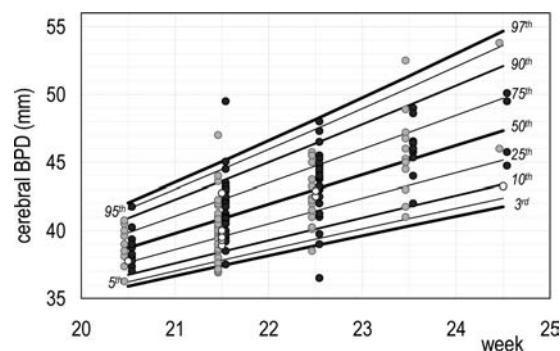


FIG 4. Reference chart for cerebral BPD growth: a whole set of computed centiles (3rd, 5th, 10th, 25th, 50th, 75th, 90th, 95th, 97th) with observed values. Females are denoted by light gray dots, males by dark gray dots, and fetuses of sex unknown by white dots.

tails are reported in On-line Table 4. GA-dependent reference centiles (5th, 50th, and 95th centiles) are given in Table 3. Figs 3 and 4 show growth charts of the cerebral FOD and BPD. The growth charts of all MR imaging traits are given in On-line Fig 8.

DISCUSSION

We provided reference linear fetal brain measurements that can be used for clinical fetal MR imaging on a single-case basis. In particular, our

study focused on GAs between 20 and 24 weeks because in many countries, crucial decisions such as pregnancy termination are possible only in the early second trimester because of laws and regulations.² Until now, most of the MR imaging fetal studies in the literature have referred to normative biometric data published by Parazzini et al in 2008⁵ to examine fetuses younger than 24 weeks of gestation. In this study, the authors did not calculate centiles but provided the minimum and maximum of each measured parameter.⁵ In our study, we conspicuously enlarged that population by doubling the number of fetuses younger than 24 weeks of gestation, and we applied a CG-LMS method to trace the reference centiles. Comparing our data with those by Parazzini et al, we observed differences for some reference limits of supratentorial measurements (eg, cerebral FOD and BPD), while no substantial difference was noted in reference limits of subtentorial structures (eg, vermian diameters and cerebellar LLD). However, our study is not directly comparable with that of Parazzini et al because of the different statistical methods used for the analyses.

We implemented the measurements by Parazzini et al,⁵ and we also added the PCF, CSA, pontine APD, pontine CCD, and mesencephalic APD. Furthermore, we provided the LCC/cerebral FOD ratio. The PCF and CSA may be useful for the assessment of posterior fossa malformations, accounting for dimensional anomalies such as Dandy-Walker malformation and closed neural tube defects.^{13,17} The diameters of the pons (ie, pontine APD and CCD) and the mesencephalic APD may be useful for the assessment of malformations involving the brain stem, such as pontocerebellar hypoplasia, molar tooth malformation, and diencephalic-mesencephalic junction dysplasia. The LCC/cerebral FOD ratio may help in assessing midline malformations, such as isolated mild-to-moderate forms of corpus callosum hypoplasia, an entity that often cannot be reliably assessed by simple visual judgment.

Data about interassessor agreement showed that almost all measurements are, in a sense, objective and independent of the idiosyncrasies of the assessor. The mesencephalic APD showed the highest variability (Table 2). This can be explained by the difficulty in obtaining a suitable orbitomeatal plane (only in 118 of 169 fetuses in our group) and in further delineating the interpeduncular fossa and the mesencephalic tectum. The vermian APD and CCD showed a high variability because of their small size and the difficulty in delineating the fastigium of the fourth ventricle. In agreement with Parazzini et al,⁵ we decided to measure the LCC as the distance between the anterior and posterior inner surfaces because they are better delineated than the outer ones due to the marked contrast with the contiguous CSF. However, as reported in Table 2, in 17 of the 169 fetuses, the LCC could not be measured by the 2 assessors because an exact midsagittal plane was not available.

The main purpose of this work was obviously to provide reliable reference limits that can be used in daily clinical practice; however, we took the opportunity of such measurement collection to acquire information about physiologic cerebral and cranial growth based on linear measurements.

The main limitation of our study is that the fetuses were not homogeneously distributed across the GAs of interest and we included only 8 fetuses at 24 weeks of GA. However, the CG-LMS method calculated the growth curves and the reference limits for

each GA, taking into account all data collected, under the sensible assumption that the growth rate does not change suddenly from one week of gestation to the subsequent week.

CONCLUSIONS

We provided new reference limits of the biometric measurements used for the MR imaging assessment of the fetal brain between 20 and 24 weeks of gestation.

REFERENCES

- Griffiths PD, Bradburn M, Campbell MJ, et al; MERIDIAN collaborative group. **Use of MRI in the diagnosis of fetal brain abnormalities in utero (MERIDIAN): a multicentre, prospective cohort study.** *Lancet* 2017;389:538–46 [CrossRef Medline](#)
- Conte G, Parazzini C, Falanga G, et al. **Diagnostic value of prenatal MR imaging in the detection of brain malformations in fetuses before the 26th week of gestational age.** *AJNR Am J Neuroradiol* 2016; 37:946–51 [CrossRef Medline](#)
- Tilea B, Alberti C, Adamsbaum C, et al. **Cerebral biometry in fetal magnetic resonance imaging: new reference data.** *Ultrasound Obstet Gynecol* 2009;33:173–81 [CrossRef Medline](#)
- Ber R, Bar-Yosef O, Hoffmann C, et al. **Normal fetal posterior fossa in MR imaging: new biometric data and possible clinical significance.** *AJNR Am J Neuroradiol* 2015;36:795–802 [CrossRef Medline](#)
- Parazzini C, Righini A, Rustico M, et al. **Prenatal magnetic resonance imaging: brain normal linear biometric values below 24 gestational weeks.** *Neuroradiology* 2008;50:877–83 [CrossRef Medline](#)
- Kyriakopoulou V, Vatansever D, Davidson A, et al. **Normative biometry of the fetal brain using magnetic resonance imaging.** *Brain Struct Funct* 2017;222:2295–2307 [CrossRef Medline](#)
- Moreira NC, Teixeira J, Themudo R, et al. **Measurements of the normal fetal brain at gestation weeks 17 to 23: a MRI study.** *Neuroradiology* 2011;53:43–48 [CrossRef Medline](#)
- Clouchoux C, Guizard N, Evans AC, et al. **Normative fetal brain growth by quantitative in vivo magnetic resonance imaging.** *Am J Obstet Gynecol* 2012;206:173.e1–8 [CrossRef](#)
- Corbett-Detig J, Habas PA, Scott JA, et al. **3D global and regional patterns of human fetal subplate growth determined in utero.** *Brain Struct Funct* 2011;215:255–63 [CrossRef Medline](#)
- Limperopoulos C, Tworetzky W, McElhinney DB, et al. **Brain volume and metabolism in fetuses with congenital heart disease: evaluation with quantitative magnetic resonance imaging and spectroscopy.** *Circulation* 2010;121:26–33 [CrossRef Medline](#)
- Scott JA, Habas PA, Kim K, et al. **Growth trajectories of the human fetal brain tissues estimated from 3D reconstructed in utero MRI.** *Int J Dev Neurosci* 2011;29:529–36 [CrossRef Medline](#)
- Grossman R, Hoffman C, Mardor Y, et al. **Quantitative MRI measurements of human fetal brain development in utero.** *Br J Anaesth* 2006;33:463–70 [Medline](#)
- Woitek R, Dvorak A, Weber M, et al. **MR-based morphometry of the posterior fossa in fetuses with neural tube defects of the spine.** *PLoS One* 2014;9:e112585 [CrossRef Medline](#)
- Garel C. **Fetal cerebral biometry: normal parenchymal findings and ventricular size.** *Eur Radiol* 2005;15:809–13 [CrossRef Medline](#)
- Weir JP. **Quantifying test-retest reliability using the intraclass correlation coefficient and the SEM.** *J Strength Cond Res* 2005;19: 231–40 [Medline](#)
- Cole TJ, Green PJ. **Smoothing reference centile curves: the LMS method and penalized likelihood.** *Stat Med* 1992;11:1305–19 [CrossRef Medline](#)
- D'Addario V, Pinto V, Del Bianco A, et al. **The clivus-supraocciput angle: a useful measurement to evaluate the shape and size of the fetal posterior fossa and to diagnose Chiari II malformation.** *Ultrasound Obstet Gynecol* 2001;18:146–49 [CrossRef Medline](#)

Differentiating Atypical Hemangiomas and Metastatic Vertebral Lesions: The Role of T1-Weighted Dynamic Contrast-Enhanced MRI

K.A. Morales, J. Arevalo-Perez, K.K. Peck, A.I. Holodny, E. Lis, and S. Karimi



ABSTRACT

BACKGROUND AND PURPOSE: Vertebral hemangiomas are benign vascular lesions that are almost always incidentally found in the spine. Their classic typical hyperintense appearance on T1- and T2-weighted MR images is diagnostic. Unfortunately, not all hemangiomas have the typical appearance, and they can mimic metastases on routine MR imaging. These are generally referred to as atypical hemangiomas and can result in misdiagnosis and ultimately additional imaging, biopsy, and unnecessary costs. Our objective was to assess the utility of dynamic contrast-enhanced MR imaging perfusion in distinguishing vertebral atypical hemangiomas and malignant vertebral metastases. We hypothesized that permeability and vascular density will be increased in metastases compared with atypical hemangiomas.

MATERIALS AND METHODS: Consecutive patients from 2011 to 2015 with confirmed diagnoses of atypical hemangiomas and spinal metastases from breast and lung carcinomas with available dynamic contrast-enhanced MR imaging were analyzed. Time-intensity curves were qualitatively compared among the groups. Perfusion parameters, plasma volume, and permeability constant were quantified using an extended Tofts 2-compartment pharmacokinetic model. Statistical significance was tested using the Mann-Whitney *U* test.

RESULTS: Qualitative inspection of dynamic contrast-enhanced MR imaging time-intensity curves demonstrated differences in signal intensity and morphology between metastases and atypical hemangiomas. Quantitative analysis of plasma volume and permeability constant perfusion parameters showed significantly higher values in metastatic lesions compared with atypical hemangiomas ($P < .001$).

CONCLUSIONS: Our data demonstrate that plasma volume and permeability constant perfusion parameters and qualitative inspection of contrast-enhancement curves can be used to differentiate atypical hemangiomas from vertebral metastatic lesions. This work highlights the benefits of adding perfusion maps to conventional sequences to improve diagnostic accuracy.

ABBREVIATIONS: DCE = dynamic contrast-enhanced; k^{trans} = permeability constant; VH = vertebral hemangioma; V_p = plasma volume

Vertebral hemangiomas (VHs) are the most common benign tumors of the spine. They compose 28% of all skeletal hemangiomas, and the thoracic spine is the most frequent location.¹ VHs are often an incidental finding, having been found in 11% of spines in a large study of postmortem examinations.² VHs are

more frequently found in women, especially in the fourth-to-sixth decades of life.³ These lesions can affect a segment or the entirety of the vertebral body, and they are multiple in roughly one-third of patients.⁴ Most are stable and asymptomatic, but they can become clinically relevant with atypical imaging characteristics when establishing the presence of metastatic disease or when dealing with an aggressive/symptomatic hemangioma, which can induce pain, fractures, and neurologic manifestations due to spinal cord compression.⁵

Histologically, VHs are characterized by vascular spaces lined with endothelial cells of mature thin-walled blood vessels and sinuses lined by flattened or attenuated endothelium. Vessels are scattered, surrounded by a fatty matrix and vertically oriented trabeculae of bone, probably causing resorption of underlying

Received October 3, 2017; accepted after revision January 18, 2018.

From the Departments of Radiology (K.A.M., J.A.-P., K.K.P., A.I.H., E.L., S.K.) and Medical Physics (K.K.P.), Memorial Sloan Kettering Cancer Center, New York, New York; and University of Puerto Rico Medical Sciences Campus (K.A.M.), San Juan, Puerto Rico.

Krystal A. Morales and Julio Arevalo-Perez contributed equally to the work as coauthors.

This research was funded, in part, through the National Institutes of Health/National Cancer Institute Cancer Center Support Grant P30 CA008748 and the National Cancer Institute of the National Institutes of Health under award No. R25CA020449.

Paper previously presented as an electronic presentation at: Annual Meeting of the American Society of Neuroradiology and the Foundation of the ASNR Symposium, May 21–26, 2016; Washington, DC.

The content is solely the responsibility of the authors and does not necessarily represent the official views of the National Institutes of Health.

Please address correspondence to Sasan Karimi, MD, Department of Radiology, Memorial Sloan-Kettering Cancer Center, 1275 York Ave, New York, NY 10065; e-mail: karimis@mskcc.org

Indicates open access to non-subscribers at www.ajnr.org

<http://dx.doi.org/10.3174/ajnr.A5630>

bone and thickening of the remaining trabeculae.³ The characteristic radiologic appearance is defined by its histologic architecture demonstrating a parallel striated pattern, “corduroy cloth,” on plain film and on sagittal or coronal CT and a spotted appearance, “polka dot,” on axial CT.^{3,6} The MR imaging appearance is also influenced by the proportion of histologic components. Postmortem specimens of VHs have been examined with MR imaging and correlated histologically, demonstrating that the signal intensity on T1- and T2-weighted imaging is associated with the fraction of the lesion occupied by adipocytes, vessels, and edema.⁷ Typical VHs are hyperintense on T1 and T2, especially on FSE sequences because of their fatty stroma and vascular components, demonstrating variable enhancement, lower in lesions with a larger fatty content.³ On the other hand, atypical VHs have low fat content and high vascularity, displaying an iso-/hypointense signal on T1- and hyperintense signal on T2-weighted images with elevated contrast enhancement. Also, some atypical VHs are more likely to show aggressive behavior when there is an increased vascular component and less fatty stroma. Cortical erosion, extradural soft tissue, expansion to the posterior elements, and even invasion of the spinal canal, are radiologic signs of aggressiveness.³ While these incidentally found lesions are benign, their appearance on routine STIR and T1- and T2-weighted MR images often mimics that of primary bone malignancies and metastatic lesions.⁸ Therefore, the ability to distinguish these commonly encountered lesions and vertebral malignancies has a direct clinical application in patient management, particularly in a patient with known malignancy.

Dynamic contrast-enhanced (DCE) MR imaging perfusion allows obtaining physiologic information about the microvascular environment of the lesion by applying a pharmacokinetic model procuring quantitative parameters such as plasma volume (V_p), representing the vascular density of the lesion of interest, and permeability constant (K^{trans}), which provides information about blood exchange between the vascular and interstitial compartments. These quantitative parameters have demonstrated their value in detecting the differences in the microvascular environment among metastatic lesions before and after treatment,⁹ benign and pathologic fractures,¹⁰ and hypovascular and hypervascular lesions.^{11,12} Vertebral metastases demonstrate very different histologic patterns, depending on the primary tumor. There is, however, a common feature in all of them: neoangiogenesis. The microenvironment of the metastasis induces secretion of proangiogenic growth factors that promote the development of new fragile and hyperpermeable vessels. The purpose of our study was to assess the utility of DCE MR imaging perfusion in distinguishing vertebral atypical hemangiomas and vertebral metastases, which otherwise can be undistinguishable in routine spine MR imaging. We hypothesized that permeability and vascular density would be increased in metastases because they are associated with a greater concentration of new aberrant and fragile vessels compared with hemangiomas.

MATERIALS AND METHODS

Our study was compliant with the Health Insurance Portability and Accountability Act and was approved by the institutional review board of Memorial Sloan Kettering Cancer Center. The need for informed consent was waived.

Atypical VH Lesions

A hospital data base was reviewed from January 2012 to June 2015. The query yielded 54 consecutive patients with the radiologic diagnosis of atypical VHs. The initial selection was based on the radiologic appearance (iso-/hypointensity on T1 and hyperintensity on STIR) and proved histology (if available). Cases without histology were included on the basis of the following criteria: the assessment of lesion stability after 1 year, negative PET/CT scan findings, and/or presence of the characteristic trabecular appearance on CT. Exclusion criteria from DCE MR imaging analysis comprised the following: lesions that did not meet the stability criteria after 1 year, a history of radiation therapy, or histology positive for malignancy. These selection criteria yielded 34 lesions present in 28 patients.

Metastatic Lesions

Consecutive patients who underwent spine needle biopsy during 2011–2013 were evaluated for vertebral metastatic lesions and classified on the basis of their primary carcinoma origin. Consecutive patients with primary carcinomas of breast ($n = 28$) and lung ($n = 14$) with available DCE MR imaging data were included for 42 metastatic lesions. Patients who had undergone radiation therapy, an operation, and/or kyphoplasty in the lesion of interest were excluded.

Data Acquisition

MR imaging sequences were acquired as a part of standard clinical protocol with a 1.5T or 3T scanner (Optima 450w or Discovery MR750w; GE Healthcare, Milwaukee, Wisconsin) using an 8-channel cervical-thoracic-lumbar surface coil. All patients underwent routine MR imaging, including sagittal T1-weighted fast spin-echo (FOV, 32–36 cm; slice thickness, 3 mm; TR, 400–650 ms; TE, 8.4 ms; flip angle, 160°; in-plane resolution, $1.4 \times 1.4 \text{ mm}^2$), T2-weighted FSE (FOV, 32–36 cm; slice thickness, 3 mm; TR, 3500–4000 ms; TE, 110 ms; flip angle, 160°; in-plane resolution, $1.4 \times 1.4 \text{ mm}^2$), and sagittal STIR FSE (FOV, 32–36 cm; slice thickness, 3 mm; TR, 3500–6000 ms; TE, 10 ms; flip angle, 160°; in-plane resolution, $1.4 \times 1.4 \text{ mm}^2$).

For DCE MR imaging, a bolus of Gd-DTPA was administered by a power injector at 0.1 mmol/kg of body weight and a rate of 2–3 mL/s. The kinetic enhancement of tissue during and after injection of Gd-DTPA was obtained before, during, and after contrast injection using a 3D T1-weighted fast-spoiled gradient recalled-echo sequence (TR, 4–5 ms; TE, 1–2 ms; slice thickness, 5 mm; flip angle, 25°; FOV, 32 cm; temporal resolution, 6–7 seconds) and consisted of 10–12 images in the sagittal plane. The duration of the DCE sequence was 200–240 seconds. Sagittal and axial T1-weighted post-Gd-DTPA MR images were acquired after DCE MR imaging.

Data Processing and Analysis

Data processing and analysis were performed using dynamic image-processing software (nordicICE; NordicNeuroLab, Bergen, Norway). Preprocessing steps integrated background noise subtraction, spatial and temporal smoothing, and detection of the arterial input function from the aorta. ROIs were manually drawn and confirmed by an experienced neuroradiologist who was blinded to the diagnosis on perfusion maps. For accurate mea-

surement of perfusion parameters, vessels, venous structures, and vertebral body endplates were carefully excluded from the ROIs. Anatomic images that matched the DCE MR images were used in ROI placements. Time-intensity curves in the ROI were then obtained. Voxel-by-voxel estimates of quantitative perfusion parameters, including vascular permeability and plasma volume, were determined on the basis of the extended Tofts 2-compartment pharmacokinetic model.¹³ For lesions with multiple slices, these perfusion values were determined for each slice and the maximum values of V_p and K^{trans} were obtained in the ROIs and were used for statistical analysis.

Imaging Analysis

Time-intensity curve morphologies were qualitatively analyzed and compared among the groups (atypical VHs versus metastatic lesions). The time-intensity curves were classified into 5 types according to Chen et al¹⁴: type A (a nearly flat time-intensity curve), type B (a slow-inclination curve), type C (rapid wash-in, followed by a plateau), type D (rapid wash-in followed by a wash-out phase), and type E (initial rapid wash-in followed by a second slowly rising phase).

For quantitative parameters, including K^{trans} and V_p , ROI values were determined for each slice of the lesion and the maximum values of V_p and K^{trans} were used for the comparison.

Statistical Analysis

A Mann-Whitney *U* test at a significance level of $P < .01$ was performed to determine the difference in the DCE MR imaging perfusion parameters, V_p and K^{trans} , between the vertebral metastases and atypical hemangiomas.

RESULTS

A sharp difference in both morphology and signal intensity is observed when comparing time-intensity curves (Fig 1). Metastatic lesions show enhancement curves resembling type D curve morphology as described by Chen et al.¹⁴ These exhibit a sharp rise (slope) and higher peak signal intensity, followed by a faster washout phase. Most atypical hemangiomas have a minimal and delayed enhancement and fall within a narrow range, except for the 4 curves highlighted in cyan in Fig 2A, which deviate significantly from this range. These 4 lesions met the stability inclusion criteria and therefore were not excluded from the analysis. Although vertebral vessels were always carefully excluded from the ROIs, some of these lesions have considerable extension through the entire vertebral body and could represent rare cases in which atypical hemangiomas display an aggressive behavior and substantial vascularity and vertebral body invasion occur. If we evaluated the curve average intensity excluding these 4 cases (Fig 2B), 88% of the atypical hemangioma curves analyzed would show a characteristic pattern with minimum and late enhancement curves with no evident washout in contrast to metastases, which display a rapid wash-in phase, higher peak, and clear washout (Fig 2C).

Quantitative analysis demonstrates higher perfusion values (V_p and K^{trans}) of metastatic lesions than atypical hemangiomas ($P < .01$), despite an almost identical appearance on T1 (Figs 3 and 4). V_p values demonstrated the greatest difference and mini-

mal overlap between atypical vertebral hemangiomas and metastatic lesions, being the best biomarker. No significant differences were found when comparing lung and breast metastases ($P > .3$).

DISCUSSION

We compared 34 atypical hemangiomas and 42 metastatic vertebral lesions and found that DCE MR perfusion assessment of the TI curves and V_p and K^{trans} parameters demonstrated higher values in vertebral metastases compared with atypical vertebral hemangiomas. V_p was considered the best parameter to differentiate the 2 groups.

Noninvasive imaging biomarkers can be of paramount importance to help distinguish atypical VHs and metastatic vertebral lesions, especially when atypical VHs can mimic the pattern observed for primary malignant and metastatic lesions. Currently, long-term stability and the classic radiologic appearance are the imaging tools available to confirm the diagnosis. However, the vertical trabecular appearance has been reported to be more difficult to visualize in atypical hemangiomas, making the diagnosis even more challenging.⁸ Furthermore, although rare, VHs display “aggressive” behavior that can manifest as pain and radiculopathies when involvement of the entire vertebral body and compression of the spinal cord and nerve roots occur. These can be easily mistaken for malignancies and may result in additional diagnostic imaging, biopsy, and, in some cases, an operation. In addition, atypical VHs have been identified concurrent with metastatic disease from primary malignancy such as colon adenocarcinoma¹⁵ and thyroid cancer.¹⁶ Consequently, their accurate identification in these cases poses a major challenge with a large impact on patient staging and management.

In the past decade, our tools to identify these lesions have been limited. Effort has been made to differentiate hemangiomas and malignant lesions with the use of diffusion-weighted imaging and apparent diffusion coefficient calculations.¹⁷ Quantitative chemical shift MR imaging has also been used, and a proportional change in signal intensity on in-phase compared with out-of-phase images showed a decrease in signal intensity in benign lesions compared with metastatic lesions.¹⁸ However, no robust method has been established to differentiate atypical hemangiomas and metastatic spine lesions.

Our study takes advantage of spine DCE MR imaging perfusion as a noninvasive method of obtaining quantitative parameters representing the physiology of the microvascular environment of each lesion. Except for the aforementioned 4 cases, atypical hemangioma time-intensity curves had a minimal and delayed enhancement, with no evident washout in contrast to metastases, which display a rapid wash-in phase, higher peak, and clear washout, a common indicator of malignancy. In addition to the benign appearance of the curves, quantitative analysis of the perfusion parameters V_p and K^{trans} also demonstrated significantly lower perfusion values in atypical hemangiomas compared with metastatic lesions, despite an almost identical appearance on T1-weighted sequences.

Our findings reflect the physiology and histologic structure of atypical vertebral hemangiomas, less fat and greater vascular content. Most hemangiomas in our study showed low plasma volume and permeability. Only 4 cases demonstrated higher V_p values,

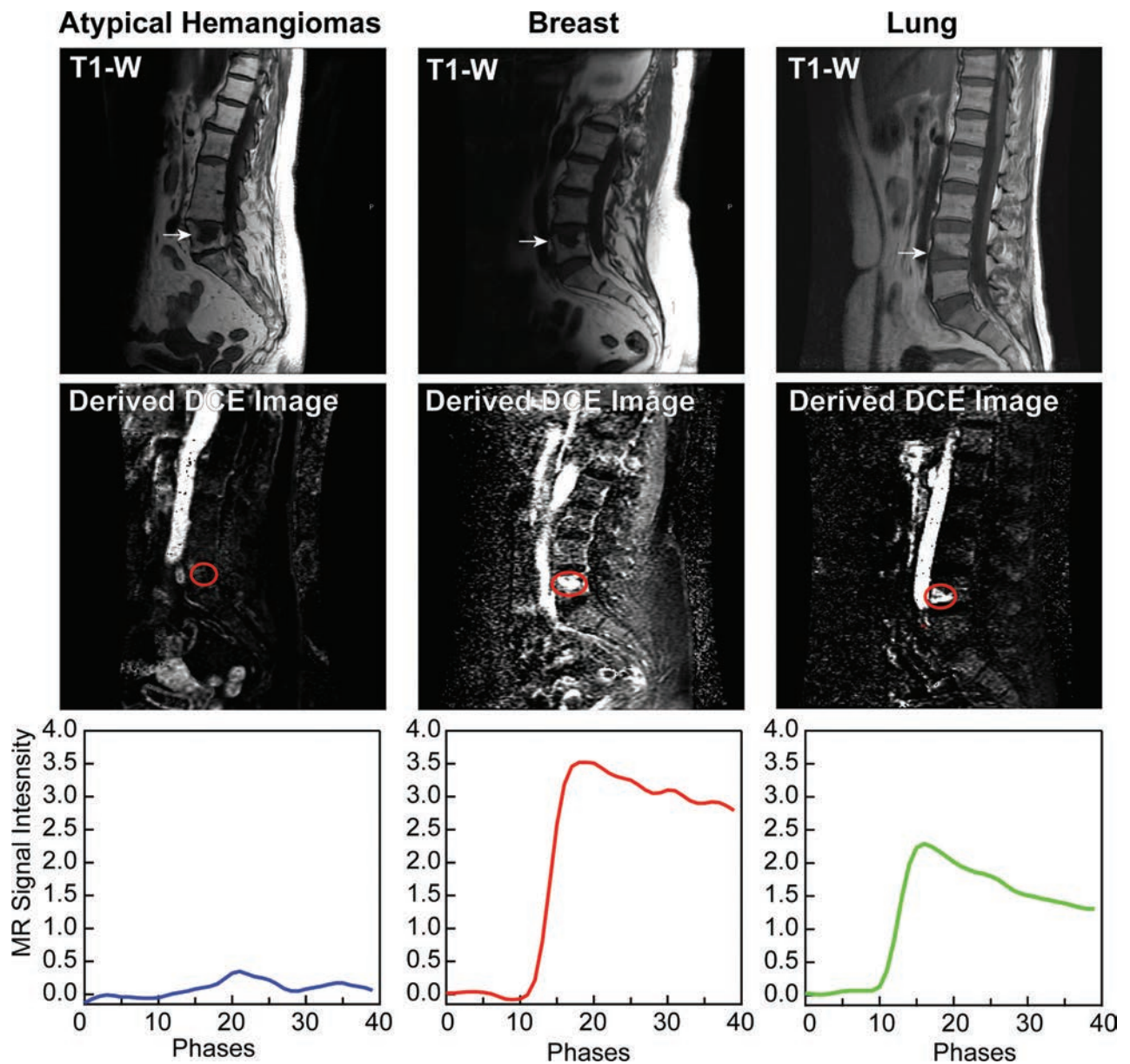


FIG 1. Representative sagittal T1-weighted and dynamic images derived from DCE MR imaging for atypical hemangiomas and spinal lesions originating from primary breast and lung carcinomas. The lower panel corresponds to the MR imaging signal enhancement curve as a function of phases (time) obtained for each representative lesion shown.

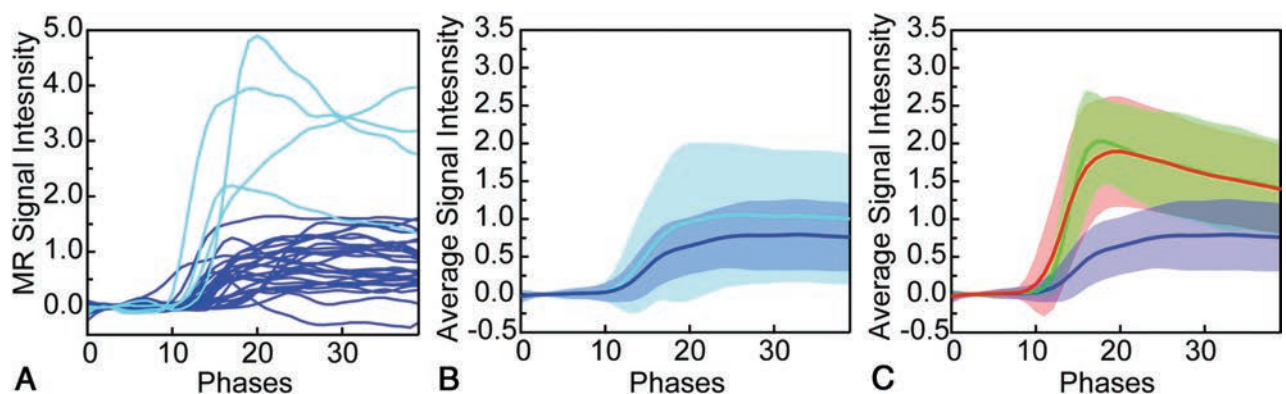


FIG 2. A, Enhancement curve for all 34 atypical hemangiomas. Curves highlighted in cyan show the 4 cases with elevated enhancement. B, Average enhancement curves for all atypical hemangiomas (cyan) excluding atypical hemangiomas with elevated enhancement (blue). C, Average enhancement curves for all atypical hemangiomas excluding enhancement curve outliers (blue) compared with breast (red) and lung (green) metastases.

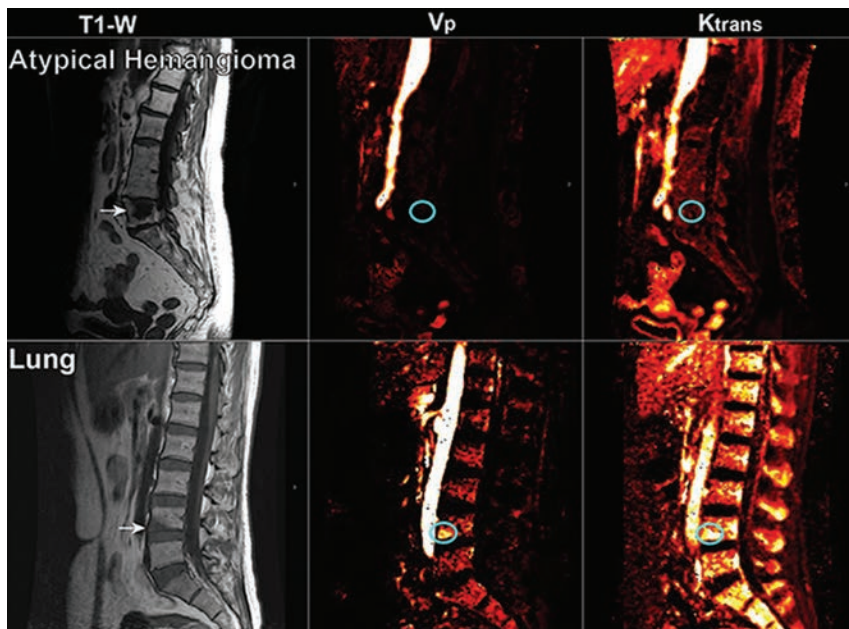


FIG 3. Representative sagittal T1-weighted imaging and the corresponding perfusion maps for V_p and K^{trans} parameters for atypical hemangiomas and metastasis from lung carcinoma. Arrows indicate the level of the lesion in T1WI, and the cyan circle highlights the region on V_p and K^{trans} maps where the lesion is located.

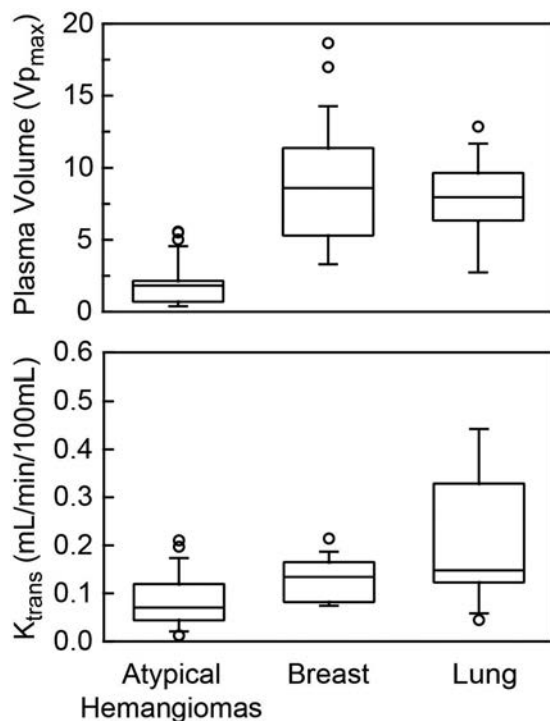


FIG 4. V_p and K^{trans} parameters obtained for atypical hemangiomas and metastatic lesions from breast and lung carcinoma. Metastases show significantly higher values ($P < .05$) for both V_p and K^{trans} compared with atypical vertebral hemangiomas. Note that the 4 outlier values representing aggressive hemangiomas account for the higher V_p values in the atypical hemangioma group that demonstrate minimal overlap with the metastatic group and remain low compared with other metastases.

which overlap those of the metastatic lesions. These 4 cases probably represent aggressive or compressive vertebral hemangiomas, which exhibit a higher degree of vascularization and an expansile soft-tissue component.¹⁹ This subgroup is associated with some features that help distinguish it from atypical quiescent hemangiomas, such as involvement of the entire vertebral body, extension into the neural arch, cortical expansion, midthoracic location, irregular honeycomb pattern, and soft-tissue mass, according to Laredo et al.¹⁹ In fact, 3 of the 4 lesions were expanding into the posterior vertebral elements, and one demonstrated ventral epidural disease. The remaining lesion was a small well-demarcated hemangioma confined to the vertebral body. However, the 4 cases demonstrated lower values of K^{trans} (0.08, 0.08, 0.09, and 0.11) than those seen on metastases (K^{trans} mean, 0.15), in keeping with the expected low permeability due to a theoretically preserved endothelium in these lesions.

As with Laredo et al,¹⁹ we suggest that DCE MR imaging perfusion can be a useful tool for differentiating quiescent atypical VHs that represent localized, relatively inactive angiomatous dysmorphies from aggressive atypical VHs that show extensive, active angiomatous tumors that can compress the spinal cord and become symptomatic.¹⁹ When there is an abnormally elevated V_p , K^{trans} can be helpful in demonstrating preservation of permeability, suggesting a benign etiology.

Our study has several limitations. First, it is a retrospective study with the possibility of selection bias. Second, there was no pathologic confirmation for most of the atypical hemangiomas; however, all these lesions were stable after 1 year, had negative findings on PET/CT, and/or had the characteristic trabecular appearance on CT. Third, the manual ROI selection, though a standard method of analyzing perfusion data, is an operator-dependent technique associated with potential interobserver and intraobserver variability. However, having 1 single trained operator performing the measurements limits the potential variation. Fourth, there is limited representation of other malignancies in the metastatic group that could have demonstrated different perfusion patterns. On the other hand, lung and breast are by far the most representative primary malignancies, accounting for 31% and 24% of all sources of spinal metastatic disease. Despite these limitations, this is the first study of its kind to compare atypical VHs and vertebral metastases using DCE MR imaging, to our knowledge.

Our study has several limitations. First, it is a retrospective study with the possibility of selection bias. Second, there was no pathologic confirmation for most of the atypical hemangiomas; however, all these lesions were stable after 1 year, had negative findings on PET/CT, and/or had the characteristic trabecular appearance on CT. Third, the manual ROI selection, though a standard method of analyzing perfusion data, is an operator-dependent technique associated with potential interobserver and intraobserver variability. However, having 1 single trained operator performing the measurements limits the potential variation. Fourth, there is limited representation of other malignancies in the metastatic group that could have demonstrated different perfusion patterns. On the other hand, lung and breast are by far the most representative primary malignancies, accounting for 31% and 24% of all sources of spinal metastatic disease. Despite these limitations, this is the first study of its kind to compare atypical VHs and vertebral metastases using DCE MR imaging, to our knowledge.

CONCLUSIONS

Our data demonstrate that qualitative inspection of contrast-enhancement curves and quantitative analysis of V_p and K^{trans} perfusion parameters can be used to differentiate atypical hemangi-

omas from vertebral metastatic lesions. The ability of DCE MR imaging to noninvasively characterize tumor vascularity has important clinical implications, which could lead to changes in patient management, reducing biopsies, hospital stay, additional imaging, and patient anxiety.

Disclosures: Krystal A. Morales—RELATED: Grant: NIH/NCI Cancer Center Support Grant P30 CA008748, National Cancer Institute R25CA020449, Comments: Medical Student Summer Fellowship Program of the Memorial Sloan Kettering Cancer Center is a research program for first- and second-year students at US medical schools who are interested in careers as physician-scientists in the field of oncology and/or related biomedical sciences. Funded since 1977 by the National Cancer Institute, this program grants students the opportunity to conduct basic laboratory or clinical research under the mentorship of Memorial Sloan Kettering faculty. Julio Arevalo-Perez—RELATED: Grant: NIH/NCI Cancer Center Support Grant P30 CA008748.* K.K. Peck—RELATED: Grant: NIH/NCI Cancer Center Support Grant P30 CA008748. A.I. Holodny—RELATED: Grant: NIH/NCI Cancer Center Support Grant P30 CA008748. Eric Lis—RELATED: Grant: NIH/NCI Cancer Center Support Grant P30 CA008748; UNRELATED: Payment for Lectures Including Service on Speakers Bureaus: Medtronic. S. Karimi—RELATED: Grant: NIH/NCI Cancer Center Support Grant P30 CA008748. *Money paid to the institution.

REFERENCES

- Murphey MD, Fairbairn KJ, Parman LM, et al. **From the archives of the AFIP: musculoskeletal angiomatous lesions: radiologic-pathologic correlation.** *Radiographics* 1995;15:893–917 [CrossRef Medline](#)
- Junghanns H, Schmorl G. *The Human Spine in Health and Disease.* New York: Grune & Stratton; 1971
- McEvoy SH, Farrell M, Brett F, et al. **Haemangioma, an uncommon cause of an extradural or intradural extramedullary mass: case series with radiological pathological correlation.** *Insights Imaging* 2016;7:87–98 [CrossRef Medline](#)
- Karlin CA, Brower AC. **Multiple primary hemangiomas of bone.** *AJR Am J Roentgenol* 1977;129:162–64 [CrossRef Medline](#)
- Alexander J, Meir A, Vrodo N, et al. **Vertebral hemangioma: an important differential in the evaluation of locally aggressive spinal lesions.** *Spine (Phila Pa 1976)* 2010;35:E917–20 [CrossRef Medline](#)
- Persaud T. **The polka-dot sign.** *Radiology* 2008;246:980–81 [CrossRef Medline](#)
- Baudrez V, Galant C, Vande Berg BC. **Benign vertebral hemangioma: MR-histological correlation.** *Skeletal Radiol* 2001;30:442–46 [CrossRef Medline](#)
- Gaudino S, Martucci M, Colantonio R, et al. **A systematic approach to vertebral hemangioma.** *Skeletal Radiol* 2015;44:25–36 [CrossRef Medline](#)
- Chu S, Karimi S, Peck KK, et al. **Measurement of blood perfusion in spinal metastases with dynamic contrast-enhanced magnetic resonance imaging: evaluation of tumor response to radiation therapy.** *Spine (Phila Pa 1976)* 2013;38:E1418–24 [CrossRef Medline](#)
- Arevalo-Perez J, Peck KK, Lyo JK, et al. **Differentiating benign from malignant vertebral fractures using T1-weighted dynamic contrast-enhanced MRI.** *J Magn Reson Imaging* 2015;42:1039–47 [CrossRef Medline](#)
- Khadem NR, Karimi S, Peck KK, et al. **Characterizing hypervascular and hypovascular metastases and normal bone marrow of the spine using dynamic contrast-enhanced MR imaging.** *AJNR Am J Neuroradiol* 2012;33:2178–85 [CrossRef Medline](#)
- Saha A, Peck KK, Lis E, et al. **Magnetic resonance perfusion characteristics of hypervascular renal and hypovascular prostate spinal metastases: clinical utilities and implications.** *Spine (Phila Pa 1976)* 2014;39:E1433–40 [CrossRef Medline](#)
- Tofts PS, Brix G, Buckley DL, et al. **Estimating kinetic parameters from dynamic contrast-enhanced T(1)-weighted MRI of a diffusible tracer: standardized quantities and symbols.** *J Magn Reson Imaging* 1999;10:223–32 [CrossRef Medline](#)
- Chen WT, Shih TT, Chen RC, et al. **Blood perfusion of vertebral lesions evaluated with gadolinium-enhanced dynamic MRI: in comparison with compression fracture and metastasis.** *J Magn Reson Imaging* 2002;15:308–14 [CrossRef Medline](#)
- Zapalowicz K, Bierzyńska-Macyszyn G, Stasiów B, et al. **Vertebral hemangioma coincident with metastasis of colon adenocarcinoma.** *J Neurosurg Spine* 2016;24:506–09 [CrossRef Medline](#)
- Laguna R, Silva F, Vazquez-Sellés J, et al. **Vertebral hemangioma mimicking a metastatic bone lesion in well-differentiated thyroid carcinoma.** *Clin Nucl Med* 2000;25:611–13 [CrossRef Medline](#)
- Leeds NE, Kumar AJ, Zhou XJ, et al. **Magnetic resonance imaging of benign spinal lesions simulating metastasis: role of diffusion-weighted imaging.** *Top Magn Reson Imaging* 2000;11:224–34 [CrossRef Medline](#)
- Zajick DC Jr, Morrison WB, Schweitzer ME, et al. **Benign and malignant processes: normal values and differentiation with chemical shift MR imaging in vertebral marrow.** *Radiology* 2005;237:590–96 [CrossRef Medline](#)
- Laredo JD, Reizine D, Bard M, et al. **Vertebral hemangiomas: radiologic evaluation.** *Radiology* 1986;161:183–89 [CrossRef Medline](#)

The Importance of Flexion MRI in Hirayama Disease with Special Reference to Laminodural Space Measurements

 D.K. Boruah,  A. Prakash,  B.B. Gogoi,  R.R. Yadav,  D.D. Dhingani, and  B. Sarma

ABSTRACT

BACKGROUND AND PURPOSE: Hirayama disease is a benign focal amyotrophy of the distal upper limbs involving C7, C8, and T1 segmental myotomes with sparing of the brachioradialis and proximal muscles of the upper limb innervated by C5–6 myotomes. The objective of the present study was to study the utility of MR imaging in young patients presenting with weakness and wasting of the distal upper extremity and to evaluate the importance of the laminodural space during flexion cervical MR imaging.

MATERIALS AND METHODS: This was a prospective cross-sectional study conducted from January 2014 to July 2017 in a tertiary care center from Northeast India. Forty-five patients with clinically definite Hirayama disease underwent electrophysiologic evaluation followed by MR imaging of the cervical spine.

RESULTS: The mean age at recruitment was 22.8 ± 5.5 years. Forty patients (88.9%) had unilateral and 5 (11.1%) had bilateral upper extremity involvement. Cervical cord T2-weighted hyperintensities were demonstrated in 16 patients (35.6%), of which 15 (33.3%) had anterior horn cell hyperintensities. Flexion MR imaging showed loss of the posterior dural attachment, forward shifting of the posterior dural sac with postcontrast enhancement, and prominent posterior epidural venous plexus in all patients. The laminodural space at maximum forward shifting of the posterior dural sac ranged from 3 to 9.8 mm, with a mean distance of 5.99 mm (95% confidence interval, 5.42–6.57 mm).

CONCLUSIONS: Flexion cervical MR imaging is a very useful investigation in diagnosing Hirayama disease. The increase in the laminodural space and the presence of cervical cord flattening during flexion are essential for diagnosis.

ABBREVIATIONS: AP = anteroposterior; HD = Hirayama disease; LDS = laminodural space; TR = transverse

Hirayama disease (HD) was initially described by Hirayama et al¹ in 1959 in a Japanese patient with unilateral atrophy of the distal upper limb. It was later coined “juvenile muscular atrophy” of distal upper limb extremity² or “monomelic amyotrophy.”³ HD is characterized by an insidious-onset asymmetric wasting with weakness of the distal muscles of the upper extremity, sparing of the brachioradialis (oblique amyotrophy), and predominant affect on the C8–T1 segmental myotomes.⁴ Very rarely, atypical HD may affect the lower limbs.⁵ The disease commonly affects young individuals in their second-to-third decades

of life with a predominant age of onset of around 15–25 years.⁶ Males are more affected than females.⁶ Initial oblique unilateral amyotrophy more frequently affects the right upper limb than the left, with subsequent contralateral upper limb affection in 50% of cases.^{3,7} Bilateral symmetric or asymmetric involvement of HD was also reported.⁸ Lai et al⁹ noted that forward shifting of the posterior cervical dural sac can occur in healthy subjects also on flexion MR imaging (ranging from 1.0 to 4.2 mm compared with those with HD ranging from 6.1 to 7.8 mm).

The aim of the study was to evaluate the utility of MR imaging in young patients presenting with distal upper extremity muscle wasting and weakness and to evaluate the importance of the laminodural space (LDS) during flexion cervical MR imaging.

MATERIALS AND METHODS

Patient Selection

The study was approved by the institutional ethics review committee. Informed and written consent was obtained from all the participants. The study group comprised patients presenting to the departments of radiodiagnosis, neurology, neurosurgery, and medicine in a tertiary care center from January 2014 to July 2017.

Received September 10, 2017; accepted after revision December 30.

From the Departments of Radiodiagnosis (D.K.B., D.D.D.) and Neurology (B.S.), Assam Medical College and Hospital, Dibrugarh, Assam, India; Department of Radiodiagnosis (A.P.), Bangalore Medical College and Research Institute, Bangalore, Karnataka, India; Department of Pathology (B.B.G.), North Eastern Indira Gandhi Regional Institute of Health and Medical Sciences, Meghalaya, India; and Department of Radiodiagnosis (R.R.Y.), Sanjay Gandhi Postgraduate Institute of Medical Sciences, Lucknow, India.

Please address correspondence to Arjun Prakash, MD, Department of Radiodiagnosis, Bangalore Medical College and Research Institute, Fort, K.R. Road, Bangalore 560002, Karnataka, India; e-mail: drarjunprakash@gmail.com

<http://dx.doi.org/10.3174/ajnr.A5577>

We included all young adults who presented to the outpatient department with weakness and wasting of the hand and/or forearm muscles with motor axonopathy in nerve-conduction studies. Patients with different etiologies with similar presentations were excluded from the study. Patients with an acute history of trauma, previous cervical spinal fixation or prosthesis, and those diagnosed with ankylosing spondylitis affecting the cervical spine were all excluded. Fifty-six patients with clinically suspected HD were recruited. We excluded 4 due to an inability to achieve adequate neck flexion (3 due to obesity and 1 due to ankylosing spondylitis). Seven patients were excluded due to excessive motion artifacts during flexion MR imaging.

Forty-five patients composed the final study group. Motor and sensory nerve conduction studies were performed under standard guidelines. The conduction velocities and compound muscle action potential amplitudes of the median and ulnar nerves were measured for analysis.

MR Imaging Protocol

MR imaging was performed using a 1.5T Magnetom Avanto B15 machine (Siemens, Erlangen, Germany). Image acquisition of the cervical spine was initially performed with patients in a supine neutral position in routine sagittal T2- and T1-weighted spin-echo, sagittal and coronal STIR, and axial T2- and T1-weighted fast spin-echo and axial 2D T2*WI gradient recalled-echo sequences. Sagittal spin-echo T1WI was acquired with a TR/TE of 450–500/9–15 ms; sagittal T2WI, with a TR/TE of 4000–4600/110–120 ms with a 3-mm slice thickness. Axial 2D T2*WI gradient recalled-echo imaging was performed with a TR/TE of 650–750/24–32 ms and a flip angle of 24°–28°.

Flexion MR imaging of the cervical spine was performed with a body coil without using a cervical coil. The optimum neck flexion of 30°–40° was obtained after putting soft MR imaging-compatible support behind the nape of neck with further support on either side of the neck to create immobility of the neck during flexion MR imaging. Postgadolinium fat-suppressed sagittal and axial T1-weighted images of the cervical spine were obtained in neck flexion with a slice thickness of 3 mm.

Image Analysis

MR images were analyzed for cord flattening, cord atrophy, and T2-weighted hyperintensities in the cord or in the region of the anterior horn cells. The maximum forward shifting of the posterior dural sac or LDS was measured in midline on postgadolinium fat-suppressed sagittal T1-weighted imaging on flexion MR imaging.

The LDS was measured at the maximum thickness of the dural detachment and enhancing posterior epidural component on postcontrast images. We also obtained the anteroposterior (AP) and transverse (TR) diameters of the cervical cord in axial images both in neutral and flexion MR imaging at the site of maximum forward shifting of the posterior dural sac. The spinal canal diameters were measured both in neutral and flexion sagittal MR images. The AP cervical spinal canal diameter on flexion MR imaging was measured at the site of maximum forward dural shift. The LDS and AP and TR diameters of the cervical cord during neutral and flexion MR imaging were measured in precontrast images and were compared with postgadolinium fat-suppressed images

Table 1: Anteroposterior spinal cord diameters in 45 patients with HD

Vertebral Levels	Minimum Cord Diameter (mm)	Maximum Cord Diameter (mm)	Mean
C2	6.27	8.11	7.13 ± 0.43
C3	5.56	7.84	6.91 ± 0.63
C4	4.99	7.54	6.50 ± 0.62
C5	4.58	7.60	6.06 ± 0.71
C6	3.97	6.98	5.64 ± 0.73
C7	4.15	6.91	5.61 ± 0.71
T1	4.75	7.73	5.93 ± 0.56

by 2 radiologists. The average value obtained from the 2 authors was compared for any variability using the *F* test and Pearson correlation. Other MR imaging findings such as cord atrophy and T2-weighted cord hyperintensities were observed by only 1 radiologist. The anteroposterior spinal cord diameters were measured at the midsagittal section from the C2 to T1 vertebral levels. The cord diameter was measured at the midvertebral level of each vertebra.

Statistical Analysis

Data were presented as percentage, mean, and SD. Calculations were performed with SPSS programs (IBM, Armonk, New York).

RESULTS

Forty-five patients comprised 44 (97.8%) males and 1 (2.2%) female. The age of presentation varied from 14 to 42 years, with a mean age of 22.8 ± 5.5 years. The duration of illness was >2 years in 30 patients (66.7%) and <2 years in 15 patients (33.3%). Forty patients (88.9%) had an affected unilateral upper extremity while 5 patients (11.1%) had bilateral involvement. All 45 patients (100%) had weakness and wasting of the affected hand muscles, 27 patients (60%) had wasting of forearm muscles, and 2 patients (4.4%) had weakness of arm muscles. Thirty patients (66.7%) had cold paresis in the affected hand, 22 patients (48.9%) had hyperaesthesia in the hand, and 23 patients (51.1%) had fasciculations in the affected muscles.

Neutral-position cervical MR imaging showed loss of cervical lordosis in 39 patients (86.7%) and localized lower cervical cord atrophy in 27 patients (60%). The cord atrophy was <2 vertebral heights in 19 patients (42.2%), 2–3 vertebral heights in 5 patients (11.1%), and >3 vertebral heights in 3 patients (6.7%). The maximum cord atrophy was observed at the C6 and C7 vertebral levels (Table 1). Asymmetric cervical cord flattening was noted in 31 patients (68.9%) (Figs 1 and 2). Intramedullary cervical cord T2-weighted hyperintensities were noted in 16 patients (35.6%), of whom 8 patients (17.8%) had an involvement of <2 vertebral heights, 6 patients (13.3%) had involvement of 2–3 vertebral heights (Fig 3), and 2 patients (4.4%) had an involvement of >3 vertebral heights. T2-weighted hyperintensities involving the anterior horn cells were noted in 15 patients (33.3%), of whom 11 patients (24.4%) had unilateral affection of the anterior horn cells and 4 patients (8.9%) had bilateral affection. Flexion cervical MR imaging showed loss of the dural attachment, forward shifting of the posterior dural sac, and a postgadolinium fat-suppressed enhancing prominent posterior epidural space in all 45 patients (100%) with HD (Figs 1 and 2).

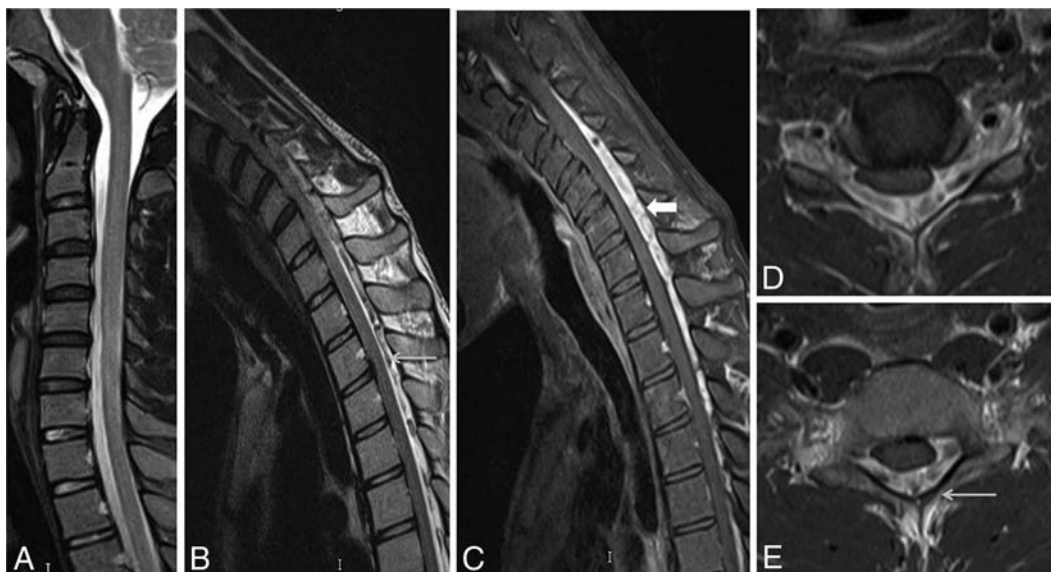


FIG 1. A 22-year-old man with wasting and weakness of the right hand and forearm muscles with cold paresis. Neutral position sagittal T2-weighted MR image (A) shows a normal appearance of the cervical cord. Flexion MR T2-weighted image (B) shows an enlarged posterior epidural space with multiple flow voids (arrow). Postgadolinium fat-suppressed sagittal T1-weighted flexion MR image (C) shows an enhancing epidural venous plexus extending from the C3 to T3 vertebral levels (block arrow). Axial postgadolinium T1 fat-suppressed images (D and E) show the enhancing posterior epidural venous plexus with flow voids within (arrow) and asymmetric flattening of the right hemicord.

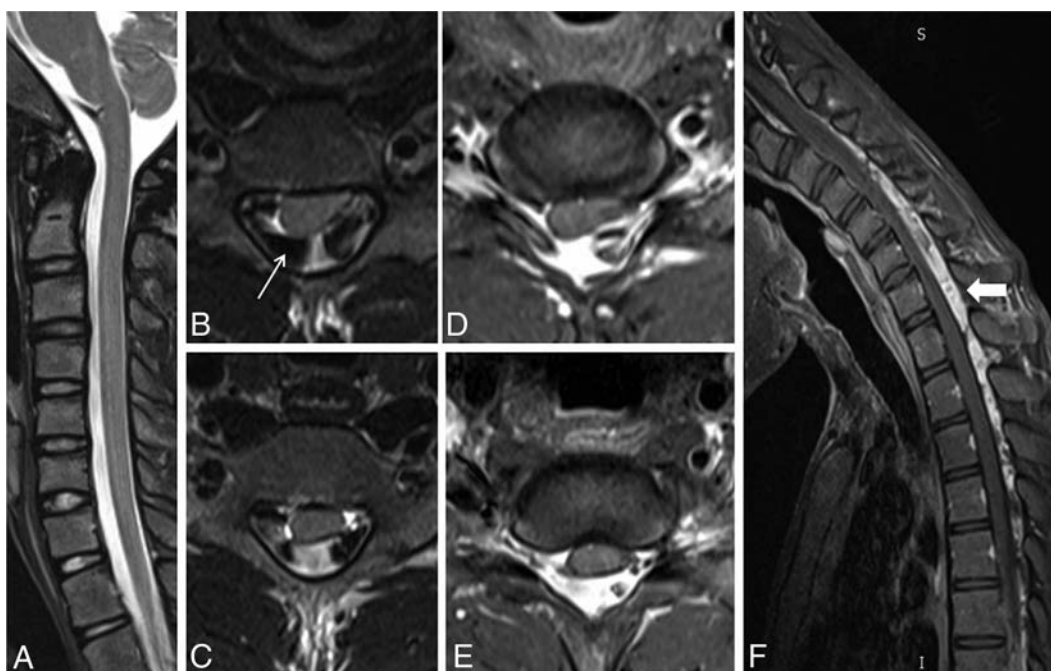


FIG 2. A 20-year-old male patient with weakness and wasting of the left hand muscles. Neutral position sagittal T2-weighted image (A) shows the normal appearance of the cervical cord. Axial T2-weighted flexion MR images (B and C) and postgadolinium T1 fat-suppressed images (D and E) show widening of the LDS with anterior displacement of the posterior dura and asymmetric cord atrophy, more on the left side, along with multiple flow voids within the posterior epidural space (arrow). Postgadolinium T1 fat-suppressed flexion MR sagittal image (F) shows an enhancing posterior epidural venous plexus extending from the C4 to T4 vertebral level (block arrow).

The measurement of LDS at the maximum forward shifting of the posterior dural sac ranged from 3 to 9.8 mm, with a mean diameter of 5.99 ± 1.90 mm (Table 2). The mean LDS measured by radiologist 1 was 5.97 ± 1.89 mm and by radiologist 2, was 6.02 ± 1.92 mm. The significance between the 2 radiologists while measuring the LDS was an F value of 0.043 and a P value of .886. The correlation between the 2 radiologists while measuring the

LDS had a Pearson correlation of 0.989 with a P value of $<.001$. A scatterplot showing various LDS measurements by the 2 radiologists has been provided in Fig 4.

Posterior epidural flow voids were noted in 21 patients (46.7%) (Fig 2). The enhancing crescentic posterior epidural space was noted only in the cervical region in 16 patients (35.6%), while 29 patients (64.4%) had involvement of the thoracic spinal



FIG 3. A 21-year-old man with asymmetric wasting of the bilateral hand muscles. Neutral MR T2-weighted sagittal and coronal (A and B) images show lower cervical cord atrophy with segmental hyperintensities in the cervical cord at the C6 and C7 vertebral levels (*white arrow*). Axial T2-weighted images (C and D) show asymmetric hyperintensities, more pronounced in the left half of the cervical cord (*arrow*). Flexion cervical MR STIR image (E) shows an enlarged posterior epidural space, which is seen as an enhancing posterior epidural venous plexus on the postgadolinium T1 fat-suppressed sagittal image (F) (*block arrow*).

Table 2: Summarized average results of measured parameters of 2 radiologists during neutral and flexion MRI in 45 patients with Hirayama disease

	Minimum	Maximum	Mean	SD
Distance of LDS	3.00	9.80	5.9978	1.90424
Spinal canal diameter in neutral MRI	10.80	15.30	12.7756	.99457
Spinal canal diameter in flexion MRI	10.90	15.50	12.9644	1.01604
AP cord diameter at neutral MRI	3.30	7.40	5.5378	1.00029
TR cord diameter at neutral MRI	7.50	14.40	12.1911	1.32593
AP cord diameter at flexion MRI	2.50	6.60	4.8089	.96903
TR cord diameter at flexion MRI	9.20	16.20	14.1022	1.39569
Ratio of LDS/spinal canal diameter in flexion MRI	0.24	0.74	0.461	0.14
Ratio of AP/TR diameter of cord in flexion MRI	0.17	0.59	0.3455	0.08634
Ratio of AP/TR diameter of cord in neutral MRI	0.26	0.72	0.4587	0.09899
Decrement of AP/TR diameter of cord during flexion MRI	0.03	0.26	0.118	0.06

Note:—Measurements are in millimeters.

posterior epidural space along with the cervical spine (Fig 2). The average spinal canal diameter at the site of maximum thickness of the posterior epidural component during flexion was 12.96 ± 1.01 mm and 12.77 ± 0.99 mm during a neutral position. This finding indicates a slight increment in the AP dimension of the spinal canal during flexion MR imaging. In our study, the average AP diameter of the spinal cord during a neutral position of the neck was 5.54 ± 1.0 mm and 4.82 ± 0.97 mm during flexion. The average TR diameter of the spinal cord during neutral MR imaging was 12.2 ± 1.33 mm and 14.1 ± 1.4 mm during flexion MR imaging. The spinal cord was compressed and anteriorly displaced by the enhancing posterior epidural component during flexion MR imaging, leading to a decrease in the AP diameter and an increase in the TR diameter of the spinal cord at the maximum compression site. The ratio of maximum anteroposterior shifting of the posterior dural sac (ie, LDS)/maximum AP diameter of the spinal canal during flexion MR imaging had an average increment value of 0.46 ± 0.14 mm (range, 0.24–0.74 mm), indicating cord

compression during flexion. The ratio of AP diameter of the cord/TR diameter of the cord during neutral MR imaging was 0.45 ± 0.09 mm (range, 0.26–0.72 mm). The ratio of AP diameter of the cord/TR diameter of the cord decreases during flexion because of cord compression and cord flattening. The decrement of the AP/TR cord ratio during flexion was 0.118 ± 0.06 mm (Fig 5).

The frequency polygon in Fig 6 shows the LDS measurements of all the cases. There was statistical significance in the LDS measurement for the diagnosis of HD with a P value of $<.001$. The 95% confidence interval was 5.42–6.57 mm with mean value of 5.99 mm.

DISCUSSION

HD was initially recognized in Japan in 1959 by Hirayama et al¹ and was initially reported under the name of juvenile muscular atrophy of unilateral upper extremity. It predominantly affects young adults and adolescents ranging from 15 to 25 years of age. However, it has also been reported in pediatric and old age groups.^{10,11} The initial symptoms of HD are slowly progressive hand weakness and fatigue, followed by cold paresthesia, tremors, and atrophy. Asymmetric distribution of symptoms and signs is characteristic, though bilaterally symmetric forms have also been reported recently.^{8,12} HD may affect C5–C7 segmental myotomes more commonly in Western countries, whereas the C7–T1 segment is predominantly affected in Asian countries.⁴ Segment C7–T1 involvement was seen in all patients in our study.

Repeated or sustained flexion movements of the neck account for necrosis of the anterior horn cells of the lower cervical cord

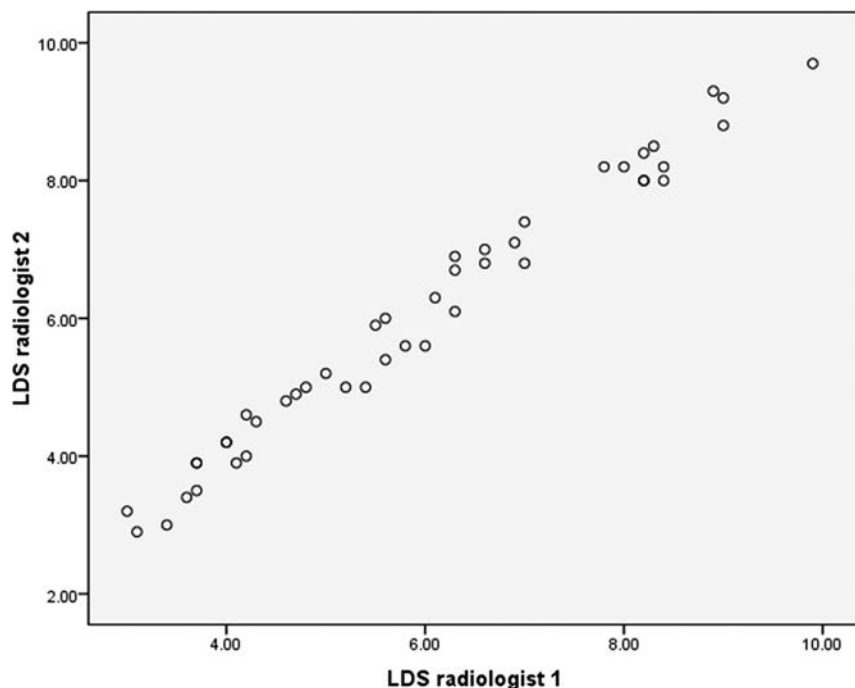


FIG 4. Scatterplot showing the various LDS measurements by the 2 radiologists.

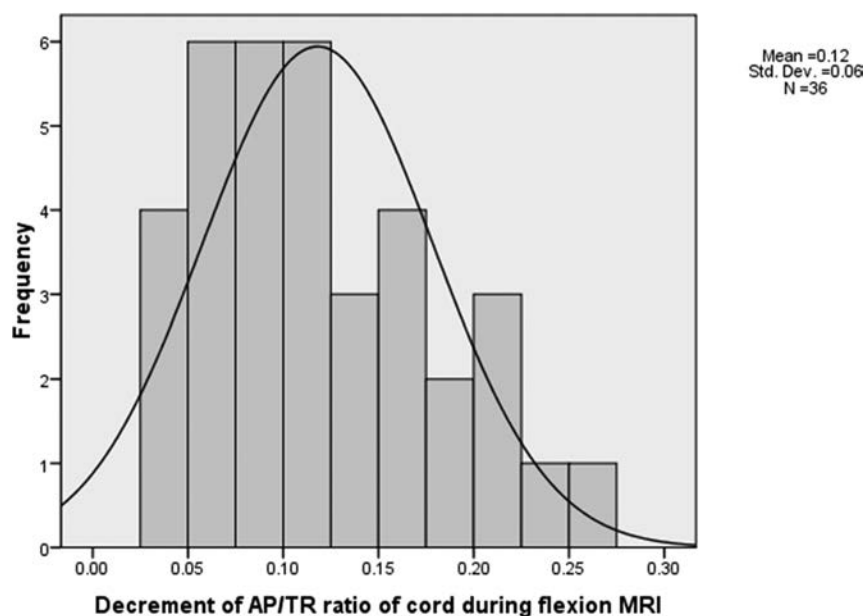


FIG 5. Histogram showing decrement in AP/TR cord diameter ratio during flexion cervical MR imaging in the 45 patients with Hirayama disease.

from chronic microcirculatory changes in the anterior spinal artery territory, which is thought to be the etiopathogenesis in HD.¹³ Another possible underlying cause might be an imbalance in growth between the individual vertebral column and spinal canal contents, which leads to abutment of the anterior spinal cord against the vertebral column and detachment of the posterior dura, leading to a widened LDS, ultimately causing microcirculatory disturbances and ischemic changes in the anterior spinal cord.¹⁴⁻¹⁷ Some authors also proposed atrophy and elevated serum immunoglobulin E levels as participating factors.¹⁸ Tanaka et al¹⁹

observed the intrathecal upregulation of proinflammatory T-helper-1 cytokines/chemokines, such as interferon- γ and macrophage inflammatory proteins-1 β chemokine, in the CSF of patients with HD, indicating the possible involvement of intrathecal immunologic processes in this condition. In 2010, Ciceri et al²⁰ proposed that venous congestion in flexion might play an additional role in determining spinal cord ischemic changes. Venous engorgement is thought to be secondary to an impaired venous drainage toward the jugular veins during neck flexion and an increased flow to the posterior internal vertebral venous plexus resulting from the negative pressure in the posterior epidural space because of anterior shifting of the dura.

Imaging plays a very important role in the diagnosis of HD. Plain radiographs may only show loss of cervical lordosis, which is a very nonspecific finding. MR imaging is the best technique in the diagnosis of this entity. Conventional neutral position MR imaging may show an atrophied lower cervical cord and asymmetric cervical cord flattening with or without abnormal T2-weighted hyperintensities in the cervical cord, especially the anterior horn cells. More important is MR imaging in neck flexion, which reveals classic findings of posterior dural detachment with forward shifting of the posterior dural sac and loss of attachment between the posterior dural sac and the subjacent lamina, leading to a widened LDS. Postgadolinium flexion MR images demonstrate moderate-to-intense enhancement in the engorged posterior epidural venous plexus, forming a crescent-shaped epidural mass, which exerts a compression effect over the cord with or without flow voids.^{14,21} Gupta et al²² proposed the use of 3D-CISS for better visualization

of the epidural flow voids on MR imaging. Although most existing literature suggests the need for flexion MR imaging in the diagnosis of HD, Lehman et al²³ in 2013 reported that neutral MR imaging itself was highly specific with moderately high sensitivity. They also reported that the findings of HD, though subtle, are often present in neutral scans, though the diagnostic confidence may be less. Chen et al¹⁵ in 2004 proposed “loss of attachment” from the posterior dural sac and subjacent lamina as the most valuable finding in the diagnosis of HD, reporting a prevalence of 93% in their study group.

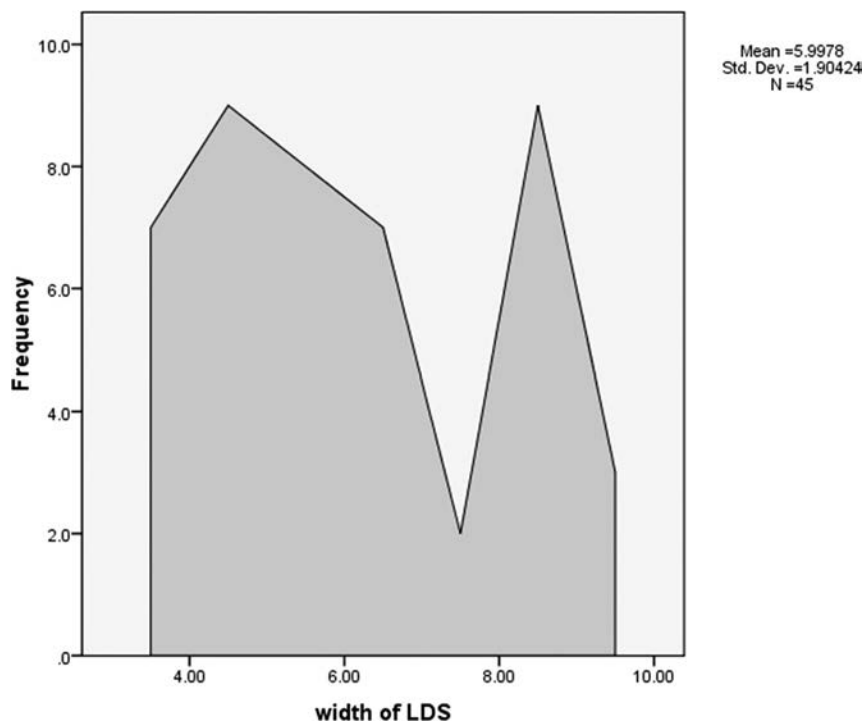


FIG 6. Frequency polygon showing the laminodural space measurements (in millimeters) during flexion cervical MR imaging in the 45 patients with HD.

However, Lai et al⁹ observed that forward shifting of the posterior dural sac was also seen in healthy subjects in up to 46% of patients, but without spinal cord compression. They further noted that the distance of such a forward shift was mild, ranging from 1.0 to 4.2 mm with a mean of 1 mm, compared with those with HD in whom it ranged from 6.1 to 7.8 mm, with a mean of 6.7 mm. They studied the increment in the ratio of the AP diameter of forward displacement of the posterior dural wall/AP diameter of the spinal canal and the decrement in the ratio of the AP diameter of the spinal cord/TR diameter of the spinal cord. They concluded that the ratio of LDS at the site of maximum forward shift to the spinal canal diameter should be increased in HD with a decreased ratio of the AP/TR diameter of the spinal cord in flexion compared with the neutral position. These ratios do not significantly change in healthy subjects.⁹ However, the major limitation of their study was the small sample size of 3 patients. We applied the findings to a larger study group. In our study of 45 patients with HD, the ratio of maximum LDS/maximum AP diameter of the spinal canal during flexion MR imaging had an average increment value of 0.46 ± 0.14 mm. The ratio of the AP diameter of the cord/TR diameter of the cord during neutral MR imaging was 0.45 ± 0.09 mm, which decreased during flexion MR imaging because of cord compression and cord flattening. The mean decrement of the AP/TR cord ratio during flexion MR imaging was 0.118 ± 0.06 mm.

We acknowledge the limitations in our study. We did not have a control group to compare LDS distance and decide the exact cutoff to label as HD. A uniform angle of neck flexion could not be achieved in all patients due to subject bias. In the future, further case-control studies are necessary to obtain the mean LDS in healthy individuals.

HD has a self-limiting course, and treatment is usually conserva-

tive. The management includes reducing repeat trauma to the cervical cord by avoiding repeat neck flexion by the use of a soft cervical collar during the progressive stage of the disease process, which is shown to arrest the disease progression.²⁴ Even surgical interventions such as cervical decompression and fusion with or without duraplasty or cervical duraplasty with tenting sutures via laminoplasty without cervical fusion may be advocated in selected patients.^{25,26} Hence, early recognition of HD is necessary because the patient can be advised to avoid or limit neck flexion movements, which helps in arresting further progression of this disease. So, a high index of clinical suspicion is necessary to diagnose this entity because neutral MR imaging may fail to diagnose it.

CONCLUSIONS

High clinical suspicion of HD is necessary in young patients with insidious onset of weakness of the hand and forearm muscles with muscle flaccidity. Flexion MR imaging sequences must be ob-

tained to look for LDS widening and anterior displacement of the posterior dura mater because it can be missed on conventional neutral position MR images.

The ratio of the LDS at maximum forward shift to the spinal canal diameter is increased in HD with decrement of the AP/TR diameter of the spinal cord during flexion MR imaging. The forward shifting of the posterior cervical dural sac on flexion MR imaging can also be seen in healthy subjects, but associated cord compression, if present, is helpful to clinch the diagnosis.

ACKNOWLEDGMENTS

We are thankful to Dr V. Preethish Kumar for his assistance in editing the manuscript.

REFERENCES

- Hirayama K, Toyokura Y, Tsubaki T. **Juvenile muscular atrophy unilateral upper extremity a new clinical entity.** *PsychiatrNeurol Jpn* 1959;61:2190–97
- Biondi A, Dormont D, Weitzner I Jr, et al. **MR imaging of the cervical cord in juvenile amyotrophy of distal upper extremity.** *AJNR Am J Neuroradiol* 1989;10:263–68 Medline
- Gourie-Devi M, Suresh TG, Shankar SK. **Monomelic amyotrophy.** *Arch Neurol* 1984;41:388–94 CrossRef Medline
- de Carvalho M, Swash M. **Monomelic neurogenic syndromes: a prospective study.** *J Neurol Sci* 2007;263:26–34 CrossRef Medline
- Di Muzio A, Delli Pizzi C, Lugaresi A, et al. **Benign monomelic amyotrophy of lower limb: a rare entity with a characteristic muscular CT.** *J Neurol Sci* 1994;126:153–61 CrossRef Medline
- Guo XM, Qin XY, Huang C. **Neuroelectrophysiological characteristics of Hirayama disease: report of 14 cases.** *Chin Med J (Engl)* 2012;125:2440–43 Medline
- Nalini A, Gourie-Devi M, Thennarasu K, et al. **Monomelic amyotrophy: clinical profile and natural history of 279 cases seen**

- over 35 years (1976–2010). *Amyotroph Lateral Scler Frontotemporal Degener* 2014;15:457–65 [CrossRef Medline](#)
8. Pradhan S. **Bilaterally symmetric form of Hirayama disease.** *Neurology* 2009;72:2083–89 [CrossRef Medline](#)
 9. Lai V, Wong YC, Poon WL, et al. **Forward shifting of posterior dural sac during flexion cervical magnetic resonance imaging in Hirayama disease: an initial study on normal subjects compared to patients with Hirayama disease.** *Eur J Radiol* 2011;80:724–28 [CrossRef Medline](#)
 10. Patel DR, Knepper L, Jones HR Jr. **Late-onset monomelic amyotrophy in a Caucasian woman.** *Muscle Nerve* 2008;37:115–19 [CrossRef Medline](#)
 11. Yilmaz O, Alemdaroglu I, Karaduman A, et al. **Benign monomelic amyotrophy in a 7-year-old girl with proximal upper limb involvement: case report.** *Turk J Pediatr* 2011;53:471–76 [Medline](#)
 12. Preethish-Kumar V, Nalini A, Singh RJ, et al. **Distal bimelic amyotrophy (DBMA): phenotypically distinct but identical on cervical spine MR imaging with brachial monomelic amyotrophy/Hirayama disease.** *Amyotroph Lateral Scler Frontotemporal Degener* 2015;16:338–44 [CrossRef Medline](#)
 13. Raval M, Kumari R, Dung AA, et al. **MRI findings in Hirayama disease.** *Indian J Radiol Imaging* 2010;20:245–49 [CrossRef Medline](#)
 14. Abraham A, Gotkine M, Drory VE, et al. **Effect of neck flexion on somatosensory and motor evoked potentials in Hirayama disease.** *J Neurol Sci* 2013;334:102–05 [CrossRef Medline](#)
 15. Chen CJ, Hsu HL, Tseng YC, et al. **Hirayama flexion myelopathy: neutral-position MR imaging findings—importance of loss of attachment.** *Radiology* 2004;231:39–44 [CrossRef Medline](#)
 16. Foster E, Tsang BK, Kam A, et al. **Mechanisms of upper limb amyotrophy in spinal disorders.** *J Clin Neurosci* 2014;21:1209–14 [CrossRef Medline](#)
 17. Gotkine M, Abraham A, Drory VE, et al. **Dynamic MRI testing of the cervical spine has prognostic significance in patients with progressive upper-limb weakness and atrophy.** *J Neurol Sci* 2014;345:168–71 [CrossRef Medline](#)
 18. Vitale V, Caranci F, Pisciotto C, et al. **Hirayama's disease: an Italian single center experience and review of the literature.** *Quant Imaging Med Surg* 2016;6:364–73 [CrossRef Medline](#)
 19. Tanaka M, Ishizu T, Ochi H, et al. **Intrathecal upregulation of IFN-gamma and MIP-1beta in juvenile muscular atrophy of the distal upper extremity.** *J Neurol Sci* 2008;275:74–77 [CrossRef Medline](#)
 20. Ciceri EF, Chiapparini L, Erbetta A, et al. **Angiographically proven cervical venous engorgement: a possible concurrent cause in the pathophysiology of Hirayama's myelopathy.** *Neurol Sci* 2010;31:845–48 [CrossRef Medline](#)
 21. Gandhi D, Goyal M, Bourque PR, et al. **Case 68: Hirayama disease.** *Radiology* 2004;230:692–96 [CrossRef Medline](#)
 22. Gupta K, Sood S, Modi J, et al. **Imaging in Hirayama disease.** *J Neurol Rural Pract* 2016;7:164–67 [CrossRef Medline](#)
 23. Lehman VT, Luetmer PH, Sorenson EJ, et al. **Cervical spine MR imaging findings of patients with Hirayama disease in North America: a multi-site study.** *AJNR Am J Neuroradiol* 2013;34:451–56 [CrossRef Medline](#)
 24. Tokumaru Y, Hirayama K. **Cervical collar therapy for juvenile muscular atrophy of distal upper extremity (Hirayama disease): results from 38 cases [in Japanese].** *Rinsho Shinkeigaku* 2001;41:173–78 [Medline](#)
 25. Chiba S, Yonekura K, Nonaka M, et al. **Advanced Hirayama disease with successful improvement of activities of daily living by operative reconstruction.** *Intern Med* 2004;43:79–81 [CrossRef Medline](#)
 26. Ito H, Takai K, Taniguchi M. **Cervical duraplasty with tenting sutures via laminoplasty for cervical flexion myelopathy in patients with Hirayama disease: successful decompression of a "tight dural canal in flexion" without spinal fusion.** *J Neurosurg Spine* 2014;21:743–52 [CrossRef Medline](#)

Percutaneous CT-Guided Biopsies of the Cervical Spine: Technique, Histopathologic and Microbiologic Yield, and Safety at a Single Academic Institution

E.L. Wiesner, T.J. Hillen, J. Long, and J.W. Jennings

ABSTRACT

BACKGROUND AND PURPOSE: Cervical spine biopsies can be challenging due to the anatomy and the adjacent critical structures. Percutaneous image-guided biopsies can obviate the need for an open biopsy, however there have been few studies looking at the approaches, safety, and efficacy of percutaneous cervical spine biopsies. This retrospective study evaluated technical considerations, histopathologic and microbiologic yield, and safety in CT-guided cervical bone biopsies.

MATERIALS AND METHODS: A retrospective review of cervical bone and/or bone/disc biopsies performed from January 2010 to January 2017 was included in this study. Clinical diagnosis and indication, patient demographics, biopsy location, biopsy needle type, technical approach, lesion size, dose-length product, conscious sedation details, complications, and diagnostic histopathologic and/or microbiologic yield were recorded for each case and summarized.

RESULTS: A total of 73 patients underwent CT-guided cervical bone biopsies. Fifty-three percent (39/73) were for clinical/imaging concern for infection and 47% (34/73) were for primary tumors or metastatic disease. Thirty-four percent (25/73) were of the inferior cervical spine (ie, C6 and C7). A sufficient sample was obtained for histopathologic and microbiologic analyses in 96% (70/73) of the biopsies. Forty-six percent (18/39) of those samples taken for infection had positive cultures. Two intraprocedural complications occurred in which the patients became hypotensive during the procedure without long-term complications.

CONCLUSIONS: Percutaneous CT-guided biopsy of the cervical spine is an effective and safe procedure with high diagnostic yield and can obviate open procedures for histopathologic and microbiologic analyses of patients with clinical and imaging findings concerning for infection or primary and metastatic osseous lesions.

ABBREVIATION: DLP = dose-length product

Biopsies of the cervical spine are more difficult to obtain than those of the thoracic or lumbar regions due to the anatomy and smaller size of the vertebral elements as well as the critical adjacent vascular and neural anatomy.

Although the demands for cervical spine biopsies are steadily increasing in our practice, few publications address the safety of such biopsies and the high diagnostic yield they can provide. To date, the largest study was published in 2016 by Cox et al¹ and looked at CT-guided cervical bone biopsies in 43 patients by combining data from 2 large tertiary care hospitals. A diagnosis was obtained in 41 of the 43 patients, for a yield of 95%. In 2008, Rimondi et al² published

a study on 430 CT-guided spinal biopsies, 10 of which were within the cervical spine (2.3% of the sample). The diagnostic accuracy for this study was 70%. Similarly, in 2004, Lis et al³ studied the accuracy of CT-guided spinal biopsies. There were 410 cases in all, with only 9 cases being of the cervical spine. Yet, for these 9 cases, there was a 100% diagnostic accuracy reported.

Using a minimally invasive percutaneous CT-guided approach to cervical spine biopsies can obviate open biopsies for both infection and primary or metastatic lesions. This technique lends itself to the increasing demands for cultures by infectious disease specialists and for tissue diagnosis of metastatic disease by oncologists.

The purpose of this retrospective study was to further evaluate technical considerations, histopathologic and microbiologic yield, and safety in CT-guided cervical bone biopsies.

MATERIALS AND METHODS

Patient Selection and Study Enrollment

Approval from the institutional review board was granted with a waiver of patient informed consent. Correlating data from a single

Received December 8, 2017; accepted after revision January 24, 2018.

From the Mallinckrodt Institute of Radiology, Washington University School of Medicine, St. Louis, Missouri.

Please address correspondence to Elizabeth L. Wiesner, BA, Mallinckrodt Institute of Radiology, 510 South Kingshighway Blvd, St. Louis, MO 63110; e-mail: wiesner.elizabeth@wustl.edu

<http://dx.doi.org/10.3174/ajnr.A5603>

academic institution on cervical bone and/or bone/disc biopsies from January 2010 to January 2017 were then gathered and included in this study. For each case, we recorded and summarized the following: patient demographics, clinical diagnosis and indication, level biopsied, biopsy needle type/gauge, technical approach, number and length of each soft-tissue/bone core biopsy, CT dose-length product, conscious sedation details including sedation time and the amount of fentanyl and/or midazolam (Versed) given, and diagnostic histopathologic and/or microbiologic yield. Procedural complications were documented according to the Society of Interventional Radiology classification.⁴ Patients were clinically monitored for at least 1 hour after each procedure for evidence of acute complications such as hematoma formation or neurologic injury. Electronic medical records were also reviewed for evidence of delayed complications within 30 days of the biopsy.

Table 1: Biopsy needles used for 34 bone lesion biopsies^a

Biopsy Needle	Bone Lesion Samples
Bonopt 14/15 (AprioMed)	8
Arrow OnControl 11/13 (Teleflex)	12
Arrow OnControl 12/14 (Teleflex)	5
Achieve 16 (CareFusion)	5
Bard 14 (Bard Peripheral Vascular)	5
Bard 16 (Bard Peripheral Vascular)	1
Tru-Cut 18 (CareFusion)	3
Tru-Cut 20 (CareFusion)	1

^a Six procedures used both bone and soft-tissue biopsy needle systems for 40 total needle systems used.

Table 2: Biopsy needles used for 39 infection biopsies^a

Biopsy Needle	Soft-Tissue Samples
Bonopt 14/15 (AprioMed)	16
Arrow OnControl 11/13 (Teleflex)	20
Arrow OnControl 12/14 (Teleflex)	3
Achieve 14 (CareFusion)	1
Achieve 16 (CareFusion)	1
Achieve 18 (CareFusion)	1
Temno Evolution 18 (CareFusion)	2
Tru-Cut 16 (CareFusion)	1
Tru-Cut 20 (CareFusion)	1

^a Seven procedures used both bone and soft-tissue biopsy needle systems, 9 procedures used only soft-tissue needle systems, and 23 procedures used only bone biopsy needle systems for 46 total needle systems used.

Biopsy Procedure

All procedures were performed by 1 of 6 board-certified fellowship-trained musculoskeletal radiologists. Most of these procedures were performed with the patient under moderate sedation except for 3 procedures performed with the patient under general anesthesia and 2 procedures in which conscious sedation was not required. In most cases, a 1:1 mixture of bupivacaine 0.25% and lidocaine 1% was administered for subcutaneous and periosteal anesthesia. Average sedation time was 67.5 minutes; average intravenous fentanyl and Versed dosages were 210.1 μ g and 3.7 mg, respectively.

The Arrow OnControl Powered Bone Lesion Biopsy System (Teleflex, Limrick, Pennsylvania) and Bonopt (AprioMed, Londonderry, New Hampshire) bone biopsy system were used for bone access and biopsy of the sites of infection, sclerotic lesions, or CT-occult lesions. In the cases in which there was a soft-tissue biopsy performed in either a lesion or the disc space, Bard (Bard Peripheral Vascular, Tempe, Arizona), Achieve (CareFusion, San Diego, California), Temno Evolution (CareFusion), and Tru-Cut (CareFusion) spring-loaded soft-tissue biopsy needles were used. Of the 73 total biopsy procedures performed, 64 procedures required the use of a bone biopsy needle system. The most commonly used bone biopsy needle system was the Arrow OnControl 11/13 needle system, used in 32 of 64 procedures. Of the 73 total biopsy procedures performed, 22 required the use of a soft-tissue biopsy needle. Nine of the 73 biopsies were performed with only a soft-tissue coaxial needle system. The most commonly used soft-tissue biopsy needle was the Achieve 16-ga biopsy needle. It was used in 6 of the 22 procedures in which a soft-tissue biopsy needle was used. Tables 1 and 2 describe in detail the different biopsy needles used for infection and lesion biopsy.

Patient positioning on the table was dependent on the location of the cervical spine lesion and the approach used to perform the biopsy. For the posterolateral and directly posterior approaches, the patient was placed prone on the table. For the directly lateral approach, the patient was placed in the decubitus position with the side of the lesion up. For the anterolateral approach, the patient was placed supine. Posterolateral (60 procedures), directly posterior (1 procedure), directly lateral (3 procedures), or anterolateral (9 procedures) approaches were used to sample the lesions (Fig 1), depending on the location of the pathology. Our most commonly used approach was a posterolateral approach through the lateral mass into the vertebral body. This approach allows avoidance of important neurovascular structures in the neck but is tedious to perform because the needle has the farthest to travel within bone to get to the site of abnormality. A direct posterior approach was used for a single spinous process lesion. The anterolateral approach was used occasionally. This approach is somewhat treacherous because the needle must be threaded among multiple important structures, includ-

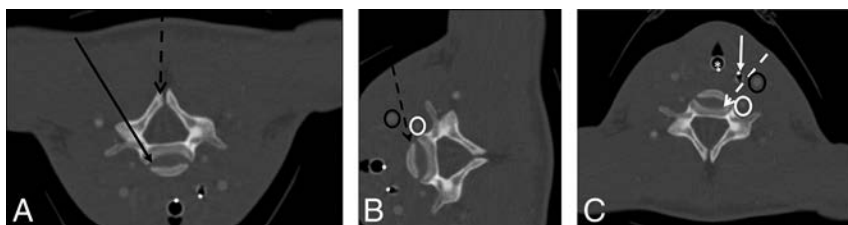


FIG 1. CT-guided cervical spine biopsies were performed using anterolateral, posterolateral, posterior, or lateral approaches. A, CT angiogram of the neck flipped vertically to depict prone positioning for a posterolateral- or posterior-approach cervical spine biopsy. The *black arrow* demonstrates a posterolateral-approach biopsy of the vertebral body or disc. The *dashed black arrow* demonstrates a directly posterior approach to a lesion in the spinous process. B, CT angiogram of the neck rotated to depict decubitus positioning for a lateral-approach biopsy to the vertebral body (*dashed black arrow*). Note that the course of the biopsy needle is between the carotid artery (*black oval*) and vertebral artery (*white oval*). C, CT angiogram of the neck with the patient in a supine position for an anterolateral-approach cervical spine biopsy. The needle (*dashed white arrow*) passes between the intubated trachea (*white asterisk*), nasogastric tube/esophagus (*solid white arrow*), carotid artery (*black oval*), and vertebral artery (*white oval*).

ing the carotid artery laterally and the trachea and esophagus medially, and it is often difficult to avoid the thyroid for lesions in the lower cervical spine. We commonly used this approach if the patient had a prior radical neck dissection because there were fewer important structures to avoid in these cases. A lateral approach was used in cases in which the mass extended into the lateral soft-tissue or was near midline at a site deemed too difficult to reach by a posterolateral approach. In this approach, the needle needs to be passed between the external and internal carotid arteries and the vertebral artery. The internal jugular vein can sometimes be avoided but not always with this approach. With this approach in the upper cervical spine, it is

imperative that the course of the vertebral artery is known because the location is variable.

CT angiography was occasionally performed immediately before the biopsy to better delineate the vascular anatomy and plan the safest biopsy path to minimize the risk of vascular injury. Of the 73 patients who underwent biopsy, 6 had corresponding CT angiograms. In these cases, an average of 80.0 mL of ioversol contrast (Optiray 350; Mallinckrodt, St. Louis, Missouri) was given intravenously to help localize vascular structures in relation to the tumor (Figs 2 and 3).

All samples were analyzed at the institution where the biopsy was performed.

RESULTS

Patient Characteristics

A total of 73 patients underwent CT-guided cervical bone biopsies. Sixty-two percent of the patients were men and 38% were women. Fifty-three percent (39/73) of the cervical biopsies were for clinical/imaging concern for infection (Fig 4), and 47% (34/73) were for primary tumors or metastatic disease. A sufficient sample was obtained for histopathologic and microbiologic analyses in 96% (70/73) of the biopsies. Forty-six percent (18/39) of those samples taken for infection had positive culture growth from a sample. Two intraoperative complications occurred. One patient became hypotensive and did not respond to the IV bolus; the procedure was terminated after 2 samples had already been obtained. The patient subsequently stabilized and had no further complications. The second patient became hypotensive and bradycardic before the biopsy needle could be placed. The patient subsequently stabilized and had no further complications. A cervical spine biopsy was performed 2 days later without complication.

Lesion Characteristics

Of the 34 CT-guided cervical bone biopsies that were for primary tumors or

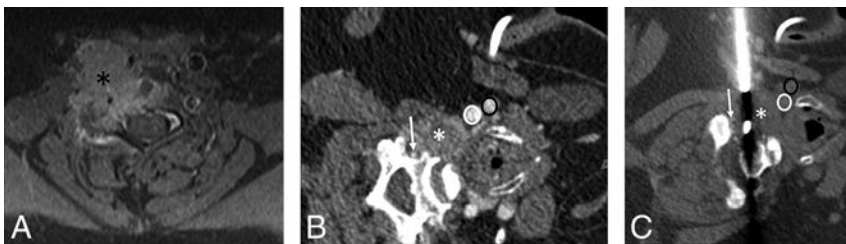


FIG 2. A 70-year-old woman with a history of lung cancer and a new right C5 mass extending into the adjacent soft tissues. A, Axial T1 fat-suppressed postcontrast MR image with a large right C5 mass (black asterisk) extending into the adjacent soft tissues and vertebral canal. B, Intraprocedural CT angiogram with the patient in a left lateral decubitus position shows the mass (white asterisk) and adjacent vascular structures (vertebral artery, white arrow; common carotid artery, white oval; jugular vein, black oval). C, Intraprocedural CT image with the patient in the left lateral decubitus position demonstrates the biopsy using a coaxial soft-tissue biopsy needle passing between vascular structures (vertebral artery, white arrow; common carotid artery, white oval; jugular vein, black oval) into the mass (white asterisk) using a lateral approach. The surgical pathology result was metastatic lung adenocarcinoma.

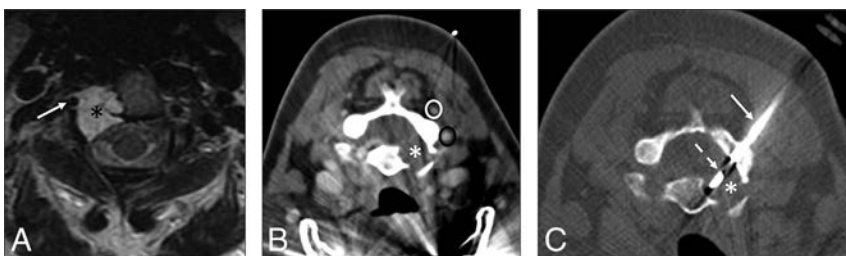


FIG 3. A 55-year-old woman with right neck and arm pain. A, Axial T2-weighted MR image with a large right C2 vertebral mass (black asterisk) surrounding the vertebral artery (white arrow). B, Intraprocedural CT angiogram soft-tissue-windowed image with the patient prone shows the mass (white asterisk) and adjacent vascular structures (deep cervical vein, white oval; vertebral artery, black oval). C, Intraprocedural CT bone-windowed image with the patient prone demonstrates the bone-access needle (white arrow) in the posterolateral right lamina of C2 and a soft-tissue biopsy needle (dashed white arrow) placed coaxially into the mass (white asterisk), using a posterolateral approach. The surgical pathology result was chordoma.

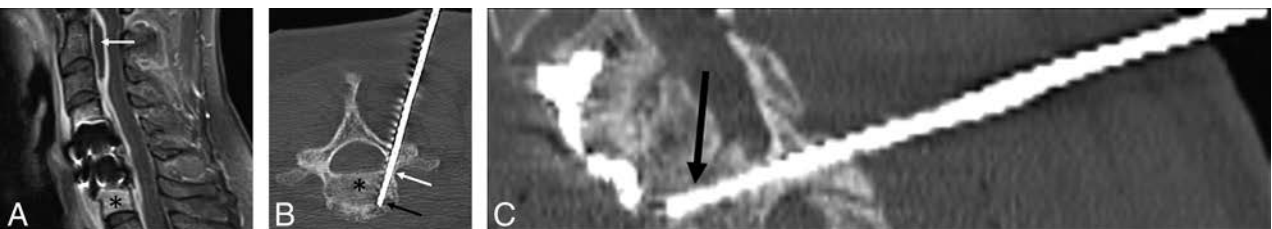


FIG 4. A 51-year-old woman with prior discectomy and interbody fusion. A, Sagittal T1 fat-suppressed postcontrast MR image with evidence of osteomyelitis at C7 (black asterisk), prevertebral inflammation, and epidural abscess (white arrow). Intraprocedural oblique axial (B) and oblique sagittal (C) CT reconstructed images during the biopsy procedure show the biopsy needle placed from a posterolateral approach, through the right C7 pedicle (white arrow) into the vertebral body (black asterisk) and subsequently the C6–C7 disc space (black arrow). Microbiology grew *Staphylococcus aureus*, and pathology showed osteomyelitis.

Table 3: Histopathologic results of CT-guided cervical bone biopsies for primary tumors or metastatic disease

Malignant (<i>n</i> = 24 cases)	
Myeloma	4
NSCLC/adenocarcinoma	4
Osteoid osteoma	3
Chordoma	2
Giant cell tumor	2
Indeterminate (abnormal)	2
Metastatic carcinoma	
Unknown primary	2
Epithelioid hemangioendothelioma	1
Metastatic carcinoma	
Breast primary	1
Metastatic papillary	
Thyroid carcinoma	1
Aneurysmal bone cyst focal	1
Eosinophilic granuloma	1
Benign (<i>n</i> = 10 cases)	
Normal ^a	6
Marrow fibrosis	1
Chronic inflammation	1
<i>Micrococcus</i> species	1
Osteomyelitis	1

Note:—NSCLC indicates non-small-cell lung carcinoma.

^a Normal means biopsy demonstrating normal bone seen on histopathology.

metastatic disease, the type of lesions biopsied included lytic, sclerotic, mixed, or CT occult. These lesions were classified as follows: 70.6% (24/34) lytic, 17.6% (6/34) mixed, 5.9% (2/34) CT occult, and 5.9% (2/34) sclerotic. Histopathologic yield per lesion type was the following: 95.8% (23/24) lytic, 83.3% (5/6) mixed, 0.0% (0/2) CT occult, and 50.0% (1/2) sclerotic.

To obtain an average size, we measured the longest axis of each lesion with an average lesion size of 18.2 mm, ranging between 5.0 and 40.0 mm. Ten lesions involved the entire vertebral body. Of the 34 biopsies performed for bone lesions in our study, the most common location of lesions, including the 10 cases in which the lesion encompassed the entire vertebral body, was the C7 cervical vertebra, which involved 29.4% (10/34) of the lesions. At this level, 5 were within the vertebral body, 3 were in the transverse process, and 2 were in the lateral mass. The locations of the lesions that made up the remaining 24/34 biopsies were as follows: C1 lesions (2/24), with both lesions in the vertebral body/anterior arch; C2 lesions (7/24), with 4 lesions centered in the vertebral body alone, 2 lesions centered within the lamina, and 1 centered in the lateral mass; C3 lesions (2/24), both of which included the entire vertebral body; C4 lesions (2/34), of which 1 lesion was centered within the vertebral body and 1 lesion was located within the C4 transverse process; C5 lesions (4/24), with 2 lesions centered within the vertebral body, 1 lesion within the C5 spinous process, and 1 lesion centered in the lateral mass; and C6 lesions (7/24), with 6 lesions centered in the vertebral body and 1 lesion centered within the lateral mass.

Of the 34 biopsies obtained, 70.6% (24) were malignant. The most common malignant lesions were myeloma and adenocarcinoma, each found in 4 patients (Table 3).

CT Radiation Dose

Our retrospective study also looked at dose-length product (DLP) in all 73 CT-guided cervical bone biopsies. For the 34 biopsies that were specific to primary tumors or metastatic disease, the range

for DLP was 122–1767 mGy × cm, with an average of 712 mGy × cm. For the 39 biopsies specific to clinical/imaging concern for infection, the range for DLP was 163–3223 mGy × cm, with an average of 932.4 mGy × cm. Combining DLPs for all 76 spinal biopsies yielded the same range of 122–3223 mGy × cm, with an overall average DLP of 829.8 mGy × cm. We accounted for the range of DLPs by equating outliers with those patients who received ablation on the same day that the cervical biopsy was performed, therefore increasing the patient's DLP and thus our calculated DLP average.

When considering the most recent spinal biopsies, specifically from January 2015 to January 2017, which accounts for 47.9% (35/73) of all biopsies performed, there was a decreased average DLP of 639 mGy × cm. This difference in average DLPs within biopsies of the last 2 years can be associated with the increasing awareness of scanning parameters, advanced scanner technology, as well as institutional emphasis on decreased diagnostic and procedural radiation doses.

DISCUSSION

Multiple publications have demonstrated the safety and utility of percutaneous bone biopsies with fewer focusing on the spine and even fewer on the cervical spine. To our knowledge, this is the largest study to date on percutaneous CT-guided cervical bone biopsies. Compared with similar studies of spinal bone biopsies, our diagnostic yield is within the average, around 96% for histopathologic and microbiologic analyses of all biopsies.

The high diagnostic yield of not just cervical bone biopsies but also biopsies throughout the entire spine is important to consider when looking at past imaging techniques and the nonspecific nature of radiologic imaging alone for yielding a definitive diagnosis. In 2012, a study by Kaltsikis et al⁵ on core needle biopsies of spinal lesions similarly emphasized the importance of the CT-guided bone biopsies themselves to render more definitive histopathologic diagnoses. For their study, 79 biopsies of the spine were performed, 5 of the cervical spine, with a diagnostic yield of 95% and a diagnostic accuracy of 97.3%. Most spinal biopsies (52%) performed in the study by Kaltsikis et al also followed our technique using the posterior lateral approach during biopsy.

Given the relatively smaller spinal anatomy and the ascending importance of the neural anatomy of the cervical spine, choosing the appropriate anatomic approach to safely perform the biopsy is an important consideration. We most commonly use a posterolateral approach for biopsy of the cervical spine, but other approaches to consider include the lateral, anterolateral, and directly posterior approach, depending on the location of the lesion. Of the 73 patients who underwent the procedure at our institution, there were only 2 minor intraprocedural complications and no postprocedural complications. There was no vascular or neurologic injury.

In 2013, Huang et al⁶ published a 2-year prospective study on the incidence of complications following percutaneous CT-guided biopsies of spinal lesions, including soft tissues and bone. Of the 386 patients, the reported rates of bruising, level of discomfort/pain, and fever did not exceed 16.1% in any category. In 2006, Peh⁷ demonstrated low complication rates on CT-guided biop-

sies of the spine, ranging from 0% to 10%, with <1% risk of major complication.

CONCLUSIONS

This study supports the addition of percutaneous cervical spine biopsies to the growing number of studies demonstrating the safety and efficacy of spine biopsies that can obviate open biopsies and their associated risks.

Disclosures: Travis J. Hillen—**UNRELATED**: Consultancy: Medtronic, Merit Medical Systems, Comments: consultant (Medtronic) and proctor training labs (Merit Medical Systems). Jack W. Jennings—**UNRELATED**: Consultancy: Merit, Medtronic, Bard, Comments: consultant (Merit, Medtronic, Bard) and advisory board (Merit, Medtronic).

REFERENCES

1. Cox M, Pukenas B, Poplawski M, et al. **CT-guided cervical bone biopsy in 43 patients: diagnostic yield and safety at two large tertiary care hospitals.** *Acad Radiol* 2016;23:1372–75 [CrossRef](#) [Medline](#)
2. Rimondi E, Staals E, Errani C, et al. **Percutaneous CT-guided biopsy of the spine: results of 430 biopsies.** *Eur Spine J* 2008;17:975–81 [CrossRef](#) [Medline](#)
3. Lis E, Bilsky M, Pisinski L, et al. **Percutaneous CT-guided biopsy of osseous lesion of the spine in patients with known or suspected malignancy.** *AJNR Am J Neuroradiol* 2004;25:1583–88 [Medline](#)
4. Omary R, Bettmann M, Cardella J, et al; Society of Interventional Radiology Standards of Practice Committee. **Quality improvement guidelines for the reporting and archiving of interventional radiology procedures.** *J Vasc Interv Radiol* 2003;14:S293–95 [CrossRef](#) [Medline](#)
5. Kaltsikis I, Chourmouzi D, Drevelegas K, et al. **Core needle biopsy of spinal lesions under CT guidance: review of 79 cases.** *J Neurol Surg A Cent Eur Neurosurg* 2012;73:199–203 [CrossRef](#) [Medline](#)
6. Huang A, Halpern E, Rosenthal DI. **Incidence of delayed complications following percutaneous CT-guided biopsy of bone and soft tissue lesions of the spine and extremities: a 2-year prospective study and analysis of risk factors.** *Skeletal Radiol* 2013;42:61–68 [CrossRef](#) [Medline](#)
7. Peh W. **CT-guided percutaneous biopsy of spinal lesions.** *Biomed Imaging Interv J* 2006;2:e25 [Medline](#)

Transforaminal Lumbar Puncture: An Alternative Technique in Patients with Challenging Access

 D.R. Nascene,  C. Ozutemiz,  H. Estby,  A.M. McKinney, and  J.B. Rykken

ABSTRACT

SUMMARY: Interlaminar lumbar puncture and cervical puncture may not be ideal in all circumstances. Recently, we have used a transforaminal approach in selected situations. Between May 2016 and December 2017, twenty-six transforaminal lumbar punctures were performed in 9 patients (25 CT-guided, 1 fluoroscopy-guided). Seven had spinal muscular atrophy and were referred for intrathecal nusinersen administration. In 2, CT myelography was performed via transforaminal lumbar puncture. The lumbar posterior elements were completely fused in 8, and there was an overlying abscess in 1. The L1–2 level was used in 2; the L2–3 level, in 10; the L3–4 level, in 12; and the L4–5 level, in 2 procedures. Post-lumbar puncture headache was observed on 4 occasions, which resolved without blood patching. One patient felt heat and pain at the injection site that resolved spontaneously within hours. One patient had radicular pain that resolved with conservative treatment. Transforaminal lumbar puncture may become an effective alternative to classic interlaminar lumbar puncture or cervical puncture.

ABBREVIATIONS: LP = lumbar puncture; SMA = spinal muscular atrophy; SMN = survival motor neuron; TFLP = transforaminal lumbar puncture

Fluoroscopy-guided lumbar puncture (LP) is a routine procedure performed by radiologists. While typically performed for CSF laboratory testing, other indications include CSF opening pressure measurement, myelography, cisternography, intrathecal drug administration, and therapeutic CSF drainage.^{1–3} LP via an interlaminar approach is a safe and ubiquitous method to access the intrathecal compartment. However, interlaminar LP may not be feasible in certain complex conditions, such as complete fusion of the posterior elements or in the presence of an infectious process in the subcutaneous tissues of the low back along the planned needle path. In those situations, C1–2 cervical puncture or suboccipital cisternal puncture under CT or fluoroscopy guidance is a possible alternative to obtain access.^{4,5} However, some institutions perform such procedures infrequently, and not all radiologists may be comfortable with these procedures, especially given the possible severity of complications. In a 2009 survey, 14% of respondents described <1 cervical puncture for myelography on average per year in their neuroradiology fellowship program.⁶ A 1990 survey of neuroradiologists reported 7 cases of paraparesis, 7

cases of quadriplegia, and 1 death attributed to cervical myelography.⁷ The same survey reported 16 cases of injection of contrast into the spinal cord, 5 cases of spinal cord puncture, and 3 cases of vertebral artery injury.⁷

Despite the risk of these feared complications, cervical puncture is considered a safe procedure in experienced hands.^{4,6,8} If available, preprocedural imaging should be reviewed to confirm the patency of the posterior spinal canal and to evaluate the position of the vertebral arteries. Unfortunately, some patients are not good candidates for interlaminar LP and have challenging cervical anatomy (eg, prior fusion procedure, spinal muscular atrophy [SMA], or ankylosing spondylitis). Therefore, cervical puncture may not be a viable option, even by the most experienced radiologists.

SMA is an autosomal recessive inherited disorder, with loss of both copies of the *SMN1* gene located on the long arm of chromosome 5 (5q), which encodes survival motor neuron (SMN), a protein necessary for motor neuron survival. SMA type 1 (Werdnig-Hoffmann disease) presents in early infancy and is the most severe form, often leading to death before 2 years of age. SMA types 2 and 3 are less severe, with SMA2 presenting later in the first year of life, and SMA3, later in childhood but sometimes in adulthood. All types of SMA cause progressive muscle wasting, frequently causing neuromuscular scoliosis and thoracic insufficiency syndrome. Severe scoliosis often requires posterior spinal fusion procedures for proper diaphragm function,⁹ which may result in complete osseous interlaminar fusion that precludes interlaminar LP.

Received December 9, 2017; accepted after revision January 24, 2018.

From the Department of Radiology (D.R.N., C.O., A.M.M., J.B.R.), Neuroradiology Section, University of Minnesota, Minneapolis, Minnesota; and University of Minnesota Medical School (H.E.), Minneapolis, Minnesota.

Please address correspondence to Can Ozutemiz, MD, Department of Radiology, University of Minnesota, MMC 292, 420 Delaware St SE, Minneapolis, MN 55455; e-mail: ozutemiz@umn.edu

<http://dx.doi.org/10.3174/ajnr.A5596>

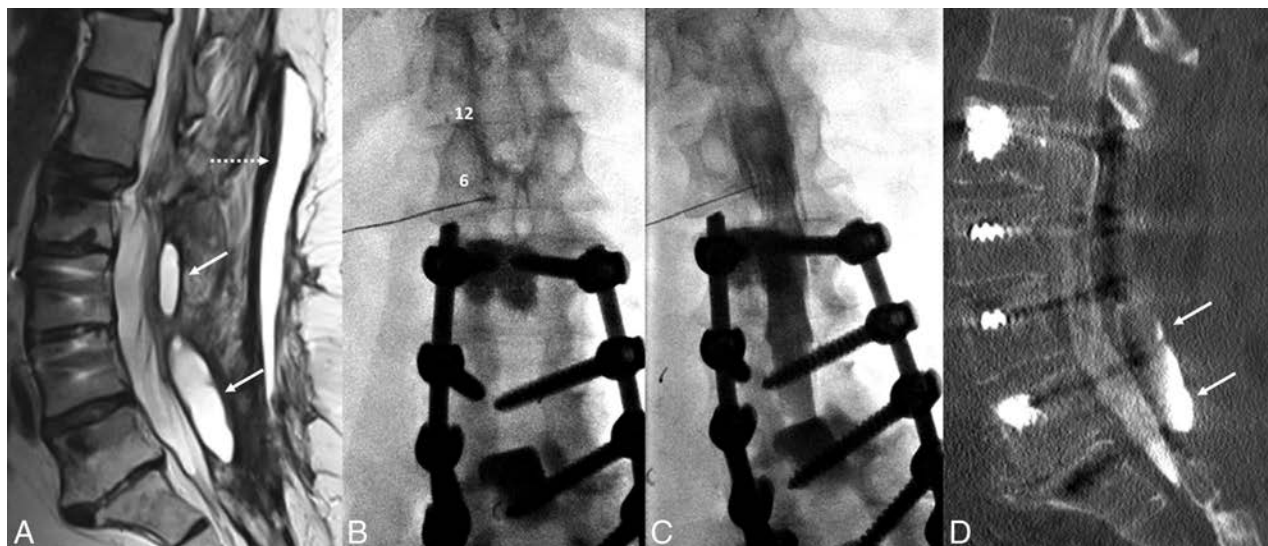


FIG 1. A 67-year-old woman with a history of multiple spinal fusions presented with newly worsening low back and radicular leg pain (case 1). Sagittal T2-weighted MR imaging (A) shows 2 paraspinous fluid collections (white arrows) within the deep paraspinal musculature and a midline subcutaneous fluid collection (dashed arrow) with rim enhancement on postcontrast series (not shown). B, Anteroposterior fluoroscopy image of myelography with TFLP. The needle tip is beyond the medial edge of the pedicle at the 5 o'clock position (relative to the pedicle). Note the position of the needle inferior to the expected location of the exiting nerve root and dorsal root ganglion. C, Oblique fluoroscopy image shows contrast extending into the intrathecal space after injection through the left L1–2 foramen. D, CT myelogram demonstrates the inferiorly located cystic collection filled with contrast, confirming a pseudomeningocele (arrows).

Recently, several patients with SMA have been referred to our institution for intrathecal nusinersen (Spinraza) injection. Nusinersen is a newly developed antisense oligonucleotide drug that alters the splicing of *SMN2* messenger RNA. The *SMN2* gene is paralogous to *SMN1* and is usually present in patients with SMA. Both genes can yield the SMN protein. However, the version of the SMN protein encoded by native *SMN2* is rapidly degraded and is not sufficient to prevent motor neuron loss. In the presence of nusinersen, the altered splicing of *SMN2* leads to a more durable and long-lived protein product that, in turn, increases the amount of functional SMN protein.^{10,11} The treatment course requires 3 loading doses separated by 2 weeks and a fourth injection 1 month after the third loading dose, followed by repeat injections every 4 months.

There are several circumstances in which there may be a need for an alternative route into the thecal sac. Recently, we have used a transforaminal approach for LP, using either fluoroscopy or CT guidance. To our knowledge, this method is not well-described in the literature. Our purpose is to describe this alternative technique and share our initial experience.

CASE SERIES

Case Selection

This retrospective case series was institutional review board–approved. Between March 2016 and November 2017, twenty-six transforaminal lumbar puncture (TFLP) procedures were performed in 9 different patients, 25 with CT and 1 with fluoroscopic guidance. Informed consent was obtained from each patient. CT-guided procedures were performed with the Sensation 64 scanner (Siemens, Erlangen, Germany), and fluoroscopy-guided procedures were performed with the OEC 9900 Mobile C-arm (GE Healthcare, Milwaukee, Wisconsin). Patient characteristics including age, sex, body mass index, and postproce-

dural complications were obtained from the electronic medical record. Used modality, puncture level, and needle length were also obtained. Of note, all patients receiving nusinersen were called by nursing staff after each procedure to identify complications.

RESULTS

Twenty-six TFLPs were performed in 7 female and 2 male patients with 100% technical success. The mean age was 39.6 years (range, 31–68 years). The mean body mass index was 21.9 (range, 12.6–40), with the body mass index not available for 1 patient. Seven patients with SMA (6 with SMA type 2 and 1 with SMA type 3) were referred for intrathecal nusinersen administration. In 2 patients, the indication for TFLP was postoperative CT myelography.

All procedures were performed using 22-ga Quincke needles (Becton-Dickinson, Washington, DC), 3.5 inch in 10 procedures, 5 inch in 14, and 7 inch in 2. For TFLP, the L1–2 spinal level was used in 2 procedures; the L2–3 level, in 10; the L3–4 level, in 12; and the L4–5 level, in 2. In cases with CT-fluoroscopy guidance, routinely, kilovolt(peak) and milliamperes-second were set as 80 and 50, respectively. In cases in which the needle tip was not seen ideally due to streak artifacts, the kilovolt(peak) was increased to 100. The total dose-length product varied between 22 and 158 with a mean of 57.5 ± 35.3 mGy \times cm. Slice thickness was either 3 or 5 mm.

Case 1

A 67-year-old woman with a history of multiple previous spinal fusion procedures presented with newly worsening low back and radicular leg pain 6 months after lumbar fusion and laminectomy. Spine MRI showed 2 paraspinous fluid collections and a large midline subcutaneous fluid collection, all of which exhibited rim enhancement (Fig 1). With clinical suspicion of abscess versus

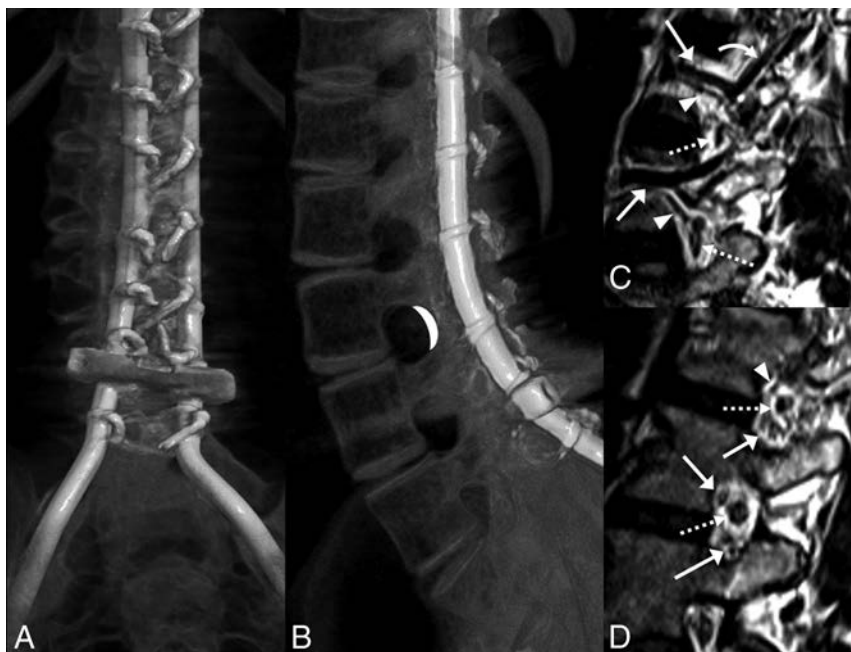


FIG 2. A and B, CT volumetric rendering of a patient with SMA2 demonstrates extensive posterior spinal fusion hardware and complete osseous interlaminar fusion without any access for a classic interlaminar LP. Note the widely patent neural foramina. The *white crescent* represents the target for TFLP. C and D, Sagittal 3D volumetric T2-weighted images of a healthy person obtained with 3T MR imaging. C, Image obtained slightly lateral to the neural foramen. D, Image obtained at the foramen. Flow voids of the lumbar arteries (*arrowheads*) and larger caliber lumbar veins (*arrows*) are seen in the anterior superior aspect of the foramen. A branching ascending lumbar vein is seen coursing toward a higher level neural foramen (*curved arrow*). More venous structures are seen in the inferior aspect of the foramen (*arrows* in D). Exiting nerve roots are shown within the center of the foramen (*dashed arrows*).

pseudomeningocele communicating with the CSF, percutaneous aspiration of the fluid collections and CT myelography were requested to determine the etiology of the pain and evaluate the provisional diagnosis of pseudomeningocele. Both procedures were scheduled on the same day at the request of the ordering surgeon, given the patient's social and transportation difficulties.

The patient was placed in a prone position under moderate sedation. The initial intent was to drain enough of the midline fluid to allow a steep oblique interlaminar approach for myelography using a combination of fluoroscopy and sonography. After 46 mL of fluid was drained, sonography showed residual fluid that, if traversed, could potentially contaminate the intrathecal compartment. Despite sedation, the patient was too agitated to safely undergo a C1–2 puncture, and rescheduling with the patient under general anesthesia was not desirable. As the back was already exposed and appropriately positioned, we elected to attempt TFLP. After re-prepping, a 5-inch 22-ga spinal needle was used to puncture the thecal sac at a 35° oblique transforaminal, infraneural approach at the L1–2 level using C-arm fluoroscopy, more oblique than usual for a transforaminal epidural injection (Fig 1). This approach was selected to minimize the risk of injury to the dorsal root ganglion, guiding the needle posterior and inferior to the known location of the ganglion seen by previous MR imaging and inferior to the conus medullaris. The patient tolerated the procedure well without any immediate complication.

Case 2

A 58-year-old man with a history of ankylosing spondylitis, morbid obesity, exaggerated thoracolumbar kyphosis, and T11 fracture had an extensive posterior surgical fusion from T4 through the pelvis. Following the operation, he developed bilateral quadriceps femoris weakness concerning for nerve compression, and an MR imaging was performed. Due to extensive metallic susceptibility, MR imaging findings were inadequate and a CT myelogram was planned. Due to ankylosing spondylitis, there was near-complete fusion of the posterior elements. An interlaminar lumbar puncture was attempted through a small L5–S1 laminectomy defect but was unsuccessful. A cervical puncture was also not ideal due to the patient's extreme cervical kyphosis secondary to ankylosing spondylitis. Therefore, a right TFLP was performed at L1–2 under CT guidance with a slightly oblique prone position using a 7 inch-long Quincke needle, with uncomplicated myelography.

Cases 3 through 9

Six patients with SMA type 2 and 1 with SMA type 3 were referred for intrathecal nusinersen injection. All patients with

SMA in this TFLP series had undergone extensive fusion procedures from the thoracic spine through the pelvis.

Preprocedural evaluation of lumbar spine radiographs and CT studies revealed extensive spinal fusion hardware and resultant complete osseous interlaminar fusion without any access for classic interlaminar LP (Fig 2). Alternative surgical options discussed with the patients included Ommaya reservoir and lumbar shunt placement (after drilling through the fused laminae). After we discussed the risks and benefits of the different approaches, these 7 patients with SMA decided to proceed with TFLP.

All procedures were successfully performed under CT guidance with the patient in the decubitus position without any need for sedation or general anesthesia.

Complications

Patient 3 experienced a post-LP headache after the second nusinersen injection, which resolved after 5 days with conservative management. Patient 4 had a post-LP headache after the first procedure, which resolved on the same day. This same patient experienced heat and pain at the injection site after the second injection, which resolved spontaneously within hours. Patient 6 had radicular pain after the third injection corresponding to the injection site, leading her to seek treatment in the emergency department. CT did not show any complications, and the pain resolved with conservative treatment. Patient 9 had post-LP headaches after 2 injections, both of which resolved the same day. In total, post-LP headache was observed following 4 procedures

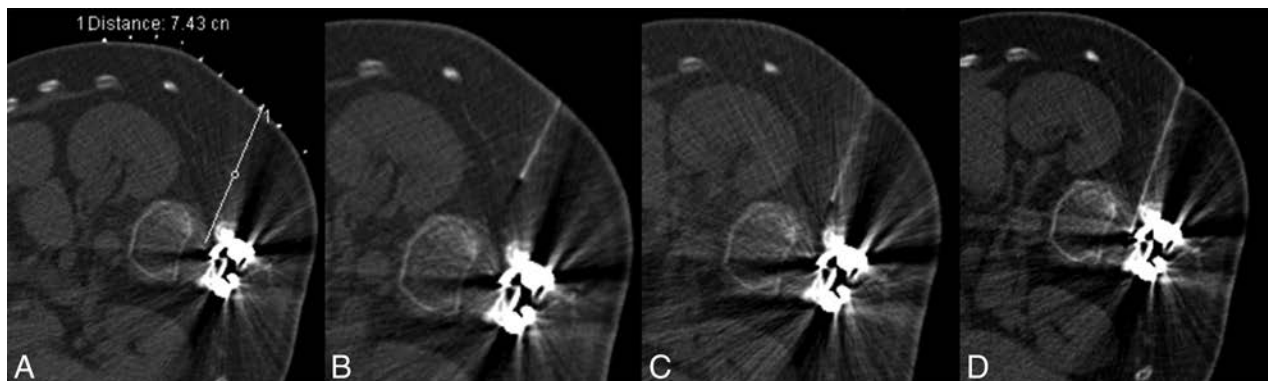


FIG 3. A 32-year-old man with SMA2 (case 5). *A*, Planning scout CT image with grid placement, obtained in the lateral decubitus position. *B*, Initial CT fluoroscopy image shows the needle more anteriorly oriented than desired. *C*, With basic needle manipulations, the needle is directed more posteriorly. *D*, Technically successful TFLP with the needle positioned immediately anterior to the facet.

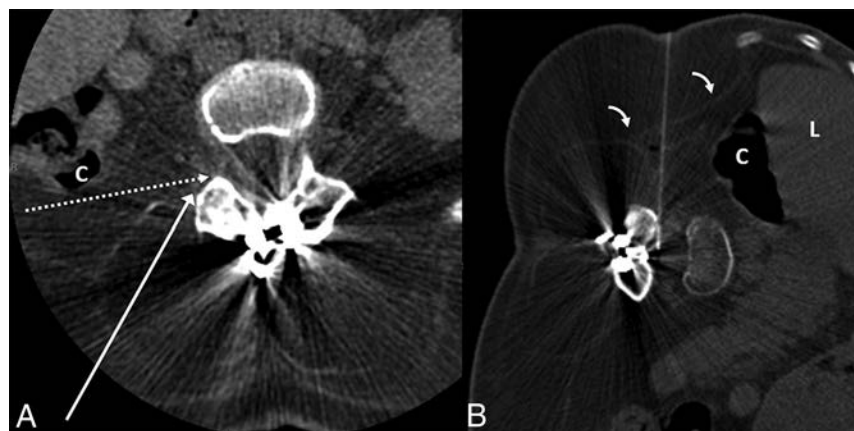


FIG 4. A 36-year-old woman with SMA2 (case 6). *A*, Preprocedural CT obtained in supine position at the level of L3–4 demonstrates extensive muscle atrophy. The *long white arrow* shows the normal needle trajectory for a transforaminal epidural steroid injection. The *dashed white arrow* indicates the needle trajectory for TFLP. Note that while supine, the posterior margin of the ascending colon (C) is along the proposed needle trajectory. *B*, CT fluoroscopy image during TFLP obtained with the patient in the left lateral decubitus position. The needle is advanced into the thecal sac with an angle slightly $>90^\circ$, just anterior to the facet. Note the anterior displacement of the liver (L) and ascending colon (C) in the decubitus position, providing a safer approach. Of note, the thin transversalis fascia (*bent arrows*) is well-visualized.

(15%), affecting 3 different patients. Only 1 of these 4 headaches lasted longer than 1 day, and all resolved with conservative management.

TFLP has been performed in our department since March 2016, and no long-term complications have been observed.

DISCUSSION

Anatomy

When performing TFLP, the proceduralist should be familiar with the anatomic location of the exiting nerve root, the radiculomedullary arteries, and, potentially, the artery of Adamkiewicz. The radiculomedullary branches are in the anterosuperior aspect of the foramen, while the ganglion and exiting nerve root are in the midportion of the foramen (Fig 2). Only smaller branch arteries and veins are found in the posterior aspect of the neural foramen.¹² In our method of TFLP, the needle is passed through the posterior portion of the foramen into the spinal canal (Figs 2–4) to minimize the risk of neurovascular injury. Thus, the operator should be proficient with transforaminal procedures as a prerequisite to TFLP.

Technique

Prior lumbar imaging is evaluated for each patient to select the safest level and side for the procedure based on the position of the conus medullaris, patency of the neural foramen, and positioning of the adjacent organs. Patients are positioned in the lateral decubitus position. In patients with scoliosis, the convex side is positioned upward. If CT is used for the procedure, an initial low-dose scout CT (80 kVp, 50–80 mAs) is performed with grid placement over the presumed injection side. Even with extensive hardware, the low-dose technique provides adequate visualization of the foramina. The planning CT is evaluated to confirm safety, and the shortest approach to the posterior neural foramen is selected, often necessitating a nearly 90° approach. The overlying skin is prepped, draped, and anesthetized

with 1% lidocaine via a 27-ga needle or J-tip. A 22-ga Quincke needle is advanced toward the posterior aspect of the neural foramen under imaging guidance (Figs 3 and 4). It is reported that during LP, orienting the cutting edge of the needle parallel to the longitudinally oriented dural fibers reduces the likelihood of CSF leaks.^{13,14}

Due to scoliosis and altered body wall anatomy, retroperitoneal organs such as the kidney and colon may be located more posteriorly than anticipated, especially as depicted by supine cross-sectional imaging. However, our experience has taught us that the decubitus position often shifts these organs anteriorly, allowing needle trajectories that did not appear feasible on the planning supine imaging (Fig 4).

While the procedure is relatively pain-free following skin anesthesia, we have noted that some patients feel sharp pain as the needle crosses the muscular portion of the posterolateral abdominal wall (Fig 4). We now advance the needle just to the transversalis fascia and administer additional lidocaine before advancing further.

Recently, Weaver et al¹⁵ reported their initial experience with

TFLP using conebeam CT for 15 transforaminal nusinersen injections in 4 adolescents with SMA (13–17 years of age). Three of their patients required general anesthesia, and 1 patient required mild sedation. In our experience, TFLP under CT guidance can be performed with any CT, ideally with CT fluoroscopy. Sedation was not necessary for the adult patients in our study. While Weaver et al did not discuss the needle positioning in detail, we believe that targeting the posterior neural foramen, preferably posteroinferiorly, will produce the fewest complications.

Safety

Lumbar transforaminal procedures are safe and effective for several indications. Transforaminal lumbar epidural steroid injections have been used commonly and safely with good clinical outcomes.^{16,17} A small number of case reports describe rare but serious adverse events, including spinal cord infarction and paraplegia following transforaminal epidural steroid injection.^{18–20} A recent multi-institutional study revealed low rates of serious adverse events in nearly 14,000 transforaminal epidural procedures, without any instance of hemorrhage, infection, or neurologic complication. Less serious effects such as increased pain, central steroid effect, and allergic reaction occurred in <5% of cases, with no statistically significant difference between interlaminar and transforaminal epidural steroid injections.²¹ Recently, CT-guided transforaminal blood patch has successfully treated ventral CSF leaks.²²

The most common complication of LP is post-LP headache, which typically occurs or worsens in the upright position and improves or resolves with lying down.²³ Younger age and female sex have been identified as significant risk factors, and these patients are more likely to receive an epidural blood patch.^{23,24} The incidence of post-LP headache varies between 2.2% and 32% with different techniques and instrumentation.^{23–25} Rodriguez et al²⁴ reported post-LP headache in 2.2% of 2141 patients who underwent fluoroscopy-guided lumbar puncture using either a 22- or 25-ga Quincke needle.

In the study by Haché et al,¹¹ 73 classic interlaminar LPs were performed in 28 patients with SMA for nusinersen injection. They reported 17 (23%) headache events, 9 with uncomplicated headache and 8 with post-lumbar puncture syndrome, consisting of headache with or without vomiting. Seven (10%) sought medical treatment and 1 (1.4%) required blood patch. In our small case series, the incidence of post-LP headache was 15%, and 1 (3.8%) sought additional medical treatment but was managed conservatively. No blood patch procedures were performed. While our post-LP headache rate was higher compared with the study of Rodriguez et al²⁴ (which contained a higher number of healthy patients), our complication rate with TFLP was lower than that for interlaminar LP compared with the study by Haché et al (containing only patients with SMA).^{11,24}

While there is evidence that cutting needles, such as the Quincke needles used in our study, lead to a higher rate of post-LP headache, the rate of headache requiring an epidural blood patch is not significantly different between the Quincke needle and non-traumatic needles.^{26,27} The study by Rodriguez et al²⁴ demonstrated that it is possible to obtain a very low rate of headache despite using Quincke needles. In addition, studies have shown a

high crossover rate from nontraumatic needles to Quincke needles, with some operators considering nontraumatic needles more difficult.^{28,29} While atraumatic needles are associated with a lower risk of headache from an interlaminar approach, it is premature to conclude that atraumatic needles will also yield a lower headache rate with TFLP. To our knowledge, our study and the study of Weaver et al¹⁵ provide the only information on this technique, and both used Quincke needles. We continue to use Quincke needles, which we can more precisely position into the posterior neural foramen. Further study will be required to compare the success rates and safety profiles of the different needle types with TFLP.

While we performed our first procedure under fluoroscopic guidance, all subsequent cases were performed with CT. With CT, the posterior portion of the neural foramen can be targeted from a lateral approach without fear of injuring the colon or kidney. Obliquity of <90° may result in the needle entering the anterolateral portion of the foramen, which, in our opinion, should be avoided if possible. Given the body wall changes in many of our patients with SMA, we elected to proceed with CT to minimize organ injury. We believe that TFLP will prove safe by fluoroscopy and, with consistent decubitus positioning, should be achievable. As a next step, we plan to incorporate sonography as an adjunct to fluoroscopy to confirm the safety of the needle path during future procedures.

Our study has several limitations. First, this is a retrospective evaluation of a method that has been used in only a few patients. Although we have not encountered any long-term complications, it has only been 18 months since our first TFLP. Additional time and further studies will be needed to characterize any long-term risks. Second, our study is largely based on our experience in patients with SMA with spinal fusion hardware and interlaminar osseous fusion. We believe that fluoroscopy-guided TFLP will likely prove feasible in patients with more typical anatomy, with CT-guided TFLP reserved for patients with more challenging anatomy, such as those with SMA, ankylosing spondylitis, or scoliosis. In summary, we believe that TFLP will prove an acceptable alternative to C1–2 puncture.

CONCLUSIONS

Although more research will be necessary to determine the relative safety of TFLP, we believe that the transforaminal approach will prove a viable alternative in patients with contraindications to classic interlaminar lumbar puncture or cervical puncture. In addition, decubitus positioning may uncover transforaminal approaches that do not appear possible when reviewing preprocedural supine imaging.

REFERENCES

1. Abel AS, Brace JR, McKinney AM, et al. **Practice patterns and opening pressure measurements using fluoroscopically guided lumbar puncture.** *AJNR Am J Neuroradiol* 2012;33:823–25 [CrossRef Medline](#)
2. Cauley KA. **Fluoroscopically guided lumbar puncture.** *AJR Am J Roentgenol* 2015;205:W442–50 [CrossRef Medline](#)
3. Ozdoba C, Gralla J, Rieke A, et al. **Myelography in the age of MRI: why we do it, and how we do it.** *Radiol Res Pract* 2011;2011:329017 [CrossRef Medline](#)
4. Gibbs WN, Skalski MR, Kim PE, et al. **C1–2 puncture: a safe, effica-**

- cious, and potentially underused technique. *Neurographics* 2017;7:1–8 CrossRef
5. Pomerantz SR, Buchbinder B, Hirsch JA. Suboccipital puncture of the cisterna magna under CT-guidance with intravenous enhancement in order to circumvent anomalous course of posterior inferior cerebellar artery (PICA). In: *Proceedings of the American Society of Spine Radiology Annual Symposium*, San Juan, Puerto Rico. February 24–27, 2005
6. Yousem DM, Gujar SK. Are C1–2 punctures for routine cervical myelography below the standard of care? *AJNR Am J Neuroradiol* 2009;30:1360–63 CrossRef Medline
7. Robertson HJ, Smith RD. Cervical myelography: survey of modes of practice and major complications. *Radiology* 1990;174:79–83 CrossRef Medline
8. Heinz ER. Development of the C1–C2 puncture in neuroradiology: a historical note. *AJNR Am J Neuroradiol* 2005;26:5–6 Medline
9. Kolb SJ, Kissel JT. Spinal muscular atrophy. *Neurol Clin* 2015;33:831–46 CrossRef Medline
10. Corey DR. Nusinersen, an antisense oligonucleotide drug for spinal muscular atrophy. *Nat Neurosci* 2017;20:497–99 CrossRef Medline
11. Haché M, Swoboda KJ, Sethna N, et al. Intrathecal injections in children with spinal muscular atrophy: nusinersen clinical trial experience. *J Child Neurol* 2016;31:899–906 CrossRef Medline
12. Demondion X, Lefebvre G, Fisch O, et al. Radiographic anatomy of the intervertebral cervical and lumbar foramina (vessels and variants). *Diagn Interv Imaging* 2012;93:690–97 CrossRef Medline
13. Flaatten H, Thorsen T, Askeland B, et al. Puncture technique and postural postdural puncture headache: a randomised, double-blind study comparing transverse and parallel puncture. *Acta Anaesthesiol Scand* 1998;42:1209–14 CrossRef Medline
14. Lybecker H, Moller JT, May O, et al. Incidence and prediction of postdural puncture headache: a prospective study of 1021 spinal anesthetics. *Anesth Analg* 1990;70:389–94 Medline
15. Weaver JJ, Natarajan N, Shaw DWW, et al. Transforaminal intrathecal delivery of nusinersen using cone-beam computed tomography for children with spinal muscular atrophy and extensive surgical instrumentation: early results of technical success and safety. *Pediatr Radiol* 2018;48:392–97 CrossRef Medline
16. Manchikanti L, Kaye AD, Manchikanti K, et al. Efficacy of epidural injections in the treatment of lumbar central spinal stenosis: a systematic review. *Anesth Pain Med* 2015;5:e23139 CrossRef Medline
17. Shim E, Lee JW, Lee E, et al. Fluoroscopically guided epidural injections of the cervical and lumbar spine. *Radiographics* 2017;37:537–61 CrossRef Medline
18. Hunttoon MA, Martin DP. Paralysis after transforaminal epidural injection and previous spinal surgery. *Reg Anesth Pain Med* 2004;29:494–95 Medline
19. Somayaji HS, Saifuddin A, Casey AT, et al. Spinal cord infarction following therapeutic computed tomography-guided left L2 nerve root injection. *Spine* 2005;30:E106–08 CrossRef Medline
20. Karaman H, Kavak GO, Tüfek A, et al. The complications of transforaminal lumbar epidural steroid injections. *Spine* 2011;36:E819–24 CrossRef Medline
21. El-Yahouchi CA, Plastaras CT, Maus TP, et al. Adverse event rates associated with transforaminal and interlaminar epidural steroid injections: a multi-institutional study. *Pain Med* 2016;17:239–49 CrossRef Medline
22. Amrhein TJ, Befera NT, Gray L, et al. CT fluoroscopy-guided blood patching of ventral CSF leaks by direct needle placement in the ventral epidural space using a transforaminal approach. *AJNR Am J Neuroradiol* 2016;37:1951–56 CrossRef Medline
23. Evans RW, Armon C, Frohman EM, et al. Assessment: prevention of post-lumbar puncture headaches: report of the therapeutics and technology assessment subcommittee of the American Academy of Neurology. *Neurology* 2000;55:909–14 CrossRef Medline
24. Rodriguez D, Branstetter BF 4th, Agarwal V, et al. Journal club: incidence of complications following fluoroscopically guided lumbar punctures and myelograms. *AJR Am J Roentgenol* 2016;206:20–25 CrossRef Medline
25. Armon C, Evans RW. Addendum to assessment: prevention of post-lumbar puncture headaches—report of the Therapeutics and Technology Assessment Subcommittee of the American Academy of Neurology. *Neurology* 2005;65:510–12 CrossRef Medline
26. Lavi R, Yarnitsky D, Rowe JM, et al. Standard vs atraumatic Whitacre needle for diagnostic lumbar puncture: a randomized trial. *Neurology* 2006;67:1492–94 CrossRef Medline
27. Strupp M, Schueler O, Straube A, et al. “Atraumatic” Sprotte needle reduces the incidence of post-lumbar puncture headaches. *Neurology* 2001;57:2310–12 CrossRef Medline
28. Castrillo A, Tabernero C, Garcia-Olmos LM, et al. Postdural puncture headache: impact of needle type, a randomized trial. *Spine J* 2015;15:1571–76 CrossRef Medline
29. Peterman SB. Postmyelography headache rates with Whitacre versus Quincke 22-gauge spinal needles. *Radiology* 1996;200:771–78 CrossRef Medline

Celebrating 35 Years of the AJNR

May 1983 edition

The Application of NMR Imaging to the Evaluation of Pituitary and Juxtaseptal Tumors

R. C. Hawkes,¹ G. N. Holland,^{1,2} W. S. Moore,¹ R. Corston,³ D. M. Kean,⁴ and B. S. Worthington⁴

Nuclear magnetic resonance (NMR) imaging was used to evaluate pituitary and juxtaseptal tumors in 37 patients representing a wide range of pathology. The value of the multiphase facility of NMR is emphasized in providing accurate volumetric information and establishing the topographical relation of tumors to adjacent structures. Current limitations of the method and possible future developments to improve diagnostic precision are discussed.

Investigation of pituitary and parasellar lesions can be particularly exciting because clinical manifestations, including visual failure and endocrinological disturbances, may occur when the lesion is in its early stages. Appropriate management demands precise localization and a distinction among various pathologies so that the appropriate operative route or field for irradiation can be chosen [1]. Early detection of suprasellar extension of pituitary adenomas is particularly important in preventing visual loss in patients undergoing medical treatment, especially when pregnancy occurs in women with prolactinomas, where there is a risk of accelerated tumor expansion [2]. Follow-up studies are valuable in assessing the effects of radiotherapy or drug therapy on tumor size. After plain skull radiography, computed tomography (CT) in the transverse axial plane is usually used to diagnose and evaluate tumors in the pituitary region [3-5]. Despite the high quality of images now available, it is sometimes difficult to determine the precise extent of extracapsular extension of pituitary tumors and to diagnose microadenomas. Invasive procedures are often required to confirm a suspected diagnosis of empty sella syndrome and to establish the relationship of any mass to the optic chiasm [6, 7].

Subjects and Methods

Proton nuclear magnetic resonance (NMR) scans using steady-state free precession (SSFP) techniques were performed with a Picker resistive NMR unit on 10 normal volunteers and 37 patients with known pathology in the pituitary region at the Queen's Medical Centre, Nottingham. The cases studied comprised 12 chromophobe pituitary adenomas; five acromegalies; four craniopharyngiomas; three cases each of prolactinoma, juxtaseptal aneurysm, and empty sella syndrome; one case each of recurrent chordoma, hypothalamic glioma, and nasopharyngeal carcinoma; and four colloid cysts of the third ventricle.

¹ Department of Physics, University of Nottingham, Nottingham, England.
² Present address: Philips International, Highfield Heights, OH 44143.
³ Department of Neurology, University of Nottingham, Nottingham, England.
⁴ Department of Academic Radiology, Queen's Medical Centre, University of Nottingham.

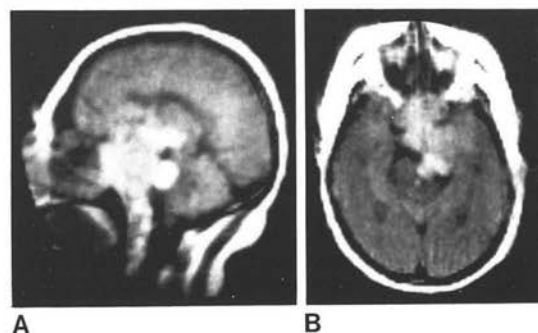
AJNR 4:221-222, May/June 1983 0195-6108/83/0403-0221 \$00.00/0 © 1983

Procedure

The normal pituitary gland is isodense with brain and is best seen on sagittal section. It is our practice to obtain a median sagittal scan and complement this with transverse and coronal scans as appropriate, using a slice thickness of 1 cm and an image time of 2 min. A typical examination of about eight sections takes 25 min. It is usually possible in no more than three attempts to obtain a section in which at least part of the third ventricle is included within the pituitary gland below. The normal gland is seen contrasted against a variable quantity of marrow and air within the basiphosphorus. The optic chiasm and optic nerves can be identified within the suprasellar cisterns on sagittal and coronal sections. The anatomy of the suprasellar cisterns shown on transverse section matches that seen with CT.

Results

NMR demonstrated clearly the presence and size of pituitary adenomas. Its multiphase facility was most valuable in delineating extracapsular extension. All tumors visualized by NMR were denser than brain tissue and all except one were homogeneous in texture. Although the bone of the fossa could not be seen, the degree of expansion of the floor could be observed from the configuration of the inferior margin of the tumor on sagittal and coronal sections. As

Preliminary Clinical Results of Proton (¹H) Imaging of Cranial Neoplasms: In vivo Measurements of T₁ and Mobile Proton Density

Thomas J. Brady,¹ Ferdinando S. Buonanno,² Ian L. Pykett,¹ Paul F. J. New,¹ Kenneth R. Davis,¹ Gerald M. Pohost,¹ and J. Philip Kistler²

Proton nuclear magnetic resonance (NMR) images reflecting T₁ relaxation time and approximating proton density were acquired and used to generate T₁ rate (1/T₁) maps. By region-of-interest selection, measurements of T₁ relaxation time were made from discrete volumes of the imaging plane. Such techniques were applied to the study of human cranial neoplasia and associated conditions of differential diagnostic importance (e.g., postoperative changes, radiation necrosis). Inversion-recovery NMR images exhibit a high lesion-detection sensitivity. In all patients, the specificity of NMR imaging is low since all abnormal areas appear as lesions darker than surrounding normal brain, reflecting a decreased proton density, prolonged T₁ values, or both. T₁ relaxation times are prolonged within neoplastic foci; however, absolute T₁ values overlap with those found in other lesions.

During the last decade, in vitro nuclear magnetic resonance (NMR) spectroscopic studies by several investigators [1-3] have demonstrated prolonged proton T₁ relaxation times in various malignant tissues when compared with values obtained from normal tissue. Prolongation of T₁ in tumors has been associated with, among other things, an increase in tissue water content [4]; however, the mechanism producing this phenomenon has not been fully elucidated.

In this preliminary study, NMR images were obtained that provide both qualitative assessment of relaxation time of normal tissue and approach attempts to detect central nervous system problems and to detect specific NMR characteristics.

Materials and Methods

The study population consisted of three patients with gliomas, abscesses, and postoperative neurologic history and of one computed tomography (CT)-guided biopsy of the Mass. Institute of Human Studies, was

T. J. Brady is a recipient of a G. M. Pohost is an established Investigator in Neurology, National Institutes of Health, Bethesda, Maryland.
¹ Center Unit, Massachusetts General Hospital.

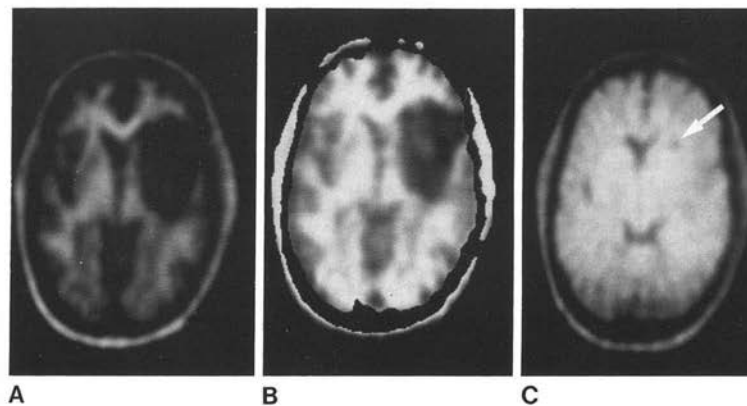
AJNR 4:223-226, May/June 1983

study. Histopathologic confirmation of the diagnosis was obtained in six patients.

NMR images were obtained using a prototype head imaging system developed by Technicare Corp. (Solon, OH). A static magnetic field of 0.147 Tesla, corresponding to a proton resonance frequency of 6.26 MHz, is generated by a four coil, resistive electromagnet. True three-dimensional volumetric data are acquired using two combined radiofrequency (RF) pulse sequences, as previously reported [5]. Postprocessing of the data allows reconstruction of images in any arbitrary plane, including levels corresponding to those of CT scans. Reconstruction of data from a saturation recovery-type technique with the 90°-90° interslice delay τ set to 1 sec generates images where the signal intensity is mainly dependent on mobile proton density (PD). Reconstruction of data from an inversion-recovery (IR) type of sequence with the 180°-90° interslice delay τ set to 400 msec provides images that are heavily T₁-weighted. The spatial resolution is about 3-4 mm and is isotropic, that is, equal in all directions.

Results and Discussion

Figure 1 contains representative images through a ventricular plane in a normal volunteer. The image that approximates PD (Fig. 1A) has uniform signal intensity within the brain parenchyma but has decreased signal intensity in regions of markedly prolonged T₁.



Pacemakers in MRI for the Neuroradiologist: Revisited

I read with interest the excellent article by Korutz et al¹ regarding their approach to MR imaging of pacemakers. The authors are to be praised for their logical and stepwise approach to device safety in the MR imaging environment. I assume that the timing of the publication of this article likely explains the omission of a reference to the sentinel publication on this topic.² That comprehensive publication also provides almost unprecedented strength of recommendations and quality of evidence quantifications.

I would like to suggest other approaches to several opinions promulgated by Korutz et al.

The 6-week waiting period of the MR imaging safety labeling condition historically results predominantly because during Phase III preclinical trials, device manufacturers did not want acute/subacute surgical postimplantation adverse events (such as spontaneous lead dislodgment) to be confused with MR imaging-related adverse events. Because these were the conditions under which these devices were studied, this same “6-week postimplantation” wording finds its way into the conditions of FDA approval. While scanning before 6 weeks postimplantation would indeed be off-label, it would be a shame for a clinically indicated or required MR imaging examination to be canceled simply because the study was needed earlier than 6 weeks postimplantation.

The article is directed to neuroradiologists, and it is indeed likely that the typical head or spine study they perform would expose at least part of the cardiovascular implantable electronic device (CIED) and/or its leads to clinically relevant transmitted radiofrequency (RF) and/or MR imaging gradient (ie, dB/dt) energies. Yet a clinically indicated MR imaging study might well be safely performed on a patient with a CIED if the requested MR imaging examination were 1) in a region where the anticipated gradient dB/dt exposure to the CIED and its leads would be minimal; and 2) there would be no significant exposure of the CIED or its components to transmitted RF energies or significant induced electric field pathways. These conditions might exist for imaging of the leg, knee, ankle, foot, and so forth of a typical-height adult, though such regions would admittedly not be routinely examined by a neuroradiologist.

The relatively recent FDA approval of the MR imaging condi-

tionally safe labeling for several brands of leadless intracardiac pacing devices is also noteworthy because such leadless devices negate most of the MR safety concerns raised in the article.

Induced Lenz forces from rapid motion of CIEDs through static magnetic spatial gradients (even for nonferrous electrically conductive materials) suggest that it might be appropriate to recommend that all patients and health care workers with implants move slowly within zone IV, especially when near or in the MR imaging scanner itself.

The authors note significant hesitation “for patients who are not awake and alert for the MR imaging examination, such as those who . . . are unable to report pain or discomfort during the examination” Because the primary CIED-related potential acute concerns associated with the gradient and RF fields are arrhythmogenesis and endocardial thermogenic damage/edema at the endocardial contact points of the intracardiac leads, it is unclear that a conscious responsive patient would be able to detect, let alone timely report, pain or discomfort in case of either thermal endocardial damage or arrhythmogenesis.

The authors conclude, “A few absolute contraindications remain for performing MR imaging in a patient with a CIED” (eg, “a device that was implanted <6 weeks before the MR imaging examination”). Our responsibility as physicians is to perform a benefit-risk assessment for each patient’s clinical scenario before providing blanket approvals—or cancellations—of any examination. MR imaging of patients with CIEDs is no exception. With appropriate clinical supervision from our electrophysiology colleagues and our ability to markedly decrease transmitted RF energies and today even imaging gradient dB/dt as needed, one might reasonably accept for MR imaging a patient with an unlabeled device with suspected cord compression, epidural abscess, device implanted for <6 weeks, and so forth. Alternatively, for even elective studies, the requested examination may be in an anatomic location for which no significant RF or imaging gradient exposure to the CIED will occur, regardless of the CIED label or the presence/absence of lead breaks. Therefore, as long as we are able to assess potential benefits and risks to our patients, I respectfully submit that absolute contraindications and carte blanche rejection of patients with devices from clinically indicated MR imaging studies without some level of case review and relative benefit-risk

ratio assessment should no longer be recommended or implemented.

Disclosures: Emanuel Kanal—*UNRELATED: Consultancy: Medtronic, St. Jude Medical.*

REFERENCES

1. Korutz AW, Obajuluwa A, Lester MS, et al. **Pacemakers in MRI for the neuroradiologist.** *AJNR Am J Neuroradiol* 2017;38:2222–30 [CrossRef](#) [Medline](#)
2. Indik JH, Gimbel JR, Alkmim-Teixeira R, et al. **2017 HRS expert consensus statement on magnetic resonance imaging and radiation exposure in patients with cardiovascular implantable electronic devices.** *Heart Rhythm* 2017;14:e97–e153 [CrossRef](#) [Medline](#)

 **E. Kanal**

Magnetic Resonance Services
Department of Radiology
University of Pittsburgh Medical Center
University of Pittsburgh
Pittsburgh, Pennsylvania

REPLY:

We would like to thank Dr Kanal for his interest in our article and his recent comments in response to our publication, “Pacemakers in MRI for the Neuroradiologist.” We agree with Dr Kanal that our responsibility as radiologists is to perform risk-benefit–based assessments on a patient-by-patient basis before approving or rejecting an MR imaging examination in a patient with a non-MR imaging–conditional device. However, we would like to reiterate that the goal of our article was to provide both a safe/conservative and practical framework that a nonexpert radi-

ologist could use in his or her own clinical practice. While certainly not exhaustive, we hope that our publication can help give patients who would have previously been deemed unsuitable for MR imaging examinations greater access to these tests in the future.

✉ **A.W. Korutz**

Department of Radiology

✉ **T.A. Hijaz**

Department of Radiology

✉ **J.D. Collins**

Department of Radiology

✉ **A.J. Nemeth**

Departments of Radiology and Neurology
Northwestern University Feinberg School of Medicine
Chicago, Illinois

<http://dx.doi.org/10.3174/ajnr.A5575>

Interaction Should Guide Management Decisions

It is with great interest that we read the recent article by Jadhav et al¹ concerning subgroup assessments in the SWIFT PRIME trial, especially for collateral status. They reported, “Outcomes stratified by collateral status had a benefit with thrombectomy across all groups: none-to-fair collaterals (33% versus 0%), good collaterals (58% versus 44%), and excellent collaterals (82% versus 28%).” They also reported, “A beneficial effect of endovascular therapy was observed over IV tPA alone across all levels of collateral flow, with the greatest effect in patients with excellent collaterals (82% versus 28%, $P = .008$).”

The authors reported that benefit persisted across multiple subgroups, but they still concluded, “Overall, this report supports the selection of patients for intra-arterial therapy on the basis of favorable patient characteristics (small core, good collateral circulation).” We do not agree with this conclusion because these patient characteristics were, foremost, assessed for prognosis, not treatment effect. Tests for statistical interaction between the predictors (treatment allocation arm and subgroups defined post hoc) were not performed, making the interpretation of data difficult.

The value and role of interaction testing and why it is not appropriate to test for superiority of a treatment in single subgroups are well presented in a *Lancet* educational series.² In short, interaction evaluates whether the combination of 2 predictors affects the outcome in other ways than expected by each variable alone. To test for superiority in single subgroups is inappropriate because both false-negative (sample size reduced) and false-positive (multiple testing) findings are possible.

In the current example, having treatment was better than not having treatment,³ and having good collaterals was better than having bad collaterals—both among those treated and among those not treated.¹ Thus, it seems that treatment is effective regardless of collateral status, and no obvious interaction is observed. A reasonable alternative hypothesis to test would have been that those with poor collaterals would do poorly, both with and without treatment; thus, the subgroup affects the treatment effect, which would be the basis for an interaction. For the sake of argument, let us assume that these results instead came from a large sample, that formal interaction tests had been performed, and that no interaction was detected. In such

circumstances, patient characteristics would have affected prognosis, but not treatment effect, an important distinction: To treat those with good collaterals will result in excellent outcome in the eyes of the interventionist (high share of recoveries), but to treat regardless of collateral status will create more patient benefit (because all benefit) but a worse outcome in the eyes of the interventionist (lower share of recoveries). We advocate that the latter is more relevant, but this is not consistent with the authors’ conclusions.

However, given the current small sample of 109 patients, divided into 6 groups, the risk of false-negative findings for interaction is high. The finding that having good collaterals was associated with a better outcome in the IV tPA arm compared with having excellent collaterals in the IV tPA arm further supports the study being underpowered and findings possibly being spurious and/or the result of multiple testing.

We encourage the authors to merge their data on a patient level with those of other recent similar trials so that these analyses will be well-powered and meaningful. We advocate against clinical decision-making based on the current preliminary data.

Disclosures: Elias Johansson—UNRELATED: Grants/Grants Pending: Several grants totaling \$520,000, all from nonprofit research bodies, the majority from the Swedish Government: Västerbotten County (\$400,000), Neurological Research Fund at Umeå University Hospital, Northern Swedish Stroke Fund, National Swedish Stroke fund, Jeansson Foundation*; Royalties: text books, Comments: about \$100–\$200 annually in royalties for 2 book chapters in a stroke book in Swedish. Jonatan Salzer—UNRELATED: Grants/Grants Pending: Synapsys, Comments: nystagmus investigation equipment donated for research*; Stock/Stock Options: Eurocine Vaccines, SensoDetect, Comments: stocks worth \$130 in 2 biomed starter companies making flu vaccines (Eurocine Vaccines) and neuropsychiatric diagnostic equipment (Sensodetect)*. *Money paid to the institution.

REFERENCES

1. Jadhav AP, Diener HC, Bonafe A, et al; SWIFT PRIME Investigators. **Correlation between clinical outcomes and baseline CT and CT angiographic findings in the SWIFT PRIME trial.** *AJNR Am J Neuroradiol* 2017;38:2270–76 CrossRef Medline
2. Rothwell PM. **Treating individuals 2: subgroup analysis in randomised controlled trials—importance, indications, and interpretation.** *Lancet* 2005;365:176–86 CrossRef Medline
3. Saver JL, Goyal M, Bonafe A, et al; SWIFT PRIME Investigators. **Stent-retriever thrombectomy after intravenous t-PA vs. t-PA alone in stroke.** *N Engl J Med* 2015;372:2285–95 CrossRef Medline

● E. Johansson
● J. Salzer

Pharmacology and Clinical Neuroscience
Umeå University
Umeå, Sweden

REPLY:

We thank Johansson and Salzer for their response to our article. We agree that several considerations of our study are limited by the small sample size. However, the main objection of the authors is with the statement in the conclusion of our article, “Overall, this report supports the selection of patients for intra-arterial therapy on the basis of favorable patient characteristics (small core, good collateral circulation) and low likelihood of recanalization with intravenous thrombolysis (large and proximal clot burden).” They fail to mention the sentence that follows, “Additional studies will be needed to further understand the continued benefit of intra-arterial treatment for patients with larger infarct burden or distal occlusions.”

Any clinical trial is powered primarily to understand main effects. This was the case even with the Solitaire With the Intention for Thrombectomy as Primary Endovascular Treatment (SWIFT PRIME) trial.¹ Subgroup analysis is to look for patterns that might help physicians make more considered assessments on prognosis and effect modification. These analyses are therefore not level 1 evidence but suggest the need for confirmatory studies within those subgroups. Some of these studies may be possible while others may never happen. Physicians then draw reasonable conclusions based on the data presented, their own heuristics, and any other current evidence to inform their practice. They can decide to wait for further confirmatory studies. This is what we suggested.

We agree that the absence of statistically significant effect modification by a variable on the relationship between the treatment and the outcome is not evidence for lack of effect modification. Small sample size is a problem with tests of effect modification in any clinical trial because the trial is invariably not powered to test for the presence or absence of such effect modification. We also agree that multiple testing within multiple subgroups increases the likelihood of type I error (stating that there is signal when there is none). Given the small sample size in our study, we therefore deliberately avoided looking for statistical interaction

(effect modification) to avoid both problems described above. Observations of our results graphically (see Figs 1 and 4 in our article) suggest that there is evidence of benefit from intra-arterial therapy versus controls in patients with a small baseline infarct core and good collateral circulation; however, we wanted to caution our readers that they should not assume from our data that a similar effect exists in patients with a large baseline core or poor collaterals. This is so because biologically, it is plausible that these patients with large baseline infarcts or very poor collaterals may have poorer outcomes on average even with good treatment. Therefore, we suggested a cautionary last sentence, “Additional studies will be needed to further understand the continued benefit of intra-arterial treatment for patients with larger infarct burden or distal occlusions,” instead of giving the readers a spurious message that patients with low ASPECTS or poor collaterals are likely to benefit to the same extent as patients with small core or good collaterals.

We therefore agree with the authors that future clinical trials and analysis of larger pooled datasets will be helpful in building more evidence for refining selection of patients who may benefit from intra-arterial therapy.² Our study is one small step in that direction.

REFERENCES

1. Saver JL, Goyal M, Bonafe A, et al; SWIFT PRIME Investigators. **Stent-retriever thrombectomy after intravenous t-PA vs. t-PA alone in stroke.** *N Engl J Med* 2015;372:2285–95 [CrossRef Medline](#)
2. Goyal M, Menon BK, van Zwam WH, et al; HERMES collaborators. **Endovascular thrombectomy after large-vessel ischaemic stroke: a meta-analysis of individual patient data from five randomised trials.** *Lancet* 2016;387:1723–31 [CrossRef Medline](#)

● **A.P. Jadhav**

Department of Neurology and Neurological Surgery
University of Pittsburgh Medical Center
Pittsburgh, Pennsylvania

● **B.K. Menon**

● **M. Goyal**

Department of Clinical Neurosciences and Radiology
University of Calgary
Calgary, Alberta, Canada

<http://dx.doi.org/10.3174/ajnr.A5617>

Triage in the Angiography Suite for Mechanical Thrombectomy in Acute Ischemic Stroke: Not Such a Good Idea

The recent evidence on the effectiveness of mechanical thrombectomy (MT) for the treatment of acute ischemic stroke (AIS) with large-vessel occlusion¹ has led to rethinking of the patient workflow. Indeed, the need to rapidly bring the patients eligible for MT into the angiography suite has caused the neurologists, interventional neuroradiologists, and anesthesiologists to find new routines to minimize, as much as possible, the time between symptom onset and the recanalization by endovascular means.¹⁻³ The main reason for this rationalization of patient management is that time to recanalization has a dramatic influence on the neurologic outcome. For instance, it has been shown in the meta-analysis of Saver et al (2016)¹ that for every 4 minutes' delay in emergency department door-to-reperfusion time, 1 of every 100 treated patients had a worse disability outcome, leading to a lower benefit of MT initiated 7.3 hours after symptom onset.

One of the options proposed to reduce this critical delay is to perform the triage directly in the angiography suite. Indeed, most of the manufacturers have developed new imaging tools to obtain, in the angiography suite, via a conebeam CT acquisition with flat panel technology, unenhanced C-arm CT, C-arm CT angiography, and perfusion acquisitions using intravenous contrast material injection. Even if the accuracy of flat panel conebeam CT perfusion has still to be demonstrated, this technique may be helpful in detecting hypoperfused brain tissue that would benefit from revascularization.

This "all-inclusive" option with C-arm CT acquisitions seems, at first glance, very seductive because it reduces the delay between imaging acquisition and groin puncture and thus the revascularization time.

However, in our opinion, some limitations weaken the validity of this workflow. Indeed, in our institution (Pitié-Salpêtrière Hospital), <30% of patients with sudden onset of neurologic deficit (ie, suspicion of acute ischemic stroke) will be eligible for mechanical thrombectomy, with the remaining patients having AIS without large-vessel occlusion or parenchymal hematoma or stroke mimics. Screening all these patients in the angiography suite would be a considerable waste of time and not cost-effective. Indeed, the average time to set up the patient on the angiography

suite table is approximately 5 minutes. The acquisition time for flat panel CT, CTA, and CT perfusion is at least 5–10 minutes. If no stroke is depicted, the angiography suite should be cleaned with a strict protocol of biocleaning (ISO7 standard) to prevent any infectious risk, because angiography suites are considered as surgical operating rooms. This biocleaning lasts at least 30 minutes. Thus, for a stroke mimic or a hematoma, the angiography suite will not be available for other procedures for at least 45 minutes to 1 hour. Due to the volume of patients admitted with suspected AIS in academic centers and to the low rate of patients who finally undergo MT among them, many patients will have a "futile" imaging in the angiography suite (ie, imaging that will not lead to an endovascular procedure).

In our opinion, triage in the angiography suite could be a potentially good option only in centers with a low volume of elective cases and/or in centers where the MR imaging or CT is rarely available or very distant geographically from the angiography suite.

One could argue that a dedicated angiography suite only for MT could be an option to overcome this limitation. However, it would not be cost-effective because the flow of patients with AIS requiring MT is highly variable.

Others would advocate that patients should be referred directly to the angiography suite on the basis of triage using clinical scores.⁴ However, it has been shown that such scores are not accurate enough to depict AIS with large-vessel occlusion.⁵

In conclusion, rethinking the workflow of patients with AIS who need MT is a major leap forward to improve the functional outcome for these patients. However, it should not penalize the other patients treated in our hospitals. These improved workflows should remain cost-effective to be valid; our enthusiasm should not lead us to use a sledgehammer to crack a nut.

ACKNOWLEDGMENTS

The authors thank M. Pierre Grare and Bénédicte Ibert for their help in the English editing of the manuscript.

Disclosures: Frédéric Clarençon—UNRELATED: Consultancy: Balt, Medtronic, Codman Neurovascular. Nader-Antoine Sourour—UNRELATED: Consultancy: Balt, Medtronic.

REFERENCES

1. Saver JL, Goyal M, van der Lugt A, et al; HERMES Collaborators. **Time to treatment with endovascular thrombectomy and outcomes from ischemic stroke: a meta-analysis.** *JAMA* 2016;316:1279–88 [CrossRef](#) [Medline](#)
2. Rinaldo L, Brinjikji W, McCutcheon BA, et al. **Hospital transfer associated with increased mortality after endovascular revascularization for acute ischemic stroke.** *J Neurointerv Surg* 2017;9:1166–72 [CrossRef](#) [Medline](#)
3. Ribo M, Boned S, Rubiera M, et al. **Direct transfer to angio suite to reduce door-to-puncture time in thrombectomy for acute stroke.** *J Neurointerv Surg* 2018;10:221–24 [CrossRef](#) [Medline](#)
4. Jadhav AP, Kenmuir CL, Aghaebrahim A, et al. **Interfacility transfer directly to the neuroangiography suite in acute ischemic stroke patients undergoing thrombectomy.** *Stroke* 2017;48:1884–89 [CrossRef](#) [Medline](#)
5. Turc G, Maier B, Naggara O, et al. **Clinical scales do not reliably identify acute ischemic stroke patients with large-artery occlusion.** *Stroke* 2016;47:1466–72 [CrossRef](#) [Medline](#)

✉ F. Clarençon

Paris VI University, Pierre et Marie Curie
Paris, France
Department of Neuroradiology, Assistance Publique–Hôpitaux de Paris
Pitié-Salpêtrière Hospital
Paris, France

✉ C. Rosso

Paris VI University, Pierre et Marie Curie
Paris, France
Urgences Cérébro-Vasculaires, Assistance Publique–Hôpitaux de Paris
Pitié-Salpêtrière Hospital
Paris, France
INSERM U 1127, CNRS UMR 7225
Sorbonne Universités, UPMC Univ Paris 06 UMR S 1127
Institut du Cerveau et de la Moelle Épinrière, ICM, F-75013
Paris, France

✉ V. Degos

Paris VI University, Pierre et Marie Curie
Paris, France
Department of Anesthesiology, Assistance Publique–Hôpitaux de Paris
Pitié-Salpêtrière Hospital
Paris, France

✉ E. Shotar

Paris VI University, Pierre et Marie Curie
Paris, France
Department of Neuroradiology, Assistance Publique–Hôpitaux de Paris
Pitié-Salpêtrière Hospital
Paris, France

✉ C. Rolla-Bigliani

Department of Neuroradiology, Assistance Publique–Hôpitaux de Paris
Pitié-Salpêtrière Hospital
Paris, France

✉ Y. Samson

Paris VI University, Pierre et Marie Curie
Paris, France
INSERM U 1127, CNRS UMR 7225
Sorbonne Universités, UPMC Univ Paris 06 UMR S 1127
Institut du Cerveau et de la Moelle Épinrière, ICM, F-75013
Paris, France

Department of Anesthesiology, Assistance Publique–Hôpitaux de Paris
Pitié-Salpêtrière Hospital
Paris, France

✉ S. Alamowitch

Paris VI University, Pierre et Marie Curie
Paris, France
Department of Vascular Neurology
Saint-Antoine Hospital
Paris, France

✉ N.-A. Sourour

Department of Neuroradiology, Assistance Publique–Hôpitaux de Paris
Pitié-Salpêtrière Hospital
Paris, France